

Thermodynamic and optical properties of naphthalene, fluorene and fluorenone derivatives

Juliana Andreia Silva Alves Oliveira

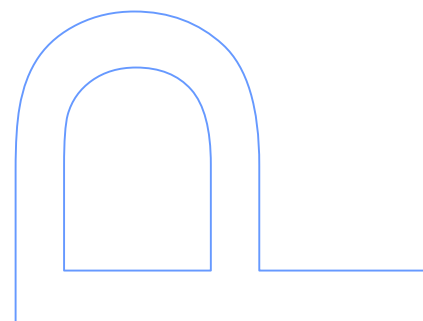
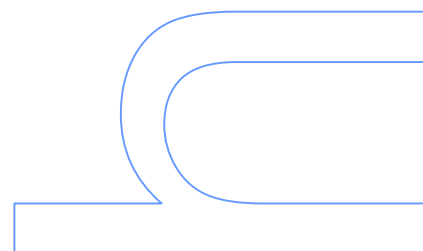
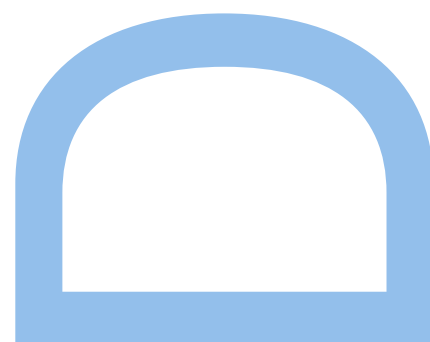
Doutoramento em Química 2016
Departamento de Química e Bioquímica
Faculdade de Ciências da Universidade do Porto

Orientador

Manuel João dos Santos Monte
Professor Associado do Departamento de Química e Bioquímica
Faculdade de Ciências da Universidade do Porto

Co-orientador

Maria das Dores Melo da Cruz Ribeiro da Silva
Professora Associada do Departamento de Química e Bioquímica
Faculdade de Ciências da Universidade do Porto



To Mom, Dad and B

Abstract

This dissertation describes the thermodynamic and optical study of 16 fluorene derivatives, 4 fluorenone derivatives and 3 naphthalene derivatives, some of which were synthesized for this purpose.

Differential scanning calorimetry analysis was performed in order to detect transitions between condensed phases and to determine their enthalpies and temperatures of transition.

The crystalline vapor pressures of all the compounds studied were measured using the Knudsen mass-loss effusion method and/or a static method based on capacitance manometers. The latter method also allowed the measurement of the liquid vapor pressures of some of the compounds, enabling phase diagram representations. Sublimation and vaporization properties (standard molar enthalpy, entropy and Gibbs energy) were determined from the vapor pressure dependency with temperature, and occasionally using also Calvet microcalorimetry.

The standard molar enthalpies of formation in the crystalline phase, were derived from the standard massic energy of combustion, at $T = 298.15$ K, measured by combustion calorimetric techniques for some of the compounds studied. For these compounds, the combination of the standard molar enthalpies of formation in the crystalline phase and the standard molar enthalpies of sublimation yielded the standard molar enthalpies of formation, in the gaseous phase. The determined results enabled the evaluation of the thermodynamic stability of the compounds by means of the Gibbs energy of formation, in crystalline and gaseous phases.

After convenient tests on a new apparatus, fluorescence spectroscopic measurements were performed to determine the fluorescence quantum yield and emission properties of the compounds studied.

Keywords: Fluorene derivatives; Fluorenone derivatives; Naphthalene derivatives; Vapor pressure; Sublimation; Vaporization; Fusion; Combustion; Enthalpy; Entropy; Gibbs energy; Fluorescence; Quantum yield; Volatility; Stability.

Resumo

Nesta dissertação é descrito o estudo termodinâmico e ótico de 16 derivados do fluoreno, 4 derivados da fluorenona e 3 derivados do naftaleno, alguns dos quais foram sintetizados neste trabalho.

Calorimetria diferencial de varrimento foi realizada com os objetivos de detetar as transições entre as fases condensadas e determinar as respectivas temperaturas e entalpias molares de fusão padrão.

As pressões de vapor da fase cristalina de todos os compostos estudados foram medidas utilizando o método de efusão de Knudsen e/ou um método estático baseado em manómetros de capacitância. O método estático também permitiu a medição pressões de vapor da fase líquida de alguns dos compostos, possibilitando a representação dos respetivos diagramas de fase. As propriedades de sublimação e vaporização (entalpia, entropia e energia de Gibbs molar padrão) foram determinados a partir da dependência da pressão do vapor com a temperatura e, ocasionalmente, usando também microcalorimetria Calvet.

As entalpias molares de formação padrão na fase cristalina, foram derivadas a partir de energias mássicas de combustão padrão, a $T = 298.15$ K, determinadas por calorimetria de combustão para alguns dos compostos estudados. Para estes compostos, a combinação das respetivas entalpias molares de formação padrão na fase cristalina com as entalpias molares de sublimação padrão permitiu o cálculo das entalpias molares de formação padrão, na fase gasosa. Estes resultados permitiram a avaliação da estabilidade termodinâmica dos compostos por meio da energia de Gibbs de formação, das fases cristalinas e gasosas.

Após testes convenientes a um novo aparelho, as propriedades de emissão dos compostos estudados, incluindo o rendimento quântico de fluorescência, foram determinadas por espectroscopia de fluorescência.

Palavras-chave: Derivados do fluoreno; Derivados da fluorenona; Derivados do naftaleno; Pressão de vapor; Sublimação; Vaporização; Fusão; Combustão; Entalpia; Entropia; Energia de Gibbs; Fluorescência; Rendimento quântico; Volatilidade; Estabilidade.

Acknowledgments

I'd like to express my deepest gratitude,

To Professor Manuel João Monte, for the guidance throughout the years, for the fruitful discussions and incentive, and for challenging me daily to develop the rational thinking essential to a good scientist, which greatly contributed to the realization of this work.

To Professor Maria da Dores Ribeiro da Silva, for the support and availability, for the transmitted knowledge and the constant encouragement.

To the late Professor Manuel Ribeiro da Silva, for always teaching me something new, for all the given opportunities that lead to this point and for all they may lead to in the future.

To all the professors and colleagues in the RG2 and RG3 groups, in which I include Mr. Carlos Torres, who in one way or another contributed to this work, I thank the regard with which I was received and all the support provided.

A special mention to Ana Rita Figueira, for being a 'partner in crime', for the contagious good mood, invaluable lessons and always prompt and unconditional assistance that cannot be put into words.

To Professor Fernanda Borges and Alexandra Gaspar, for kindly welcoming me into their group and providing me with the necessary tools for what was to be a brief collaboration and ended up becoming a long 'synthetic' endeavor.

To Joana, Tiago, Maria João and Sílvia, for representing the purest definition of friendship. The past years wouldn't have been the same without you.

To my loving parents and my dear B, for the never ending patience, encouragement, support and love. For the constant reminder that it would all be worth it.

Again and always, to Professor Alice.

Thanks are also due to the Department of Chemistry and Biochemistry of the Faculty of Sciences, University of Porto, and to CIQ-UP (Centro de Investigação em Química), for providing the facilities and conditions necessary for the execution of this work.

And, finally, to FCT (Fundação para a Ciência e Tecnologia) for the award of the Ph. D. research grant (SFRH/BD/80372/2011), included in the research project PTDC/QUI-QUI/102814/2008, and for granting the financial support for the presentation of this research in international scientific conferences.



General index

	Page
Abstract	III
Resumo	IV
Acknowledgments	V
General index	VII
Figure index	XV
Table index	XX
1. Introduction	1
1.1. Aim of the study	3
1.2. Compounds studied	4
1.3. Methods used	7
References	9
2. Synthesis	13
2.1. Introduction	15
2.2. General information	15
2.2.1. Reagents and solvents	15
2.2.2. General procedures and instrumentation	15
2.2.3. Synthetic yields and purity degrees	17
2.3. Synthetic procedures	18
2.3.1. Halogenated fluorene derivatives	18
2.3.1.1. 2,7-Difluorofluorene	18
2.3.1.2. 2,7-Dichlorofluorene	19
2.3.1.3. 2,7-Diiodofluorene	19
2.3.1.4. 2-Chlorofluorene	20
2.3.1.5. 9-Chlorofluorene	24
2.3.1.6. 9-Iodofluorene	25
2.3.2. Halogenated fluorenone derivatives	27
References	28
3. Experimental methods	29
3.1. Purification and characterization	31
3.1.1. Purification methods	31
3.1.2. Purity analysis	31

3.2. Calorimetric methods	33
3.2.1. Differential calorimetry	33
3.2.1.1. Introduction to differential calorimetry	33
3.2.1.2. Power compensation calorimetry: Differential scanning calorimeter	34
3.2.1.2.1. Typical thermogram and treatment of experimental results	35
3.2.1.2.2. Calibration	36
3.2.1.2.3. Description of the apparatuses	37
3.2.1.2.4. Experimental procedure	38
3.2.1.3. Heat flux calorimetry: Calvet Microcalorimeter	39
3.2.1.3.1. Typical thermogram and treatment of experimental results	40
3.2.1.3.2. Calibration	42
Temperature calibration	42
Blank calibration	43
Calorimeter calibration	43
3.2.1.3.3. Description of the apparatus	44
Calvet microcalorimeter	44
Vacuum pumping system	45
Vacuum line and calorimetric cells	45
3.2.1.3.4. Experimental procedure	46
3.2.2. Combustion calorimetry	47
3.2.2.1. Introduction to combustion calorimetry	47
3.2.2.1.1. Combustion of organic compounds containing bromine	48
3.2.2.2. Theoretical and technical basis of the method	49
3.2.2.2.1. Variation of temperature in adiabatic conditions	49
3.2.2.2.2. Variation of temperature in adiabatic conditions in rotating bomb combustion calorimetry	52
3.2.2.2.3. Calibration of the calorimeter: Energy equivalent calculation	54
3.2.2.2.4. Combustion auxiliaries	58
3.2.2.2.5. Standard massic energy of combustion: Washburn corrections	59
3.2.2.2.6. Standard molar enthalpy of combustion and formation	62
3.2.2.3. Description of the combustion calorimetric systems	63
3.2.2.3.1. Static bomb combustion calorimeter	64
Static combustion bomb	64
Calorimetric vessel	65
Thermostatic bath	66
3.2.2.3.2. Experimental procedure	66
3.2.2.3.3. Rotating bomb combustion calorimeter	67
Rotating combustion bomb	67
Calorimetric vessel	68
Thermostatic bath	69

3.2.2.3.4. Experimental procedure	69
3.2.2.3.5. Analysis of combustion products	70
Carbon dioxide recovery	70
Unburned compound and / or carbon residue	71
Analysis of nitric acid	71
Analysis of arsenic(III) oxide	72
3.3. Vapor pressure measurement methods	73
3.3.1. Introduction to the study of vapor pressures	73
3.3.1.1. Experimental methods for vapor pressure measurement	73
Ebulliometric methods	73
Gas saturation methods	74
Effusion methods	74
Static methods	74
Association of different methods	74
3.3.1.2. Vapor pressure equations	74
3.3.1.2.1. Clausius-Clapeyron equation	75
3.3.1.2.2. Thermodynamic properties at a reference temperature	77
3.3.1.2.3. Clarke-Glew equation	78
3.3.1.2.4. Thermodynamic characterization of phase transitions: temperature and pressure variables	79
3.3.2. Description of the vapor pressure measurement systems	81
3.3.2.1. Knudsen mass-loss effusion method	81
3.3.2.1.1. Ideal and real effusion processes	81
3.3.2.1.2. Deviations from the ideal conditions	82
Molecular flow	82
Probability of transmission	83
Condensation coefficient	84
Orifice area and equilibrium conditions	84
Surface diffusion	85
Alteration of vapor molar mass	85
3.3.2.1.3. Description of the apparatus	86
Pumping system	86
Sublimation chamber	86
Temperature measurement and control	87
Effusion cells	88
3.3.2.1.4. Experimental procedure	89
3.3.2.2. Static method with capacitance manometers	90
3.3.2.2.1. Thermal transpiration and other sources of error in a static method	90
3.3.2.2.2. Description of the apparatus	91
Capacitance manometer	91

Tubing system	93
Sample cell and thermostatic bath	93
Pumping system	93
Auxiliary and data acquisition systems	94
3.3.2.2.3. Experimental procedure	95
3.4. Photoluminescence spectroscopy	96
3.4.1. Introduction to photoluminescence	96
3.4.1.1. Fluorescence	97
3.4.1.2. Phosphorescence	98
3.4.2. Excited-state lifetimes and luminescence quantum yield	99
3.4.3. Quantification of emission and instrumentation	100
3.4.3.1. Integrating sphere based methods	100
3.4.4. Factors affecting accuracy	101
Temperature and pH	101
Solvent polarity and oxygen quenching	102
Self-absorption	102
Impurities and structural effects	102
Excimers and exciplexes	103
Light scattering	103
3.4.5. Spectroscopic apparatuses	103
3.4.6. Experimental procedure	106
3.4.6.1. Solution fluorescence	106
3.4.6.2. Solid state fluorescence	107
References	108
4. Experimental results	113
4.1. Introduction to experimental results	115
4.2. Thermodynamic results	117
4.2.1. General remarks	117
4.2.1.1. Thermodynamic properties of combustion	118
4.2.1.1.1. Calibration of the combustion calorimetric systems	118
4.2.1.1.2. Massic and molar energies and molar enthalpies of combustion	119
4.2.1.1.3. Apparent mass to true mass correction	120
4.2.1.2. Thermodynamic properties of phase transition	120
4.2.1.2.1. Temperatures and standard molar properties of fusion	120
4.2.1.2.2. Standard molar enthalpies of sublimation and vaporization	121
4.2.1.2.3. Enthalpies of sublimation and vaporization at a reference temperature	123
4.2.1.2.4. Standard molar entropies and Gibbs energies of sublimation and vaporization	125

4.2.1.2.5. Calorimetric determination of standard molar enthalpies of sublimation	125
4.2.1.3. Standard molar properties of formation, in crystalline and gaseous phases	126
4.2.2. Experimental results	129
4.2.2.1. 2-Substituted fluorenes	129
4.2.2.1.1. 2-Fluorencarboxaldehyde	129
Vapor pressures and thermodynamic properties of phase transition	129
Combustion calorimetry and thermodynamic properties of formation	132
4.2.2.1.2. 2-Aminofluorene	133
Vapor pressures and thermodynamic properties of phase transition	133
Combustion calorimetry and thermodynamic properties of formation	136
4.2.2.1.3. 2-Nitrofluorene	138
Vapor pressures and thermodynamic properties of phase transition	138
Combustion calorimetry and thermodynamic properties of formation	141
4.2.2.1.4. 2-Fluorofluorene	143
Vapor pressures and thermodynamic properties of phase transition	143
Combustion calorimetry and thermodynamic properties of formation	146
4.2.2.1.5. 2-Bromofluorene	147
Vapor pressures and thermodynamic properties of phase transition	147
Combustion calorimetry and thermodynamic properties of formation	150
4.2.2.1.6. 2-Iodofluorene	153
Vapor pressures and thermodynamic properties of phase transition	153
4.2.2.2. 2,7-Disubstituted fluorenes	157
4.2.2.2.1. 2,7-Di- <i>tert</i> -butylfluorene	157
Vapor pressures and thermodynamic properties of phase transition	157
Combustion calorimetry and thermodynamic properties of formation	162
4.2.2.2.2. 2,7-Difluorofluorene	164
Vapor pressures and thermodynamic properties of phase transition	164
4.2.2.2.3. 2,7-Dichlorofluorene	167
Vapor pressures and thermodynamic properties of phase transition	167
4.2.2.2.4. 2,7-Dibromofluorene	170
Vapor pressures and thermodynamic properties of phase transition	170
Combustion calorimetry and thermodynamic properties of formation	173
4.2.2.2.5. 2,7-Diodofluorene	176
Vapor pressures and thermodynamic properties of phase transition	176
4.2.2.3. 9-Substituted fluorenes	179
4.2.2.3.1. 9-Fluorencarboxylic Acid	179
Vapor pressures and thermodynamic properties of phase transition	180
Combustion calorimetry and thermodynamic properties of formation	183
4.2.2.3.2. 9-Phenyl-9-fluorenol	186

Vapor pressures and thermodynamic properties of phase transition	186
Combustion calorimetry and thermodynamic properties of formation	188
4.2.2.3.3. 9-Benzylidene fluorene	190
Vapor pressures and thermodynamic properties of phase transition	190
Combustion calorimetry and thermodynamic properties of formation	193
4.2.2.3.4. 9-Fluorene methanol	195
Vapor pressures and thermodynamic properties of phase transition	195
Combustion calorimetry and thermodynamic properties of formation	197
4.2.2.3.5. 9-Chlorofluorene	199
Vapor pressures and thermodynamic properties of phase transition	199
4.2.2.4. 2-Substituted fluorenes	202
4.2.2.4.1. 2-Aminofluorene	202
Vapor pressures and thermodynamic properties of phase transition	202
4.2.2.4.2. 2-Hydroxyfluorene	205
Vapor pressures and thermodynamic properties of phase transition	205
4.2.2.4.3. 2-Fluorofluorene	208
Vapor pressures and thermodynamic properties of phase transition	208
4.2.2.5. 2,7-Substituted fluorene	212
4.2.2.5.1. 2,7-Dibromofluorene	212
Vapor pressures and thermodynamic properties of phase transition	212
4.2.2.6. 2,6-Substituted naphthalenes	215
4.2.2.6.1. 2,6-Diethylnaphthalene	215
Vapor pressures and thermodynamic properties of phase transition	215
Combustion calorimetry and thermodynamic properties of formation	218
4.2.2.6.2. 2,6-Diisopropylnaphthalene	219
Vapor pressures and thermodynamic properties of phase transition	219
Combustion calorimetry and thermodynamic properties of formation	221
4.2.2.6.3. 2,6-Di- <i>tert</i> -butylnaphthalene	223
Vapor pressures and thermodynamic properties of phase transition	223
Combustion calorimetry and thermodynamic properties of formation	225
4.3. Photoluminescence properties	227
4.3.1. General remarks	227
4.3.2. Experimental results	229
4.3.2.1. Fluorene and fluorene derivatives	229
4.3.2.1.1. Fluorene	229
4.3.2.1.2. 2-Aminofluorene	233
4.3.2.1.3. 2-Fluorofluorene	234
4.3.2.1.4. 2,7-Di- <i>tert</i> -butylfluorene	235
4.3.2.2. Naphthalene and naphthalene derivatives	237

4.3.2.2.1. Naphthalene	237
4.3.2.2.2. 2,6-Diethylnaphthalene	240
4.3.2.2.3. 2,6-Diisopropylnaphthalene	241
4.3.2.2.4. 2,6-Di- <i>tert</i> -butylnaphthalene	243
4.3.2.3. Fluoranthene	245
References	247
5. Discussion and conclusions	253
5.1. Introduction	255
5.2. Thermodynamic properties	256
5.2.1. Thermodynamic properties of fusion	256
5.2.2. Thermodynamic properties of sublimation and vaporization	261
5.2.2.1. Fluorene and fluorene derivatives	261
5.2.2.1.1. Correlations and estimation equations	263
5.2.2.1.2. Enthalpic and entropic contributions to the standard Gibbs energies of sublimation	268
i) 2-Fluorencarboxaldehyde, 2-aminofluorene and 2-nitrofluorene	268
ii) 2- and 2,7- halogenated fluorenes	270
iii) 9-Substituted fluorenes	273
5.2.2.2. Fluorenone and fluorenone derivatives	276
5.2.2.2.1. Correlations and estimation equations	277
5.2.2.2.2. Enthalpic and entropic contributions to the standard Gibbs energies of sublimation	278
5.2.2.3. Naphthalene and naphthalene derivatives	280
5.2.2.3.1. Correlation between enthalpy and standard Gibbs energy of sublimation	280
5.2.2.3.2. Enthalpic and entropic contributions to the standard Gibbs energies of sublimation	282
5.2.3. Thermodynamic properties of formation	283
5.2.3.1. Thermodynamic stability	284
5.2.3.2. Enthalpic increments	286
5.3. Photoluminescence properties	289
5.3.1. Challenges and technical difficulties	289
5.3.2. Fluorescence properties of the compounds studied	290
5.3.2.1. Fluorene and 2,7-di- <i>tert</i> -butylfluorene	290
5.3.2.2. Naphthalene and naphthalene derivatives	294
5.4. Conclusions	297
References	298

Annexes	301
Annex A.	303
A.1. Units and conversions	303
A.2. Constants	303
Annex B.	304
B.1. Abbreviation, acronym and symbol list	304
Annex C.	308
C.1. ¹ H NMR, ¹³ C NMR and mass spectral data	308
C.1.1. 2,7-Difluorofluorene	308
C.1.2. 2,7-Dichlorofluorene	308
C.1.3. 2,7-Diiodofluorene	309
C.1.4. 9-Chlorofluorene	309
C.1.5. 2-Bromofluorenone	309
C.1.6. 2-Iodofluorenone	309
C.1.7. 2,7-Dichlorofluorenone	310
C.1.8. 2,7-Diiodofluorenone	310
C.2. Experimental results of test substances	311
C.2.1. Benzoic Acid	311
C.2.2. <i>N</i> -Methylnicotinamide	314
C.2.3. Pyrene	316
References	318

Figure index

	Page
1. Introduction	
Figure 1.1	3
Structure formulae and numbering of fluorene, fluorenone and naphthalene.	
2. Synthesis	
Figure 2.1.	16
General scheme of the starting materials and the final molecules synthesized in the course of this work (crossed arrows represent non-successful synthetic paths).	
3. Experimental methods	
Figure 3.1.	34
General schematic representation of a power compensation calorimeter.	
Figure 3.2.	36
Schematic representation of a typical power compensation DSC thermogram.	
Figure 3.3.	39
General schematic representation of a heat flux Calvet microcalorimeter.	
Figure 3.4.	41
Schematic representation of a typical Calvet microcalorimetry thermogram.	
Figure 3.5.	42
Representative thermodynamic cycle of the processes occurring during a Calvet microcalorimetry sublimation or vaporization experiment.	
Figure 3.6.	45
Schematic representation of the complete Calvet microcalorimeter.	
Figure 3.7.	50
Typical curve of the calorimetric temperature versus time during a combustion experiment.	
Figure 3.8.	56
Thermochemical cycle for the calculation of the energy equivalent of the calorimeter, ε_{cal} .	
Figure 3.9.	60
Thermochemical cycle for deriving the standard energy of combustion, $\Delta_c U^p$, at $T = 298.15$ K.	
Figure 3.10.	64
Schematic representation of the static combustion bomb and assembling parts.	
Figure 3.11.	65
Schematic representation of the static bomb calorimetric system.	
Figure 3.12.	67
Schematic representation of the rotating combustion bomb and calorimetric vessel.	
Figure 3.13.	68
Global schematic representation of the rotating bomb combustion calorimeter.	
Figure 3.14.	70
Carbon dioxide recovery system.	
Figure 3.15.	87
Schematic representation of the Knudsen mass loss effusion apparatus.	
Figure 3.16.	88
Schematic representation of the ovens inside the vacuum chamber and of the effusion cell.	

Figure 3.17.	Schematic representation of the static method apparatus.	92
Figure 3.18.	Image of the HP-VEE software data acquisition display.	94
Figure 3.19.	Simplified Jablonski diagram.	96
Figure 3.20.	Simple schematic representation of the interior of the integrating sphere of the Hamamatsu Quantaaurus-QY spectrometer.	104
Figure 3.21.	Image of the U6039-05 software data acquisition display.	105
Figure 3.22.	Example of excitation light and emission spectra on reference and sample.	105
Figure 3.23.	Quartz cuvette and lidded petri dish used for the fluorescence measurements in solution and in the solid state, respectively.	106
Figure 3.24.	Typical amounts of sample used for the solid state fluorescence measurements.	107

4. Experimental results

Figure 4.1.	Thermodynamic cycle for deriving the dependence of the enthalpy of sublimation or vaporization enthalpy with pressure.	121
Figure 4.2.	Plots of $\ln(p/\text{Pa})$ against $1000(K/T)$ of 2-fluorencarboxaldehyde.	130
Figure 4.3.	Plots of $\ln(p/\text{Pa})$ against $1000(K/T)$ of 2-aminofluorene.	135
Figure 4.4.	Plots of $\ln(p/\text{Pa})$ against $1000(K/T)$ of 2-nitrofluorene.	140
Figure 4.5.	Phase diagram ($\ln(p/\text{Pa})$ against $1000(K/T)$) of 2-fluorofluorene.	145
Figure 4.6.	Phase diagram ($\ln(p/\text{Pa})$ against $1000(K/T)$) of 2-bromofluorene.	148
Figure 4.7.	Phase diagram ($\ln(p/\text{Pa})$ against $1000(K/T)$) of 2-iodofluorene.	155
Figure 4.8.	Typical DSC thermogram of 2,7-di- <i>tert</i> -butylfluorene.	158
Figure 4.9.	Phase diagram ($\ln(p/\text{Pa})$ against $1000(K/T)$) of 2,7-di- <i>tert</i> -butylfluorene.	160
Figure 4.10.	Plots of $\ln(p/\text{Pa})$ against $1000(K/T)$ of 2,7-difluorofluorene.	165
Figure 4.11.	Phase diagram ($\ln(p/\text{Pa})$ against $1000(K/T)$) of 2,7-dichlorofluorene.	168
Figure 4.12.	Plots of $\ln(p/\text{Pa})$ against $1000(K/T)$ of 2,7-dibromofluorene.	172
Figure 4.13.	Plots of $\ln(p/\text{Pa})$ against $1000(K/T)$ of 2,7-diiodofluorene.	177
Figure 4.14.	Plots of $\ln(p/\text{Pa})$ against $1000(K/T)$ of 9-fluorencarboxylic acid.	182
Figure 4.15.	Plots of $\ln(p/\text{Pa})$ against $1000(K/T)$ of 9-phenyl-9-fluorenol.	187
Figure 4.16.	Plots of $\ln(p/\text{Pa})$ against $1000(K/T)$ of 9-benzylidene-fluorene.	192
Figure 4.17.	Phase diagram ($\ln(p/\text{Pa})$ against $1000(K/T)$) of 9-fluorene-methanol.	196
Figure 4.18.	Plots of $\ln(p/\text{Pa})$ against $1000(K/T)$ of 9-chlorofluorene.	200
Figure 4.19.	Plots of $\ln(p/\text{Pa})$ against $1000(K/T)$ of 2-aminofluorenone.	203
Figure 4.20.	Plots of $\ln(p/\text{Pa})$ against $1000(K/T)$ of 2-hydroxyfluorenone.	206
Figure 4.21.	Plots of $\ln(p/\text{Pa})$ against $1000(K/T)$ of 2-hydroxyfluorenone.	210
Figure 4.22.	Plots of $\ln(p/\text{Pa})$ against $1000(K/T)$ of 2,7-dibromofluorenone.	213

Figure 4.23.	Phase diagram ($\ln(p/\text{Pa})$ against $1000(K/T)$) of 2,6-diethylnaphthalene.	217
Figure 4.24.	Plots of $\ln(p/\text{Pa})$ against $1000(K/T)$ of 2,6-diisopropylnaphthalene.	220
Figure 4.25.	Plots of $\ln(p/\text{Pa})$ against $1000(K/T)$ of 2,6-di- <i>tert</i> -butylnaphthalene.	224
Figure 4.26.	Normalized UV-Vis absorption and fluorescence emission spectra of fluorene.	231
Figure 4.27.	Normalized fluorescence emission spectra of fluorene powder samples.	232
Figure 4.28.	Fluorescence emission spectra of 2-aminofluorene in powder form.	233
Figure 4.29.	Fluorescence emission spectra of 2-fluorofluorene in powder form.	234
Figure 4.30.	Normalized UV-Vis absorption and fluorescence emission spectra of 2,7-di- <i>tert</i> -butylfluorene.	236
Figure 4.31.	Normalized UV-Vis absorption and relative fluorescence emission spectra of naphthalene.	239
Figure 4.32.	Normalized UV-Vis absorption and relative fluorescence emission spectra of 2,6-diethylnaphthalene.	240
Figure 4.33.	Normalized UV-Vis absorption and relative fluorescence emission spectra of 2,6-diisopropylnaphthalene.	242
Figure 4.34.	Normalized UV-Vis absorption and relative fluorescence emission spectra of 2,6-di- <i>tert</i> -butylnaphthalene.	244
Figure 4.35.	Fluorescence emission spectra of fluoranthene in powder form.	246

5. Discussion and conclusions

Figure 5.1.	Correlation between the temperature and enthalpy of fusion of the compounds studied.	258
Figure 5.2.	Temperature of fusion versus entropy of fusion of the compounds studied.	259
Figure 5.3.	Correlation between experimental and estimated results of T_{fus} of halogenated fluorenes.	260
Figure 5.4.	Correlation between experimental and estimated results of thermodynamic properties of sublimation or vaporization for the halogenated fluorenes studied.	265
Figure 5.5.	Correlation between $\Delta_{\text{cr}}^{\text{g}}H_{\text{m}}^{\circ}$ and $\Delta_{\text{cr}}^{\text{g}}G_{\text{m}}^{\circ}$ determined experimentally.	266
Figure 5.6.	Correlation between experimental and estimated results of $\Delta_{\text{cr}}^{\text{g}}G_{\text{m}}^{\circ}$ for the 2-substituted and 2,7-disubstituted fluorenes.	267
Figure 5.7.	Correlation between experimental and estimated results of $\Delta_{\text{cr}}^{\text{g}}G_{\text{m}}^{\circ}$ for the 9-substituted fluorenes.	268
Figure 5.8.	Relation between the enthalpic and entropic contributions to $\Delta_{\text{cr}}^{\text{g}}G_{\text{m}}^{\circ}$ of the carboxaldehyde, amine and nitro derivatives of fluorene in position 2.	269
Figure 5.9.	Packing diagram of 2-fluorencarboxaldehyde, C–H...O interactions are represented as dashed lines.	269

Figure 5.10.	Packing diagram of 2-aminofluorene, N–H... π interactions are represented as dashed lines.	270
Figure 5.11.	Relation between the enthalpic and entropic contributions to $\Delta_{cr}^g G_m^o$ of the monohalogenated derivatives of fluorene in position 2.	271
Figure 5.12.	Relation between the enthalpic and entropic contributions to $\Delta_{cr}^g G_m^o$ of the dihalogenated derivatives of fluorene in positions 2,7.	271
Figure 5.13.	Correlation between the enthalpies and entropies of sublimation of the monohalogenated and the dihalogenated derivatives of fluorene.	272
Figure 5.14.	Relation between the enthalpic and entropic contributions to $\Delta_l^g G_m^o$ of the monohalogenated derivatives of fluorene in position 2.	272
Figure 5.15.	Relation between the enthalpic and entropic contributions to $\Delta_{cr}^g G_m^o$ of the 9-fluorene derivatives.	273
Figure 5.16.	Scheme of the crystalline structure of 9-fluorene-methanol. Hydrogen bonds (O–H...O) are represented as dashed lines.	274
Figure 5.17.	Scheme of the crystalline structure of 9-phenyl-9-fluorene. Hydrogen bonds are represented as dashed lines and O–H... π interactions as double dashed lines.	275
Figure 5.18.	Scheme of the crystalline structures of A and B fluorene-9-carboxylic acid cyclic dimers. Hydrogen bonds are represented as dashed lines and centers of symmetry as dots.	275
Figure 5.19.	Correlation between $\Delta_{cr}^g H_m^o$ and $\Delta_{cr}^g G_m^o$ determined experimentally.	277
Figure 5.20.	Relation between the enthalpic and entropic contributions to $\Delta_{cr}^g G_m^o$ of the fluorenone derivatives.	279
Figure 5.21.	Packing arrangement of 2-aminofluorenone within the unit cell.	279
Figure 5.22.	Correlation between experimental and estimated results of $\Delta_{cr}^g G_m^o$.	281
Figure 5.23.	Relation between the enthalpic and entropic contributions to $\Delta_{cr}^g G_m^o$ of naphthalene, 2,6-dimethylnaphthalene and of the 2,6-dialkylnaphthalene studied in this work.	282
Figure 5.24.	Standard molar Gibbs energies of formation, in the crystalline phase and in the gaseous phase, of fluorene, naphthalene and some of their derivatives, plotted in order of increasing thermodynamic stability of the crystals.	285
Figure 5.25.	Decrease of the standard molar enthalpies of formation, in the gaseous and crystal phases, with increasing molar mass of naphthalene and the 2,6-dialkylnaphthalenes studied in this work.	286
Figure 5.26.	Normalized fluorescence emission spectra of fluorene and 2,7-di- <i>tert</i> -butylfluorene.	291
Figure 5.27.	Normalized fluorescence emission spectra of fluorene in cyclohexane solution at different concentrations.	293
Figure 5.28.	Normalized fluorescence emission spectra of 2,7-di- <i>tert</i> -butylfluorene in cyclohexane solution at different concentrations.	293

Figure 5.29.	Normalized fluorescence emission spectra of naphthalene and of the 2,6-dialkyl derivatives studied in cyclohexane solution.	295
Figure 5.30.	Normalized fluorescence emission spectra of naphthalene and of the 2,6-dialkyl derivatives studied in the solid state.	295

Annexes

Figure C1.	Structures, and IUPAC numbering, of fluorene and fluorenone.	308
Figure C.2.	Plots of $\ln(p/\text{Pa})$ against $1000(K/T)$ of benzoic acid: effusion vapor pressures.	312
Figure C.3.	Plots of $\ln(p/\text{Pa})$ against $1000(K/T)$ of benzoic acid: static vapor pressures.	312
Figure C.4	Plots of $\ln(p/\text{Pa})$ against $1000(K/T)$ of <i>N</i> -methylnicotinamide.	314
Figure C.5.	Normalized UV/vis absorption and fluorescence emission spectra of pyrene.	317

Table index

	Page
1. Introduction	
Table 1.1. Compounds covered in this work and respective origin.	7
3. Experimental methods	
Table 3.1. Reference materials used for the calibration of temperature and enthalpy of fusion.	38
Table 3.2. Reference materials used for the calibration of the Calvet microcalorimeter.	44
Table 3.3. Diameters, areas and transmission probability factors of the effusion orifices.	89
Table 3.4. Possible radiative and non-radiative de-excitation pathways of excited fluorophores and average time scales.	97
4. Experimental results	
Table 4.1. Experimental techniques used to determine thermodynamic and fluorescence properties of each of compound studied in this work.	115
Table 4.2. Data used for the estimation of $\Delta_{cr/l}^{\circ} C_{p,m}^{\circ}$ (298.15 K) of the compounds studied.	124
Table 4.3. Standard molar enthalpies of formation of the product compounds formed in the combustion reactions.	126
Table 4.4. Standard molar entropy values of the constituent elements.	128
Table 4.5. Source, purification and analysis details of 2-fluorencarboxaldehyde.	129
Table 4.6. Temperatures, molar enthalpies and entropies of fusion of 2-fluorencarboxaldehyde.	129
Table 4.7. Vapor pressures of 2-fluorencarboxaldehyde determined by the Knudsen effusion method.	130
Table 4.8. Standard ($p^{\circ} = 0.1$ MPa) molar properties of sublimation of 2-fluorene carboxaldehyde, derived from the vapor pressure results determined experimentally and available in the literature.	131
Table 4.9. Standard ($p^{\circ} = 0.1$ MPa) massic energy of combustion of 2-fluorene carboxaldehyde, at $T = 298.15$ K.	132
Table 4.10. Standard ($p^{\circ} = 0.1$ MPa) molar energy and enthalpy of combustion, and derived standard molar enthalpies of formation of the crystalline and gaseous phases of 2-fluorencarboxaldehyde, at $T = 298.15$ K.	132
Table 4.11. Source, purification and analysis details of 2-aminofluorene.	133

Table 4.12.	Temperatures, molar enthalpies and entropies of fusion of 2-aminofluorene.	133
Table 4.13.	Standard ($p^\circ = 0.1$ MPa) molar enthalpy of sublimation of 2-aminofluorene, determined by Calvet microcalorimetry.	134
Table 4.14.	Vapor pressures of 2-aminofluorene determined by the Knudsen effusion method.	134
Table 4.15.	Standard ($p^\circ = 0.1$ MPa) molar properties of sublimation of 2-aminofluorene, derived from the experimental vapor pressure results.	135
Table 4.16.	Standard ($p^\circ = 0.1$ MPa) massic energy of combustion of 2-aminofluorene, at $T = 298.15$ K.	136
Table 4.17.	Standard ($p^\circ = 0.1$ MPa) molar energy and enthalpy of combustion, and derived standard molar enthalpies of formation of the crystalline and gaseous phases of 2-aminofluorene, at $T = 298.15$ K.	136
Table 4.18.	Standard ($p^\circ = 0.1$ MPa) molar absolute entropies and standard molar entropies, enthalpies and Gibbs energies of formation of the crystalline and gaseous phases of 2-aminofluorene, at $T = 298.15$ K.	137
Table 4.19.	Source, purification and analysis details of 2-nitrofluorene.	138
Table 4.20.	Temperatures, molar enthalpies and entropies of fusion of 2-nitrofluorene.	138
Table 4.21.	Standard ($p^\circ = 0.1$ MPa) molar enthalpy of sublimation of 2-nitrofluorene, determined by Calvet microcalorimetry.	139
Table 4.22.	Vapor pressures of 2-nitrofluorene determined by the Knudsen effusion method.	139
Table 4.23.	Standard ($p^\circ = 0.1$ MPa) molar properties of sublimation of 2-nitrofluorene, derived from the vapor pressure results determined experimentally and available in the literature.	140
Table 4.24.	Standard ($p^\circ = 0.1$ MPa) massic energy of combustion of 2-nitrofluorene, at $T = 298.15$ K.	141
Table 4.25.	Standard ($p^\circ = 0.1$ MPa) molar energy and enthalpy of combustion, and derived standard molar enthalpies of formation of the crystalline and gaseous phases of 2-nitrofluorene, at $T = 298.15$ K.	142
Table 4.26.	Standard ($p^\circ = 0.1$ MPa) molar absolute entropies and standard molar entropies, enthalpies and Gibbs energies of formation of the crystalline and gaseous phases of 2-nitrofluorene, at $T = 298.15$ K.	142
Table 4.27.	Source, purification and analysis details of 2-fluorofluorene.	143
Table 4.28.	Temperatures, molar enthalpies and entropies of fusion of 2-fluorofluorene.	143
Table 4.29.	Vapor pressures of 2-fluorofluorene determined by the static method with capacitance manometers.	144
Table 4.30.	Standard ($p^\circ = 0.1$ MPa) molar properties of sublimation and vaporization of 2-fluorofluorene, derived from the experimental vapor pressure results.	145

Table 4.31.	Preliminary results for the standard ($p^\circ = 0.1$ MPa) molar energy and enthalpy of combustion, and derived standard molar enthalpies of formation of the crystalline and gaseous phases of 2-fluorofluorene, at $T = 298.15$ K.	146
Table 4.32.	Source, purification and analysis details of 2-bromofluorene.	147
Table 4.33.	Temperatures, molar enthalpies and entropies of fusion of 2-bromofluorene.	147
Table 4.34.	Vapor pressures of 2-bromofluorene determined by the Knudsen effusion method.	148
Table 4.35.	Vapor pressures of 2-bromofluorene determined by the static method with capacitance manometers.	149
Table 4.36.	Standard ($p^\circ = 0.1$ MPa) molar properties of sublimation and vaporization of 2-bromofluorene, derived from the vapor pressure results determined experimentally and available in the literature.	149
Table 4.37.	Standard ($p^\circ = 0.1$ MPa) massic energy of combustion of 2-bromofluorene, at $T = 298.15$ K.	151
Table 4.38.	Standard ($p^\circ = 0.1$ MPa) molar energy and enthalpy of combustion, and derived standard molar enthalpies of formation of the crystalline and gaseous phases of 2-bromofluorene, at $T = 298.15$ K.	151
Table 4.39.	Standard ($p^\circ = 0.1$ MPa) molar absolute entropies and standard molar entropies, enthalpies and Gibbs energies of formation of the crystalline and gaseous phases of 2-bromofluorene, at $T = 298.15$ K.	152
Table 4.40.	Source, purification and analysis details of 2-iodofluorene.	153
Table 4.41.	Temperatures, molar enthalpies and entropies of fusion of 2-iodofluorene.	153
Table 4.42.	Vapor pressures of 2-iodofluorene determined by the Knudsen effusion and static methods.	154
Table 4.43.	Standard ($p^\circ = 0.1$ MPa) molar properties of sublimation and vaporization of 2-iodofluorene, derived from experimental and literature vapor pressure results.	155
Table 4.44.	Source, purification and analysis details of 2,7-di- <i>tert</i> -butylfluorene.	157
Table 4.45.	Temperatures and standard molar enthalpies and entropies of condensed phase transitions of 2,7-di- <i>tert</i> -butylfluorene.	157
Table 4.46.	Standard ($p^\circ = 0.1$ MPa) molar enthalpy of sublimation of 2,7-di- <i>tert</i> -butylfluorene, determined by Calvet microcalorimetry.	158
Table 4.47.	Vapor pressures of 2,7-di- <i>tert</i> -butylfluorene determined by the Knudsen effusion method.	159
Table 4.48.	Vapor pressures of 2,7-di- <i>tert</i> -butylfluorene determined by the static method with capacitance manometers.	160
Table 4.49.	Standard ($p^\circ = 0.1$ MPa) molar properties of sublimation and vaporization of 2,7-di- <i>tert</i> -butylfluorene, derived from the experimental vapor pressure results.	161

Table 4.50.	Standard ($p^\circ = 0.1$ MPa) massic energy of combustion of 2,7-di- <i>tert</i> -butylfluorene, at $T = 298.15$ K.	162
Table 4.51.	Standard ($p^\circ = 0.1$ MPa) molar energy and enthalpy of combustion, and derived standard molar enthalpies of formation of the crystalline and gaseous phases of 2,7-di- <i>tert</i> -butylfluorene, at $T = 298.15$ K.	163
Table 4.52.	Standard ($p^\circ = 0.1$ MPa) molar absolute entropies and standard molar entropies, enthalpies and Gibbs energies of formation of the crystalline and gaseous phases of 2,7-di- <i>tert</i> -butylfluorene, at $T = 298.15$ K.	163
Table 4.53.	Source, purification and analysis details of 2,7-difluorofluorene.	164
Table 4.54.	Temperatures, molar enthalpies and entropies of fusion of 2,7-difluorofluorene.	164
Table 4.55.	Vapor pressures of 2,7-difluorofluorene determined by the Knudsen effusion method	165
Table 4.56.	Standard ($p^\circ = 0.1$ MPa) molar properties of sublimation and vaporization of 2,7-difluorofluorene, derived from the experimental vapor pressure results.	166
Table 4.57.	Source, purification and analysis details of 2,7-dichlorofluorene.	167
Table 4.58.	Temperatures, molar enthalpies and entropies of fusion of 2,7-dichlorofluorene.	167
Table 4.59.	Vapor pressures of 2,7-dichlorofluorene determined by the static method with capacitance manometers.	168
Table 4.60.	Standard ($p^\circ = 0.1$ MPa) molar properties of sublimation of 2,7-dichlorofluorene, derived from experimental and literature vapor pressure results.	169
Table 4.61.	Source, purification and analysis details of 2,7-dibromofluorene.	170
Table 4.62.	Temperatures, molar enthalpies and entropies of fusion of 2,7-dibromofluorene.	170
Table 4.63.	Vapor pressures of 2,7-dibromofluorene, determined by the Knudsen effusion method.	171
Table 4.64.	Vapor pressures of 2,7-dibromofluorene determined by the static method with capacitance manometers.	171
Table 4.65.	Standard ($p^\circ = 0.1$ MPa) molar properties of sublimation of 2,7-dibromofluorene derived from the vapor pressure results determined experimentally and available in the literature.	172
Table 4.66.	Standard ($p^\circ = 0.1$ MPa) massic energy of combustion of 2,7-dibromofluorene, at $T = 298.15$ K.	174
Table 4.67.	Standard ($p^\circ = 0.1$ MPa) molar energy and enthalpy of combustion, and derived standard molar enthalpies of formation of the crystalline and gaseous phases of 2,7-dibromofluorene, at $T = 298.15$ K.	174
Table 4.68.	Standard ($p^\circ = 0.1$ MPa) molar absolute entropies and standard molar entropies, enthalpies and Gibbs energies of formation of the crystalline and gaseous phases of 2,7-dibromofluorene, at $T = 298.15$ K.	175

Table 4.69.	Source, purification and analysis details of 2,7-diiodofluorene.	176
Table 4.70.	Temperatures, molar enthalpies and entropies of fusion of 2,7-diiodofluorene.	176
Table 4.71.	Vapor pressures of 2,7-diiodofluorene determined by the Knudsen effusion method.	177
Table 4.72.	Standard ($p^\circ = 0.1$ MPa) molar properties of sublimation of 2,7-diiodofluorene derived from the experimental vapor pressure results.	178
Table 4.73.	Source, purification and analysis details of 9-fluorene-carboxylic acid.	179
Table 4.74.	Temperatures, molar enthalpies and entropies of fusion of 9-fluorene-carboxylic acid.	180
Table 4.75.	Standard ($p^\circ = 0.1$ MPa) molar enthalpy of sublimation of 9-fluorene-carboxylic acid, determined by Calvet microcalorimetry.	180
Table 4.76.	Vapor pressures of 9-fluorene-carboxylic acid determined by the Knudsen effusion method.	181
Table 4.77.	Standard ($p^\circ = 0.1$ MPa) molar properties of sublimation of 9-fluorene-carboxylic acid derived from the vapor pressure results determined experimentally and available in the literature.	182
Table 4.78.	Standard ($p^\circ = 0.1$ MPa) massic energy of combustion of 9-fluorene-carboxylic acid, at $T = 298.15$ K.	184
Table 4.79.	Standard ($p^\circ = 0.1$ MPa) molar energy and enthalpy of combustion, and derived standard molar enthalpies of formation of the crystalline and gaseous phases of 9-fluorene-carboxylic acid, at $T = 298.15$ K.	184
Table 4.80.	Standard ($p^\circ = 0.1$ MPa) molar absolute entropies and standard molar entropies, enthalpies and Gibbs energies of formation of the crystalline and gaseous phases of 9-fluorene-carboxylic acid, at $T = 298.15$ K.	185
Table 4.81.	Source, purification and analysis details of 9-phenyl-9-fluorene.	186
Table 4.82.	Temperatures, molar enthalpies and entropies of fusion of 9-phenyl-9-fluorene available in the literature.	186
Table 4.83.	Vapor pressures of 9-phenyl-9-fluorene, determined by the Knudsen effusion method.	187
Table 4.84.	Standard ($p^\circ = 0.1$ MPa) molar properties of sublimation of 9-phenyl-9-fluorene derived from the experimental vapor pressure results.	188
Table 4.85.	Standard ($p^\circ = 0.1$ MPa) massic energy of combustion of 9-phenyl-9-fluorene, at $T = 298.15$ K.	189
Table 4.86.	Standard ($p^\circ = 0.1$ MPa) molar energy and enthalpy of combustion, and derived standard molar enthalpies of formation of the crystalline and gaseous phases of 9-phenyl-9-fluorene, at $T = 298.15$ K.	189
Table 4.87.	Source, purification and analysis details of 9-benzylidene-fluorene.	190
Table 4.88.	Temperatures, molar enthalpies and entropies of fusion of 9-benzylidene-fluorene.	190
Table 4.89.	Vapor pressures of 9-benzylidene-fluorene determined by the Knudsen effusion method.	191

Table 4.90.	Standard ($p^\circ = 0.1$ MPa) molar properties of sublimation of 9-benzylidene fluorene derived from the experimental vapor pressure results.	192
Table 4.91.	Standard ($p^\circ = 0.1$ MPa) massic energy of combustion of 9-benzylidene fluorene, at $T = 298.15$ K.	193
Table 4.92.	Standard ($p^\circ = 0.1$ MPa) molar energy and enthalpy of combustion, and derived standard molar enthalpies of formation of the crystalline and gaseous phases of 9-phenyl-9-fluorenol, at $T = 298.15$ K.	194
Table 4.93.	Source, purification and analysis details of 9-fluorenemethanol.	195
Table 4.94.	Temperatures, molar enthalpies and entropies of fusion of 9-fluorenemethanol.	195
Table 4.95.	Vapor pressures of 9-fluorenemethanol determined by the Knudsen effusion method.	196
Table 4.96.	Standard ($p^\circ = 0.1$ MPa) molar properties of sublimation and vaporization of 9-fluorenemethanol derived from the vapor pressure results determined experimentally and available in the literature.	197
Table 4.97.	Standard ($p^\circ = 0.1$ MPa) molar energy and enthalpy of combustion, and derived standard molar enthalpies of formation of the crystalline and gaseous phases 9-fluorenemethanol, at $T = 298.15$ K.	198
Table 4.98.	Standard ($p^\circ = 0.1$ MPa) molar absolute entropies and standard molar entropies, enthalpies and Gibbs energies of formation of the crystalline and gaseous phases 9-fluorenemethanol, at $T = 298.15$ K.	198
Table 4.99.	Source, purification and analysis details of 9-chlorofluorene.	199
Table 4.100.	Temperatures, molar enthalpies and entropies of fusion of 9-chlorofluorene.	199
Table 4.101.	Vapor pressures of 9-chlorofluorene determined by the Knudsen effusion method.	200
Table 4.102.	Standard ($p^\circ = 0.1$ MPa) molar properties of sublimation of 9-chlorofluorene derived from the vapor pressure results determined experimentally and available in the literature.	201
Table 4.103.	Source, purification and analysis details of 2-aminofluorenone.	202
Table 4.104.	Temperatures, molar enthalpies and entropies of fusion of 2-aminofluorenone.	202
Table 4.105.	Vapor pressures of 2-aminofluorenone determined by the Knudsen effusion method.	203
Table 4.106.	Standard ($p^\circ = 0.1$ MPa) molar properties of sublimation of 2-aminofluorenone derived from the experimental vapor pressure results.	204
Table 4.107.	Source, purification and analysis details of 2-hydroxyfluorenone.	205
Table 4.108.	Temperatures, molar enthalpies and entropies of fusion of 2-hydroxyfluorenone.	205
Table 4.109.	Vapor pressures of 2-hydroxyfluorenone determined by the Knudsen effusion method.	206

Table 4.110.	Standard ($p^\circ = 0.1$ MPa) molar properties of sublimation of 2-hydroxyfluorenone derived from the experimental vapor pressure results.	207
Table 4.111.	Source, purification and analysis details of 2-fluorofluorenone.	208
Table 4.112.	Temperatures, molar enthalpies and entropies of fusion of 2-fluorofluorenone.	208
Table 4.113.	Vapor pressures of 2-fluorofluorenone determined by the Knudsen effusion method.	209
Table 4.114.	Vapor pressures of 2-fluorofluorenone determined by the static method with capacitance manometers.	209
Table 4.115.	Standard ($p^\circ = 0.1$ MPa) molar properties of sublimation of 2-fluorofluorenone derived from the vapor pressure results determined experimentally.	210
Table 4.116.	Source, purification and analysis details of 2,7-dibromofluorenone.	212
Table 4.117.	Temperatures, molar enthalpies and entropies of fusion of 2,7-dibromofluorenone	212
Table 4.118.	Vapor pressures of 2,7-dibromofluorenone determined by the Knudsen effusion method.	213
Table 4.119.	Standard ($p^\circ = 0.1$ MPa) molar properties of sublimation of 2,7-dibromofluorenone derived from the vapor pressure results determined experimentally.	214
Table 4.120.	Source, purification and analysis details of 2,6-diethylnaphthalene.	215
Table 4.121.	Temperatures, molar enthalpies and entropies of fusion of 2,6-diethylnaphthalene.	215
Table 4.122.	Vapor pressures of 2,6-diethylnaphthalene determined by the static method with capacitance manometers.	216
Table 4.123.	Standard ($p^\circ = 0.1$ MPa) molar properties of sublimation and vaporization of 2,6-diethylnaphthalene, derived from the experimental vapor pressure results.	217
Table 4.124.	Standard ($p^\circ = 0.1$ MPa) molar energy and enthalpy of combustion, and derived standard molar enthalpies of formation of the crystalline and gaseous phases of 2,6-diethylnaphthalene, at $T = 298.15$ K.	218
Table 4.125.	Standard ($p^\circ = 0.1$ MPa) molar absolute entropies and standard molar entropies, enthalpies and Gibbs energies of formation of the crystalline and gaseous phases of 2,6-diethylnaphthalene, at $T = 298.15$ K.	218
Table 4.126.	Source, purification and analysis details of 2,6-diisopropylnaphthalene.	219
Table 4.127.	Temperatures, molar enthalpies and entropies of fusion of 2,6-diisopropylnaphthalene available in the literature.	219
Table 4.128.	Vapor pressures of 2,6-diisopropylnaphthalene determined by the Knudsen effusion method.	220
Table 4.129.	Standard ($p^\circ = 0.1$ MPa) molar properties of sublimation of 2,6-diisopropylnaphthalene, derived from the experimental vapor pressure results.	221

Table 4.130.	Standard ($p^\circ = 0.1$ MPa) molar energy and enthalpy of combustion, and derived standard molar enthalpies of formation of the crystalline and gaseous phases of 2,6-diisopropylnaphthalene, at $T = 298.15$ K.	221
Table 4.131.	Standard ($p^\circ = 0.1$ MPa) molar absolute entropies and standard molar entropies, enthalpies and Gibbs energies of formation of the crystalline and gaseous phases of 2,6-diisopropylnaphthalene, at $T = 298.15$ K.	222
Table 4.132.	Source, purification and analysis details of 2,6-di- <i>tert</i> -butylnaphthalene.	223
Table 4.133.	Temperatures, molar enthalpies and entropies of fusion of 2,6-di- <i>tert</i> -butylnaphthalene available in the literature.	223
Table 4.134.	Vapor pressures of 2,6-di- <i>tert</i> -butylnaphthalene determined by the Knudsen effusion method.	224
Table 4.135.	Standard ($p^\circ = 0.1$ MPa) molar properties of sublimation of 2,6-di- <i>tert</i> -butylnaphthalene, derived from the experimental vapor pressure results.	225
Table 4.136.	Standard ($p^\circ = 0.1$ MPa) molar energy and enthalpy of combustion, and derived standard molar enthalpies of formation of the crystalline and gaseous phases of 2,6-di- <i>tert</i> -butylnaphthalene, at $T = 298.15$ K.	225
Table 4.137.	Standard ($p^\circ = 0.1$ MPa) molar absolute entropies and standard molar entropies, enthalpies and Gibbs energies of formation of the crystalline and gaseous phases of 2,6-di- <i>tert</i> -butylnaphthalene, at $T = 298.15$ K.	226
Table 4.138.	Fluorescence quantum yields of the weakly/non fluorescent compounds, in powder form, studied in this work.	228
Table 4.139.	Source, purification and analysis details of fluorene.	229
Table 4.140.	Literature results for the fluorescence quantum yield of fluorene in different solvents.	229
Table 4.141.	Fluorescence spectroscopic data of fluorene in cyclohexane solutions, at room temperature.	230
Table 4.142.	Absorption and fluorescence spectroscopic data of fluorene in powder form (Supelco), for different amounts of sample.	231
Table 4.143.	Absorption and fluorescence spectroscopic data of 2-aminofluorene in powder form, for different amounts of sample.	233
Table 4.144.	Absorption and fluorescence spectroscopic data of 2-fluorofluorene in powder form, for different amounts of sample.	234
Table 4.145.	Fluorescence spectroscopic data of 2,7-di- <i>tert</i> -butylfluorene in cyclohexane solutions, at room temperature.	235
Table 4.146.	Absorption and fluorescence spectroscopic data of 2,7-di- <i>tert</i> -butylfluorene in powder form, for different amounts of sample.	235
Table 4.147.	Source, purification and analysis details of naphthalene.	237
Table 4.148.	Literature results for the fluorescence quantum yield of naphthalene in different solvents.	237
Table 4.149.	Fluorescence spectroscopic data of naphthalene in cyclohexane solutions, at room temperature.	238

Table 4.150.	Absorption and fluorescence spectroscopic data of naphthalene in powder form, for different amounts of sample.	238
Table 4.151.	Fluorescence spectroscopic data of 2,6-diethylnaphthalene in cyclohexane solutions, at room temperature.	240
Table 4.152.	Fluorescence spectroscopic data of 2,6-diisopropylnaphthalene in cyclohexane solutions, at room temperature.	241
Table 4.153.	Absorption and fluorescence spectroscopic data of 2,6-diisopropyl naphthalene in powder form, for different amounts of sample.	241
Table 4.154.	Fluorescence spectroscopic data of 2,6-di- <i>tert</i> -butylnaphthalene in cyclohexane solution and in powder form, at room temperature.	243
Table 4.155.	Absorption and fluorescence spectroscopic data of 2,6-di- <i>tert</i> -butylnaphthalene in powder form, for different amounts of sample.	243
Table 4.156.	Source, purification and analysis details of fluoranthene.	245
Table 4.157.	Absorption and fluorescence spectroscopic data of fluoranthene in powder form, for different amounts of sample.	245

5. Discussion and conclusions

Table 5.1.	Temperatures, molar enthalpies and entropies of fusion of the compounds studied, determined by DSC.	256
Table 5.2.	Bondi radius, and absolute and excess volumes and electron affinities of the halogen atoms.	260
Table 5.3.	Thermodynamic properties of sublimation and vaporization of fluorene and its derivatives, as well as their vapor pressures at $T = 298.15$ K.	261
Table 5.4.	Thermodynamic properties of sublimation and vaporization of fluorenone and its derivatives, as well as their vapor pressures at $T = 298.15$ K.	276
Table 5.5.	Thermodynamic properties of sublimation and vaporization of naphthalene and its derivatives, as well as their vapor pressures at $T = 298.15$ K.	280
Table 5.6.	Thermodynamic properties of formation, in the crystalline and gaseous phases, of fluorene, naphthalene and some of its derivatives studied in this work, at $T = 298.15$ K.	283
Table 5.7.	Gaseous phase increments on enthalpies of formation associated to the insertion of different substituents in benzene, in positions 2,6 of naphthalene and in positions 2,7 of fluorene.	287
Table 5.8.	Fluorescence quantum yields of fluorene and 2,7-di- <i>tert</i> -butylfluorene in cyclohexane solution and in powder form.	292
Table 5.9.	Fluorescence quantum yields of naphthalene and of the 2,6-dialkyl derivatives studied in cyclohexane solution and in powder form.	296

Annexes

Table B.1.	List of abbreviations, acronyms and symbols used and respective meanings.	304
Table C.1.	Vapor pressures of benzoic acid determined by the Knudsen effusion method.	311
Table C.2.	Vapor pressures of benzoic acid determined by the static method with capacitance manometers.	311
Table C.3.	Standard ($p^\circ = 0.1$ MPa) molar properties of sublimation of benzoic acid, derived from the vapor pressure results determined experimentally and available in the literature.	313
Table C.4.	Vapor pressures of <i>N</i> -methylnicotinamide determined by the Knudsen effusion method.	314
Table C.5.	Standard ($p^\circ = 0.1$ MPa) molar properties of sublimation and vaporization of <i>N</i> -methylnicotinamide, derived from the experimental vapor pressure results.	315
Table C.6.	Literature results for the fluorescence quantum yield of pyrene in different solvents, and in powder form	316
Table C.7.	Fluorescence spectroscopic data of pyrene in cyclohexane solution and in powder form, at room temperature.	316
Table C.8.	Absorption and fluorescence quantum yield results of pyrene in powder form, for different amounts of sample.	317

Chapter

Introduction

1

- 1.1. Aim of the study
- 1.2. Compounds studied
- 1.3. Methods used

References

1.1. Aim of the study

The present study is mainly focused on the evaluation of the volatility of fluorene, fluorenone and naphthalene derivatives (figure 1.1), as well as the characterization of their fluorescence properties, and on the measurement of the thermodynamic stability of some of them.

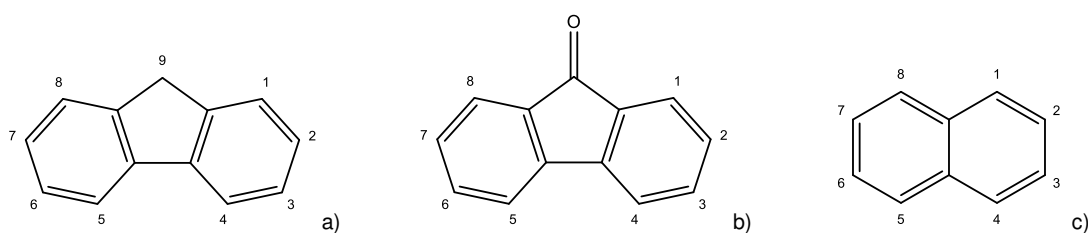


Figure 1.1. Structure formulae and numbering of fluorene (a), fluorenone (b) and naphthalene (c).

Fluorene and naphthalene are polycyclic aromatic hydrocarbons (PAHs) while fluorenone is an oxygenated polycyclic aromatic hydrocarbon (OPAH) that may result from the oxidation of fluorene. The relative abundance of PAHs in atmospheric air, water vapor and particulate matter is to a large extent conditioned by their volatility [1]. The knowledge of accurate vapor pressure and water solubility is fundamental to assess the dispersion and permanence of these compounds in the atmosphere as well as their accumulation in living beings and in soils, sediments and underground waters [2]. A compound's volatility is also very important from the industrial point of view. The quantification of vapor pressures is often required for the planning and monitoring of various industrial processes [3], as well as for optimizing storage conditions of hazardous substances according to safety standards.

The vapor pressures and thermodynamic properties of derivatives of fluorene and fluorenone have been studied over the past 50 years, mostly since the last decade [4-10]. Their low volatility hinders the accurate experimental determination of their vapor pressures and, consequently, the derived thermodynamic properties. So, data on thermodynamic properties of these compounds is scarce and often inaccurate. The quality of the currently available experimental thermochemical and thermophysical data for these compounds is also lessened by the frequent use of samples with purity levels much lower than what would be recommended. Vapor pressures results determined by effusion methods using low-purity samples (ca. 95 %) are still being published nowadays [8,9], which contribute to the lack of

reliability of vapor pressure results of several of these compounds. Apart from these examples, the availability of reliable vapor pressure data fortunately continues to grow, and with it the possibility to establish estimation methods for predicting vapor pressures of aromatic compounds, as the ones suggested by Chickos and Hosseini [11], Coutsikos [12], Crampon [13], and more recently by Monte and collaborators [14,15].

The assessment of the thermodynamic stability of PAHs is also of great importance when evaluating the reactivity of these compounds. It is a powerful tool for predicting chemical reactions leading to their degradation, namely its eventual oxidation or hydrolysis. Also, PAH derivatives are commonly applied on optoelectronic devices, whose durability depends to great extent on the thermodynamic stability of its components.

When considering the design of new photoluminescent materials, one of the main properties that significantly affects the performance of these devices is the quantum yield (QY) in the solid state [16], in addition to their chemical and thermal stability and volatility. Furthermore, the characterization of the luminescent properties of PAHs is also very useful to selectively detect and identify these pollutant compounds in the environment, using highly sensitive analytical techniques [17-20].

1.2. Compounds studied

PAHs constitute one of the main classes of persistent organic pollutants that are harmful to living beings. Several of them appear in the USEPA (United States Environmental Protection Agency) priority pollutant list [21] and also in the list of priority regulated substances by the European Union [22]. PAHs are originated from a variety of natural and anthropogenic sources. Their major sources in the environment are related to human activities, being mainly associated with oil spills, gas exploration, industrial waste and incomplete combustion of coal, other fossil fuels and organic matter [1,23,24]. Most have relatively low vapor pressures and therefore tend to accumulate in soil and sediments, water and animal tissue [25]. They are often resistant to biological degradation and are not efficiently removed by conventional physicochemical methods [26].

PAHs may induce genotoxic effects in humans and some have been proved to be carcinogenic and potentially tumorigenic [27,28]. PAHs can be “activated” by light irradiation to form highly reactive oxidized species [29,30], which can cause various adverse health effects, such as premature aging, acute and chronic respiratory and inflammatory conditions, among others. As carcinogen compounds, several PAHs have been frequently studied, giving particular attention to nitro-PAHs [31], such as 2-nitrofluorene listed as

“possibly carcinogenic to humans” by the International Agency for Research on Cancer [32], and halogenated PAHs, mainly the chlorinated ones [33]. Some PAHs are susceptible to oxidation and photo-degradation in the presence of light. 9-Fluorenone, for example, may occur as the result of aerobic oxidation in position 9 of fluorene [34].

Fluorene, fluorenone and naphthalene derivatives have important applications in a variety of areas. They are widely used as precursors in peptide synthesis [35,36], in active ingredients for drugs and pharmaceuticals [37], base materials for organic dyes [38-40], organic semiconductor materials for the application in the field of organic electronics [41-44], etc.

The use of PAHs derivatives due to their semiconductor properties has exponentially increased in the past decades. Presently, fluorene, fluorenone and naphthalene derivatives as well as their derived oligomers and polymers have been successfully used as active components on a new generation of electronic devices such as organic light emitting diodes (OLEDs) and organic solar cells (OSCs), drawing the attention of the scientific and technological communities, evidenced by a great number of diverse studies published in literature [45-49].

Due to their aromatic structures, several PAHs show intrinsic fluorescence emission in the UV and blue spectral regions [50]. In general, red and green emitting OLEDs have proven to be more efficient in terms of luminescence and durability. Nowadays there is a pressing demand for new organic compounds with high chemical and thermal stabilities and high fluorescence efficiency for blue emitting OLEDs [51]. The structure of fluorene and fluorenone add rigidity to the derived oligomers and polymers improving their thermal and morphological stability and consequently their durability. One of the problems that occur in blue emitting materials is called “green emission defect” [49], due to the appearance of an additional undesirable low energy “green emission band” which reduces the emission efficiency and prevents the emission of pure blue color [52,53]. Occasionally, fluorene-based polymers are not sufficiently stable, while smaller PAHs building molecules, as well as being easier to purify and characterize, are generally more thermally stable [54,55]. Functionalizing fluorene and fluorenone molecules with electron donor/acceptor substituents, or π chromophore groups with good thermal and chemical stability, can help to achieve blue emitting materials that can be applied in OLEDs [46,49,56,57].

Recent developments in organic photovoltaics devices (OPVs) sensitized with chromophores demonstrated greater efficiency and lower costs compared to crystalline silicon technology that has been dominant in terms of commercial production. Fluorene derivatives have been used successfully as components in this type of voltaic cells [58-61],

and a growing industrial interest on these compounds is expected in addition to its use as OLEDs.

The development of oligomeric and polymeric hybrids of fluorene with triphenylamine, carbazole, quinoline and pyrene [62-65], among others, has proved to be successful in overcoming the problems associated with thermal and chemical stability of some OLEDs and OPVs components and simultaneously allows the modulating and customization of the material's optoelectronic properties.

The compounds covered in this work are listed in table 1.1 and can be separated into three classes, according to the core molecule:

- Fluorene derivatives with substituents in positions 2, 2,7 and 9;
- Fluorenone derivatives with substituents in positions 2 and 2,7;
- Naphthalene derivatives with substituents in positions 2,6.

The selected fluorene and fluorenone derivatives are substituted at its most electronegative centers - positions 2 and 2,7 - granting the highest linearity and, therefore, conjugation efficiency. Additionally, some fluorene derivatives substituted in position 9 were also studied. Later in the course of this project, the study was further extended to some alkyl derivatives of naphthalene in positions 2,6.

Most of the compounds were acquired commercially, but a few were synthesized in the present work employing methods described in the literature for similar compounds. The detailed description of these procedures can be found in section 2.3. After conveniently purified, the synthesized compounds were identified by Nuclear Magnetic Resonance (NMR) and mass spectroscopy.

Table 1.1. Compounds covered in this work and respective origin ^a.

Compound	Origin	Compound	Origin
FLUORENE DERIVATIVES			
2-Fluorencarboxaldehyde	○	2,7-Dichlorofluorene	●
2-Aminofluorene	○	2,7-Dibromofluorene	○
2-Nitrofluorene	○	2,7-Diodofluorene	●
2-Fluorofluorene	○	9-Fluorencarboxylic acid	○
2-Bromofluorene	○	9-Phenyl-9-fluorenol	○
2-Iodofluorene	○	9-Benzylidene fluorene	○
2,7-Di- <i>tert</i> -butylfluorene	○	9-Fluorene methanol	○
2,7-Difluorofluorene	●	9-Chlorofluorene	●
FLUORENONE DERIVATIVES			
2-Aminofluorenone	○	2,7-diNitrofluorenone	○
2-Hydroxifluorenone	○	2,7-diBromofluorenone	○
2-Fluorofluorenone	○		
NAPHTHALENE DERIVATIVES			
2,6-Diethylnaphthalene	○	2,6-Di- <i>tert</i> -butylnaphthalene	○
2,6-Diisopropylnaphthalene	○		

^a ○, acquired commercially; ●, successfully synthesized in the present work.

1.3. Methods used

The following experimental methods used for determining the thermodynamic and luminescence properties have been applied in this work:

Differential Scanning Calorimetry (DSC)

The compounds were analyzed by DSC in order to determine the temperatures of fusion and the standard molar enthalpies and entropies of fusion. This calorimetric study also allowed the detection of eventual transitions between crystalline phases and the determination of the respective temperatures and enthalpies of transition.

Measurement of vapor pressures

The measurement of vapor pressures at different temperatures was carried out using a Knudsen effusion method and/or a static method based on capacitance manometers. Together with estimated heat capacities, the vapor pressure results allow the determination of standard molar enthalpies, entropies and Gibbs energies of sublimation (and sometimes also vaporization) at reference temperatures.

Calvet microcalorimetry

For a few compounds, the standard molar enthalpies of sublimation were also obtained by Calvet microcalorimetry.

Combustion calorimetry

For the compounds with enough available quantity of purified sample, the standard massic energies of combustion were determined by combustion calorimetry in static or rotating bomb, depending on the compound's chemical composition. From the determined standard massic energy of combustion, the standard molar enthalpy of formation in the crystalline phase at the temperature 298.15 K was derived.

Photoluminescence spectroscopy

The study of fluorescence spectral properties and quantum yield of some of the compounds studied was performed by fluorescence spectroscopy. The fluorescence emission wavelength, relative emission intensity and absolute quantum yield were determined in powder form and also in solution for some of the compounds studied, using a fluorescence spectrophotometer.

References

- [1] K. Ravindra, R. Sokhi, R. Van Grieken, *Atmos. Environ.* 42 (2008) 2895-2921;
- [2] A. Delle Site, *J. Phys. Chem. Ref. Data* 26 (1997) 157-193;
- [3] T.E. Dauber, *J. Chem. Eng. Data* 41 (1996) 942-946;
- [4] K. Rakus, S.P. Verevkin, J. Schaezter, H.-D. Beckhaus, C. Rüdhardt, *Chem. Ber.* 127 (1994) 1095-1103;
- [5] Y.D. Lei, R. Chankalal, A. Chan, F. Wania, *J. Chem. Eng. Data* 47 (2002) 801-806;
- [6] S. P. Verevkin, *Fluid Phase Equilib.* 225 (2004) 145-152;
- [7] W. Hanshaw, M. Nutt, J.S. Chickos, *J. Chem. Eng. Data* 53 (2008) 1903-1913; 53 (2008) 2721-2722;
- [8] J.L. Goldfarb, E.M. Suuberg, *Environ. Toxicol. Chem.* 27 (2008) 1244-1249;
- [9] J. Fu, E.M. Suuberg, *Environ. Toxicol. Chem.* 31 (2012) 486-493;
- [10] M.J.S. Monte, R. Notario, M.M.G. Calvinho, A.R.R.P. Almeida, L.M.P.F. Amaral, A.I.M.C. Lobo Ferreira, M.D.M.C. Ribeiro da Silva, *J. Chem. Eng. Data* 57 (2012) 2486-2496;
- [11] J. S. Chickos, S. Hosseini, J.F. Liebman, *J. Org. Chem.* 58 (1993) 5345-5350;
- [12] P. Coutsikos, E. Voutsas, K. Magoulas, D.P. Tassios, *Fluid Phase Equilib.* 207 (2003) 263-281;
- [13] C. Crampon, L. Trassy, L. Avauillée, E. Neau, L. Coniglio, *Fluid Phase Equilib.* 216 (2004) 95-109;
- [14] M.J.S. Monte, A.R.R.P. Almeida, *Struct. Chem.* 24 (2013) 2001-2016;
- [15] M.J.S. Monte, A.R.R.P. Almeida, J.F. Liebman, *Chemosphere* 138 (2015) 478-485;
- [16] Geffroy, P. le Roy, C. Prat, *Polym. Int.* 55 (2006) 572-582;
- [17] K.R.R. Mahanama, L.A. Gundel, J.M. Daisey, *Intern. J. Environ. Anal. Chem.* 56 (1994) 289-309;
- [18] J.J.S. Rodríguez, C.P. Sanz, *Analisis* 28 (2000) 710-717;
- [19] Y. Huang, J. Wei, J. Song, M. Chen, Y. Luo, *Chemosphere* 92 (2013) 1010-1016;
- [20] N. Ferretto, M. Tedetti, C. Guigue, S. Mounier, R. Redon, M. Goutx, *Chemosphere* 107 (2014) 344-353;

- [21] USEPA, Priority Pollutant List (<https://www.epa.gov/sites/production/files/2015-09/documents/priority-pollutant-list-epa.pdf>, accessed in February 2016);
- [22] Directive 2013/39/EU of the European Parliament and of the Council, *Official Journal of the European Union* (24.8.2013) L 226/1-17;
- [23] B.-K. Lee, V.T. Vu, chapter 5, in: *Air Pollution*, V. Villanyi (Ed.), Sciyo (2010) (Open Access: <http://www.intechopen.com/books/air-pollution>);
- [24] H.I. Abdel-Shafy, M.S.M. Mansour, *Egypt. J. Petrol.* 25 (2015) 107-123;
- [25] R.G. Harvey, *Polycyclic Aromatic Hydrocarbons: Chemistry and Carcinogenicity*, Cambridge University Press, Cambridge (1991);
- [26] R.E. Hinchee, B.C. Alleman, R.E. Hoeppe, R.N. Miller (Eds.), *Hydrocarbon Bioremediation*, CRC Press, Boca Raton, USA (1994);
- [27] K.L. White, *J. Environ. Sci. Health* 4 (1986) 163-202;
- [28] A. Luch (Ed.), *The Carcinogenic Effects of Polycyclic Aromatic Hydrocarbons*, Imperial College Press, London, UK (2005);
- [29] H.T. Yu, *J. Environ. Sci. Health, C* 20 (2002) 149-183;
- [30] P.P. Fu, Q. Xia, X. Sun, H. Yu, *J. Environ. Sci. Heal.* C30 (2012) 1-41;
- [31] V. Purohit, A.K. Basu, *Chem. Res. Toxicol.* 13 (2000) 673-692;
- [32] International Agency for Research on Cancer (http://monographs.iarc.fr/ENG/Classification/latest_classif.php, accessed in February 2016);
- [33] P.P. Fu, L.S. Von Tungeln, L.H. Chiu, Z.Y. Own, *J. Environ. Sci. Heal.* C17 (1999) 71-109;
- [34] X. Zhang, X. Ji, S. Jiang, L. Liu, B.L. Weeks, Z. Zhang, *Green Chem.* 13 (2011) 1891-1896;
- [35] K.D. Stigers, M.R. Koutroulis, D.M. Chung, J.S. Nowick, *J. Org. Chem.* 65 (2000) 3858-3860;
- [36] R. Chinchilla, D.J. Dodsworth, C. Nájera, J.M. Soriano, *Bioorg. Med. Chem. Lett.* 12 (2002) 1817-1820;
- [37] T. Motomura, H. Nagamori, K. Suzawa, H. Ito, T. Morita, S. Kobayashi, H. Shinkai, *Fluorene compound and pharmaceutical use thereof*. US Patent no. 2013/0274240 A1;
- [38] I.V. Kurdyukova, A.A. Ishchenko, *Russ. Chem. Rev.* 81 (2012) 258-290;

- [39] D. Kumar, K.R. Justin Thomas, C.-P. Lee, K.-C. Ho, *J. Org. Chem.* 79 (2014) 3159-3172;
- [40] Y.D. Kima, J.H. Choa, C.R. Parka, J.-H. Choib, C. Yoonc, J.P. Kima, *Dyes Pigm.* 89 (2011) 1-8;
- [41] J. Locklin, M.M. Ling, A. Sung, M.E. Roberts, Z. Bao, *Adv. Mater.* 18 (2006) 2989-2992;
- [42] S. Fratiloiu, S.M. Fonseca, F.C. Grozema, H.D. Burrows, M.L. Costa, A. Charas, J. Morgado, L.D.A. Siebbeles, *J. Phys. Chem. C* 111 (2007) 5812-5820;
- [43] X. Guo, F.S. Kim, M.J. Seger, S.A. Jenekhe, M.D. Watson, *Chem. Mater.* 24 (2012) 1434-1442;
- [44] T.J. Marks, M.R. Wasielewski, A. Facchetti, B.A. Jones, *Naphthalene-based semiconductor materials and methods of preparing and use thereof*. US Patent no. 7,569,693 B2 (2009);
- [45] C. Sekine, Y. Tsubata, T. Yamada, M. Kitano, S. Doi, *Sci. Technol. Adv. Mater.* 15 (2014) 034203;
- [46] G.L. Eakins, J.S. Alfordb, B.J. Tiegsa, B.E. Breyfoglea, C.J. Stearman, *J. Phys. Org. Chem.* 24 (2011) 1119-1128;
- [47] J.H. Oh, J.-H. Kim, Y.T. Kim, W.S. Shin, S.C. Yoon, S.-J. Moon, C. Lee, I.-N. Kang, D.-H. Hwang, *J. Nanosci. Nanotechnol.* 12 (2012) 4132-4136;
- [48] L.-H. Xie, S.-H. Yang, J.-Y. Lin, M.-D. Yi, W. Huang, *Phil. Trans. R. Soc. A* 371 (2013) 20120337;
- [49] A. Goel, S. Chaurasia, M. Dixit, V. Kumar, S. Prakash, B. Jena, J. K. Verma, M. Jain, R.S. Anand, S. Sundar Manoharan, *Org. Lett.* 11 (2009) 1289-1292;
- [50] R. Dabestani, I.N. Ivanov, *Photochem. Photobiol.* 70 (1999) 10-34;
- [51] M. Zhu, C. Yang, *Chem. Soc. Rev.* 42 (2013) 4963-4976;
- [52] M. Sims, D.D.C. Bradley, M. Ariu, M. Koeberg, A. Asimakis, M. Grell, D.G. Lidzey, *Adv. Funct. Mater.* 14 (2004) 765-781;
- [53] A.P. Kulkarni, X. Kong, S.A. Jenekhe, *J. Phys. Chem. B* 108 (2004) 8689-8701;
- [54] T. Yu, L. Liu, Z. Xie, Y. Ma, *Sci. China Chem.* 58 (2015) 907-915;
- [55] N.J. Findlay, B. Breig, C. Forbes, A.R. Inigo, A.L. Kanibolotsky, P.J. Skabara, *J. Mater. Chem. C* 4 (2016) 3774-3780;

- [56] Z. Peng, S. Tao, X. Zhang, J. Tang, C.S. Lee, S.-T. Lee, *J. Phys. Chem. C* 112 (2008) 2165-2169;
- [57] P. Song, F. Ma, *J. Phys. Chem. A* 114 (2010) 2230-2234;
- [58] P. Singh, A. Baheti, K.R.J. Thomas, C.-P. Lee, K.-C. Ho, *Dyes Pigm.* 95 (2012) 523-533;
- [59] S. Ma, Y. Fu, D. Ni, J. Mao, Z. Xie, G. Tu, *Chem. Commun.* 48 (2012) 11847-11849;
- [60] M. Fakis, M. Dori, E. Stathatos, H.-H. Chou, Y.-S. Yen, J.T. Lin, V. Giannetas, P. Persephonis, *J. Photochem. Photobiol. A* 251 (2013) 18-24;
- [61] K.R.J. Thomas, A. Baheti, *Mater. Technol.* 28 (2013) 71-87;
- [62] Z. Fan, N. Li, Y. Quan, Q. Chen, S. Ye, Q. Fan, W. Huang, H. Xu, *J. Mater. Chem. C* 2 (2014) 9754-9759;
- [63] W. Li, J. Qiao, L. Duan, L. Wang, Y. Qiu, *Tetrahedron* 63 (2007) 10161-10168;
- [64] A. Slodek, M. Matussek, M. Filapek, G. Szafraniec-Gorol, A. Szlapa, I. Grudzka-Flak, M. Szczurek, J.G. Malecki, A. Maron, E. Schab-Balcerzak, E.M. Nowak, J. Sanetra, M. Olejnik, W. Danikiewicz, S. Krompiec, *Eur. J. Org. Chem.* (2016) 2500-2508;
- [65] K.R.J. Thomas, N. Kapoor, M.N.K.P. Bolisetty, J.-H. Jou, Y.-L. Chen, Y.-C. Jou, *J. Org. Chem.* 77 (2012) 3921-3932.

Chapter

Synthesis

2

- 2.1. Introduction
- 2.2. General information
- 2.3. Synthetic procedures

References

2.1. Introduction

The progress of this work led to the study of compounds that were not commercially available or that were too expensive to purchase in the necessary amounts. Within this framework, halogenated derivatives in positions 2, 9 and 2,7 of fluorene, as well as in positions 2 and 2,7 positions of fluorenone, were obtained by organic synthesis, using adaptations of procedures published in the literature. Figure 2.1 shows a general scheme of the starting materials and the final molecules synthesized in the course of this work.

Each synthetic procedure was initially tested in microscale and after a satisfactory outcome of this initial test, the procedure was adapted to a bigger scale and repeated until the necessary amount of compound was obtained. The details of the materials, instrumentation and synthetic procedures used will be described as follows, as well as the techniques used for product characterization.

2.2. General information

2.2.1. Reagents and solvents

The starting materials and other additional reagents used in the synthesis of fluorene and fluorenone derivatives, presented in figure 2.1, were acquired commercially from Sigma-Aldrich (3, 6, 9, 14) and TCI Chemicals (1, 12) and used without additional purification. The solvents used were pro analysis (p.a.) grade and also commercially acquired from Merck, Sigma-Aldrich, Carlo Erba, Alfa Aesar and Fluka.

2.2.2. General procedures and instrumentation

The progression of the synthetic reactions was monitored by thin layer chromatography (TLC) using aluminum plates pre-coated with silica gel 60 F₂₅₄ (Merck) with layer thickness of 0.2 mm. For analytical control, several elution systems were used: diethyl ether/petroleum ether (in various proportions), petroleum ether/dichloromethane (in various proportions), hexane/dichloromethane (8:2), dichloromethane/methanol (9:1), hexane/ethyl

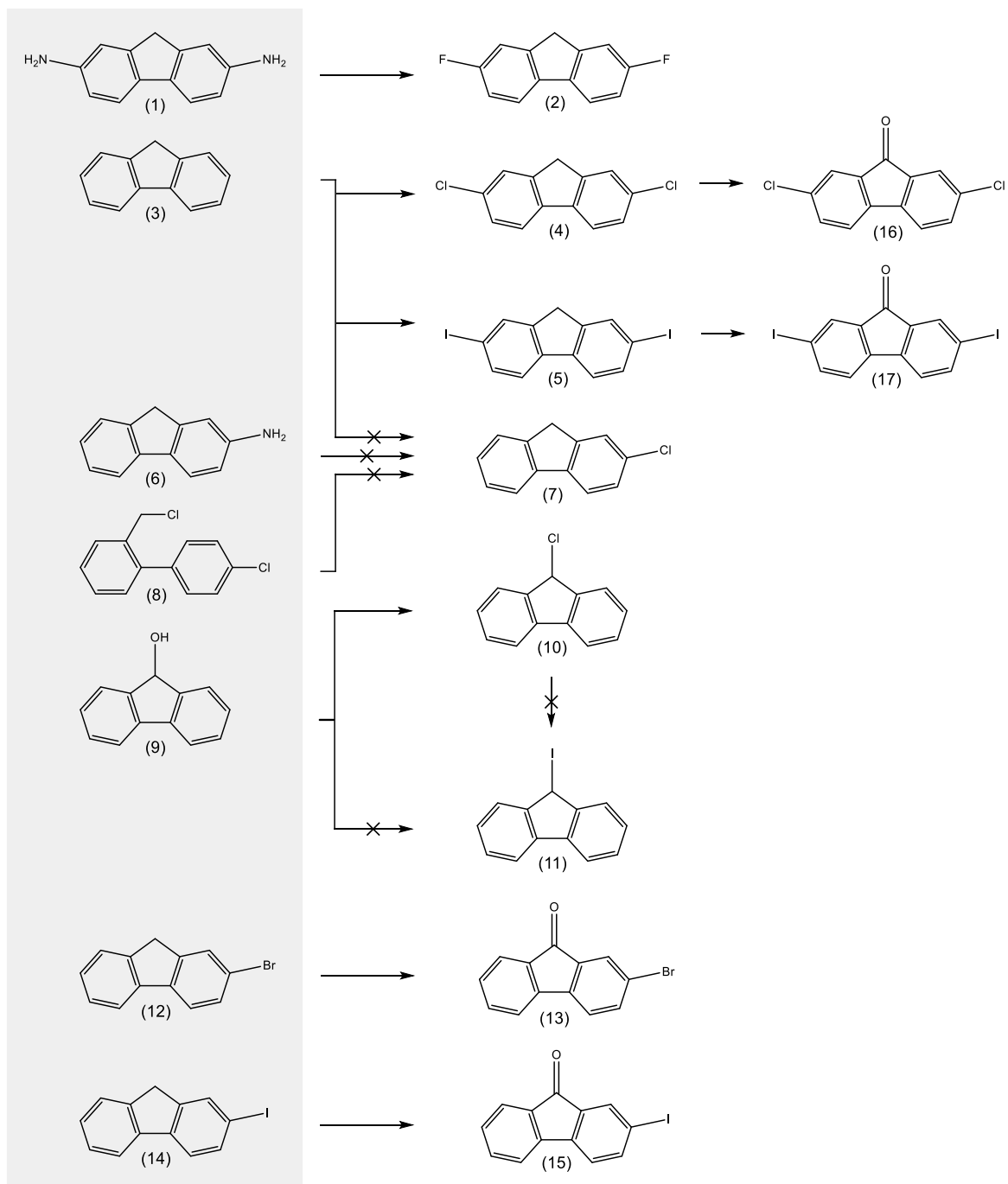


Figure 2.1. General scheme of the starting materials and the final molecules synthesized in the course of this work (crossed arrows represent non-successful synthetic paths).

acetate (in various proportions). The spots in the chromatographic plates were visualized under UV light (254 and/or 366 nm). Silica gel 60 (0.040 - 0.063 mm) (Carlo Erba) was used as stationary phase for the purification by flash column chromatography. The mobile phases used, as well as the volumetric proportions of each component when mixtures were used, will be specifically mentioned for each compound.

Reagents were weighed on a Kern ABJ-NM/ABS-N balance. Microwave assisted synthesis was performed in a Biotage Initiator 2.5 synthesizer. Solvents were evaporated under reduced pressure using a Büchi Rotavapor R-210 and synthesized samples were dried in a MTI Corporation vacuum oven, at a temperature of 323 K.

The synthesized compounds were identified by nuclear magnetic resonance (NMR) and mass spectrometry (MS). The ^1H NMR and ^{13}C NMR data were acquired, at room temperature, on a Brüker AMX 400 spectrometer operating at 400.15 MHz and 101.0 MHz, respectively. Electron impact mass spectrometry (EI-MS) was carried out on a VG AutoSpec instrument. Additional details regarding the spectroscopic characterization, as well as the spectroscopic data, are presented in section C of the annexes.

2.2.3. Synthetic yields and purity degrees

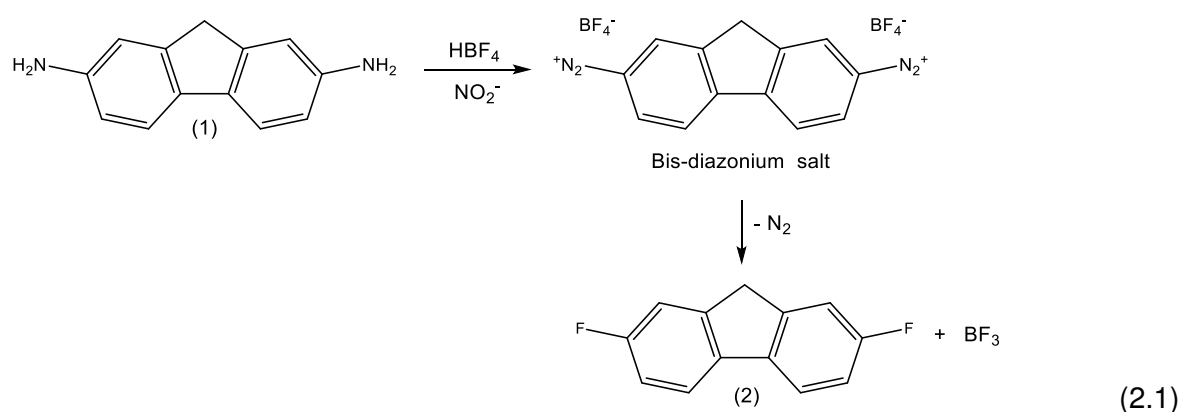
The purity degree and synthetic yield of each isolated compound are presented after the description of the respective synthetic procedure. The (mass fraction) purity degrees were determined by gas-liquid chromatography (GC) and are related to the isolated compounds, before further purification by sublimation under reduced pressure (section 3.1.1.). The synthetic yields were calculated as the ratio, in percentage, of the obtained molar amount of isolated compound to that theoretically predicted by stoichiometric calculation, based on the amount of the limiting reagent.

2.3. Synthetic procedures

2.3.1. Halogenated fluorene derivatives

2.3.1.1. 2,7-Difluorofluorene

The synthesis of 2,7-difluorofluorene (2) was performed by Balz-Schiemann reaction [1] (reaction 2.1), according to a procedure described in the literature [2].



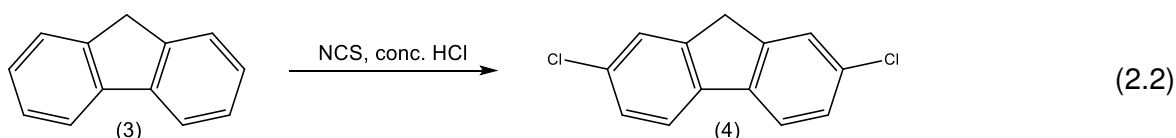
To a solution of 2,7-diaminofluorene (1) (1.55 g, 7.9 mmol) in tetrahydrofuran (15 mL), protected from the light, 15 mL of tetrafluoroboric acid (HBF_4 , 48 wt. % in H_2O) was added. Then, a saturated aqueous solution of sodium nitrite (NaNO_2) (1.47 g, 17 mmol) was added dropwise at a temperature between 278 and 283 K. After addition, the mixture was stirred for 30 min, then filtered and washed with a 5 % HBF_4 solution, methanol and finally with diethyl ether. The crude product, the bis-diazonium salt, was thoroughly dried in a vacuum oven at 323 K. It was then mixed with boiling xylenes and heated for 30 min yielding a dark tar like residue. After cooling to room temperature, the residue was triturated with diethyl ether. The solvent was evaporated and the resulting residue was purified by flash column chromatography (diethyl ether/petroleum ether 3:7). The collected fractions were monitored by TLC and the ones containing the desired product were combined and evaporated to dryness.

Purity: 0.891

Synthetic yield: 68.3 %

2.3.1.2. 2,7-Dichlorofluorene

Fluorene can undergo chlorination at its most electronegative centers yielding 2,7-dichloro derivatives [3]. In this work, 2,7-dichlorofluorene (4) was synthesized from fluorene (3) using *N*-chlorosuccinimide (NCS) in acetonitrile and hydrochloric acid (HCl) (reaction 2.2), following the procedure proposed by Perumattam *et al.* [3].



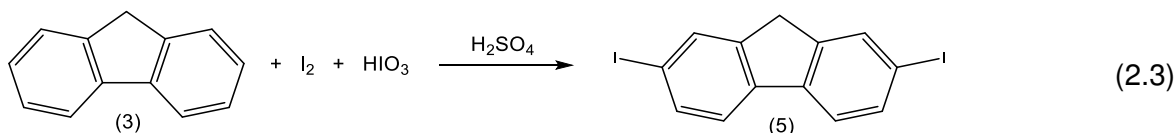
To a solution of fluorene (3) (2.01 g, 12 mmol) and NCS (3.87 g, 29 mmol) in acetonitrile (15 mL), stirred at a temperature between 278 and 283 K, concentrated HCl (1.4 mL) was added dropwise. After the exothermic reaction stopped, the mixture was stirred for 4 h at room temperature. The resulting precipitate was filtered and dissolved in dichloromethane. The solution was then washed with 5 % sodium bicarbonate (NaHCO₃) solution (2 × 10 mL). The organic phase was dried over anhydrous sodium sulphate (Na₂SO₄), filtered, and evaporated to dryness originating a pale yellow powder. The product was recrystallized from ethanol yielding white needles.

Purity: 0.976

Synthetic yield: 65.0 %

2.3.1.3. 2,7-Diiodofluorene

2,7-Diiodofluorene (5) was synthesized by the iodination of fluorene (3) with iodine (I₂) in the presence of iodic acid (HIO₃) and sulfuric acid (H₂SO₄) (reaction 2.3), following the procedure of Anémian *et al.* [4] with minor modifications.



A solution of fluorene (3) (2.04 g, 12 mmol), I₂ (2.27 g, 8.9 mmol), HIO₃ (1.06 g, 6.0 mmol), concentrated H₂SO₄ (0.7 mL) and chloroform (2 mL) in acetic acid (15 mL) was warmed at 353 K for 5 h. The resulting precipitate was filtered and dissolved in chloroform. The solution was then washed with an aqueous solution of sodium dithionite (Na₂S₂O₄, 0.5M) to remove the remaining iodine (2 × 10 mL). The organic phase was dried over anhydrous Na₂SO₄ and evaporated to dryness. A pale yellow product was obtained and then recrystallized from ethyl acetate yielding white needles.

Purity: 0.979

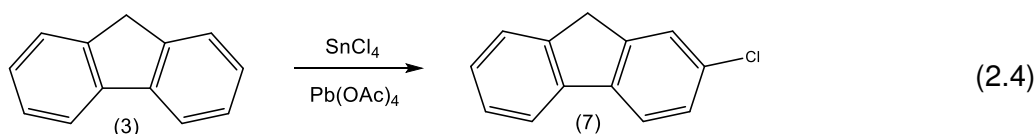
Synthetic yield: 91.7 %

2.3.1.4. 2-Chlorofluorene

Along this work, the synthesis of 2-chlorofluorene (7) was also attempted following different procedures described in the literature [5-8]. Although, for different reasons, the compound was not obtained, the attempts performed so far are described as follows.

Procedure I

Initially, following the procedure described by Muathen [5], the chlorination of fluorene (3) was attempted using a combination of tin(IV) chloride (SnCl₄) and lead(IV) acetate (Pb(OAc)₄) under mild conditions (reaction 2.4).



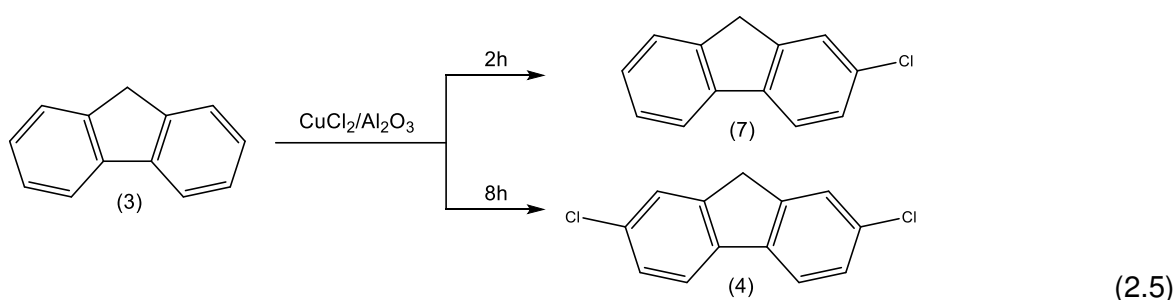
Lead(IV) acetate (0.68 g, 1.5 mmol) was added portion wise over 5 min to a vigorously stirred solution of fluorene (3) (0.26 g, 1.5 mmol) and tin(IV) chloride (0.5 mL, 4.3 mmol) in anhydrous ethyl acetate (7.5 mL). The mixture was stirred for 20 min and then diluted with ethyl acetate (7.5 mL). The resulting solid was filtered off and the filtrate washed successively with 1M HCl solution (2 × 10 mL) and 5 % NaHCO₃ solution (2 × 10 mL). The

organic phase was dried over anhydrous Na_2SO_4 , evaporated to dryness and recrystallized from ethyl acetate.

The ^1H NMR analysis of the product showed a mixture of several components, from which it was not possible to isolate 2-chlorofluorene. Several elution systems were tested and the mixture was further purified by flash column chromatography (dichloromethane/*n*-hexane 2:8). The collected fractions were monitored by TLC and the ones expected to contain the desired product were combined and evaporated to dryness. The ^1H NMR analysis of the product obtained by flash column chromatography showed again a mixture of components.

Procedure II

After the outcome of procedure I, the chlorination of fluorene (3) using alumina-supported copper(II) chloride as reported by Kodomari *et al.* [6] was attempted. The authors described the successful chlorination of fluorene with the formation of 2-chloro and 2,7-dichlorofluorene in high yields (reaction 2.5).



Alumina-supported copper(II) chloride was prepared by adding neutral alumina (10 g, 0.1 mol) to a solution of copper(II) chloride (7 g, 0.05 mol) in 15 mL of water. The water was evaporated at 353 K under reduced pressure and the resulting reagent was dried at 373 K overnight. To prepare 2-chlorofluorene (7), activated alumina (8 g) was added to a solution of fluorene (3) (0.2 g, 1.2 mmol) in chlorobenzene (30 mL). The mixture was stirred vigorously for 2h at 403 K. The activated alumina was filtered out and washed with chlorobenzene (10 mL). The combined filtrate was evaporated to dryness to yield the synthesized product.

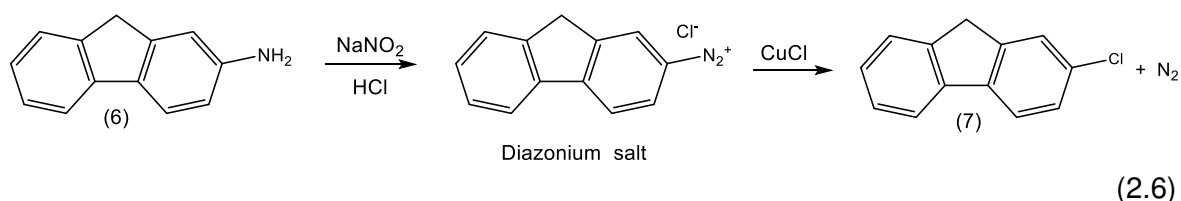
Even though the results reported by the authors were replicated, the isolation of 2-chlorofluorene was not successful as the ^1H NMR spectra of the product revealed the presence of a mixture of two compounds that were identified as the mono and dichlorinated

derivatives. Even when the reaction time was reduced, there was always the formation of a small amount of 2,7-dichlorofluorene. In addition, other solvents (toluene and dioxane) have been used but the reaction had the same outcome. The separation of the two derivatives by column chromatography was not successful as they present similar polarities and the same retention factor in TLC, although several elution systems were tested. The separation of the two chlorinated derivatives was also attempted by reduced pressure sublimation, however the two derivatives present similar volatilities and their separation was unsuccessful even at low temperatures.

Procedure III

The synthesis of 2-chlorofluorene (7) was also attempted by Sandmeyer reaction using 2-aminofluorene (6) as starting material. In this reaction, a primary aromatic amine is treated with concentrated HCl and NaNO₂ to produce a diazonium salt, which is then converted to an aryl halide, under copper(I) catalysis [9].

The procedure used for the synthesis of 2-chlorofluorene (reaction 2.6) was adapted from a literature procedure used for the synthesis of *p*-chlorotoluene [7].



To a solution of 2-aminofluorene (6) (0.20 g, 1.1 mmol) in tetrahydrofuran (4 mL), concentrated HCl (1 mL) was added while stirring. The solution was thoroughly cooled in an ice bath and a saturated aqueous solution of NaNO₂ (0.10 g, 1.4 mmol) was added dropwise with vigorous stirring while keeping the temperature under 278 K. A few minutes after completing this addition, copper(I) chloride (CuCl) (0.15 g, 1.5 mmol) dissolved in concentrated HCl (1 mL) was added. The mixture was removed from the ice bath, allowed to slowly warm to room temperature and then heated for 1 h at 333 K.

After cooling to room temperature, the reaction mixture was washed with aqueous sodium hydroxide (NaOH) (2 M, 2 × 10 mL) and water (2 × 10 mL). The organic phase was dried over anhydrous Na₂SO₄ and evaporated to dryness. The resulting residue was purified by flash column chromatography (diethyl ether/petroleum ether 0.5:9.5). The collected

fractions were monitored by TLC and the ones expected to contain the desired product were combined and the solvent evaporated.

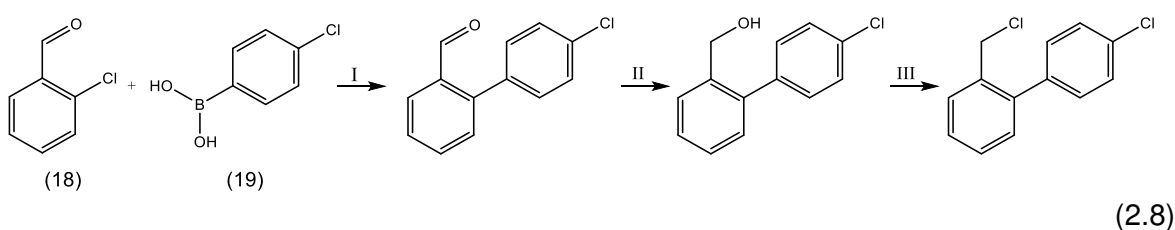
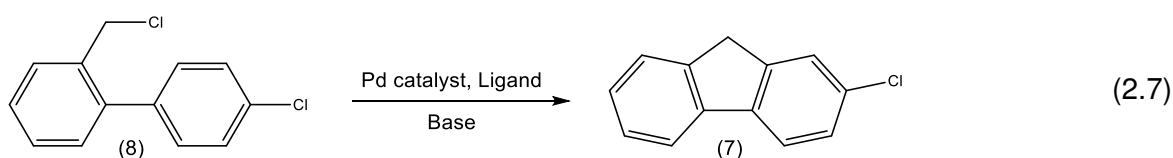
After work-up, it was observed that the reaction unexpectedly yielded a mixture. It was possible to identify one of the products as 2-chlorofluorene by the ^1H NMR spectra, however, it was not possible to identify the other constituent from the NMR spectra or gas chromatography analysis. The mixture components were, again, not possible to separate using the already mentioned methods.

One of the byproducts of this reaction can be the phenol derivative [7], resulting from a competing reaction with the water in the reaction mixture. This hypothesis, however, was not consistent with the obtained spectral results.

Lastly, no alteration of the product composition was observed when different experimental conditions were used, such as the reaction temperature after CuCl addition or the stoichiometric amount of CuCl.

Procedure IV

Since the chlorination of fluorene by previously described methods was not successful, another synthetic approach not involving fluorene or a derivative of fluorene as a starting material was considered. Instead, the synthesis of 2-chlorofluorene (7) can be performed by the Pd-catalyzed cyclization of 4'-chloro-2-phenylbenzylchloride (8) (reaction 2.7), using the procedure proposed by Hwang *et al.* [8]. As the starting material is not commercially available, the synthetic strategy described by reaction 2.8 was developed in order to obtain it.

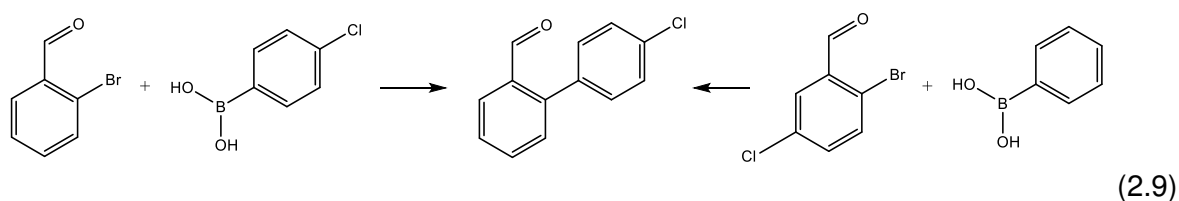


Step I of this strategy was attempted by Suzuki-Miyaura cross-coupling reaction [10, 11]. In Suzuki-Miyaura reactions, organohalides react with organoboranes originating coupled products using a palladium catalyst and base.

For this reaction, 2-chlorobenzaldehyde (18) (0.23 mL, 2.0 mmol), (4-chlorophenyl) boronic acid (19) (0.32 g, 2.0 mmol), sodium carbonate (0.24 g, 2.3 mmol) and the Pd catalyst, PdOAc₂ (11 mg, 0.05 mmol), were mixed with dimethylformamide (4 mL) and water (2 mL). The mixture was agitated for 5 min at room temperature and then heated under reflux until complete consumption of the aldehyde. Upon completion, the reaction mixture was filtered with a cotton plug, to discard the palladium residue, and washed with aqueous NaOH (2 M, 2 × 10 mL) and HCl (1M, 2 × 10 mL). The organic layer was dried over anhydrous Na₂SO₄ and evaporated to dryness. The resulting residue was purified by flash column chromatography (dichloromethane). The collected fractions were monitored by TLC and the ones expected to contain the desired product were combined and the solvent evaporated.

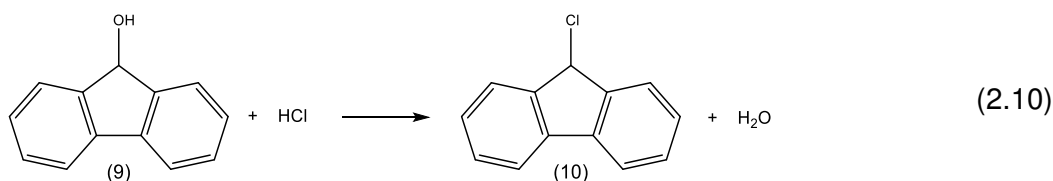
This step was unfortunately not successful, as the spectral data indicates a mixture of components not easy to identify. This synthesis was repeated using different experimental conditions such as microwave heating (at different temperatures and different reaction times), solvents and bases, with no improvement.

Alternatives to step I involving organobromides as starting materials instead of organochlorides were considered (reaction 2.9), however, due to time restrictions, the synthesis of this compound and its cyclization could not be pursued.



2.3.1.5. 9-Chlorofluorene

Alcohols react with hydrogen halides, yielding the corresponding alkyl halide through an acid catalyzed nucleophilic substitution. By treating 9-fluorenone (9) with concentrated HCl, 9-chlorofluorene (10) was obtained (reaction 2.10), following the procedure in the literature [12].



A solution of 9-fluorenol (9) (2.05 g, 11.3 mmol) in water (100 mL) and concentrated HCl (25 mL) was heated for 15 min to 333 K. After this time, the mixture was removed from heating and cooled in an ice bath to induce the precipitation of the product. The precipitate was filtered and washed with ice cold water. The resulting product was dissolved in dichloromethane and then washed with aqueous NaOH (2 M, 2 × 10 mL) to neutralize any traces of the concentrated acid. The organic phase was dried over anhydrous Na₂SO₄, filtered and evaporated to dryness yielding a pale yellow powder. The product was recrystallized from ethanol yielding translucent needles.

Purity: sample not analyzed before further purification.

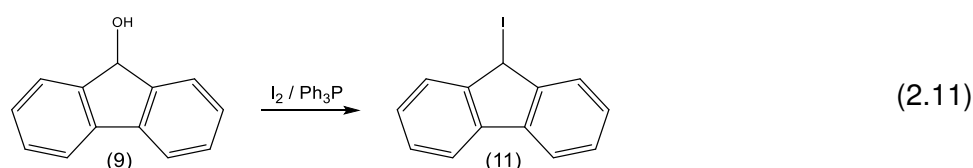
Synthetic yield: 84.5 %

2.3.1.6. 9-Iodofluorene

In this work, the synthesis of 9-iodofluorene (11) was attempted following different procedures described in the literature [13,14]. Even though the compound was not obtained, the two attempts performed so far are described as follows.

Procedure I

The synthesis of 9-iodofluorene (11) from 9-fluorenol (9) was attempted through an adaptation of the procedure published by Hajipour *et al.* [13]. The authors have described the solvent-free iodination of alcohols with iodine (I₂) and triphenylphosphine (Ph₃P), using microwave heating (reaction 2.11).

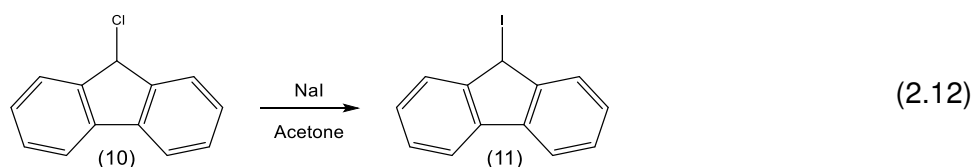


In a mortar, a mixture of 9-fluorenone (9) (0.25 g, 1.4 mmol), iodine (0.34 g, 1.3 mmol) and triphenylphosphine (0.37 g, 1.4 mmol) was ground with a pestle to a homogeneous mixture. The reaction mixture was transferred to a microwave reaction vial, sealed, and irradiated for 5 min at 373 K. After this reaction period, the resulting mixture was diluted in dichloromethane and filtered to remove any solid residue. It was then washed with aqueous $\text{Na}_2\text{S}_2\text{O}_4$ (0.5M, 2×10 mL) to remove the excess iodine, and water (2×10 mL). The organic layer was dried over anhydrous Na_2SO_4 , filtered and evaporated to dryness.

It was confirmed by TLC of the obtained product that the starting material was completely consumed and a new product was formed. It was isolated by column chromatography (dichloromethane/methanol, 9:1), and identified by NMR as the byproduct triphenylphosphine oxide.

Procedure II

For the second attempt, the synthesis of 9-iodofluorene from 9-chlorofluorene by Finkelstein reaction (reaction 2.12) was tried, following the procedure described by Baughman *et al.* [14]. This reaction features the displacement of chloride using sodium iodide (NaI) in acetone solution and the formation of the respective alkyl iodide.

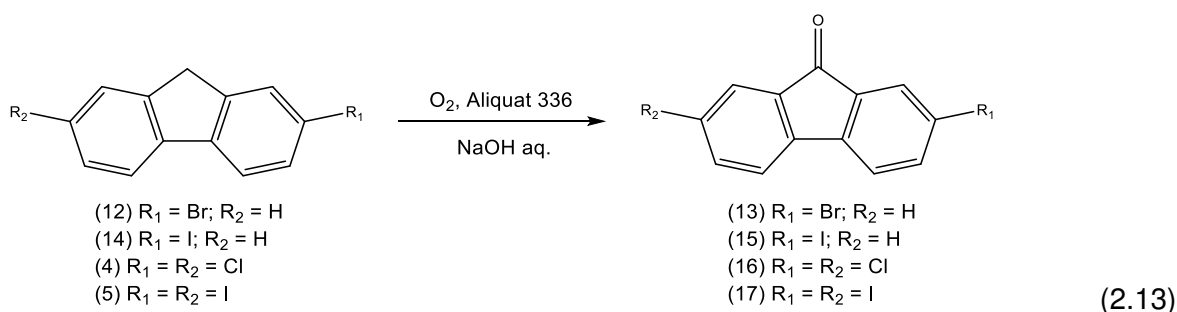


Sodium iodide (0.26 g, 1.3 mmol) and 9-chlorofluorene (0.33 g, 2.2 mmol) were dissolved in acetone (15 mL) and allowed to reflux for 3 days. The reaction mixture was cooled and flooded with diethyl ether (15 mL). Any precipitate was filtered off and the ether solution was washed with water (2×10 mL). The organic layer was dried over anhydrous Na_2SO_4 , filtered and the solvent evaporated. The reaction yielded a mixture of two components that were separated by column chromatography (diethyl ether/petroleum ether, 3:7). The collected fractions were monitored by TLC, combined according to composition and the solvent evaporated. None of the isolated components were identified as 9-iodofluorene by ^1H and ^{13}C NMR. One of the components was identified as 9-fluorenone, while the other component was not possible to identify by the NMR spectral data.

Due to time restrictions, the synthesis of these compounds was not revisited.

2.3.2. Halogenated fluorenone derivatives

Halogenated fluorenone derivatives were synthesized from the respective halogenated fluorenes by air oxidation, using a base-catalyzed reaction in the presence of a phase-transfer catalyst, Aliquat[®] 336, also known as Starks' catalyst [9] (reaction 2.13). The general procedure was validated by synthesizing 9-fluorenone ($R_1 = R_2 = H$) from fluorene, and after a satisfactory outcome of this initial test, the procedure was adapted to synthesize 2-bromofluorenone (13), 2-iodofluorenone (15), 2,7-dichlorofluorenone (16) and 2,7-diiodofluorenone (17).



To a solution of the halofluorene (1mmol) in toluene (10 mL), aqueous NaOH (10M, 10 mL) was added. The mixture was stirred vigorously while 6 drops of aliquat were added. The mixture was kept under agitation for further 30 min After this period, the organic layer was separated and washed with aqueous HCl (1M, 2 × 10 mL) and brine (2 × 10 mL). The organic phase was dried over anhydrous Na_2SO_4 and evaporated to dryness yielding a bright yellow powder, characteristic of fluorenone derivatives. The resulting products were purified by flash column chromatography (dichloromethane/petroleum ether 4:6). The collected fractions were monitored by TLC and the ones expected to contain the desired product were combined and evaporated to dryness.

Purities: (13) 0.983; (15) 0.961; (16) 0.975; (17) 0.981.

Synthetic yields: (15) 55.9 %; (16) 58.1 %; (17) 76.7 %. Negligently, the obtained mass of (13) after synthesis was not registered which prevented the yield calculation.

References

- [1] A.J. Cresswell, S.G. Davies, P.M. Roberts, J.E. Thomson, *Chem. Rev.* 115 (2015) 566-611;
- [2] B.M. York Jr., *Spiro-(fluoren-9,4'-imidazolidine)-2',5'-diones*. US Patent no. 4,438,272 (1984);
- [3] J. Perumattam, C. Shao, W.L. Confer, *Synthesis* 11 (1994) 1181-1184;
- [4] R. Anémian, Y. Morel, P.L. Baldeck, B. Paci, K. Kretsch, J.-M. Nunzic, C. Andraud, *J. Mater. Chem.* 13 (2003) 2157-2163;
- [5] H.A. Muathen, *Tetrahedron* 52 (1996) 8863-8866;
- [6] M. Kodomari, H. Satoh, S. Yoshitomi, *J. Org. Chem.* 53 (1988) 2093-2094;
- [7] "The Sandmeyer Reaction: Substitution for an NH_2 on an Aromatic Ring", <http://web.mnstate.edu/jasperse/chem365/sandmeyer.doc.pdf>, accessed in September 2015;
- [8] S.J. Hwang, H.J. Kim, S. Chang, *Org. Lett.* 11 (2009) 4588-4591;
- [9] K.L. Williamson, K.M. Masters, *Macroscale and Microscale Organic Experiments* (6th Ed.), Brooks/Cole Cengage Learning, Belmont (2010);
- [10] N. Miyaura, K. Yamada, A. Suzuki, *Tetrahedron Lett.* 20 (1979) 3437-3440;
- [11] N. Miyaura, A. Suzuki, *Chem. Rev.* 95 (1995) 2457-2483;
- [12] F.H. Greenberg, *J. Chem. Educ.* 73 (1996) 1043-1045;
- [13] A.R. Hajipour, A.R. Falahati, A.E. Ruoho, *Tetrahedron Lett.* 47 (2006) 4191-4196;
- [14] T.W. Baughman, J.C. Sworen, K.B. Wagener, *Tetrahedron* 60 (2004) 10943-10948.

Chapter

3

Experimental methods

- 3.1. Purification and characterization
- 3.2. Calorimetric methods
- 3.3. Vapor pressure measurement methods
- 3.4. Photoluminescence spectroscopy

References

3.1. Purification and characterization

3.1.1. Purification methods

With the exception of the synthesized compounds, all the other ones studied in this work were commercially acquired from Sigma-Aldrich Co., Tokyo Chemical Industry and Acros Organics, with a degree of purity ranging between 0.97 and 0.99 according to the information available in the respective certificates of analysis provided by the suppliers.

The high sensitivity of the techniques used in this work demands the use of samples with a high degree of purity. All the compounds studied in this work, solid at room temperature, were routinely purified by successive sublimation under reduced pressure (ca. 1 Pa) until a convenient degree of purity was achieved. Additionally, when proved necessary, some of the compounds were further purified by successive recrystallization in an adequate solvent and, afterwards, thoroughly dried and sublimed under reduced pressure.

3.1.2. Purity analysis

The purity monitoring throughout the purification process and the determination of the mass fraction of impurities of the purified samples was performed by GC. This analysis was performed on an Agilent 4890D chromatograph, equipped with a HP-5 semi-capillary column (15 m length, 0.53 mm inner diameter and 1.5 μm film thickness), whose stationary phase consists of 0.05 diphenyl and 0.95 dimethylpolysiloxane (mole fraction).

The signal detection at the end of the column is carried out by a flame ionization detector (FID), under a flow of hydrogen ($0.47 \text{ cm}^3\cdot\text{s}^{-1}$). The mobile phase consists of compressed air, used as carrier gas ($5.1 \text{ cm}^3\cdot\text{s}^{-1}$), and nitrogen, as auxiliary gas ($0.50 \text{ cm}^3\cdot\text{s}^{-1}$). The *HP GC Chem Station Rev* software, supplied by the manufacturer, displays the detected signal in real time, which is proportional to the mass of ionized material in the detector.

A sample of the compound to be analyzed was dissolved in a suitable solvent (spectroscopic grade), and injected into the chromatograph (about 1 μL). To allow the solvent to be vaporized and quickly detected, the sample is kept at an initial predefined temperature during a stabilization period of 1 minute, followed by a heating ramp at 0.17

K·s⁻¹ to a final predefined temperature kept constant during a suitable period of time to ensure that the sample is completely eliminated from the column. Chromatographic conditions, such as the injector and detector temperatures, as well as the initial and final predefined oven temperatures were optimized according to the characteristics of each compound.

All data regarding the source of the compounds (acquired or synthesized), lot number and respective degree of purity certified by the supplier (when acquired), purification details and the final degree of purity of the compounds studied are fully presented in chapter 4.

3.2. Calorimetric methods

3.2.1. Differential calorimetry

3.2.1.1. Introduction to differential calorimetry

Differential thermal analysis by calorimetric methods provides qualitative and quantitative information on the change of physical properties of a substance associated with processes that result in release or absorption of heat as a function of temperature. In this group of methods are included calorimetric methods like differential scanning calorimetry (DSC) and Calvet microcalorimetry.

Calorimetric differential analysis is extremely versatile, allowing the direct determination of temperatures and transition enthalpies in condensed phases, the measurement of temperature-dependent properties such as heat capacity, detection of thermal decomposition processes, identification of different polymorphic forms, etc, on a vast diversity of materials such as liquid crystals, drugs, biological materials, metals, polymers, glass and ceramics, etc. [1].

In differential measuring systems, the calorimeter's signal depends on the difference between the responses of a reference and a sample to a temperature variation. The advantage of the differential principle is that disturbances to the system, with the exception of those occurring in the sample, affect both the sample and the reference equally and are compensated by the difference between the individual signals. Differential calorimeters also present the advantages of being easy to work with, the experiments are fast, require only small amounts of sample (about 5-10 mg), can be performed at temperatures significantly above ambient and allow the study of "slow" reactions, which are outside the normal operating range of most adiabatic calorimeters. These advantages, however, have some costs in terms of accuracy, yielding results generally less accurate than the corresponding measurements by adiabatic calorimetry [2].

Two general types of differential calorimeters must be distinguished, according to their operation principle [3,4]:

- **Power compensation** calorimeters, where the output signal of the calorimeter is proportional to the difference between the heat flow rates supplied to the sample and the reference, in separate furnaces;

- and **Heat flux** calorimeters, where the temperature difference between the sample and reference, in the same furnace, is directly converted in a difference in potential, proportional to a difference in heat flow rate to the sample and to the reference.

Differential calorimeters can be operated in a dynamic (non-isothermal) mode, where the sample is subjected to heating and/or cooling, or in an isothermal mode, in which the temperature is maintained constant.

Both types of differential calorimeters and modes of operation were used in this work to determine phase transition properties. The respective apparatuses and experimental procedures will be described as follows (sections 3.2.1.2 and 3.2.1.3).

3.2.1.2. Power compensation calorimetry: Differential scanning calorimeter

A power compensation calorimeter, simply schematized in figure 3.1, consists of two identical microfurnaces, thermally decoupled, one containing the sample (S) and other the reference (R), each associated to a temperature sensor (1) and a heating resistance (2) controlled by independent electrical circuits.

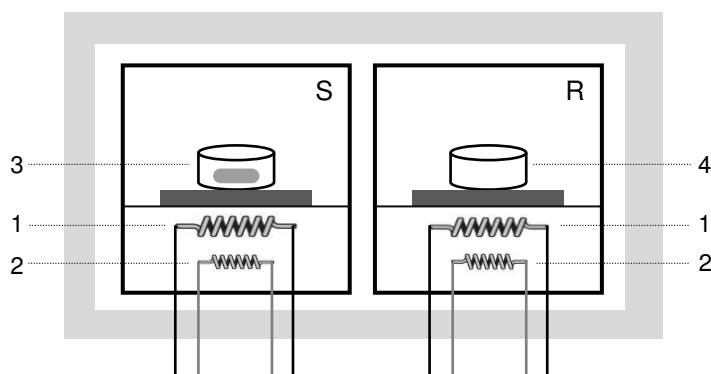


Figure 3.1. General schematic representation of a power compensation calorimeter (S. sample furnace; R. reference furnace; 1. temperature sensors; 2. heating resistances; 3. sample crucible; 4. reference crucible).

The samples are enclosed in crucibles (3), made of high thermal conductivity materials (e.g., aluminum, copper), which may or may not be hermetically sealed, depending on the type of application. The selection of the appropriate crucibles depends on the characteristics of the sample to be analyzed and the properties to be determined. The reference generally consists of an empty crucible (4) with a mass as similar as possible to

that of the sample crucible. During the experiments, a purging gas (e.g., helium, argon, nitrogen) is flowed through the furnaces at a constant rate to ensure that the ambient conditions are as uniform as possible in all experiments.

During a thermal characterization study, the same heating power is supplied to both furnaces in order to change their temperature in accordance to a preset heating rate. If there is ideal thermal symmetry between both furnaces, their temperature is the same. When thermal asymmetry occurs, after the release or consumption of heat due to a certain physical or chemical process in the sample, the system compensates the temperature difference, adjusting the heat flow rate by Joule heating (in the mW range) through a heating resistance, to reduce the difference between the temperature of the sample and reference furnaces.

3.2.1.2.1. Typical thermogram and treatment of experimental results

DSC results are usually displayed as thermal analysis curves, or thermograms, in which the instrument signal, heat flow rate, is plotted as a function of time and temperature. In the absence of any changes in the sample, the sample and reference furnaces are at the same temperature and heat flow rate is approximately constant, establishing the baseline. The baseline is related to the heat capacity of the sample in the absence of phase transitions, and its good definition is crucial for the reproducibility and accuracy of experimental results.

Prior to heating, the sample is subjected to an isothermal period to reach equilibrium with the furnace conditions. The sample is then heated, according to a preset heating rate, and when a thermic transformation occurs, the resulting change in heat flow rate causes a deviation from the baseline in the form of a peak. In the DSC experiments performed in the present work, a negative deviation corresponds to an endothermic process (e.g., melting), whereas a positive deviation corresponds to an exothermic process (e.g., crystallization).

Figure 3.2 represents a typical thermogram of an endothermic process based on a dynamic method, showing the temperature ramp (dashed line) and the heat flow rate, ϕ , associated with the occurring transitions (solid line). To characterize the transition associated to the peak, it is necessary to define the onset temperature and area of the peak, which are respectively related to the temperature and enthalpy of transition. The transition temperature, T_{tr} , is the onset temperature defined by the intersection between the tangent that follows the downslope of the peak and the extrapolated baseline. The heat associated to the process is determined by the area of the peak, defined from the interpolation of the

baseline connecting the beginning and end of the transition. Assuming that the experiment occurs at constant pressure, the measured heat corresponds to the change in enthalpy during the process.

The difference between the baseline before and after the transition will depend on the change in heat capacity of the sample with temperature. In the case of figure 3.2, they are nearly collinear, which means that the sample transformation occurs with no significant change in heat capacity.

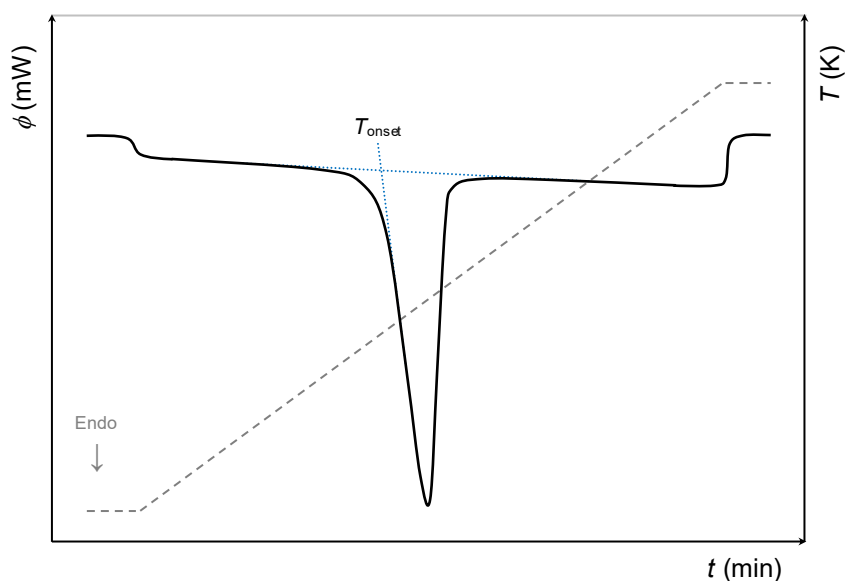


Figure 3.2. Schematic representation of a typical power compensation DSC thermogram.

3.2.1.2.2. Calibration

The calorimeter's signal does not depend solely on the occurring thermal process but also on a number of factors inherent to the calorimeter, namely heating rate, thermal conductivity of the crucible material, nature and flow of the purge gas, etc. To account for thermal gradients between the crucibles, the sample and the reference, it's crucial to carefully calibrate the apparatus [5].

In order to achieve reproducibility and accuracy of the results, it is necessary to perform the calibration in terms of temperature and in terms of heat flow. The aim of this calibration is to assign the correct values of temperature and heat flow rates to those indicated by the instrument. Therefore, the determined calibration constants are factors of

proportionality between quantities measured by the device and the actual values. Because the calibration constants are complex and generally unknown functions of various parameters, the calibration experiments should be carried under the same experimental conditions used for the sample experiments.

The recommended calibration method for a dynamic operated DSC involves the determination of the temperature of fusion of several standard substances for thermal analysis, as some of those recommended by Sabbah *et al.* [6], over the temperature range of the equipment and using various heating rates.

A number of the recommended temperature standards have well established enthalpies of transition, allowing both temperature and enthalpy calibration to be performed simultaneously.

3.2.1.2.3. Description of the apparatuses

Two differential scanning calorimeters were used in this work, both with power compensation in a dynamic mode. Initially, a DSC 141 SETARAM calorimeter was used. Later this apparatus was replaced by a PerkinElmer Diamond Pyris 1 calorimeter. The detailed description and mode of operation of both apparatuses can be found in the respective manuals provided with the devices [7,8].

DSC studies were carried out using hermetically sealed aluminum crucibles (30 or 50 μL capacity) and a flow of nitrogen used as purging gas. For some of the compounds studied in the SETARAM calorimeter, it was necessary to use a pressed aluminum disk between the crucible and the lid to ensure its tightness.

The calibration of both calorimeters was performed by other researchers, using high purity reference materials and test substances (details in table 3.1) and the same heating rate and aluminum crucibles used in the sample study.

In case of the SETARAM calorimeter, the heat flow and temperature scales of the calorimeter were calibrated independently, at a $2 \text{ K}\cdot\text{min}^{-1}$ heating rate. The heat flow scale was calibrated using indium and the temperature scale was calibrated by measuring the melting temperature of indium, tin, benzoic acid, *o*-terphenyl, 4-methoxybenzoic acid and lead [9]. In case of the PerkinElmer calorimeter, the power and temperature scales of the calorimeter were calibrated simultaneously, at 2, 5 and $10 \text{ K}\cdot\text{min}^{-1}$ heating rates, by measuring the melting temperature of the following substances [10]: naphthalene, benzoic acid, diphenylacetic acid, triphenylene, perylene, *o*-terphenyl 1,3,5-triphenylbenzene, 4-methoxybenzoic acid and anthracene.

Table 3.1. Reference materials used for the calibration of temperature and enthalpy of fusion (literature data collected from ref. [6], unless otherwise indicated).

Calibrant	T_{fus} K	$\Delta_{\text{fus}} H_{\text{m}}^{\circ}(T_{\text{fus}})$ kJ·mol ⁻¹	Classification
Indium	429.75	3.29 ± 0.1	Primary standard
Tin	505.08	7.17 ± 0.4	Primary standard
Naphthalene	353.35	19.06 ± 0.8	Primary standard
Benzoic acid	395.50	18.06 ± 0.4	Primary standard
Diphenylacetic acid	420.41	31.27 ± 0.4	Secondary standard
Triphenylene	471.02	24.74 ± 0.8	Secondary standard
Perylene	551.25	31.87 ± 0.8	Secondary standard
<i>o</i> -Terphenyl	329.35 [11]	17.19 ± 0.01 [12]	Test substance
1,3,5-Triphenylbenzene	447.9 [13]	32.4 ± 1.3 [12]	Test substance
4-Methoxybenzoic acid	456.43 [5]	28.33 ± 0.14 [14]	Test substance
Anthracene	488.93 [15]	29.4 ± 0.1 [12]	Test substance
Lead	600.61 [5]	4.78 ± 0.2 [5]	Test substance

3.2.1.2.4. Experimental procedure

In each experiment, two aluminum crucibles, very close in mass, are used. A small sample (5 to 10 mg) of pulverized crystalline compound is placed in one of the crucibles, while the other is kept empty for reference.

Once prepared and sealed, both crucibles are accurately weighed (Mettler Toledo XS105, ±1·10⁻⁵ g or Mettler Toledo UMT2, ±1·10⁻⁷ g). The amount of sample is determined by the difference in mass of the crucible containing the sample and empty. The crucibles are placed in their respective measuring chambers and the desired temperature program is set. For each compound, four to six independent thermal scans were performed on fresh samples under a constant flow of nitrogen, starting at room temperature to about 15 K above the melting temperature, at a heating rate of 2 K·min⁻¹, and then cooled back to room temperature. The recorded thermogram is analyzed, using the instrument's dedicated software, to compute the onset temperatures and the enthalpies of occurring condensed phase transitions. After the scan, the sample crucible is weighed again to ensure that no mass loss occurred during the experiment. The absence of decomposition and the thermodynamic reversibility of the condensed phase transitions is confirmed by a second run with the same sample recrystallized *in situ*.

3.2.1.3. Heat flux calorimetry: Calvet microcalorimeter

In heat flow calorimeters, the heat associated with a given process occurring in a reaction vessel – calorimetric cell – is exchanged by conduction with a heat sink kept at a constant temperature – an isothermal block – where they are inserted.

Tian [16] was one of the first scientists to use the heat conduction principle for constructing calorimeters. Later, Calvet [17,18] developed a calorimeter based on twin Tian systems, symmetrically placed inside an isothermal block, providing an effective compensation for irregular heat effects. Its theoretical and operating principles are fully described in the literature [19,20].

Calvet microcalorimeters are particularly suited for the study of slow reactions and the measurement of very small amounts of energy, hence the designation ‘microcalorimeter’. They can be divided into two groups: high temperatures calorimeters applied to slow thermal processes, phase transitions and heat capacities determinations, and the low-temperature calorimeters for the study of biological processes. Calvet microcalorimeters, however, have the downsides of having much longer response times and very slow heating and cooling rates, when compared to a DSC for example.

The Calvet microcalorimeter, as shown in figure 3.3, is basically composed of two identical calorimetric cells, placed in symmetrically arranged cavities in a large metal block (1). The process under study occurs in the sample cell (2), while the other cell operates as a reference (3). The heat transfer between the cells and the isothermal block is monitored by high thermal conductivity thermopiles containing large numbers of identical thermocouples, connected in series, regularly arranged around the calorimetric cells.

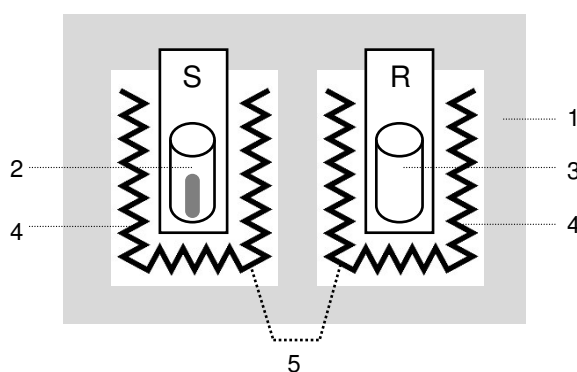


Figure 3.3. General schematic representation of a heat flux Calvet microcalorimeter (S. sample cavity; R. reference cavity; 1. isothermal block; 2. sample cell; 3. reference cell; 4. thermopiles; 5. differential connection between thermopiles).

The thermopiles (4) act as the measuring sensor of the temperature difference between the outer surface of the calorimetric cell and the inner surface of the isothermal block and, simultaneously, as a thermal bridge between the cells and the isothermal block. The thermopiles of the two calorimetric cells are connected in opposition (5) so that the measured output signal is a difference in potential generated by the two thermopiles. The resulting heat flow, directly proportional to the temperature gradient between the two calorimetric cells, is compensated by Peltier effect (for exothermic processes) or Joule heating (for endothermic processes), in order to keep the temperature constant.

The experimental procedure commonly used for this type of calorimetry, known as the “drop calorimetric technique”, was developed by Skinner *et al.* [21] for the determination of enthalpies of sublimation. In this procedure, a known mass of sample contained in a small glass capillary at room temperature is dropped into the sample cell of the calorimeter. To compensate the thermal disturbance produced by dropping the glass capillary into the sample cell, a similar but empty capillary is simultaneously dropped into the reference cell. This allows the determination of the heat associated solely with the process taking place in the sample cell. This technique has been adapted to the study of liquid compounds by Ribeiro da Silva and colleagues [22] in order to determine molar enthalpies of vaporization.

In this calorimetric technique, the processes do not occur under equilibrium conditions, which can compromise the accuracy of the experimental results. Studies by Skinner *et al.* [21] showed that the results obtained by microcalorimetry Calvet can differ up to 5 % from the results derived from vapor pressures determined by the Knudsen mass-loss effusion method. For the Calvet microcalorimeter used in this work [23], it was concluded that the uncertainty of the method may be better than 2 %, however conditioned by the compound’s purity and thermal stability, the appropriate choice of the reference compounds used in calibration (section 3.2.1.3.2), and the uncertainty introduced by the enthalpic corrective term, $\Delta_{298.15\text{ K}}^T H_m^{\circ}(\text{g})$.

3.2.1.3.1. Typical thermogram and treatment of experimental results

The study of the thermal process occurring in the calorimeter is performed by measuring the heat flow, ϕ , over time, defining a thermogram similar to the curve illustrated in figure 3.4.

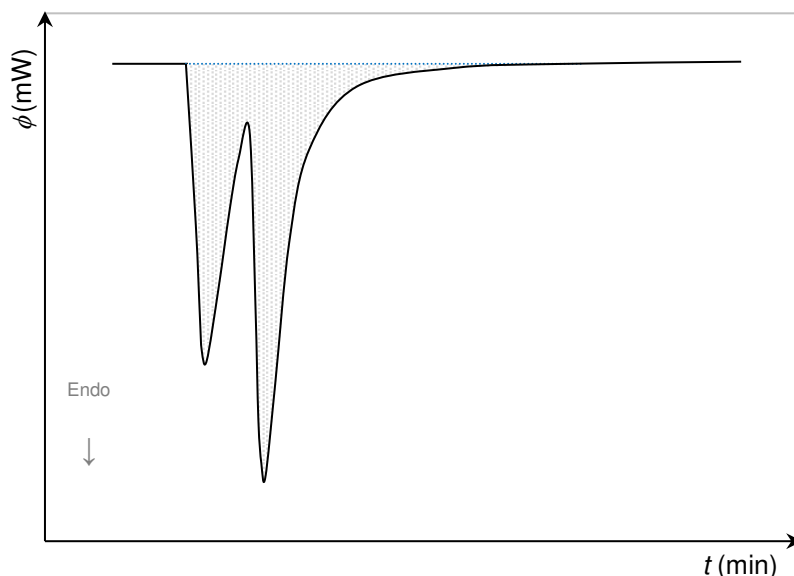


Figure 3.4. Schematic representation of a typical Calvet microcalorimetry thermogram.

After thermal equilibrium is reached between the cells and the calorimetric block, held at a predefined temperature T , the initial baseline is defined. When the capillary tubes are simultaneously dropped at room temperature (ca. 298 K) in the respective calorimetric cells, the first endothermic peak is observed due to the heating of the sample from 298 K to the temperature of the calorimeter, if T is smaller than the temperature of fusion of the compound. If T is larger than the temperature of fusion, the first endothermic peak includes the heating of the sample from 298 K to the temperature of the calorimeter as well as the enthalpy of fusion. Once the capillaries reach thermal stability inside the calorimeter, the system is evacuated and the sample is rapidly removed from the calorimetric cell originating a second endothermic curve in the thermogram.

The enthalpy variation of the total process, $\Delta_{cr/l,298.15\text{ K}}^{g,T} H_m$, can be determined from the integration of the total area under the baseline of the thermogram. This thermogram includes the following enthalpic contributions:

- Thermal disturbances produced by dropping the glass capillaries into the calorimetric cells;
- Heating of the glass capillaries and sample, in the condensed state, from 298 K to the temperature of the calorimeter;
- Phase transition(s).

The determination of the standard molar enthalpy of sublimation or vaporization, at the reference temperature $T = 298.15 \text{ K}$, is obtained from the experimental result $\Delta_{\text{cr/l},298.15 \text{ K}}^{\text{g},T} H_{\text{m}}^{\circ}$, according to the thermodynamic cycle shown in figure 3.5.

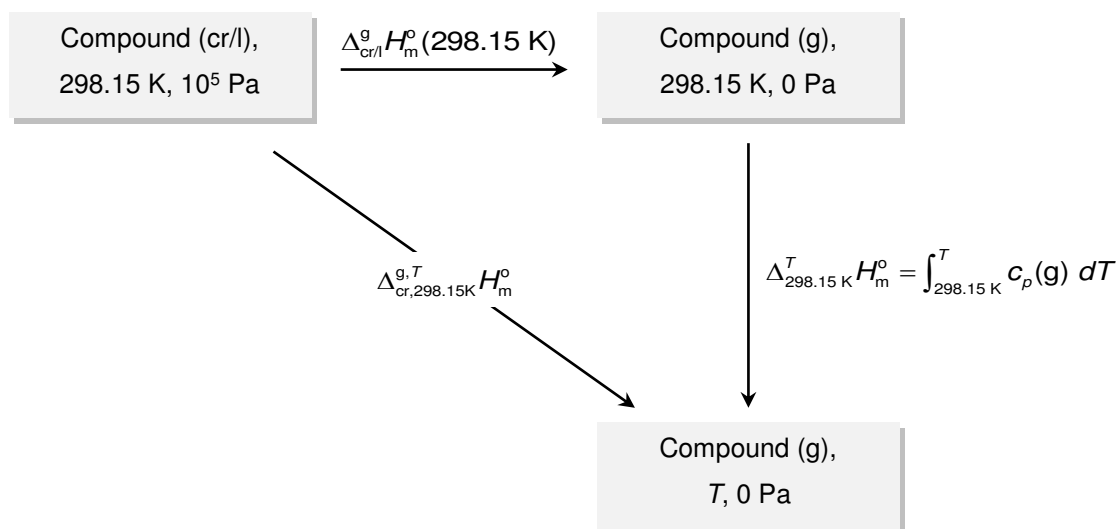


Figure 3.5. Representative thermodynamic cycle of the processes occurring during a Calvet microcalorimetry sublimation or vaporization experiment.

The standard molar enthalpy of sublimation or vaporization, at the reference temperature $T = 298.15 \text{ K}$, can then be determined from the following expression:

$$\Delta_{\text{cr/l}}^{\text{g}} H_{\text{m}}^{\circ} (298.15 \text{ K}) = \Delta_{\text{cr/l},298.15\text{K}}^{\text{g},T} H_{\text{m}}^{\circ} - \Delta_{298.15\text{K}}^T H_{\text{m}}^{\circ}(\text{g}) \quad (3.1)$$

where the term $\Delta_{298.15\text{K}}^T H_{\text{m}}^{\circ}(\text{g})$ corresponds to the thermal adjustment of the enthalpy, in the gaseous state, and can be estimated by computational methods or by group additivity methods derived from the data of Stull *et al.* [2].

3.2.1.3.2. Calibration

Temperature calibration

The calibration of the temperature of the isothermal block of the calorimeter, performed by other investigators [23], was achieved by establishing a relation (given by

expression 2.2) between the actual temperature of the calorimetric cells, measured by a PT100 temperature sensor calibrated against a SPRT temperature probe (25 Ω ; Tinsley, 5187A), and that indicated by the Setaram G11 controller.

$$\theta_{\text{real}}/^{\circ}\text{C} = 1.0054 \theta_{\text{G11}}/^{\circ}\text{C} - 3.822 \quad (3.2)$$

Blank calibration

Because the mass of the capillaries (sample and reference) is not exactly the same, the heat capacities of the capillary tubes do not cancel each other totally, and their contributions are not negligible for the total enthalpy change. Therefore, to account for the difference in mass of both capillaries and, also, the different sensibilities of the two measuring cells, the additional enthalpic contribution is determined through blank experiments, at various temperatures, where empty capillary tubes of similar masses are simultaneously dropped into both calorimetric cells.

For the calorimetric system used, blank experiments were performed by other investigators [23], using capillaries with masses ranging between (20 and 30) mg. Expression 3.3 was used for the determination of the enthalpic blank correction, $\Delta H_{\text{corr}}(\text{blank})$, as a function of the temperature difference between the calorimetric cell and the temperature 298.15 K, and the masses of the reference, m_{ref} , and empty sample capillary tubes, m_{exp} ($a = -20.3902$, $b = -0.88204$, $c = 0.816818$, $d = 1.814894$ [23]).

$$\Delta H_{\text{corr}}(\text{blank})/\text{mJ} = a + [b(m_{\text{exp}}/\text{mg}) + c(m_{\text{ref}}/\text{mg}) + d][(T/\text{K}) - 298.15] \quad (3.3)$$

Calorimeter calibration

The entrance of the calorimetric cells is not covered by thermocouples. Through this small uncovered area some thermal leakage can occur by convection and radiation processes. In order to account for this and other heat transfer processes, calibration experiments are performed, under the same conditions carried out in the experiments with the compounds under study, to determine a proportionality factor, k_{cal} , between the heat involved in the reaction and the area of the thermogram obtained experimentally, according to equation 3.4.

$$k_{\text{cal}}(T) = \frac{\Delta_{\text{cr}/1,298.15\text{K}}^{\text{g},T} H_{\text{m}}^{\circ}}{\Delta_{\text{cr}/1,298.15\text{K}}^{\text{g},T} H_{\text{m}}^{\circ}(\text{cal})} \quad (3.4)$$

The standard substance selected as calibrant should present volatility comparable to that of the compound under study, within the experimental temperature range. In this work, the calibration was performed using recommended primary standard substances [6], anthracene and naphthalene, whose molar enthalpies of sublimation are rigorously established (table 3.2). The average calibration constant, at the temperature T , $\langle k_{\text{cal}} \rangle$, used in the calculation of enthalpies of sublimation of the studied compounds is determined as the mean of at least six agreeing values.

Table 3.2. Reference materials used for the calibration of the Calvet microcalorimeter.

Calibrant	T_{fus} K	Temp. range K	$\Delta_{\text{cr}}^{\text{g}} H_{\text{m}}^{\circ}(298.15 \text{ K})$ kJ·mol ⁻¹	Classification
Naphthalene	353.35	[250 - 353]	72.6 ± 0.6 [6]	Primary standard
Anthracene	488.93	[338 - 360]	100.4 ± 0.4 [23]	Primary standard

3.2.1.3.3. Description of the apparatus

The calorimetric system used is based on a commercial high temperature Calvet microcalorimeter Setaram HT1000D, in isothermal mode, which can be operated from room temperature to $1.3 \cdot 10^3$ K, using the drop calorimetric technique referred to above. Both the apparatus and technique have been previously described in the literature [23].

The complete system, schematized in figure 3.6, includes, in addition to the Calvet microcalorimeter (A), a pumping system (B) and a glass vacuum line (C), which will be briefly described as follows.

Calvet microcalorimeter

The Calvet microcalorimeter Setaram HT1000D consists of an inner isothermal metal block of high heat capacity (1) externally lined with ceramic material (2), containing two identical cavities in which the calorimetric cells (3) are introduced. The base of each cavity is surrounded by a thermopile (4) composed of 496 thermocouples (Pt-Pt/Rh) connected in series and radially arranged around each cavity.

The temperature of the metal block is regulated by a Setaram G11 control system, which also has the function of amplifying and registering the electronic signal from the thermocouples. The temperature is programmed through the Setaram 3.20 software,

installed in an interfaced computer that is also used for the data acquisition, graphical representation of the thermogram in real time, and for the related calculations.

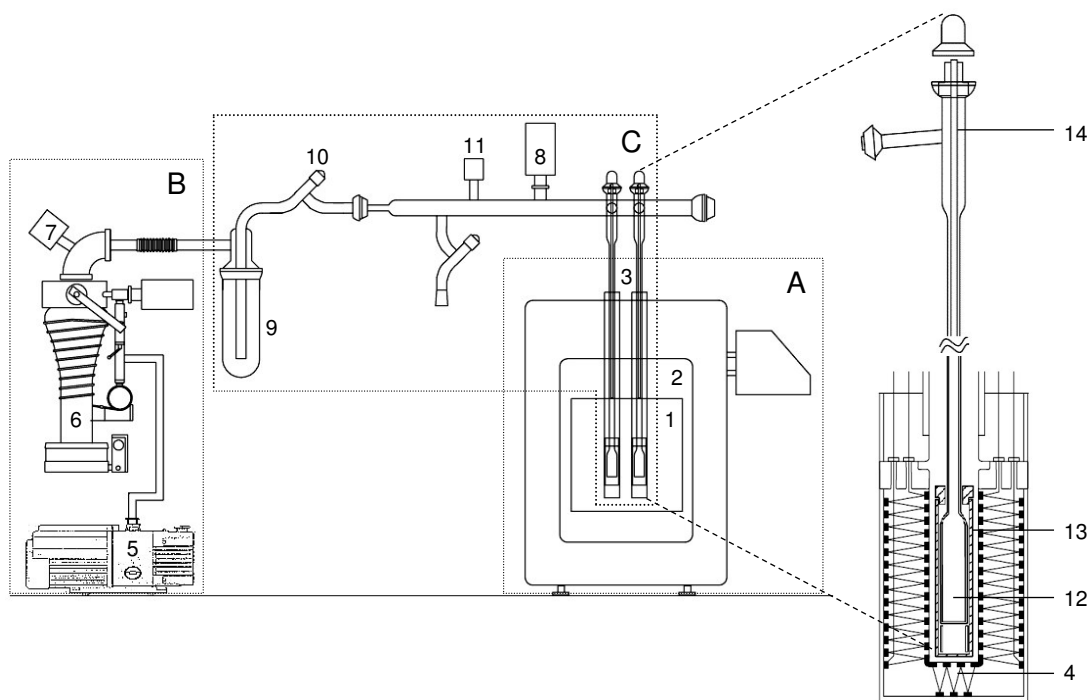


Figure 3.6. Schematic representation of the complete Calvet microcalorimeter: A. Calvet microcalorimeter Setaram HT1000D (1. isothermal metal block; 2. ceramic lining; 3. calorimetric cells; 4. thermopile); B. Vacuum pumping system (5. rotary pump; 6. oil diffusion pump; 7. Pirani gauge; 8. Penning gauge); C. Vacuum line (9. Liquid nitrogen glass trap; 10. isolation teflon valve; 11. air inlet teflon valve; 12. pyrex vessel; 13. kanthal cylinder; 14. Inner pyrex tube). Image adapted from ref. [23].

Vacuum pumping system

The pumping system consists of an Edwards RV5 rotary pump (5), which is used both for pre-evacuating the system and for backing the Edwards Diffstak 63 oil diffusion pump (6). An Edwards APG-M Pirani gauge (7) is used to measure the pressure of the system during the pre-evacuation process and an Edwards AIM-S Penning gauge (8) is used to measure the pressure kept throughout the sublimation process.

Vacuum line and calorimetric cells

The twin calorimetric cells are connected to the vacuum pumping system through a glass line that includes a liquid nitrogen trap (9) to condense the sublimated samples preventing contamination of the pumping system. Between the trap and the calorimetric cells, there are two valves, one allowing the isolation of the pumping system (10) and the

other used to admit air in the system (11) for restoring the atmospheric pressure. All glass connections in the system are made of greaseless spherical joints from Young.

The calorimetric cells (3) consist of long inlet tubes made of pyrex[®] glass that extend to the inside of the thermal block ending in small vessels (12), cylindrical in shape. The vessels are tightly fitted into cylinders made of kanthal[®] (iron-chromium-aluminum alloy used for high-temperature applications) (13), which promote good thermal contact between the calorimetric vessel and the isothermal block. The calorimetric cells are equipped with inner tubes (14), through which the capillaries are dropped, easy to remove and clean without removing the calorimetric cells, and therefore without significant disturbance to the thermal equilibrium, allowing multiple consecutive experiments.

3.2.1.3.4. Experimental procedure

In each experiment, a pair of glass capillary tubes (Marienfeld Superior, $\phi_{\text{ext}} = 1.5 - 1.6$ mm), sealed at one end, with a mass difference between them inferior to 0.1 mg, was selected and accurately weighed (Mettler Toledo UMT2, $\pm 1 \cdot 10^{-7}$ g). A pulverized sample of a crystalline compound (3 to 5 mg) is placed in one of the capillaries while the other is kept empty as a reference. The capillary containing the sample is weighed again and the amount of sample is determined by the difference in mass. Preliminary experiments were performed to determine the appropriate experimental temperature for each compound.

After thermal equilibrium is reached between the cells and the calorimetric block, the capillary tubes are simultaneously dropped at ca. 298 K in the respective calorimetric cells. The system is then sealed and once the capillaries reach thermal stability inside the calorimetric cells, the system is evacuated and the sample is spontaneously removed by sublimation. When the signal returns to the baseline and the experiment is finished, the pumping system is isolated and air is slowly admitted in the system. The acquired data is processed using the instrument's dedicated software, to compute the experimental enthalpy changes.

When the experimental study of the compound is finished, this procedure is repeated at the same experimental temperature for the calibration using capillaries filled with a selected calibrant.

3.2.2. Combustion Calorimetry

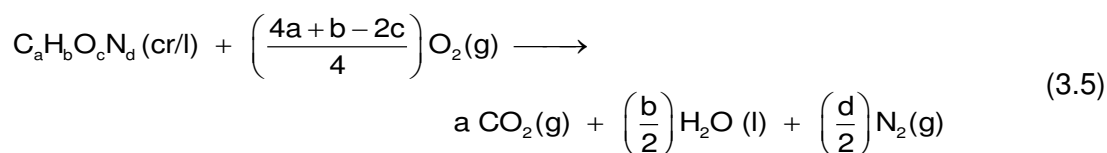
3.2.2.1 Introduction to combustion calorimetry

Combustion calorimetry is one of the most precise and accurate calorimetric techniques for the determination of enthalpies of formation of organic compounds in a condensed state [24,25]. The calorimetric study of a combustion reaction allows the measurement of the amount of energy, at constant volume, associated to the complete oxidation of a compound under controlled experimental conditions. The combustion must occur rapidly, with no side reactions, and originate identifiable and quantifiable products, as well as an amount of energy per mass unit easily measurable. Rigorous characterization of the initial and final states of each calorimetric experiment ensures the reproducibility and reliability of the experimental results.

The calorimeters used in the combustion study are frequently of the isoperibol type, and consist of a calorimetric vessel in controlled thermal contact with its surroundings – a thermostatic bath – which is kept at a constant temperature, independent of the course of the experiment. The heat flow between the calorimeter vessel and the surroundings is allowed, though limited, and accurately controlled to ensure that the amount of heat exchanged between them is proportional to the respective temperature difference, following Newton's law of cooling.

The combustion reaction takes place in a reaction chamber located within the calorimetric vessel – a combustion bomb – and consists of a sealed metal container with thick walls, suitable to withstand high pressures, where the combustion reaction is triggered by the ignition of a fuse in a pressurized oxidizing atmosphere, to promote a fast and complete reaction. The heat released in the reaction is calculated from the temperature rise of the calorimetric fluid (water or other high thermal conductivity fluid) placed inside the calorimetric vessel, where the sealed combustion bomb is immersed during the combustion process.

The selection of the appropriate system and procedure for the calorimetric study of a certain compound will depend, above all, on its composition and, consequently, the nature of the combustion products formed. In the case of organic compounds constituted of carbon, hydrogen, oxygen and/or nitrogen, combustion calorimetry in a static bomb is the suitable method, leading generally to a rapid and complete combustion reaction with simple and easily-defined products.



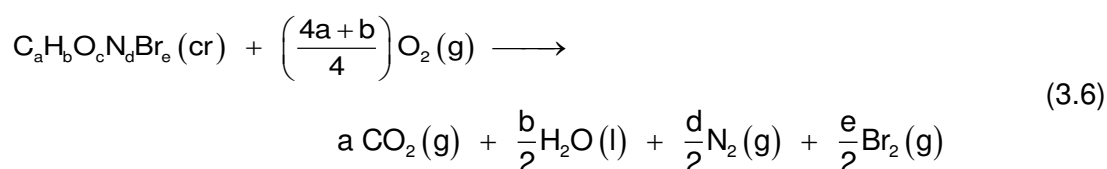
Organic compounds with other elements, such as sulfur or halogens, present additional difficulties due to the corrosive nature of some of their combustion products and the difficulty to characterize unambiguously the final state of the combustion process. For this type of compounds, combustion calorimetry in a rotating bomb, internally lined with corrosive resistant materials such as platinum or tantalum, is the appropriate method. This type of calorimeter allows the rotation of the bomb in two orthogonal axes, after the complete combustion of the sample till the end of calorimetric experiment. The presence of a suitable bomb solution, in combination with the rotation movement to wash the inner walls of the bomb, promotes the complete dissolution of the combustion products and a homogeneous oxidation state of the species in the bomb content, facilitating its analysis and accurate characterization.

The apparatuses and experimental procedures for both methods will be described in more detail ahead in this work (section 3.2.2.3).

3.2.2.1.1. Combustion of organic compounds containing bromine

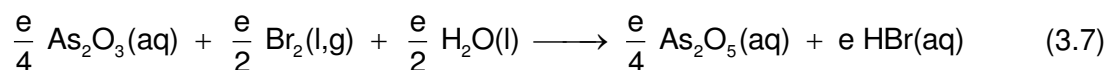
In this work, some organic compounds containing bromine were studied by rotating bomb combustion calorimetry.

The combustion reaction of brominated organic compounds with empirical formula $\text{C}_a\text{H}_b\text{O}_c\text{N}_d\text{Br}_e$, in oxygen atmosphere, yields reaction products containing bromine in different proportions and in different oxidation states: (3 to 10) % of HBr and (90 to 97) % of Br_2 [25], according to the reaction represented by chemical equation (3.6).

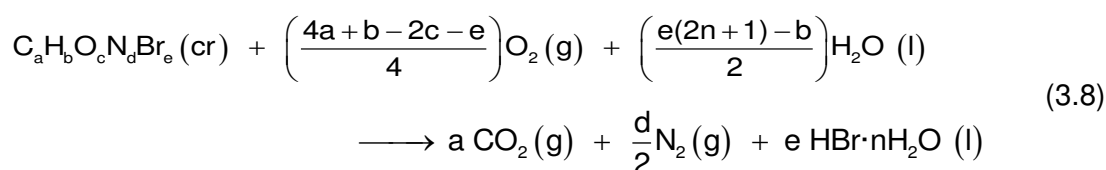


Bjellerup [26] was the pioneer in using rotating bomb combustion calorimetry for the study of organic compounds containing bromine, using a bomb solution of arsenic(III) oxide

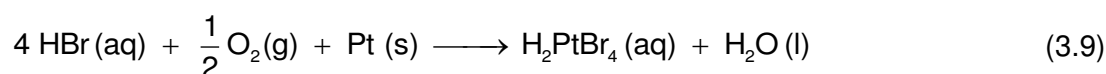
as a reducing agent to promote the conversion of the molecular bromine to bromide ion, according to the reaction in equation 3.7,



in order to achieve a homogeneous and well-defined final state, with hydrobromic acid as the only combustion product containing bromine:



The hydrobromic acid formed in the combustion process reacts with the platinum crucible and fittings, though to a very small extent, dissolving it in the bomb solution. So it is necessary to account for the energy contribution associated with the side reaction 3.9.



3.2.2.2. Theoretical and technical basis of the method

3.2.2.2.1. Variation of temperature in adiabatic conditions

In a combustion calorimetric experiment, the heat involved in the combustion process will cause a variation in the calorimeter's temperature. The temperature variation during a combustion experiment on an isoperibol system is typically represented by the thermogram schematized in figure 3.7. The calorimetric curve can be divided into three distinct periods: the initial and final periods, where temperature variation is due mainly to the heat transfer between the calorimeter and the surroundings, and the heat of stirring; and the main period, where there is a sudden rise in temperature fundamentally due to the combustion reaction taking place within the bomb.

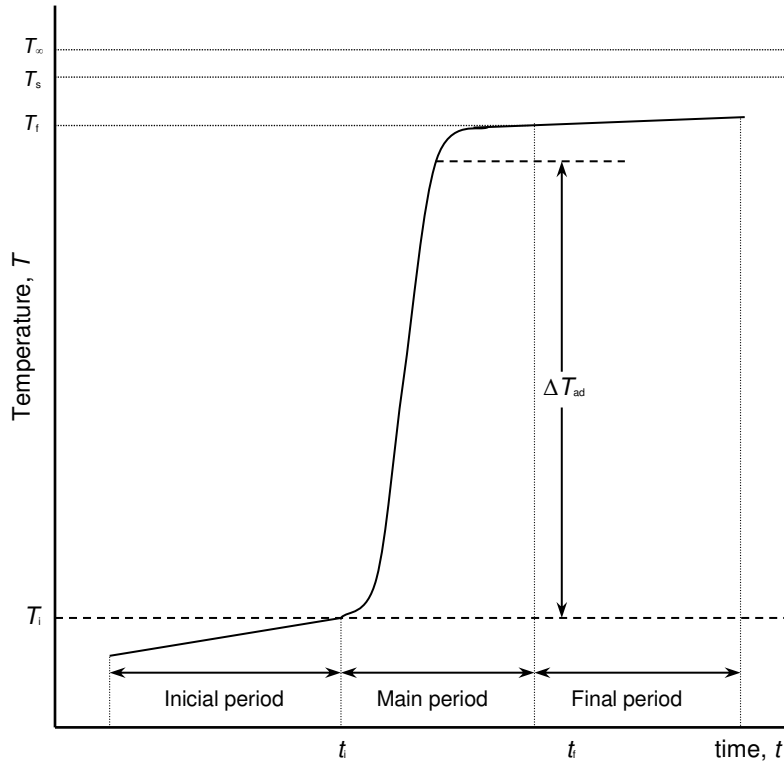


Figure 3.7. Typical curve of the calorimetric temperature versus time during a combustion experiment.

The observed temperature rise during the combustion experiment, corrected for adiabatic conditions, ΔT_{ad} , is determined from $T_f - T_i$, taking into consideration the heat exchange between the calorimetric vessel and the surroundings and the heat produced by the stirring of the calorimetric fluid. These effects are taken into account with a corrective term, ΔT_{corr} , in the calculation of the variation of temperature in adiabatic conditions, according to expression 3.10, T_i and T_f being, respectively, the calorimeter temperature at the start and end of the main period.

$$\Delta T_{ad} = (T_f - T_i) - \Delta T_{corr} \quad (3.10)$$

The thermal corrective term can be determined following the method described by Coops *et al.* [27], which assumes the variation in temperature caused by heat of stirring of the calorimetric fluid, u , as being constant throughout the experiment and the variation in temperature due to heat transfer between the calorimeter and the surroundings is proportional the difference between the temperatures of the calorimeter, T , and surroundings, T_s , according to the Newton's cooling law.

The temperature variation of the calorimeter, during the initial and final periods, can be translated by expression 3.11, where k is a cooling constant of the calorimetric system.

$$\frac{dT}{dt} = u + k(T_s - T) \quad (3.11)$$

After an infinite period of time, and considering k and T_s as being constant, the calorimeter temperature will tend to a constant limit value, T_∞ , called convergence temperature (temperature of the calorimetric fluid after an infinite time, with constant stirring at a controlled speed). Then the system reaches an equilibrium state in which the temperature variation rate is canceled, $(dT/dt) = 0$, and consequently:

$$u = k(T_\infty - T_s) \quad (3.12)$$

Replacing u in the equation 3.11:

$$\frac{dT}{dt} = k(T_\infty - T) \quad (3.13)$$

Defining g_i and g_f , as the values of (dT/dt) at the average temperatures \bar{T}_i and \bar{T}_f of the initial and final periods, respectively, then k and T_∞ can be defined by the expressions 3.14 and 3.15, respectively:

$$k = \frac{g_i - g_f}{\bar{T}_f - \bar{T}_i} \quad (3.14)$$

$$T_\infty = \bar{T}_i + \frac{g_i}{k} = \bar{T}_f + \frac{g_f}{k} = \frac{g_i \bar{T}_f - g_f \bar{T}_i}{g_i - g_f} \quad (3.15)$$

During the initial and final periods, temperature variations as a function of time are not linear, but in fact defined by exponential curves, as a result of the secondary thermal effects mentioned above. However, a linear behavior can be assumed when considering relatively short periods of time. The error introduced by this approximation is not relevant and can be eliminated if the same calculation method and experimental period intervals are employed in both the calibration and compound combustion experiments. This approach allows the

determination of g_i and g_f values, by the least squares regression method, from linear functions $T = f(t)$ adjusted to (t, T) values in the initial and final periods.

The corrective term, ΔT_{corr} , for the secondary thermal effects that occur during the main period can be determined by the integration of equation 3.13, according to the mean value theorem:

$$\Delta T_{\text{corr}} = \int_{t_i}^{t_f} k(T_{\infty} - T) dt = k(T_{\infty} - T_m)(t_f - t_i) \quad (3.16)$$

where T_m is the mean temperature of the main period, which can be determined by:

$$T_m = \frac{1}{t_f - t_i} \int_{t_i}^{t_f} T dt \quad (3.17)$$

However, the determination of T_m using equation 3.17 is not possible because there is no known simple analytical expression $T = f(t)$ to express the temperature rise during the main period of a calorimetric experiment. Therefore, T_m is obtained by numerical integration using Regnault-Pfaundler method, also called the trapezoid rule [27,28], which allows the determination of the area under the curve that defines the main period by dividing it into an appropriate number of trapezoids, in order to obtain a good geometric approximation of the area. To each trapezoid corresponds a mean temperature ($T_m', T_m'', T_m''' \dots$) and T_m corresponds to the weighted average of the mean temperature values of all trapezoids:

$$T_m = \frac{aT_m' + bT_m'' + cT_m''' + \dots}{a + b + c + \dots} \quad (3.18)$$

where a, b, c, \dots are the lengths of the base of each trapezium corresponding to regular time intervals between consecutive temperature measurements.

3.2.2.2.2. Variation of temperature in adiabatic conditions in rotating bomb combustion calorimetry

When considering rotating bomb calorimetry, since the bomb rotation is initiated during the main period, the temperature variation of the calorimeter during final period

cannot be translated by expression 3.11 because it is necessary to consider an additional factor that differentiates it from the initial period, corresponding to the heat of rotation, r , constant over time. The temperature variation of the calorimeter during the final period can then be translated by the expression:

$$\left(\frac{dT}{dt}\right)_f = u + r + k(T_s - T) \quad (3.19)$$

Consequently, the convergence temperature of the final period is not coincident with that obtained in the initial period. Considering $(dT/dt) = 0$, $T = T_{\infty,i}$ for the initial period and $T = T_{\infty,f}$ for the final period, and solving equations 3.11 and 3.19 in order to u and r , respectively:

$$u = k(T_{\infty,i} - T_s) \quad (3.20)$$

$$r = k(T_{\infty,f} - T_{\infty,i}) \quad (3.21)$$

Replacing u and r in expressions 3.11 and 3.19:

$$\left(\frac{dT}{dt}\right)_i = k(T_{\infty,i} - T) \quad (3.22)$$

$$\left(\frac{dT}{dt}\right)_f = k(T_{\infty,i} - T) \quad (3.23)$$

For rotating bomb combustion calorimetry, we must also account for the heat produced by the rotation of the bomb, at a constant speed, in the calculation of ΔT_{corr} :

$$\Delta T_{\text{corr}} = \int_{t_i}^{t_f} k(T_{\infty,i} - T) dt + \int_{t_f}^{t_i} k(T_{\infty,f} - T) dt \quad (3.24)$$

considering t_f as the instant when the bomb rotation is initiated and maintained until the end of the experiment, so that:

$$\int_{t_i}^{t_f} (T - T_i) dt = \int_{t_f}^{t_i} (T_f - T) dt \quad (3.25)$$

As demonstrated by Good *et al.* [29], if the bomb rotation is initiated when the temperature rise is about 63 % of the total temperature variation observed in the main period, the calorimeter temperature variation due to the heat generated by the rotation of the bomb is included in the correction for the other thermal effects. Keeping the rotation of the bomb until the end of the experiment, besides promoting the equilibrium and homogeneity of the final state, also has the advantage of allowing the detection of any eventual malfunctions of the rotation mechanism, resulting in an erratic convergence temperature. Admitting that the temperature variation during the main period is exponential, the value of the mean temperature, T_m , can be calculated as:

$$T_m = 0.63(T_f - T_i) \quad (3.26)$$

3.2.2.2.3. Calibration of the calorimeter: Energy equivalent calculation

The calibration of the calorimetric system establishes the relation between the temperature variation and the energy inherent to a combustion reaction, and allows the determination of the energy equivalent of the calorimeter, E , defined as the amount of energy that must be supplied to the calorimeter and its contents to raise its temperature by one unit,

$$E = \frac{Q}{\Delta T_{ad}} \quad (3.27)$$

where Q is the amount of heat necessary to produce the corrected temperature variation ΔT_{ad} .

The energy equivalent of a bomb calorimeter, determined by supplying an accurately known amount of energy to the system under study and measuring the corresponding temperature rise, can be determined by two methods: an electrical calibration, by the dissipation of an accurately known quantity of electrical energy by Joule heating effect; and a chemical calibration, by the combustion of a precisely known mass of a standard substance, whose massic energy of combustion was accurately determined by a certified laboratory [27].

In this work, the determination of the energy equivalent of the calorimetric systems used was performed by chemical calibration using the recommended thermochemical standard, benzoic acid, reproducing as closely as possible the experimental conditions used

in the compound combustion experiments, in order to minimize/eliminate eventual systematic errors.

The energy equivalent of the calorimeter, E , translated by the sum of the heat capacities of all its components, is generally taken as the sum of two parts: the energy equivalent of the calorimeter with the empty combustion bomb, ε_{cal} , and the energy equivalent of the bomb contents. During a combustion experience, there is a change of the calorimeter's content due to the conversion of reactants to products, with different heat capacities. Therefore, there is a need to define two equivalents of bomb content: for the initial state, ε_i , with the bomb containing only the reactants; and for the final state, ε_f , with the bomb containing only the products formed. The energy equivalent of the calorimeter can then be defined for the initial and the final states, according to:

$$E_i = \varepsilon_{\text{cal}} + \varepsilon_i \quad (3.28)$$

$$E_f = \varepsilon_{\text{cal}} + \varepsilon_f \quad (3.29)$$

The values of ε_i and ε_f for each calibration experiment are determined by the sum of the heat capacities of the components of the bomb, respectively, before and after combustion reaction, by the following expressions [27]:

$$\varepsilon_i = C_v(\text{O}_2) n_i(\text{O}_2) + c_p(\text{H}_2\text{O}, \text{l}) m(\text{H}_2\text{O}, \text{l}) + C_v(\text{H}_2\text{O}, \text{g}) n_i(\text{H}_2\text{O}, \text{g}) + c_p(\text{BA}) m(\text{BA}) + c_p(\text{fuse}) m(\text{fuse}) + c_p(\text{Pt}) m_i(\text{Pt}) \quad (3.30)$$

and

$$\varepsilon_f = C_v(\text{O}_2) n_f(\text{O}_2) + C_v(\text{CO}_2) n(\text{CO}_2) + C_v(\text{H}_2\text{O}, \text{g}) n_f(\text{H}_2\text{O}, \text{g}) + c_p(\text{Pt}) m_f(\text{Pt}) + c_p(\text{sol}) m(\text{sol}) \quad (3.31)$$

In these expressions:

$C_v(\text{O}_2)$, $C_v(\text{CO}_2)$, $C_v(\text{H}_2\text{O}, \text{g})$ represent, respectively, the molar heat capacity, at constant volume, of oxygen, carbon dioxide and water vapor;

$c_p(\text{H}_2\text{O}, \text{l})$, $c_p(\text{BA})$, $c_p(\text{fuse})$, $c_p(\text{Pt})$, $c_p(\text{sol})$ represent, respectively, the specific heat capacity, at constant pressure of liquid water, benzoic acid, cotton fuse, platinum and final bomb solution;

$n_i(\text{O}_2)$, $n_i(\text{H}_2\text{O}, \text{g})$ represent, respectively, the initial amount of oxygen and water vapor;

$m(\text{H}_2\text{O},\text{l}), m(\text{BA}),$ represent, respectively, the initial masses of liquid water, benzoic acid,
 $m_i(\text{Pt}), m(\text{fuse})$ platinum and cotton fuse;
 $n_f(\text{O}_2), n(\text{CO}_2,\text{g}),$ represent, respectively, the final amounts of oxygen, carbon dioxide and
 $n_f(\text{H}_2\text{O},\text{g})$ water vapor;
 $m_f(\text{Pt}), m(\text{sol})$ represent, respectively, the final masses of platinum and final bomb
 solution.

The determination of ε_{cal} , from the calibration experiments, is based on the following thermochemical cycle:

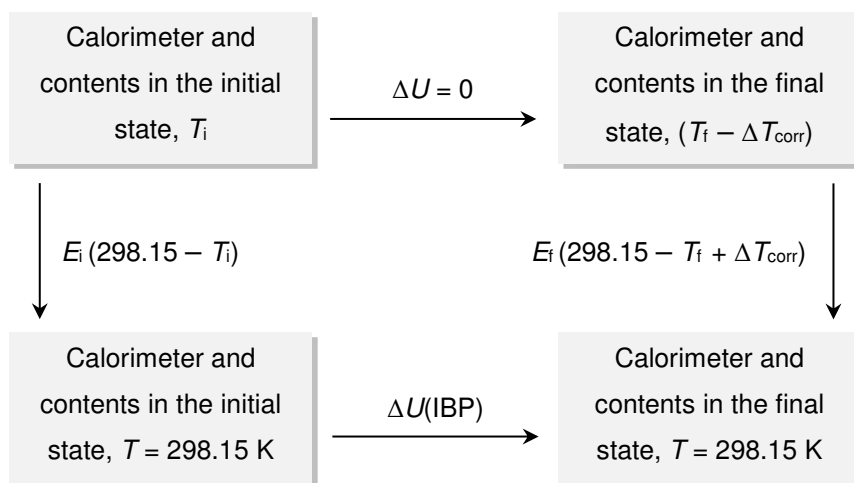


Figure 3.8. Thermochemical cycle for the calculation of the energy equivalent of the calorimeter, ε_{cal} .

from which the following expression was deduced:

$$\varepsilon_{\text{cal}} = \frac{[-\Delta U(\text{IBP}) + \varepsilon_i \cdot (T_i - 298.15) + \varepsilon_f \cdot (298.15 - T_f + \Delta T_{\text{corr}})]}{\Delta T_{\text{ad}}} \quad (3.32)$$

A correction of ε_{cal} will be required when the mass of water placed in the calorimeter vessel differs from the reference mass of water, according to,

$$\varepsilon_{\text{cal}}(\text{corr}) = \varepsilon_{\text{cal}} + C_p(\text{H}_2\text{O},\text{l}) \cdot \Delta m(\text{H}_2\text{O},\text{l}) \quad (3.33)$$

in which $C_p(\text{H}_2\text{O},\text{l})$ is the heat capacity of liquid water at constant pressure and $\Delta m(\text{H}_2\text{O},\text{l})$ is the difference between the net mass of water placed in the calorimetric vessel and the reference mass.

For calibration experiments, the variation of internal energy associated to the isothermal bomb process, $\Delta U(\text{IBP})$, at $T = 298.15$ K, includes the energetic contributions due to the combustion of benzoic acid and cotton fuse, and other side reactions:

$$\Delta U(\text{IBP}) = \Delta U(\text{BA}) + \Delta U(\text{HNO}_3) + \Delta U(\text{fuse}) + \Delta U(\text{ign}) - \Delta U(\text{carb}) \quad (3.34)$$

In this expression:

$\Delta U(\text{BA})$ is the variation of internal energy associated to the combustion of benzoic acid, given by the product of the mass of benzoic acid by the respective certified value of massic energy of combustion: $\Delta U(\text{BA}) = m(\text{BA}) \cdot \Delta_c u(\text{BA}, \text{cert})$;

$\Delta U(\text{HNO}_3)$ is the variation of internal energy associated to the formation of a nitric acid aqueous solution of $0.1 \text{ mol}\cdot\text{dm}^{-3}$ from $\text{N}_2(\text{g})$, $\text{O}_2(\text{g})$ and $\text{H}_2\text{O}(\text{l})$, described by the chemical equation: $1/2 \text{N}_2(\text{g}) + 5/4 \text{O}_2(\text{g}) + 1/2 \text{H}_2\text{O}(\text{l}) \rightarrow \text{HNO}_3(\text{aq})$, with $\Delta U_m^\circ(\text{HNO}_3) = -59.7 \text{ kJ}\cdot\text{mol}^{-1}$ [30];

$\Delta U(\text{fuse})$ is the variation of internal energy associated to the combustion of the cotton fuse (empirical formula $\text{CH}_{1.686}\text{O}_{0.843}$) given by the product of the mass of fuse by the standard massic energy of combustion of cotton, $\Delta_c u^\circ(\text{cotton}) = -16240 \text{ J}\cdot\text{g}^{-1}$ [27];

$\Delta U(\text{ign})$ is the energy supplied for the ignition, calculated as: $\Delta U(\text{ign}) = -1/2 C(V_i^2 - V_f^2)$, where C is the capacitance of the capacitor and V_i and V_f are, respectively, the initial and final voltages of the capacitor;

$\Delta U(\text{carb})$ is the variation of internal energy associated to the combustion of carbon soot formed in case of an incomplete combustion, $\Delta_c u^\circ(\text{carb}) = -33 \text{ kJ}\cdot\text{g}^{-1}$ [27].

The calorimetric systems used in this work were calibrated by combustion of benzoic acid NBS Standard Reference Material[®] 39j, with the certified massic energy of combustion, $\Delta_c u(\text{BA}, \text{cert}) = -(26434 \pm 3) \text{ J}\cdot\text{g}^{-1}$ [31], for the following certification conditions:

- the combustion reaction is referred to 298.15 K;
- the sample is burned in a bomb of constant volume in pure oxygen at an initial pressure of $p = 3.04 \text{ MPa}$ at a temperature of 298.15 K;

- the mass of benzoic acid and water, expressed in grams, added to the bomb before combustion is numerically equal to three times the internal volume of the bomb, expressed in liters.

When deviations occur to the experimental conditions described above, the massic energy of combustion, $\Delta_c u(\text{BA, cert})$, can be corrected by multiplying the certified value by a corrective factor, f [27]:

$$f = 1 + 1 \cdot 10^{-6} \left[197(p - 3.04) + 42 \left(\frac{m(\text{BA})}{V} - 3 \right) + 30 \left(\frac{m(\text{H}_2\text{O})}{V} - 3 \right) - 45(T - 298.15) \right] \quad (3.35)$$

where p is the initial oxygen pressure (MPa), V is the internal volume of the combustion bomb (dm^3), T is the temperature the combustion reaction refers to (K), $m(\text{BA})$ is the mass of burned benzoic acid (g) and $m(\text{H}_2\text{O})$ is the mass of water placed inside the bomb (g). This corrective factor can be applied without appreciable error [27] for the following ranges of experimental conditions: $2.03 \text{ MPa} < p < 4.05 \text{ MPa}$; $2 \text{ g} \cdot \text{dm}^{-3} < m(\text{BA})/V < 4 \text{ g} \cdot \text{dm}^{-3}$; $2 \text{ g} \cdot \text{dm}^{-3} < m(\text{H}_2\text{O})/V < 4 \text{ g} \cdot \text{dm}^{-3}$ and $293.15 \text{ K} < T < 303.5 \text{ K}$.

3.2.2.2.4. Combustion auxiliaries

Combustion aids are substances that may be useful in a calorimetric study to start or moderate the combustion reaction. Auxiliary substances are primarily used to promote the occurrence of complete combustion reactions, preventing the formation of undesired side products [32], like carbon residue. To this end, these substances must be easily combustible and present a rigorously known combustion energy.

They may also be important in controlling the stoichiometry of the combustion reaction, for example, as a source of hydrogen in the combustion of substances with low molecular fraction of this element. Additionally, in the study of liquid compounds, the substance used as combustion aid can also be used to enclose the sample during the experiment.

Among the most common combustion aids are benzoic acid, hydrocarbons (such as *n*-hexadecane) and polymers (such as polyethylene and polyester, commercially known as melinex®).

3.2.2.2.5. Standard massic energy of combustion: Washburn corrections

After determining the energy equivalent of the calorimeter, ε_{cal} , it is possible to calculate the variation of internal energy for the isothermal bomb process, $\Delta U(\text{IBP})$, from the value of ΔT_{ad} , in experimental conditions and at the reference temperature $T = 298.15$ K, by the following expression:

$$\Delta U(\text{IBP}) = -\varepsilon_{\text{cal}}(\text{corr}) \cdot \Delta T_{\text{ad}} + \varepsilon_i \cdot (T_i - 298.15) + \varepsilon_f \cdot (298.15 - T_f + \Delta T_{\text{corr}}) \quad (3.36)$$

As mentioned above, the values of the equivalent energy, ε_i and ε_f , are calculated by the sum of the heat capacities of the bomb contents, respectively, before and after combustion, by expressions similar to 3.30 and 3.31, but now taking into account the mass and heat capacity of the compound under study and eventual auxiliary substances.

In experiments on a static bomb combustion calorimeter, the sample ignition is performed at the temperature $T_i = 298.15$ K, and it is sufficient to define ε_i , as the term $\varepsilon_i \cdot (T_i - 298.15)$ of the previous equation is annulled. On the other hand, for the rotating bomb combustion calorimeter, the temperature of ignition is planned so that T_f is as close as possible to 298.15 K so that the term $\varepsilon_f \cdot (298.15 - T_f - \Delta T_{\text{corr}})$ of the above equation is minimized.

The value of $\Delta U(\text{IBP})$ determined experimentally, in addition to the energy variation associated with the combustion reaction of the compound under study, also includes the energy contributions of the combustion of eventual auxiliary substances, side reactions and formation of any carbon residue, with both the reactants and the products in the used experimental conditions. In order to determine the energy of combustion in the standard conditions ($p^\circ = 0.1$ MPa), $\Delta_c U^\circ$, at the reference temperature, it's necessary to correct the experimental value of $\Delta U(\text{IBP})$ to the standard state. Washburn developed a calculation method, known as the Washburn corrections [33], that allows correction for the standard conditions of all energy contributions of the processes carried out in bomb experimental conditions. Initially his method was only applicable to compounds containing carbon, hydrogen and oxygen. Subsequently, due to the need for determining the standard energy of combustion of compounds containing other elements, the method has been developed to be employed on a wider range of organic compounds with nitrogen [34], sulfur [35] and halogens [36-38] in their composition.

The variation of the internal energy associated to the combustion process in the experimental conditions to the standard conditions, at the reference temperature of 298.15 K, can be deduced from the following thermochemical cycle:

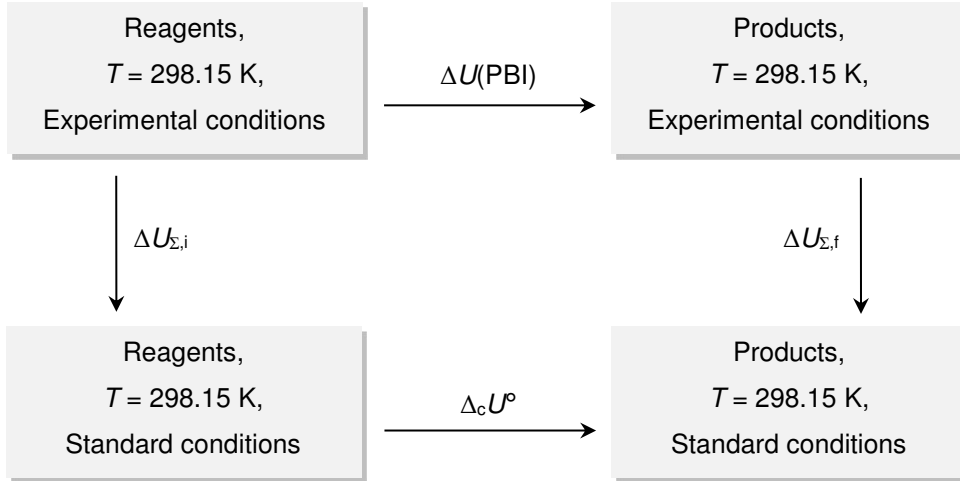


Figure 3.9. Thermochemical cycle for deriving the standard energy of combustion, $\Delta_c U^\circ$, at $T = 298.15\text{ K}$.

Given the previous thermochemical cycle:

$$\Delta_c U^\circ = \Delta U(\text{IBP}) + \Delta U_\Sigma \tag{3.37}$$

where ΔU_Σ is the energy variation associated to the Washburn corrections, calculated by:

$$\Delta U_\Sigma = \Delta U_{\Sigma,f} - \Delta U_{\Sigma,i} \tag{3.38}$$

$\Delta U_{\Sigma,i}$ and $\Delta U_{\Sigma,f}$ are the energy variations associated to the Washburn corrections of the initial and final states, respectively. Although individually $\Delta U_{\Sigma,i}$ and $\Delta U_{\Sigma,f}$ can have high values, the overall correction calculated by the difference between these two terms is relatively small. The main contributions to the energy correction term, are due to the following processes [25]:

Initial state:

Compression of the gaseous, liquid and solid phases from 0.10 to 3.04 MPa;
 Vaporization of the water inside the bomb, until saturation of gas phase;
 Dissolution of gaseous O₂ and N₂ in the liquid phase.

Final state:

Decompression of the gaseous, liquid and solid phases to 0.1 MPa;
 Removal of gaseous CO₂, O₂ and N₂ from the liquid phase;
 Condensation of the water vapor formed;
 Dilution of the liquid phase to obtain a solution with a reference concentration.

The standard massic energy of combustion of a given compound, $\Delta_c u^\circ$, at the reference temperature, can be calculated from the value of $\Delta U(\text{IBP})$ corrected to the standard state and the mass of burned compound expressed in grams, $m(\text{cpd})$:

$$\Delta_c u^\circ (\text{cpd}) = \frac{\Delta U(\text{IBP}) - \sum_i \Delta_c U_i - \sum_j \Delta_r U_j - \Delta U_\Sigma + \Delta U(\text{carb})}{m(\text{cpd})} \quad (3.39)$$

Considering the compounds studied in this work:

$\sum_i \Delta_c U_i$, is the sum of the energetic contributions of the combustion of auxiliary substances:

$$\sum_i \Delta_c U_i = \Delta U(\text{fuse}) + \Delta U(\text{aux}) \quad (3.40)$$

$\sum_j \Delta_r U_j$, is the sum of the energetic contributions of processes and side reactions:

$$\sum_j \Delta_r U_j = \Delta U(\text{ign}) + \Delta U(\text{HNO}_3) + \Delta U(\text{As}_2\text{O}_3) + \Delta U(\text{H}_2\text{PtBr}_4) \quad (3.41)$$

In addition to the meanings already assigned:

$\Delta U(\text{aux})$ is the internal energy variation associated to the combustion of auxiliary substances, calculated as: $\Delta U(\text{aux}) = m(\text{aux}) \cdot \Delta_c u^\circ(\text{aux})$;

$\Delta U(\text{As}_2\text{O}_3)$ is the energetic contribution of the oxidation of the arsenic(III) oxide bomb solution according to equation 3.7, determined following the procedure described by Hu *et al.* [39];

$\Delta U(\text{H}_2\text{PtBr}_4)$ is the energetic contribution of the formation of H_2PtBr_4 (aq), according to equation 3.9, determined from the mass loss of the platinum crucible and its supporting ring and $\Delta_f H_m^\circ(\text{H}_2\text{PtBr}_4, \text{aq}) = -(368.2 \pm 0.1) \text{ kJ}\cdot\text{mol}^{-1}$ [30].

The $\Delta U(\text{As}_2\text{O}_3)$ and $\Delta U(\text{H}_2\text{PtBr}_4)$ contributions were only considered for the combustion study of the bromine containing compounds.

3.2.2.2.6. Standard molar enthalpy of combustion and formation

The standard molar enthalpy of combustion of a compound, $\Delta_c H_m^\circ$, is determined from the respective standard molar energy of combustion using expression 3.42, where ΔV corresponds to the variation of molar volume of all gaseous species (reactants and products) involved in the reaction, at the standard pressure p° , and $\Delta_c U_m^\circ$ is the standard molar energy of combustion.

$$\Delta_c H_m^\circ = \Delta_c U_m^\circ + p^\circ \Delta V \quad (3.42)$$

$\Delta_c U_m^\circ$ is derived from the product of the respective standard massic energy of combustion molar mass by the compound's molar mass, M :

$$\Delta_c U_m^\circ = \Delta_c u^\circ \cdot M \quad (3.43)$$

Considering the molar volumes of solid or liquid species negligible when compared to their molar volumes in the gaseous state and assuming that the intervening gaseous species present close to ideal behavior, consequently:

$$\Delta_c H_m^\circ = \Delta_c U_m^\circ + \Delta n RT \quad (3.44)$$

in which R is the gas constant and Δn is the variation of the amount of substance of the gaseous species involved in the combustion reaction.

Taking into consideration Hess's law and the chemical reaction that represents the combustion of a given compound,

$$\Delta_c H_m^o = \sum_i v_i \Delta_f H_m^o (\text{products}) - \sum_i v_i \Delta_f H_m^o (\text{reactants}) \quad (3.45)$$

where v_n represent the stoichiometric coefficients of the reactants and products involved in the reaction.

The standard molar enthalpy of formation of a compound in the condensed phase can be calculated from the values of the standard molar enthalpy of combustion, as long as the enthalpies of formation of all the species involved in the reaction are known.

Thus, from the relation of the previous equation with the equations that represents the combustion reaction of compounds of empirical formula $C_aH_bO_cN_d$ and $C_aH_bO_cN_dBr_e$ (equations 3.5 and 3.8, respectively) studied in this work, it is possible to deduce the following expressions for determining the standard molar enthalpy of formation in the condensed phase. The values of $\Delta_f H_m^o$ of the species involved in these reactions were taken from literature [40].

$$\Delta_f H_m^o (C_aH_bO_cN_d, cr/l) = a \Delta_f H_m^o (CO_2, g) + b/2 \Delta_f H_m^o (H_2O, l) - \Delta_c H_m^o (C_aH_bO_cN_d, cr/l) \quad (3.46)$$

$$\begin{aligned} \Delta_f H_m^o (C_aH_bO_cN_dBr_e, cr/l) = a \Delta_f H_m^o (CO_2, g) + e \Delta_f H_m^o (HBr \cdot 600H_2O, l) + \\ + \left(\frac{1201e - b}{2} \right) \Delta_f H_m^o (H_2O, l) - \Delta_c H_m^o (C_aH_bO_cN_dBr_e, cr/l) \end{aligned} \quad (3.47)$$

3.2.2.3. Description of the combustion calorimetric systems

Along this work, the calorimetric studies were performed in two isoperibol calorimetric systems: a static bomb combustion calorimeter, used for compounds containing carbon, hydrogen, oxygen and/or nitrogen; and a rotating bomb combustion calorimeter, used for halogenated compounds, namely brominated fluorenes. Both calorimetric systems used were originally built at the National Physical Laboratory in Teddington, England, and are extensively described in the literature [41,42]. They were later transferred to the University of Manchester [43,44], and finally to the Faculty of Sciences in the University of Porto where, once installed, several adaptations were made to the equipment, as well as the automatization of their peripherals [45,46].

The calorimetric systems are essentially constituted by the combustion bomb, the calorimetric vessel, the thermostatic bath, and a set of peripheral components for inducing

the ignition, temperature measurement and data acquisition. These will be briefly described as follows, along with a summary of the respective experimental procedures.

3.2.2.3.1. Static bomb combustion calorimeter

Static combustion bomb

The static bomb combustion (A), schematized in figure 3.10, is constructed of stainless steel and consists of three mountable parts: the bomb body, the bomb head and the sealing ring. The bomb body (B) is internally coated with platinum and has an internal volume of 0.290 dm³. The bomb head (C) is equipped with two twin valves for inlet (1) and outlet (2) of gases, and two electrodes, one isolated (3) (through which the electrical discharge is made for the ignition of the sample) and other in electrical contact with the bomb (4). A tube (5) adapted to the inlet valve directs the oxygen flow to the base of the bomb, in order not to avoid disturbing the crucible and its contents during pressurization and deaeration of the bomb. To this tube is also adapted the crucible ring holder (6).

The head is adapted to the body of the bomb and the entire system is closed by screwing the sealing ring (D) to the external surface of the bomb body. The hermeticity of the bomb is assured by an o-ring placed between the head and the body.

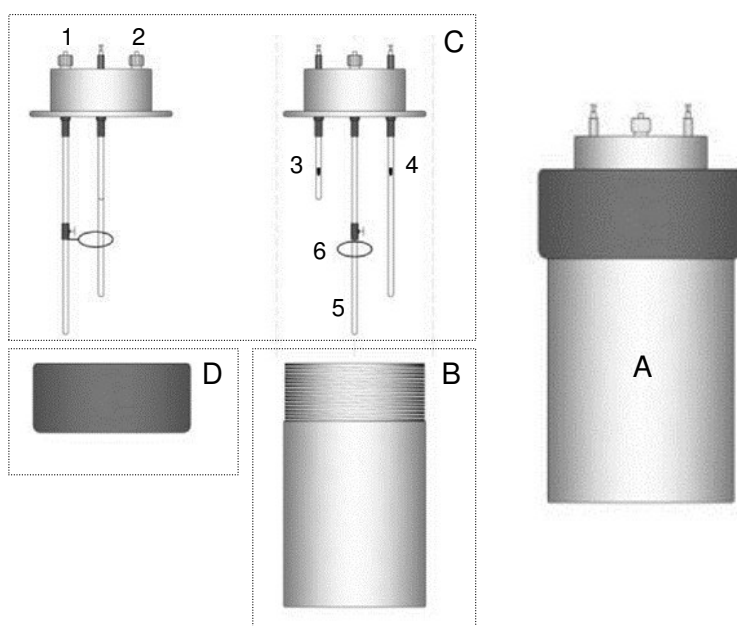


Figure 3.10. Schematic representation of the static combustion bomb (A) and assembling parts: B. body of the bomb; C. head of the bomb (side and front views; 1. inlet gas valve; 2. outlet gas valve; 3. isolated electrode; 4. non-isolated electrode; 5. tube; 6. crucible ring holder); D. sealing ring. Image adapted from ref. [9].

Calorimetric vessel

The cylindrical calorimetric vessel (E), represented in figure 3.11, is made of copper coated with rhodium. Its lid (7) has a propeller (8) coupled to a motor to ensure the water surrounding the combustion bomb, the internal electrical resistance (9) and the temperature sensor (10, Thermometrics, standard serial No. 1030, $\pm 1 \cdot 10^{-4}$ K) is in constant circulation.

The metal container (11) surrounding the propeller axis, is filled with silicon oil whose functions are to prevent loss of water vapor, regulate the propeller rotation movement and allow for a small expansion of the air existing in the calorimeter.

The calorimetric vessel and respective lid are fitted in an isothermal vessel constructed of copper and coated on the outside with agglomerated cork. Inside there are three metal pillars that support the calorimeter vessel and fix the distance between the calorimeter and the side wall and base of the vessel.

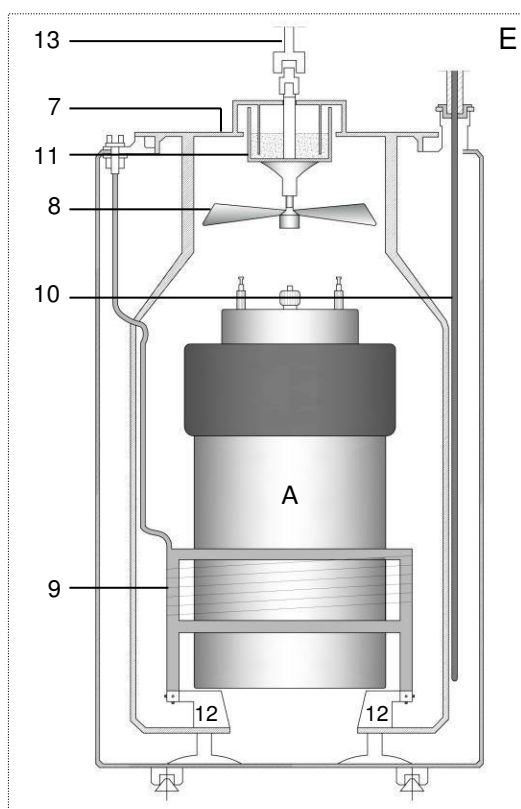


Figure 3.11. Schematic representation of the static bomb calorimetric system: A. combustion bomb; E. calorimetric vessel (7. calorimeter lid; 8. propeller; 9. internal electrical resistance; 10. temperature sensor; 11. metal container containing silicone oil; 12. circular steel support; 13. axis for connection to the agitation motor). Image adapted from ref. [9].

Thermostatic bath

The isothermal vessel and its head are connected to an external thermostatic bath containing a volume of water kept at a controlled temperature of (301.000 ± 0.001) K by a temperature controller TRONAC PTC41. The thermostatic bath is equipped with a temperature sensor, an auxiliary heating resistance, a cooling coil and a centrifugal pump to uniformly pump the water into the isothermal vessel and its head.

3.2.2.3.2. Experimental procedure

For the combustion experiment of a solid compound, the sample is pulverized and pressed into a pellet form. After the cotton fuse, platinum crucible, sample and eventual auxiliary substance are successively and accurately weighed (Mettler AE240, $\pm 1 \cdot 10^{-5}$ g), the sample is carefully assembled in the head of the bomb: the crucible with the sample is placed in the ring holder, the two electrodes are connected by a platinum wire (Goodfellow, 99.99 %, $\phi = 0.05$ mm), to which one end of the cotton thread is fastened and the other end is carefully placed under the sample pellet, inside the crucible.

After placing 1.00 cm^3 of deionized water inside the body of the bomb, the bomb is sealed and degassed twice with oxygen to a pressure of 1.52 MPa, followed by pressurization to 3.04 MPa. The bomb is placed inside the calorimetric vessel and the necessary electric terminals are connected. The propeller is adapted to the top of the calorimeter, which is then positioned inside the isothermal vessel. Approximately 2900.0 g (reference mass) of distilled water, used as calorimetric fluid, is weighed (Mettler PM11-N, $\pm 1 \cdot 10^{-1}$ g) and added to the calorimeter. The temperature of calorimetric fluid is measured in 10 second intervals using a temperature sensor ($\pm 1 \cdot 10^{-4}$ K).

The temperature is recorded throughout the initial period, and at $T = 298.150 \pm 0.002$ K, the discharge of electric current of a capacitor (1400 μF) through the platinum wire causes the combustion of the cotton fuse and the ignition of sample, thus marking the start of the main period. The temperature is recorded throughout the main period and until the end of the final period. At the end of the experiment, all electrical contacts are disconnected and the system is disassembled. The bomb is removed from the calorimetric vessel, to proceed to the analysis of the combustion products. Finally, the crucible is calcined.

3.2.2.3.3. Rotating bomb combustion calorimeter

Rotating combustion bomb

The rotating combustion bomb (A), depicted in figure 3.12, is constructed of stainless steel and consists of three mountable parts: the bomb body, the bomb head and the sealing ring. The bomb head, with all internal fittings made of tantalum, is equipped with two valves for inlet (1) and outlet (2) of gases, an electrical contact (3), and two electrodes, one isolated (through which the electrical discharge is made for the ignition of the sample) and another in electrical contact with the bomb. The bifurcated shape of the non-insulated electrode (4), has the additional function of supporting the ring where the platinum crucible (5) is placed and allows it to fall after the activation of the bomb's rotation. The bifurcated shape of the non-insulated electrode (4), has the additional function of supporting the ring where the platinum crucible (5) is placed and allows it to fall after the activation of the bomb's rotation.

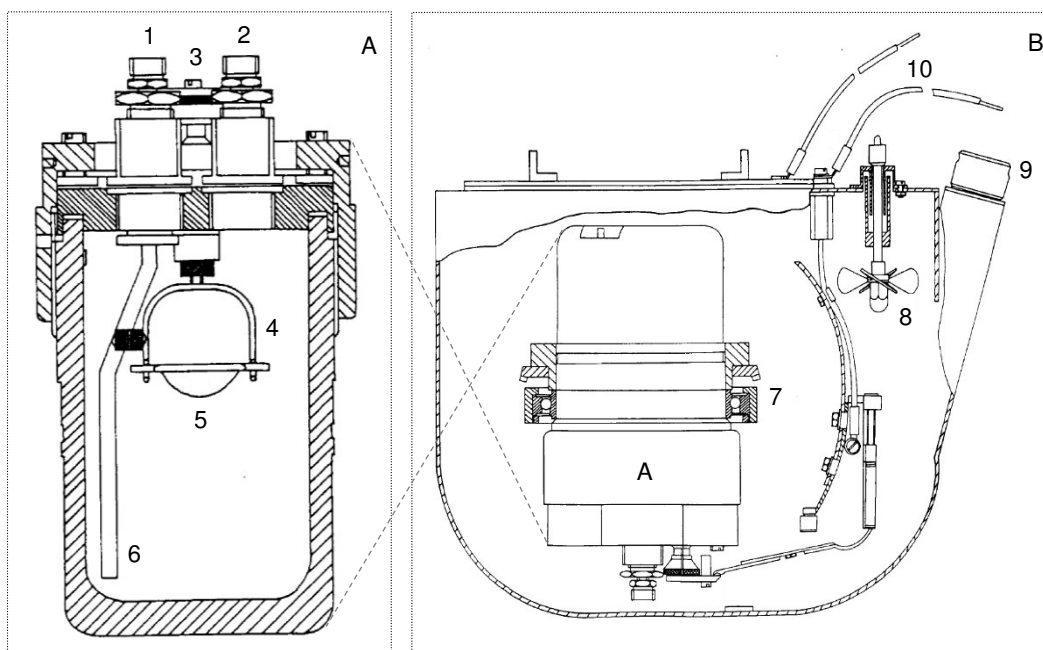


Figure 3.12. Schematic representation of the rotating combustion bomb and calorimetric vessel: A. Combustion bomb (1. inlet gas valve; 2. outlet gas valve; 3. electrical contact; 4. crucible holder; 5. platinum crucible; 6. tube; 7. ball bearing system); B. Calorimetric vessel (8. stirrer; 9. thermometer hole; 10. electric connections). Image adapted from ref. [46].

There is a tube (6) connected to the inlet valve through which oxygen is introduced near the bottom of the bomb, preventing disruption of the contents of the crucible during pressurization and deaeration of the bomb.

The bomb body is internally coated with tantalum (internal volume 0.329 dm^3) and externally equipped with a ball bearing system (7) that allows the simultaneous axial and

longitudinal rotation of the bomb, after appropriate adjustment to the calorimetric vessel. The bomb is closed by adapting the head to the body, with an o-ring placed between them, and hand tightening the sealing ring by means of a screw system.

Calorimetric vessel

The calorimetric vessel (B) is a metallic container, internally coated with gold, where the combustion bomb is suspended, engaged in the rotation system in an inverted position, as shown in figure 3.12. In the inverted position, the valves are kept away from the ignition source and protected from the resulting gases while submerged by the bomb solution.

The vessel is equipped with a stirrer (8) that promotes efficient circulation of the calorimetric fluid, whose temperature is measured by a quartz thermometer (Hewlett-Packard 2804A, $\pm 1 \cdot 10^{-4}$ K) inserted into hole (9). The vessel is closed and introduced in the respective cavity in the thermostatic bath.

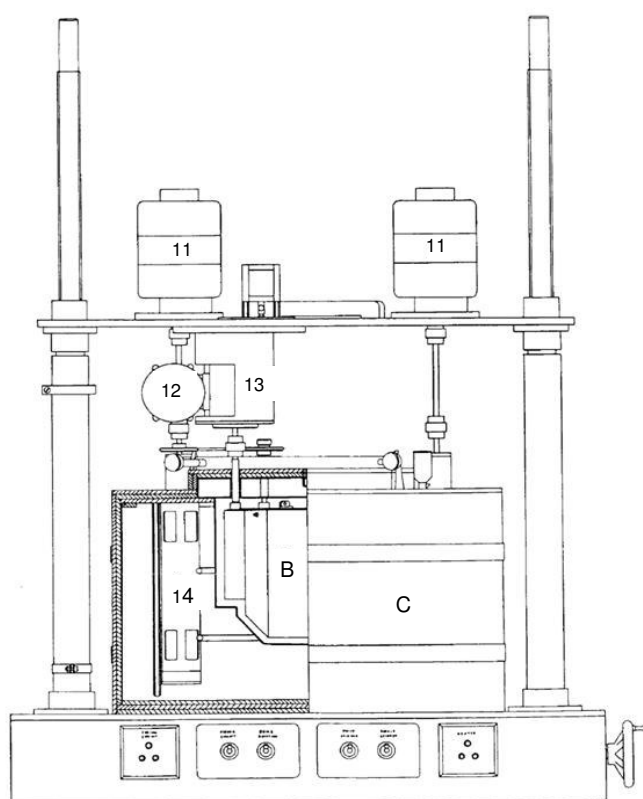


Figure 3.13. Global schematic representation of the rotating bomb combustion calorimeter: B. Calorimetric vessel; C. thermostatic bath (11. thermostatic bath agitation motor; 12. calorimetric vessel agitation motor; 13. bomb rotation motor; 14. water circulation system). Image adapted from ref. [46].

Thermostatic bath

The thermostatic bath (C), depicted in the global scheme of the calorimetric system in figure 3.13, consists of a recipient containing a volume of water kept at a controlled temperature of (299.050 ± 0.001) K by a temperature controller TRONAC PTC41. The calorimeter vessel is introduced into the respective cavity and the system is closed with a lid, where there are a set of holes for the passage of electric connections (10) and the axes of the motors responsible for the water stirring (11, 12) and the bomb rotation (13), located on a support plate of variable height above the thermostatic bath. The homogeneity of the temperature is ensured by a circulation system (14) which circulates water throughout the thermostatic bath and inside its lid.

3.2.2.3.4. Experimental procedure

For the combustion experiment of a solid compound, the sample is pulverized and pressed into a pellet form. The cotton fuse, platinum crucible, sample and eventual auxiliary substance are successively and accurately weighed (Mettler AE240, $\pm 1 \cdot 10^{-5}$ g). With the head of the bomb in an inverted position, the sample is carefully assembled inside the crucible placed in the ring holder, the two electrodes are connected by a platinum wire (Goodfellow, 99.99 %, $\phi = 0.05$ mm), to which one end of the cotton thread is fastened and the other end is carefully placed under the sample pellet, inside the crucible.

After placing an adequate volume of arsenic(III) oxide solution (≈ 0.09 mol·dm⁻³), measured with a volumetric pipet, inside the body of the bomb, the bomb is then sealed and degassed twice with oxygen to a pressure of 1.52 MPa, followed by pressurization to 3.04 MPa. The calorimetric vessel is placed in its cavity inside the thermostatic bath, the bomb is manually inverted and adapted to the rotation mechanism inside the calorimeter vessel. All the necessary electric contacts are established between the pump and approximately 3965.0 g (reference mass) of distilled water, used as calorimetric fluid, are weighed (Mettler PM11-N, $\pm 1 \cdot 10^{-1}$ g) and added to the calorimeter. The lid of the thermostatic bath is closed, the quartz thermometer is placed in the respective hole and the motor axis for the agitation of the thermostatic bath and rotation of the bomb are properly adapted.

After reaching thermal equilibrium, the temperature of calorimetric fluid is recorded in 10 second intervals using a temperature sensor ($\pm 1 \cdot 10^{-4}$ K), throughout the initial period. At a predetermined temperature, a discharge of electric current of a capacitor (1288 μ F) through the platinum wire causes the combustion of the cotton fuse and the ignition of sample, thus initiating the main period. The rotation of the pump is started when the

temperature corresponds to about 63 % of the variation in temperature of the main period, and kept till the end of the experiment.

The temperature is recorded throughout the main period and until the end of the final period. At the end of the experiment, all electrical contacts are disconnected and the system is disassembled. The bomb is removed from the calorimetric vessel, to proceed to the analysis of the combustion products. Finally, the crucible is calcined.

3.2.2.3.5. Analysis of combustion products

Carbon dioxide recovery

The extent of the combustion reaction of a compound is determined by the total mass of carbon dioxide produced, after considering the necessary corrections for the contributions of combustion auxiliaries (cotton fuse, eventual auxiliary substances...).

After each combustion experiment, the bomb is connected through the outlet gas valve to a carbon dioxide recovery system (figure 3.14), constituted by a U-shaped glass tube (A), containing anhydrous magnesium perchlorate to retain the water vapor escaping from the bomb, followed by two glass absorption tubes (B) connected in series to a manometer (C), containing butyl phthalate as manometric liquid to control the gas output flow.

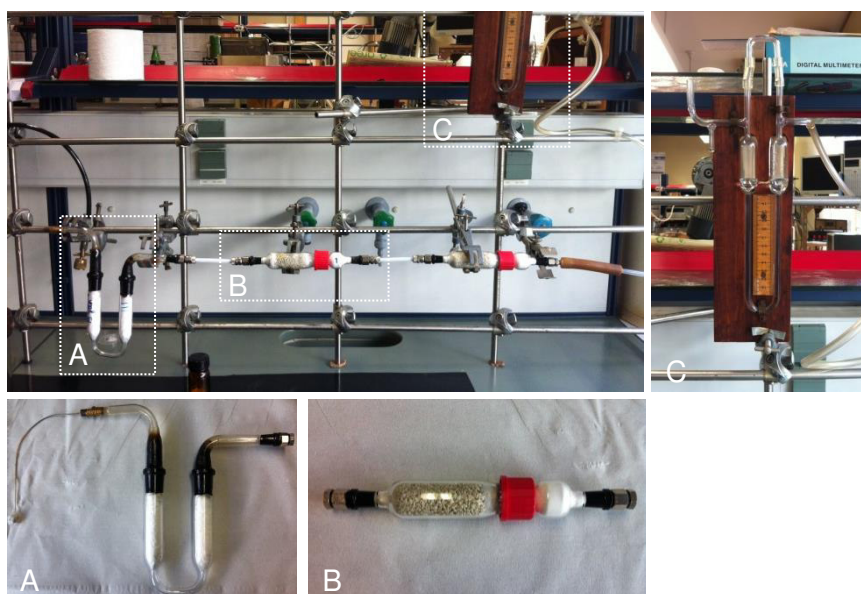
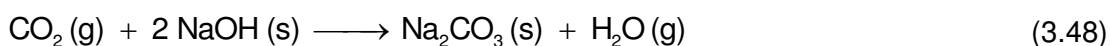


Figure 3.14. Carbon dioxide recovery system: A. U-shaped tube; B. absorption tubes; C. liquid column manometer.

The gases contained within the bomb are collected by a gravimetric method, in the two absorption tubes containing ascarite[®] saturated with O₂. This material consists of small fragments of silica functionalized with sodium hydroxide, which reacts with carbon dioxide forming sodium carbonate, according to the chemical equation 3.48. The water vapor formed is adsorbed by anhydrous magnesium perchlorate also present in the tubes.



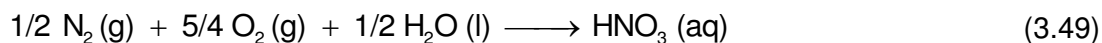
The gases contained in the bomb are slowly evacuated, until the pressure within the bomb equals atmospheric pressure. After that, the bomb is twice pressurized to 1.5 MPa with oxygen and again evacuated through the system, to ensure that all the carbon dioxide remaining in the bomb is effectively removed. The absorption tubes are accurately weighed (Mettler Toledo AT201, $\pm 1 \cdot 10^{-5}$ g) before and after the recovery process, and the mass of carbon dioxide formed is determined. From the ratio between the mass of carbon dioxide formed to that calculated from the mass of sample used in each experiment, it's possible to assess the percentage of compound burned.

Unburned compound and / or carbon residue

After the carbon dioxide recovery, the bomb is opened. In the case there is evidence of unburned compound or carbon residue inside the bomb in areas other than the crucible, indicative of incomplete combustion reaction, the experiment should be rejected. If the carbon residue is confined to interior of the crucible and its mass, determined by accurately weighing the crucible before and after calcination (Mettler AE240, $\pm 1 \cdot 10^{-5}$ g), does not exceed 1 mg the experiment can be considered and the energy of combustion associated to the determined mass of carbon residue will subsequently be considered in the calculation of the energy of the total process.

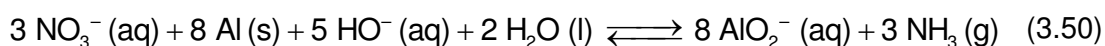
Analysis of nitric acid

For the correct calculation of the massic energy of combustion resulting from a calorimetric experiment, it is necessary to account for the energy involved in the formation of nitric acid. Nitrogen can be found in the bomb as molecular nitrogen, added to the bomb as a contaminant of the oxygen used to pressurize the bomb, and/or as a constituent element of the compound under study. About 10 % [47] of all the nitrogen present in the bomb undergoes oxidation during the combustion process forming nitrogen oxides which, in turn, react with the water in the bomb solution forming nitric acid:



The remaining 90 % of the nitrogen in the reaction products presents in the elemental form. In order to quantitatively determine the amount of nitric acid formed, the crucible and the internal surfaces and contents of the bomb are rinsed with deionized water, and the amount of nitric acid in the resulting solution is determined by acid-base volumetry using a sodium hydroxide solution, in the presence of an indicator (methyl red).

In case of rotating bomb combustion calorimetry, the amount of nitric acid formed is determined by the Devarda method [48]. In this method, the nitrate anion is reduced by Devarda's alloy (50 % copper, 45 % aluminum and 5 % zinc) to form ammonia gas, under alkaline conditions, according to chemical equation 3.50.



Devarda's alloy and a saturated potassium hydroxide solution are added to the rinsing water in a round bottom flask, which is then adapted to a distillation system. The ammonia distillate is collected in a flask containing a hydrochloric acid solution ($\approx 0.1 \text{ mol}\cdot\text{dm}^{-3}$) and when the distillation is complete, an accurate volume of a sodium hydroxide solution ($\approx 0.2 \text{ mol}\cdot\text{dm}^{-3}$) is added to the distillate solution. The amount of nitric acid is determined from the hydroxide excess, by acid-base back titration with a hydrochloric acid stock solution ($0.1000 \text{ mol}\cdot\text{dm}^{-3}$) using methyl red as indicator, based on the difference in titrant volume in the experiment and in a blank test.

Analysis of arsenic(III) oxide

The amount of the hydrobromic acid formed as a combustion product is determined by the extent of the arsenic (III) oxide oxidation reaction, in which the excess of arsenic(III) oxide after the combustion process is quantified by iodometry [48], according to the chemical equation:



The analysis is performed by redox titration using a triiodide solution ($0.05 \text{ mol}\cdot\text{dm}^{-3}$) as titrant and starch solution as indicator.

The weight of platinum that reacted with the final bomb solution is determined by weighing the platinum crucible at the end of combustion experiment.

3.3. Vapor pressure measurement methods

3.3.1. Introduction to the study of vapor pressures

Vapor pressure is the pressure exerted by a vapor when in thermodynamic equilibrium with its condensed phase (liquid or solid), at a given temperature. In kinetic terms, this equilibrium is established when the rate at which condensed phase molecules sublime/vaporize equals the rate at which vapor molecules return to the condensed phase. This rate increases exponentially with temperature. Vapor pressure is also a measure of a substance's volatility and from its variation with temperature it's possible to determine the standard enthalpy, entropy and Gibbs energy of sublimation and/or vaporization. These properties can be used to determine other thermodynamic properties, such as the enthalpy of formation in the gaseous state and Gibbs energies of formation, either in gas phase or in condensed phase. This indirect method for the determination of phase transition properties presents advantages over some direct calorimetric methods that, in general, appear to lead to less reliable results [49]. Furthermore it can also be useful for performing internal consistency of the results to evaluate their reliability [50]. However, the experimental techniques require careful control of experimental conditions because eventual errors performed during the vapor pressure measurements may strongly affect the calculated slopes of the referred to above variation.

3.3.1.1. Experimental methods of vapor pressure measurement

The available methods for the experimental determination of vapor pressures can be divided into four categories: ebulliometric, gas saturation, effusion and static methods. The choice of the appropriate method depends on a number of factors, among which are specific characteristics of the compounds under study, such as physical state and volatility.

Ebulliometric methods

Ebulliometry is used for the study of liquid compounds and is based on the dependency of a substance's boiling temperature with pressure, that is, the temperature at which its vapor pressure equals the well-defined pressure of the system in which the substance is placed. The devices for the application of this method are called ebulliometers.

Gas saturation methods

In the gas saturation method [51,52], also called transpiration method, a flow of inert gas (carrier gas) is slowly passed through the surface of a sample, liquid or solid, over a given time interval. The saturated vapor, transported by the carrier gas, is subsequently condensed in a cooled trap and quantitatively determined by a suitable method. Correlating the amount of condensed vapor at different flow rates of carrier gas, and extrapolating to zero flow, it is possible to determine the vapor pressure of the substance in equilibrium conditions.

Effusion methods

In effusion methods, the vapor in equilibrium with its condensed phase flows under reduced pressure from an isothermal cell through an effusion orifice of accurately known area. The orifice should be sufficiently small so that equilibrium conditions are not significantly disturbed. One of the most used effusion methods is the Knudsen mass-loss effusion (KMLE). In this method, the amount of substance effused, at a given temperature, is related to the vapor pressure through equations, developed by Knudsen, based in the kinetic theory of gases. This method will be addressed in detail in section 3.3.2.1.

Static methods

In static methods, the vapor pressure is measured at constant temperature and under equilibrium conditions between the vapor and its condensed phase (crystalline or liquid), inside a closed system. Currently the most used techniques are based on modern manometers. Due to their high sensitivity, the capacitance diaphragm gauges are the frequently used [53,54]. This method will be addressed in detail in section 3.3.2.2.

Association of different methods

By combining methods that are dependent (for example, KMLE) and independent (for example, static methods) of the vapor's molar mass, it is possible to detect and study eventual association (formation of dimers, for example) or dissociation processes occurring in the gas phase.

3.3.1.2. Vapor pressure equations

Several equations have been developed to mathematically describe the dependence of vapor pressure with temperature, however, none is universally used by the scientific

community. Choosing the most convenient expression will depend, among other factors, on the range of the vapor pressures under study.

The Clausius-Clapeyron, and Clarke-Glew equations, described as follows, are the expressions used in this work to correlate vapor pressure with temperature allowing the determination of the thermodynamic properties of phase transition between the condensed phases and the gas phase. There are, however, several other empirical equations [55], like the Antoine equation [56], that enable the correlation of vapor pressure with temperature.

3.3.1.2.1. Clausius-Clapeyron equation

In a phase diagram, sublimation and vaporization curves establish the pressure and temperature conditions at which the crystalline or liquid phases of a compound are in equilibrium with its vapor. For this condition, the chemical potential, μ , is equal in both phases.

$$\mu(\text{cr/l}, p, T) = \mu(\text{g}, p, T) \quad (3.52)$$

For one mole of a pure substance, the chemical potential is equivalent to the molar Gibbs energy, G_m , and therefore:

$$G_m(\text{cr/l}, p, T) = G_m(\text{g}, p, T) \quad (3.53)$$

Applying an infinitesimal variation to the system's pressure, dp , and temperature, dT , a new equilibrium will be established between the two phases:

$$G_m(\text{cr/l}, p + dp, T + dT) = G_m(\text{g}, p + dp, T + dT) \quad (3.54)$$

and so,

$$dG_m(\text{cr/l}) = dG_m(\text{g}) \quad (3.55)$$

Knowing that:

$$dG_m = -S_m dT + V_m dp \quad (3.56)$$

and relating 3.55 and 3.56 for the condensed phase and the gas phase,

$$-S_m(\text{cr/l})dT + V_m(\text{cr/l})dp = -S_m(\text{g})dT + V_m(\text{g})dp \quad (3.57)$$

where $S_m(\text{cr/l})$ and $S_m(\text{g})$ are, respectively, the molar entropy of the condensed and gas phases and $V_m(\text{cr/l})$ and $V_m(\text{g})$ the respective molar volumes.

Rearranging equation 3.57, the Clapeyron equation is obtained,

$$\frac{dp}{dT} = \frac{\Delta_{\text{cr/l}}^g S_m}{\Delta_{\text{cr/l}}^g V_m} \quad (3.58)$$

where $\Delta_{\text{cr/l}}^g S_m$ and $\Delta_{\text{cr/l}}^g V_m$ are, respectively, the variations in molar entropy and molar volume between the phases in equilibrium.

In equilibrium conditions, at the temperature T and at the corresponding vapor pressure, the molar entropy of sublimation/vaporization is related to the molar enthalpy of sublimation/vaporization, according to equation 3.59,

$$\Delta_{\text{cr/l}}^g S_m = \frac{\Delta_{\text{cr/l}}^g H_m}{T} \quad (3.59)$$

and equation 3.58 can be transformed into Equation 3.60.

$$\frac{dp}{dT} = \frac{\Delta_{\text{cr/l}}^g H_m}{T \Delta_{\text{cr/l}}^g V_m} \quad (3.60)$$

Assuming that, for vapor pressures smaller than 0.1 MPa, the gas presents an ideal behavior and that the molar volume of the condensed phases is negligible when compared to the molar volume of the gas phase ($V_m(\text{cr/l}) \ll V_m(\text{g})$), $\Delta_{\text{cr/l}}^g V_m$ is approximately equal to $V_m(\text{g})$ and can be calculated as:

$$\Delta_{\text{cr/l}}^g V_m \approx V_m(\text{g}) = \frac{R \cdot T}{p} \quad (3.61)$$

These approximations allow the transformation of the Clapeyron equation in the Clausius-Clapeyron equation.

$$\frac{d \ln p}{dT} = \frac{\Delta_{cr/l}^g H_m}{R \cdot T^2} \quad (3.62)$$

For vapor pressure measurements performed in a limited temperature interval, it may be assumed that the enthalpy of sublimation/vaporization is approximately constant ($d(\Delta_{cr/l}^g H_m)/dT \approx 0$), allowing the integration of equation 3.62, where p° is a reference pressure.

$$\ln\left(\frac{p}{p^\circ}\right) = -\frac{\Delta_{cr/l}^g H_m}{R \cdot T} + a \quad (3.63)$$

Or simply,

$$\ln\left(\frac{p}{p^\circ}\right) = a - \frac{b}{T} \quad (3.64)$$

Plotting the logarithm of the vapor pressure as a function of temperature, $\ln(p/\text{Pa}) = f(K/T)$, the slope b is related to the enthalpy of sublimation or vaporization (equation 3.66) at the mean temperature of the experimental interval, $\langle T \rangle$, and the parameter a is related to the molar entropy of sublimation or vaporization, for $p^\circ = p(\langle T \rangle)$ and temperature $\langle T \rangle$ (equation 3.65).

$$a = \Delta_{cr/l}^g S_m[\langle T \rangle, p(\langle T \rangle)]/R \quad (3.65) \quad b = \Delta_{cr/l}^g H_m(\langle T \rangle)/R \quad (3.66)$$

3.3.1.2.2. Thermodynamic properties at a reference temperature

The Clausius-Clapeyron equation allows the calculation of $\Delta_{cr/l}^g H_m^o(\langle T \rangle)$ for the average temperature $\langle T \rangle$ of a short experimental interval. The correction for any other reference temperature, θ , different from $\langle T \rangle$ may be carried out using the relation translated by equation 3.67.

$$\Delta_{cr/l}^g H_m^o(\theta) = \Delta_{cr/l}^g H_m^o(\langle T \rangle) + \int_{\langle T \rangle}^{\theta} \Delta_{cr/l}^g C_{p,m}^o(T) dT \quad (3.67)$$

In this equation, $\Delta_{cr/l}^g C_{p,m}^o$ represents the difference between the standard molar heat capacities of the gas phase (with assumed ideal behavior), $C_{p,m}^o(g)$, and the crystalline, $C_{p,m}^o(cr)$, or liquid phases, $C_{p,m}^o(l)$. If the difference between the standard molar heat capacities, at constant pressure, of the condensed and gaseous phases, is constant, the integration of equation 3.67 yields:

$$\Delta_{cr/l}^g H_m^o(\theta) = \Delta_{cr/l}^g H_m^o(\langle T \rangle) + (\theta - \langle T \rangle) \Delta_{cr/l}^g C_{p,m}^o \quad (3.68)$$

3.3.1.2.3. Clarke-Glew equation

For a temperature range greater than 20 K, the Clausius-Clapeyron equation is not the appropriate adjustment to the vapor pressure values, since the variation of the difference in heat capacity between the gas and condensed phases in the considered temperature interval is not null and consequently $\Delta_{cr/l}^g H_m^o$ varies with temperature according to the equation 3.69.

$$d\left(\frac{\Delta_{cr/l}^g H_m^o}{dT}\right)_p = \Delta_{cr/l}^g C_{p,m}^o \quad (3.69)$$

For more extended temperature ranges, one of the most used equations is the Clarke-Glew equation [57]:

$$\begin{aligned} R \ln\left(\frac{p}{p^o}\right) = & -\frac{\Delta_{cr/l}^g G_m^o(\theta)}{\theta} + \Delta_{cr/l}^g H_m^o(\theta) \left(\frac{1}{\theta} - \frac{1}{T}\right) + \Delta_{cr/l}^g C_{p,m}^o(\theta) \left[\left(\frac{\theta}{T}\right) - 1 + \ln\left(\frac{T}{\theta}\right)\right] + \\ & + \left(\frac{\theta}{2}\right) \left(\frac{\partial \Delta_{cr/l}^g C_{p,m}^o}{\partial T}\right) (\theta) \left(\frac{T}{\theta} - \frac{\theta}{T} - 2 \ln\left(\frac{T}{\theta}\right)\right) + \dots \end{aligned} \quad (3.70)$$

where:

- p is the vapor pressure at the temperature T ;
- p^o is a reference pressure (in this work, standard pressure $p^o = 0.1$ MPa);
- θ is a reference temperature (in this work, $\theta = 298.15$ K);
- $\Delta_{cr/l}^g G_m^o$ is the standard molar Gibbs energy of sublimation/vaporization;

$\Delta_{\text{cr/l}}^{\text{g}} H_{\text{m}}^{\circ}$ is the standard molar enthalpy of sublimation/vaporization;

$\Delta_{\text{cr/l}}^{\text{g}} C_{\rho,\text{m}}^{\circ}$ is the difference between the standard molar isobaric heat capacities of the gas, $C_{\rho,\text{m}}^{\circ}(\text{g})$, and the solid, $C_{\rho,\text{m}}^{\circ}(\text{cr})$, or liquid, $C_{\rho,\text{m}}^{\circ}(\text{l})$.

A key advantage of the Clarke-Glew equation is that it may allow determination of $\Delta_{\text{cr/l}}^{\text{g}} C_{\rho,\text{m}}^{\circ}$. Assuming, as approximation, that the $\Delta_{\text{cr/l}}^{\text{g}} C_{\rho,\text{m}}^{\circ}$ variation with temperature is not significant, equation 3.70 can be simplified to equation 3.71 and, if accurate experimental results are available over a sufficiently large temperature range, a constant value of $\Delta_{\text{cr/l}}^{\text{g}} C_{\rho,\text{m}}^{\circ}$ can be derived.

$$R \ln \left(\frac{p}{p^{\circ}} \right) = - \frac{\Delta_{\text{cr/l}}^{\text{g}} G_{\text{m}}^{\circ}(\theta)}{\theta} + \Delta_{\text{cr/l}}^{\text{g}} H_{\text{m}}^{\circ}(\theta) \left(\frac{1}{\theta} - \frac{1}{T} \right) + \Delta_{\text{cr/l}}^{\text{g}} C_{\rho,\text{m}}^{\circ}(\theta) \left[\left(\frac{\theta}{T} \right) - 1 + \ln \left(\frac{T}{\theta} \right) \right] \quad (3.71)$$

For small intervals of temperature, the third term of the second member of equation 3.71 may be neglected and the so truncated equation is equivalent to the Clausius-Clapeyron equation.

If $T = \theta$, equation 3.71 is reduced to equation 3.72 with which is possible to calculate the vapor pressure at any reference temperature θ .

$$\ln p = \ln p^{\circ} - \frac{\Delta_{\text{cr/l}}^{\text{g}} G_{\text{m}}^{\circ}(\theta)}{\theta R} \quad (3.72)$$

Or:

$$\Delta_{\text{cr/l}}^{\text{g}} G_{\text{m}}^{\circ}(\theta) = -\theta R \ln K_{\text{p}} \quad (3.73)$$

Equation 3.73 is a particular case of the well-known relation between standard Gibbs energy and equilibrium constant, where $K_{\text{p}} = (p/p^{\circ})_{\text{eq}}$.

3.3.1.2.4. Thermodynamic characterization of phase transitions: temperature and pressure variables

The measurement of vapor pressures at different temperatures for the condensed phases of a pure compound enables the construction of its phase diagram. In a phase

diagram of a pure substance, vapor pressures are plotted against temperature, defining the boundaries between the different phases in equilibrium.

For a given system, the vapor pressure of two condensed phases is equal at the temperature, T_{tr} , at which they are in equilibrium with the gaseous phase. Thus, considering equation 3.71 and the equilibrium between liquid-vapor and crystalline-vapor phases of a compound, equation 3.74 allows the determination of the triple point temperature T_{tr} when the values of the related thermodynamic properties of the phase transitions are known.

$$-\frac{\Delta_{cr}^g G_m^o(\theta)}{\theta} + \Delta_{cr}^g H_m^o(\theta) \left(\frac{1}{\theta} - \frac{1}{T_{tr}} \right) + \Delta_{cr}^g C_{p,m}^o(\theta) \left[\left(\frac{\theta}{T_{tr}} \right) - 1 + \ln \left(\frac{T_{tr}}{\theta} \right) \right] =$$

$$-\frac{\Delta_l^g G_m^o(\theta)}{\theta} + \Delta_l^g H_m^o(\theta) \left(\frac{1}{\theta} - \frac{1}{T_{tr}} \right) + \Delta_l^g C_{p,m}^o(\theta) \left[\left(\frac{\theta}{T_{tr}} \right) - 1 + \ln \left(\frac{T_{tr}}{\theta} \right) \right] \quad (3.74)$$

Once T_{tr} is determined, it is possible to calculate the pressure of the triple point, p_{tr} , solving equation 3.71 for $T = T_{tr}$:

$$R \ln \left(\frac{p_{tr}}{p^o} \right) = -\frac{\Delta_{cr/l}^g G_m^o(\theta)}{\theta} + \Delta_{cr/l}^g H_m^o(\theta) \left(\frac{1}{\theta} - \frac{1}{T_{tr}} \right) + \Delta_{cr/l}^g C_{p,m}^o(\theta) \left[\left(\frac{\theta}{T_{tr}} \right) - 1 + \ln \left(\frac{T_{tr}}{\theta} \right) \right] \quad (3.75)$$

The value of p_{tr} can also be determined directly from the equation 3.72, if $\Delta_{cr/l}^g G_m^o(T_{tr})$ is known. Furthermore, from the difference between the standard molar enthalpies of sublimation and vaporization, at a certain temperature, it is possible to obtain the standard molar enthalpy of fusion.

$$\Delta_{cr}^l H_m^o(T) = \Delta_{cr}^g H_m^o(T) - \Delta_l^g H_m^o(T) \quad (3.76)$$

3.3.2. Description of the vapor pressure measurement systems

3.3.2.1. Knudsen mass-loss effusion method

3.3.2.1.1. Ideal and real effusion processes

KMLE method is mainly used for measuring vapor pressures of pure substances in the solid state, in the interval between (0.1 and 1) Pa [58-60]. It was first developed by Martin Knudsen [61-63] from the study of isothermal gas flow through cylindrical tubes, at reduced pressures that promote molecular flow conditions. Knudsen concluded that, under those conditions, the Lambert's cosine law applies to the reflection of the gas molecules colliding to the inner wall of the tube, since they are reflected in a direction independent of the angle of incidence. The experimental observations of Knudsen were an important contribution for the validation the Kinetic Theory of Gases. From his experimental work, Knudsen deduced the expression 3.77, which applies to the gaseous flow from a recipient with pressure p_1 to an adjacent recipient with pressure p_2 connected by an orifice of null thickness and diameter inferior to a tenth of the mean free path of the molecules.

$$p_1 - p_2 = \frac{m}{t} \cdot \frac{w_1 + w_2}{\sqrt{d}} \quad (3.77)$$

In this equation, m is the mass of gas which passes through the orifice over the time interval t , d is the density of the gas. w_1 and w_2 represent, respectively, the orifice and the tube's resistance to gas flow. Considering that the tube width is much greater than that of the orifice, w_2 is negligible when compared to w_1 , calculated by equation 3.78 where A_0 is the area of the orifice.

$$w_1 = \frac{\sqrt{2\pi}}{A_0} \quad (3.78)$$

Assuming ideal gas behavior, the relation $d = M/RT$ (where M is the molar mass of the gas, T is the absolute temperature and R the constant of gases) is valid. So, if p_2 is negligible when compared to p_1 , equation 3.77 can be rewritten as the equation (3.79) applied by Knudsen [63] for determining the vapor pressure p_1 of a pure substance at the temperature T .

$$p_1 = \frac{m}{tA_0} \cdot \sqrt{\frac{2\pi RT}{M}} \quad (3.79)$$

3.3.2.1.2. Deviations from the ideal conditions

The application of equation 3.79 is only valid under the following conditions:

- Regime of molecular flow through the orifice;
- Orifice of null thickness;
- Thermal equilibrium between the isothermal cell and the sample;
- Saturated vapor throughout the cell;
- Collisions between vapor molecules and cell walls obeying the Lambert's cosine law;
- Unitary vapor condensation coefficient;
- Absence of chemical reaction between the sample and the cell;
- Absence of surface diffusion phenomena.

Some of the listed ideal conditions cannot be strictly replicated experimentally. The conditions used in real experiments may affect the calculated vapor pressure values. It is possible, however, to minimize the inherent errors to the deviations from ideal to real conditions:

Molecular flow

Gas flow can be classified into one of three types depending on the pressure and on the size of the effusion orifice [64]:

- Molecular flow, occurs at reduced pressures of the vapor where the intermolecular collisions are rare and the flow is only conditioned by the molecular collisions with the walls of the orifice;
- Viscous flow, occurs at high vapor pressures where the intermolecular collisions are more frequent than collisions with the walls of the effusion orifice;
- Transition flow (with characteristics between molecular and viscous flow), occurs at a pressure range in which the flow is conditioned by both intermolecular collisions and with the orifice's walls.

The mean free path, λ , defined as the average distance covered by a particle between collisions with other moving particles, can be calculated the by equation 3.80 [64,65],

$$\lambda = \frac{1}{\sqrt{2}\pi\sigma^2 n} \quad (3.80)$$

where n represents the number of molecules per unit of volume and σ , the diameter of molecular collision, a characteristic parameter related to a molecule's dimensions.

The accepted limits between types of flow are established by the Knudsen number, K_n , defined as the ratio of the mean free path and the diameter of the effusion orifice. Accordingly:

$K_n > 1$, Molecular flow; $1 > K_n > 0.01$, Transitional flow; $K_n < 0.01$, Viscous flow.

Although there is no unanimity concerning the limit value between transitional and molecular flows, in practice it is assumed that the flow is molecular for vapor pressures lower than 1 Pa. Some researchers believe that molecular flow regime only occurs when the ratio (r/λ) approaches zero, and consider an additional correction factor, K_{hp} , defined by Hiby and Pahl [66] by equation 3.81.

$$K_{hp} = 1 + \frac{K' r}{2\lambda} \quad (3.81)$$

where $K' = 0.48$. The use of this correction, however, implies the knowledge of λ , usually determined by estimating the diameter of molecular collision.

Effusion under a non-molecular flow conditions would lead to calculated vapor pressures bigger than the actual and, consequently, overestimated enthalpies of sublimation [58].

Probability of transmission

The vapor's molecular flow should ideally be carried out through an orifice of null thickness. The finite thickness of the real orifices prevents the use of equation 3.79. It is therefore necessary to include a parameter that considers the fraction of vapor molecules that after collision with the orifice wall are reflected back into the cell. The transmission probability factor, w_o , accounts for this effect providing an estimate of the probability of transmission of vapor molecules through the effusion orifice, according to its geometric dimension. So, for real effusion orifices, equation 3.79 leads to equation 3.82.

$$p_1 = \frac{1}{w_o} \cdot \frac{m}{tA_o} \cdot \sqrt{\frac{2\pi RT}{M}} \quad (3.82)$$

Saul Dushman [64] deduced the expression 3.83 for an approximate calculation of w_0 for short tubes,

$$w_0 = 1/[1+(3l/8r)] \quad (3.83)$$

where l is the thickness of the tube and r its radius. Later, Pieter Clausing [67] developed, for the transmission through shorter tubes (orifices), a rigorous mathematical formula, whose approximate solution is expressed by equation 3.84.

$$w_0 = 1/[1+(l/2r)] \quad (3.84)$$

For l/r values smaller than 0.1, values of w_0 calculated by equation 3.83 are less than 1 % higher than the values calculated by the expression 3.84 [58].

Condensation coefficient

Within the vapor saturated effusion cell, there is a fraction of molecules that undergoes condensation after collision with the surface of the condensed phase. Defining the condensation coefficient, α , as the ratio of molecules that condense after collision with the surface of the condensed phase and $(1-\alpha)$ as the ratio of molecules that are reflected back to the effusion orifice, contributing to the effusion flow, equation 3.79 becomes equation 3.85.

$$p_1 = \frac{1}{\alpha w_0} \cdot \frac{m}{tA_0} \cdot \sqrt{\frac{2\pi RT}{M}} \quad (3.85)$$

The condensation coefficient is usually assumed to be unitary for most solid compounds.

Orifice area and equilibrium conditions

The area of the orifice must be sufficiently small to ensure that the cell is saturated with vapor and to minimize the pressure gradient within the cell. Under these conditions the vapor effusion rate should be compensated by the sublimation rate. However, for larger orifices, the heat absorbed by the sample during the sublimation may not be compensated by the heat transfer from the vicinity of the cell to the sample. In this case, self-cooling of the sample may occur which will cause the measured vapor pressure to be lower than the

effective vapor pressure. The self-cooling effect increases with temperature and leads to default errors in sublimation enthalpy values calculated from the pressure-temperature relationship [58].

Surface diffusion

Langmuir [68,69] and Volmer and Estermann [70] demonstrated that gaseous molecules are reflected by the solid surfaces with which they collide, not by a simple bounce mechanism, but by a mechanism involving surface diffusion. As a result of collisions, the molecules are adsorbed by the inner surface of the cell, move along this surface and, after a period of time, suffer desorption or may migrate through the orifice to the outside of the cell.

Surface diffusion coefficient values are difficult to obtain since they depend on the nature of the vapor and of the material constituting the cell. The errors inherent to this process can be minimized when taking into consideration that the ratio between the diffusion flow and the effusion flow increases with decreasing radius and thickness of the orifice as well as with decreasing vapor pressure within the cell [58].

Alteration of vapor molar mass

The vapor pressure calculated from the equation 3.79 is dependent on the molar mass of the effusing vapor. Considering, for example, the occurrence of total dimerization of the effusing vapor, the vapor pressure of the dimer, p_{dim} , (the real vapor pressure) would be given by equation 3.86, in which M is the molar mass of the monomer.

$$p_{\text{dim}} = \frac{1}{w_o} \cdot \frac{m}{tA_o} \cdot \sqrt{\frac{2\pi RT}{2M}} \quad (3.86)$$

If the occurrence of dimerization was ignored, the ratio between the calculated and real pressures would be:

$$\frac{p_{\text{mon}}}{p_{\text{dim}}} = \frac{1}{w_o} \cdot \frac{m}{tA_o} \cdot \sqrt{\frac{2\pi RT}{M}} \Big/ \frac{1}{w_o} \cdot \frac{m}{tA_o} \cdot \sqrt{\frac{2\pi RT}{2M}} = \sqrt{2} \quad (3.87)$$

Therefore ignoring this eventual process would result on a calculated vapor pressure larger than the real pressure. In the case of partial vapor dimerization, a similar analysis to the one above would be performed, by determining an average molar mass if the degree of dimerization is known. Dissociation processes can also occur in the gaseous phase, yielding

vapor molecules of smaller molar mass and resulting on a calculated vapor pressure smaller than the real pressure.

By comparing the pressures determined by the Knudsen mass-loss effusion method with vapor pressures measured using methods that are independent of the vapor's molar mass (like torsion-effusion or static method), it is possible to test the existence of association or dissociation in the gas phase under experimental conditions.

3.3.2.1.3. Description of the apparatus

The Knudsen effusion apparatus used in this work for the measurement of vapor pressures was built and tested in our laboratory. Its detailed description can be found in the literature [60], but the most relevant aspects of the equipment and of the respective experimental procedure will be described here.

The apparatus, schematically represented in figure 3.15, allows the simultaneous operation of nine effusion cells at three different temperatures, for the determination of vapor pressures of crystalline samples in the range of (0.1 to 1) Pa, and in a temperature interval within room temperature and 423 K. It's essentially constituted by a pumping system (A), a sublimation chamber (B), a set of peripheral components for the temperature measurement and control, and data acquisition (C) and the effusion cells (D).

Pumping system

The pumping system is constituted by an Edwards RV12 rotary pump (1), which is used for pre-evacuating the system and for backing the Edwards Cryo-cooled Diffstack CR160 oil diffusion pump (2).

The system's pressure is monitored in different points by two Edwards Active Pirani APG-M manometers (3) and by an Edwards Active Inverted magnetron AIM-S manometer, for high-vacuum (4). All metal-metal joints are ISO KF connections. The pumping system is connected to the sublimation chamber through a glass line with a glass-metal connection to a flexible tube.

Sublimation chamber

The sublimation chamber consists of a glass bell jar, with an aluminum lid and base. The hermeticity of the glass-aluminum joints is ensured by neoprene L-gaskets, lubricated with Apiezon L.

The sublimation chamber is connected to the pumping system through a glass vacuum line (5) with a glass-metal connection to a flexible metal tube. To prevent the sample contamination of the vacuum pumps, the vacuum line includes a glass cold finger (6), for liquid nitrogen, adapted to the chamber by a hole in its lid. The sublimation chamber sits on a sliding platform to facilitate the connection to the pumping system.

Inside the sublimation chamber are three separate ovens (7), consisting of cylindrical aluminum blocks, each supported by three ceramic pillars (8) that thermally insulate them from the base of the chamber. Each oven contains three symmetrically arranged cylindrical cavities (9), of dimensions similar to the effusion cells for good thermal contact.

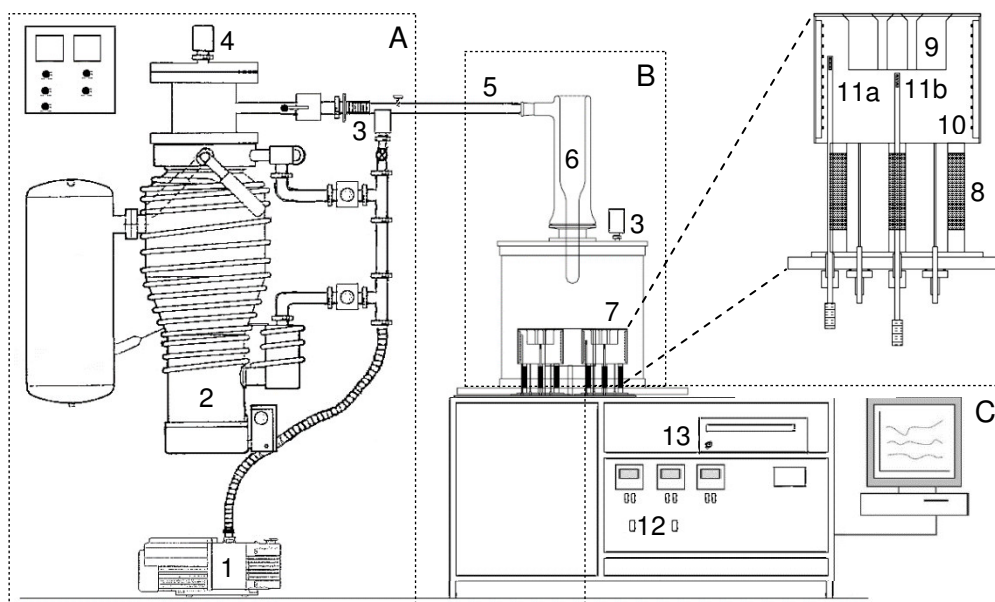


Figure 3.15. Schematic representation of the Knudsen mass loss effusion apparatus: A. pumping system (1. rotary pump; 2. oil diffusion pump; 3. Pirani manometers; 4. inverted magnetron gauge); B. sublimation chamber (5. glass vacuum line; 6. glass cold finger; 7. aluminum blocks (ovens); 8. ceramic pillars; 9. effusion cell cavities; 10. heating resistances; 11. platinum resistance thermometers); C. peripherals for temperature measurement, control, and data acquisition (12. PID temperature controllers Omron E5CN; 13. data logger Agilent 34970A). Image adapted from ref. [60,71].

Temperature measurement and control

The thermostatic system of each oven consists of two circular electrical heating resistances Ari Aerorod BXX (10), connected in parallel to a power source and two platinum resistance thermometers Pt-100 1/10, calibrated against a SPRT temperature probe (25 Ω ; Tinsley, 5187A). The thermometer located near the heating resistances (11a) is connected to a PID controller Omron E5CN (12), responsible for the oven temperature control, while

the thermometer located at the center of the block, equidistant to the basis of cell cavities (11b), is responsible for measuring the accurate temperature of the oven and the respective cells, assumed to be in thermal equilibrium with each block. These thermometers are connected to an automatic data acquisition system, Agilent 34970A (13), interfaced to a computer equipped with an Agilent BenchLink Data Logger software, which processes the data and continuously displays the temperature of the ovens, collected at regular intervals for the duration of the experience, with a resolution of 10^{-3} K.

Effusion cells

The cylindrical effusion cells and the respective screw caps are made in aluminum. Inside each cap there is a thin platinum disc (0.0125 ± 0.0012 mm thickness) with a laser perforated effusion orifice in the center, placed between a brass and a teflon[®] washer that are secured in place by a screw thread brass ring.

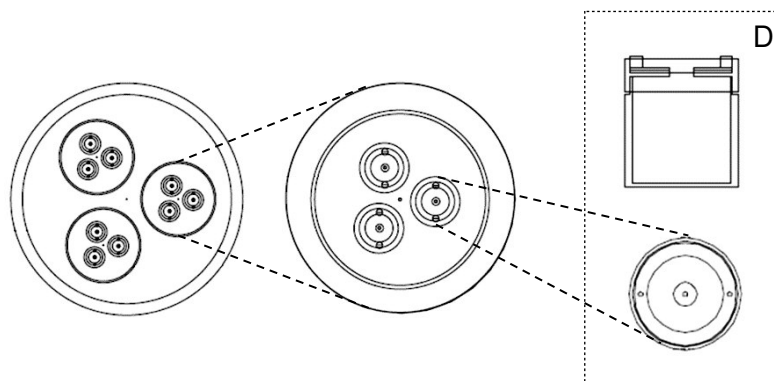


Figure 3.16. Schematic representation of the ovens inside the vacuum chamber (top view) and of the effusion cell (side and top views). Image adapted from ref. [60].

The nine effusion cells are grouped into three series according to effusion orifice diameters: series A - small orifices; B - medium orifices; B - large orifices. During the course of this work, the effusion cells were subjected to maintenance and the platinum discs were replaced. The geometric parameters of both sets of orifices used are presented in the table 3.3. For the first set of orifices – A, B, C – the transmission probability factor, w_0 , was calculated using equation 3.83. For the second set of orifices – A', B', C' – w_0 was calculated using equation 3.84, using diameter values provided by the supplier.

Table 3.3. Diameters, areas and transmission probability factors of the effusion orifices.

Orifices		ϕ (mm)	A_o (mm ²)	w_o	$A_o w_o$
Small	A ₁	0.800	0.503	0.988	0.497
	A ₂	0.805	0.509	0.989	0.503
	A ₃	0.800	0.503	0.988	0.497
	A ₁ ' , A ₂ ' , A ₃ '	0.900	0.636	0.986	0.627
Medium	B ₄	0.992	0.774	0.991	0.766
	B ₅	0.999	0.783	0.991	0.776
	B ₆	1.004	0.792	0.991	0.784
	B ₄ ' , B ₅ ' , B ₆ '	1.000	0.785	0.988	0.776
Large	C ₇	1.183	1.099	0.992	1.090
	C ₈	1.197	1.125	0.992	1.116
	C ₉	1.200	1.131	0.992	1.122
	C ₇ ' , C ₈ ' , C ₉ '	1.120	0.985	0.989	0.974

To test the new orifices, experiments were successfully performed with benzoic acid and with another compound which had previously been studied by this and/or other complementary techniques: benzoic acid and *N*-methylnicotinamide. These experimental results are presented in annex C.2.

3.3.2.1.4. Experimental procedure

A properly pulverized sample of the crystalline compound under study is placed and pressed inside the effusion cells with a brass piston, in order to achieve a flat surface and to ensure good thermal contact. The cells are sealed with the respective caps and then weighed on an analytical balance (Mettler AE163, ± 0.01 mg).

After weighing, the cells are lubricated with a thin Apiezon L layer, for improved thermal contact, and are introduced inside the respective cavities in the aluminum blocks, so that each contains three cells with different effusion orifice size.

The sublimation chamber is closed with its lid, the cold finger is assembled and fixed with a metal clamp. The blocks containing the cells are heated to the desired temperatures and, after allowing for thermal stabilization of the cells, the system is vacuum-pumped and when the pressure is lower than 1 Pa, the cold finger is filled with liquid nitrogen. A valve that enables the connection to the oil diffuser pump is opened and when the pressure in the

sublimation chamber is below 10^{-2} Pa, the effusion time counter is initiated. The pressure of the system keeps decreasing toward the ultimate pressure of $5 \cdot 10^{-4}$ Pa.

When the suitable effusion time period is finished, the system is isolated from the pumping system, air is slowly admitted in the sublimation chamber and the effusion time counter is stopped. The cells are removed from the ovens and thoroughly cleaned to remove the Apiezon L. After cooled to room temperature, the cells are weighed to assess the mass loss.

3.3.2.2. Static method with capacitance manometers

As previously mentioned, a static method was also used in this work for the direct measurement of equilibrium vapor pressures of compounds in the solid and/or liquid phases.

Although there are several techniques based on the static method, more recent manometric variants employ capacitance diaphragm gauges. In this technique, the deflection of a metal diaphragm induced by the pressure of the vapor is related to the capacitance variation of a capacitor that includes a flexible electrode – the diaphragm – and a set of fixed electrodes. The variation in capacitance is proportional to the measured vapor pressure.

3.3.2.2.1. Thermal transpiration and other sources of error in a static method

Static methods based on capacitance diaphragm gauges are susceptible to some sources of systematic errors. This method is very sensitive to volatile impurities and to dissolved or adsorbed gases in the sample. The presence of residual gas in the sample will result in overestimated vapor pressure values and underestimated enthalpies of phase transition, since the lower vapor pressures are relatively more affected. Therefore, it is crucial to thoroughly degas the sample previously to its study, which will ensure the consistency of the measured pressure values.

Another major problem in the use of static methods for measurement of low pressures ($p < 1$ Pa) is the possibility of thermal transpiration, generally negligible for higher pressures. When the temperature of the pressure gauge is kept above the temperature of the sample to prevent sample condensation inside the gauge, as is the case in the used experimental apparatus, thermal transpiration may occur. Tests made on the apparatus used in this study

revealed no significant influence of thermal transpiration on measured values, even for pressure values near the lower limit of the gauge's applicability range (0.5 Pa) [53] which is essentially due to the relatively large internal diameter of the tubing ($\phi_{\text{int}} = 17$ mm) used in the apparatus.

It is also important to ensure the mechanical and thermal stability of the system. The deflection of the diaphragm in response to pressure difference may be in the nanometer range, so the used apparatus is equipped with flexible metal tubes to minimize possible vibrations which would influence the pressure measurement. The maintenance of the gauge at a constant temperature is essential to avoid thermal expansion of its components that would lead to changes in the zero and calibration of the gauge, and consequently measurement errors.

3.3.2.2.2. Description of the apparatus

The static apparatus used in this work was built and tested in our laboratory and is reported in detail in the literature [53]. Nevertheless, a description of the main characteristics of the equipment and experimental procedure will be presented here.

This apparatus, schematically represented in figure 3.17, is equipped with capacitance diaphragm gauges and was used to measure the vapor pressures of solid and liquid samples, above ca. 1 Pa until $1.3 \cdot 10^3$ Pa, in temperature intervals included within (243 and 473) K. It is essentially constituted by a diaphragm capacitance gauge (A) connected to a metallic tubing system (B), a sample cell thermostated at selected temperatures controlled by a thermostatic bath (C), a pumping system (D) and a set of peripheral components for temperature control and measurement, pressure measurement and automatic data acquisition.

Capacitance manometer

The vapor pressure is directly measured using MKS Baratron capacitance diaphragm absolute gauges (A). During this study, two models were used, operating at different maximum pressures and at controlled constant temperatures:

- MKS Baratron 631A01TBEH applicable to measuring vapor pressures up to $1.3 \cdot 10^2$ Pa at an auto-controlled temperature of 423 K;
- MKS Baratron 631A11TBFP applicable to measuring vapor pressures up to $1.3 \cdot 10^3$ Pa at an auto-controlled temperature of 473 K.

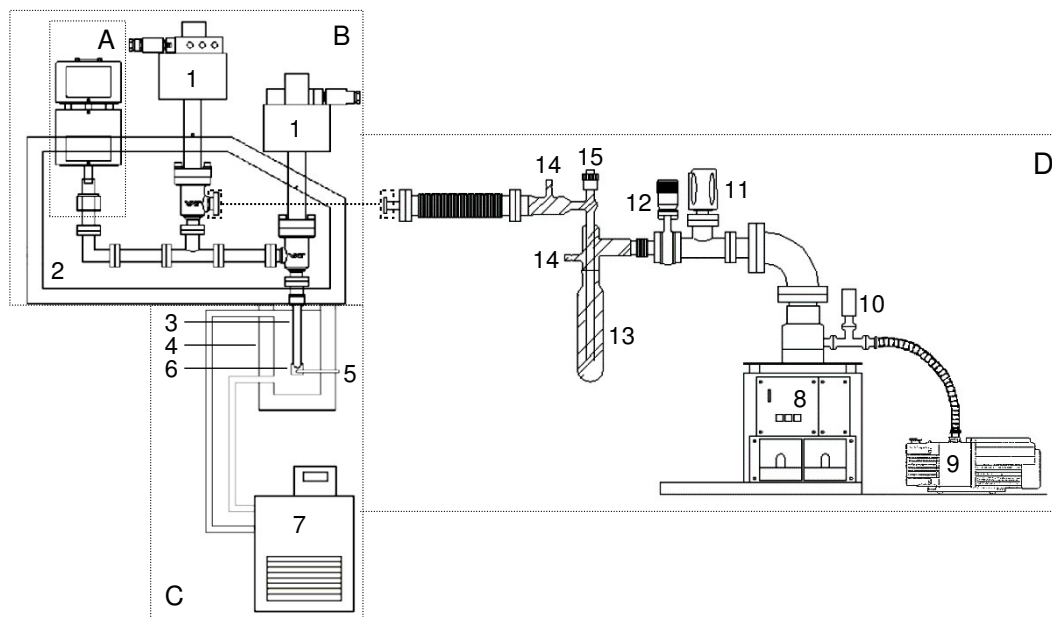


Figure 3.17. Schematic representation of the static method apparatus: A. Capacitance diaphragm absolute gauge; B. Pressure line (1. all-metal angle VAT valves; 2. insulated thermostated box); C. Sample cell and thermostatic bath (3. sample cell; 4. double-jacked vessel; 5. platinum resistance thermometer; 6. brass block; 7. thermostatic bath); D. Pumping system (8. turbomolecular pump; 9. rotary pump; 10. Pirani manometer; 11. WRG-S manometer; 12. UHV gate valve; 13. glass trap for liquid nitrogen; 14. teflon air inlet valves; 15. teflon in-line tap isolation valve). Image adapted from ref. [53,71].

Each capacitance manometer contains two compartments. The lower compartment has two chambers – one that receives the vapor of the sample, and the reference chamber. The latter contains a system of fixed circular electrodes and a getter which removes residual amounts of gas from the evacuate space by absorption or adsorption, maintaining its pressure negligible. So, the vapor pressure of the sample is related to the deflection of the flexible metal diaphragm, made of Inconel, which separates the two chambers. The upper gauge compartment contains the electronic components required to operate the gauge and electronic systems for noise reduction, ensuring a good resolution and high sensitivity. The manometer is connected to the tubing system by a Swagelok/Cajon VCR connection with an 8-VCR-CF DN 16 adapter, in which silver-plated copper gaskets are compressed between the ends of the connecting tubes, which facilitates the exchange between the two gauges.

Tubing system

The pressure gauge connects to the sample cell by a line constructed of stainless steel tubing with ConFlat DN 16 CF connections and two all-metal angle valves VAT series 57 (1), operated pneumatically.

The tubing and the lower compartment of the pressure gauge, are kept in a thermal insulated stainless steel box (2) with a removable front. This box is kept at a controlled temperature slightly higher than that of the sample, in order to avoid condensation of its vapor, but lower than the gauge's operating temperature. The box is thermostated by air forced convection through a heating resistance, by means of a fan, and is controlled by a Eurotherm 2116 PID temperature controller connected to a platinum resistance thermometer Pt-100 (± 0.1 K).

Sample cell and thermostatic bath

The sample cell (3) consists of a stainless steel tube, closed at the lower end, which is connected to the pressure line through one of the electro-pneumatic valves by a metal-metal 8-VCR connection, described above. The cell containing the sample is introduced in a cylindrical cavity of a double-jacketed copper vessel (4), responsible for its thermal stability, supplied by a constant flow of a thermal fluid (Julabo Thermal H10S oil) whose temperature determines that of the sample cell by thermal equilibrium. The temperature of the thermal fluid near the sample is measured by a platinum resistance thermometer Pt-100 1/10 (5), inserted in a narrow cavity in the thermostated vessel located near the bottom of the sample cell. The sample cell and thermometer cavities end in an inner small block of made of brass (6), with the function to improve thermal contact between them and the circulating fluid. The temperature of the circulating fluid is regulated by a Julabo F33-MW thermostatic bath (7), equipped with a cooling system, which allows the temperature control between 253 K and 473 K (± 0.01 K).

Pumping system

The pumping system is constituted by an Edwards EXT70 turbo-molecular pump (8) coupled to an Edwards RV3 rotary pump (9), responsible for the primary vacuum. The turbomolecular pump is installed on an Edwards EXPB 1.5 base, equipped with an Edwards EXC120 controller and two Edwards AGD pressure gauges connected to an Edwards Active Pirani APG-M manometer (10), that measures the pressure at a point between pumps, and an Edwards WRG-S manometer (11), that measures the pressure near the exit of the turbomolecular pump.

At the exit of the turbo-molecular pump, there is also a VAT 010 series valve (UHV gate valve) (12), which facilitates the rapid isolation of the pumping system. This valve communicates with a glass vacuum line that establishes the connection between the pumping system and the pressure line. The glass line includes a glass trap cooled (13) with liquid nitrogen, and is equipped with two air inlet ASL1 J. Young valves (14), and a J. Young in-line tap SPOR25 isolation valve (15), all made of teflon.

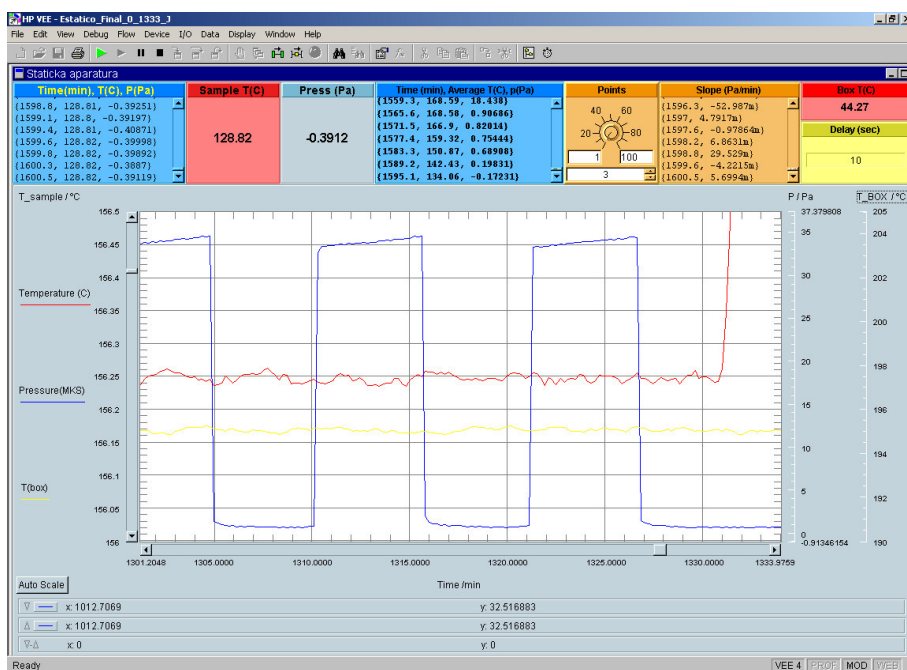


Figure 3.18. Image of the HP-VEE software data acquisition display.

Auxiliary and data acquisition systems

The pressure and temperature experimental data are collected through a data acquisition system, Keithley 2700, programmed to read the vapor pressure and the temperatures of the sample and of the thermostated box at regular intervals. This data is monitored by of an HP-VEE software (figure 3.18) configured for this purpose.

The Julabo thermostatic bath and the electro-pneumatic valves are also connected to the computer, and controlled using respectively the EasyTemp software (v2.2) supplied by Julabo Lobortechnik GmbH for programing and controlling the temperature of the circulating fluid and ADAM software (v1.1) [72] for automatically operating the electro-pneumatic valves.

3.3.2.2.3. Experimental procedure

In a typical experiment, the sample cell containing a small amount of sample is connected to the tubing system and introduced into the double-jacked thermostatic vessel. Prior to vapor pressure measurements, the sample is thoroughly degassed until consecutive measurements at a selected temperature deliver consistent pressure results. When the degassing process is completed, an experimental temperature is selected and the pressure baseline is established with the sample cell closed and the rest of the system connected to the pumping system. The sample cell is then opened allowing the capacitance manometer to be filled with the sample's vapor. There is a sudden increase in the pressure read by the pressure gauge and, when it stabilizes, the (p, T) data is registered. After the vapor pressure is determined, the sample cell is again closed and the pressure returns to the baseline. This process is repeated at different temperatures over a chosen temperature interval, following increasing and decreasing temperature sequences in order to test the quality of results and detect eventual systematic errors caused by insufficient degassing of the sample.

3.4. Photoluminescence spectroscopy

3.4.1. Introduction to photoluminescence

Luminescence is the emission of light (usually in the UV-Vis region) that occurs from the deactivation of electronically excited species [73]. The various types of luminescence are classified according to the mode of excitation. Fluorescence and phosphorescence are particular cases of photoluminescence, in which the mode of excitation is the absorption of photons. A molecule, or part of a molecule, that is capable of re-emitting light upon absorption of photons is called fluorophore.

At any electronic energy level, S_n , a fluorophore can exist in a number of vibrational energy levels ($v = 0, 1, 2, \dots$). At room temperature, most fluorophores occupy the lowest vibrational energy level of the ground electronic state, S_0 . Following light absorption, a fluorophore is excited to any of the higher vibrational levels of an excited electronic state. The excited state exists for a finite time and then the fluorophore returns to S_0 dissipating part of its energy through a number of radiative and non-radiative pathways, as is illustrated in the simplified Jablonski diagram in figure 3.19.

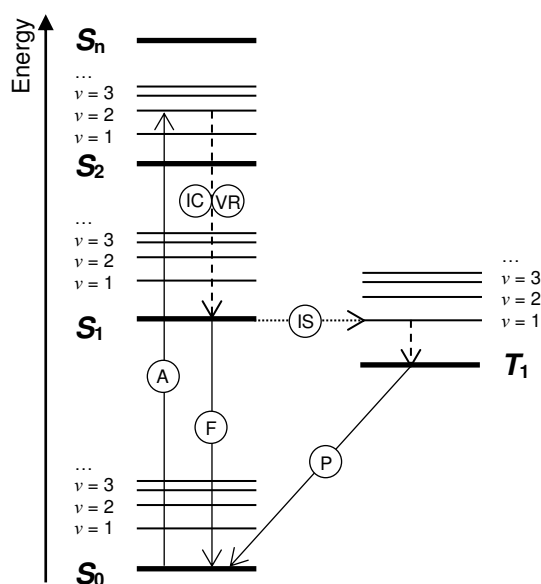


Figure 3.19. Simplified Jablonski diagram: S_0 - ground state; S_1 - first singlet excited state; S_n - singlet excited state; T_1 - first triplet excited state; A - photon absorption; F - fluorescence; P - phosphorescence; VR - vibrational relaxation; IC - internal conversion; IS - intersystem crossing.

Table 3.4. Possible radiative and non-radiative de-excitation pathways of excited fluorophores and average time scales.

		Type	Transition	Time scale / s
A	Absorption	Radiative	$S_1 \rightarrow S_n$	10^{-15}
IC	Internal conversion	Non-radiative	$S_n \rightarrow S_1, T_n \rightarrow T_1$ $S_1 \rightarrow S_0$	10^{-14} – 10^{-10} 10^{-7} – 10^{-6}
VR	Vibrational relaxation	Non-radiative	$S_{1, v=n} \rightarrow S_{1, v=0}$	10^{-12} – 10^{-10}
F	Fluorescence	Radiative	$S_1 \rightarrow S_0$	10^{-9} – 10^{-7}
IS	Intersystem crossing	Non-radiative	$S_1 \rightarrow T_1, S_n \rightarrow T_n$ $T_n \rightarrow S_n$	10^{-8} – 10^{-5}
P	Phosphorescence	Radiative	$T_1 \rightarrow S_0$	10^{-2} – 10^3

The probability of each transition is related to the respective time scale [74] (table 3.4): the faster the transition, the more likely it is to happen.

An excited fluorophore in any higher vibrational level of S_n , quickly relaxes to the lowest vibrational state of the first excited electronic state with the same multiplicity, S_1 , by vibrational relaxation (between vibrational levels of the same electronic level) and interval conversion (between different electronic levels) through collisions with other molecules. From S_1 , a fluorophore may reach S_0 emitting radiation through different processes: fluorescence and phosphorescence. Owing to the loss of vibrational energy, radiation emission will always occur at a lower energy than that of absorption, and therefore at larger wavelengths.

The ground state and first excited state have similar energy spacing between vibrational energy levels and, consequently, the absorption and fluorescence spectra are approximate mirror images of each other [74]. This mirror-image relationship, however, is affected by interactions of the fluorophore in the excited state with the surrounding medium.

3.4.1.1. Fluorescence

From the lowest vibrational level of S_1 , the fluorophore can return to any of the vibrational levels of the ground state, emitting fluorescence radiation [73].



Because the emission of fluorescence takes place from the lowest vibrational level of S_1 , the emission maximum and the spectra profile are typically independent of the excitation

wavelength. Different excitation wavelengths, however, will produce variations in fluorescence emission intensity [75,76].

Absorption overlaps fluorescence at the wavelength corresponding to the 0-0 transition: $S_{0, v=0} \leftrightarrow S_{1, v=0}$. It should actually occur at the same wavelength, but in practice they rarely coincide, as a result of a small energy loss by the interaction of fluorophore with the surrounding environment. Due to energy dissipation, the energy of the emitted photon is lower and therefore of longer wavelength than the absorption wavelength. This difference in energy/wavelength is known as Stokes shift (gap between the maximum of the first absorption band and the maximum of fluorescence emission) [73,74].

3.4.1.2. Phosphorescence

Fluorophores in S_1 can also undergo a spin conversion to the first triplet state, T_1 , through intersystem crossing (non-radiative transition between isoenergetic vibrational levels belonging to electronic states with different multiplicities). The probability of intersystem crossing increases if the vibrational levels of S_1 overlap with those of T_1 . From T_1 , the fluorophore can return to any of the vibrational levels of S_0 , emitting phosphorescence radiation [73].



Because T_1 has smaller energy than S_1 , phosphorescence spectrum is located at longer wavelengths than the fluorescence spectrum. Since the theoretically forbidden excitation to a triplet state is less probable, the return to S_0 from T_1 will take longer than from S_1 . While fluorescence emission occurs within nanoseconds, phosphorescence lifetime can take up to several hours in certain materials [76,77].

Phosphorescence in solution at room temperature is not likely to occur because many deactivation processes compete with phosphorescence emission (table 3.4), but it can be observed at very low temperatures and/or in rigid mediums. Molecules containing heavy atoms, such as bromine or iodine, are frequently phosphorescent. In heavy atoms, a spin-orbit interaction is substantial facilitating intersystem crossing [78].

3.4.2. Excited-state lifetimes and luminescence quantum yield

Two key parameters for fluorophore characterization and comparison are the excited-state lifetime and the luminescence quantum yield. These parameters can be defined for fluorescence and phosphorescence transitions.

Excited-state lifetime is the average time that a fluorophore remains in an excited singlet or triplet state before returning to S_0 [75], and can be described as the decrease of the number of excited fluorophores in time following excitation. Luminescence quantum yield provides a direct measure of the efficiency of the conversion of absorbed light into emitted light [79]. The fluorescence quantum yield, ϕ_F , can be calculated as the ratio of photons absorbed to photons emitted through fluorescence [75]:

$$\phi_F = \frac{\text{number of photons emitted}}{\text{number of photons absorbed}} \quad (3.90)$$

Other processes, however, contribute to the fluorophore deactivation, such as internal conversion, intersystem crossing, inter and intramolecular interaction. So, in other words, the fluorescence quantum yield can also be associated to the probability of the excited state being deactivated to S_0 by fluorescence rather than by another non-radiative mechanism,

$$\phi_F = \frac{k_F}{k_F + k_{nr}} \quad (3.91)$$

where, k_F , is the rate constant for fluorescence deactivation, and k_{nr} is the rate constant for non-radiative deactivation, including all other possible competing deactivation pathways. The weaker the competitive processes are, the larger is the de-excitation via fluorescence. Fluorophores with quantum yields approaching unity, will be more efficient and display the brightest emissions. Fluorophores with quantum yields as low as 0.1, however, are already considered fluorescent [80].

3.4.3. Quantification of emission and instrumentation

The radiation emitted by a fluorophore, in solution or in solid phase, can be characterized by the emission spectra, quantum yield and lifetime. These properties are related to the fluorophore structure and its chemical environment.

Emission data is usually presented in the form of emission spectra, where emission intensity is plotted as a function of emission wavelength (or wavenumber, cm^{-1}). Energy spacing between vibrational levels is illustrated in the emission spectrum by different bands corresponding to the vibrational levels of the ground state [81]. Most rigid organic molecules have restricted vibrational levels and can show simpler spectra with broader bands devoid of vibrational structure.

Emission spectra can be readily obtained using a conventional spectrometer while the determination of lifetime requires time-resolved spectroscopy, where the emission of the sample is monitored as a function of time after excitation by a pulse of light. Comparatively, emission quantum yields are more difficult to determine, particularly for crystalline samples. In general, photoluminescence quantum yields can be determined through comparative and absolute methods [79]:

- In comparative methods, photoluminescence measurements of a sample are compared with those of a well characterized standard [82] with optical properties closely matching those of the investigated sample under identical experimental conditions. The accuracy of these methods depend on the accuracy of the standard determination;
- In absolute methods, the quantum efficiency can be determined by optical methods, by directly measuring the portion of absorbed photons emitted as luminescence, or by calorimetric methods such as photoacoustic and thermal lensing [83], by directly measuring the portion of photons lost by non-radiative recombinations.

3.4.3.1. Integrating sphere based methods

In this work, photoluminescence quantum yields were performed using an absolute optical technique based on an integrating sphere.

An integrating sphere is a spherical cavity whose inner surface is coated with a highly reflective (diffuse) surface which enables spacial integration of incoming light flux while minimizing issues related to the angular dependence of reflection, emission and scattering [84]. While conventional fluorescence spectrometers can detect only a certain fraction of

the emitted light, those equipped with an integrating sphere detect all light emitted by the excited sample, and hence allow for the absolute determination of the fluorescence quantum yield [79].

By using an integrating sphere, much of the optical anisotropy (dependence with the direction of propagation of the radiation) is eliminated by multiple reflections on the inner surface of the integrating sphere [85]. For this reason, the use of integrating spheres, particularly for the determination of quantum yield on the solid state, is becoming increasingly common. Recent commercial instruments based on an integrating sphere are found to yield reliable results in various set-ups [85].

3.4.4. Factors affecting accuracy

The accurate characterization of fluorescence can often be difficult and troublesome, because it is highly sensitive to changes in environment conditions (temperature, solvent, fluorophore interaction with other molecules, etc.) that can distort the emission spectra and influence the quantum yield, both in solution and in the solid state. Decrease of fluorescence intensity by interaction of the fluorophore in its excited state with the local molecular environment is known as quenching. Fluorescence quenching can occur due to the presence of oxidizing agents, inner filter effects (as self-absorption) and formation of excited state dimers.

Temperature and pH

At room temperature, most molecules are in the lowest vibrational level of the ground state. At higher temperatures, higher vibrational levels of the ground state are populated (Boltzmann distribution) and more transitions occur from these levels to higher vibrational levels of excited electronic states. This leads to broader absorption and emission spectra since the superposition of the different levels blurs most of the fine vibrational structure of the band. An increase in temperature also results in a decrease in the fluorescence quantum yield and lifetime because non-radiative processes related to thermal agitation are more efficient at higher temperatures [73]. Conversely, at lower temperatures, the spectral widths are reduced and the spectra shows enhanced vibrational structure [74].

When in solution, small changes in pH can also affect the intensity and spectral characteristics of fluorescence. As a result, pH sensitive fluorophores in different ionization states have distinct absorption and emission spectra in aqueous solution. This principle is used in fluorescence sensors for the measurement of pH changes within cells [75].

Solvent polarity and oxygen quenching

Solution fluorescence emission spectrum and quantum yield strongly depend on the polarity of the solvent. A fluorophore on higher vibrational levels of an excited state, loses excess vibrational energy to surrounding solvent molecules. The interaction with the solvent molecules decreases the energy of the excited fluorophore, reducing the energy separation between the ground and excited states. This results in a shift of the fluorescence emission to longer wavelengths and an increase of the Stokes shift, which will be more prominent with increasing solvent polarity. The polarity of the fluorophore also determines the sensitivity of the excited state to solvent effects. Polar and charged fluorophores exhibit a far stronger effect than non-polar fluorophores [75].

When in solution, the presence of trace oxidizing agents, for example, dissolved molecular oxygen can severely reduce fluorescence intensity. Oxygen quenching is more significant in nonpolar solvents in which oxygen is more soluble than in aqueous solution. The dissolved oxygen can be removed by bubbling the solution with an inert non-quenching gas such as nitrogen [86,87].

Self-absorption

Either in solution or in the solid state, if the sample shows significant overlap of the absorption and luminescence spectra, some of the photons emitted by the fluorophore may be reabsorbed causing a distortion of the shape of the fluorescence spectrum in the overlap region [73] and a decrease of the observed fluorescence intensity and inaccurate quantum yield values. Self-absorption is unfortunately an undesired consequence of using integrating sphere setups, particularly when measuring solid samples [88]. Because a fraction of the emitted light is redirected onto the sample, there is a probability of it being reabsorbed. These effects can be lessened by using very dilute solutions or by reducing the volume of the emissive material if in the solid state. Alternatively, corrections can be applied by comparing emission spectra taken inside and outside the sphere.

Impurities and structural effects

The presence of impurities in the sample (and/or the solvent if in solution) can dramatically affect the accuracy of results, increasing or decreasing the fluorescence emission depending on the fluorescent nature of the impurity. Fluorescent impurities can decrease the sensitivity or even prevent the distinct detection of individual fluorophores.

Solid state fluorescence properties are sensitive to chemical impurities, structural defects and the already referred to above self-absorption of fluorescence, which may cause

fluorescence quenching of the material. Single crystals, powders with different size particles or even thin film will present distinct fluorescence spectra [89].

In some cases, however, a trace amount of impurity can act as a doping agent, particularly in the solid state, increasing the emission intensity of the fluorophore. In solid-state electronics, doping is widely used in the manufacture of semiconductors with the intention of modulating and enhancing its electrical properties [81,90].

Excimers and exciplexes

At higher concentrations and/or in the solid state, a fluorophore in the excited state can interact with an unexcited neighbor to form an excited state dimer, called excimer. The formation of such excited dimers is short-lived, existing only in the excited state, and is quite common in polycyclic aromatic hydrocarbons. The energy change associated with the excimer emission is smaller than that of the monomer. Thus, the fluorescence band corresponding to excimer emission is shifted to longer wavelengths and does not show vibrational structure. Analogous phenomena can also occur as a result of the interaction between different molecules in the excited state, forming excited complexes, called exciplexes. While excimers are nonpolar, exciplexes are polar species [81].

Light scattering

Scattering of excitation radiation, either from solvent molecules (Raman inelastic scattering), molecules in solution (Rayleigh elastic scattering) or from small particles in colloidal suspension (Tyndall scattering) will lead to radiation intensity fluctuations and to inaccurate emission results.

3.4.5. Spectroscopic apparatuses

In this work, the UV-Vis absorption spectra were obtained by means of an Agilent 8453 UV-Vis diode array system, and were used to determine the maximum absorption wavelength which was used as the excitation wavelength for the solution fluorescence study. The fluorescence spectra and the absolute emission quantum yields (ϕ_F) of the samples, in the solid state (powder form) and in solution, were measured using the absolute photoluminescence quantum yield spectrometer Hamamatsu Quantaaurus-QY C11347-11. The detailed description and mode of operation of both apparatuses can be found in the respective manuals provided with the devices [91,92].

The fluorometer is equipped with a 150 W xenon lamp, as a monochromatic light source, coupled to a monochromator for wavelength discrimination, an integrating sphere as sample chamber, and a multichannel (back-thinned CCD) detector. The apparatus allows the excitation of the sample in the wavelength range (250 to 850) nm and the photoluminescence measurement in the range (300 to 950) nm.

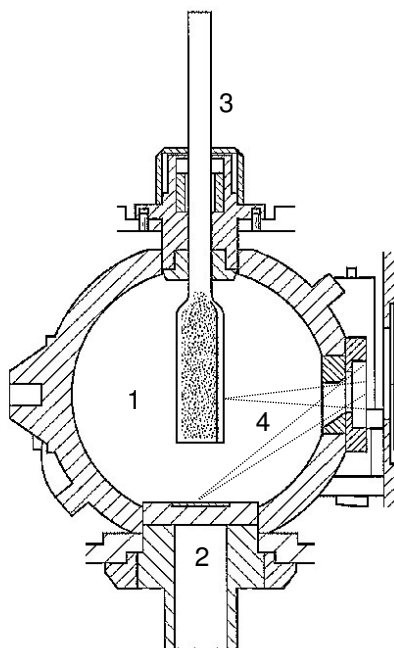


Figure 3.20. Simple schematic representation of the interior (sectional view) of the integrating sphere of the Hamamatsu Quantaurus-QY spectrometer (1. integrating sphere cavity; 2. sample holder for solid samples; 3. quartz cuvette for liquid samples; 4. exciting light). Image adapted from ref. [93].

The inner surface of the integrating sphere is made of Spectralon[®], a polytetrafluoroethylene-based material which has the highest diffuse reflectance of any known material over the ultraviolet, visible, and near-infrared regions of the spectrum [94]. The integrating sphere is equipped with a sample holder for solid samples located at the bottom of the sphere and an attachment for a quartz cuvette for liquid samples at the top (figure 3.20).

The system utilizes dedicated software, U6039-05 Quantaurus-QY (V3.7.0, figure 3.21), to automatically control the excitation wavelengths, measure fluorescence intensity and determine absolute photoluminescence quantum yields. The absolute fluorescence quantum yield is determined as the ratio of the number of photons emitted from the excited sample to the number of absorbed photons (equation 3.92). The number of absorbed

photons is determined from the difference between the incident excitation light intensity of the reference and of the absorbing sample, depicted in blue in figure 3.22.

$$\phi_F = \frac{\text{number of photons emitted as fluorescence from sample}}{\text{number of photons absorbed by sample}} \quad (3.92)$$

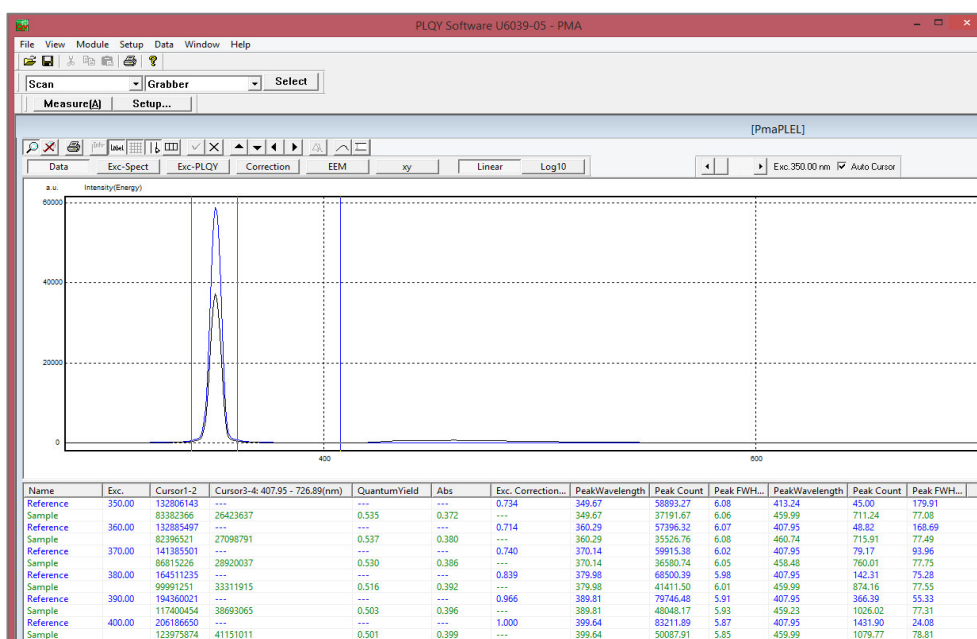


Figure 3.21. Image of the U6039-05 software data acquisition display.

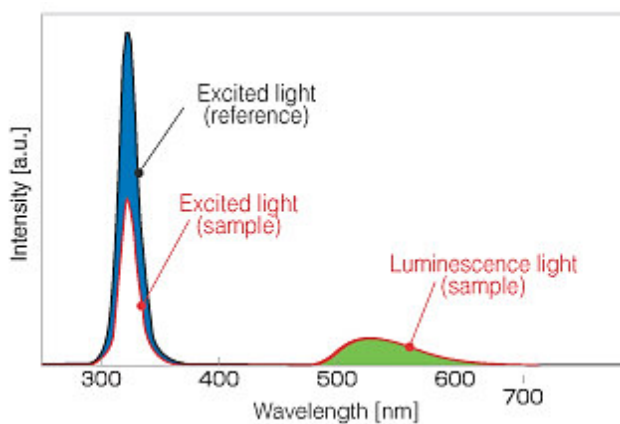


Figure 3.22. Example of excitation light and emission spectra on reference and sample (image adapted from ref. [95]).

The UV-Vis absorption and fluorescence spectra were acquired at room temperature ($T \approx 295$ K). The fluorescence measurements of the solutions were carried out using a 1 cm path length quartz cuvette with a tube extension (Hamamatsu A10095-02, figure 3.23-a), and the fluorescence measurements in the solid state were performed using a quartz lidded Petri dish with 17 mm of external diameter (Hamamatsu A10095-03, figure 3.23-b).



Figure 3.23. Quartz cuvette (a) and lidded petri dish (b) used for the fluorescence measurements in solution and in the solid state, respectively.

3.4.6. Experimental procedure

3.4.6.1. Solution fluorescence

The solutions used for the absorption and fluorescence measurements, with concentrations ranging from $(1 \cdot 10^{-6}$ to $1 \cdot 10^{-3})$ mol·dm⁻³, were prepared by rigorous dilution of a known mass of compound in cyclohexane (VWR Chemicals, spectroscopic grade).

The UV-Vis absorption spectra of the solvent background were recorded to define the corresponding base line, followed by that of the sample solutions to determine the maximum absorption wavelength.

Just before the fluorescence measurements, each solution was thoroughly deoxygenated by bubbling with nitrogen for about 20 minutes to reduce/eliminate oxygen quenching. The fluorescence spectra of the solutions were then recorded, in order of increasing concentration, using the maximum absorption wavelength determined by UV-Vis as the excitation wavelength.

3.4.6.2. Solid state fluorescence

For the fluorescence measurements in the solid state, a loose powder sample, obtained by milling the sublimed crystals, was placed in a quartz Petri dish and the fluorescence spectrum was recorded over a range of excitation wavelengths at regular intervals of 10 nm. Whenever possible, the excitation wavelength range was selected in accordance with data available in the literature.

For each compound, three measurements were performed with increasing amounts of sample (as represented in figure 3.24) to test the dependence of quantum yield with amount of sample and eventual self-absorption effects in the solid phase.



Figure 3.24. Typical amounts of sample used for the solid state fluorescence measurements (approximate percentage of the area of the base of the dish covered by powder sample: a. 15 %; b. 40 %, c. 100 %).

References

- [1] P.J. Haines (Ed.), *Principles of Thermal Analysis and Calorimetry*, RSC Paperbacks, Royal Society of Chemistry, Cambridge (2002);
- [2] D.R. Stull, E.F. Westrum Jr., G.C. Sinke, *The Chemical Thermodynamics of Organic Compounds*, John Wiley & Sons, Inc., New York (1969);
- [3] J.A. Martinho Simões, M.E. Minas da Piedade, chapter 12, in: *Molecular Energetics: Condensed-Phase Thermochemical Techniques*, University Press, Oxford (2008);
- [4] G. Höhne, W. Hemminger, H.-J. Flammersheim, *Differential Scanning Calorimetry: An Introduction for Practitioners*, Springer-Verlag, Berlin (1996);
- [5] G.D. Gatta, M.J. Richardson, S.M. Sarge, S. Stølen, *Pure Appl. Chem.* 78 (2006) 1455-1476;
- [6] R. Sabbah, A. Xu-Wu, J.S. Chickos, M.L. Planas Leitão, M.V. Roux, L.A. Torres, *Thermochim. Acta* 331 (1999) 93-204;
- [7] *DSC 141 User Manual*, Setaram Group, Lyon, France (1997);
- [8] *Pyris User Manual* (<http://mdi.as.nyu.edu/docs/CP/4738/DSC.Manual.pdf>);
- [9] A.L.R. Silva, *Ph. D. Thesis*, Faculty of Sciences, University of Porto (2015);
- [10] A.P.S.M.C. Carvalho, L.M.P.F. Amaral, private communication (2015);
- [11] S.S. Chang, A.B. Bestul, *J. Chem. Phys.* 56 (1972) 503-516;
- [12] M.V. Roux, M. Temprado, J.S. Chickos, Y. Nagano, *J. Phys. Chem. Ref. Data* 37 (2008) 1855-1996;
- [13] J.S. Chickos, W. Hanshaw, *J. Chem. Eng. Data* 49 (2004) 620-630;
- [14] R. Sabbah, L. El Watik, *J. Therm. Anal.* 38 (1992) 855-863;
- [15] P. Goursot, H.L. Girdhar, E.F. Westrum Jr., *J. Phys. Chem.* 74 (1970) 2538-2541;
- [16] A. Tian, *Bull. Soc. Chim. Fr. Ser. 4* (33) (1923) 427, cited in [23];
- [17] E. Calvet, *C. R. Acad. Sci. Paris* 226 (1948) 1702, cited in [23];
- [18] E. Calvet, H. Prat, *Recent Progress in Microcalorimetry*, Pergamon Press, New York (1963);
- [19] E. Calvet, chapter 12, in: *Experimental Thermochemistry*, vol. 1, F.D. Rossini (Ed.), Interscience, New York (1956);
- [20] E. Calvet, chapter 17, in: *Experimental Thermochemistry*, vol. 2, H.A. Skinner (Ed.), Interscience, New York (1962);

- [21] F.A. Adedeji, D.L.S. Brown, J.A. Connor, M.L. Leung, M.I. Paz-Andrade, H.A. Skinner, *J. Organomet. Chem.* 97 (1975) 221-228;
- [22] M.A.V. Ribeiro da Silva, M.A.R. Matos, L.M.P.F. Amaral, *J. Chem. Thermodyn.* 27 (1995) 565-574;
- [23] L.M.N.B.F. Santos, B. Schröder, O.O.P. Fernandes, M.A.V. Ribeiro da Silva, *Thermochim. Acta* 415 (2004) 15-20;
- [24] F.D. Rossini (Ed.), *Experimental Thermochemistry*, vol. 1, Interscience, New York (1956);
- [25] J.D. Cox, G. Pilcher, *Thermochemistry of Organic and Organometallic Compounds*, Academic Press, London/New York (1970);
- [26] L. Bjellerup, *Acta Chem. Scand.* 13 (1959) 1511-1531;
- [27] J. Coops, R.S. Jessup, K. Van Nes, chapter 3, in: *Experimental Thermochemistry*, vol. 1, F.D. Rossini (Ed.), Interscience, New York (1956);
- [28] I. Wadsö, *Sci. Tools* 13 (1966) 33-39;
- [29] W.D. Good, D.W. Scott, G. Waddington, *J. Phys. Chem.* 60 (1956) 1080-1089;
- [30] The NBS Tables of Chemical Thermodynamics Properties, *J. Phys. Chem. Ref. Data*, vol. 11, suppl. 2. (1982);
- [31] *Certificate of Analysis*, Standard Reference Material® 39j Benzoic Acid, N.I.S.T., Gaithersburg (2007);
- [32] J.D. Cox, chapter 4, in: S. Sunner, M. Månsson, (Eds.), *Experimental Chemical Thermodynamics*, vol.1, Pergamon Press, Oxford (1979);
- [33] E.W. Washburn, *J. Res. Nat. Bur. Stand.* 10 (1933) 525-558;
- [34] E.J. Prosen, *Natl. Bur. Stand. Report (USA)*, No. 1119 (1951), cited in ref. [35];
- [35] W.N. Hubbard, D.W. Scott, G. Waddington, chapter 5, in: *Experimental Thermochemistry*, vol. 1, F.D. Rossini (Ed.), Interscience, New York (1956);
- [36] W.D. Good, D.W. Scott, chapter 2, in: *Experimental Thermochemistry*, vol. 2, H.A. Skinner (Ed.), Interscience, New York (1962);
- [37] L. Smith, W.N. Hubbard, chapter 8, in: *Experimental Thermochemistry*, vol. 1, F.D. Rossini (Ed.), Interscience, New York (1956);
- [38] L. Bjellerup, chapter 3, in: *Experimental Thermochemistry*, vol. 2, H.A. Skinner (Ed.), Interscience, New York (1962);
- [39] A.T. Hu, G.C. Sinke, M. Månsson, B. Ringnér, *J Chem Thermodyn.* 4 (1972) 283-299;

- [40] J.D. Cox, D.D. Wagman, V.A. Medvedev, *CODATA key values for Thermodynamics*, Hemisphere Publishing Corp., New York (1989);
- [41] H.A. Gundry, D. Harrop, A.J. Head, G.B. Lewis, *J. Chem. Thermodyn.* 1 (1969) 321-332;
- [42] J.D. Cox, H.A. Gundry, A.J. Head, *Trans. Faraday Soc.* 60 (1964) 653-665;
- [43] J. Bickerton, G. Pilcher, G. Al-Takhin, *J. Chem. Thermodyn.* 16 (1984) 373-378;
- [44] M.D.M.C. Ribeiro da Silva, P. Souza, G. Pilcher, *J. Chem. Thermodyn.* 21 (1989) 173-178;
- [45] M.D.M.C. Ribeiro da Silva, L.M.N.B.F. Santos, A.L.R. Silva, O. Fernandes, W.E. Acree Jr., *J. Chem. Thermodyn.* 35 (2003) 1093-1100;
- [46] J.M. Gonçalves, *Ph. D. Thesis*, Faculty of Sciences, University of Porto (1996);
- [47] A.J. Head, W.D. Good, chapter 9, in: S. Sunner, M. Månsson, (Eds.), *Experimental Chemical Thermodynamics*, Vol.1, Pergamon Press, Oxford (1979);
- [48] A.I. Vogel, *A textbook of quantitative inorganic analysis including elementary instrumental analysis*, Longmans, London (1961);
- [49] A.R.R.P. Almeida, M.J.S. Monte, *Struct. Chem.* 24 (2013) 1993-1997;
- [50] M.J.S. Monte, in: M. E. Minas da Piedade (Ed.), *Energetics of Stable Molecules and Reactive Intermediates*, NATO ASI Series C, Kluwer Academic Publishers, Dordrecht (1999);
- [51] J.D. Cox, H.A. Gundry, D. Harrop, A.J. Head, *J. Chem. Thermodyn.* 1 (1969) 77-87;
- [52] S.P. Verevkin, V.N. Emel'yanenko, *Fluid Phase Equilib.* 266 (2008) 64-75;
- [53] M.J.S. Monte, L.M.N.B.F. Santos, M. Fulem, J.M.S. Fonseca, C.A.D. Sousa, *J. Chem. Eng. Data* 51 (2006) 757-766;
- [54] M. Fulem, K. Růžička, V. Růžička, T. Šimeček, E. Hulicius, J. Pangrác, *J. Chem. Thermodyn.* 38 (2006) 312-322;
- [55] K. Růžička, V. Majer, *AIChE J.* 42 (1996) 1723-1740;
- [56] C. Antoine, *CR Hebd. Acad. Sci.* 107 (1888) 681-684;
- [57] E.C.W. Clarke, D.N. Glew, *Trans. Faraday Soc.* 62 (1966) 539-547;
- [58] M.J.S. Monte, *Ph. D. Thesis*, Faculty of Sciences, University of Porto (1990);
- [59] M.A.V.R. Silva, M.J.S. Monte, *Thermochim. Acta.* 171 (1990) 169-183;
- [60] M.A.V.R. Silva, M.J.S. Monte, L.M.N.B.F. Santos, *J. Chem. Therm.* 38 (2006) 778-787;
- [61] M. Knudsen, *Ann. Physik* 28 (1909) 75-130, cited in [60];

- [62] M. Knudsen, *Ann. Physik* 28 (1909) 999-1016, cited in [60];
- [63] M. Knudsen, *Ann. Physik* 29 (1909) 179-193, cited in [60];
- [64] S. Dushman, *Scientific Foundations of Vacuum Technique*, John Wiley & Sons, Inc., New York (1989);
- [65] J.F. O'Halon, *User's Guide to Vacuum Technology*, John Wiley & Sons, New York (1989);
- [66] J.W. Hiby, M. Pahl, *Z. Naturforsch 7a* (1952) 542-553, cited in [58];
- [67] P. Clausing, *Ann. Physik* 12 (1932) 961-989, cited in [58];
- [68] I. Langmuir, *Phys. Rev.* 8 (1916) 149-176;
- [69] I. Langmuir, *J. Am. Chem. Soc.* 38 (1916) 2221-2295;
- [70] M.Z. Volmer, I. Estermann, *Z. Physik* 7 (1921) 13-17;
- [71] J.M.S. Fonseca, *M. Sc. Thesis*, Faculty of Sciences, University of Porto (2004);
- [72] L.M.N.B.F. Santos, *ADAM Control*, v1.1 (2006);
- [73] B. Valeur, *Molecular Fluorescence: Principles and Applications*, Wiley-VCH Verlag & Co., Weinheim, Germany (2001);
- [74] M. Sauer, J. Hofkens, Jörg Enderlein, *Handbook of Fluorescence Spectroscopy and Imaging - From Single Molecules to Ensembles*, Wiley-VCH Verlag & Co., Weinheim, Germany (2011);
- [75] J.R. Lakowicz, *Principles of fluorescence spectroscopy* (3rd Ed.), Springer, New York (2006);
- [76] J.R. Albani, *Principles and Applications of Fluorescence Spectroscopy*, Blackwell Publishing, Oxford, UK (2007);
- [77] Z. Pan, Y.-Y. Lu, F. Liu, *Nat. Mater.* 11 (2012) 58-63;
- [78] J.C. Koziar, D.O. Cowan, *Acc. Chem. Res.* 11 (1978) 334-341;
- [79] C. Würth, M. Grabolle, J. Pauli, M. Spieles, U. Resch-Genger, *Nat Protoc.* 8 (2013) 1535-1550;
- [80] <http://www.acktar.com/category/FluorescenceCrossword>, accessed in February 2016;
- [81] B. Wardle, *Principles and Applications of Photochemistry*, John Wiley & Sons, West Sussex, UK (2009);
- [82] A.M. Brouwer, *Pure Appl. Chem.* 83 (2011) 2213-2228;

- [83] K. Rurack, Springer Ser. Fluoresc. 5 (2008) 101-145;
- [84] J. Valenta, *Nanosci. Methods* 3 (2014) 11-27;
- [85] K. Suzuki, A. Kobayashi, S. Kaneko, K. Takehira, T. Yoshihara, H. Ishida, Y. Shiina, S. Oishi, S. Tobita, *Phys. Chem. Chem. Phys.* 11 (2009) 9850-9860;
- [86] I.B. Berlman, *Handbook of Fluorescence Spectra of Aromatic Molecules* (2nd Ed.), Academic Press, New York (1971);
- [87] T. Pagano, A.J. Biacchi, J.E. Kenny, *Appl. Spectrosc.* 62 (2008) 333-336;
- [88] T.-S. Ahn, R.O. Al-Kaysi, A.M. Müller, K.M. Wentz, C.J. Bardeen, *Rev. Sci. Instrum.* 78 (2007) 086105;
- [89] R. Kato, K. Suzuki, A. Furube, M. Kotani, K. Tokumaru, *J. Phys. Chem. C* 113 (2009) 2961-2965;
- [90] D.J. Norris, A.L. Efros, S.C. Erwin, *Science* 319 (2008) 1776-1779;
- [91] Agilent Technologies, *Agilent 8453 UV-Visible Spectroscopy System Operator's Manual*, G1115-90042 (July 2011);
- [92] Hamamatsu Photonics, *Absolute PL Quantum Yield Spectrometer Instruction Manual*, V1.12E (May 2012); Hamamatsu Photonics, *PLQY Measurement Software U6039-05 Instruction Manual*, V3.7.0.E (April 2014);
- [93] K. Iguchi (Hamamatsu Photonics K.K.), *Quantum-yield measurement device*. US Patent no. 8,592,780 B2 (2013);
- [94] G.T. Georgiev, J.J. Butler, *Appl Opt.* 46 (2007) 7892-7899;
- [95] K. Suzuki, (Application Note) *Nature Photonics* 5 (2011).

Chapter

4

Experimental results

- 4.1. Introduction to experimental results
- 4.2. Thermodynamic properties
- 4.3. Fluorescence properties

References

4.1. Introduction to the experimental results

In this chapter, it is presented all the detailed information regarding the origin and purification of the samples for study, as well as, all the experimental results for each compound studied, according to table 4.1. The experimental results of the test substances are presented in section C of the annexes.

Table 4.1. Experimental techniques used to determine thermodynamic and fluorescence properties of each of compound studied in this work.

Compound	DSC ^a	CM ^b	CC ^c	VP ^d	FS ^e
Fluorene					●
Naphthalene					●
Fluoranthene					●
2-SUBSTITUTED FLUORENES					
2-Fluorencarboxaldehyde	●		●	●	
2-Aminofluorene	●	●	●	●	●
2-Nitrofluorene	●	●	●	●	
2-Fluorofluorene	●		⊙	●	●
2-Bromofluorene	●		●	●	
2-Iodofluorene	●			●	
2,7-DISUBSTITUTED FLUORENES					
2,7-Di- <i>tert</i> -butylfluorene	●	○	●	●	●
2,7-Difluorofluorene	●			●	
2,7-Dichlorofluorene	●			●	
2,7-Dibromofluorene	●		●	●	
2,7-Diiodofluorene	●			●	
9-SUBSTITUTED FLUORENES					
9-Fluorencarboxylic acid	●	●	●	●	
9-Phenyl-9-fluorenol	○		●	○	
9-Benzylidene fluorene	●		●	●	
9-Fluorenemethanol	○		○	●	
9-Chlorofluorene	●			●	

.../...

.../...

2-SUBSTITUTED FLUORENONES				
2-Aminofluorenone	●	⊙	●	
2-Hydroxyfluorenone	●		●	
2-Fluorofluorenone	●		●	
2,7-SUBSTITUTED FLUORENONES				
2,7-Dinitrofluorenone			⊙	
2,7-Dibromofluorenone	●		●	
2,6-SUBSTITUTED NAPHTHALENES				
2,6-diethylnaphthalene	○	○	●	●
2,6-diisopropylnaphthalene	○	○	●	●
2,6-di- <i>tert</i> -butylnaphthalene	○	○	●	●
Test substances ^f				
Benzoic acid			●	
<i>N</i> -Methylnicotinamide			●	
Pyrene				●

^aDSC: temperatures and enthalpies of condensed phase transition determined by differential scanning calorimetry;

^bCM: sublimation enthalpies determined directly by Calvet microcalorimetry;

^cCC: massic energies of combustion determined by static or rotating bomb combustion calorimetry;

^dVP: vapor pressures of the condensed phases, determined by the Knudsen effusion method and/or the static method based on the diaphragm capacitance gauges;

^eFS: fluorescence properties, determined by fluorescence spectroscopy;

^fExperimental results presented in annex C.2.

(●, performed in this work; ⊙, incomplete study; ○, performed by other researchers.)

The experimental results are presented in tables and figures, when applicable. The following thermodynamic and fluorescence properties are reported:

Fusion

- Melting temperatures, enthalpies and entropies of fusion determined by differential scanning calorimetry and, for some compounds, also determined indirectly from the enthalpies of sublimation and vaporization;

Sublimation and vaporization

- Vapor pressures at different temperatures (determined by the Knudsen effusion method and/or the static method) and the derived standard molar ($p^{\circ} = 0.1$ MPa) enthalpies, entropies and Gibbs energies of sublimation and/or vaporization at the reference temperatures: $T = 298.15$ K, mean experimental temperature and triple

point temperature (when applicable); standard ($p^\circ = 0.1$ MPa) molar enthalpies of sublimation directly determined by Calvet microcalorimetry, at $T = 298.15$ K;

Combustion and formation reactions

- Standard massic energies of combustion, determined by combustion calorimetry and derived standard molar enthalpies of formation in the crystalline phase, at $T = 298.15$ K, which combined with the corresponding enthalpies of sublimation, enabled the determination of the standard molar enthalpies of formation in the gaseous phase;

Thermodynamic stability

- Standard molar Gibbs energies of formation in the crystalline and gaseous phases, determined from standard molar enthalpies of formation and standard molar entropy values;

Fluorescence properties

- Fluorescence spectroscopic data and quantum yield of the compounds in solution and in powder form, at room temperature.

4.2. Thermodynamic properties

4.2.1. General remarks

Contrary to what was anticipated in the beginning of this project, it was not possible to perform a complete thermodynamic study of all the compounds referred to above, particularly in what concerns the combustion calorimetry study.

This highly sensitive technique requires the use of samples with a very high degree of purity (ideally >0.999). The purification to the desired degree of some of the compounds studied proved to be extremely difficult or, in some cases, impossible with the available purification techniques. Consequently, the failure to get enough quantity of samples with the minimum degree of purity was the limiting factor that prevented the thermochemical study of 2-iodofluorene, 2-hydroxyfluorenone, 2-fluorofluorenone, 2,7-dinitrofluorenone and 2,7-dibromofluorenone.

The combustion study of 2-aminofluorenone was attempted, however, the compound presented an explosive behavior upon ignition and originated large amounts

of non-quantifiable carbon soot in the inner walls of the combustion bomb. Several combustion aids and experimental conditions were tested without success and the combustion study of 2-aminofluorenone is, so far, incomplete.

The measurement of the vapor pressures of 2,7-dinitrofluorenone by the Knudsen effusion method was tested, using both sets of effusion orifices used throughout this work. Both tests yielded vapor pressure results equally scattered and inaccurate, even upon repetition. The reason for this behavior was not possible to clarify.

In the case of the synthesized compounds, its study was conditioned by the amount of sample obtained. For the synthesized halofluorenes, it was possible to perform the vapor pressure measurements and phase transition studies. For the synthesized halofluorenones, only the microscale synthetic test was performed and the amount of sample obtained was limited. Macroscale repetitions of these syntheses were required, but were not possible due to time limitations in the course of this work.

For the compounds studied with success, the thermodynamic properties and respective uncertainties were derived from the obtained experimental results according to the calculations explained in detail the following points.

4.2.1.1. Thermodynamic properties of combustion

4.2.1.1.1. Calibration of the combustion calorimetric systems

The energy equivalents, ε_{cal} , of the used calorimetric systems were determined from the combustion benzoic acid (NIST Standard Reference Material 39j), in the presence of oxygen at a pressure $p = 3.04$ MPa and of 1.00 cm³ of deionized water.

For the static bomb combustion calorimeter, the energy equivalent had previously been determined by another researcher [1], $\varepsilon_{\text{cal}} = (15551.7 \pm 1.2)$ J·K⁻¹, and was periodically confirmed in the course of this work. For the rotating bomb combustion calorimeter used during this work, calibration experiments were performed without bomb rotation and the energy equivalent of the calorimeter, also determined by another researcher [2], was $\varepsilon_{\text{cal}} = (20361.4 \pm 0.6)$ J·K⁻¹.

The value for the pressure coefficient of massic energy for the compounds studied was assumed to be $(\partial u/\partial p)_T = -0.2$ J·g⁻¹·MPa⁻¹ [3], at $T = 298.15$ K, a typical value for most organic compounds.

4.2.1.1.2. Massic and molar energies and molar enthalpies of combustion

For the organic compounds of molecular formula $C_aH_bO_cN_d$ studied in this work, the massic energy, $\Delta_c u^0$, of the combustion reaction represented by the general chemical equation 3.5, was calculated by the procedure given by Hubbard *et al.* [4].

The accuracy of the calorimetric and analytical procedures used for the combustion of the organobromine compounds of molecular formula $C_aH_bO_cN_dBr_e$ studied in this work (general chemical equation 3.8) has been reported by other researchers [5,6] by measuring the standard massic combustion energy of the test substance 4-bromobenzoic acid, recommended by Bjellerup [7]. The applied standard state corrections were calculated by the procedure proposed by Bjellerup [8], and Sellers and Sunner [9].

In this work, the variation of adiabatic temperature was calculated using the LABTERMO software [10], specifically adapted to the each calorimetric system used. The standard massic and molar internal energies, and the molar enthalpies of combustion of the compounds studied were calculated according to the equations 3.39, 3.43 and 3.44, respectively, presented in section 3.2.2.2. The uncertainty associated to the mean standard massic energy of combustion refers the standard deviation of the mean of the independent results, σ , calculated through equation 4.1, where \bar{x} is the arithmetic average of n experimental results.

$$\sigma = \sqrt{\frac{\sum_{i=1}^n (x_i - \bar{x})^2}{n(n-1)}} \quad (4.1)$$

Adopting what was proposed by Rossini [11] and, later on, by Olofsson [12], the uncertainty interval associated with the standard molar energies of combustion is twice the standard deviation of the mean ($\pm 2\sigma$), of at least six results, ensuring a confidence level of 95 %. It was calculated by equation 4.2 and includes the uncertainties associated to the energy equivalent, and to the combustion of the calibrant and eventual auxiliary substances:

$$\frac{\sigma_{\Delta_c U_m^0}}{\Delta_c U_m^0} = 2 \sqrt{\left(\frac{\sigma_{\epsilon_{\text{cal}}}}{\epsilon_{\text{cal}}}\right)^2 + \left(\frac{\sigma_{\Delta_c u(\text{BA})}}{\Delta_c u(\text{BA})}\right)^2 + \left(\frac{\sigma_{\Delta_c u^0(\text{aux})}}{\Delta_c u^0(\text{aux})}\right)^2 + \left(\frac{\sigma_{\Delta_c u^0(\text{cpd})}}{\Delta_c u^0(\text{cpd})}\right)^2} \quad (4.2)$$

where:

$\varepsilon_{\text{cal}}, \sigma_{\varepsilon_{\text{cal}}}$	represent the mean value of the energy equivalent of the calorimeter and the corresponding standard deviation of the mean;
$\Delta_c u(\text{BA}), \sigma_{\Delta_c u(\text{BA})}$	represent the mean massic energy of combustion of benzoic acid, used as calibrant, and the corresponding standard deviation of the mean;
$\Delta_c u^\circ(\text{aux}), \sigma_{\Delta_c u^\circ(\text{aux})}$	represent the mean massic energy of combustion of auxiliary substances and the corresponding standard deviation of the mean;
$\Delta_c u^\circ(\text{cpd}), \sigma_{\Delta_c u^\circ(\text{cpd})}$	represent the mean massic energy of combustion of the compound under study and the corresponding standard deviation of the mean.

4.2.1.1.3. Apparent mass to true mass correction

All the necessary weightings for the combustion experiments were corrected from apparent mass values to true mass, under vacuum conditions, using the density, ρ . The values of ρ used, presented for each compound throughout this chapter, were compiled from the information contained in commercial catalogs, the literature database of the Royal Chemical Society (ChemSpider) [13], Yaws' book of thermophysical properties [14] and other literature sources. When it was not possible to source values in the literature, the density of the compounds was determined from the mass and volume ratio of pressed pellets of the samples. The pellets were weighed on an analytical balance Mettler Toledo AG 245 (with an accuracy of $\pm 10^{-5}$ g) and the dimensions of the tablets (diameter, $2r$, and height, h) were measured with a manual micrometer, enabling the determination of the respective volume V , according to the following expression:

$$V = \pi r^2 h \quad (4.3)$$

4.2.1.2. Thermodynamic properties of phase transition

4.2.1.2.1. Temperatures and standard molar properties of fusion

The phase transitions between condensed phases of the compounds studied were characterized by DSC. To characterize the transition associated to a peak, the onset temperatures and respective enthalpies of transition were determined. The uncertainties associated to these properties are twice the standard deviation of the mean of the individual results ($\pm 2\sigma$), where σ is calculated through equation 4.1.

4.2.1.2.2. Standard molar enthalpies of sublimation and vaporization

Thermodynamic properties of sublimation or vaporization often refer to the mean experimental temperature, $\langle T \rangle$, of the determinations. At the temperature $\langle T \rangle$, the standard molar enthalpy of sublimation or vaporization, $\Delta_{cr/l}^g H_m^o(\langle T \rangle)$, is the change in enthalpy of the isothermal process described by:



The standard states referred to in this process can be defined as follows [15]:

- For a crystalline compound is the state related to its most stable crystalline form, at a temperature T and a standard pressure of 0.1 MPa;
- For a liquid compound, as the state corresponding to the pure liquid, at a temperature T and a standard pressure of 0.1 MPa;
- For a gas, as the state of an ideal gas, at a temperature T and a standard pressure of 0.1 MPa, which is enthalpically equivalent to the real gas at the same temperature and zero pressure.

Considering the following thermochemical cycle, expression 4.4 can be deduced which relates the standard molar enthalpy of sublimation or vaporization at a given temperature T , with the molar enthalpy of sublimation or vaporization at the same temperature and at the equilibrium vapor pressure, $p(T)$:

$$\Delta_{cr/l}^g H_m^o(T) = \Delta H_1 + \Delta_{cr/l}^g H_m(T) + \Delta H_2 \quad (4.4)$$

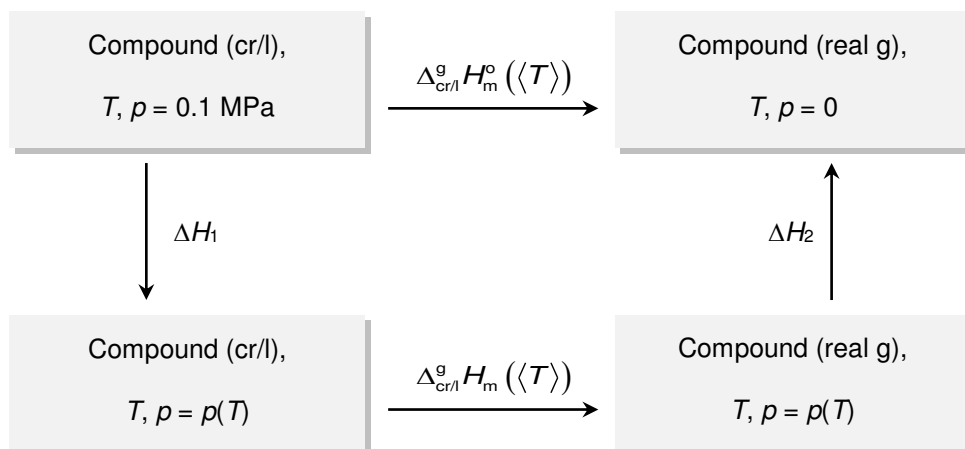


Figure 4.1. Thermodynamic cycle for deriving the dependence of the enthalpy of sublimation or vaporization enthalpy with pressure.

The ΔH_1 and ΔH_2 values can be calculated by equations 4.5 and 4.6, where V_m is the molar volume, relative to the solid or liquid phases in equation 4.5, and to the gas phase in equation 4.6. The contribution of the ΔH_1 and ΔH_2 terms in equation 4.4 will depend on the magnitude of p .

$$\Delta H_1 = \int_{0.1 \text{ MPa}}^{p(T)} \left[-T(\partial V/\partial T)_p + V_m \right] dp \quad (4.5)$$

$$\Delta H_2 = \int_{p(T)}^0 \left[-T(\partial V/\partial T)_p + V_m \right] dp \quad (4.6)$$

For one mole of a solid or liquid compound, the value of the integrand in equation 4.5, at $T = 298.15$ K, is about $10^{-1} \text{ dm}^3 \cdot \text{mol}^{-1}$ and can be considered independent of pressure [15,16]. Considering $p \approx 0$, the maximum value of ΔH_1 will be about $10 \text{ J} \cdot \text{mol}^{-1}$ which comparatively to a typical value of $\Delta_{\text{cr/l}}^{\text{g}} H_m(T)$ with a magnitude of (10^4 to 10^5) $\text{J} \cdot \text{mol}^{-1}$, can be neglected for the calculation of $\Delta_{\text{cr/l}}^{\text{g}} H_m(T)$.

Similarly, for one mole of a gaseous compound, the value of the integrand in equation 4.5, at $T = 298.15$ K, is between $(2-3) \cdot 10^{-2} \text{ m}^3 \cdot \text{mol}^{-1}$ and approximately independent of pressure [15,16]. Since low volatile (crystalline and liquid) organic compounds have vapor pressures far inferior than 0.1 MPa , at 298.15 K , the result of the difference $[(p = 0) - (p = p(T))]$, is usually very small, and ΔH_2 value is negligible when compared to ΔH_1 .

Considering these approximations, $\Delta_{\text{cr/l}}^{\text{g}} H_m(T) \approx \Delta_{\text{cr/l}}^{\text{g}} H_m^{\text{p}}(T)$ can be admitted without introducing significant errors.

Throughout this work, solid and liquid vapor pressures were fitted by a truncated form of Clarke-Glew equation (3.71), using the software SigmaPlot (version 10.0), in order to determine the standard molar thermodynamic properties of sublimation and vaporization of the compounds studied at selected reference temperatures: $T = 298.15$ K, the mean temperature of the experimental interval, and (when applicable) the triple point temperature. The uncertainties associated to the parameters are calculated from the standard deviations of the least squares regressions of the fitting.

For some of the compounds studied, the thermodynamic properties of sublimation were obtained by two different methods. In these cases, the weighed mean of both results, \bar{x}_w , is presented with the corresponding standard deviation, $\sigma_{\bar{x}_w}$, calculated through equations 4.7 and 4.8, where x_A and x_B are the individual values and σ_A and σ_B are the standard uncertainties associated to each value [12,17].

$$\bar{x}_w = \left(\frac{x_A}{\sigma_A^2} + \frac{x_B}{\sigma_B^2} \right) / \left(\frac{1}{\sigma_A^2} + \frac{1}{\sigma_B^2} \right) \quad (4.7)$$

$$\sigma_{\bar{x}_w} = \frac{1}{\sqrt{\frac{1}{\sigma_A^2} + \frac{1}{\sigma_B^2}}} \quad (4.8)$$

4.2.1.2.3. Enthalpies of sublimation and vaporization at a reference temperature

The standard molar enthalpy of sublimation or vaporization of a compound at $T = 298.25 \text{ K}$, $\Delta_{\text{cr/l}}^{\text{g}} H_{\text{m}}^{\circ}(298.15 \text{ K})$, can be related to its standard molar enthalpy of sublimation or vaporization at a temperature $\langle T \rangle$, $\Delta_{\text{cr/l}}^{\text{g}} H_{\text{m}}^{\circ}(\langle T \rangle)$, by the equation 4.9 (see section 3.3.1.3.2).

$$\Delta_{\text{cr/l}}^{\text{g}} H_{\text{m}}^{\circ}(298.15 \text{ K}) = \Delta_{\text{cr/l}}^{\text{g}} H_{\text{m}}^{\circ}(\langle T \rangle) + (298.15 \text{ K} - \langle T \rangle) \Delta_{\text{cr/l}}^{\text{g}} C_{\rho, \text{m}}^{\circ} \quad (4.9)$$

In this work, some of the $\Delta_{\text{cr/l}}^{\text{g}} C_{\rho, \text{m}}^{\circ}(298.15 \text{ K})$ values, assumed as constant for the considered temperature intervals, were estimated from the standard molar heat capacities of the crystalline, $C_{\rho, \text{m}}^{\circ}(\text{cr})$, and liquid phases, $C_{\rho, \text{m}}^{\circ}(\text{l})$, using respectively equations 4.10 and 4.11, developed by Chickos *et al.* [18],

$$\Delta_{\text{cr}}^{\text{g}} C_{\rho, \text{m}}^{\circ}(298.15 \text{ K}) / \text{J} \cdot \text{K}^{-1} \cdot \text{mol}^{-1} = -[0.75 + 0.15 C_{\rho, \text{m}}^{\circ}(\text{cr}, 298.15 \text{ K}) / \text{J} \cdot \text{K}^{-1} \cdot \text{mol}^{-1}] \quad (4.10)$$

$$\Delta_{\text{l}}^{\text{g}} C_{\rho, \text{m}}^{\circ}(298.15 \text{ K}) / \text{J} \cdot \text{K}^{-1} \cdot \text{mol}^{-1} = -[10.58 + 0.26 C_{\rho, \text{m}}^{\circ}(\text{l}, 298.15 \text{ K}) / \text{J} \cdot \text{K}^{-1} \cdot \text{mol}^{-1}] \quad (4.11)$$

or from the standard molar heat capacities of the gaseous phase, $C_{\rho, \text{m}}^{\circ}(\text{g}, 298.15 \text{ K})$, applying rearrangements of these equations, suggested by Monte and collaborators [19,20]:

$$\Delta_{\text{cr}}^{\text{g}} C_{\rho, \text{m}}^{\circ}(298.15 \text{ K}) / \text{J} \cdot \text{K}^{-1} \cdot \text{mol}^{-1} = -[0.9 + 0.176 C_{\rho, \text{m}}^{\circ}(\text{g}, 298.15 \text{ K}) / \text{J} \cdot \text{K}^{-1} \cdot \text{mol}^{-1}] \quad (4.12)$$

$$\Delta_{\rho,m}^g C_{\rho,m}^{\circ}(298.15 \text{ K}) / \text{J} \cdot \text{K}^{-1} \cdot \text{mol}^{-1} = -[14.3 + 0.35 C_{\rho,m}^{\circ}(\text{g}, 298.15 \text{ K}) / \text{J} \cdot \text{K}^{-1} \cdot \text{mol}^{-1}] \quad (4.13)$$

In the absence of experimental values of $C_{\rho,m}^{\circ}(\text{cr/l})$ and of computational values of $C_{\rho,m}^{\circ}(\text{g})$, they were estimated from those of fluorene and fluorenone through group contribution methods using data of structurally relevant molecules and/or group contributions proposed by Domalski and Hearing [21], and Chickos *et al.* [22], listed in table 4.2. For some of the compounds studied, vapor pressures measured over temperature ranges larger than 50 K enabled the estimation of a constant value of $\Delta_{\text{cr/l}}^g C_{\rho,m}^{\circ}$ through the Clarke-Glew equation (3.71).

Table 4.2. Data used for the estimation of $\Delta_{\text{cr/l}}^g C_{\rho,m}^{\circ}(298.15 \text{ K})$ of the compounds studied.

Molecules	$C_{\rho,m}^{\circ}(\text{g}, 298.15 \text{ K})$	$C_{\rho,m}^{\circ}(\text{l}, 298.15 \text{ K})$	$C_{\rho,m}^{\circ}(\text{cr}, 298.15 \text{ K})$
	J·K ⁻¹ ·mol ⁻¹		
Fluorene	173.1 [23]	261.5 [24]	203.13 [25]
Fluorenone	173.98 [26]		
Benzene	82.44 [27]		
Benzaldehyde	111.7 [28]		
Biphenylmethane			233.5 [29]
Triphenylmethanol			318.8 [29]
Triphenylethylene			309.2 [29]
Cyclopentane	82.8 [30]		
Chlorocyclopentane	98.86 [31]		
Groups^a			
C_B-(H)(C_B)₂	13.61 [21]		
C_B-(F)(C_B)₂	26.10 [21]		
C_B-(Cl)(C_B)₂	29.33 [21]		
C_B-(Br)(C_B)₂	29.65 [21]		
C_B-(I)(C_B)₂	32.70 [21]		
C_B-(O)(C_B)₂	15.86 [21]		
C_B-(N)(C_B)₂	16.07 [21]		
O-(C_B)(H)	18.16 [21]		
N-(C_B)(H)₂	24.35 [21]		
C_B(H)		21.8 [22]	
			.../...

.../...

C_B-(C)	15.3 [22]
C_c(H)-(C_c)₂(C)^b	25.9 [22]
C(H)₂-(C)₂	31.9 [22]
HO-(C)	53.1 [22]

^a According to Benson notation;

^b Subscript 'c', adopted in ref. [22] refers to ring atoms (not in Benson notation).

4.2.1.2.4. Standard molar entropies and Gibbs energies of sublimation and vaporization

The application of the Clarke-Glew equation (3.71) to the experimental vapor pressures results at different temperatures yields the determination of $\Delta_{\text{cr/l}}^{\text{g}}H_{\text{m}}^{\circ}(\theta)$ and $\Delta_{\text{cr/l}}^{\text{g}}G_{\text{m}}^{\circ}(\theta)$. The standard molar entropy of sublimation or vaporization, $\Delta_{\text{cr/l}}^{\text{g}}S_{\text{m}}^{\circ}(\theta)$, is easily calculated using equation 4.14.

$$\Delta_{\text{cr/l}}^{\text{g}}S_{\text{m}}^{\circ}(\theta) = \frac{\Delta_{\text{cr/l}}^{\text{g}}H_{\text{m}}^{\circ}(\theta) - \Delta_{\text{cr/l}}^{\text{g}}G_{\text{m}}^{\circ}(\theta)}{\theta} \quad (4.14)$$

The standard molar Gibbs energy of sublimation or vaporization, $\Delta_{\text{cr/l}}^{\text{g}}G_{\text{m}}^{\circ}$, at a reference temperature θ , is a measure of the volatility of a compound at that temperature, being related by equation 4.15 to its vapor pressure.

$$\Delta_{\text{cr/l}}^{\text{g}}G_{\text{m}}^{\circ}(\theta) = -R\theta \ln(p(\theta)/p^{\circ}) \quad (4.15)$$

4.2.1.2.5. Calorimetric determination of standard molar enthalpies of sublimation

The experimental uncertainty associated with $\Delta_{\text{cr}}^{\text{g}}H_{\text{m}}^{\circ}(298.15 \text{ K})$ determined by Calvet microcalorimetry, is twice the standard deviation of the mean, calculated by equation 4.16, and includes the uncertainties associated to the calibration constant, to the standard molar enthalpies of sublimation of the compound under study and of the substance used as calibrant.

$$\frac{\sigma_{\Delta_{cr}^g H_m^o(298.15\text{ K})}}{\Delta_{cr}^g H_m^o(298.15\text{ K})} = 2 \sqrt{\left(\frac{\sigma_{\langle k_{cal}(T) \rangle}}{\langle k_{cal}(T) \rangle} \right)^2 + \left(\frac{\sigma_{\Delta_{cr,298.15K}^{g,T} H_m^o}}{\Delta_{cr,298.15K}^{g,T} H_m^o} \right)^2 + \left(\frac{\sigma_{\Delta_{cr}^g H_m^o(\text{cal}, 298.15\text{ K})}}{\Delta_{cr}^g H_m^o(\text{cal}, 298.15\text{ K})} \right)^2} \quad (4.16)$$

where:

$\langle k_{cal}(T) \rangle$, $\sigma_{\langle k_{cal}(T) \rangle}$ represent the mean value of the calibration constant at the predefined temperature T , and the corresponding standard deviation of the mean;

$\Delta_{cr,298.15K}^{g,T} H_m^o$, $\sigma_{\Delta_{cr,298.15K}^{g,T} H_m^o}$ represent the standard molar enthalpy of sublimation of the compound under study at the predefined temperature T , and the corresponding standard deviation of the mean;

$\Delta_{cr}^g H_m^o(\text{cal}, 298.15\text{ K})$, represent the standard molar enthalpy of sublimation of the substance used as calibrant and the corresponding standard deviation of the mean.

4.2.1.3. Standard molar properties of formation, in crystalline and gaseous phases

The standard molar enthalpies of formation, in the crystalline phase, of some compounds studied were determined by equations 3.46 and 3.47 (deduced in section 3.2.2.2). Those equations are based on the standard molar enthalpies of combustion and on the standard molar enthalpies of formation of the other species involved in the combustion reaction. The values of $\Delta_f H_m^o$ of these species were taken from the literature and are recorded in table 4.3.

Table 4.3. Standard molar enthalpies of formation of the product compounds formed in the combustion reactions.

	$-\Delta_f H_m^o(298.15\text{ K})$ $\text{kJ} \cdot \text{mol}^{-1}$
CO ₂ , g	393.51 ± 0.13 [32]
H ₂ O, l	285.830 ± 0.040 [32]
HBr·600H ₂ O, l	120.924 ± 0.005 [32]
HF·10H ₂ O, l	322.034 ± 0.650 [33]

The experimental uncertainty associated to the values of standard molar enthalpies of formation include, in addition to the uncertainty associated with the standard molar enthalpy of combustion, the uncertainties related to the standard molar enthalpies of formation of the products formed in the combustion reaction, calculated through equation 4.17,

$$\sigma_{\Delta_f H_m^{\circ}(\text{cpd,cr})} = \sqrt{\left(\sigma_{\Delta_c H_m^{\circ}(\text{cpd,cr})}\right)^2 + \left(\nu_i \cdot \sigma_{\Delta_f H_m^{\circ}(\text{CO}_2,\text{g})}\right)^2 + \left(\nu_i \cdot \sigma_{\Delta_f H_m^{\circ}(\text{H}_2\text{O,l})}\right)^2 + \left(\nu_i \cdot \sigma_{\Delta_f H_m^{\circ}(\text{HBr}\cdot 600\text{H}_2\text{O,l})}\right)^2} \quad (4.17)$$

where ν_i represent the respective stoichiometric coefficients of all species in the equation that represents the combustion reaction.

The standard molar enthalpy of formation, in the gas phase, at $T = 298.15$ K, was determined from the standard molar enthalpy of formation, in the crystalline phase, and the standard molar enthalpy of sublimation by expression 4.18.

$$\Delta_f H_m^{\circ}(\text{g}, 298.15 \text{ K}) = \Delta_f H_m^{\circ}(\text{cr/l}, 298.15 \text{ K}) + \Delta_{\text{cr/l}}^{\text{g}} H_m^{\circ}(298.15 \text{ K}) \quad (4.18)$$

In addition to the standard enthalpies of formation, the standard molar entropies and Gibbs energies of formation, in crystalline and gaseous phases were also determined. From the standard molar entropy in the gas phase, $S_m^{\circ}(\text{g}, 298.15 \text{ K})$ (determined by other researchers using computational methods), it was possible to determine the standard molar entropies of formation in the gaseous phase, using equation 4.19, where all the properties refer to the temperature 298.15 K.

$$\Delta_f S_m^{\circ}(\text{g}) = S_m^{\circ}(\text{g}) - \sum_i \nu_i S_{m,i}^{\circ} \quad (4.19)$$

In this equation, $\sum_i \nu_i S_{m,i}^{\circ}$ is the sum of the standard molar entropies of the constituent elements, at standard state, multiplied by the stoichiometric coefficients according to the respective equations of formation of the compounds. In table 4.4 are listed the standard molar entropy values published in the literature [34], that were used in this work.

Table 4.4. Standard molar entropy values of the constituent elements.

Element	$\frac{S_m^\circ(298.15\text{ K})}{\text{J} \cdot \text{K}^{-1} \cdot \text{mol}^{-1}}$
C (graphite)	5.740
H ₂ (g)	130.680
N ₂ (g)	191.609
O ₂ (g)	205.147
Br ₂ (l)	152.206

Finally, the standard molar Gibbs energy of formation, in both crystalline and gaseous phases, were obtained through equations 4.20 and 4.21, respectively, by combining the standard molar enthalpies and entropies of formation, where all properties refer to $T = 298.15\text{ K}$.

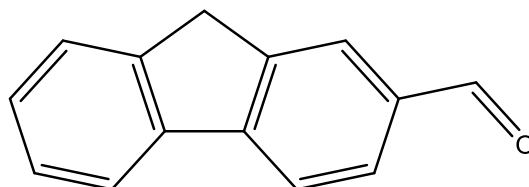
$$\Delta_f G_m^\circ(\text{g}) = \Delta_f H_m^\circ(\text{g}) - T \Delta_f S_m^\circ(\text{g}) \quad (4.20)$$

$$\Delta_f G_m^\circ(\text{cr}) = \Delta_f G_m^\circ(\text{g}) - \Delta_{\text{cr}}^{\text{g}} G_m^\circ \quad (4.21)$$

4.2.2. Experimental results

4.2.2.1. 2-Substituted fluorenes

4.2.2.1.1. 2-Fluorencarboxaldehyde



Molecular formula	CAS Number	Molar Mass	Density
C ₁₄ H ₁₀ O	30084-90-3	194.2276 g·mol ⁻¹	1.213 [35]

Table 4.5. Source, purification and analysis details of 2-fluorencarboxaldehyde.

Source	Lot	Minimum initial purity ^a	Purification method	Final mass fraction purity ^b
Sigma-Aldrich	S45338	0.992	Sublimation under reduced pressure	0.9995

^a Determined by GC, as stated in the certificate of analysis of the manufacturer;

^b Determined by GC.

Vapor pressures and thermodynamic properties of phase transition

Table 4.6. Temperatures, molar enthalpies and entropies of fusion of 2-fluorencarboxaldehyde.

Exp.	T_{fus} (onset)	$\Delta_{\text{cr}}^{\text{l}} H_{\text{m}}^{\circ}(T_{\text{fus}})$	$\Delta_{\text{cr}}^{\text{l}} S_{\text{m}}^{\circ}(T_{\text{fus}})$
	K	kJ·mol ⁻¹	J·K ⁻¹ ·mol ⁻¹
1	357.66	22.11	
2	357.68	22.09	
3	357.59	22.07	
4	357.53	22.01	
5	357.50	21.96	
6	357.69	22.08	
Mean	357.61 ± 0.07	22.05 ± 0.05	61.7 ± 0.1
Literature ^a	356 - 358		

^a Sigma-Aldrich, MSDS.

Table 4.7. Vapor pressures of 2-fluorene-carboxaldehyde determined by the Knudsen effusion method. ^a

T / K	t / s	Orifices	m / mg			p / Pa			
			m_{small}	m_{medium}	m_{large}	p_{small}	p_{medium}	p_{large}	p_{mean}
335.16	21894	A ₃ -B ₆ -C ₉	4.49	6.86	9.76	0.121	0.120	0.119	0.120
337.16	16533	A ₃ -B ₆ -C ₉	4.16	6.29	8.87	0.149	0.146	0.144	0.146
339.09	21894	A ₁ -B ₄ -C ₇	6.65	10.32	14.57	0.185	0.186	0.184	0.185
341.16	17397	A ₃ -B ₆ -C ₉			14.58			0.226	
341.11	16533	A ₂ -B ₅ -C ₈	6.36	9.73		0.232	0.230		
343.14	17397	A ₂ -B ₅ -C ₈			18.35			0.287	
343.08	16533	A ₁ -B ₄ -C ₇	7.77	11.98		0.287	0.287		
345.09	17397	A ₁ -B ₄ -C ₇	10.27	15.69	22.41	0.362	0.359	0.360	0.360
347.16	10254	A ₃ -B ₆ -C ₉	7.88	11.64	16.68	0.461	0.442	0.443	0.449
349.11	10254	A ₂ -B ₅ -C ₈	9.34	14.32	20.14	0.555	0.552	0.539	0.548
351.09	10254	A ₁ -B ₄ -C ₇	11.24	17.47	24.92	0.678	0.683	0.685	0.682
353.10	10263	A ₂ -B ₅ -C ₈	14.34	22.19	31.42	0.856	0.859	0.845	0.853
355.09	10263	A ₁ -B ₄ -C ₇	17.22	26.82	38.83	1.044	1.054	1.072	1.057

^a $u(T/K) = \pm 0.01$, $u(p/\text{Pa}) = \pm 0.01$.

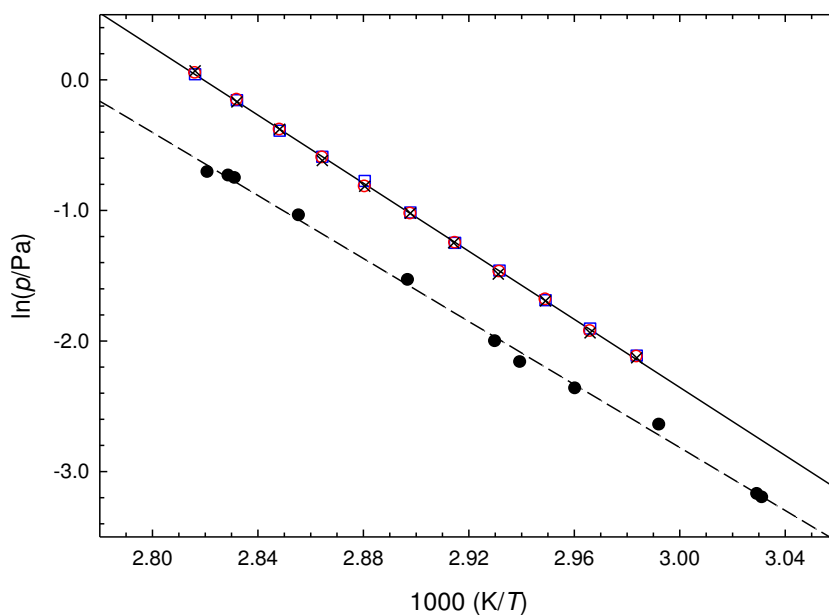


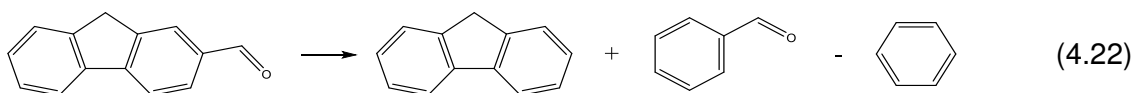
Figure 4.2. Plots of $\ln(p/\text{Pa})$ against $1000(K/T)$ of 2-fluorene-carboxaldehyde: effusion vapor pressures for the different effusion orifices - \square , small; \circ , medium; \times , large; \bullet , literature vapor pressure results [36].

Table 4.8. Standard ($p^\circ = 0.1$ MPa) molar properties of sublimation of 2-fluorene-carboxaldehyde, derived from the vapor pressure results determined experimentally and available in the literature.

$\Delta T / K$	θ / K	$\frac{\Delta_{cr}^g G_m^\circ(\theta)}{kJ \cdot mol^{-1}}$	$\frac{\Delta_{cr}^g H_m^\circ(\theta)}{kJ \cdot mol^{-1}}$	$\frac{\Delta_{cr}^g S_m^\circ(\theta)^a}{J \cdot K^{-1} \cdot mol^{-1}}$	$p(\theta)^b$ Pa	R^2	$\frac{\Delta_g^{cr} C_{p,m}^\circ}{J \cdot K^{-1} \cdot mol^{-1}}$	s^d
<i>Crystalline phase, effusion method</i>								
335.16-355.09	298.15	45.94 ± 0.08	110.1 ± 0.6	215.2 ± 2.0	$8.9 \cdot 10^{-4}$	0.9998	36.5	0.012
	345.13^e	35.96 ± 0.01	108.4 ± 0.6	209.9 ± 1.7	$3.6 \cdot 10^{-1}$			
<i>Crystalline phase, literature^f</i>								
329.9-354.5	298.15	46.21 ± 0.21	101.9 ± 1.6	186.8 ± 8.7	$8.0 \cdot 10^{-4}$	0.9977	36.5	0.048

^a Calculated through equation 4.14; ^b Calculated through equation 4.15; ^c Estimated value; ^d Standard deviation of the fit defined as $s = \sqrt{\left(\sum_{i=1}^n (\ln p - \ln p_{calc})_i^2\right) / (n - m)}$, where n is the number of experimental points used in the fit and m is the number of adjustable parameters in the Clarke and Glew equation; ^e Mean temperature; ^f Calculated from the literature vapor pressure results [36] using the value of $\Delta_{cr}^g C_{p,m}^\circ$ estimated in this work.

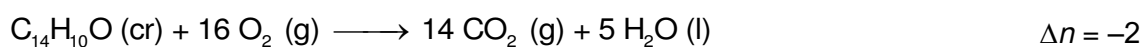
The value $C_{p,m}^\circ(g, 298.15K) = 202.36 J \cdot K^{-1} \cdot mol^{-1}$, estimated for this compound from the $C_{p,m}^\circ(g, 298.15K)$ values of fluorene [23], benzaldehyde [28] and benzene [27], using a group additivity approach according to equation 4.22 and data provided in table 4.2., was inserted into equation 4.12 yielding the result $\Delta_{cr}^g C_{p,m}^\circ = -36.5 J \cdot K^{-1} \cdot mol^{-1}$.



In figure 4.2, the experimental vapor pressure results for 2-fluorene-carboxaldehyde are represented with the literature vapor pressures previously reported by Goldfarb and Suuberg [36]. The literature's vapor pressure results are systematically smaller when compared to those of the present work. The standard molar enthalpy of sublimation, reported by Goldfarb and Suuberg, which refers to the mean experimental temperature, was corrected to $T = 298.15$ K, using the $\Delta_{cr}^g C_{p,m}^\circ$ value estimated in this work, yielding the value $\Delta_{cr}^g H_m^\circ(298.15 K) = (101.9 \pm 1.6) kJ \cdot mol^{-1}$, which is not in agreement with the one determined in the present work. These discrepancies may be related to the insufficient purity of the samples used by Goldfarb and Suuberg (minimum purity 0.95).

Combustion calorimetry and thermodynamic properties of formation

Combustion equation:

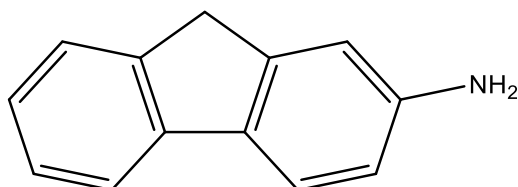
Table 4.9. Standard ($p^\circ = 0.1 \text{ MPa}$) massic energy of combustion of 2-fluorene-carboxaldehyde, at $T = 298.15 \text{ K}$.^a

Exp.	1	2	3	4	5	6	7
$m(\text{CO}_2, \text{total}) / \text{g}$	1.72227	1.73348	1.67135	1.57191	1.60672	1.66965	1.65070
$m(\text{cpd}) / \text{g}$	0.54141	0.54520	0.52568	0.49392	0.50513	0.52498	0.51910
$m(\text{fuse}) / \text{g}$	0.00296	0.00246	0.00233	0.00314	0.00268	0.00264	0.00246
$\Delta T_{\text{ad}} / \text{K}$	1.23774	1.24589	1.20055	1.12888	1.15411	1.19987	1.18478
$\varepsilon / \text{J}\cdot\text{K}^{-1}$	14.23	14.23	14.19	14.16	14.14	14.19	14.22
$\Delta m(\text{H}_2\text{O}) / \text{g}$	0.2	0.8	0.9	0.3	-0.4	-0.2	1.4
$-\Delta U(\text{IBP}) / \text{J}$	19266.94	19396.89	18691.06	17572.71	17962.09	18676.73	18449.99
$\Delta U(\text{fuse}) / \text{J}$	48.07	39.95	37.84	50.99	43.52	42.87	39.95
$\Delta U(\text{HNO}_3) / \text{J}$	0.20	1.48	0.33	0.48	0.48	0.22	0.18
$\Delta U(\text{ign}) / \text{J}$	0.67	0.72	1.09	0.70	0.67	0.69	0.86
$\Delta U_{\Sigma} / \text{J}$	12.01	12.10	11.61	10.85	11.11	11.60	11.44
$-\Delta_c u^\circ / \text{J}\cdot\text{g}^{-1}$	35475.26	35479.38	35461.27	35451.87	35450.24	35471.90	35442.92
$-\langle \Delta_c u^\circ \rangle = (35461.8 \pm 5.3) \text{ J}\cdot\text{g}^{-1}$							
$\langle \% \text{CO}_2 \rangle = (100.011 \pm 0.009) \%$							

^a $\varepsilon_{\text{cal}} = (15551.7 \pm 1.2) \text{ J}\cdot\text{K}^{-1}$.Table 4.10. Standard ($p^\circ = 0.1 \text{ MPa}$) molar energy and enthalpy of combustion, and derived standard molar enthalpies of formation of the crystalline and gaseous phases of 2-fluorene-carboxaldehyde, at $T = 298.15 \text{ K}$.

$-\Delta_c U_m^\circ(\text{cr})$	$-\Delta_c H_m^\circ(\text{cr})$	$-\Delta_f H_m^\circ(\text{cr})$	$\Delta_{\text{cr}}^g H_m^\circ$	$\Delta_f H_m^\circ(\text{g})$
$\text{kJ}\cdot\text{mol}^{-1}$	$\text{kJ}\cdot\text{mol}^{-1}$	$\text{kJ}\cdot\text{mol}^{-1}$	$\text{kJ}\cdot\text{mol}^{-1}$	$\text{kJ}\cdot\text{mol}^{-1}$
6887.7 ± 2.5	6892.6 ± 2.5	45.7 ± 3.1	110.2 ± 0.6	64.5 ± 3.2

4.2.2.1.2. 2-Aminofluorene



Molecular formula	CAS Number	Molar Mass	Density
C ₁₃ H ₁₁ N	153-78-6	181.2331 g·mol ⁻¹	1.0458 [14]

Table 4.11. Source, purification and analysis details of 2-aminofluorene.

Source	Lot	Minimum initial purity ^a	Purification method	Final mass fraction purity ^b
Sigma-Aldrich	S90850V	0.995	Sublimation under reduced pressure	0.9998

^a Determined by HPLC (area %), as stated in the certificate of analysis of the manufacturer;^b Determined by GC.

Vapor pressures and thermodynamic properties of phase transition

Table 4.12. Temperatures, molar enthalpies and entropies of fusion of 2-aminofluorene.

Exp.	T_{fus} (onset)	$\Delta_{\text{cr}}^{\text{l}} H_{\text{m}}^{\circ}(T_{\text{fus}})$	$\Delta_{\text{cr}}^{\text{l}} S_{\text{m}}^{\circ}(T_{\text{fus}})$
	K	kJ·mol ⁻¹	J·K ⁻¹ ·mol ⁻¹
1	401.11	23.78	
2	401.07	23.80	
3	400.96	23.78	
4	400.81	23.75	
5	400.85	23.81	
6	400.83	23.92	
Mean	400.9 ± 0.1	23.81 ± 0.05	59.4 ± 0.1
Literature	397 - 401 ^a		
	404.15 ^b		

^a Sigma-Aldrich, MSDS;^b Ref. [37], minimum purity 0.98.

Table 4.13. Standard ($p^\circ = 0.1$ MPa) molar enthalpy of sublimation of 2-aminofluorene, determined by Calvet microcalorimetry.

Exp.	m / mg	T / K	$\Delta_{\text{cr}, 298.15 \text{ K}}^{\text{g}, T} H_{\text{m}}^{\circ}$	$\Delta_{298.15 \text{ K}}^T H_{\text{m}}^{\circ}(\text{g})$	$\Delta_{\text{cr}}^{\text{g}} H_{\text{m}}^{\circ}(298.15 \text{ K})$
			$\text{kJ}\cdot\text{mol}^{-1}$	$\text{kJ}\cdot\text{mol}^{-1}$	$\text{kJ}\cdot\text{mol}^{-1}$
1	5.21	427.21	140.08	30.26	109.82
2	4.04	427.21	139.97	30.26	109.71
3	5.33	427.21	139.91	30.26	109.65
4	3.68	427.09	141.50	30.23	111.26
5	3.96	427.13	141.75	30.24	111.51
Mean		427.17			110.4 ± 1.7

The calorimeter was calibrated with high purity anthracene (details in table 3.2), and the calibration constant, k_{cal} , for the mean experimental temperature, $T = 427.2$ K, was found to be $k_{\text{cal}} = (1.0200 \pm 0.0020)$. The term $\Delta_{298.15 \text{ K}}^T H_{\text{m}}^{\circ}(\text{g})$ was calculated from the integration of the fitting of a 2nd degree polynomial to the $C_{p,m}^{\circ}(\text{g})$ results calculated at the B3LYP/6-31G(2df,p) level of theory [38], between $T = (290$ and $500)$ K:

$$C_{p,m}^{\circ}(\text{g}) = -4.99 \cdot 10^{-4} T^2 + 0.986 T - 56.79 \quad (4.23)$$

Table 4.14. Vapor pressures of 2-aminofluorene determined by the Knudsen effusion method. ^a

T / K	t / s	Orifices	m / mg			p / Pa			
			m_{small}	m_{medium}	m_{large}	p_{small}	p_{medium}	p_{large}	p_{mean}
345.16	43616	A ₃ -B ₆ -C ₉	8.51	13.03	18.36	0.121	0.120	0.118	0.120
347.13	43616	A ₂ -B ₅ -C ₈	10.65	16.57	22.81	0.154	0.155	0.148	0.152
349.17	27013	A ₃ -B ₆ -C ₉	8.02	12.63	17.39	0.190	0.189	0.182	0.187
351.15	27013	A ₂ -B ₅ -C ₈	10.18	15.69	21.44	0.238	0.238	0.226	0.234
353.10	27013	A ₁ -B ₄ -C ₇	12.24	18.59	26.12	0.291	0.286	0.283	0.287
355.17	10816	A ₃ -B ₆ -C ₉	6.08	9.28	13.21	0.362	0.350	0.348	0.353
357.13	10816	A ₂ -B ₅ -C ₈	7.32	11.69	16.42	0.432	0.447	0.436	0.438
359.16	10989	A ₃ -B ₆ -C ₉	9.35	14.64	20.02	0.551	0.546	0.522	0.540
361.13	10989	A ₂ -B ₅ -C ₈	11.38	17.83	24.59	0.664	0.675	0.647	0.662
363.10	10989	A ₁ -B ₄ -C ₇	13.57	21.14	29.22	0.805	0.811	0.789	0.802
365.09	10229	A ₁ -B ₄ -B ₆	15.55	24.11	24.29	0.994	0.997	0.981	0.991

^a $u(T/\text{K}) = \pm 0.01$, $u(p/\text{Pa}) = \pm 0.01$.

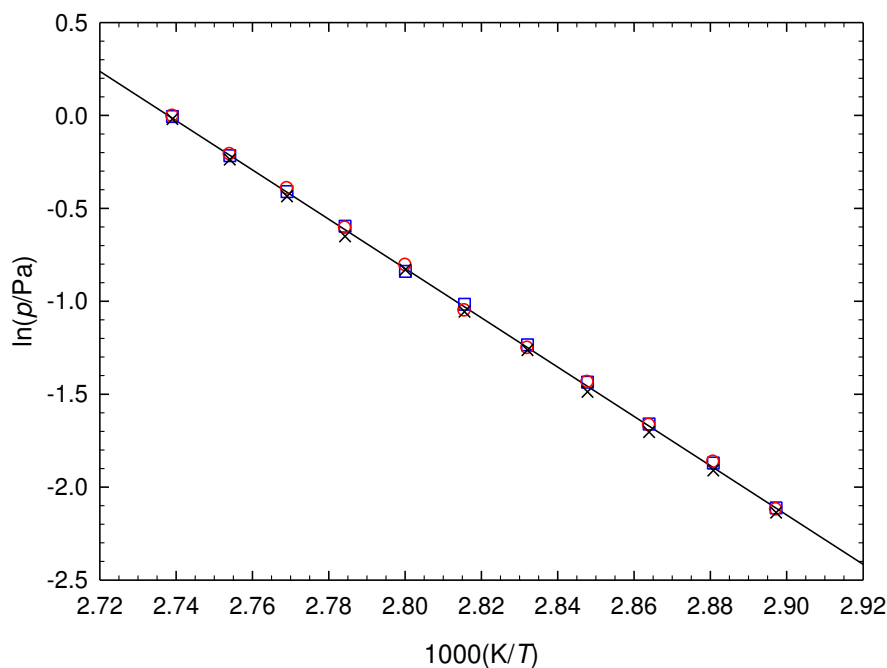


Figure 4.3. Plots of $\ln(p/\text{Pa})$ against $1000(K/T)$ of 2-aminofluorene: effusion vapor pressures for the different effusion orifices - \square , small; \circ , medium; \times , large.

Table 4.15. Standard ($p^\circ = 0.1$ MPa) molar properties of sublimation of 2-aminofluorene, derived from the experimental vapor pressure results.

$\Delta T / \text{K}$	θ / K	$\frac{\Delta_{\text{cr}}^{\text{g}} G_{\text{m}}^{\circ}(\theta)}{\text{kJ}\cdot\text{mol}^{-1}}$	$\frac{\Delta_{\text{cr}}^{\text{g}} H_{\text{m}}^{\circ}(\theta)}{\text{kJ}\cdot\text{mol}^{-1}}$	$\frac{\Delta_{\text{cr}}^{\text{g}} S_{\text{m}}^{\circ}(\theta)^{\text{a}}}{\text{J}\cdot\text{K}^{-1}\cdot\text{mol}^{-1}}$	$p(\theta)^{\text{b}}$ Pa	R^2	$\frac{\Delta_{\text{g}}^{\text{cr}} C_{\text{p,m}}^{\circ \text{c}}}{\text{J}\cdot\text{K}^{-1}\cdot\text{mol}^{-1}}$	s^{d}
<i>Crystalline phase, effusion method</i>								
345.16-365.09	298.15	48.97 ± 0.06	112.3 ± 0.4	212.4 ± 1.4	$2.8 \cdot 10^{-4}$	0.9999	34.8	0.007
	355.13^{e}	37.05 ± 0.01	110.3 ± 0.4	206.3 ± 1.1	$3.6 \cdot 10^{-1}$			

^a Calculated through equation 4.14; ^b Calculated through equation 4.15; ^c Estimated value; ^d Standard deviation of the fit defined as $s = \sqrt{\left(\sum_{i=1}^n (\ln p - \ln p_{\text{calc},i})^2\right) / (n - m)}$, where n is the number of experimental points used in the fit and m is the number of adjustable parameters in the Clarke and Glew equation; ^e Mean temperature.

The value of $C_{\text{p,m}}^{\circ}(\text{g}, 298.15\text{K}) = 192.85 \text{ J}\cdot\text{K}^{-1}\cdot\text{mol}^{-1}$, calculated at the B3LYP/6-31G(2df,p) level of theory [38], was inserted into equation 4.12, yielding the result $\Delta_{\text{cr}}^{\text{g}} C_{\text{p,m}}^{\circ} = -34.8 \text{ J}\cdot\text{K}^{-1}\cdot\text{mol}^{-1}$.

Combustion calorimetry and thermodynamic properties of formation

Combustion equation:



$$\Delta n = -2.25$$

Table 4.16. Standard ($p^\circ = 0.1 \text{ MPa}$) massic energy of combustion of 2-aminofluorene, at $T = 298.15 \text{ K}$.^a

Exp.	1	2	3	4	5	6
$m(\text{CO}_2, \text{ total}) / \text{g}$	1.12520	1.29003	1.63814	1.63504	1.55207	1.55451
$m(\text{cpd}) / \text{g}$	0.35491	0.40741	0.51742	0.51654	0.48982	0.49062
$m(\text{fuse}) / \text{g}$	0.00298	0.00313	0.00319	0.00274	0.00359	0.00353
$\Delta T_{\text{ad}} / \text{K}$	0.85587	0.98162	1.24594	1.24378	1.18105	1.18233
$\varepsilon / \text{J}\cdot\text{K}^{-1}$	13.74	13.90	14.15	14.14	14.05	14.09
$\Delta m(\text{H}_2\text{O}) / \text{g}$	-1.1	0.0	-1.1	0.0	-0.3	0.2
$-\Delta U(\text{IBP}) / \text{J}$	13317.25	15278.66	19387.58	19359.65	18381.56	18403.93
$\Delta U(\text{fuse}) / \text{J}$	48.40	50.83	51.81	44.50	58.30	57.33
$\Delta U(\text{HNO}_3) / \text{J}$	19.08	21.35	26.28	26.80	28.68	25.11
$\Delta U(\text{ign}) / \text{J}$	0.81	0.84	0.80	0.83	0.83	0.92
$\Delta U(\text{carb}) / \text{J}$		10.23	3.63			
$\Delta U_{\Sigma} / \text{J}$	7.64	8.86	11.51	11.47	10.82	10.86
$-\Delta_c U^\circ / \text{J}\cdot\text{g}^{-1}$	37311.23	37328.12	37303.56	37319.24	37327.51	37321.41
$-\langle \Delta_c U^\circ \rangle = (37318.5 \pm 3.9) \text{ J}\cdot\text{g}^{-1}$						
$\langle \% \text{ CO}_2 \rangle = (100.001 \pm 0.011) \%$						

^a $\varepsilon_{\text{cal}} = (15551.7 \pm 1.2) \text{ J}\cdot\text{K}^{-1}$.Table 4.17. Standard ($p^\circ = 0.1 \text{ MPa}$) molar energy and enthalpy of combustion, and derived standard molar enthalpies of formation of the crystalline and gaseous phases of 2-aminofluorene, at $T = 298.15 \text{ K}$.

$-\Delta_c U_m^\circ(\text{cr})$	$-\Delta_c H_m^\circ(\text{cr})$	$\Delta_f H_m^\circ(\text{cr})$	$\Delta_{\text{cr}}^g H_m^\circ$	$\Delta_f H_m^\circ(\text{g})$
$\text{kJ}\cdot\text{mol}^{-1}$	$\text{kJ}\cdot\text{mol}^{-1}$	$\text{kJ}\cdot\text{mol}^{-1}$	$\text{kJ}\cdot\text{mol}^{-1}$	$\text{kJ}\cdot\text{mol}^{-1}$
6763.3 ± 2.1	6768.9 ± 2.1	81.3 ± 2.7	112.3 ± 0.4^a	193.6 ± 2.7
			110.4 ± 1.7^b	191.7 ± 3.2
Mean			112.2 ± 0.4^c	193.5 ± 2.7

^a Derived from vapor pressure results;^b Derived from calorimetric results;^c Calculated as the weighted mean of the results.

Table 4.18. Standard ($p^\circ = 0.1$ MPa) molar absolute entropies and standard molar entropies, enthalpies and Gibbs energies of formation of the crystalline and gaseous phases of 2-aminofluorene, at $T = 298.15$ K.

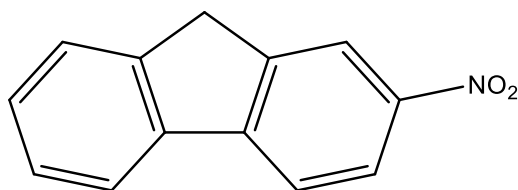
Phase	S_m°	$-T\Delta_f S_m^\circ$	$\Delta_f H_m^\circ$	$\Delta_f G_m^\circ$
	$\text{J}\cdot\text{K}^{-1}\cdot\text{mol}^{-1}$	$\text{kJ}\cdot\text{mol}^{-1}$	$\text{kJ}\cdot\text{mol}^{-1}$	$\text{kJ}\cdot\text{mol}^{-1}$
g	412.0 ^a	142.3	193.6 ± 2.7 ^c	335.9 ± 2.7
cr	199.6 ± 1.4 ^b	205.6 ± 1.4	81.3 ± 2.7	286.9 ± 2.7

^a Calculated at the B3LYP/6-31G(2df,p) level [38];

^b $S_m^\circ(\text{cr}) = S_m^\circ(\text{g}) - \Delta_{\text{cr}}^\circ S_m^\circ$;

^c Derived from vapor pressure results.

4.2.2.1.3. 2-Nitrofluorene



Molecular formula	CAS Number	Molar Mass	Density
C ₁₃ H ₉ NO ₂	607-57-8	211.2161 g·mol ⁻¹	1.1685 [14]

Table 4.19. Source, purification and analysis details of 2-nitrofluorene.

Source	Lot	Minimum initial purity ^a	Purification method	Final mass fraction purity ^b
Sigma-Aldrich	S43858	0.979	Recrystallization; Sublimation under reduced pressure	0.9996

^a Determined by HPLC (area %), as stated in the certificate of analysis of the manufacturer;^b Determined by GC.

During the purification process, the compound was subjected to successive recrystallizations using ethanol until the desired degree of purity was reached. The recrystallized compound was further subjected to sublimation under reduced pressure.

Vapor pressures and thermodynamic properties of phase transition

Table 4.20. Temperatures, molar enthalpies and entropies of fusion of 2-nitrofluorene.

Exp.	T_{fus} (onset)	$\Delta_{\text{cr}}^{\text{l}} H_{\text{m}}^{\circ}(T_{\text{fus}})$	$\Delta_{\text{cr}}^{\text{l}} S_{\text{m}}^{\circ}(T_{\text{fus}})$
	K	kJ·mol ⁻¹	J·K ⁻¹ ·mol ⁻¹
1	429.77	24.76	
2	429.61	24.79	
3	429.60	24.72	
4	429.71	24.82	
5	430.77	24.67	
Mean	429.9 ± 0.4	24.75 ± 0.05	57.6 ± 0.1
Literature ^a	429 - 431		

^a Sigma-Aldrich, MSDS.

Table 4.21. Standard ($p^\circ = 0.1$ MPa) molar enthalpy of sublimation of 2-nitrofluorene, determined by Calvet microcalorimetry.

Exp.	m / mg	T / K	$\Delta_{\text{cr}, 298.15 \text{ K}}^{\text{g}, T} H_{\text{m}}^{\circ}$	$\Delta_{298.15 \text{ K}}^T H_{\text{m}}^{\circ}(\text{g})$	$\Delta_{\text{cr}}^{\text{g}} H_{\text{m}}^{\circ}(298.15 \text{ K})$
			$\text{kJ}\cdot\text{mol}^{-1}$	$\text{kJ}\cdot\text{mol}^{-1}$	$\text{kJ}\cdot\text{mol}^{-1}$
1	3.21	432.11	146.83	33.08	113.75
2	2.98	432.14	147.71	33.09	114.63
3	2.48	432.09	147.71	33.07	114.64
4	3.16	432.19	146.99	33.10	113.89
5	2.43	432.07	147.41	33.07	114.34
Mean		432.12			114.2 ± 2.5

The calibration was performed with high purity anthracene (details in table 3.2), and the calibration constant k_{cal} , for the mean experimental temperature $T = 432.1$ K was found to be $k_{\text{cal}} = (1.0113 \pm 0.0107)$. The term $\Delta_{298.15 \text{ K}}^T H_{\text{m}}^{\circ}(\text{g})$ was calculated from the integration of the fitting of a 2nd degree polynomial to the $C_{\rho, \text{m}}^{\circ}(\text{g})$ results calculated at the B3LYP/6-31G(2df,p) level of theory [38], between $T = (290$ and $500)$ K:

$$C_{\rho, \text{m}}^{\circ}(\text{g}) = -5.05 \cdot 10^{-4} T^2 + 1.00 T - 51.20 \quad (4.24)$$

 Table 4.22. Vapor pressures of 2-nitrofluorene determined by the Knudsen effusion method. ^a

T / K	t / s	Orifices	m / mg			p / Pa			
			m_{small}	m_{medium}	m_{large}	ρ_{small}	ρ_{medium}	ρ_{large}	ρ_{mean}
357.16	46967	A ₃ -B ₆ -C ₉	7.25	11.4	16.03	0.090	0.092	0.090	0.091
359.13	46967	A ₂ -B ₅ -C ₈	9.07	14.03	19.47	0.114	0.115	0.111	0.113
361.11	46967	A ₁ -B ₄ -C ₇	10.91	16.94	23.90	0.140	0.141	0.139	0.140
363.16	25135	A ₃ -B ₆ -C ₉	7.15	11.3	15.95	0.172	0.172	0.170	0.171
365.14	25135	A ₂ -B ₅ -C ₈	8.96	14.08	19.54	0.213	0.217	0.209	0.213
367.11	25135	A ₁ -B ₄ -C ₇	10.68	16.7	23.42	0.258	0.261	0.258	0.259
369.16	14496	A ₃ -B ₆ -C ₉	7.68	11.86	16.95	0.322	0.315	0.315	0.317
371.13	14496	A ₂ -B ₅ -C ₈	9.42	14.78	20.13	0.392	0.398	0.377	0.389
373.10	14496	A ₁ -B ₄ -C ₇	11.23	17.51	24.56	0.474	0.478	0.472	0.475
375.15	10130	A ₃ -B ₆ -C ₉	9.56	14.76	20.92	0.578	0.565	0.561	0.568
377.14	10130	A ₂ -B ₅ -C ₈	11.61	18.20	25.09	0.696	0.707	0.678	0.694
379.12	11149	A ₁ -B ₄ -C ₇	15.15	23.56	32.89	0.839	0.844	0.829	0.837

^a $u(T/\text{K}) = \pm 0.01$, $u(p/\text{Pa}) = \pm 0.01$.

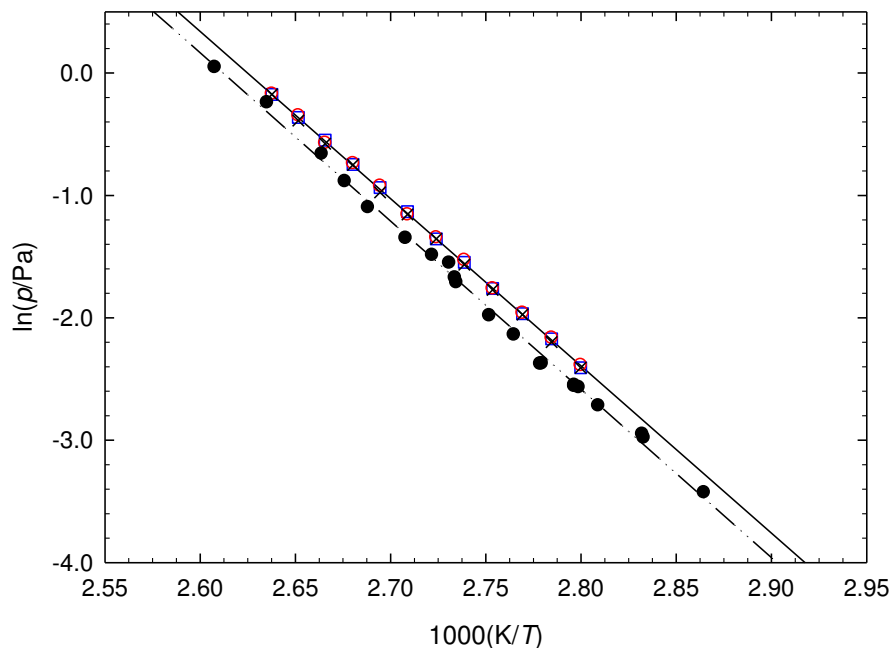


Figure 4.4. Plots of $\ln(p/\text{Pa})$ against $1000(\text{K}/T)$ of 2-nitrofluorene: effusion vapor pressures for the different effusion orifices - \square , small; \circ , medium; \times , large; \bullet , literature vapor pressure results [36].

Table 4.23. Standard ($p^\circ = 0.1 \text{ MPa}$) molar properties of sublimation of 2-nitrofluorene, derived from the vapor pressure results determined experimentally and available in the literature.

$\Delta T / \text{K}$	θ / K	$\frac{\Delta_{\text{cr}}^{\text{g}} G_{\text{m}}^{\circ}(\theta)}{\text{kJ}\cdot\text{mol}^{-1}}$	$\frac{\Delta_{\text{cr}}^{\text{g}} H_{\text{m}}^{\circ}(\theta)}{\text{kJ}\cdot\text{mol}^{-1}}$	$\frac{\Delta_{\text{cr}}^{\text{g}} S_{\text{m}}^{\circ}(\theta)^a}{\text{J}\cdot\text{K}^{-1}\cdot\text{mol}^{-1}}$	$p(\theta)^b$ Pa	R^2	$\frac{\Delta_{\text{g}}^{\text{cr}} C_{\rho,\text{m}}^{\circ c}}{\text{J}\cdot\text{K}^{-1}\cdot\text{mol}^{-1}}$	s^d
<i>Crystalline phase, effusion method</i>								
357.16-379.12	298.15	53.49 ± 0.06	116.2 ± 0.3	210.3 ± 1.0	$4.7\cdot 10^{-5}$	0.9999	36.6	0.007
	368.14 ^e	39.06 ± 0.01	113.6 ± 0.3	202.5 ± 0.8	$2.9\cdot 10^{-1}$			
<i>Crystalline phase, literature^f</i>								
349.1-384.5	298.15	54.07 ± 0.26	116.7 ± 1.4	210.1 ± 4.8	$3.4\cdot 10^{-5}$	0.9972	36.6	0.052

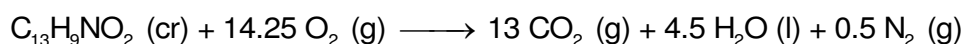
^a Calculated through equation 4.14; ^b Calculated through equation 4.15; ^c Estimated value; ^d Standard deviation of the fit defined as $s = \sqrt{\frac{\sum_{i=1}^n (\ln p - \ln p_{\text{calc}})^2}{(n - m)}}$, where n is the number of experimental points used in the fit and m is the number of adjustable parameters in the Clarke and Glew equation; ^e Mean temperature; ^f Calculated from the literature vapor pressure results [36] using the value of $\Delta_{\text{g}}^{\text{cr}} C_{\rho,\text{m}}^{\circ}$ estimated in this work..

The value of $C_{\rho,\text{m}}^{\circ}(\text{g}, 298.15\text{K}) = 192.85 \text{ J}\cdot\text{K}^{-1}\cdot\text{mol}^{-1}$, calculated at the B3LYP/6-31G(2df,p) level of theory [38], was inserted into equation 4.12, yielding the result $\Delta_{\text{cr}}^{\text{g}} C_{\rho,\text{m}}^{\circ} = -36.6 \text{ J}\cdot\text{K}^{-1}\cdot\text{mol}^{-1}$.

In figure 4.4, the experimental vapor pressure results are shown together with literature vapor pressures results previously reported by Goldfarb and Suuberg [36]. The present work's vapor pressures are systematically slightly higher when compared to those of the literature, but both regressions present identical slopes and consequently agreeing enthalpies of sublimation. The reported standard molar enthalpy of sublimation, which is referred to the mean experimental temperature, was corrected to the temperature $T = 298.15$ K, using the $\Delta_{\text{cr}}^{\text{g}}C_{p,m}^{\text{o}}$ value estimated in the present work, yielding the value $\Delta_{\text{cr}}^{\text{g}}H_{\text{m}}^{\text{o}}(298.15 \text{ K}) = (116.7 \pm 1.4) \text{ kJ}\cdot\text{mol}^{-1}$, that is within experimental uncertainty of the result determined in the present work.

Combustion calorimetry and thermodynamic properties of formation

Combustion equation:



$$\Delta n = -0.75$$

Table 4.24. Standard ($p^{\circ} = 0.1$ MPa) massic energy of combustion of 2-nitrofluorene, at $T = 298.15$ K.^a

Exp.	1	2	3	4	5	6
$m(\text{CO}_2, \text{total}) / \text{g}$	1.08487	1.51549	1.63924	1.02196	1.44683	1.20875
$m(\text{cpd}) / \text{g}$	0.39897	0.55790	0.60349	0.37578	0.53253	0.44477
$m(\text{fuse}) / \text{g}$	0.00258	0.00290	0.00280	0.00251	0.00268	0.00264
$\Delta T_{\text{ad}} / \text{K}$	0.78728	1.09883	1.19083	0.74180	1.04997	0.87727
$\bar{\alpha}_1 / \text{J}\cdot\text{K}^{-1}$	13.65	13.80	13.97	13.62	13.81	13.76
$\Delta m(\text{H}_2\text{O}) / \text{g}$	0.5	0.6	-1.5	-1.3	-1.1	-1.6
$-\Delta U(\text{IBP}) / \text{J}$	12255.09	17105.66	18527.70	11541.71	16337.79	13648.67
$\Delta U(\text{fuse}) / \text{J}$	41.90	47.10	45.47	40.76	43.52	42.87
$\Delta U(\text{HNO}_3) / \text{J}$	19.88	35.07	32.07	18.50	32.67	19.10
$\Delta U(\text{ign}) / \text{J}$	0.85	0.93	0.86	0.64	0.70	0.56
$\Delta U(\text{carb}) / \text{J}$		3.63				2.64
$\Delta U_{\Sigma} / \text{J}$	8.40	11.97	13.10	7.88	11.40	9.44
$-\Delta_c U^{\circ} / \text{J}\cdot\text{g}^{-1}$	30540.92	30498.57	30550.73	30535.34	30515.09	30532.41
	$-\langle \Delta_c U^{\circ} \rangle = (30528.8 \pm 7.7) \text{ J}\cdot\text{g}^{-1}$					
	$\langle \% \text{ CO}_2 \rangle = (100.009 \pm 0.020) \%$					

^a $\epsilon_{\text{cal}} = (15551.7 \pm 1.2) \text{ J}\cdot\text{K}^{-1}$.

Table 4.25. Standard ($p^\circ = 0.1$ MPa) molar energy and enthalpy of combustion, and derived standard molar enthalpies of formation of the crystalline and gaseous phases of 2-nitrofluorene, at $T = 298.15$ K.

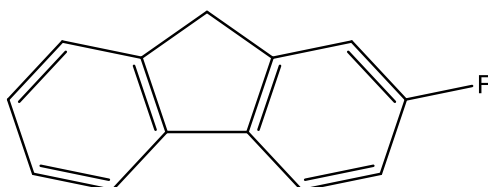
$-\Delta_c U_m^\circ(\text{cr})$	$-\Delta_c H_m^\circ(\text{cr})$	$\Delta_f H_m^\circ(\text{cr})$	$\Delta_{\text{cr}}^g H_m^\circ$	$\Delta_f H_m^\circ(\text{g})$
$\text{kJ}\cdot\text{mol}^{-1}$	$\text{kJ}\cdot\text{mol}^{-1}$	$\text{kJ}\cdot\text{mol}^{-1}$	$\text{kJ}\cdot\text{mol}^{-1}$	$\text{kJ}\cdot\text{mol}^{-1}$
6448.2 ± 3.5	6450.0 ± 3.5	48.2 ± 3.9	116.2 ± 0.3^a	164.4 ± 3.9
			114.2 ± 2.5^b	162.4 ± 4.6
		Mean	116.2 ± 0.3^c	164.4 ± 3.9

^a Derived from vapor pressure results;^b Derived from calorimetric results;^c Calculated as the weighted mean of the results.Table 4.26. Standard ($p^\circ = 0.1$ MPa) molar absolute entropies and standard molar entropies, enthalpies and Gibbs energies of formation of the crystalline and gaseous phases of 2-nitrofluorene, at $T = 298.15$ K.

Phase	S_m°	$-T\Delta_f S_m^\circ$	$\Delta_f H_m^\circ$	$\Delta_f G_m^\circ$
	$\text{J}\cdot\text{K}^{-1}\cdot\text{mol}^{-1}$	$\text{kJ}\cdot\text{mol}^{-1}$	$\text{kJ}\cdot\text{mol}^{-1}$	$\text{kJ}\cdot\text{mol}^{-1}$
g	443.1^a	155.2	164.4 ± 3.9^c	319.6 ± 3.9
cr	232.8 ± 1.0^b	217.9 ± 1.0	48.2 ± 3.9	266.1 ± 3.9

^a Calculated at the B3LYP/6-31G(2df,p) level [38];^b $S_m^\circ(\text{cr}) = S_m^\circ(\text{g}) - \Delta_{\text{cr}}^g S_m^\circ$;^c Derived from vapor pressure results.

4.2.2.1.4. 2-Fluorofluorene



Molecular formula	CAS Number	Molar Mass	Density
C ₁₃ H ₉ F	343-43-1	184.2080 g·mol ⁻¹	1.207 [39]

Table 4.27. Source, purification and analysis details of 2-fluorofluorene.

Source	Lot	Minimum initial purity ^a	Purification method	Final mass fraction purity ^b
TCI Europe	FCO01	0.998	Sublimation under reduced pressure	0.9999

^a Determined by GC, as stated in the certificate of analysis of the manufacturer;

^b Determined by GC.

Vapor pressures and thermodynamic properties of phase transition

Table 4.28. Temperatures, molar enthalpies and entropies of fusion of 2-fluorofluorene.

Exp.	T_{fus} (onset) K	$\Delta_{\text{cr}}^{\text{l}} H_{\text{m}}^{\circ}(T_{\text{fus}})$ kJ·mol ⁻¹	$\Delta_{\text{cr}}^{\text{l}} S_{\text{m}}^{\circ}(T_{\text{fus}})$ J·K ⁻¹ ·mol ⁻¹	T_{tp}^{a} K	$\Delta_{\text{cr}}^{\text{l}} H_{\text{m}}^{\circ}(T_{\text{tp}})^{\text{b}}$ kJ·mol ⁻¹	$\Delta_{\text{cr}}^{\text{l}} S_{\text{m}}^{\circ}(T_{\text{tp}})$ J·K ⁻¹ ·mol ⁻¹
1	373.06	22.43				
2	373.20	22.37				
3	372.99	22.45				
4	373.07	22.40				
5	373.23	22.36				
Mean	373.11 ± 0.09	22.40 ± 0.03	60.04 ± 0.08	372.56	22.78 ± 0.09	61.1 ± 0.2
Lit. ^c	371.65					

^a Triple point temperature derived indirectly from vapor pressure results;

^b Determined indirectly from the $\Delta_{\text{cr}}^{\text{g}} H_{\text{m}}^{\circ}(T_{\text{tp}})$ and $\Delta_{\text{cr}}^{\text{g}} S_{\text{m}}^{\circ}(T_{\text{tp}})$ values presented in table 4.30;

^c TCI Europe, certificate of analysis.

Table 4.29. Vapor pressures of 2-fluorofluorene determined by the static method with capacitance manometers. ^a

<i>T/K</i>	<i>p/Pa</i>	$100\Delta p/p^b$	<i>T/K</i>	<i>p/Pa</i>	$100\Delta p/p^b$	<i>T/K</i>	<i>p/Pa</i>	$100\Delta p/p^b$
<i>Crystalline phase</i>								
321.04	0.963	−0.6	338.98	5.878	0.5	354.64	24.11	0.5
323.02	1.195	0.1	340.85	6.991	0.2	356.58	28.41	0.3
325.03	1.456	−1.1	342.80	8.387	0.3	358.73	33.77	−0.6
327.00	1.795	−0.4	344.75	9.981	−0.2	360.45	39.15	−0.1
329.01	2.214	0.2	346.73	11.91	−0.5	362.68	47.13	0
330.92	2.665	−0.4	348.84	14.48	0.2	364.51	54.25	−0.8
332.94	3.286	0.5	350.67	17.20	1.2	366.63	64.54	−0.5
335.02	4.027	0.6	352.67	20.39	0.7	368.46	74.46	−0.8
336.92	4.841	0.7						
<i>Liquid phase^c</i>								
350.71	26.65	−0.3	372.43	102.6	0	394.26	332.1	0
352.68	30.61	0.6	374.49	114.9	−0.5	396.11	364.1	0
354.63	34.50	−0.2	376.39	128.4	−0.1	398.19	402.3	−0.3
356.66	39.38	−0.1	378.44	144.1	0	4004	442.3	0.2
358.59	44.47	−0.1	380.29	159.9	0.2	402.12	486.2	−0.4
360.58	50.53	0.2	382.45	179.9	0.2	404.10	537.4	0.2
362.56	56.89	−0.2	384.27	198.1	0.1	406.06	586.3	−0.3
364.55	64.42	0	386.38	221.4	0	408.03	644.9	0.1
366.49	72.53	0.2	388.21	243.7	0	409.98	705.6	0.1
368.47	81.56	0.2	390.33	271.8	−0.1	411.88	768.8	0.1
370.45	91.57	0.1	392.25	300.8	0.3			

^a $u(T) = \pm 0.01$ K, $u(p/\text{Pa}) = 0.01 + 0.0025(p/\text{Pa})$ for gauge I;^b $\Delta p = p - p_{\text{calc}}$, where p_{calc} is calculated from the Clarke and Glew equation with parameters given in table 4.30;^c Including supercooled liquid.

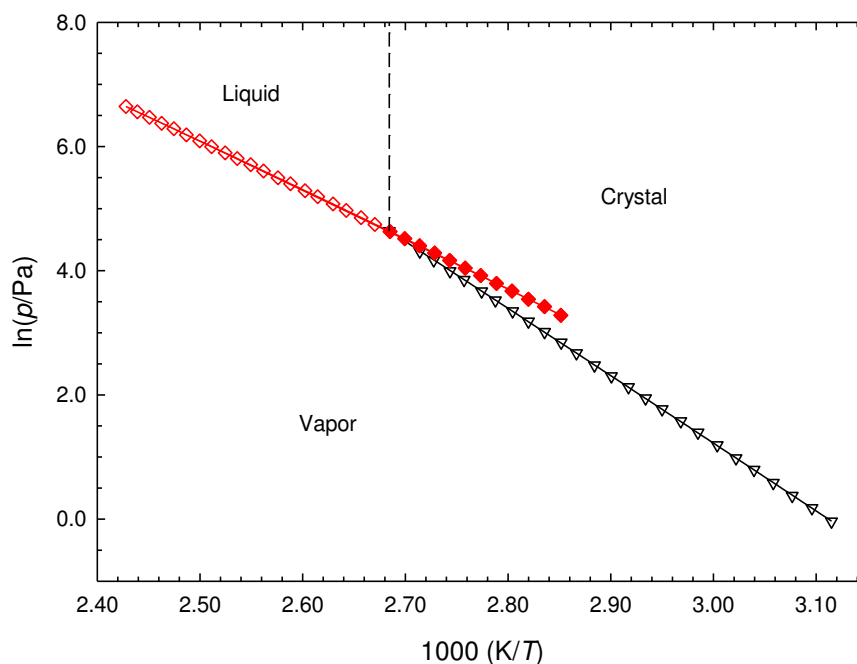


Figure 4.5. Phase diagram ($\ln(p/\text{Pa})$ against $1000(K/T)$) of 2-fluorofluorene: ∇ , crystal vapor pressures; \diamond , liquid vapor pressures; \blacklozenge , supercooled liquid vapor pressures (triple point coordinates: $T_{\text{tp}} = 372.56 \text{ K}$; $p_{\text{p}} = 103.5 \text{ Pa}$).

Table 4.30. Standard ($p^\circ = 0.1 \text{ MPa}$) molar properties of sublimation and vaporization of 2-fluorofluorene, derived from the experimental vapor pressure results.

$\Delta T / \text{K}$	θ / K	$\frac{\Delta_{\text{cr/l}}^g G_m^\circ(\theta)}{\text{kJ}\cdot\text{mol}^{-1}}$	$\frac{\Delta_{\text{cr/l}}^g H_m^\circ(\theta)}{\text{kJ}\cdot\text{mol}^{-1}}$	$\frac{\Delta_{\text{cr/l}}^g S_m^\circ(\theta)^a}{\text{J}\cdot\text{K}^{-1}\cdot\text{mol}^{-1}}$	$p(\theta)^b$ Pa	R^2	$\frac{\Delta_{\text{g}}^{\text{cr/l}} C_{p,m}^\circ}{\text{J}\cdot\text{K}^{-1}\cdot\text{mol}^{-1}}$	s^c
<i>Crystalline phase, static method</i>								
	298.15	35.13 ± 0.01	91.72 ± 0.08	189.8 ± 0.3	$7.0 \cdot 10^{-2}$			
321.04-368.46	345.13^d	26.33 ± 0.01	90.15 ± 0.08	184.9 ± 0.2	$1.0 \cdot 10^1$	1.0000	33.6^f	0.006
	372.56^e	21.29 ± 0.01	89.23 ± 0.08	182.4 ± 0.2	$1.0 \cdot 10^2$			
<i>Liquid phase, static method^g</i>								
	298.15	30.89 ± 0.03	71.86 ± 0.26	137.4 ± 0.9	$3.9 \cdot 10^{-1}$			
350.71-411.88	381.30^d	20.24 ± 0.01	65.82 ± 0.03	119.5 ± 0.1	$1.7 \cdot 10^2$	1.0000	72.7 ± 3.2^h	0.002
	372.56^e	21.29 ± 0.01	66.45 ± 0.04	121.2 ± 0.1	$1.0 \cdot 10^2$			

^a Calculated through equation 4.14; ^b Calculated through equation 4.15; ^c Standard deviation of the fit defined as

$$s = \sqrt{\left(\sum_{i=1}^n (\ln p - \ln p_{\text{calc}})^2 \right) / (n - m)},$$

where n is the number of experimental points used in the fit and m is the number of

adjustable parameters in the Clarke and Glew equation; ^d Mean temperature; ^e Triple point temperature; ^f Estimated value;

^g Including supercooled liquid; ^h Adjustable parameter.

The value $C_{\rho,m}^{\circ}$ (g, 298.15 K) was estimated for this compound from the value $C_{\rho,m}^{\circ}$ (g, 298.15 K) of fluorene [23] using a group additivity approach according to equation 4.25 and data provided in table 4.2. The resulting value, $C_{\rho,m}^{\circ}$ (g, 298.15 K) = 185.6 J·K⁻¹·mol⁻¹, was inserted into equation 4.12 yielding the result: $\Delta_{cr}^g C_{\rho,m}^{\circ} = -33.6$ J·K⁻¹·mol⁻¹.

$$C_{\rho,m}^{\circ}(\text{Fluorene}) - [1 \times \mathbf{C}_B\text{-(H)}(\mathbf{C}_B)_2] + [1 \times \mathbf{C}_B\text{-(F)}(\mathbf{C}_B)_2] \quad (4.25)$$

The value $\Delta_1^g C_{\rho,m}^{\circ} = -(72.7 \pm 3.2)$ J·K⁻¹·mol⁻¹ was obtained by adjusting the Clarke and Glew equation (eq. 3.71) to the experimental vapor pressures results of the liquid phase.

Combustion calorimetry and thermodynamic properties of formation

Combustion equation:



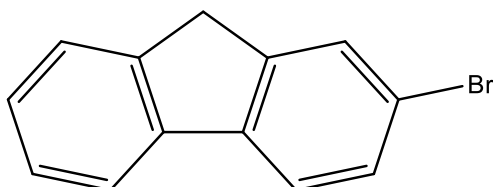
The study of 2-fluorofluorene by rotating bomb combustion calorimetry was performed by another researcher [40], but not completed due to lack of compound and an equipment operating problem. The preliminary values, however, determined from the mean of four experimental combustion experiments, are presented bellow and provide an approximation of the enthalpy of formation of the crystalline and gaseous phases of 2-fluorofluorene.

Table 4.31. Preliminary results for the standard ($p^{\circ} = 0.1$ MPa) molar energy and enthalpy of combustion, and derived standard molar enthalpies of formation of the crystalline and gaseous phases of 2-fluorofluorene, at $T = 298.15$ K.

$-\langle \Delta_c U^{\circ} \rangle^a$	$-\Delta_c U_m^{\circ}(\text{cr})$	$-\Delta_c H_m^{\circ}(\text{cr})$	$-\Delta_f H_m^{\circ}(\text{cr})$	$\Delta_{cr}^g H_m^{\circ}$	$-\Delta_f H_m^{\circ}(\text{g})$
J·g ⁻¹	kJ·mol ⁻¹	kJ·mol ⁻¹	kJ·mol ⁻¹	kJ·mol ⁻¹	kJ·mol ⁻¹
35190.6 ± 4.8	6482.4 ± 2.1	6487.3 ± 2.1	93.6 ± 2.8	91.72 ± 0.08	1.9 ± 2.8

^a $\epsilon_{\text{cal}} = (25146,4 \pm 1.3)$ J·K⁻¹ [41].

4.2.2.1.5. 2-Bromofluorene



Molecular formula	CAS Number	Molar Mass	Density
C ₁₃ H ₉ Br	1133-80-8	245.1136 g·mol ⁻¹	1.4168 [14]

Table 4.32. Source, purification and analysis details of 2-bromofluorene.

Source	Lot	Minimum initial purity ^a	Purification method	Final mass fraction purity ^b
TCI Europe	EHZXB	0.999	Sublimation under reduced pressure	0.9999

^a Determined by GC, as stated in the certificate of analysis of the manufacturer;

^b Determined by GC.

Vapor pressures and thermodynamic properties of phase transition

Table 4.33. Temperatures, molar enthalpies and entropies of fusion of 2-bromofluorene.

Exp.	T_{fus} (onset) K	$\Delta_{\text{cr}}^{\text{l}} H_{\text{m}}^{\circ}(T_{\text{fus}})$ kJ·mol ⁻¹	$\Delta_{\text{cr}}^{\text{l}} S_{\text{m}}^{\circ}(T_{\text{fus}})$ J·K ⁻¹ ·mol ⁻¹	T_{tp}^{a} K	$\Delta_{\text{cr}}^{\text{l}} H_{\text{m}}^{\circ}(T_{\text{tp}})^{\text{b}}$ kJ·mol ⁻¹	$\Delta_{\text{cr}}^{\text{l}} S_{\text{m}}^{\circ}(T_{\text{tp}})$ J·K ⁻¹ ·mol ⁻¹
1	387.42	16.81				
2	387.38	17.21				
3	387.40	17.07				
4	387.40	17.02				
5	387.34	16.99				
Mean	387.39 ± 0.03	17.0 ± 0.1	43.9 ± 0.3	385.08	18.8 ± 0.2	48.8 ± 0.5
Lit.	381.5-383.1 ^c	16.02 ^c	41.90 ^c			
	387.55 ^d					

^a Triple point temperature derived indirectly from vapor pressure results;

^b Determined indirectly from the $\Delta_{\text{cr}}^{\text{g}} H_{\text{m}}^{\circ}(T_{\text{tp}})$ and $\Delta_{\text{f}}^{\text{g}} H_{\text{m}}^{\circ}(T_{\text{tp}})$ values presented in table 4.36;

^c Ref. [42], minimum purity 0.95;

^d TCI Europe, certificate of analysis.

Table 4.34. Vapor pressures of 2-bromofluorene determined by the Knudsen effusion method.^a

T / K	t/s	Orifices	m / mg			p / Pa			
			m_{small}	m_{medium}	m_{large}	p_{small}	p_{medium}	p_{large}	p_{mean}
327.17	37154	A ₃ -B ₆ -C ₉	8.44	13.04	18.61	0.118	0.119	0.118	0.118
329.13	37154	A ₂ -B ₅ -C ₈	10.44	16.31	23.07	0.148	0.150	0.148	0.149
331.09	37154	A ₁ -B ₄ -C ₇	12.68	19.85	28.34	0.183	0.186	0.186	0.185
333.16	20435	A ₃ -B ₆ -C ₉	8.70	13.39	19.35	0.229	0.223	0.225	0.226
335.14	20435	A ₂ -B ₅ -C ₈	10.70	16.55	23.45	0.279	0.280	0.275	0.278
337.11	20435	A ₁ -B ₄ -C ₇	12.93	20.21	28.72	0.343	0.347	0.346	0.345
339.16	10172	A ₃ -B ₆ -C ₉	7.97	12.34	17.63	0.425	0.417	0.416	0.419
341.14	10172	A ₂ -B ₅ -C ₈	9.48	15.01	21.05	0.501	0.515	0.501	0.506
343.10	10172	A ₁ -B ₄ -C ₇	11.78	18.03	25.60	0.634	0.627	0.626	0.629
345.16	10213	A ₃ -B ₆ -C ₉	14.13	22.07	31.47	0.758	0.749	0.747	0.751
347.09	10213	A ₂ -B ₅ -C ₈	17.46	26.99	38.01	0.928	0.929	0.909	0.922
349.09	10213	A ₁ -B ₄ -C ₇	20.73	32.19	45.87	1.120	1.125	1.127	1.124

^a $u(T/K) = \pm 0.01$, $u(p/\text{Pa}) = \pm 0.01$.

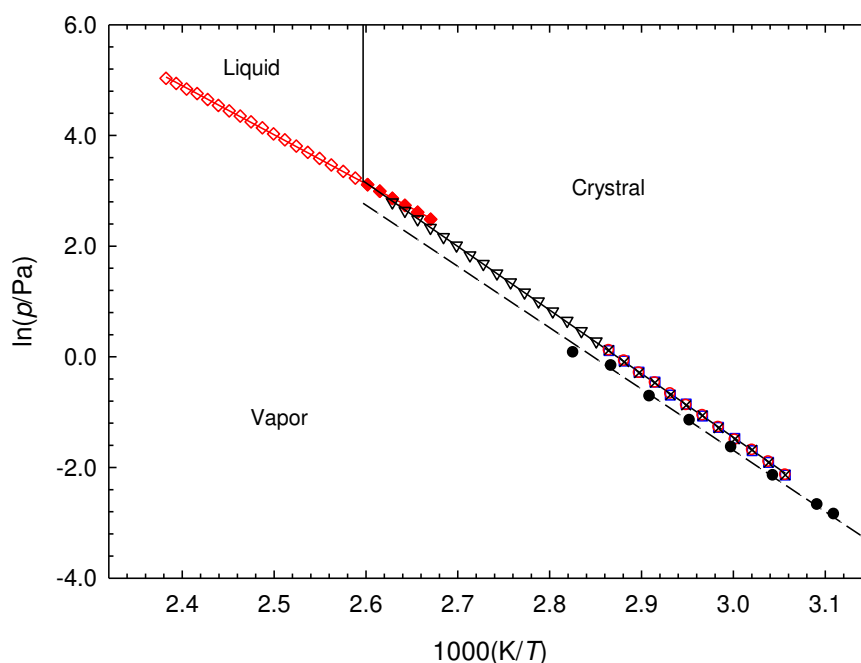


Figure 4.6. Phase diagram ($\ln(p/\text{Pa})$ against $1000(K/T)$) of 2-bromofluorene: effusion crystal vapor pressures for the different effusion orifices - \square , small; \circ , medium; \times , large; static vapor pressures - ∇ , crystal vapor pressures; \diamond , liquid vapor pressures; \blacklozenge , supercooled liquid vapor pressures (triple point coordinates: $T_{\text{tp}} = 385.08 \text{ K}$; $p_{\text{tp}} = 23.44 \text{ Pa}$); \bullet , literature vapor pressure results [42].

Table 4.35. Vapor pressures of 2-bromofluorene determined by the static method with capacitance manometers. ^a

<i>T</i> /K	<i>p</i> /Pa	100Δ <i>p</i> / <i>p</i> ^{<i>b</i>}	<i>T</i> /K	<i>p</i> /Pa	100Δ <i>p</i> / <i>p</i> ^{<i>b</i>}	<i>T</i> /K	<i>p</i> /Pa	100Δ <i>p</i> / <i>p</i> ^{<i>b</i>}
<i>Crystalline phase</i>								
350.80	1.323	−0.5	362.65	3.848	0.5	372.53	8.716	−0.4
352.79	1.593	−0.2	364.63	4.520	−0.3	374.50	10.30	0.4
354.74	1.921	0.8	366.60	5.367	0.2	376.47	12.02	0.1
356.73	2.274	−0.2	368.56	6.271	−0.7	378.44	14.03	−0.1
358.70	2.726	0.5	370.56	7.492	0.6	380.40	16.34	−0.1
360.67	3.206	−0.6						
<i>Liquid phase</i> ^{<i>c</i>}								
374.47	12.00	−0.5	390.28	32.01	0.2	405.99	77.40	0.8
376.47	13.62	−0.7	392.25	36.02	0.5	407.97	84.99	−0.4
378.44	15.41	−0.9	394.21	40.22	0.3	409.95	93.80	−0.6
380.40	17.49	−0.5	396.18	45.06	0.4	411.90	104.5	−0.1
382.39	19.92	0.2	398.13	50.46	0.8	413.88	116.4	0.6
384.36	22.44	0	400.11	56.25	0.7	415.84	126.4	−1.1
386.34	25.29	0	402.06	62.80	1.0	417.81	139.8	−0.8
388.31	28.54	0.4	404.05	69.88	0.9	419.77	153.4	−1.2

^a $u(T) = \pm 0.01$ K, $u(p/\text{Pa}) = 0.01 + 0.0025(p/\text{Pa})$ for gauge I and $u(p/\text{Pa}) = 0.1 + 0.0025(p/\text{Pa})$ for gauge II;

^b $\Delta p = p - p_{\text{calc}}$, where p_{calc} is calculated from the Clarke and Glew equation with parameters given in table 4.36;

^c Including supercooled liquid.

 Table 4.36. Standard ($p^\circ = 0.1$ MPa) molar properties of sublimation and vaporization of 2-bromofluorene, derived from the vapor pressure results determined experimentally and available in the literature.

ΔT /K	θ /K	$\frac{\Delta_{\text{cr/l}}^g G_m^\circ(\theta)}{\text{kJ}\cdot\text{mol}^{-1}}$	$\frac{\Delta_{\text{cr/l}}^g H_m^\circ(\theta)}{\text{kJ}\cdot\text{mol}^{-1}}$	$\frac{\Delta_{\text{cr/l}}^g S_m^\circ(\theta)^a}{\text{J}\cdot\text{K}^{-1}\cdot\text{mol}^{-1}}$	$\frac{p(\theta)^b}{\text{Pa}}$	R^2	$\frac{\Delta_{\text{g}}^{\text{cr/l}} C_{p,m}^\circ}{\text{J}\cdot\text{K}^{-1}\cdot\text{mol}^{-1}}$	s^d
<i>Crystalline phase, effusion method</i>								
327.17-349.09	298.15	42.46 ± 0.05	98.05 ± 0.44	186.4 ± 1.5	3.6·10 ^{−3}	0.9998	34.7	0.011
	338.13 ^e	35.09 ± 0.01	96.66 ± 0.44	182.1 ± 1.3	3.8·10 ^{−1}			
<i>Crystalline phase, static method</i>								
	298.15	42.18 ± 0.03	96.43 ± 0.14	182.0 ± 0.5	3.4·10 ^{−3}			
350.80-380.40	365.60 ^e	30.15 ± 0.01	94.08 ± 0.14	174.9 ± 0.4	4.9	1.0000	34.7	0.005
	385.08 ^f	26.76 ± 0.01	93.41 ± 0.14	173.1 ± 0.4	2.3·10 ¹			
<i>Crystalline phase, literature</i> ^{<i>g</i>}								
303.9-353.9	298.15	42.64 ± 0.15	94.2 ± 1.5	172.9 ± 5.1	3.4·10 ^{−3}	0.9970	34.7	0.095

.../...

.../...

Liquid phase, static method^h

298.15	38.44 ± 0.03	81.72 ± 0.13	145.2 ± 0.4	1.8·10 ⁻²				
374.47-419.77	397.12 ^e	25.28 ± 0.01	73.64 ± 0.13	121.8 ± 0.3	4.7·10 ¹	0.9999	81.6	0.007
385.08 ^f	26.76 ± 0.01	74.63 ± 0.13	124.3 ± 0.3	2.3·10 ¹				

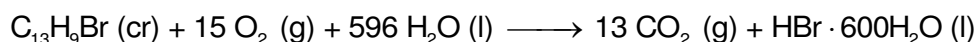
^a Calculated through equation 4.14; ^b Calculated through equation 4.15; ^c Estimated values; ^d Standard deviation of the fit defined as $s = \sqrt{\left(\sum_{i=1}^n (\ln p - \ln p_{\text{calc}})_i^2\right) / (n - m)}$, where n is the number of experimental points used in the fit and m is the number of adjustable parameters in the Clarke and Glew equation; ^e Mean temperature; ^f Triple point temperature; ^g Calculated from the literature vapor pressure results [42] using the value of $\Delta_{\text{cr}}^{\text{g}}C_{\rho,m}^{\text{o}}$ estimated in this work; ^h Including supercooled liquid.

The value of $C_{\rho,m}^{\text{o}}(\text{g}, 298.15\text{K}) = 192.16 \text{ J}\cdot\text{K}^{-1}\cdot\text{mol}^{-1}$ was calculated at the B3LYP/6-311++G(d,p) level of theory [20], and inserted into equations 4.12 and 4.13, respectively yielding the results $\Delta_{\text{cr}}^{\text{g}}C_{\rho,m}^{\text{o}} = -34.7 \text{ J}\cdot\text{K}^{-1}\cdot\text{mol}^{-1}$ and $\Delta_1^{\text{g}}C_{\rho,m}^{\text{o}} = -81.6 \text{ J}\cdot\text{K}^{-1}\cdot\text{mol}^{-1}$.

The vapor pressure results previously reported by Fu and Suuberg [42] are slightly smaller when compared to those of the present work. Their reported standard molar enthalpy of sublimation, which refers to the mean experimental temperature, was corrected to $T = 298.15 \text{ K}$, using the $\Delta_{\text{cr}}^{\text{g}}C_{\rho,m}^{\text{o}}$ estimated in the present work, yielding the values compiled in table 4.36. The enthalpy of sublimation, $\Delta_{\text{cr}}^{\text{g}}H_{\text{m}}^{\text{o}}(298.15 \text{ K}) = (94.2 \pm 1.5) \text{ kJ}\cdot\text{mol}^{-1}$, presents a mean variation of approximately $-3 \text{ kJ}\cdot\text{mol}^{-1}$ when compared to the mean of the results obtained in this work with the effusion and static methods. These discrepancies may be related to the insufficient purity of the samples used by Fu and Suuberg (minimum purity 0.95).

Combustion calorimetry and thermodynamic properties of formation

Combustion equation:



$$\Delta n = -2$$

Table 4.37. Standard ($p^\circ = 0.1$ MPa) massic energy of combustion of 2-bromofluorene, at $T = 298.15$ K.^a

Exp.	1	2	3	4	5	6
$m(\text{cpd}) / \text{g}$	0.48935	0.67978	0.66958	0.70230	0.70014	0.67599
$m(\text{fuse}) / \text{g}$	0.00301	0.00315	0.00252	0.00212	0.00239	0.00234
T_i / K	297.3129	297.2191	297.2636	297.2010	297.1953	297.1939
T_f / K	297.9995	298.1508	298.1801	298.1612	298.1539	298.1217
$\Delta T_{\text{ad}} / \text{K}$	0.64526	0.89494	0.88155	0.92411	0.92106	0.89031
$\epsilon_i / \text{J}\cdot\text{K}^{-1}$	53.75	53.91	53.90	53.93	53.93	53.91
$\epsilon_f / \text{J}\cdot\text{K}^{-1}$	53.00	53.18	53.19	53.20	53.19	53.18
$\Delta m(\text{H}_2\text{O}) / \text{g}$	3.8	2.5	1.7	0.8	3.1	-0.9
$-\Delta U(\text{IBP}) / \text{J}$	13182.36	18278.78	18002.26	18867.96	18814.62	18171.50
$\Delta U(\text{fuse}) / \text{J}$	48.88	51.16	40.92	34.43	38.81	38.00
$\Delta U(\text{HNO}_3) / \text{J}$	4.66	2.39	5.01	3.46	2.75	3.58
$\Delta U(\text{As}_2\text{O}_3)^a / \text{J}$	161.07	220.94	217.52	228.40	229.07	220.56
$\Delta U(\text{H}_2\text{PtBr}_6) / \text{J}$	0.06	0.11	0.02	0.06	0.04	0.04
$\Delta U(\text{ign}) / \text{J}$	1.12	1.12	1.11	1.12	1.12	1.12
$\Delta U(\text{carb}) / \text{J}$		0.99				
$\Delta U_\Sigma / \text{J}$	15.11	20.92	20.58	21.57	21.51	20.77
$-\Delta_c U^\circ / \text{J}\cdot\text{g}^{-1}$	26468.95	26455.99	26461.68	26455.99	26455.34	26462.74
$-\langle \Delta_c U^\circ \rangle = (26460.1 \pm 2.2) \text{ J}\cdot\text{g}^{-1}$						

^a $\epsilon_{\text{cal}} = (20361.4 \pm 0.6) \text{ J}\cdot\text{K}^{-1}$;

^bThe compound was burnt in the presence of 10.00 cm^3 of an aqueous solution of As_2O_3 ($0.1154 \text{ mol}\cdot\text{dm}^{-3}$).

 Table 4.38. Standard ($p^\circ = 0.1$ MPa) molar energy and enthalpy of combustion, and derived standard molar enthalpies of formation of the crystalline and gaseous phases of 2-bromofluorene, at $T = 298.15$ K.

$-\Delta_c U_m^\circ(\text{cr})$	$-\Delta_c H_m^\circ(\text{cr})$	$\Delta_f H_m^\circ(\text{cr})$	$\Delta_{\text{cr}}^g H_m^\circ$	$\Delta_f H_m^\circ(\text{g})$
$\text{kJ}\cdot\text{mol}^{-1}$	$\text{kJ}\cdot\text{mol}^{-1}$	$\text{kJ}\cdot\text{mol}^{-1}$	$\text{kJ}\cdot\text{mol}^{-1}$	$\text{kJ}\cdot\text{mol}^{-1}$
6485.7 ± 1.4	6490.7 ± 1.4	110.8 ± 2.2	98.05 ± 0.44^a	208.9 ± 2.2
			96.43 ± 0.14^b	207.2 ± 2.2
Mean			96.58 ± 0.13^c	207.4 ± 2.2

^aDerived from vapor pressure results determined by the effusion method;

^bDerived from vapor pressure results determined by the static method;

^cCalculated as the weighted mean of the results..

Table 4.39. Standard ($p^\circ = 0.1$ MPa) molar absolute entropies and standard molar entropies, enthalpies and Gibbs energies of formation of the crystalline and gaseous phases of 2-bromofluorene, at $T = 298.15$ K.

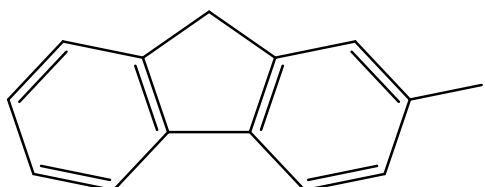
Phase	S_m°	$-T\Delta_f S_m^\circ$	$\Delta_f H_m^\circ$	$\Delta_f G_m^\circ$
	$\text{J}\cdot\text{K}^{-1}\cdot\text{mol}^{-1}$	$\text{kJ}\cdot\text{mol}^{-1}$	$\text{kJ}\cdot\text{mol}^{-1}$	$\text{kJ}\cdot\text{mol}^{-1}$
g	435.42 ^a	90.4	207.4 ± 2.2 ^c	297.8 ± 2.2
cr	253.1 ± 0.2 ^b	144.8 ± 0.1	110.8 ± 2.2	255.6 ± 2.2

^a Calculated at the B3LYP/6-311++G(d,p) level [20];

^b $S_m^\circ(\text{cr}) = S_m^\circ(\text{g}) - \Delta_{\text{cr}}^g S_m^\circ$;

^c Weighted mean of the values determined in this work using the effusion and static methods presented in table 4.36.

4.2.2.1.6. 2-Iodofluorene



Molecular formula	CAS Number	Molar Mass	Density
C ₁₃ H ₉ I	2523-42-4	292.1140 g·mol ⁻¹	1.714 [43]

Table 4.40. Source, purification and analysis details of 2-iodofluorene.

Source	Lot	Minimum initial purity	Purification method	Final mass fraction purity ^c
Sigma-Aldrich	MKBB2762	0.990 ^a	Sublimation under reduced pressure	0.9960
	MKBD5491V	0.993 ^b		

^a Determined by GC, as stated in the certificate of analysis of the manufacturer (May 2009);

^b Determined by GC, as stated in the certificate of analysis of the manufacturer (May 2010);

^c Determined by GC.

Vapor pressures and thermodynamic properties of phase transition

Table 4.41. Temperatures, molar enthalpies and entropies of fusion of 2-iodofluorene.

Exp.	T_{fus} (onset) K	$\Delta_{\text{cr}}^{\text{l}} H_{\text{m}}^{\circ}(T_{\text{fus}})$ kJ·mol ⁻¹	$\Delta_{\text{cr}}^{\text{l}} S_{\text{m}}^{\circ}(T_{\text{fus}})$ J·K ⁻¹ ·mol ⁻¹	T_{tp}^{a} K	$\Delta_{\text{cr}}^{\text{l}} H_{\text{m}}^{\circ}(T_{\text{tp}})^{\text{b}}$ kJ·mol ⁻¹	$\Delta_{\text{cr}}^{\text{l}} S_{\text{m}}^{\circ}(T_{\text{tp}})$ J·K ⁻¹ ·mol ⁻¹
1	404.13	17.50				
2	404.14	17.46				
3	404.19	17.60				
4	404.08	17.51				
5	404.12	17.56				
Mean	404.13 ± 0.04	17.53 ± 0.05	43.4 ± 0.1	402.17	20.0 ± 0.1	49.7 ± 0.2
Lit. ^c	399-402					

^a Triple point temperature derived indirectly from vapor pressure results;

^b Determined indirectly from the $\Delta_{\text{cr}}^{\text{g}} H_{\text{m}}^{\circ}(T_{\text{tp}})$ and $\Delta_{\text{f}}^{\text{g}} H_{\text{m}}^{\circ}(T_{\text{tp}})$ values presented in table 4.43;

^c Sigma-Aldrich, MSDS.

The vapor pressure study of this compound was done in collaboration with another researcher [40], who performed the Knudsen effusion experimental study. These results will be compiled in the table below, along with the vapor pressures determined in this work using the static method based on capacitance manometers.

Table 4.42. Vapor pressures of 2-iodofluorene determined by the Knudsen effusion and static methods.

<i>T/K</i>	<i>p/Pa</i>	$100\Delta p/p^a$	<i>T/K</i>	<i>p/Pa</i>	$100\Delta p/p^a$	<i>T/K</i>	<i>p/Pa</i>	$100\Delta p/p^a$
<i>Crystalline phase, effusion method^b</i>								
341.16	0.119	0	349.21	0.275	1.1	355.12	0.485	0
343.22	0.150	1.3	350.12	0.296	-0.7	357.16	0.583	-1.2
345.11	0.179	-0.6	352.17	0.357	-2.0	359.20	0.725	1.4
347.16	0.220	-0.5	353.21	0.405	0.5	361.12	0.859	0.3
<i>Crystalline phase, static method^c</i>								
362.63	0.966	-0.4	376.45	3.290	0.3	388.31	8.743	0.8
364.62	1.157	-0.5	378.45	3.888	0.2	390.26	10.11	0
366.60	1.384	-0.4	380.39	4.564	0	392.21	11.77	-0.1
368.57	1.667	0.6	382.39	5.393	0.2	394.20	13.67	-0.4
370.55	1.974	0.1	384.32	6.314	0.3	396.16	15.91	-0.3
372.51	2.337	-0.2	386.36	7.414	-0.1	398.18	18.49	-0.5
374.49	2.790	0.5						
<i>Liquid phase, static method^{c,d}</i>								
392.08	13.59	0.1	4000	21.97	-0.1	407.96	34.89	-0.1
394.08	15.35	-0.1	402.08	24.79	-0.2	409.94	39.07	0.1
396.17	17.46	0	403.96	27.76	0.1	411.91	43.60	0.1
398.00	19.54	0.2	405.93	30.99	-0.3	413.86	48.52	0.1

^a $\Delta p = p - p_{\text{calc}}$, where p_{calc} is calculated from the Clarke and Glew equation with parameters given in table 4.43;

^b Ref. [40];

^c $u(T) = \pm 0.01$ K, $u(p/\text{Pa}) = 0.01 + 0.0025(p/\text{Pa})$ for gauge I and $u(p/\text{Pa}) = 0.1 + 0.0025(p/\text{Pa})$ for gauge II;

^d Including supercooled liquid.

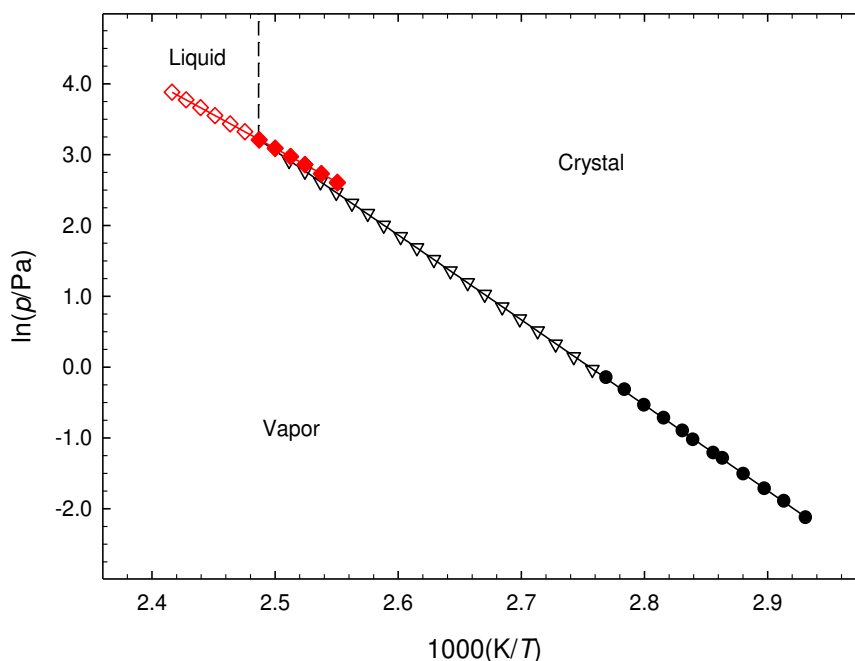


Figure 4.7. Phase diagram ($\ln(p/\text{Pa})$ against $1000(K/T)$) of 2-iodofluorene: ∇ , crystal vapor pressures; \diamond , liquid vapor pressures; \blacklozenge , supercooled liquid vapor pressures (triple point coordinates: $T_{\text{tp}} = 402.17$ K; $p_{\text{tp}} = 24.99$ Pa); \bullet , literature solid vapor pressure results.

Table 4.43. Standard ($p^\circ = 0.1$ MPa) molar properties of sublimation and vaporization of 2-iodofluorene, derived from experimental and literature vapor pressure results.

$\Delta T / \text{K}$	θ / K	$\frac{\Delta_{\text{cr/l}}^g G_m^\circ(\theta)}{\text{kJ}\cdot\text{mol}^{-1}}$	$\frac{\Delta_{\text{cr/l}}^g H_m^\circ(\theta)}{\text{kJ}\cdot\text{mol}^{-1}}$	$\frac{\Delta_{\text{cr/l}}^g S_m^\circ(\theta)^a}{\text{J}\cdot\text{K}^{-1}\cdot\text{mol}^{-1}}$	$p(\theta)^b$ Pa	R^2	$\frac{\Delta_{\text{g}}^{\text{cr/l}} C_{p,m}^\circ}{\text{J}\cdot\text{K}^{-1}\cdot\text{mol}^{-1}}^c$	s^d
<i>Crystalline phase, effusion method^e</i>								
341.16-361.12	298.15	46.70 ± 0.08	103.0 ± 0.5	188.8 ± 1.7	$6.6 \cdot 10^{-4}$	0.9997	34.7	0.011
<i>Crystalline phase, static method</i>								
	298.15	46.66 ± 0.02	102.5 ± 0.1	187.3 ± 0.3	$6.7 \cdot 10^{-4}$			
362.63-398.18	380.41^f	31.61 ± 0.01	99.69 ± 0.10	179.0 ± 0.3	4.6	1.0000	34.7	0.004
	402.17^g	27.73 ± 0.01	98.93 ± 0.10	177.0 ± 0.2	$2.5 \cdot 10^1$			
<i>Liquid phase, static method^h</i>								
	298.15	42.18 ± 0.02	87.41 ± 0.09	151.7 ± 0.3	$4.1 \cdot 10^{-3}$			
392.08-413.86	402.97^f	27.63 ± 0.01	78.86 ± 0.09	127.1 ± 0.2	$2.6 \cdot 10^1$	1.0000	81.6	0.002
	402.17^g	27.73 ± 0.01	78.92 ± 0.09	127.2 ± 0.2	$2.5 \cdot 10^1$			

^a Calculated through equation 4.14; ^b Calculated through equation 4.15; ^c Estimated value; ^d Standard deviation of the fit defined as $s = \sqrt{\left(\sum_{i=1}^n (\ln p - \ln p_{\text{calc}})_i^2\right) / (n - m)}$, where n is the number of experimental points used in the fit and m is the number of adjustable parameters in the Clarke and Glew equation; ^e Calculated from the vapor pressure results presented in reference [40] using the value of $\Delta_{\text{cr}}^g C_{p,m}^\circ$ estimated in this work. ^f Mean temperature; ^g Triple point temperature;

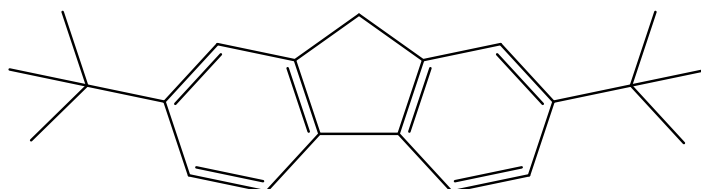
^h Including supercooled liquid.

The values $\Delta_{\text{cr}}^{\text{g}} C_{\rho,\text{m}}^{\text{o}} = -34.7 \text{ J}\cdot\text{K}^{-1}\cdot\text{mol}^{-1}$ and $\Delta_{\text{cr}}^{\text{g}} C_{\rho,\text{m}}^{\text{o}} = -81.6 \text{ J}\cdot\text{K}^{-1}\cdot\text{mol}^{-1}$ were estimated in this work by means of equations 4.12 and 4.13 with the value $C_{\rho,\text{m}}^{\text{o}}(\text{g}, 298.15 \text{ K}) = 192.2 \text{ J}\cdot\text{K}^{-1}\cdot\text{mol}^{-1}$. This value was estimated from that of fluorene [23], using a group additivity approach according to equation 4.26 and data provided in table 4.2.

$$C_{\rho,\text{m}}^{\text{o}}(\text{Fluorene}) = [1 \times \mathbf{C}_{\text{B}}\text{-(H)}(\text{C}_{\text{B}})_2] + [1 \times \mathbf{C}_{\text{B}}\text{-(F)}(\text{C}_{\text{B}})_2] \quad (4.26)$$

4.2.2.2. 2,7-Disubstituted fluorenes

4.2.2.2.1. 2,7-Di-*tert*-butylfluorene



Molecular formula	CAS Number	Molar Mass	Density
C ₂₁ H ₂₆	58775-05-6	278.4300 g·mol ⁻¹	0.988 [44]

Table 4.44. Source, purification and analysis details of 2,7-di-*tert*-butylfluorene.

Source	Lot	Minimum initial purity ^a	Purification method	Final mass fraction purity ^b
Aldrich	MKBG0052	0.995	Sublimation under reduced pressure	0.9996

^a Determined by HPLC (area %), as stated in the certificate of analysis of the manufacturer;

^b Determined by GC.

Vapor pressures and thermodynamic properties of phase transition

Table 4.45. Temperatures and standard molar enthalpies and entropies of condensed phase transitions of 2,7-di-*tert*-butylfluorene.

Exp.	$T_{\text{crl-crl}}$ (onset)	$\Delta_{\text{crl}}^{\text{crl}} H_{\text{m}}^{\circ}(T_{\text{crl-crl}})$	$\Delta_{\text{crl}}^{\text{crl}} S_{\text{m}}^{\circ}(T_{\text{crl-crl}})$	T_{fus} (onset)	$\Delta_{\text{cr}}^{\text{l}} H_{\text{m}}^{\circ}(T_{\text{fus}})$	$\Delta_{\text{cr}}^{\text{l}} S_{\text{m}}^{\circ}(T_{\text{fus}})$
	K	kJ·mol ⁻¹	J·K ⁻¹ ·mol ⁻¹	K	kJ·mol ⁻¹	J·K ⁻¹ ·mol ⁻¹
1	367.05	10.04		395.92	15.50	
2	367.26	9.92		396.26	15.52	
3	366.94	9.93		396.01	16.07	
4	366.76	10.03		395.77	15.82	
5	367.09	10.09		395.70	15.30	
Mean	367.0 ± 0.2	10.00 ± 0.07	27.2 ± 0.2	395.9 ± 0.2	15.6 ± 0.3	39.4 ± 0.8
VP ^a	366.8	12.7 ± 0.4	34.6 ± 1.1	394.8	14.5 ± 0.3	36.7 ± 0.8
Lit. ^b				394 - 397		

^a Derived indirectly from vapor pressure results;

^b Sigma-Aldrich, MSDS.

The DSC thermograms of 2,7-di-*tert*-butylfluorene reveal the existence of a crystalline transition at $T_{\text{crI-crI}} = (367.0 \pm 0.2)$ K (example shown in figure 4.8), before the fusion transition at $T_{\text{fus}} = (395.9 \pm 0.2)$ K. The crystalline transition is thermodynamically reversible, yielding the same values of transition temperature and enthalpy either using fresh samples or recrystallized *in situ*.

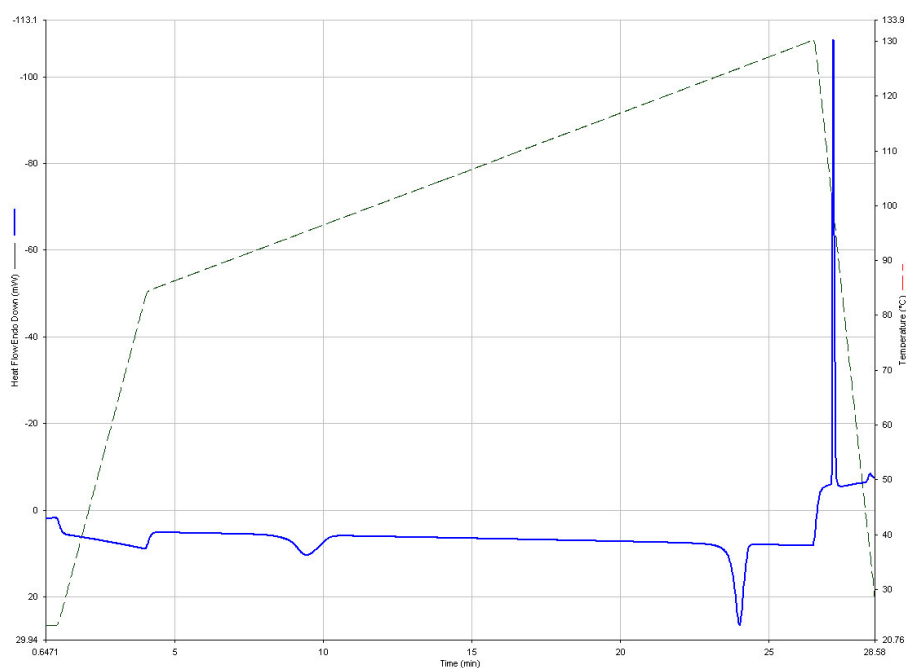


Figure 4.8. Typical DSC thermogram of 2,7-di-*tert*-butylfluorene: solid line, heat flow (mW); dashed line, temperature (°C).

The calorimetric determination of the enthalpy of sublimation of this compound was performed by another researcher [45].

Table 4.46. Standard ($p^\circ = 0.1$ MPa) molar enthalpy of sublimation of 2,7-di-*tert*-butylfluorene, determined by Calvet microcalorimetry.

T / K	$\Delta_{\text{cr}, 298.15 \text{ K}}^{\text{g}, T} H_{\text{m}}^{\circ}$ $\text{kJ}\cdot\text{mol}^{-1}$	$\Delta_{298.15 \text{ K}}^T H_{\text{m}}^{\circ} (\text{g})$ $\text{kJ}\cdot\text{mol}^{-1}$	$\Delta_{\text{cr}}^{\text{g}} H_{\text{m}}^{\circ} (298.15 \text{ K})$ $\text{kJ}\cdot\text{mol}^{-1}$
406.57 ± 0.01^a	164.6 ± 0.4^a	44.74	119.9 ± 0.9^b

^aUncertainties are the estimated standard deviation of the mean of six independent experiments;

^bThe uncertainty is the expanded uncertainty of the mean (0.95 level of confidence, $k = 2$), and includes the uncertainty due to the calibration.

The calorimeter was calibrated with high purity anthracene (details in table 3.2), and the calibration constant, k_{cal} , for the mean experimental temperature, $T = 406.57$ K, was found to be $k_{\text{cal}} = (1.0557 \pm 0.0022)$, calculated as the average of six independent sublimation experiments. The system was also tested at the same temperature by determining the enthalpy of sublimation of pyrene (purity mass fraction 0.9989), yielding the result $\Delta_{\text{cr}}^{\text{g}} H_{\text{m}}^{\text{o}}(298.15 \text{ K}) = (100.3 \pm 1.3) \text{ kJ}\cdot\text{mol}^{-1}$, which is in excellent agreement with the value recently reported in the literature [46].

The term $\Delta_{298.15 \text{ K}}^T H_{\text{m}}^{\text{o}}(\text{g})$ was calculated from the integration of the fitting of a 3rd degree polynomial to the $C_{\rho, \text{m}}^{\text{o}}(\text{g}, 298.15 \text{ K})$ results calculated at the B3LYP/6-31G(2df,p) level of theory [45], between $T = (290 \text{ and } 500) \text{ K}$:

$$C_{\rho, \text{m}}^{\text{o}} = 53.99 + 7.16 \cdot 10^{-1}(T/\text{K}) + 1.50 \cdot 10^{-3}(T/\text{K})^2 - 1.82 \cdot 10^{-6}(T/\text{K})^3 \quad (4.27)$$

Table 4.47. Vapor pressures of 2,7-di-*tert*-butylfluorene determined by the Knudsen effusion method.^a

T / K	t / s	Orifices	m / mg			p / Pa			
			m_{small}	m_{medium}	m_{large}	p_{small}	p_{medium}	p_{large}	p_{mean}
349.14	20029	A'1-B'4-C'7	5.22		7.99	0.106		0.105	0.106
351.14	21123	A'1-B'4-C'7	6.99	8.45	10.88	0.135	0.132	0.136	0.134
353.30	20029	A'2-B'5-C'8		10.34	12.79		0.171	0.169	0.17
355.28	21123	A'2-B'5-C'8	11.06	13.78	17.00	0.215	0.217	0.213	0.215
357.20	20029	A'3-B'6-C'9	12.68	16.24	20.14	0.261	0.271	0.267	0.266
359.19	22815	A'3-B'6-C'9	18.20	21.91	28.75	0.330	0.321	0.336	0.329
361.14	10798	A'1-B'4-C'7	10.64	13.12	16.52	0.409	0.408	0.409	0.409
363.27	10389	A'2-B'5-C'8	12.83	15.72	19.64	0.514	0.509	0.507	0.51
368.20	10389	A'3-B'6-C'9	19.97	25.02	31.89	0.805	0.816	0.828	0.816
369.13	11379	A'1-B'4-C'7	24.05	29.79	37.46	0.886	0.888	0.889	0.888
370.26	11379	A'2-B'5-C'8		32.89	41.23		0.979	0.975	0.977
371.21	11522	A'3-B'6-C'9	29.65	36.23	45.88	1.082	1.070	1.079	1.077
372.21	11379	A'3-B'6-C'9		39.35	49.50		1.178	1.180	1.179

^a $u(T/\text{K}) = \pm 0.01$, $u(p/\text{Pa}) = \pm 0.01$.

Table 4.48. Vapor pressures of 2,7-di-*tert*-butylfluorene determined by the static method with capacitance manometers. ^a

<i>T</i> /K	<i>p</i> /Pa	100Δ <i>p</i> / <i>p</i> ^{<i>b</i>}	<i>T</i> /K	<i>p</i> /Pa	100Δ <i>p</i> / <i>p</i> ^{<i>b</i>}	<i>T</i> /K	<i>p</i> /Pa	100Δ <i>p</i> / <i>p</i> ^{<i>b</i>}
<i>Crystalline phase</i>								
368.55	0.873	-0.1	376.45	1.778	0	384.34	3.492	-0.2
370.54	1.055	0.6	378.41	2.106	-0.2	386.30	4.126	0.1
372.50	1.246	-0.5	380.40	2.524	0.7	388.27	4.862	0.3
374.50	1.492	-0.3	382.38	2.965	-0.1	390.24	5.670	-0.4
<i>Liquid phase</i> ^{<i>c</i>}								
384.34	3.946	0.3	392.22	6.859	-0.2	400.05	11.64	0.1
386.32	4.548	0.2	394.20	7.843	-0.3	402.07	13.27	0.1
388.28	5.217	0	396.17	8.987	0	404.04	15.08	0.2
390.28	5.976	-0.5	398.15	10.26	0			

^a $u(T/K) = \pm 0.01$, $u(T) = \pm 0.01$ K, $u(p/Pa) = 0.01 + 0.0025(p/Pa)$ for gauge I;

^b $\Delta p = p - p_{calc}$, where p_{calc} is calculated from the Clarke and Glew equation with parameters given in table 4.49;

^c Including supercooled liquid.

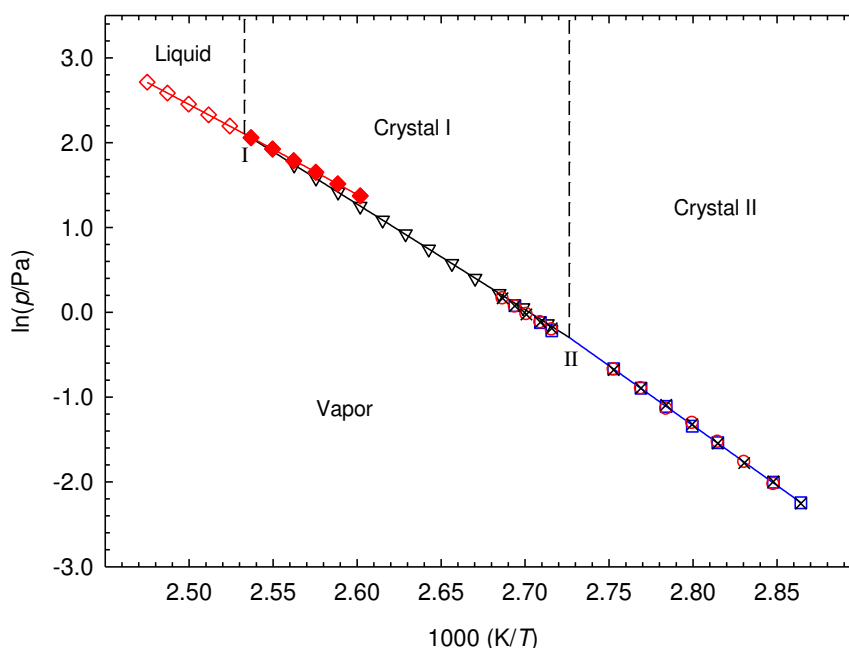


Figure 4.9. Phase diagram ($\ln(p/Pa)$ against $1000(K/T)$) of 2,7-di-*tert*-butylfluorene: effusion crystal vapor pressures for the different effusion orifices - \square , small; \circ , medium; \times , large; static vapor pressures - ∇ , crystal vapor pressures; \diamond , liquid vapor pressures; \blacklozenge , supercooled liquid vapor pressures (triple point coordinates: $T_{tp}(I) = 394.80$ K, $p_{tp}(I) = 8.19$ Pa); $T_{tp}(II) = 366.79$ K, $p_{tp}(II) = 0.74$ Pa.

Table 4.49. Standard ($p^\circ = 0.1$ MPa) molar properties of sublimation and vaporization of 2,7-di-*tert*-butylfluorene, derived from the experimental vapor pressure results.

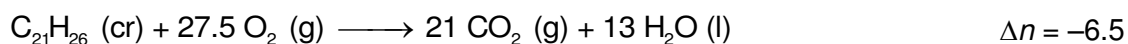
$\Delta T / \text{K}$	θ / K	$\frac{\Delta_{\text{cr/l}}^{\text{g}} G_{\text{m}}^{\circ}(\theta)}{\text{kJ}\cdot\text{mol}^{-1}}$	$\frac{\Delta_{\text{cr/l}}^{\text{g}} H_{\text{m}}^{\circ}(\theta)}{\text{kJ}\cdot\text{mol}^{-1}}$	$\frac{\Delta_{\text{cr/l}}^{\text{g}} S_{\text{m}}^{\circ}(\theta)^{\text{a}}}{\text{J}\cdot\text{K}^{-1}\cdot\text{mol}^{-1}}$	$p(\theta)^{\text{b}}$ Pa	R^2	$\frac{\Delta_{\text{g}}^{\text{cr/l}} C_{\text{p,m}}^{\circ \text{c}}}{\text{J}\cdot\text{K}^{-1}\cdot\text{mol}^{-1}}$	s^{d}
<i>Crystalline phase II, effusion method</i>								
	298.15	51.57 ± 0.06	121.1 ± 0.4	233.2 ± 1.4	$9.2\cdot 10^{-5}$			
349.14-363.27	356.21^{e}	38.36 ± 0.01	117.5 ± 0.4	222.2 ± 1.1	$2.4\cdot 10^{-1}$	0.9999	63.0	0.005
	366.79^{f}	36.02 ± 0.01	116.8 ± 0.4	220.2 ± 1.1	$7.4\cdot 10^{-1}$			
<i>Crystalline phase I, effusion method</i>								
	298.15	49.45 ± 0.36	109.3 ± 1.8	200.7 ± 6.2	$2.2\cdot 10^{-4}$			
368.20-372.21	370.21^{e}	35.50 ± 0.01	104.7 ± 1.8	186.9 ± 4.9	$9.8\cdot 10^{-1}$	0.9991	63.0	0.005
<i>Crystalline phase I, static method</i>								
	298.15	49.19 ± 0.04	108.4 ± 0.2	198.6 ± 0.7	$2.1\cdot 10^{-4}$			
	379.40^{e}	33.69 ± 0.01	103.3 ± 0.2	183.5 ± 0.5	2.3			
368.55-390.24	366.79^{f}	36.02 ± 0.01	104.1 ± 0.2	185.6 ± 0.5	$7.4\cdot 10^{-1}$	1.0000	63.0	0.004
	394.80^{g}	30.89 ± 0.01	102.3 ± 0.2	180.9 ± 0.5	8.2			
<i>Liquid phase, static method^h</i>								
	298.15	46.61 ± 0.04	101.2 ± 0.2	183.1 ± 0.7	$6.8\cdot 10^{-4}$			
384.34-404.04	394.19^{e}	30.97 ± 0.01	87.93 ± 0.15	144.5 ± 0.4	7.8	1.0000	137.7	0.002
	394.80^{g}	30.89 ± 0.01	87.85 ± 0.15	144.3 ± 0.4	8.2			

^a Calculated through equation 4.14; ^b Calculated through equation 4.15; ^c Estimated values; ^d Standard deviation of the fit defined as $s = \sqrt{\left(\sum_{i=1}^n (\ln p - \ln p_{\text{calc}})_i^2\right) / (n - m)}$, where n is the number of experimental points used in the fit and m is the number of adjustable parameters in the Clarke and Glew equation; ^e Mean temperature; ^f Temperature of triple point (crl, crl, g); ^g Temperature of the triple point (crl, liq, g); ^h Including supercooled liquid.

The value of $C_{\text{p,m}}^{\circ}(\text{g}, 298.15\text{K}) = 352.65 \text{ J}\cdot\text{K}^{-1}\cdot\text{mol}^{-1}$ [45] was calculated at the B3LYP/6-31G(2df,p) level of theory, and inserted into equations 4.12 and 4.13, respectively yielding the $\Delta_{\text{cr}}^{\text{g}} C_{\text{p,m}}^{\circ} = -63.0 \text{ J}\cdot\text{K}^{-1}\cdot\text{mol}^{-1}$ and $\Delta_{\text{l}}^{\text{g}} C_{\text{p,m}}^{\circ} = -137.7 \text{ J}\cdot\text{K}^{-1}\cdot\text{mol}^{-1}$.

Combustion calorimetry and thermodynamic properties of formation

Combustion equation:



In the study of 2,7-di-*tert*-butylfluorene using static bomb combustion calorimetry, two combustion aids were tested to prevent the formation of carbon soot residue. Firstly, the sample pellet was enclosed in melinex[®] bags, using the technique described by Skinner and Snelson [47]. The use of this combustion aid, however, didn't prove successful and *n*-hexadecane (Aldrich Gold Label, mass fraction >0.999) was tested with better results.

Table 4.50. Standard ($p^\circ = 0.1 \text{ MPa}$) massic energy of combustion of 2,7-di-*tert*-butylfluorene, at $T = 298.15 \text{ K}$.^a

Exp.	1	2	3	4	5	6
$m(\text{CO}_2, \text{ total}) / \text{g}$	1.62291	1.45839	1.56279	1.46598	1.40955	
$m(\text{cpd}) / \text{g}$	0.48788	0.40911	0.41354	0.40747	0.40290	0.41266
$m(\text{fuse}) / \text{g}$	0.00259	0.00289	0.00295	0.00299	0.00283	0.00288
$m(\text{c.aid}) / \text{g}$		0.04230 ^b	0.08121 ^b	0.03492 ^c	0.02175 ^c	0.02177 ^c
T_i / K	298.15116	298.15073	298.15189	298.15550	298.15144	298.15143
T_f / K	299.55510	299.40766	299.47515	299.45182	299.39494	299.42001
$\Delta T_{\text{ad}} / \text{K}$	1.33381	1.18254	1.25155	1.22361	1.16907	1.19646
$\bar{\epsilon} / \text{J}\cdot\text{K}^{-1}$	14.70	14.50	14.58	14.65	14.55	14.56
$\Delta m(\text{H}_2\text{O}) / \text{g}$	0	-1.7	-0.4	-9.4	-0.8	-0.1
$-\Delta U(\text{IBP}) / \text{J}$	20762.04	18398.57	19479.19	18998.28	18193.40	18623.23
$\Delta U(\text{fuse}) / \text{J}$	42.06	46.93	47.91	48.56	45.96	46.77
$\Delta U(\text{c.aid}) / \text{J}$		968.85 ^b	1859.79 ^b	1647.05 ^c	1025.63 ^c	1026.57 ^c
$\Delta U(\text{HNO}_3) / \text{J}$	10.52	10.25	11.61	5.04	5.77	8.05
$\Delta U(\text{ign}) / \text{J}$	0.58	0.69	0.66	0.77	0.78	0.70
$\Delta U(\text{carb}) / \text{J}$	6.60	10.23	5.61			
$\Delta U_{\Sigma} / \text{J}$	9.12	8.35	9.25	7.92	7.65	7.85
$-\Delta_c U^\circ / \text{J}\cdot\text{g}^{-1}$	42442.69	42468.82	42453.55	42431.86	42463.12	42491.16
$-\langle \Delta_c U^\circ \rangle = (42458.5 \pm 8.5) \text{ J}\cdot\text{g}^{-1}$						
$\langle \% \text{ CO}_2 \rangle = (99.963 \pm 0.011) \%$						

^a $\bar{\epsilon}_{\text{cal}} = (15551.7 \pm 1.2) \text{ J}\cdot\text{K}^{-1}$;^b Combustion aid: Melinex[®];^c Combustion aid: *n*-Hexadecane.

The energies of combustion of melinex[®] and *n*-hexadecane in each experiment, were calculated using the respective massic energies of combustion: $\Delta_c U^\rho(\text{melinex}) = -(22902 \pm 5) \text{ J}\cdot\text{g}^{-1}$ [47] and $\Delta_c U^\rho(n\text{-hex}) = -(47161.9 \pm 1.3) \text{ J}\cdot\text{g}^{-1}$. The later one was determined as the mean of results obtained by other researchers in our laboratory and is in good agreement with that reported in the literature [48].

Table 4.51. Standard ($p^\circ = 0.1 \text{ MPa}$) molar energy and enthalpy of combustion, and derived standard molar enthalpies of formation of the crystalline and gaseous phases of 2,7-di-*tert*-butylfluorene, at $T = 298.15 \text{ K}$.

$-\Delta_c U_m^\circ(\text{cr})$	$-\Delta_c H_m^\circ(\text{cr})$	$-\Delta_f H_m^\circ(\text{cr})$	$\Delta_{\text{cr}}^\circ H_m^\circ$	$-\Delta_f H_m^\circ(\text{g})$
$\text{kJ}\cdot\text{mol}^{-1}$	$\text{kJ}\cdot\text{mol}^{-1}$	$\text{kJ}\cdot\text{mol}^{-1}$	$\text{kJ}\cdot\text{mol}^{-1}$	$\text{kJ}\cdot\text{mol}^{-1}$
11821.7 ± 5.9	11837.8 ± 5.9	141.7 ± 6.5	121.1 ± 0.4^a	20.6 ± 6.5
			119.9 ± 0.9^b	21.8 ± 6.6
Mean			120.9 ± 0.4^c	20.8 ± 6.5

^a Derived from effusion vapor pressure results of crystalline phase II;

^b Derived from calorimetric results;

^c Calculated as the weighted mean of the results.

Table 4.52. Standard ($p^\circ = 0.1 \text{ MPa}$) molar absolute entropies and standard molar entropies, enthalpies and Gibbs energies of formation of the crystalline and gaseous phases of 2,7-di-*tert*-butylfluorene, at $T = 298.15 \text{ K}$.

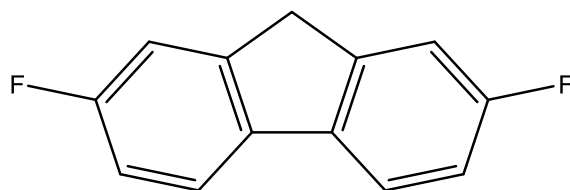
Phase	S_m°	$-T\Delta_f S_m^\circ$	$-\Delta_f H_m^\circ$	$\Delta_f G_m^\circ$
	$\text{J}\cdot\text{K}^{-1}\cdot\text{mol}^{-1}$	$\text{kJ}\cdot\text{mol}^{-1}$	$\text{kJ}\cdot\text{mol}^{-1}$	$\text{kJ}\cdot\text{mol}^{-1}$
g	602.2^a	362.9	20.6 ± 6.5^c	342.3 ± 6.5
cr	369.0 ± 1.4^b	432.4 ± 0.4	141.7 ± 6.5	290.7 ± 6.5

^a Calculated at the B3LYP/6-31G(2df,p) level [45];

^b $S_m^\circ(\text{cr}) = S_m^\circ(\text{g}) - \Delta_{\text{cr}}^\circ S_m^\circ$;

^c Derived from effusion vapor pressure results of crystalline phase II.

4.2.2.2.2. 2,7-Difluorofluorene



Molecular formula	CAS Number	Molar Mass	Density
C ₁₃ H ₈ F ₂	2195-50-8	202.1984 g·mol ⁻¹	1.289 [49]

Table 4.53. Source, purification and analysis details of 2,7-difluorofluorene.

Source	Initial purity ^{a,b}	Purification method	Final mass fraction purity ^a
Synthesis	0.891	Sublimation under reduced pressure	0.9992

^a Purity after synthesis;^b Determined by GC.**Vapor pressures and thermodynamic properties of phase transition**

Table 4.54. Temperatures, molar enthalpies and entropies of fusion of 2,7-difluorofluorene.

Exp.	T_{fus} (onset)	$\Delta_{\text{cr}}^{\text{l}} H_{\text{m}}^{\circ}(T_{\text{fus}})$	$\Delta_{\text{cr}}^{\text{l}} S_{\text{m}}^{\circ}(T_{\text{fus}})$
	K	kJ·mol ⁻¹	J·K ⁻¹ ·mol ⁻¹
1	356.00	18.03	
2	355.97	18.13	
3	356.50	18.06	
4	356.65	18.00	
5	356.73	18.05	
Mean	356.4 ± 0.3	18.05 ± 0.04	50.6 ± 0.1
Literature ^a	353 - 355.5		

^a Ref. [50], no information regarding minimum purity.

Table 4.55. Vapor pressures of 2,7-difluorofluorene determined by the Knudsen effusion method. ^a

T / K	t / s	Orifices	m / mg			p / Pa			
			m_{small}	m_{medium}	m_{large}	p_{small}	p_{medium}	p_{large}	p_{mean}
299.17	25637	A ₁ '-B ₄ '-C ₇	5.37	6.56	8.22	0.093	0.092	0.091	0.092
301.37	25637	A ₂ '-B ₅ '-C ₈	6.87	8.48	10.81	0.119	0.119	0.121	0.120
303.20	25637	A ₃ '-B ₆ '-C ₉	8.75	10.64	13.36	0.152	0.150	0.150	0.151
305.14	14537	A ₁ '-B ₄ '-C ₇	6.11	7.58	9.36	0.188	0.189	0.186	0.187
307.34	14537	A ₂ '-B ₅ '-C ₈	7.76	9.63	12.11	0.240	0.241	0.241	0.240
309.20	14537	A ₃ '-B ₆ '-C ₉	9.73	11.96	15.10	0.302	0.300	0.301	0.301
311.13	10086	A ₁ '-B ₄ '-C ₇	8.34	10.17	12.85	0.374	0.369	0.371	0.371
313.18	10086	A ₂ '-B ₅ '-C ₈	10.41	12.99	16.26	0.468	0.472	0.471	0.470
315.21	10086	A ₃ '-B ₆ '-C ₉	13.07	15.93	20.45	0.589	0.581	0.594	0.588
317.11	10029	A ₁ '-B ₄ '-C ₇	16.27	19.72	24.70	0.740	0.726	0.724	0.730
319.16	10029	A ₂ '-B ₅ '-C ₈	20.42	25.12	31.48	0.932	0.927	0.925	0.928
321.19	10029	A ₃ '-B ₆ '-C ₉	25.25	30.43	38.82	1.156	1.127	1.144	1.142

^a $u(T/K) = \pm 0.01$, $u(p/\text{Pa}) = \pm 0.01$.

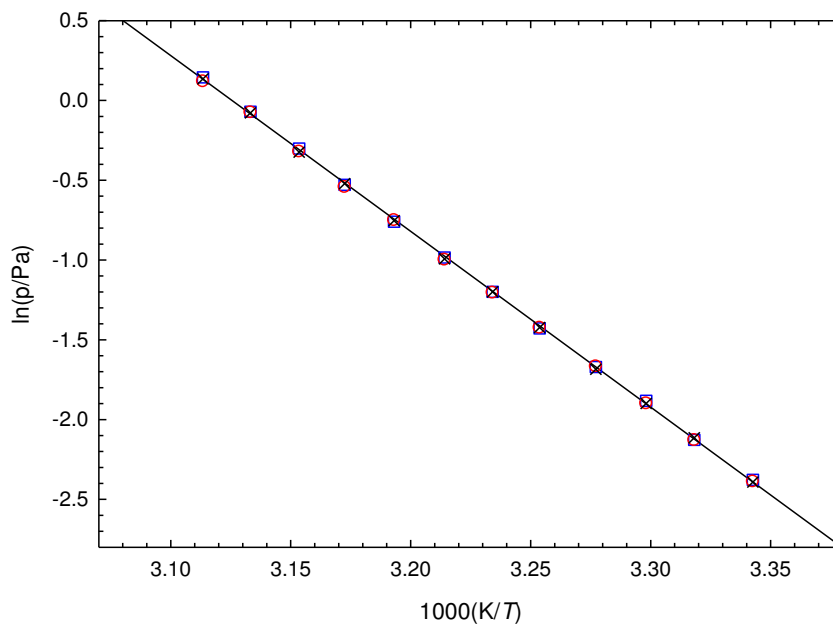


Figure 4.10. Plots of $\ln(p/\text{Pa})$ against $1000(K/T)$ of 2,7-difluorofluorene: effusion vapor pressures for the different effusion orifices - \square , small; \circ , medium; \times , large.

Table 4.56. Standard ($p^\circ = 0.1$ MPa) molar properties of sublimation and vaporization of 2,7-difluorofluorene, derived from the experimental vapor pressure results.

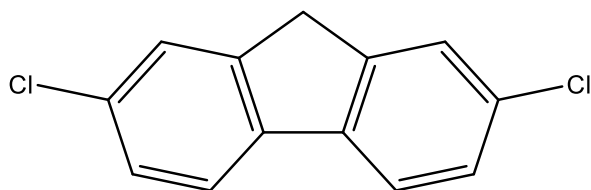
$\Delta T / \text{K}$	θ / K	$\frac{\Delta_{\text{cr}}^{\text{g}} G_{\text{m}}^{\circ}(\theta)}{\text{kJ}\cdot\text{mol}^{-1}}$	$\frac{\Delta_{\text{cr}}^{\text{g}} H_{\text{m}}^{\circ}(\theta)}{\text{kJ}\cdot\text{mol}^{-1}}$	$\frac{\Delta_{\text{cr}}^{\text{g}} S_{\text{m}}^{\circ}(\theta)^{\text{a}}}{\text{J}\cdot\text{K}^{-1}\cdot\text{mol}^{-1}}$	$\frac{p(\theta)^{\text{b}}}{\text{Pa}}$	R^2	$\frac{\Delta_{\text{g}}^{\text{cr}} C_{\rho,\text{m}}^{\circ\text{c}}}{\text{J}\cdot\text{K}^{-1}\cdot\text{mol}^{-1}}$	s^{d}
<i>Crystalline phase, effusion method</i>								
299.17-321.19	298.15	34.79 ± 0.02	91.78 ± 0.35	191.1 ± 1.2	$8.0\cdot 10^{-2}$	0.9999	35.8	0.010
	310.18 ^e	32.49 ± 0.01	91.35 ± 0.35	189.8 ± 1.1	$3.4\cdot 10^{-1}$			

^a Calculated through equation 4.14; ^b Calculated through equation 4.15; ^c Estimated value; ^d Standard deviation of the fit defined as $s = \sqrt{\left(\sum_{i=1}^n (\ln p - \ln p_{\text{calc},i})^2\right) / (n - m)}$, where n is the number of experimental points used in the fit and m is the number of adjustable parameters in the Clarke and Glew equation; ^e Mean temperature.

The value $\Delta_{\text{cr}}^{\text{g}} C_{\rho,\text{m}}^{\circ} = -35.8 \text{ J}\cdot\text{K}^{-1}\cdot\text{mol}^{-1}$ was estimated in this work by means of equation 4.12 and the value $C_{\rho,\text{m}}^{\circ}(\text{g}, 298.15 \text{ K}) = 198.1 \text{ J}\cdot\text{K}^{-1}\cdot\text{mol}^{-1}$, estimated for this compound from the value $C_{\rho,\text{m}}^{\circ}(\text{g}, 298.15 \text{ K})$ of fluorene [23] using a group additivity approach according to equation 4.28 and data provided in table 4.2.

$$C_{\rho,\text{m}}^{\circ}(\text{Fluorene}) - [2 \times \mathbf{C}_{\text{B}}^{\text{-(H)}}(\text{C}_{\text{B}})_2] + [2 \times \mathbf{C}_{\text{B}}^{\text{-(F)}}(\text{C}_{\text{B}})_2] \quad (4.28)$$

4.2.2.2.3. 2,7-Dichlorofluorene



Molecular formula	CAS Number	Molar Mass	Density
C ₁₃ H ₈ Cl ₂	7012-16-0	235.1046 g·mol ⁻¹	1.2845 [14]

Table 4.57. Source, purification and analysis details of 2,7-dichlorofluorene.

Source	Initial purity ^{a,b}	Purification method	Final mass fraction purity ^b
Synthesis	0.976	Recrystallization; Sublimation under reduced pressure	0.9994

^aPurity after synthesis;^bDetermined by GC.

Vapor pressures and phase transition thermodynamic properties

Table 4.58. Temperatures, molar enthalpies and entropies of fusion of 2,7-dichlorofluorene.

Exp.	T_{fus} (onset)	$\Delta_{\text{cr}}^{\text{l}} H_{\text{m}}^{\circ}(T_{\text{fus}})$	$\Delta_{\text{cr}}^{\text{l}} S_{\text{m}}^{\circ}(T_{\text{fus}})$
	K	kJ·mol ⁻¹	J·K ⁻¹ ·mol ⁻¹
1	396.77	18.23	
2	396.99	18.60	
3	396.94	18.26	
4	396.89	18.31	
5	396.91	18.16	
6	396.87	18.59	
Mean	396.90 ± 0.06	18.4 ± 0.2	46.4 ± 0.5
Literature	397.6 - 398.5 ^a		
	398.5 - 399.5 ^b		

^aRef. [42], minimum purity 0.97;^bRef. [51], no information regarding minimum purity.

Table 4.59. Vapor pressures of 2,7-dichlorofluorene determined by the static method with capacitance manometers. ^a

<i>T</i> /K	<i>p</i> /Pa	100Δ <i>p</i> / <i>p</i> ^{<i>b</i>}	<i>T</i> /K	<i>p</i> /Pa	100Δ <i>p</i> / <i>p</i> ^{<i>b</i>}	<i>T</i> /K	<i>p</i> /Pa	100Δ <i>p</i> / <i>p</i> ^{<i>b</i>}
<i>Crystalline phase</i>								
364.64	1.50	−0.7	376.33	4.22	0.2	386.28	9.58	0.2
366.48	1.78	0	378.44	5.05	0.4	388.32	11.25	0
368.59	2.15	0	380.30	5.89	0.3	390.20	12.98	−0.4
370.46	2.54	0	382.22	6.92	0.6	392.25	15.23	−0.5
372.51	3.03	0	384.26	8.17	0.5	394.22	17.74	−0.5
374.51	3.61	0						

^a $u(T) = \pm 0.01$ K, $u(p) = 0.01 + 0.0025p$ Pa.

^b $\Delta p = p - p_{\text{calc}}$, where p_{calc} is calculated from the Clarke and Glew equation with parameters given in table 4.60.

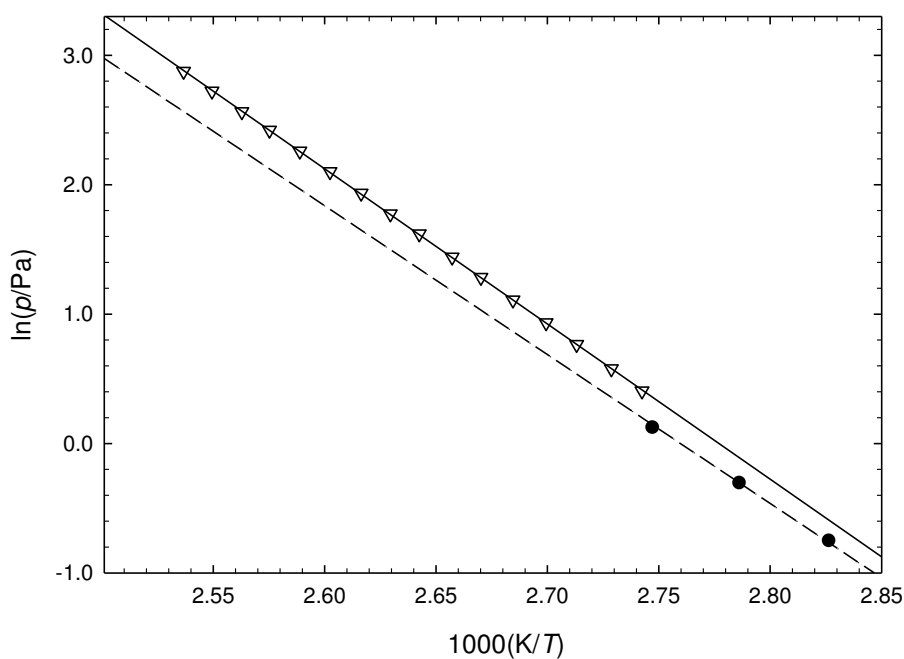


Figure 4.11. Plots of $\ln(p/\text{Pa})$ against $1000(K/T)$ of 2,7-dichlorofluorene: ∇ , crystal vapor pressures; \bullet , literature vapor pressure results [42].

Table 4.60. Standard ($p^\circ = 0.1$ MPa) molar properties of sublimation of 2,7-dichlorofluorene, derived from experimental and literature vapor pressure results.

$\Delta T / K$	θ / K	$\frac{\Delta_{cr}^g G_m^\circ(\theta)}{kJ \cdot mol^{-1}}$	$\frac{\Delta_{cr}^g H_m^\circ(\theta)}{kJ \cdot mol^{-1}}$	$\frac{\Delta_{cr}^g S_m^\circ(\theta)^a}{J \cdot K^{-1} \cdot mol^{-1}}$	$\frac{p(\theta)^b}{Pa}$	R^2	$\frac{\Delta_g^{cr} C_{p,m}^\circ}{J \cdot K^{-1} \cdot mol^{-1}}$	s^d
<i>Crystalline phase, static method</i>								
364.64-394.22	298.15	46.03 ± 0.03	102.7 ± 0.1	190.1 ± 0.4	$8.6 \cdot 10^{-4}$	1.0000	36.9	0.004
	379.43 ^e	30.96 ± 0.01	99.7 ± 0.1	181.2 ± 0.3	5.5			
<i>Crystalline phase, literature^f</i>								
318.5-364.0	298.15	45.57 ± 0.08	97.16 ± 0.62	173.0 ± 0.6	$1.1 \cdot 10^{-3}$	0.9997	36.9	0.029

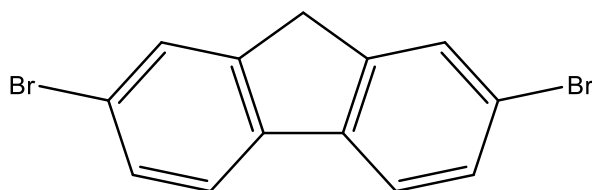
^a Calculated through equation 4.14; ^b Calculated through equation 4.15; ^c Estimated value; ^d Standard deviation of the fit defined as $s = \sqrt{\left(\sum_{i=1}^n (\ln p - \ln p_{calc})^2\right) / (n - m)}$, where n is the number of experimental points used in the fit and m is the number of adjustable parameters in the Clarke and Glew equation; ^e Mean temperature; ^f Calculated from the vapor pressure results presented in reference [42] using the value of $\Delta_{cr}^g C_{p,m}^\circ$ estimated in this work.

The value $\Delta_{cr}^g C_{p,m}^\circ = -36.9 J \cdot K^{-1} \cdot mol^{-1}$ was estimated in this work by means of equation 4.12 and the value $C_{p,m}^\circ(g, 298.15 K) = 204.5 J \cdot K^{-1} \cdot mol^{-1}$, estimated for this compound from the value $C_{p,m}^\circ(g, 298.15 K)$ of fluorene [23] using a group additivity approach according to equation 4.29 and data provided in table 4.2.

$$C_{p,m}^\circ(\text{Fluorene}) - [2 \times \mathbf{C}_B\text{-(H)}(\mathbf{C}_B)_2] + [2 \times \mathbf{C}_B\text{-(F)}(\mathbf{C}_B)_2] \quad (4.29)$$

The vapor pressure results reported by Fu and Suuberg [42], also shown in figure 4.11, are slightly smaller than the ones determined in this work. Their reported standard molar enthalpy of sublimation, which refers to the mean experimental temperature, was corrected to $T = 298.15$ K, using the $\Delta_{cr}^g C_{p,m}^\circ$ value estimated in the present work, yielding the values compiled in table 4.60. The enthalpy of sublimation, $\Delta_{cr}^g H_m^\circ(298.15 K) = (97.16 \pm 0.62) kJ \cdot mol^{-1}$, differs by $-5.5 kJ \cdot mol^{-1}$ from the result derived in this work. These discrepancies may be related to the purity of the samples (minimum purity 0.97), used without further purification by Fu and Suuberg.

4.2.2.2.4. 2,7-Dibromofluorene



Molecular formula	CAS Number	Molar Mass	Density
C ₁₃ H ₈ Br ₂	16433-88-8	324.0096 g·mol ⁻¹	1.7203 [14]

Table 4.61. Source, purification and analysis details of 2,7-dibromofluorene.

Source	Lot	Minimum initial purity ^a	Purification method	Final mass fraction purity ^b
TCI Europe	SLUTA	0.997	Sublimation under reduced pressure	0.9998

^a Determined by GC, as stated in the certificate of analysis of the manufacturer;^b Determined by GC.

Vapor pressures and phase transition thermodynamic properties

Table 4.62. Temperatures, molar enthalpies and entropies of fusion of 2,7-dibromofluorene.

Exp.	T_{fus} (onset)	$\Delta_{\text{cr}}^{\text{l}} H_{\text{m}}^{\circ}(T_{\text{fus}})$	$\Delta_{\text{cr}}^{\text{l}} S_{\text{m}}^{\circ}(T_{\text{fus}})$
	K	kJ·mol ⁻¹	J·K ⁻¹ ·mol ⁻¹
1	438.87	22.72	
2	438.63	22.70	
3	438.85	22.67	
4	438.73	22.80	
5	438.88	22.72	
Mean	438.8 ± 0.1	22.72 ± 0.04	51.78 ± 0.09
Literature	438.5 - 439.5 ^a 439.85 ^b	22.08 ^a	50.30 ^a

^a TCI Europe, certificate of analysis;^b Ref. [42], minimum purity 0.97.

Table 4.63. Vapor pressures of 2,7-dibromofluorene, determined by the Knudsen effusion method. ^a

<i>T</i> / K	<i>t</i> / s	Orifices	<i>m</i> / mg			<i>p</i> / Pa			
			<i>m</i> _{small}	<i>m</i> _{medium}	<i>m</i> _{large}	<i>p</i> _{small}	<i>p</i> _{medium}	<i>p</i> _{large}	<i>p</i> _{mean}
361.15	43682	A ₃ -B ₆ -C ₉	8.75	13.71	19.43	0.095	0.097	0.096	0.096
363.14	43682	A ₂ -B ₅ -C ₈	10.74	16.65	23.73	0.119	0.119	0.118	0.119
365.11	43682	A ₁ -B ₄ -C ₇	12.84	20.25	28.92	0.144	0.147	0.148	0.146
367.16	23786	A ₃ -B ₆ -C ₉	8.66	13.54	19.42	0.179	0.177	0.177	0.178
369.11	23786	A ₂ -B ₅ -C ₈	10.52	16.40	23.28	0.215	0.218	0.214	0.216
371.10	23786	A ₁ -B ₄ -C ₇	12.56	19.84	28.26	0.261	0.267	0.267	0.265
373.15	12809	A ₃ -B ₆ -C ₉	8.26	13.01	18.43	0.319	0.318	0.315	0.318
375.12	12809	A ₂ -B ₅ -C ₈	9.98	15.79	22.48	0.382	0.392	0.388	0.387
377.12	12809	A ₁ -B ₄ -C ₇	11.89	18.73	26.99	0.463	0.472	0.478	0.471
379.15	10755	A ₃ -B ₆ -C ₉	12.13	18.92	12.13	0.563	0.556	0.560	0.560
381.12	10755	A ₂ -B ₅ -C ₈	14.74	23.05	14.74	0.678	0.687	0.674	0.680
383.12	10755	A ₁ -B ₄ -C ₇	17.30	27.36	17.30	0.809	0.827	0.832	0.823

^a $u(T/K) = \pm 0.01$, $u(p/Pa) = \pm 0.01$.

 Table 4.64. Vapor pressures of 2,7-dibromofluorene determined by the static method with capacitance manometers. ^a

<i>T</i> / K	<i>p</i> / Pa	100Δ <i>p</i> / <i>p</i> ^b	<i>T</i> / K	<i>p</i> / Pa	100Δ <i>p</i> / <i>p</i> ^b	<i>T</i> / K	<i>p</i> / Pa	100Δ <i>p</i> / <i>p</i> ^b
<i>Crystalline phase</i>								
382.23	0.732	0.4	388.21	1.254	0.5	394.16	2.104	0.5
384.26	0.874	-0.2	390.11	1.472	-0.5	396.08	2.489	1.6
386.08	1.029	-0.4	392.14	1.751	-1.2	398.07	2.922	-0.4

^a $u(T) = \pm 0.01$ K, $u(p) = 0.01 + 0.0025p$ Pa;

^b $\Delta p = p - p_{\text{calc}}$, where p_{calc} is calculated from the Clarke and Glew equation with parameters given in table 4.65.

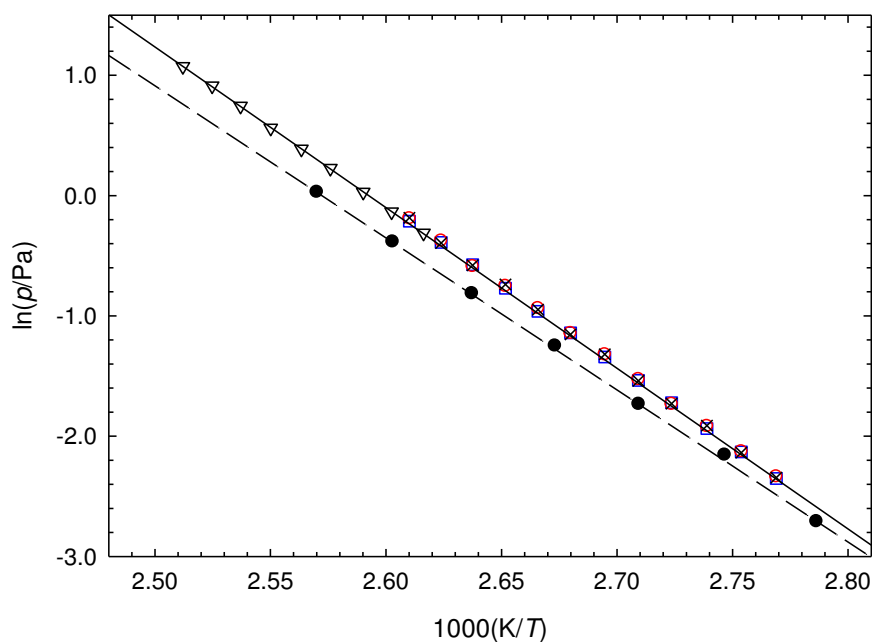


Figure 4.12. Plots of $\ln(p/\text{Pa})$ against $1000(K/T)$ of 2,7-dibromofluorene: effusion crystal vapor pressures for the different effusion orifices - □, small; ○, medium; ×, large; static vapor pressures - ▽, crystal vapor pressures; ●, literature vapor pressure results [42].

Table 4.65. Standard ($p^\circ = 0.1 \text{ MPa}$) molar properties of sublimation of 2,7-dibromofluorene derived from the vapor pressure results determined experimentally and available in the literature.

$\Delta T / \text{K}$	θ / K	$\frac{\Delta_{\text{cr}}^{\text{g}} G_{\text{m}}^{\circ}(\theta)}{\text{kJ}\cdot\text{mol}^{-1}}$	$\frac{\Delta_{\text{cr}}^{\text{g}} H_{\text{m}}^{\circ}(\theta)}{\text{kJ}\cdot\text{mol}^{-1}}$	$\frac{\Delta_{\text{cr}}^{\text{g}} S_{\text{m}}^{\circ}(\theta)^{\text{a}}}{\text{J}\cdot\text{K}^{-1}\cdot\text{mol}^{-1}}$	$p(\theta)^{\text{b}}$ Pa	R^2	$\frac{\Delta_{\text{g}}^{\text{cr}} C_{p,m}^{\circ \text{c}}}{\text{J}\cdot\text{K}^{-1}\cdot\text{mol}^{-1}}$	s^{d}
<i>Crystalline phase, effusion method</i>								
361.15-383.12	298.15	54.12 ± 0.07	114.6 ± 0.3	202.9 ± 1.0	$3.3 \cdot 10^{-5}$	0.9999	37.9	0.007
	372.14^{e}	39.44 ± 0.01	111.8 ± 0.3	194.4 ± 0.8	$2.9 \cdot 10^{-1}$			
<i>Crystalline phase, static method</i>								
382.23-398.07	298.15	54.21 ± 0.10	114.6 ± 0.4	202.5 ± 1.4	$3.2 \cdot 10^{-5}$	0.9999	37.9	0.005
	390.15^{e}	36.07 ± 0.01	111.1 ± 0.4	192.3 ± 1.0	1.5			
<i>Crystalline phase, literature^f</i>								
328.7-389.1	298.15	53.22 ± 0.21	107.3 ± 1.2	181.4 ± 4.1	$4.8 \cdot 10^{-5}$	0.9985	37.9	0.078

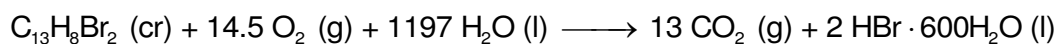
^a Calculated through equation 4.14; ^b Calculated through equation 4.15; ^c Estimated value; ^d Standard deviation of the fit defined as $s = \sqrt{\left(\sum_{i=1}^n (\ln p - \ln p_{\text{calc}})_i^2\right) / (n - m)}$, where n is the number of experimental points used in the fit and m is the number of adjustable parameters in the Clarke and Glew equation; ^e Mean temperature; ^f Calculated from the literature vapor pressure results [42] using the value of $\Delta_{\text{cr}}^{\text{g}} C_{p,m}^{\circ}$ estimated in this work.

The value of $C_{p,m}^{\circ}(\text{g}, 298.15\text{K}) = 210.09 \text{ J}\cdot\text{K}^{-1}\cdot\text{mol}^{-1}$ was calculated at the B3LYP/6-311++G(d,p) level of theory [20], and inserted into equation 4.12, yielding the result $\Delta_{\text{cr}}^{\circ} C_{p,m}^{\circ} = -34.7 \text{ J}\cdot\text{K}^{-1}\cdot\text{mol}^{-1}$.

The vapor pressure results reported by Fu and Suuberg [42], also shown in figure 4.12, are slightly smaller than the ones determined in this work. Although the variation in vapor pressure is only slight, the difference in enthalpy is significant. Their reported standard molar enthalpy of sublimation, which refers to the mean experimental temperature, was corrected to $T = 298.15 \text{ K}$, using the $\Delta_{\text{cr}}^{\circ} C_{p,m}^{\circ}$ value estimated in the present work, yielding the values compiled in table 4.65. The enthalpy of sublimation, $\Delta_{\text{cr}}^{\circ} H_{\text{m}}^{\circ}(298.15 \text{ K}) = (107.3 \pm 1.2) \text{ kJ}\cdot\text{mol}^{-1}$, differs by $-7.3 \text{ kJ}\cdot\text{mol}^{-1}$ from our result. These discrepancies may be related, again, to the insufficient purity of the samples used by Fu and Suuberg (minimum purity 0.97).

Combustion calorimetry and thermodynamic properties of formation

Combustion equation:



$$\Delta n = -1.5$$

For the study of 2,7-dibromofluorene by rotating bomb combustion calorimetry, the use of *n*-hexadecane (Aldrich Gold Label, mass fraction > 0.999) as a combustion auxiliary was needed to avoid the formation of carbon soot residue. The energy of combustion of the *n*-hexadecane used in each experiment, $\Delta U(n\text{-hex})$, was calculated using the value of the massic energy of combustion of $\Delta_c u^{\circ} = -(47150.4 \pm 1.3) \text{ J}\cdot\text{g}^{-1}$, determined in our laboratory as the mean of results obtained by a number of experimentalists in our laboratory and is in good agreement with that reported in the literature [48].

Table 4.66. Standard ($p^\circ = 0.1$ MPa) massic energy of combustion of 2,7-dibromofluorene, at $T = 298.15$ K.^a

Exp.	1	2	3	4	5	6
$m(\text{cpd}) / \text{g}$	0.92474	0.88317	0.81559	0.91887	0.79031	0.77473
$m(\text{fuse}) / \text{g}$	0.00223	0.00265	0.00230	0.00289	0.00239	0.00223
$m(n\text{-hex}) / \text{g}$			0.04746	0.05254	0.05108	0.05244
T_i / K	297.2000	297.2544	297.1986	297.1198	297.2155	297.2239
T_f / K	298.1466	298.1600	299.1466	298.1785	298.1454	298.1419
$\Delta T_{\text{ad}} / \text{K}$	0.90836	0.86768	0.91191	1.02375	0.89487	0.88278
$\varepsilon_i / \text{J}\cdot\text{K}^{-1}$	75.00	74.97	75.03	75.11	75.02	75.01
$\varepsilon_f / \text{J}\cdot\text{K}^{-1}$	73.21	73.23	73.48	73.52	73.47	73.50
$\Delta m(\text{H}_2\text{O}) / \text{g}$	2.0	0.0	-3.0	3.3	2.0	0.6
$-\Delta U(\text{IBP}) / \text{J}$	18570.19	17731.16	18623.65	20934.91	18294.41	18042.02
$\Delta U(\text{fuse}) / \text{J}$	36.22	43.04	37.35	46.93	38.81	36.22
$\Delta U(n\text{-hex}) / \text{J}$			2237.61	2477.47	2408.53	2472.75
$\Delta U(\text{HNO}_3) / \text{J}$	1.43	3.22	4.30	2.27	0.84	3.94
$\Delta U(\text{As}_2\text{O}_3)^b / \text{J}$	451.58	428.03	400.42	444.26	387.05	378.73
$\Delta U(\text{H}_2\text{PtBr}_6) / \text{J}$	0.08	0.04	0.03	0.03	0.03	0.02
$\Delta U(\text{ign}) / \text{J}$	1.12	1.12	1.11	1.11	1.11	1.11
$\Delta U(\text{carb}) / \text{J}$	4.62	4.62	3.30			5.61
$\Delta U_{\Sigma} / \text{J}$	26.59	25.48	25.81	28.91	25.33	24.92
$-\Delta_c U^\circ / \text{J}\cdot\text{g}^{-1}$	19528.64	19516.03	19521.36	19518.58	19528.82	19530.74
$-\langle \Delta_c U^\circ \rangle = (19524.0 \pm 2.5) \text{ J}\cdot\text{g}^{-1}$						

^a $\varepsilon_{\text{cal}} = (20361.4 \pm 0.6) \text{ J}\cdot\text{K}^{-1}$;^b The compound was burnt in the presence of 15.00 cm³ of an aqueous solution of As₂O₃ (0.1154 mol·dm³).Table 4.67. Standard ($p^\circ = 0.1$ MPa) molar energy and enthalpy of combustion, and derived standard molar enthalpies of formation of the crystalline and gaseous phases of 2,7-dibromofluorene, at $T = 298.15$ K.

$-\Delta_c U_m^\circ(\text{cr})$	$-\Delta_c H_m^\circ(\text{cr})$	$\Delta_f H_m^\circ(\text{cr})$	$\Delta_{\text{cr}}^g H_m^\circ$	$\Delta_f H_m^\circ(\text{g})$
$\text{kJ}\cdot\text{mol}^{-1}$	$\text{kJ}\cdot\text{mol}^{-1}$	$\text{kJ}\cdot\text{mol}^{-1}$	$\text{kJ}\cdot\text{mol}^{-1}$	$\text{kJ}\cdot\text{mol}^{-1}$
6326.0 ± 1.8	6329.7 ± 1.8	114.7 ± 2.5	114.6 ± 0.3^a	229.3 ± 2.5
			114.6 ± 0.4^b	
Mean			114.6 ± 0.2^c	229.3 ± 2.5^c

^a Derived from vapor pressure results determined by the effusion method;^b Derived from vapor pressure results determined by the static method;^c Calculated as the weighted mean.

Table 4.68. Standard ($p^\circ = 0.1$ MPa) molar absolute entropies and standard molar entropies, enthalpies and Gibbs energies of formation of the crystalline and gaseous phases of 2,7-dibromofluorene, at $T = 298.15$ K.

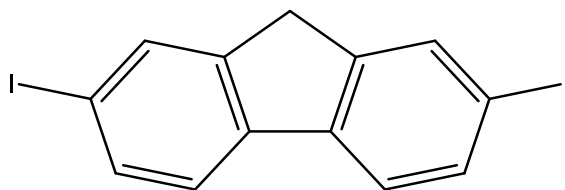
Phase	S_m°	$-T\Delta_f S_m^\circ$	$\Delta_f H_m^\circ$	$\Delta_f G_m^\circ$
	$\text{J}\cdot\text{K}^{-1}\cdot\text{mol}^{-1}$	$\text{kJ}\cdot\text{mol}^{-1}$	$\text{kJ}\cdot\text{mol}^{-1}$	$\text{kJ}\cdot\text{mol}^{-1}$
g	478.16 ^a	80.9	229.3 ± 2.5 ^c	310.2 ± 2.5
cr	275.5 ± 0.8 ^b	141.3 ± 0.2	114.7 ± 2.5	256.0 ± 2.5

^a Calculated at the B3LYP/6-311++G(d,p) level [20];

^b $S_m^\circ(\text{cr}) = S_m^\circ(\text{g}) - \Delta_{\text{cr}}^g S_m^\circ$;

^c Weighted mean of the values determined in this work using the effusion and static methods presented in table 4.65.

4.2.2.2.5. 2,7-Diiodofluorene



Molecular formula	CAS Number	Molar Mass	Density
C ₁₃ H ₈ I ₂	16218-28-3	418.0105 g·mol ⁻¹	2.171 [52]

Table 4.69. Source, purification and analysis details of 2,7-diiodofluorene.

Source	Initial purity ^a	Purification method	Final mass fraction purity ^b
Synthesis	0.979	Sublimation under reduced pressure	0.9969

^a Purity after synthesis;^b Determined by GC.

Vapor pressures and phase transition thermodynamic properties

Table 4.70. Temperatures, molar enthalpies and entropies of fusion of 2,7-diiodofluorene.

Exp.	T_{fus} (onset)	$\Delta_{\text{cr}}^{\text{l}} H_{\text{m}}^{\circ}(T_{\text{fus}})$	$\Delta_{\text{cr}}^{\text{l}} S_{\text{m}}^{\circ}(T_{\text{fus}})$
	K	kJ·mol ⁻¹	J·K ⁻¹ ·mol ⁻¹
1	490.94	24.21	
2	490.95	24.36	
3	490.83	24.26	
4	491.01	24.12	
5	490.87	24.40	
6	490.62	24.34	
Mean	490.9 ± 0.1	24.28 ± 0.09	49.5 ± 0.2
Literature	487 - 490 ^a		
	489 - 491 ^b		

^a Ref. [53,54], no information regarding minimum purity;^b Sigma-Aldrich, MSDS.

Table 4.71. Vapor pressures of 2,7-diiodofluorene determined by the Knudsen effusion method. ^a

T / K	t/s	Orifices	m / mg			p / Pa			
			m _{small}	m _{medium}	m _{large}	p _{small}	p _{medium}	p _{large}	p _{mean}
393.19	21402	A ₁ -B ₄ ¹ -C ₇	5.52	6.61	7.66	0.115	0.113	0.115	0.114
395.24	21402	A ₂ -B ₅ -C ₈	8.38	10.29	12.23	0.136	0.137	0.138	0.137
397.15	21402	A ₃ -B ₆ -C ₉	12.12	14.82	17.45	0.16	0.162	0.162	0.161
399.19	12765	A ₁ -B ₄ ¹ -C ₇	5.83	6.87	8.26	0.206	0.203	0.201	0.203
401.22	12765	A ₂ -B ₅ -C ₈	8.91	10.67	12.88	0.240	0.241	0.239	0.240
403.14	12765	A ₃ -B ₆ -C ₉	12.54	15.22	18.02	0.292	0.289	0.282	0.288
405.21	11404	A ₁ -B ₄ ¹ -C ₇		10.53	12.21		0.347	0.347	0.347
407.25	11404	A ₂ -B ₅ -C ₈	13.47	16.13	19.17	0.414	0.410	0.409	0.411
409.15	11404	A ₃ -B ₆ -C ₉	19.16	23.10	26.92	0.487	0.484	0.476	0.482
411.22	10885	A ₁ -B ₄ ¹ -C ₇	14.34	16.84	19.41	0.602	0.592	0.593	0.596
413.25	10885	A ₂ -B ₅ -C ₈	21.80	25.79	30.73	0.699	0.692	0.693	0.695
415.14	10885	A ₃ -B ₆ -C ₉	31.06	37.06		0.817	0.819		0.818

^a $u(T/K) = \pm 0.01$, $u(p/Pa) = \pm 0.01$.

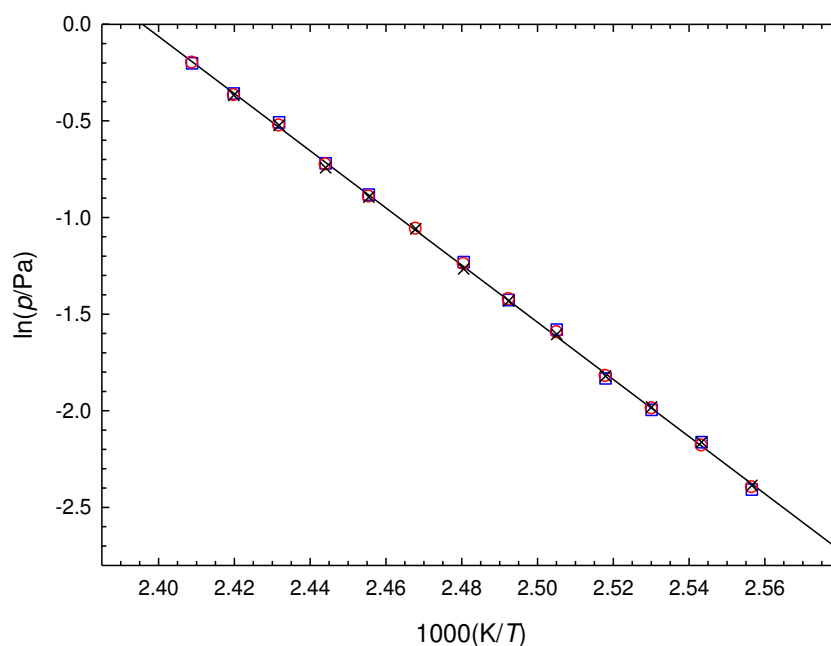


Figure 4.13. Plots of $\ln(p/Pa)$ against $1000(K/T)$ of 2,7-diiodofluorene: effusion vapor pressures for the different effusion orifices - \square , small; \circ , medium; \times , large.

Table 4.72. Standard ($p^\circ = 0.1$ MPa) molar properties of sublimation of 2,7-diiodofluorene derived from the experimental vapor pressure results.

$\Delta T / K$	θ / K	$\frac{\Delta_{cr}^g G_m^\circ(\theta)}{kJ \cdot mol^{-1}}$	$\frac{\Delta_{cr}^g H_m^\circ(\theta)}{kJ \cdot mol^{-1}}$	$\frac{\Delta_{cr}^g S_m^\circ(\theta)^a}{J \cdot K^{-1} \cdot mol^{-1}}$	$\frac{p(\theta)^b}{Pa}$	R^2	$\frac{\Delta_g^{cr} C_{p,m}^\circ}{J \cdot K^{-1} \cdot mol^{-1}}$	s^d
<i>Crystalline phase, effusion method</i>								
393.19-415.14	298.15	64.11 ± 0.19	126.5 ± 0.7	209.3 ± 2.4	$5.9 \cdot 10^{-7}$	0.9997	38.1	0.012
	404.16^e	42.58 ± 0.01	122.4 ± 0.7	197.5 ± 1.7	$3.1 \cdot 10^{-1}$			

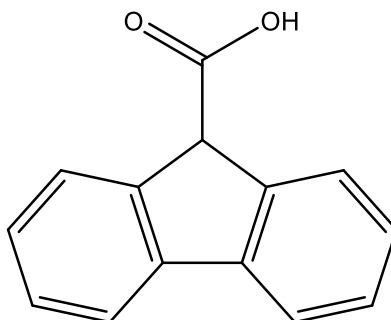
^a Calculated through equation 4.14; ^b Calculated through equation 4.15; ^c Estimated value; ^d Standard deviation of the fit defined as $s = \sqrt{\left(\sum_{i=1}^n (\ln p - \ln p_{calc,i})^2\right) / (n - m)}$, where n is the number of experimental points used in the fit and m is the number of adjustable parameters in the Clarke and Glew equation; ^e Mean temperature.

The values $\Delta_{cr}^g C_{p,m}^\circ = -38.1 J \cdot K^{-1} \cdot mol^{-1}$ was estimated in this work by means of equation 4.12 with the value $C_{p,m}^\circ(g, 298.15 K) = 211.3 J \cdot K^{-1} \cdot mol^{-1}$, which was estimated from that of fluorene [23], using a group additivity approach according to equation 4.30 and data provided in table 4.2.

$$C_{p,m}^\circ(\text{Fluorene}) - [2 \times \mathbf{C}_B\text{-(H)}(\mathbf{C}_B)_2] + [2 \times \mathbf{C}_B\text{-(F)}(\mathbf{C}_B)_2] \quad (4.30)$$

4.2.2.3. 9-Substituted fluorenes

4.2.2.3.1. 9-Fluorencarboxylic Acid



Molecular formula	CAS Number	Molar Mass	Density
C ₁₄ H ₁₀ O ₂	1989-33-9	210.2276 g·mol ⁻¹	1.164 ^a

^a Calculated from the mass/volume ratio of a pellet of the compound.

Table 4.73. Source, purification and analysis details of 9-fluorencarboxylic acid.

Source	Lot	Minimum initial purity ^a	Purification method	Final mass fraction purity ^b
Sigma-Aldrich	STBB0096	0.986	Sublimation under reduced pressure	0.9979
	STBB4311	0.966		

^a Determined by HPLC (area %), as stated in the certificate of analysis of the manufacturer (July 2009);

^b Determined by HPLC (area %), as stated in the certificate of analysis of the manufacturer (April 2010);

^b Determined by GC.

Vapor pressures and phase transition thermodynamic properties

Table 4.74. Temperatures, molar enthalpies and entropies of fusion of 9-fluorene-carboxylic acid.

Exp.	$T_{\text{fus}}(\text{onset})$	$\Delta_{\text{cr}}^{\text{l}} H_{\text{m}}^{\circ}(T_{\text{fus}})$	$\Delta_{\text{cr}}^{\text{l}} S_{\text{m}}^{\circ}(T_{\text{fus}})$
	K	$\text{kJ}\cdot\text{mol}^{-1}$	$\text{J}\cdot\text{K}^{-1}\cdot\text{mol}^{-1}$
1	503.35	30.87	
2	504.01	30.00	
3	504.14	30.34	
4	503.30	29.80	
5	503.86	30.05	
6	504.33	30.41	
Mean	503.8 ± 0.3	30.2 ± 0.3	59.9 ± 0.6
Literature ^a	501 - 504		

^a Sigma-Aldrich, MSDS.Table 4.75. Standard ($p^{\circ} = 0.1$ MPa) molar enthalpy of sublimation of 9-fluorene-carboxylic acid, determined by Calvet microcalorimetry.

Exp.	m / mg	T / K	$\Delta_{\text{cr}, 298.15 \text{ K}}^{\text{g}, T} H_{\text{m}}^{\circ}$	$\Delta_{298.15 \text{ K}}^T H_{\text{m}}^{\circ}(\text{g})$	$\Delta_{\text{cr}}^{\text{g}} H_{\text{m}}^{\circ}(298.15 \text{ K})$
			$\text{kJ}\cdot\text{mol}^{-1}$	$\text{kJ}\cdot\text{mol}^{-1}$	$\text{kJ}\cdot\text{mol}^{-1}$
1	5.776	462.46	171.14	43.44	127.70
2	5.338	462.56	170.85	43.47	127.38
3	4.578	462.55	170.51	43.47	127.04
4	5.150	462.46	170.09	43.44	126.65
5	6.549	462.46	170.29	43.44	126.85
6	5.615	462.46	171.17	43.44	127.73
Mean		462.49			127.2 ± 2.0

The calorimeter was calibrated with high purity anthracene (details in table 3.2), and the calibration constant, k_{cal} , for the mean experimental temperature, $T = 462.69$ K, was found to be $k_{\text{cal}} = (1.0015 \pm 0.0074)$, where the uncertainty is twice the standard deviation of the mean of the six independent experiments.

The term $\Delta_{298.15 \text{ K}}^T H_{\text{m}}^{\circ}(\text{g})$ was calculated from the integration of the fitting of a 2nd degree polynomial to the $C_{p,m}^{\circ}(\text{g})$ results calculated at the B3LYP/6-31G(2df,p) level of theory [55], between $T = (290 \text{ and } 500)$ K.

$$C_{p,m}^{\circ}(\text{g}) = -5.43 \cdot 10^{-4} T^2 + 1.06 T - 57.64 \quad (4.31)$$

 Table 4.76. Vapor pressures of 9-fluorene-carboxylic acid determined by the Knudsen effusion method. ^a

<i>T</i> / K	<i>t</i> / s	Orifices	<i>m</i> / mg			<i>p</i> / Pa			
			<i>m</i> _{small}	<i>m</i> _{medium}	<i>m</i> _{large}	<i>p</i> _{small}	<i>p</i> _{medium}	<i>p</i> _{large}	<i>p</i> _{zero}
384.16	26294	A ₂ -B ₅ -C ₈	5.52	8.25	11.28	0.129	0.125	0.119	0.139
386.13	26294	A ₁ -B ₄ -C ₇	6.71	9.96	13.58	0.159	0.153	0.147	0.171
388.15	21676	A ₃ -B ₆ -C ₉	6.99	10.20	14.06	0.197	0.186	0.180	0.211
390.15	21676	A ₂ -B ₅ -C ₈	8.15	12.33		0.233	0.228		
392.13	21676	A ₁ -B ₄ -C ₇	9.96	14.65	20.35	0.289	0.275	0.269	0.307
394.15	21967	A ₂ -B ₅ -C ₈	12.34	18.73	25.32	0.350	0.344	0.323	0.378
396.15	11058	A ₃ -B ₆ -C ₉	7.90	11.40	15.79	0.440	0.412	0.399	0.474
398.15	11058	A ₂ -B ₅ -C ₈	9.21	13.79	18.95	0.521	0.506	0.483	0.558
400.15	11058	A ₁ -B ₄ -C ₇	11.18	16.33	22.63	0.643	0.608	0.592	0.689
402.15	10297	A ₃ -B ₆ -C ₉	12.22	18.89	25.96	0.763	0.739	0.710	0.811
404.15	10297	A ₂ -B ₅ -C ₈	15.13	22.68	31.09	0.926	0.900	0.857	0.994
406.16	10297	A ₁ -B ₄ -C ₇	18.03	26.97	37.19	1.120	1.085	1.052	1.182

^a *u*(*T*/K) = ±0.01, *u*(*p*/Pa) = ±0.01.

The plot of the vapor pressure results as a function of temperature (figure 4.14) reveals a slight systematic decrease of vapor pressure with increasing area of the effusion orifice. In order to correct the measured vapor pressure for an hypothetical effusion orifice with zero area, the equilibrium vapor pressure at each experimental temperature, *p*_{zero}, was calculated as the intercept of the plot of *p*_{*i*} against *p*_{*i*}*w*₀*A*₀, where *p*_{*i*} represents the vapor pressure values for each experimental temperature presented in table 4.76, according to the procedure suggested by Whitman-Motzfeldt [56,57].

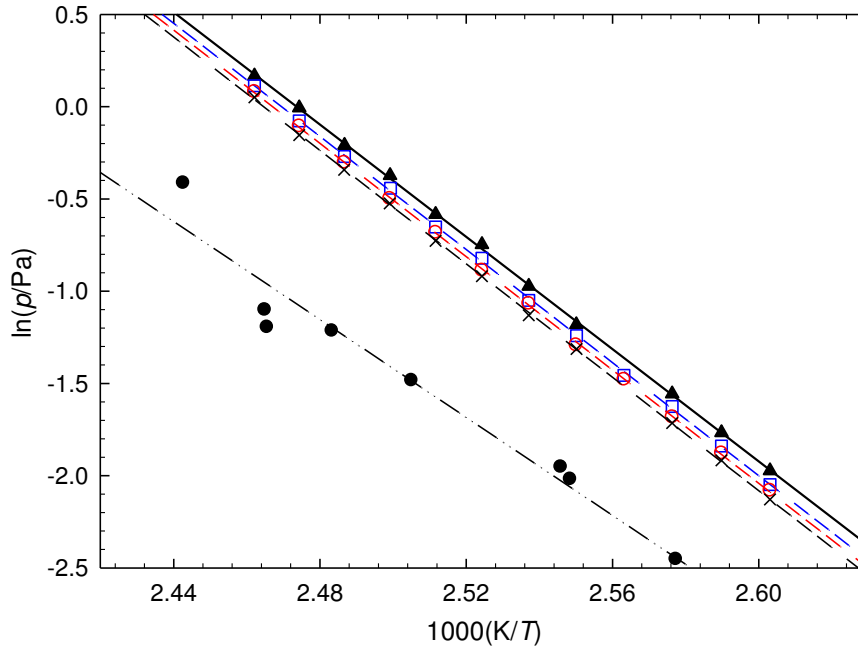


Figure 4.14. Plots of $\ln(p/\text{Pa})$ against $1000(K/T)$ of 9-fluorenicarboxylic acid: effusion vapor pressures for the different effusion orifices - \square , small; \circ , medium; \times , large; \blacktriangle , extrapolation for hypothetical effusion orifice of zero area; \bullet , literature vapor pressure results [36].

Table 4.77. Standard ($p^\circ = 0.1 \text{ MPa}$) molar properties of sublimation of 9-fluorenicarboxylic acid derived from the vapor pressure results determined experimentally and available in the literature.

$\Delta T / \text{K}$	θ / K	$\frac{\Delta_{\text{cr}}^{\text{g}} G_{\text{m}}^{\circ}(\theta)}{\text{kJ}\cdot\text{mol}^{-1}}$	$\frac{\Delta_{\text{cr}}^{\text{g}} H_{\text{m}}^{\circ}(\theta)}{\text{kJ}\cdot\text{mol}^{-1}}$	$\frac{\Delta_{\text{cr}}^{\text{g}} S_{\text{m}}^{\circ}(\theta)^{\text{a}}}{\text{J}\cdot\text{K}^{-1}\cdot\text{mol}^{-1}}$	$p(\theta)^{\text{b}}$ Pa	R^2	$\frac{\Delta_{\text{g}}^{\text{cr}} C_{\text{p,m}}^{\circ \text{c}}}{\text{J}\cdot\text{K}^{-1}\cdot\text{mol}^{-1}}$	s^{d}
<i>Crystalline phase, effusion method^e</i>								
384.16-406.16	298.15	62.30 ± 0.20	130.4 ± 0.8	228.4 ± 2.8	$1.2 \cdot 10^{-6}$	0.9997	37.7	0.013
	395.16 ^f	40.67 ± 0.01	126.8 ± 0.8	218.0 ± 2.0	$4.2 \cdot 10^{-1}$			
<i>Crystalline phase, literature^g</i>								
349.1-418.4	298.15	60.53 ± 0.49	113.5 ± 2.1	177.7 ± 0.8	$2.5 \cdot 10^{-6}$	0.9950	37.7	0.119

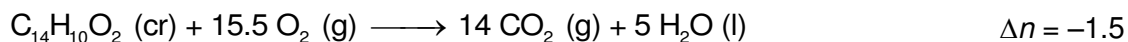
^a Calculated through equation 4.14; ^b Calculated through equation 4.15; ^c Estimated value; ^d Standard deviation of the fit defined as $s = \sqrt{\left(\sum_{i=1}^n (\ln p - \ln p_{\text{calc},i})^2\right) / (n - m)}$, where n is the number of experimental points used in the fit and m is the number of adjustable parameters in the Clarke and Glew equation; ^e Considering equilibrium vapor pressures p_{zero} ; ^f Mean temperature; ^g Calculated from the literature vapor pressure results [36] using the value of $\Delta_{\text{cr}}^{\text{g}} C_{\text{p,m}}^{\circ}$ estimated in this work.

The value of $C_{p,m}^{\circ}(\text{g}, 298.15\text{K}) = 209.09 \text{ J}\cdot\text{K}^{-1}\cdot\text{mol}^{-1}$ was calculated at the B3LYP/6-31G(2df,p) level of theory [55], and inserted into equation 4.12, yielding the result $\Delta_{\text{cr}}^{\text{g}}C_{p,m}^{\circ} = -37.7 \text{ J}\cdot\text{K}^{-1}\cdot\text{mol}^{-1}$.

The vapor pressure results reported by Goldfarb and Suuberg [36], also shown in figure 4.14, appear to be in clear disagreement with the results determined in the present work. Their reported standard molar enthalpy of sublimation, which refers to the mean experimental temperature, was corrected to $T = 298.15 \text{ K}$, using the $\Delta_{\text{cr}}^{\text{g}}C_{p,m}^{\circ}$ estimated in the present work, yielding the values compiled in table 4.77. These discrepancies may be related to insufficient purity of the sample used by Goldfarb and Suuberg (minimum purity 0.97). Also, the very low pressures measured by these authors (minimum measured vapor pressure 0.002 Pa), if not accurate, may also have contributed to such a marked inconsistency between the enthalpy of sublimation determined in this work and the one reported by them.

Combustion calorimetry and thermodynamic properties of formation

Combustion equation:



Given the brittle nature of the pressed samples, in some of the combustion experiments of 9-fluorene-carboxylic acid, the sample pellets were burnt inclosed in melinex[®] bags, using the technique described by Skinner and Snelson [47]. The energy of combustion of melinex used in each experiment, $\Delta U(\text{mel})$, was calculated using the reported value of the massic energy of combustion of melinex, $\Delta_c U^{\circ} = -(22902 \pm 5) \text{ J}\cdot\text{g}^{-1}$ [47], routinely confirmed by the combustion of melinex samples in our laboratory.

Table 4.78. Standard ($p^\circ = 0.1$ MPa) massic energy of combustion of 9-fluorene-carboxylic acid, at $T = 298.15$ K.^a

Exp.	1	2	3	4	5	6	7
$m(\text{CO}_2, \text{total}) / \text{g}$	1.46106	1.78640	1.73998	1.55600	1.61901	1.52040	1.54277
$m(\text{cpd}) / \text{g}$	0.49699	0.60797	0.59226	0.52942	0.51426	0.48100	0.49033
$m(\text{fuse}) / \text{g}$	0.00277	0.00282	0.00259	0.00282	0.00257	0.00265	0.00266
$m(\text{mel}) / \text{g}$					0.04701	0.04646	0.04428
$\Delta T_{\text{ad}} / \text{K}$	1.01037	1.23694	1.20424	1.07577	1.11562	1.04704	1.06242
$\varepsilon / \text{J}\cdot\text{K}^{-1}$	14.11	14.31	14.32	14.18	14.23	14.15	14.16
$\Delta m(\text{H}_2\text{O}) / \text{g}$	-1.1	-0.1	1.0	1.1	-2.7	-0.4	0.8
$-\Delta U(\text{IBP}) / \text{J}$	15721.88	19253.03	18749.58	16749.60	17352.25	16295.52	16540.33
$\Delta U(\text{fuse}) / \text{J}$	44.98	45.80	42.06	45.80	41.74	43.04	43.20
$\Delta U(\text{melinex}) / \text{J}$					1076.67	1064.11	1014.08
$\Delta U(\text{HNO}_3) / \text{J}$	0.15	0.69	0.31	0.60	1.57	2.16	2.22
$\Delta U(\text{ign}) / \text{J}$	0.70	0.67	0.68	0.66	0.81	0.80	0.71
$\Delta U(\text{carb}) / \text{J}$				1.65			
$\Delta U_{\Sigma} / \text{J}$	10.46	13.08	12.69	11.21	11.84	11.05	11.22
$-\Delta_c U^\circ / \text{J}\cdot\text{g}^{-1}$	31522.34	31569.75	31564.72	31531.94	31541.30	31549.19	31549.32
$-\langle \Delta_c U^\circ \rangle = (31546.5 \pm 6.4) \text{ J}\cdot\text{g}^{-1}$							
$\langle \% \text{CO}_2 \rangle = (100.015 \pm 0.012) \%$							

^a $\varepsilon_{\text{cal}} = (15551.7 \pm 1.2) \text{ J}\cdot\text{K}^{-1}$.Table 4.79. Standard ($p^\circ = 0.1$ MPa) molar energy and enthalpy of combustion, and derived standard molar enthalpies of formation of the crystalline and gaseous phases of 9-fluorene-carboxylic acid, at $T = 298.15$ K.

$-\Delta_c U_m^\circ(\text{cr})$	$-\Delta_c H_m^\circ(\text{cr})$	$-\Delta_f H_m^\circ(\text{cr})$	$\Delta_{\text{cr}}^g H_m^\circ$	$-\Delta_f H_m^\circ(\text{g})$
$\text{kJ}\cdot\text{mol}^{-1}$	$\text{kJ}\cdot\text{mol}^{-1}$	$\text{kJ}\cdot\text{mol}^{-1}$	$\text{kJ}\cdot\text{mol}^{-1}$	$\text{kJ}\cdot\text{mol}^{-1}$
6632.0 ± 2.9	6635.8 ± 2.9	302.5 ± 3.4	130.4 ± 0.8^a	172.1 ± 3.5
			127.2 ± 2.0^b	175.3 ± 3.9
		Mean	130.0 ± 0.7^c	172.5 ± 3.5

^a Derived from vapor pressure results;^b Derived from calorimetric results;^c Calculated as the weighted mean of the results.

Table 4.80. Standard ($p^\circ = 0.1$ MPa) molar absolute entropies and standard molar entropies, enthalpies and Gibbs energies of formation of the crystalline and gaseous phases of 9-fluorene-carboxylic acid, at $T = 298.15$ K.

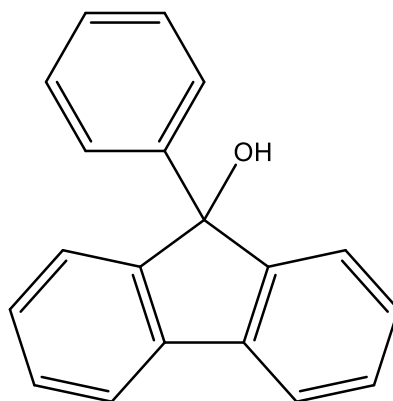
Phase	S_m°	$-T\Delta_f S_m^\circ$	$-\Delta_f H_m^\circ$	$-\Delta_f G_m^\circ$
	$\text{J}\cdot\text{K}^{-1}\cdot\text{mol}^{-1}$	$\text{kJ}\cdot\text{mol}^{-1}$	$\text{kJ}\cdot\text{mol}^{-1}$	$\text{kJ}\cdot\text{mol}^{-1}$
g	451.58 ^a	145.3	172.1 ± 3.5 ^c	26.8 ± 3.5
cr	223.18 ± 2.8 ^b	213.4 ± 0.8	302.5 ± 3.4	89.1 ± 3.5

^a Calculated at the B3LYP/6-31G(2df,p) level [55];

^b $S_m^\circ(\text{cr}) = S_m^\circ(\text{g}) - \Delta_{\text{cr}}^\circ S_m^\circ$;

^c Derived from vapor pressure results.

4.2.2.3.2. 9-Phenyl-9-fluoreno



Molecular formula	CAS Number	Molar Mass	Density
C ₁₉ H ₁₄ O	25603-67-2	258.3125 g·mol ⁻¹	1.242 [58]

Table 4.81. Source, purification and analysis details of 9-phenyl-9-fluoreno.

Source	Lot	Minimum initial purity ^a	Purification method	Final mass fraction purity ^b
Aldrich	1442505v	0.999	Sublimation under reduced pressure	0.9994

^a Determined by HPLC (area %), as stated in the certificate of analysis of the manufacturer;^b Determined by GC.**Vapor pressures and phase transition thermodynamic properties**

Table 4.82. Temperatures, molar enthalpies and entropies of fusion of 9-phenyl-9-fluoreno available in the literature.

T_{fus} (onset)	$\Delta_{\text{cr}}^{\text{l}} H_{\text{m}}^{\circ}(T_{\text{fus}})$	$\Delta_{\text{cr}}^{\text{l}} S_{\text{m}}^{\circ}(T_{\text{fus}})$
K	kJ·mol ⁻¹	J·K ⁻¹ ·mol ⁻¹
382.7 ± 0.1 ^a	22.7 ± 0.1 ^a	59.3 ± 0.3
382 - 386 ^b		

^a Ref. [59], mass fraction purity 0.9994;^b TCI Chemicals, MSDS.

Table 4.83. Vapor pressures of 9-phenyl-9-fluoreno1, determined by the Knudsen effusion method.^a

T / K	t/s	Orifices	m / mg			p / Pa			
			m_{small}	m_{medium}	m_{large}	p_{small}	p_{medium}	p_{large}	p_{mean}
359.16	36171	A ₃ -B ₆ -C ₉	8.78	12.48	18.16	0.128	0.119	0.121	0.123
361.15	22569	A ₂ -B ₅ -C ₈	6.38	10.16	13.84	0.152	0.157	0.148	0.152
363.10	36171	A ₁ -B ₄ -C ₇	12.55	19.44	27.42	0.189	0.190	0.188	0.189
365.15	18286	A ₂ -B ₅ -C ₈	8.08	12.44	17.36	0.239	0.238	0.231	0.236
367.11	18286	A ₁ -B ₄ -C ₇	10.06	14.89	21.45	0.302	0.290	0.293	0.295
369.16	14828	A ₃ -B ₆ -C ₉	10.68	15.12	22.07	0.386	0.355	0.362	0.368
371.13	14828	A ₂ -B ₅ -C ₈	12.59	19.67	26.80	0.462	0.468	0.443	0.458
373.10	14828	A ₁ -B ₄ -C ₇	15.37	23.39	32.98	0.573	0.565	0.56	0.566
375.15	10335	A ₃ -B ₆ -C ₉	13.70	20.24	28.78	0.717	0.688	0.684	0.696
377.15	10335	A ₂ -B ₅ -C ₈	15.96	25.09	34.93	0.848	0.864	0.836	0.849
379.12	10335	A ₁ -B ₄ -C ₇	18.97	30.07	42.77	1.024	1.051	1.051	1.042

^a $u(T/K) = \pm 0.01$, $u(p/\text{Pa}) = \pm 0.01$.

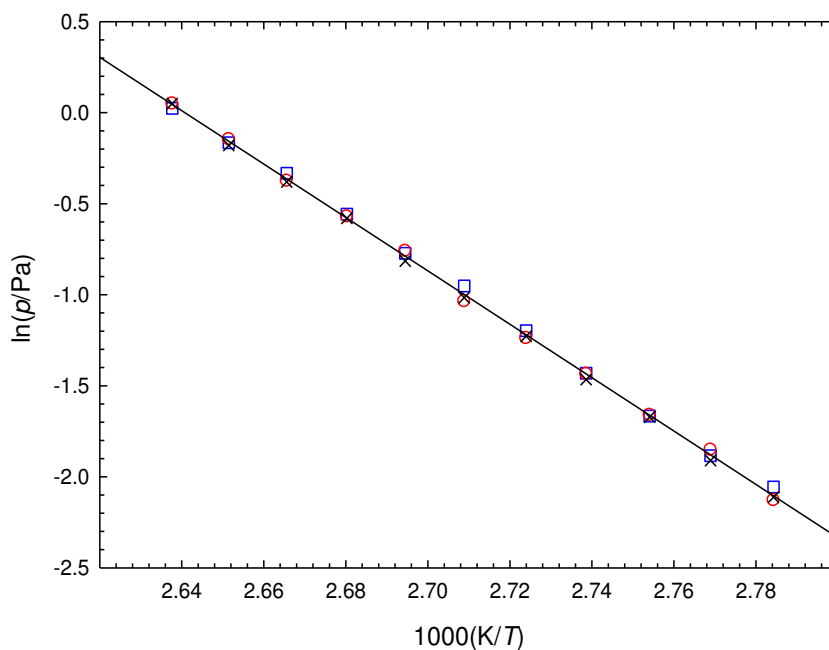


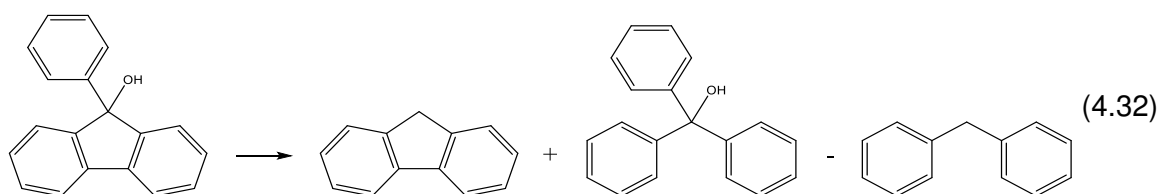
Figure 4.15. Plots of $\ln(p/\text{Pa})$ against $1000(K/T)$ of 9-phenyl-9-fluoreno1: effusion vapor pressures for the different effusion orifices - \square , small; \circ , medium; \times , large.

Table 4.84. Standard ($p^\circ = 0.1$ MPa) molar properties of sublimation of 9-phenyl-9-fluorene derived from the experimental vapor pressure results.

$\Delta T / K$	θ / K	$\frac{\Delta_{cr}^g G_m^\circ(\theta)}{kJ \cdot mol^{-1}}$	$\frac{\Delta_{cr}^g H_m^\circ(\theta)}{kJ \cdot mol^{-1}}$	$\frac{\Delta_{cr}^g S_m^\circ(\theta)^a}{J \cdot K^{-1} \cdot mol^{-1}}$	$\frac{p(\theta)^b}{Pa}$	R^2	$\frac{\Delta_{g}^{cr} C_{p,m}^\circ}{J \cdot K^{-1} \cdot mol^{-1}}$	s^d
<i>Crystalline phase, effusion method</i>								
359.16-379.12	298.15	54.79 ± 0.06	125.0 ± 0.3	235.5 ± 1.0	$2.5 \cdot 10^{-5}$	0.9999	44.0	0.006
	369.14^e	38.41 ± 0.01	121.9 ± 0.3	226.2 ± 0.8	$3.7 \cdot 10^{-1}$			

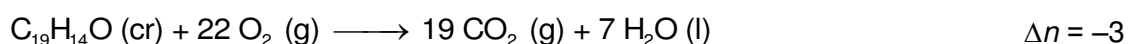
^a Calculated through equation 4.14; ^b Calculated through equation 4.15; ^c Estimated value; ^d Standard deviation of the fit defined as $s = \sqrt{\left(\sum_{i=1}^n (\ln p - \ln p_{calc})_i^2\right) / (n - m)}$, where n is the number of experimental points used in the fit and m is the number of adjustable parameters in the Clarke and Glew equation; ^e Mean temperature.

The value of $C_{p,m}^\circ$ (cr, 298.15K) of 9-phenyl-9-fluorene was inserted into equation 4.10, yielding the result $\Delta_{cr}^g C_{p,m}^\circ = -44.0 J \cdot K^{-1} \cdot mol^{-1}$. The value of $C_{p,m}^\circ$ (cr, 298.15K) = $288.4 J \cdot K^{-1} \cdot mol^{-1}$ was estimated by adding an increment to the $C_{p,m}^\circ$ (cr, 298.15K) of fluorene [25] corresponding to the substitution of the hydrogen atoms in position 9 of fluorene by an hydroxyl group and a phenyl group. This increment was estimated from the difference between the values of $C_{p,m}^\circ$ (cr, 298.5K) of triphenylmethanol [29] and diphenylmethane [29], as illustrated by equation 4.32, using data provided in table 4.2.



Combustion calorimetry and thermodynamic properties of formation

Combustion equation:



The study of 9-phenyl-9-fluorene by static bomb combustion calorimetry was initiated by another researcher [59], and completed in this work. The experimental results obtained by both researchers, presented in table 4.85, were used to derive

the standard molar enthalpies of formation in crystalline and gaseous phases presented in table 4.86.

Table 4.85. Standard ($p^\circ = 0.1$ MPa) massic energy of combustion of 9-phenyl-9-fluoreno1, at $T = 298.15$ K.^a

Exp.	1	2	3	4	5	6 ^b	7 ^b
$m(\text{CO}_2, \text{total}) / \text{g}$	1.66755	1.63665	1.69734	1.76750	1.60377	1.60314	1.59663
$m(\text{cpd}) / \text{g}$	0.51398	0.50467	0.52299	0.54476	0.49410	0.49387	0.49186
$m(\text{fuse}) / \text{g}$	0.00231	0.00213	0.00271	0.00251	0.00267	0.00275	0.00288
$\Delta T_{\text{ad}} / \text{K}$	1.21481	1.19206	1.23581	1.28746	1.16788	1.16777	1.16288
$\varepsilon / \text{J}\cdot\text{K}^{-1}$	14.20	14.22	13.88	14.33	14.16	14.21	14.20
$\Delta m(\text{H}_2\text{O}) / \text{g}$	-1.2	-0.3	0.8	-1.3	-0.7	-1.3	-0.6
$-\Delta U(\text{IBP}) / \text{J}$	18902.67	18553.12	19239.33	20032.80	18174.91	18170.39	18097.65
$\Delta U(\text{fuse}) / \text{J}$	37.51	34.59	44.01	40.76	43.36	44.66	46.77
$\Delta U(\text{HNO}_3) / \text{J}$	1.33	1.13	1.54	0.81	0.74	0.14	0.18
$\Delta U(\text{ign}) / \text{J}$	0.84	0.90	0.90	0.83	0.72	0.66	0.71
$\Delta U(\text{carb}) / \text{J}$		4.29					1.98
$\Delta U_{\Sigma} / \text{J}$	11.36	11.13	11.15	12.14	10.89	10.88	10.84
$-\Delta_c U^\circ / \text{J}\cdot\text{g}^{-1}$	36679.38	36678.54	36678.77	36675.03	36672.58	36679.11	36680.84
$-\langle \Delta_c U^\circ \rangle = (35577.8 \pm 1.1) \text{ J}\cdot\text{g}^{-1}$							
$\langle \% \text{CO}_2 \rangle = (100.09 \pm 0.03) \%$							

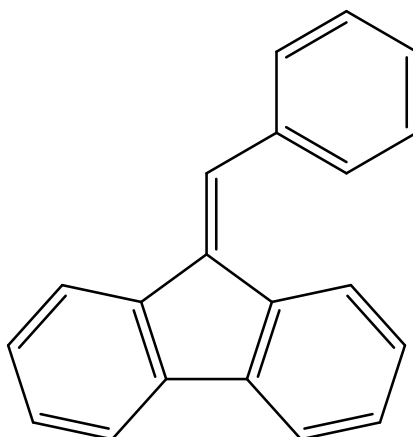
^a $\varepsilon_{\text{cal}} = (15551.7 \pm 1.2) \text{ J}\cdot\text{K}^{-1}$;

^b Experimental results obtained in this work.

Table 4.86. Standard ($p^\circ = 0.1$ MPa) molar energy and enthalpy of combustion, and derived standard molar enthalpies of formation of the crystalline and gaseous phases of 9-phenyl-9-fluoreno1, at $T = 298.15$ K.

$-\Delta_c U_m^\circ(\text{cr})$	$-\Delta_c H_m^\circ(\text{cr})$	$\Delta_f H_m^\circ(\text{cr})$	$\Delta_{\text{cr}}^g H_m^\circ$	$\Delta_f H_m^\circ(\text{g})$
$\text{kJ}\cdot\text{mol}^{-1}$	$\text{kJ}\cdot\text{mol}^{-1}$	$\text{kJ}\cdot\text{mol}^{-1}$	$\text{kJ}\cdot\text{mol}^{-1}$	$\text{kJ}\cdot\text{mol}^{-1}$
9475.3 ± 1.1	9482.8 ± 1.1	5.3 ± 2.7	125.0 ± 0.3	130.3 ± 2.7

4.2.2.3.3. 9-Benzylidene fluorene



Molecular formula	CAS Number	Molar Mass	Density
C ₂₀ H ₁₄	1836-87-9	254.3237 g·mol ⁻¹	1.176 [60]

Table 4.87. Source, purification and analysis details of 9-benzylidene fluorene.

Source	Lot	Minimum initial purity ^a	Purification method	Final mass fraction purity ^b
Aldrich	20711BA	0.994	Sublimation under reduced pressure	0.9989

^a Determined by HPLC (area %), as stated in the certificate of analysis of the manufacturer;^b Determined by GC.**Vapor pressures and phase transition thermodynamic properties**

Table 4.88. Temperatures, molar enthalpies and entropies of fusion of 9-benzylidene fluorene.

Exp.	T_{fus} (onset)	$\Delta_{\text{cr}}^{\text{l}} H_{\text{m}}^{\circ}(T_{\text{fus}})$	$\Delta_{\text{cr}}^{\text{l}} S_{\text{m}}^{\circ}(T_{\text{fus}})$
	K	kJ·mol ⁻¹	J·K ⁻¹ ·mol ⁻¹
1	348.76	16.87	
2	348.71	17.12	
3	348.71	16.99	
4	348.64	17.09	
5	348.62	16.84	
Mean	348.69 ± 0.05	17.0 ± 0.1	48.8 ± 0.3
Literature ^a	347.85-349.95		

^a Sigma-Aldrich, certificate of analysis.

Table 4.89. Vapor pressures of 9-benzylidene fluorene determined by the Knudsen effusion method.^a

<i>T</i> / K	<i>t</i> / s	Orifices	<i>m</i> / mg		<i>p</i> / Pa		
			<i>m</i> _{small}	<i>m</i> _{large}	<i>p</i> _{small}	<i>p</i> _{large}	<i>p</i> _{mean}
339.23	124030	A ₁ '-C ₇ '	5.18	5.08	0.0113	0.0111	0.0112
340.31	124030	A ₂ '-C ₈ '	5.86	5.82	0.0128	0.0127	0.0128
341.21	93808	A ₁ '-C ₇ '	4.79	4.8	0.0139	0.0139	0.0141
342.26	93808	A ₂ '-C ₈ '	5.46	5.49	0.0158	0.0159	0.0159
343.24	86483	A ₂ '-C ₈ '	5.64	5.72	0.0178	0.0180	0.0179
344.26	86483	A ₃ '-C ₉ '	6.48	6.3	0.0205	0.0199	0.0202
345.22	65244	A ₁ '-C ₇ '	5.40	5.39	0.0226	0.0226	0.0226
346.30	65244	A ₂ '-C ₈ '	6.15	6.08	0.0258	0.0255	0.0257
347.24	65244	A ₃ '-C ₉ '	6.89	6.85	0.0289	0.0288	0.0289

^a $u(T/K) = \pm 0.01$, $u(p/\text{Pa}) = \pm 0.01$.

As the amount of compound available was limited, the vapor pressure measurements of 9-benzylidene fluorene using the Knudsen effusion method was performed using only the effusion orifices of series A and C, corresponding respectively to the effusion orifices of smaller and larger effusion diameters.

Due to its very low volatility, it was only possible to determine the crystal vapor pressures of 9-benzylidene fluorene over an unusually short experimental temperature interval (≈ 8 K). Even for vapor pressures one order of magnitude smaller than those usually measured by this technique, the effusion time periods were extremely long, between (18 and 34) h. Also, considering that it is a relatively 'large' molecule, there may be a possible influence on its mean free path and consequently in the molecular flow of the gas molecules through the orifice, affecting the vapor pressure results.

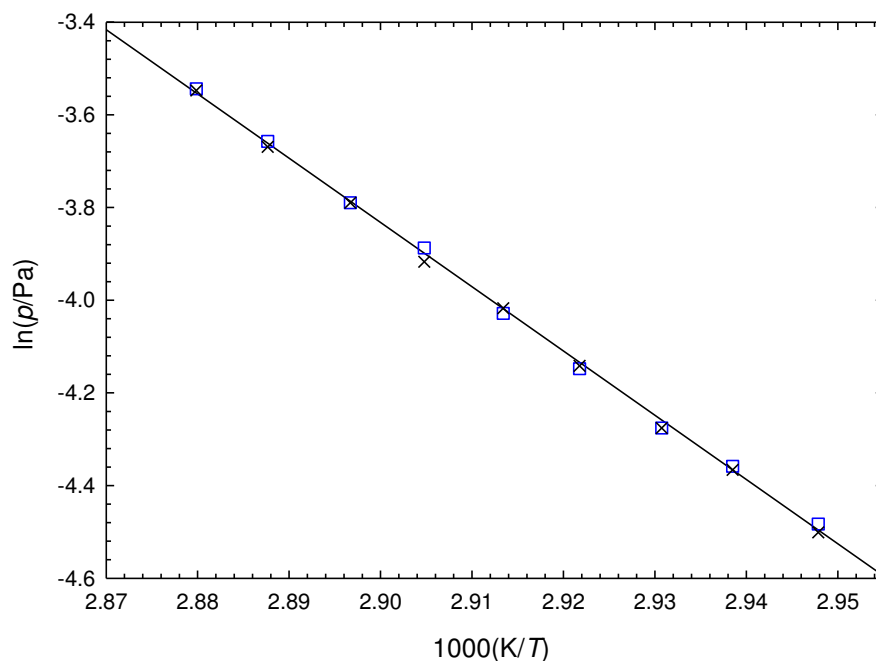


Figure 4.16. Plots of $\ln(p/\text{Pa})$ against $1000(K/T)$ of 9-benzylidene fluorene: effusion vapor pressures for the different effusion orifices - \square , small; \times , large.

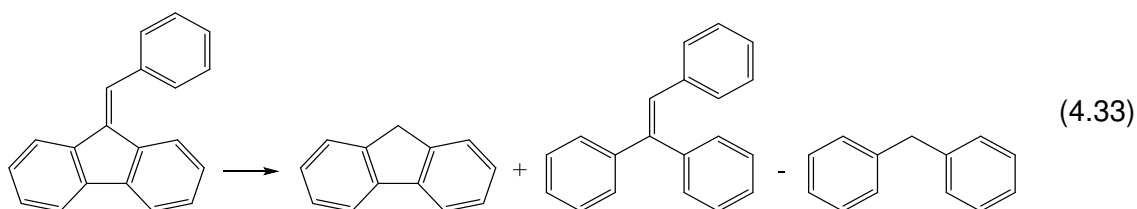
Table 4.90. Standard ($p^\circ = 0.1 \text{ MPa}$) molar properties of sublimation of 9-benzylidene fluorene derived from the experimental vapor pressure results.

$\Delta T / \text{K}$	θ / K	$\Delta_{\text{cr}}^{\text{g}} G_{\text{m}}^{\circ}(\theta)$ $\text{kJ}\cdot\text{mol}^{-1}$	$\Delta_{\text{cr}}^{\text{g}} H_{\text{m}}^{\circ}(\theta)$ $\text{kJ}\cdot\text{mol}^{-1}$	$\Delta_{\text{cr}}^{\text{g}} S_{\text{m}}^{\circ}(\theta)^{\text{a}}$ $\text{J}\cdot\text{K}^{-1}\cdot\text{mol}^{-1}$	$p(\theta)^{\text{b}}$ Pa	R^2	$\Delta_{\text{g}}^{\text{cr}} C_{\rho, \text{m}}^{\circ \text{c}}$ $\text{J}\cdot\text{K}^{-1}\cdot\text{mol}^{-1}$	s^{d}
<i>Crystalline phase, effusion method</i>								
339.23-347.24	298.15	53.8 ± 0.1	117.7 ± 1.1	214.3 ± 3.7	$3.8 \cdot 10^{-5}$	0.9994	42.6	0.009
	343.24^{e}	44.33 ± 0.01	115.8 ± 1.1	208.2 ± 3.2	$1.8 \cdot 10^{-2}$			

^a Calculated through equation 4.14; ^b Calculated through equation 4.15; ^c Estimated value; ^d Standard deviation of the fit defined as $s = \sqrt{\left(\sum_{i=1}^n (\ln p - \ln p_{\text{calc}, i})^2\right) / (n - m)}$, where n is the number of experimental points used in the fit and m is the number of adjustable parameters in the Clarke and Glew equation; ^e Mean temperature.

The value of $C_{\rho, \text{m}}^{\circ}(\text{cr}, 298.15\text{K})$ of 9-benzylidene fluorene was inserted into equation 4.10, yielding the result $\Delta_{\text{cr}}^{\text{g}} C_{\rho, \text{m}}^{\circ} = -42.6 \text{ J}\cdot\text{K}^{-1}\cdot\text{mol}^{-1}$. The value of $C_{\rho, \text{m}}^{\circ}(\text{cr}, 298.15\text{K}) = 278.8 \text{ J}\cdot\text{K}^{-1}\cdot\text{mol}^{-1}$ was estimated by adding an increment to the $C_{\rho, \text{m}}^{\circ}(\text{cr}, 298.15\text{K})$ of fluorene [25] corresponding to the substitution of the hydrogen atoms in position 9 of fluorene by a styryl group. This increment was estimated from the difference

between the values of $C_{p,m}^{\circ}$ (cr, 298.5K) of triphenylethylene [29] and diphenylmethane [29], as illustrated by equation 4.33, using data provided in table 4.2.



Combustion calorimetry and thermodynamic properties of formation

Combustion equation:

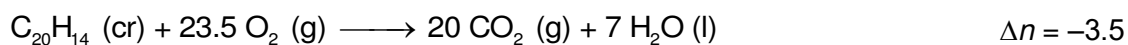


Table 4.91. Standard ($p^{\circ} = 0.1 \text{ MPa}$) massic energy of combustion of 9-benzylidene fluorene, at $T = 298.15 \text{ K}$.^a

Exp.	1	2	3	4	5	6
$m(\text{CO}_2, \text{total}) / \text{g}$	1.67596	1.41511	1.40051	1.46144	1.43938	1.30158
$m(\text{cpd}) / \text{g}$	0.48288	0.40752	0.40341	0.42113	0.41466	0.37449
$m(\text{fuse}) / \text{g}$	0.00294	0.00290	0.00269	0.00243	0.00263	0.00340
$\Delta T_{\text{ad}} / \text{K}$	1.23659	1.04325	1.03328	1.07851	1.06151	0.96004
$c_{\text{cal}} / \text{J}\cdot\text{K}^{-1}$	14.15	13.96	13.95	13.99	13.97	13.88
$\Delta m(\text{H}_2\text{O}) / \text{g}$	2.0	3.1	1.9	1.8	1.5	1.3
$-\Delta U(\text{IBP}) / \text{J}$	19258.92	16252.41	16091.89	16795.87	16529.78	14948.81
$\Delta U(\text{fuse}) / \text{J}$	47.75	47.10	43.69	39.46	42.71	55.22
$\Delta U(\text{HNO}_3) / \text{J}$	0.70	0.87	0.76	1.24	1.06	0.94
$\Delta U(\text{ign}) / \text{J}$	0.84	0.82	0.67	0.73	0.83	0.95
$\Delta U_{\Sigma} / \text{J}$	11.16	9.26	9.15	9.59	9.43	8.44
$-\Delta_c U^{\circ} / \text{J}\cdot\text{g}^{-1}$	-39758.43	39738.35	39755.60	39761.60	39732.79	39743.03

$$-\langle \Delta_c U^{\circ} \rangle = (39748.30 \pm 4.8) \text{ J}\cdot\text{g}^{-1}$$

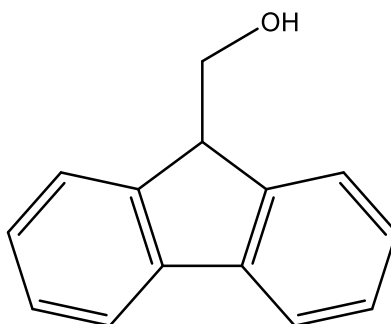
$$\langle \% \text{CO}_2 \rangle = (100.053 \pm 0.008) \%$$

^a $c_{\text{cal}} = (15551.7 \pm 1.2) \text{ J}\cdot\text{K}^{-1}$.

Table 4.92. Standard ($p^\circ = 0.1$ MPa) molar energy and enthalpy of combustion, and derived standard molar enthalpies of formation of the crystalline and gaseous phases of 9-phenyl-9-fluoreno1, at $T = 298.15$ K.

$-\Delta_c U_m^\circ(\text{cr})$	$-\Delta_c H_m^\circ(\text{cr})$	$\Delta_f H_m^\circ(\text{cr})$	$\Delta_{\text{cr}}^g H_m^\circ$	$\Delta_f H_m^\circ(\text{g})$
$\text{kJ}\cdot\text{mol}^{-1}$	$\text{kJ}\cdot\text{mol}^{-1}$	$\text{kJ}\cdot\text{mol}^{-1}$	$\text{kJ}\cdot\text{mol}^{-1}$	$\text{kJ}\cdot\text{mol}^{-1}$
10108.9 ± 3.0	10117.6 ± 3.0	246.6 ± 4.0	117.7 ± 1.1	364.3 ± 4.1

4.2.2.3.4. 9-Fluorenemethanol



Molecular formula	CAS Number	Molar Mass	Density
C ₁₄ H ₁₂ O	24324-17-2	196.2440 g·mol ⁻¹	1.084 ^a

^a Calculated from the mass/volume ratio of a pellet of the compound.

Table 4.93. Source, purification and analysis details of 9-fluorenemethanol.

Source	Lot	Minimum initial purity ^a	Purification method	Final mass fraction purity ^b
Aldrich	1428746	0.993	Sublimation under reduced pressure	0.9998

^a Determined by HPLC (area %), as stated in the certificate of analysis of the manufacturer;

^b Determined by GC.

Vapor pressures and phase transition thermodynamic properties

Table 4.94. Temperatures, molar enthalpies and entropies of fusion of 9-fluorenemethanol.

T_{fus} (onset)	$\Delta_{\text{cr}}^{\text{l}} H_{\text{m}}^{\circ}(T_{\text{fus}})$	$\Delta_{\text{cr}}^{\text{l}} S_{\text{m}}^{\circ}(T_{\text{fus}})$	T_{tp}	$\Delta_{\text{cr}}^{\text{l}} H_{\text{m}}^{\circ}(T_{\text{tp}})$	$\Delta_{\text{cr}}^{\text{l}} S_{\text{m}}^{\circ}(T_{\text{tp}})$
K	kJ·mol ⁻¹	J·K ⁻¹ ·mol ⁻¹	K	kJ·mol ⁻¹	J·K ⁻¹ ·mol ⁻¹
377.1 ± 0.1 ^a	27.9 ± 0.2 ^a	74.0 ± 0.5	376.43 ^b	29.2 ± 0.2 ^c	77.6 ± 0.5
376-378 ^d					

^a Ref. [61], mass fraction purity 0.9998;

^b Triple point temperature derived indirectly from vapor pressure results;

^c Determined indirectly from the $\Delta_{\text{cr}}^{\text{g}} H_{\text{m}}^{\circ}(T_{\text{tp}})$ and $\Delta_{\text{f}}^{\text{g}} H_{\text{m}}^{\circ}(T_{\text{tp}})$ values presented in table 4.96;

^d Sigma-Aldrich, MSDS.

Table 4.95. Vapor pressures of 9-fluorene-methanol determined by the Knudsen effusion method. ^a

T / K	t / s	Orifices	m / mg			p / Pa			
			m_{small}	m_{medium}	m_{large}	p_{small}	p_{medium}	p_{large}	p_{mean}
337.18	54616	A ₃ -B ₆ -C ₉	29.11	23.42	18.43	0.092	0.092	0.090	337.18
339.17	54616	A ₂ -B ₅ -C ₈	20.77	16.73	13.16	0.117	0.119	0.115	339.17
341.10	54616	A ₁ -B ₄ -C ₇	13.53	10.72	8.53	0.150	0.150	0.147	341.10
343.17	26450	A ₃ -B ₆ -C ₉	8.55	13.05	18.37	0.197	0.190	0.187	343.17
345.21	26450	A ₂ -B ₅ -C ₈	10.68	16.69	23.32	0.243	0.247	0.239	345.21
347.13	26450	A ₁ -B ₄ -C ₇	13.04	20.40	28.74	0.302	0.306	0.303	347.13
349.16	18500	A ₃ -B ₆ -C ₉	11.77	18.07	25.92	0.390	0.380	0.381	349.16
351.22	18500	A ₂ -B ₅ -C ₈	14.86	23.13	32.15	0.488	0.493	0.476	351.22
353.14	18500	A ₁ -B ₄ -C ₇	18.18	28.27	39.60	0.607	0.611	0.602	353.14
355.17	10704	A ₃ -B ₆ -C ₉	13.36	20.43	28.86	0.772	0.748	0.739	355.17
357.16	10704	A ₂ -B ₅ -C ₈	16.60	25.72	35.77	0.950	0.955	0.923	357.16
359.10	10704	A ₁ -B ₄ -C ₇	20.28	31.41	44.14	1.180	1.184	1.169	359.10

^a $u(T/K) = \pm 0.01$, $u(p/\text{Pa}) = \pm 0.01$.

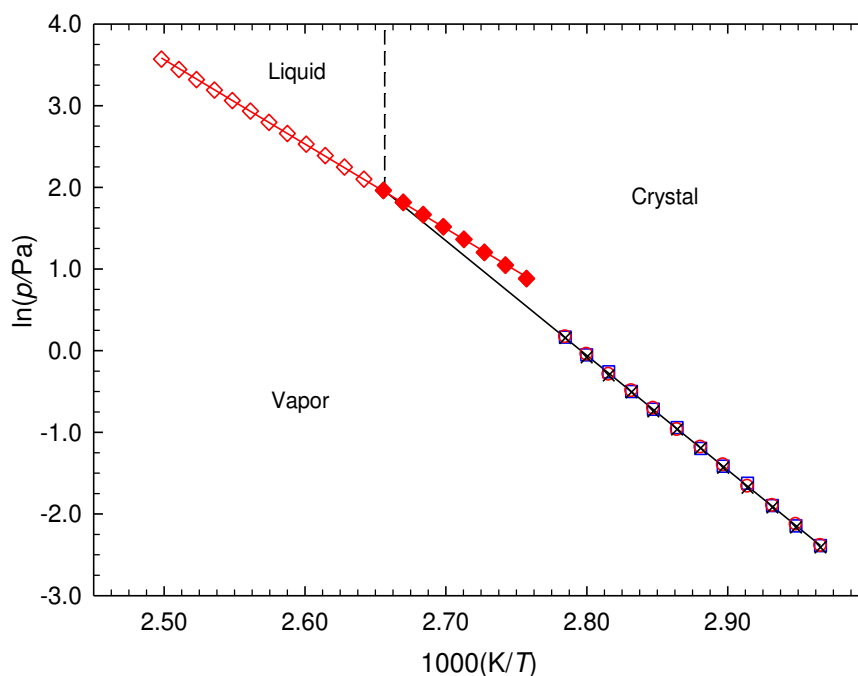


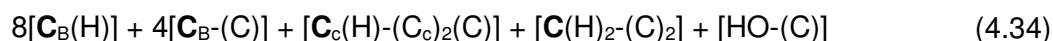
Figure 4.17. Phase diagram ($\ln(p/\text{Pa})$ against $1000(K/T)$) of 9-fluorene-methanol: effusion crystal vapor pressures for the different effusion orifices - \square , small; \circ , medium; \times , large; literature static vapor pressure results [61] - \diamond , liquid vapor pressures; \blacklozenge , supercooled liquid vapor pressures (triple point coordinates: $T_{\text{tp}} = 376.43 \text{ K}$; $p_{\text{tp}} = 7.03 \text{ Pa}$).

Table 4.96. Standard ($p^\circ = 0.1$ MPa) molar properties of sublimation and vaporization of 9-fluorenemethanol derived from the vapor pressure results determined experimentally and available in the literature.

$\Delta T / \text{K}$	θ / K	$\frac{\Delta_{\text{cr/l}}^g G_m^\circ(\theta)}{\text{kJ}\cdot\text{mol}^{-1}}$	$\frac{\Delta_{\text{cr/l}}^g H_m^\circ(\theta)}{\text{kJ}\cdot\text{mol}^{-1}}$	$\frac{\Delta_{\text{cr/l}}^g S_m^\circ(\theta)^a}{\text{J}\cdot\text{K}^{-1}\cdot\text{mol}^{-1}}$	$p(\theta)^b$ Pa	R^2	$\frac{\Delta_{\text{g}}^{\text{cr/l}} C_{\rho,m}^\circ^c}{\text{J}\cdot\text{K}^{-1}\cdot\text{mol}^{-1}}$	s^d
<i>Crystalline phase, effusion method</i>								
	298.15	48.14 ± 0.03	118.8 ± 0.2	237.0 ± 0.7	$3.7 \cdot 10^{-4}$			
337.18-359.10	348.14^e	36.43 ± 0.01	117.0 ± 0.2	231.4 ± 0.6	$3.4 \cdot 10^{-1}$	0.9999	37.0	0.014
	376.43^f	29.93 ± 0.02	115.9 ± 0.2	228.4 ± 0.5	7.0			
<i>Liquid phase, literature^g</i>								
	298.15	42.98 ± 0.01	97.8 ± 0.1	183.7 ± 0.3	$3.0 \cdot 10^{-3}$			
362.69-400.30	381.50^e	29.17 ± 0.01	86.0 ± 0.1	149.0 ± 0.3	10.1	1.0000	141.5	0.003
	376.43^f	29.93 ± 0.01	86.7 ± 0.1	150.8 ± 0.3	7.0			

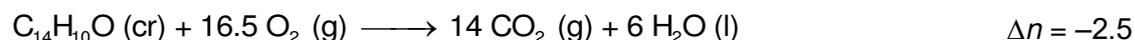
^a Calculated through equation 4.14; ^b Calculated through equation 4.15; ^c Estimated values. ^d Standard deviation of the fit defined as $s = \sqrt{\left(\sum_{i=1}^n (\ln p - \ln p_{\text{calc},i})^2\right) / (n - m)}$, where n is the number of experimental points used in the fit and m is the number of adjustable parameters in the Clarke and Glew equation; ^e Mean temperature; ^f Triple point temperature; ^g Including supercooled liquid and calculated from the literature vapor pressure results [55] using the value of $\Delta_f^g C_{\rho,m}^\circ$ estimated in this work.

The value of $C_{\rho,m}^\circ(\text{g}, 298.15\text{K}) = 205.03 \text{ J}\cdot\text{K}^{-1}\cdot\text{mol}^{-1}$ [55] was calculated at the B3LYP/6-31G(2df,p) level of theory, and inserted into equation 4.12, yielding the result $\Delta_{\text{cr}}^g C_{\rho,m}^\circ = -37.0 \text{ J}\cdot\text{K}^{-1}\cdot\text{mol}^{-1}$. The value $\Delta_{\text{cr}}^g C_{\rho,m}^\circ = 141.5 \text{ J}\cdot\text{K}^{-1}\cdot\text{mol}^{-1}$ was estimated from the difference of between $C_{\rho,m}^\circ(\text{g}, 298.15\text{K})$, referred to above, and $C_{\rho,m}^\circ(\text{l}, 298.15\text{K}) = 346.5 \text{ J}\cdot\text{K}^{-1}\cdot\text{mol}^{-1}$ estimated using group contribution values proposed by Chickos *et al.* [22], according to equation 4.34, using data provided in table 4.2.



Combustion calorimetry and thermodynamic properties of formation

Combustion equation:



The study of 9-fluorenemethanol by static bomb combustion calorimetry was performed by another researcher [61], whose results were used to derive the

standard molar enthalpies of formation in crystalline and gaseous phases presented in table 4.97.

Table 4.97. Standard ($p^\circ = 0.1$ MPa) molar energy and enthalpy of combustion, and derived standard molar enthalpies of formation of the crystalline and gaseous phases 9-fluorene-methanol, at $T = 298.15$ K.

$-\Delta_c U_m^\circ(\text{cr})$	$-\Delta_c H_m^\circ(\text{cr})$	$-\Delta_f H_m^\circ(\text{cr})$	$\Delta_{\text{cr}}^g H_m^\circ$	$\Delta_f H_m^\circ(\text{g})$
$\text{kJ}\cdot\text{mol}^{-1}$	$\text{kJ}\cdot\text{mol}^{-1}$	$\text{kJ}\cdot\text{mol}^{-1}$	$\text{kJ}\cdot\text{mol}^{-1}$	$\text{kJ}\cdot\text{mol}^{-1}$
7108.3 ± 2.3	7114.5 ± 2.3	109.6 ± 2.9	118.8 ± 0.2	9.2 ± 2.9

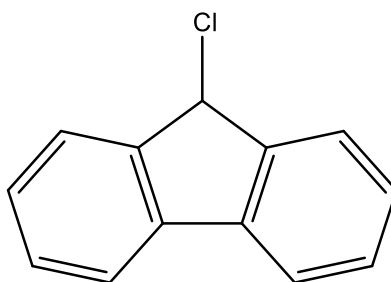
Table 4.98. Standard ($p^\circ = 0.1$ MPa) molar absolute entropies and standard molar entropies, enthalpies and Gibbs energies of formation of the crystalline and gaseous phases 9-fluorene-methanol, at $T = 298.15$ K.

Phase	S_m°	$-T\Delta_f S_m^\circ$	$\Delta_f H_m^\circ$	$\Delta_f G_m^\circ$
	$\text{J}\cdot\text{K}^{-1}\cdot\text{mol}^{-1}$	$\text{kJ}\cdot\text{mol}^{-1}$	$\text{kJ}\cdot\text{mol}^{-1}$	$\text{kJ}\cdot\text{mol}^{-1}$
g	435.52^a	158.5	9.2 ± 2.9	167.7 ± 2.9
cr	198.52 ± 0.7^b	229.1 ± 0.2	-109.6 ± 2.9	119.5 ± 2.9

^a Calculated at the B3LYP/6-31G(2df,p) level [55];

^b $S_m^\circ(\text{cr}) = S_m^\circ(\text{g}) - \Delta_{\text{cr}}^g S_m^\circ$.

4.2.2.3.5. 9-Chlorofluorene



Molecular formula	CAS Number	Molar Mass	Density
C ₁₃ H ₉ Cl	6630-65-5	200.6611 g·mol ⁻¹	1.25 [62]

Table 4.99. Source, purification and analysis details of 9-chlorofluorene.

Source	Initial purity	Purification method	Final mass fraction purity
Synthesis	— ^a	Sublimation under reduced pressure	0.9982 ^b

^a Sample not analyzed by GC previous to further purification;

^b Determined by GC.

Vapor pressures and phase transition thermodynamic properties

Table 4.100. Temperatures, molar enthalpies and entropies of fusion of 9-chlorofluorene.

Exp.	T_{fus} (onset)	$\Delta_{\text{cr}}^{\text{l}} H_{\text{m}}^{\circ}(T_{\text{fus}})$	$\Delta_{\text{cr}}^{\text{l}} S_{\text{m}}^{\circ}(T_{\text{fus}})$
	K	kJ·mol ⁻¹	J·K ⁻¹ ·mol ⁻¹
1	362.11	17.50	
2	361.86	17.50	
3	362.43	17.78	
4	361.85	17.63	
5	362.64	17.62	
Mean	362.2 ± 0.3	17.6 ± 0.1	48.6 ± 0.3
Literature	360.5 - 361.9 ^a	14.21	39.34
	359 - 361 ^b		

^a Ref. [42], minimum purity 0.97;

^b Alfa Aesar, MSDS.

Table 4.101. Vapor pressures of 9-chlorofluorene determined by the Knudsen effusion method. ^a

<i>T</i> / K	<i>t</i> / s	Orifices	<i>m</i> / mg			<i>p</i> / Pa			
			<i>m</i> _{sml}	<i>m</i> _{med}	<i>m</i> _{lrg}	<i>p</i> _{sml}	<i>p</i> _{med}	<i>p</i> _{lrg}	<i>p</i> _{mean}
309.18	40502	A ₃ -B ₆ -C ₉	7.00	10.41	14.86	0.096	0.093	0.093	0.094
311.14	40502	A ₂ -B ₅ -C ₈	8.86	13.14	18.55	0.124	0.119	0.117	0.120
313.10	40502	A ₁ -B ₄ -C ₇	10.39	16.19	22.77	0.148	0.149	0.147	0.148
315.18	19965	A ₃ -B ₆ -C ₉	6.76	10.16	14.43	0.195	0.186	0.185	0.186
317.15	19965	A ₂ -B ₅ -C ₈	8.49	12.69	17.91	0.243	0.235	0.231	0.236
319.10	19965	A ₁ -B ₄ -C ₇	9.98	15.59	22.01	0.29	0.293	0.291	0.291
321.17	10183	A ₃ -B ₆ -C ₉	6.69	9.82	13.85	0.382	0.355	0.351	0.363
323.13	10183	A ₂ -B ₅ -C ₈	8.10	12.46	17.29	0.459	0.457	0.441	0.452
325.09	10183	A ₁ -B ₄ -C ₇	9.65	14.95	21.05	0.556	0.557	0.552	0.555
327.17	10178	A ₃ -B ₆ -C ₉		19.14	27.30		0.699	0.698	0.699
329.11	10178	A ₂ -B ₅ -C ₈	15.80	23.87	33.22	0.904	0.885	0.856	0.882
331.08	10178	A ₁ -B ₄ -C ₇	18.30	28.57	40.63	1.064	1.074	1.075	1.071

^a $u(T/K) = \pm 0.01$, $u(p/Pa) = \pm 0.01$.

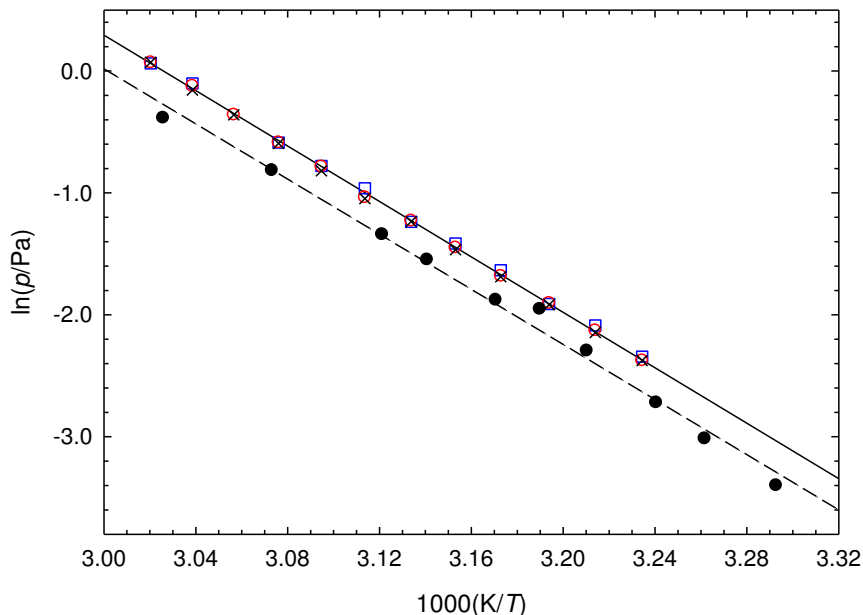


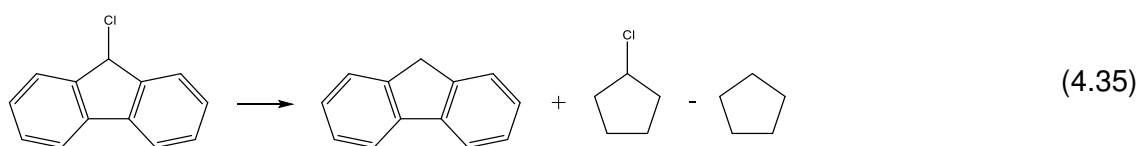
Figure 4.18. Plots of $\ln(p/Pa)$ against $1000(K/T)$ of 9-chlorofluorene: effusion crystal vapor pressures for the different effusion orifices - \square , small; \circ , medium; \times , large; \bullet , literature vapor pressure results [42].

Table 4.102. Standard ($p^\circ = 0.1$ MPa) molar properties of sublimation of 9-chlorofluorene derived from the vapor pressure results determined experimentally and available in the literature.

$\Delta T / K$	θ / K	$\frac{\Delta_{\text{cr}}^{\text{g}} G_{\text{m}}^{\circ}(\theta)}{\text{kJ}\cdot\text{mol}^{-1}}$	$\frac{\Delta_{\text{cr}}^{\text{g}} H_{\text{m}}^{\circ}(\theta)}{\text{kJ}\cdot\text{mol}^{-1}}$	$\frac{\Delta_{\text{cr}}^{\text{g}} S_{\text{m}}^{\circ}(\theta)^{\text{a}}}{\text{J}\cdot\text{K}^{-1}\cdot\text{mol}^{-1}}$	$\frac{p(\theta)^{\text{b}}}{\text{Pa}}$	R^2	$\frac{\Delta_{\text{g}}^{\text{cr}} C_{\rho,\text{m}}^{\circ\text{c}}}{\text{J}\cdot\text{K}^{-1}\cdot\text{mol}^{-1}}$	s^{d}
<i>Crystalline phase, effusion method</i>								
309.18-331.08	298.15	37.80 ± 0.03	95.0 ± 0.5	191.8 ± 1.7	$2.4 \cdot 10^{-2}$	0.9998	34.2	0.013
	320.13 ^e	33.61 ± 0.01	94.3 ± 0.5	189.6 ± 1.6	$3.3 \cdot 10^{-1}$			
<i>Crystalline phase, literature^f</i>								
349.1-418.4	298.15	38.43 ± 0.18	94.6 ± 3.0	198 ± 10	$1.9 \cdot 10^{-2}$	0.9920	34.2	0.090

^a Calculated through equation 4.14; ^b Calculated through equation 4.15; ^c Estimated value; ^d Standard deviation of the fit defined as $s = \sqrt{\left(\sum_{i=1}^n (\ln p - \ln p_{\text{calc}})^2\right) / (n - m)}$, where n is the number of experimental points used in the fit and m is the number of adjustable parameters in the Clarke and Glew equation; ^e Mean temperature; ^f Calculated from the literature vapor pressure results [42] using the value of $\Delta_{\text{cr}}^{\text{g}} C_{\rho,\text{m}}^{\circ}$ estimated in this work.

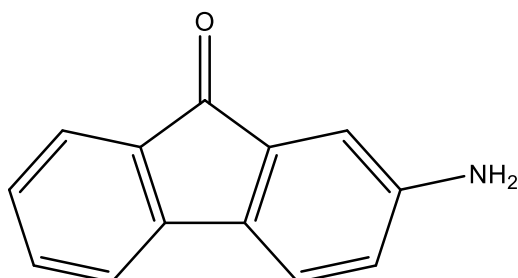
The value of $C_{\rho,\text{m}}^{\circ}$ (g, 298.15K) of 9-chlorofluorene was inserted into equation 4.12, yielding the result $\Delta_{\text{cr}}^{\text{g}} C_{\rho,\text{m}}^{\circ} = -34.2 \text{ J}\cdot\text{K}^{-1}\cdot\text{mol}^{-1}$. The value of $C_{\rho,\text{m}}^{\circ}$ (g, 298.15K) = 189.2 $\text{J}\cdot\text{K}^{-1}\cdot\text{mol}^{-1}$ was estimated by adding an increment to the $C_{\rho,\text{m}}^{\circ}$ (g, 298.15K) of fluorene corresponding to the substitution of an hydrogen atom by a chlorine atom in position 9 of fluorene. The increment for the chlorine atom was estimated from the difference between the values of $C_{\rho,\text{m}}^{\circ}$ (g, 298.15K) of chlorocyclopentane [31] and cyclopentane [30], as illustrated in equation 4.35, using data provided in table 4.2.



The vapor pressure results reported by Fu and Suuberg [42], also shown in figure 4.18, are systematically slightly smaller than the ones determined in this work, but present identical tendencies with temperature (regression slopes). Their reported standard molar enthalpy of sublimation, which refers to the mean experimental temperature, was corrected to $T = 298.15$ K, using the $\Delta_{\text{cr}}^{\text{g}} C_{\rho,\text{m}}^{\circ}$ value estimated in the present work, yielding the values compiled in table 4.102. The enthalpy of sublimation, $\Delta_{\text{cr}}^{\text{g}} H_{\text{m}}^{\circ}$ (298.15 K) = $(94.6 \pm 3.0) \text{ kJ}\cdot\text{mol}^{-1}$, is within experimental uncertainty of the result determined in the present work, and vapor pressures extrapolated to $T = 298.15$ K only differ by $5 \cdot 10^{-3}$ Pa.

4.2.2.4. 2-Substituted fluorenones

4.2.2.4.1. 2-Aminofluorenone



Molecular formula	CAS Number	Molar Mass	Density
C ₁₃ H ₉ NO	3096-57-9	195.2158 g·mol ⁻¹	1.327 [63]

Table 4.103. Source, purification and analysis details of 2-aminofluorenone.

Source	Lot	Minimum initial purity ^a	Purification method	Final mass fraction purity ^b
Aldrich	04618LHV	0.991	Sublimation under reduced pressure	0.9985

^a Determined by HPLC (area %), as stated in the certificate of analysis of the manufacturer;^b Determined by GC.

Vapor pressures and phase transition thermodynamic properties

Table 4.104. Temperatures, molar enthalpies and entropies of fusion of 2-aminofluorenone.

Exp.	T_{fus} (onset)	$\Delta_{\text{cr}}^{\text{l}} H_{\text{m}}^{\circ}(T_{\text{fus}})$	$\Delta_{\text{cr}}^{\text{l}} S_{\text{m}}^{\circ}(T_{\text{fus}})$
	K	kJ·mol ⁻¹	J·K ⁻¹ ·mol ⁻¹
1	429.62	23.96	
2	429.63	24.14	
3	429.51	24.00	
4	429.57	24.19	
5	429.28	24.02	
Mean	429.5 ± 0.1	24.06 ± 0.09	56.0 ± 0.2
Literature ^a	430 - 433		

^a Sigma Aldrich, MSDS.

Table 4.105. Vapor pressures of 2-aminofluorenone determined by the Knudsen effusion method.^a

T / K	t / s	Orifices	m / mg			p / Pa			
			m_{sml}	m_{med}	m_{lrq}	p_{sml}	p_{med}	p_{lrq}	p_{mean}
373.14	41403	A ₃ -B ₆ -C ₉	7.10	10.59	14.48	0.106	0.103	0.099	0.103
375.09	41403	A ₂ -B ₅ -C ₈	8.41	12.66	17.60	0.128	0.125	0.121	0.125
377.10	41403	A ₁ -B ₄ -C ₇	9.94	15.18	21.17	0.154	0.152	0.149	0.152
379.15	19912	A ₃ -B ₆ -C ₉	6.14	8.79	12.41	0.198	0.179	0.177	0.185
381.10	19912	A ₂ -B ₅ -C ₈	7.20	10.93	15.34	0.230	0.226	0.220	0.225
383.11	19912	A ₁ -B ₄ -C ₇	8.47	13.04	18.27	0.275	0.273	0.269	0.272
385.15	10995	A ₃ -B ₆ -C ₉	5.99	9.00	12.68	0.352	0.335	0.33	0.339
387.08	10995	A ₂ -B ₅ -C ₈	7.26	11.32	15.46	0.423	0.427	0.406	0.419
389.10	10995	A ₁ -B ₄ -C ₇	8.32	13.18	18.64	0.492	0.504	0.502	0.499
391.15	10222	A ₃ -B ₆ -C ₉	10.02	14.52	20.93	0.638	0.586	0.59	0.605
393.09	10222	A ₂ -B ₅ -C ₈	11.97	18.00	25.04	0.755	0.736	0.712	0.734
395.11	10222	A ₁ -B ₄ -C ₇	13.85	21.14	29.84	0.888	0.877	0.871	0.879

^a $u(T/K) = \pm 0.01$, $u(p/\text{Pa}) = \pm 0.01$.

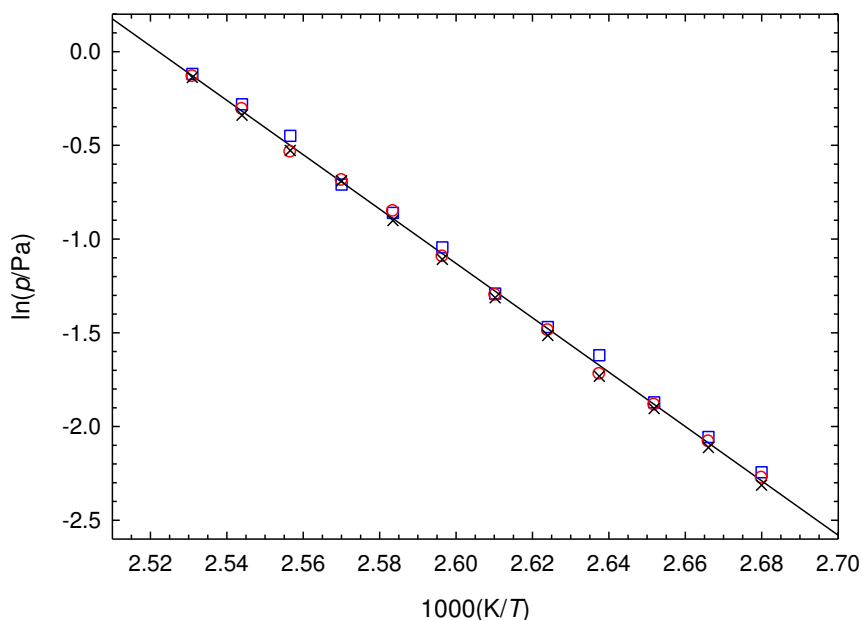


Figure 4.19. Plots of $\ln(p/\text{Pa})$ against $1000(K/T)$ of 2-aminofluorenone: effusion crystal vapor pressures for the different effusion orifices - \square , small; \circ , medium; \times , large.

Table 4.106. Standard ($p^\circ = 0.1$ MPa) molar properties of sublimation of 2-aminofluorenone derived from the experimental vapor pressure results.

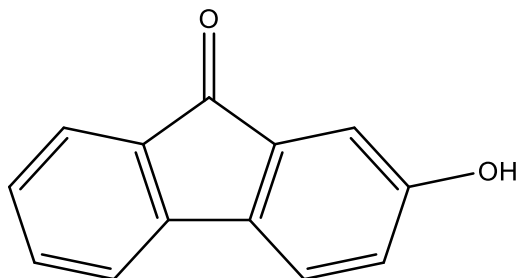
$\Delta T / K$	θ / K	$\frac{\Delta_{cr}^g G_m^\circ(\theta)}{kJ \cdot mol^{-1}}$	$\frac{\Delta_{cr}^g H_m^\circ(\theta)}{kJ \cdot mol^{-1}}$	$\frac{\Delta_{cr}^g S_m^\circ(\theta)^a}{J \cdot K^{-1} \cdot mol^{-1}}$	$\frac{p(\theta)^b}{Pa}$	R^2	$\frac{\Delta_{g}^{cr} C_{p,m}^\circ}{J \cdot K^{-1} \cdot mol^{-1}}$	s^d
<i>Crystalline phase, effusion method</i>								
373.14-395.11	298.15	58.82 ± 0.16	123.7 ± 0.7	217.6 ± 2.4	$5.0 \cdot 10^{-6}$	0.9997	36.2	0.014
	384.13^e	40.53 ± 0.01	120.6 ± 0.7	208.4 ± 1.8	$3.1 \cdot 10^{-1}$			

^a Calculated through equation 4.14; ^b Calculated through equation 4.15; ^c Estimated value; ^d Standard deviation of the fit defined as $s = \sqrt{\left(\sum_{i=1}^n (\ln p - \ln p_{calc,i})^2\right) / (n - m)}$, where n is the number of experimental points used in the fit and m is the number of adjustable parameters in the Clarke and Glew equation; ^e Mean temperature.

The value $\Delta_{cr}^g C_{p,m}^\circ = -36.2 J \cdot K^{-1} \cdot mol^{-1}$ was estimated in this work by means of equation 4.12 with the value $C_{p,m}^\circ(g, 298.15 K) = 200.8 J \cdot K^{-1} \cdot mol^{-1}$, estimated for this compound from the value $C_{p,m}^\circ(g, 298.15 K)$ of fluorenone [26] using a group additivity approach according to equation 4.36 and data provided in table 4.2.

$$C_{p,m}^\circ(\text{Fluorenone}) - [1 \times \mathbf{C}_B\text{-(H)}(\mathbf{C}_B)_2] + [1 \times \mathbf{C}_B\text{-(N)}(\mathbf{C}_B)_2] + [1 \times \mathbf{N}\text{-(C}_B\text{)}(\mathbf{H})_2] \quad (4.36)$$

4.2.2.4.2. 2-Hydroxyfluorenone



Molecular formula	CAS Number	Molar Mass	Density
C ₁₃ H ₈ O ₂	6949-73-1	196.2004 g·mol ⁻¹	1.2272 [14]

Table 4.107. Source, purification and analysis details of 2-hydroxyfluorenone.

Source	Lot	Minimum initial purity ^a	Purification method	Final mass fraction purity ^a
Acros Organics	A0137718	0.9939	Sublimation under reduced pressure	0.9986

^a Determined by GC.

Vapor pressures and phase transition thermodynamic properties

Table 4.108. Temperatures, molar enthalpies and entropies of fusion of 2-hydroxyfluorenone.

Exp.	T_{fus} (onset)	$\Delta_{\text{cr}}^{\text{l}} H_{\text{m}}^{\circ}(T_{\text{fus}})$	$\Delta_{\text{cr}}^{\text{l}} S_{\text{m}}^{\circ}(T_{\text{fus}})$
	K	kJ·mol ⁻¹	J·K ⁻¹ ·mol ⁻¹
1	482.49	29.37	
2	482.22	29.58	
3	482.41	29.36	
4	482.42	29.42	
5	481.92	29.13	
Mean	482.3 ± 0.2	29.4 ± 0.1	61.0 ± 0.2
Literature ^a	477 - 479		

^a Sigma Aldrich, MSDS.

Table 4.109. Vapor pressures of 2-hydroxyfluorenone determined by the Knudsen effusion method.^a

T / K	t / s	Orifices	m / mg			p / Pa			
			m_{sml}	m_{med}	m_{lrg}	p_{sml}	p_{med}	p_{lrg}	p_{mean}
387.16	21287	A ₁ '-B ₄ '-C ₇ '	3.70	4.48	5.54	0.089	0.087	0.086	0.087
389.22	21287	A ₂ '-B ₅ '-C ₈ '	4.62	5.65	6.66	0.111	0.110	0.103	0.108
391.26	21287	A ₃ '-B ₆ '-C ₉ '	5.47	6.65	8.10	0.132	0.130	0.126	0.129
393.17	14621	A ₁ '-B ₄ '-C ₇ '	4.70	5.66	6.81	0.166	0.161	0.155	0.161
395.23	14621	A ₂ '-B ₅ '-C ₈ '	5.80		8.14	0.205		0.185	0.195
397.26	14621	A ₃ '-B ₆ '-C ₉ '	6.74	8.14	10.05	0.239	0.233	0.229	0.234
399.18	10663	A ₁ '-B ₄ '-C ₇ '	5.99	7.33	8.87	0.292	0.289	0.278	0.286
401.21	11897	A ₂ '-B ₅ '-C ₈ '			12.74			0.359	
401.26	10663	A ₂ '-B ₅ '-C ₈ '	7.25	8.78	10.62	0.354	0.347		
403.25	11897	A ₃ '-B ₆ '-C ₉ '	10.05	12.43	15.63	0.441	0.441	0.442	0.441
405.18	10246	A ₁ '-B ₄ '-C ₇ '			15.81			0.52	
405.26	10663	A ₃ '-B ₆ '-C ₉ '	10.36	12.59		0.509	0.500		
407.23	10246	A ₂ '-B ₅ '-C ₈ '	12.41	15.05	18.78	0.636	0.624	0.619	0.626
409.26	10246	A ₃ '-B ₆ '-C ₉ '	14.89	18.38	22.51	0.765	0.763	0.744	0.757

^a $u(T/K) = \pm 0.01$, $u(p/Pa) = \pm 0.01$.

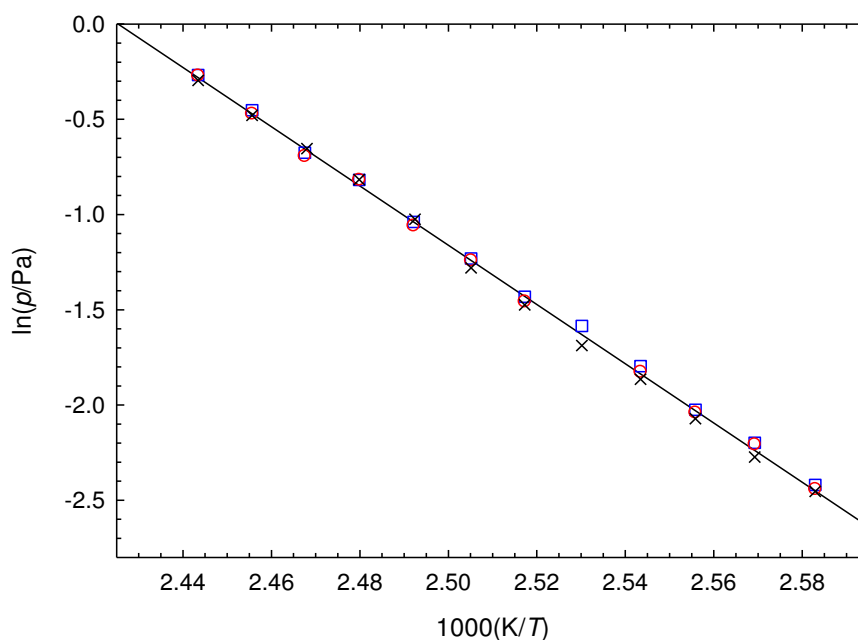


Figure 4.20. Plots of $\ln(p/Pa)$ against $1000(K/T)$ of 2-hydroxyfluorenone: effusion crystal vapor pressures for the different effusion orifices - \square , small; \circ , medium; \times , large.

Table 4.110. Standard ($p^\circ = 0.1$ MPa) molar properties of sublimation of 2-hydroxyfluorenone derived from the experimental vapor pressure results.

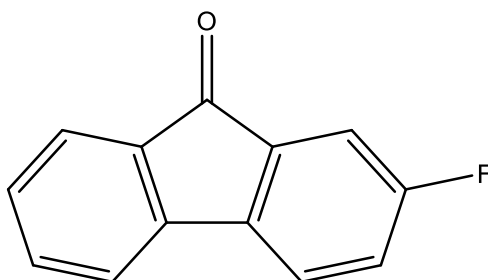
$\Delta T / K$	θ / K	$\frac{\Delta_{cr}^g G_m^\circ(\theta)}{kJ \cdot mol^{-1}}$	$\frac{\Delta_{cr}^g H_m^\circ(\theta)}{kJ \cdot mol^{-1}}$	$\frac{\Delta_{cr}^g S_m^\circ(\theta)^a}{J \cdot K^{-1} \cdot mol^{-1}}$	$\frac{p(\theta)^b}{Pa}$	R^2	$\frac{\Delta_g^{cr} C_{p,m}^\circ}{J \cdot K^{-1} \cdot mol^{-1}}$	s^d
<i>Crystalline phase, effusion method</i>								
387.16-409.26	298.15	64.83 ± 0.21	132.9 ± 0.8	228.3 ± 2.8	$4.4 \cdot 10^{-7}$	0.9996	35.1	0.015
	398.21^e	42.54 ± 0.01	129.3 ± 0.8	217.9 ± 2.0	$2.6 \cdot 10^{-1}$			

^a Calculated through equation 4.14; ^b Calculated through equation 4.15; ^c Estimated value; ^d Standard deviation of the fit defined as $s = \sqrt{\left(\sum_{i=1}^n (\ln p - \ln p_{calc,i})^2 \right) / (n - m)}$, where n is the number of experimental points used in the fit and m is the number of adjustable parameters in the Clarke and Glew equation; ^e Mean temperature.

The value $\Delta_{cr}^g C_{p,m}^\circ = -35.1 J \cdot K^{-1} \cdot mol^{-1}$ was estimated in this work by means of equation 4.12 with the value $C_{p,m}^\circ(g, 298.15 K) = 194.4 J \cdot K^{-1} \cdot mol^{-1}$, estimated for this compound from the value $C_{p,m}^\circ(g, 298.15 K)$ of fluorenone [26] according to equation 4.37 using a group additivity approach and data provided in table 4.2.

$$C_{p,m}^\circ(\text{Fluorenone}) - [1 \times \mathbf{C}_B\text{-(H)}(\mathbf{C}_B)_2] + [1 \times \mathbf{C}_B\text{-(O)}(\mathbf{C}_B)_2] + [1 \times \mathbf{O}\text{-(C}_B\text{)}(\mathbf{H})] \quad (4.37)$$

4.2.2.4.3. 2-Fluorofluorenone



Molecular formula	CAS Number	Molar Mass	Density
C ₁₃ H ₇ OF	343-01-1	198.1914 g·mol ⁻¹	1.2415 [14]

Table 4.111. Source, purification and analysis details of 2-fluorofluorenone.

Source	Lot	Minimum initial purity ^a	Purification method	Final mass fraction purity ^a
Aldrich	11720JZ	0.9798	Sublimation under reduced pressure	0.9966
	11720JZV	0.9838		

^a Determined by GC.**Vapor pressures and phase transition thermodynamic properties**

Table 4.112. Temperatures, molar enthalpies and entropies of fusion of 2-fluorofluorenone.

Exp.	T_{fus} (onset)	$\Delta_{\text{cr}}^{\text{l}} H_{\text{m}}^{\circ}(T_{\text{fus}})$	$\Delta_{\text{cr}}^{\text{l}} S_{\text{m}}^{\circ}(T_{\text{fus}})$
	K	kJ·mol ⁻¹	J·K ⁻¹ ·mol ⁻¹
1	388.53	18.95	
2	388.53	18.97	
3	388.51	18.87	
4	388.48	18.83	
5	388.54	18.95	
6	388.49	18.98	
Mean	388.51 ± 0.02	18.93 ± 0.05	48.7 ± 0.1
Literature ^a	388 - 390		

^a Sigma-Aldrich, MSDS.

Table 4.113. Vapor pressures of 2-fluorofluorenone determined by the Knudsen effusion method. ^a

<i>T</i> / K	<i>t</i> / s	Orifices	<i>m</i> / mg			<i>p</i> / Pa			
			<i>m</i> _{small}	<i>m</i> _{medium}	<i>m</i> _{large}	<i>p</i> _{small}	<i>p</i> _{medium}	<i>p</i> _{large}	<i>p</i> _{mean}
317.15	27969	A ₁ '-B ₄ '-C ₇ '	5.11	6.16	7.71	0.084	0.082	0.082	0.083
319.19	27969	A ₂ '-B ₅ '-C ₈ '	6.31	7.70	9.60	0.104	0.103	0.102	0.103
321.26	27969	A ₃ '-B ₆ '-C ₉ '	8.09	9.75	12.32	0.134	0.131	0.132	0.132
323.15	20477	A ₁ '-B ₄ '-C ₇ '		9.10	11.24		0.167	0.164	0.166
325.17	20477	A ₂ '-B ₅ '-C ₈ '	9.26	11.40	14.03	0.211	0.210	0.206	0.209
327.27	20477	A ₃ '-B ₆ '-C ₉ '	11.44	14.04	17.65	0.262	0.260	0.260	0.260
329.15	10787	A ₁ '-B ₄ '-C ₇ '	7.37	8.72	11.13	0.321	0.307	0.312	0.313
331.15	10787	A ₂ '-B ₅ '-C ₈ '	8.76	11.12	13.79	0.382	0.393	0.388	0.388
333.27	10787	A ₃ '-B ₆ '-C ₉ '	11.14	13.75	17.22	0.488	0.487	0.486	0.487
335.16	10979	A ₁ '-B ₄ '-C ₇ '	14.05	17.11	21.25	0.606	0.597	0.590	0.598
337.17	10979	A ₂ '-B ₅ '-C ₈ '	17.22	21.18	26.04	0.745	0.741	0.726	0.737
339.27	10979	A ₃ '-B ₆ '-C ₉ '	21.06	25.83	32.34	0.914	0.907	0.904	0.908

^a $u(T/K) = \pm 0.01$, $u(p/\text{Pa}) = \pm 0.01$.

 Table 4.114. Vapor pressures of 2-fluorofluorenone determined by the static method with capacitance manometers. ^a

<i>T</i> / K	<i>p</i> / Pa	100Δ <i>p</i> / <i>p</i> ^b	<i>T</i> / K	<i>p</i> / Pa	100Δ <i>p</i> / <i>p</i> ^b	<i>T</i> / K	<i>p</i> / Pa	100Δ <i>p</i> / <i>p</i> ^b
<i>Crystalline phase, static method</i> ^c								
344.88	1.661	0.7	358.71	5.880	-0.8	372.54	19.32	0.3
346.86	1.991	-0.2	360.68	7.013	-0.6	374.48	22.59	0.1
348.83	2.405	0.0	362.67	8.391	0.0	376.47	26.59	0.4
350.82	2.877	-0.7	364.65	9.939	-0.1	378.45	31.09	0.3
352.79	3.471	-0.1	366.60	11.82	0.6	380.44	36.16	-0.3
354.77	4.183	0.5	368.60	13.94	0.2	382.39	41.97	-0.6
356.74	4.985	0.2	370.56	16.41	0.2			

^a $u(T) = \pm 0.01$ K, $u(p) = 0.01 + 0.0025p$ Pa;

^b $\Delta p = p - p_{\text{calc}}$, where p_{calc} is calculated from the Clarke and Glew equation with parameters given in table 4.115.

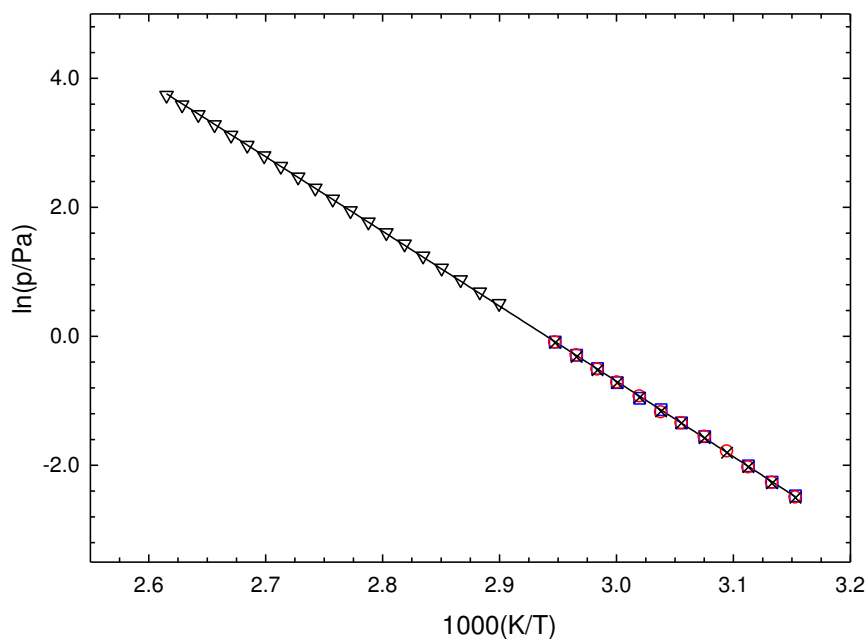


Figure 4.21. Plots of $\ln(p/\text{Pa})$ against $1000(K/T)$ of 2-fluorofluorenone: effusion crystal vapor pressures for the different effusion orifices - \square , small; \circ , medium; \times , large; static vapor pressures - ∇ , crystal vapor pressures.

Table 4.115. Standard ($p^\circ = 0.1 \text{ MPa}$) molar properties of sublimation of 2-fluorofluorenone derived from the vapor pressure results determined experimentally.

$\Delta T / \text{K}$	θ / K	$\frac{\Delta_{\text{cr}}^{\text{g}} G_{\text{m}}^{\circ}(\theta)}{\text{kJ}\cdot\text{mol}^{-1}}$	$\frac{\Delta_{\text{cr}}^{\text{g}} H_{\text{m}}^{\circ}(\theta)}{\text{kJ}\cdot\text{mol}^{-1}}$	$\frac{\Delta_{\text{cr}}^{\text{g}} S_{\text{m}}^{\circ}(\theta)^{\text{a}}}{\text{J}\cdot\text{K}^{-1}\cdot\text{mol}^{-1}}$	$p(\theta)^{\text{b}}$ Pa	R^2	$\frac{\Delta_{\text{g}}^{\text{cr}} C_{p,m}^{\circ \text{c}}}{\text{J}\cdot\text{K}^{-1}\cdot\text{mol}^{-1}}$	s^{d}
<i>Crystalline phase, effusion method</i>								
317.15-339.27	298.15	40.56 ± 0.04	97.9 ± 0.4	192.3 ± 1.3	$7.8 \cdot 10^{-3}$	0.9998	33.7	0.011
	328.21 ^e	34.83 ± 0.01	96.9 ± 0.4	189.1 ± 1.2	$2.9 \cdot 10^{-1}$			
<i>Crystalline phase, static method</i>								
344.88-382.39	298.15	40.33 ± 0.02	97.0 ± 0.1	190.1 ± 0.3	$8.6 \cdot 10^{-3}$	1.0000	33.7	0.004
	363.64 ^e	28.12 ± 0.01	94.6 ± 0.1	182.3 ± 0.3	9.1			

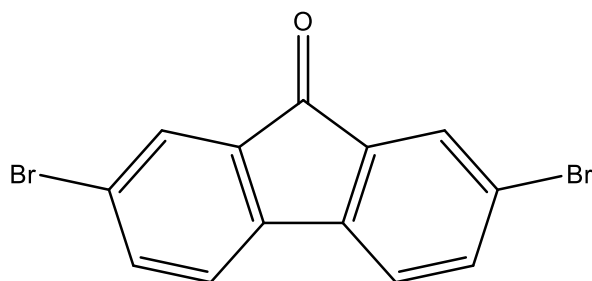
^a Calculated through equation 4.14; ^b Calculated through equation 4.15; ^c Estimated value; ^d Standard deviation of the fit defined as $s = \sqrt{\left(\sum_{i=1}^n (\ln p - \ln p_{\text{calc}})_i^2\right) / (n - m)}$, where n is the number of experimental points used in the fit and m is the number of adjustable parameters in the Clarke and Glew equation; ^e Mean temperature.

The value $\Delta_{\text{cr}}^{\text{g}} C_{\rho, \text{m}}^{\text{o}} = -33.7 \text{ J}\cdot\text{K}^{-1}\cdot\text{mol}^{-1}$ was estimated in this work by means of equation 4.12 and the value $C_{\rho, \text{m}}^{\text{o}}(\text{g}, 298.15 \text{ K}) = 186.5 \text{ J}\cdot\text{K}^{-1}\cdot\text{mol}^{-1}$, estimated for this compound from the value $C_{\rho, \text{m}}^{\text{o}}(\text{g}, 298.15 \text{ K})$ of fluorenone [26] using a group additivity approach according to equation 4.38 and data provided in table 4.2.

$$C_{\rho, \text{m}}^{\text{o}}(\text{Fluorenone}) - [1 \times \mathbf{C}_{\text{B}}\text{-(H)}(\text{C}_{\text{B}})_2] + [1 \times \mathbf{C}_{\text{B}}\text{-(F)}(\text{C}_{\text{B}})_2] \quad (4.38)$$

4.2.2.5. 2,7-Substituted fluorenone

4.2.2.5.1. 2,7-Dibromofluorenone



Molecular formula	CAS Number	Molar Mass	Density
C ₁₃ H ₆ OBr ₂	14348-75-5	337.9931 g·mol ⁻¹	1.907 [64]

Table 4.116. Source, purification and analysis details of 2,7-dibromofluorenone.

Source	Lot	Minimum initial purity ^a	Purification method	Final mass fraction purity ^b
Aldrich	MK BK2818V	0.989	Sublimation under reduced pressure	0.9964

^b Determined by GC.**Vapor pressures and phase transition thermodynamic properties**

Table 4.117. Temperatures, molar enthalpies and entropies of fusion of 2,7-dibromofluorenone.

Exp.	T_{fus} (onset)	$\Delta_{\text{cr}}^{\text{l}} H_{\text{m}}^{\circ}(T_{\text{fus}})$	$\Delta_{\text{cr}}^{\text{l}} S_{\text{m}}^{\circ}(T_{\text{fus}})$
	K	kJ·mol ⁻¹	J·K ⁻¹ ·mol ⁻¹
1	477.89	27.11	
2	478.27	27.03	
3	477.74	26.85	
4	477.63	26.73	
5	477.53	26.64	
Mean	477.8 ± 0.3	26.9 ± 0.2	56.3 ± 0.4
Literature ^a	476 - 478		

^a Sigma-Aldrich, MSDS

Table 4.118. Vapor pressures of 2,7-dibromofluorenone determined by the Knudsen effusion method.^a

T / K	t / s	Orifices	m / mg			p / Pa			
			m_{small}	m_{medium}	m_{large}	p_{small}	p_{medium}	p_{large}	p_{mean}
381.17	25297	A ₁ '-B ₄ '-C ₇ '	7.04	8.49	10.41	0.108	0.105	0.103	0.105
383.16	25297	A ₂ '-B ₅ '-C ₈ '	8.08	10.36	12.77	0.124	0.128	0.126	0.126
385.25	25297	A ₃ '-B ₆ '-C ₉ '	10.17	12.54	15.65	0.156	0.156	0.155	0.156
387.17	10750	A ₁ '-B ₄ '-C ₇ '	5.28	6.34	7.87	0.191	0.186	0.184	0.187
389.14	10750	A ₂ '-B ₅ '-C ₈ '	6.23	7.82	9.52	0.227	0.230	0.223	0.226
391.25	10750	A ₃ '-B ₆ '-C ₉ '	7.39	9.18	11.55	0.269	0.271	0.271	0.270
393.19	10989	A ₁ '-B ₄ '-C ₇ '	9.29	11.52	14.23	0.332	0.333	0.328	0.331
395.16	10989	A ₂ '-B ₅ '-C ₈ '	10.77	13.79	17.00	0.386	0.400	0.392	0.393
397.25	10989	A ₃ '-B ₆ '-C ₉ '	13.29	16.42	20.43	0.478	0.477	0.473	0.476
399.19	11471	A ₁ '-B ₄ '-C ₇ '	16.66	20.44	25.12	0.575	0.571	0.558	0.568
401.15	11471	A ₂ '-B ₅ '-C ₈ '		24.05	29.69		0.673	0.661	0.667
403.25	11471	A ₃ '-B ₆ '-C ₉ '	23.44	28.71	36.17	0.813	0.806	0.808	0.809

^a $u(T/K) = \pm 0.01$, $u(p/Pa) = \pm 0.01$.

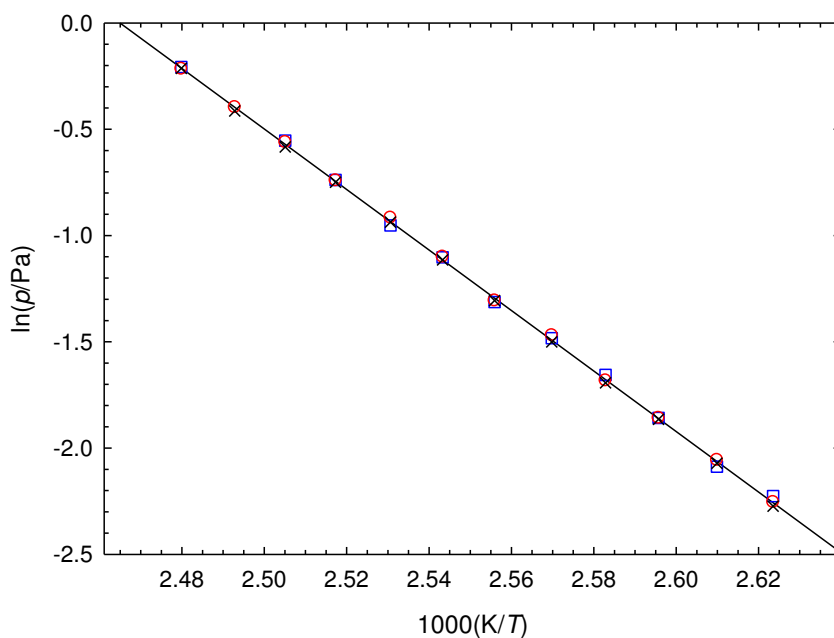


Figure 4.22. Plots of $\ln(p/Pa)$ against $1000(K/T)$ of 2,7-dibromofluorenone: effusion crystal vapor pressures for the different effusion orifices - \square , small; \circ , medium; \times , large.

Table 4.119. Standard ($p^\circ = 0.1$ MPa) molar properties of sublimation of 2,7-dibromofluorenone derived from the vapor pressure results determined experimentally.

$\Delta T / K$	θ / K	$\frac{\Delta_{cr}^g G_m^\circ(\theta)}{kJ \cdot mol^{-1}}$	$\frac{\Delta_{cr}^g H_m^\circ(\theta)}{kJ \cdot mol^{-1}}$	$\frac{\Delta_{cr}^g S_m^\circ(\theta)^a}{J \cdot K^{-1} \cdot mol^{-1}}$	$\frac{p(\theta)^b}{Pa}$	R^2	$\frac{\Delta_g^{cr} C_{p,m}^\circ{}^c}{J \cdot K^{-1} \cdot mol^{-1}}$	s^d
<i>Crystalline phase, effusion method</i>								
381.17-403.25	298.15	60.37 ± 0.09	121.9 ± 0.4	206.4 ± 1.4	$2.7 \cdot 10^{-6}$	0.9999	37.2	0.007
	392.21 ^e	41.47 ± 0.01	118.4 ± 0.4	196.1 ± 1.0	$3.0 \cdot 10^{-1}$			

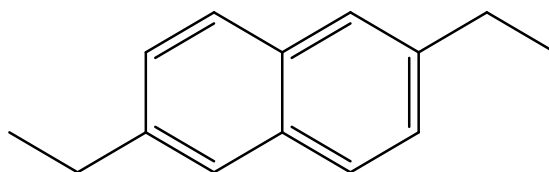
^a Calculated through equation 4.14; ^b Calculated through equation 4.15; ^c Estimated value; ^d Standard deviation of the fit defined as $s = \sqrt{\left(\sum_{i=1}^n (\ln p - \ln p_{calc,i})^2\right) / (n - m)}$, where n is the number of experimental points used in the fit and m is the number of adjustable parameters in the Clarke and Glew equation; ^e Mean temperature.

The value $\Delta_{cr}^g C_{p,m}^\circ = -37.2 \text{ J} \cdot \text{K}^{-1} \cdot \text{mol}^{-1}$ was estimated in this work by means of equation 4.12 and the value $C_{p,m}^\circ(\text{g}, 298.15 \text{ K}) = 206.06 \text{ J} \cdot \text{K}^{-1} \cdot \text{mol}^{-1}$, estimated for this compound from the value $C_{p,m}^\circ(\text{g}, 298.15 \text{ K})$ of fluorenone [26] using a group additivity approach according to equation 4.39 and data provided in table 4.2.

$$C_{p,m}^\circ(\text{Fluorenone}) - [2 \times \mathbf{C}_B\text{-(H)}(\mathbf{C}_B)_2] + [2 \times \mathbf{C}_B\text{-(Br)}(\mathbf{C}_B)_2] \quad (4.39)$$

4.2.2.6. 2,6-Substitued naphthalenes

4.2.2.6.1. 2,6-Diethylnaphthalene



Molecular formula	CAS Number	Molar Mass	Density
C ₁₄ H ₁₆	59919-41-4	184.2760 g·mol ⁻¹	0.974 [65]

Table 4.120. Source, purification and analysis details of 2,6-diethylnaphthalene.

Source	Lot	Minimum initial purity ^a	Purification method	Final mass fraction purity ^b
Aldrich	05010AIV	0.999	Sublimation under reduced pressure	0.9994

^a Determined by HPLC (area %), as stated in the certificate of analysis of the manufacturer;

^b Determined by GC.

Vapor pressures and phase transition thermodynamic properties

Table 4.121. Temperatures, molar enthalpies and entropies of fusion of 2,6-diethylnaphthalene.

T_{fus} (onset)	$\Delta_{\text{cr}}^{\text{l}} H_{\text{m}}^{\circ}(T_{\text{fus}})$	$\Delta_{\text{cr}}^{\text{l}} S_{\text{m}}^{\circ}(T_{\text{fus}})$	T_{tp}	$\Delta_{\text{cr}}^{\text{l}} H_{\text{m}}^{\circ}(T_{\text{tp}})$	$\Delta_{\text{cr}}^{\text{l}} S_{\text{m}}^{\circ}(T_{\text{tp}})$
K	kJ·mol ⁻¹	J·K ⁻¹ ·mol ⁻¹	K	kJ·mol ⁻¹	J·K ⁻¹ ·mol ⁻¹
322.5 ± 0.1 ^a	22.36 ± 0.06 ^a	69.3 ± 0.2	321.98 ^b	21.5 ± 0.1 ^c	66.8 ± 0.3
322.45-323.85 ^d					

^a Ref. [66], mass fraction purity 0.9994;

^b Triple point temperature derived indirectly from vapor pressure results;

^c Determined indirectly from the $\Delta_{\text{cr}}^{\text{g}} H_{\text{m}}^{\circ}(T_{\text{tp}})$ and $\Delta_{\text{cr}}^{\text{g}} S_{\text{m}}^{\circ}(T_{\text{tp}})$ values presented in table 4.123;

^d Sigma-Aldrich, certificate of analysis.

Table 4.122. Vapor pressures of 2,6-diethylnaphthalene determined by the static method with capacitance manometers.^a

<i>T/K</i>	<i>p/Pa</i>	$100\Delta p/p^b$	<i>T/K</i>	<i>p/Pa</i>	$100\Delta p/p^b$	<i>T/K</i>	<i>p/Pa</i>	$100\Delta p/p^b$
<i>Crystalline phase</i>								
305.16	0.582	0	311.07	1.173	0.3	316.98	2.287	0
306.21	0.660	0	312.15	1.326	0.1	318.02	2.571	0.2
307.09	0.734	0	313.05	1.468	-0.1	319.00	2.853	-0.2
308.13	0.829	-0.1	314.05	1.647	0	320.02	3.193	-0.1
309.09	0.924	-0.5	315.05	1.849	0.3	321.0	3.550	-0.2
310.09	1.048	0.3	316.05	2.067	0.2			
<i>Liquid phase^c</i>								
305.14	0.888	0.1	328.86	6.915	0.1	352.66	38.11	-0.4
307.10	1.067	0	330.92	8.096	-0.2	354.66	43.70	0.3
309.09	1.282	-0.1	332.91	9.445	0	356.62	49.43	0
311.11	1.540	-0.2	334.90	11.00	0.1	358.60	56.18	0.2
313.08	1.841	0	336.86	12.79	0.6	360.57	63.35	0
315.03	2.186	-0.1	338.84	14.69	-0.1	362.55	71.59	0
317.03	2.607	0.1	340.82	17.02	0.3	364.52	80.51	-0.2
319.01	3.093	0.2	342.80	19.55	0.1	366.48	90.73	0
320.94	3.645	0.4	344.76	22.43	0	368.45	101.8	-0.1
322.96	4.296	0	346.75	25.70	-0.1	370.45	114.5	0.1
324.95	5.067	0.3	348.72	29.35	-0.2	372.40	128.3	0.2
326.90	5.869	-0.8	350.71	33.48	-0.4			

^a $u(T) = \pm 0.01$ K, $u(p) = 0.01 + 0.0025p$ Pa;^b $\Delta p = p - p_{\text{calc}}$, where p_{calc} is calculated from the Clarke and Glew equation with parameters given in table 4.123;^c Including supercooled liquid.

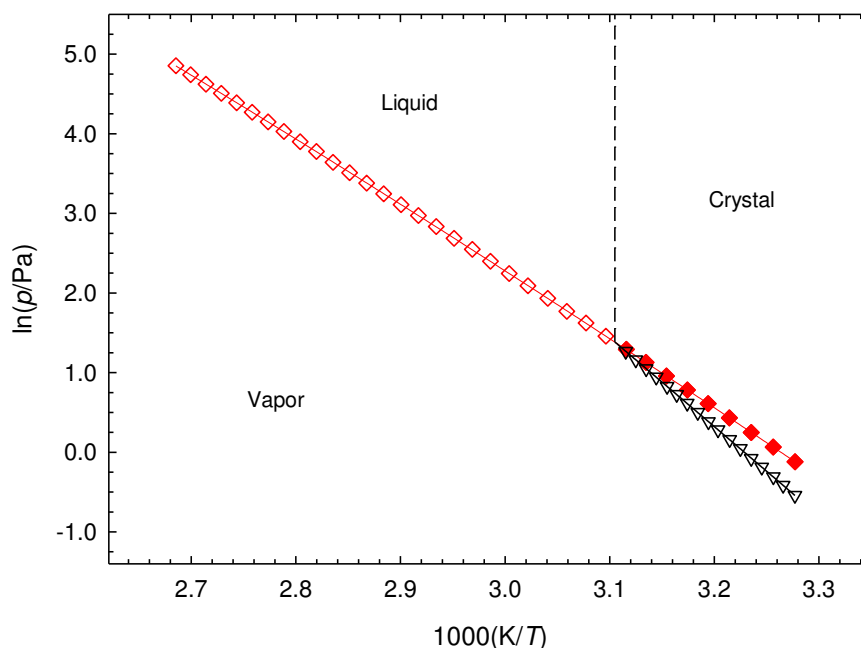


Figure 4.23. Phase diagram ($\ln(p/\text{Pa})$ against $1000(K/T)$) of 2,6-diethylnaphthalene: ∇ , crystal vapor pressures; \diamond , liquid vapor pressures; \blacklozenge , supercooled liquid vapor pressures (triple point coordinates: $T_{\text{tp}} = 321.98 \text{ K}$; $p_{\text{tp}} = 3.96 \text{ Pa}$).

Table 4.123. Standard ($p^\circ = 0.1 \text{ MPa}$) molar properties of sublimation and vaporization of 2,6-diethylnaphthalene, derived from the experimental vapor pressure results.

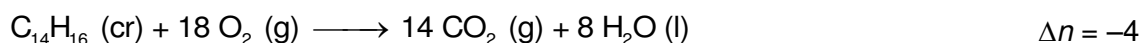
$\Delta T / \text{K}$	θ / K	$\frac{\Delta_{\text{cr/l}}^{\text{g}} G_{\text{m}}^{\circ}(\theta)}{\text{kJ}\cdot\text{mol}^{-1}}$	$\frac{\Delta_{\text{cr/l}}^{\text{g}} H_{\text{m}}^{\circ}(\theta)}{\text{kJ}\cdot\text{mol}^{-1}}$	$\frac{\Delta_{\text{cr/l}}^{\text{g}} S_{\text{m}}^{\circ}(\theta)^{\text{a}}}{\text{J}\cdot\text{K}^{-1}\cdot\text{mol}^{-1}}$	$p(\theta)^{\text{b}}$ Pa	R^2	$\frac{\Delta_{\text{g}}^{\text{cr/l}} C_{\text{p,m}}^{\circ \text{c}}}{\text{J}\cdot\text{K}^{-1}\cdot\text{mol}^{-1}}$	s^{d}
<i>Crystalline phase, static method</i>								
305.16-321.00	298.15	32.03 ± 0.01	93.63 ± 0.09	206.6 ± 0.3	$2.4\cdot 10^{-1}$			
	313.08 ^e	28.96 ± 0.01	93.02 ± 0.09	204.6 ± 0.3	1.5	1.0000	40.9	0.002
	321.98 ^f	27.14 ± 0.01	92.66 ± 0.09	203.5 ± 0.3	4.0			
<i>Liquid phase, static method^g</i>								
	298.15	30.49 ± 0.01	73.42 ± 0.04	144.0 ± 0.1	$4.6\cdot 10^{-1}$			
305.14-372.40	338.77 ^e	24.89 ± 0.01	69.62 ± 0.04	132.0 ± 0.1	$1.5\cdot 10^1$	1.0000	93.8	0.005
	321.98 ^f	27.14 ± 0.01	71.19 ± 0.04	136.8 ± 0.1	4.0			

^a Calculated through equation 4.14; ^b Calculated through equation 4.15; ^c Estimated value; ^d Standard deviation of the fit defined as $s = \sqrt{\left(\sum_{i=1}^n (\ln p - \ln p_{\text{calc}})_i^2\right) / (n - m)}$, where n is the number of experimental points used in the fit and m is the number of adjustable parameters in the Clarke and Glew equation; ^e Mean temperature; ^f Triple point temperature; ^g Including supercooled liquid.

The value of $C_{p,m}^{\circ}(\text{g}, 298.15\text{K}) = 227.1 \text{ J}\cdot\text{K}^{-1}\cdot\text{mol}^{-1}$ [66] was calculated at the B3LYP/6-31G(d) level of theory, and inserted into equations 4.12 and 4.13, respectively yielding the results $\Delta_{\text{cr}}^{\text{g}}C_{p,m}^{\circ} = -40.9 \text{ J}\cdot\text{K}^{-1}\cdot\text{mol}^{-1}$ and $\Delta_{\text{f}}^{\text{g}}C_{p,m}^{\circ} = -93.8 \text{ J}\cdot\text{K}^{-1}\cdot\text{mol}^{-1}$.

Combustion calorimetry and thermodynamic properties of formation

Combustion equation:



The study of 2,6-diethylnaphthalene by static bomb combustion calorimetry was performed by another researcher [66], whose results were used to derive the standard molar enthalpies of formation in crystalline and gaseous phases presented in table 4.124.

Table 4.124. Standard ($p^{\circ} = 0.1 \text{ MPa}$) molar energy and enthalpy of combustion, and derived standard molar enthalpies of formation of the crystalline and gaseous phases of 2,6-diethylnaphthalene, at $T = 298.15 \text{ K}$.

$-\langle\Delta_{\text{c}}U^{\circ}\rangle$	$-\Delta_{\text{c}}U_{\text{m}}^{\circ}(\text{cr})$	$-\Delta_{\text{c}}H_{\text{m}}^{\circ}(\text{cr})$	$-\Delta_{\text{f}}H_{\text{m}}^{\circ}(\text{cr})$	$\Delta_{\text{cr}}^{\text{g}}H_{\text{m}}^{\circ}$	$\Delta_{\text{f}}H_{\text{m}}^{\circ}(\text{g})$
$\text{J}\cdot\text{g}^{-1}$	$\text{kJ}\cdot\text{mol}^{-1}$	$\text{kJ}\cdot\text{mol}^{-1}$	$\text{kJ}\cdot\text{mol}^{-1}$	$\text{kJ}\cdot\text{mol}^{-1}$	$\text{kJ}\cdot\text{mol}^{-1}$
41915.4 ± 1.7	7724.0 ± 2.5	7733.9 ± 2.5	61.9 ± 3.1	93.63 ± 0.09	31.7 ± 3.1

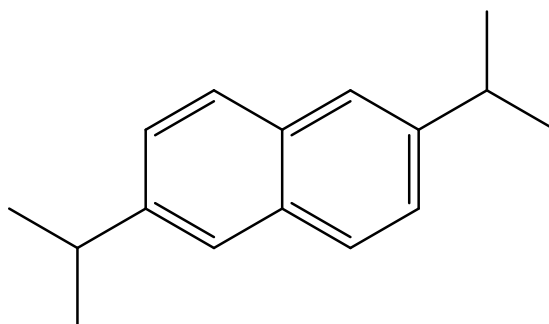
Table 4.125. Standard ($p^{\circ} = 0.1 \text{ MPa}$) molar absolute entropies and standard molar entropies, enthalpies and Gibbs energies of formation of the crystalline and gaseous phases of 2,6-diethylnaphthalene, at $T = 298.15 \text{ K}$.

Phase	S_{m}°	$-T\Delta_{\text{f}}S_{\text{m}}^{\circ}$	$\Delta_{\text{f}}H_{\text{m}}^{\circ}$	$\Delta_{\text{f}}G_{\text{m}}^{\circ}$
	$\text{J}\cdot\text{K}^{-1}\cdot\text{mol}^{-1}$	$\text{kJ}\cdot\text{mol}^{-1}$	$\text{kJ}\cdot\text{mol}^{-1}$	$\text{kJ}\cdot\text{mol}^{-1}$
g	480.62^{a}	192.4	31.7 ± 3.1	224.1 ± 3.1
cr	$274.0 \pm 0.3^{\text{b}}$	254.0 ± 0.1	-61.9 ± 3.1	192.1 ± 3.1

^a Calculated at the B3LYP/6-31G(d) level [66];

^b $S_{\text{m}}^{\circ}(\text{cr}) = S_{\text{m}}^{\circ}(\text{g}) - \Delta_{\text{cr}}^{\text{g}}S_{\text{m}}^{\circ}$.

4.2.2.6.2. 2,6-Diisopropylnaphthalene



Molecular formula	CAS Number	Molar Mass	Density
C ₁₆ H ₂₀	24157-81-1	212.3291 g·mol ⁻¹	0.949 [67]

Table 4.126. Source, purification and analysis details of 2,6-diisopropylnaphthalene.

Source	Lot	Minimum initial purity ^a	Purification method	Final mass fraction purity ^b
TCI Europe	VRQIF	0.999	Used without further purification	0.9998

^a Determined by GC, as stated in the certificate of analysis of the manufacturer;

^b Determined by GC.

Vapor pressures and phase transition thermodynamic properties

Table 4.127. Temperatures, molar enthalpies and entropies of fusion of 2,6-diisopropylnaphthalene available in the literature.

T_{fus} (onset)	$\Delta_{\text{cr}}^{\text{l}} H_{\text{m}}^{\circ}(T_{\text{fus}})$	$\Delta_{\text{cr}}^{\text{l}} S_{\text{m}}^{\circ}(T_{\text{fus}})$
K	kJ·mol ⁻¹	J·K ⁻¹ ·mol ⁻¹
343.0 ± 0.2 ^a	18.8 ± 0.1 ^a	54.8 ± 0.3
343.25 ^b		

^a Ref. [66], mass fraction purity 0.9998;

^b TCI Europe, certificate of analysis.

Table 4.128. Vapor pressures of 2,6-diisopropylnaphthalene determined by the Knudsen effusion method. ^a

<i>T</i> / K	<i>t</i> / s	Orifices	<i>m</i> / mg			<i>p</i> / Pa			
			<i>m</i> _{small}	<i>m</i> _{medium}	<i>m</i> _{large}	<i>p</i> _{small}	<i>p</i> _{medium}	<i>p</i> _{large}	<i>p</i> _{mean}
301.12	26976	A ₁ '-B ₄ '-C ₇ '	4.63	5.69	7.22	0.074	0.074	0.075	0.074
303.20	26976	A ₂ '-B ₅ '-C ₈ '	6.06	7.47	9.34	0.098	0.098	0.097	0.098
305.19	26976	A ₃ '-B ₆ '-C ₉ '	7.73	9.54	11.93	0.125	0.125	0.124	0.125
307.11	14278	A ₁ '-B ₄ '-C ₇ '	5.32	6.51	8.09	0.163	0.162	0.160	0.162
309.19	14278	A ₂ '-B ₅ '-C ₈ '	6.79	8.33	10.39	0.209	0.207	0.206	0.207
311.20	14278	A ₃ '-B ₆ '-C ₉ '	8.45	10.47	13.11	0.261	0.262	0.261	0.261
313.11	10626	A ₁ '-B ₄ '-C ₇ '	7.92	9.90	12.29	0.330	0.333	0.329	0.331
315.18	10626	A ₂ '-B ₅ '-C ₈ '	10.10	12.50	15.55	0.422	0.422	0.418	0.421
317.09	11769	A ₃ '-B ₆ '-C ₉ '	14.09	17.31	21.74	0.533	0.530	0.530	0.531
319.16	11769	A ₁ '-B ₄ '-C ₇ '	17.73	21.96	27.54	0.673	0.674	0.673	0.673
321.19	11769	A ₂ '-B ₅ '-C ₈ '	22.37	27.48	34.61	0.852	0.846	0.848	0.849
323.19	10626	A ₃ '-B ₆ '-C ₉ '	25.14	30.93	38.55	1.063	1.058	1.050	1.057

^a *u*(*T*/K) = ±0.01, *u*(*p*/Pa) = ±0.01.

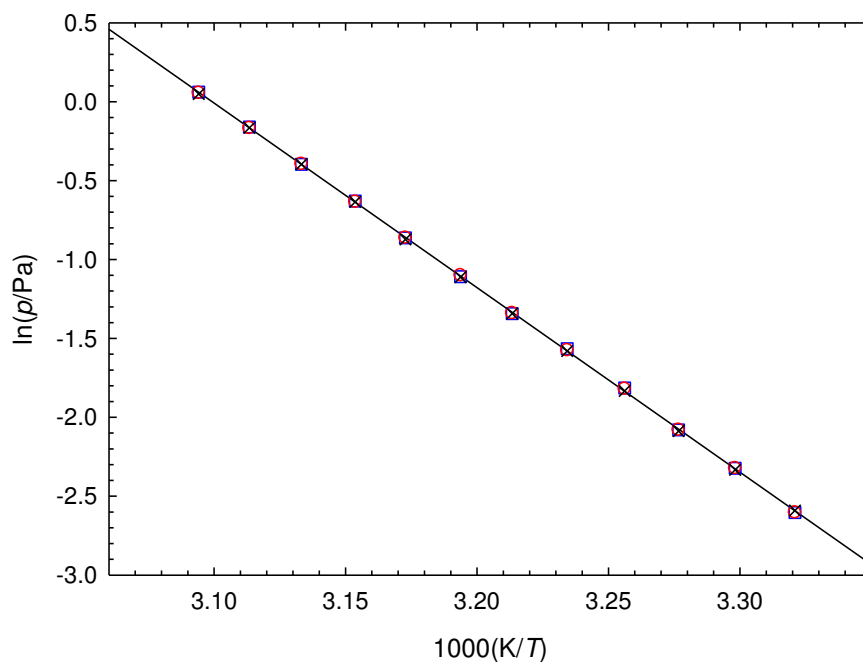


Figure 4.24. Plots of ln(*p*/Pa) against 1000(*K*/*T*) of 2,6-diisopropylnaphthalene: effusion vapor pressures for the different effusion orifices - □, small; ○, medium; ×, large.

Table 4.129. Standard ($p^\circ = 0.1$ MPa) molar properties of sublimation of 2,6-diisopropylnaphthalene, derived from the experimental vapor pressure results.

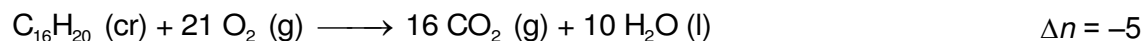
$\Delta T / K$	θ / K	$\frac{\Delta_{cr}^g G_m^\circ(\theta)}{kJ \cdot mol^{-1}}$	$\frac{\Delta_{cr}^g H_m^\circ(\theta)}{kJ \cdot mol^{-1}}$	$\frac{\Delta_{cr}^g S_m^\circ(\theta)^a}{J \cdot K^{-1} \cdot mol^{-1}}$	$\frac{p(\theta)^b}{Pa}$	R^2	$\frac{\Delta_g^{cr} C_{p,m}^{\circ c}}{J \cdot K^{-1} \cdot mol^{-1}}$	s^d
<i>Crystalline phase, effusion method</i>								
301.12-323.19	298.15	35.94 ± 0.01	97.96 ± 0.24	208.0 ± 0.8	$5.1 \cdot 10^{-2}$	0.9999	49.2 ^f	0.007
	312.16 ^e	33.04 ± 0.01	97.27 ± 0.24	205.8 ± 0.8	$3.0 \cdot 10^{-1}$			

^a Calculated through equation 4.14; ^b Calculated through equation 4.15; ^c Estimated value; ^d Standard deviation of the fit defined as $s = \sqrt{\left(\sum_{i=1}^n (\ln p - \ln p_{calc,i})^2\right) / (n - m)}$, where n is the number of experimental points used in the fit and m is the number of adjustable parameters in the Clarke and Glew equation; ^e Mean temperature.

The value of $C_{p,m}^\circ(g, 298.15K) = 274.4 J \cdot K^{-1} \cdot mol^{-1}$ [66] was calculated at the B3LYP/6-31G(d) level of theory, and inserted into equation 4.12, yielding the result $\Delta_{cr}^g C_{p,m}^\circ = -49.2 J \cdot K^{-1} \cdot mol^{-1}$.

Combustion calorimetry and thermodynamic properties of formation

Combustion equation:



The study of 2,6-diisopropylnaphthalene by static bomb combustion calorimetry was performed by another researcher [66], whose results were used to derive the standard molar enthalpies of formation in crystalline and gaseous phases presented in table 4.130.

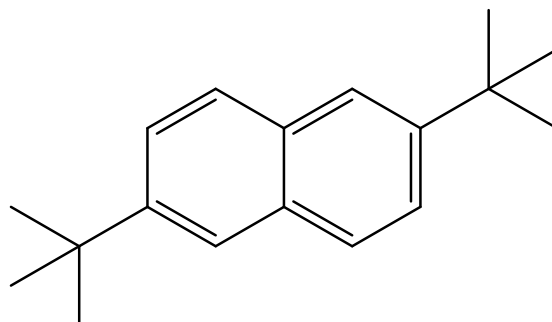
 Table 4.130. Standard ($p^\circ = 0.1$ MPa) molar energy and enthalpy of combustion, and derived standard molar enthalpies of formation of the crystalline and gaseous phases of 2,6-diisopropylnaphthalene, at $T = 298.15$ K.

$-\langle \Delta_c U^\circ \rangle$	$-\Delta_c U_m^\circ(cr)$	$-\Delta_c H_m^\circ(cr)$	$-\Delta_f H_m^\circ(cr)$	$\Delta_{cr}^g H_m^\circ$	$-\Delta_f H_m^\circ(g)$
$J \cdot g^{-1}$	$kJ \cdot mol^{-1}$	$kJ \cdot mol^{-1}$	$kJ \cdot mol^{-1}$	$kJ \cdot mol^{-1}$	$kJ \cdot mol^{-1}$
42481.1 ± 3.9	9020.0 ± 3.3	9032.4 ± 3.3	122.1 ± 3.9	97.96 ± 0.24	24.1 ± 3.9

Table 4.131. Standard ($p^\circ = 0.1$ MPa) molar absolute entropies and standard molar entropies, enthalpies and Gibbs energies of formation of the crystalline and gaseous phases of 2,6-diisopropylnaphthalene, at $T = 298.15$ K.

Phase	S_m°	$-T\Delta_f S_m^\circ$	$-\Delta_f H_m^\circ$	$\Delta_f G_m^\circ$
	$\text{J}\cdot\text{K}^{-1}\cdot\text{mol}^{-1}$	$\text{kJ}\cdot\text{mol}^{-1}$	$\text{kJ}\cdot\text{mol}^{-1}$	$\text{kJ}\cdot\text{mol}^{-1}$
g	529.62 ^a	259.1	24.1 ± 3.9	235.0 ± 3.9
cr	321.6 ± 0.8 ^b	321.1 ± 0.2	122.1 ± 3.9	199.0 ± 3.9

^a Calculated at the B3LYP/6-31G(d) level [66];^b $S_m^\circ(\text{cr}) = S_m^\circ(\text{g}) - \Delta_{\text{cr}}^\circ S_m^\circ$.

4.2.2.6.3. 2,6-Di-*tert*-butylnaphthalene

Molecular formula	CAS Number	Molar Mass	Density
C ₁₈ H ₂₄	3905-64-4	240.3822 g·mol ⁻¹	0.936 [14]

Table 4.132. Source, purification and analysis details of 2,6-di-*tert*-butylnaphthalene.

Source	Lot	Minimum initial purity ^a	Purification method	Final mass fraction purity ^b
TCI Europe	Z2CGB	0.999	Used without further purification	0.9993

^a Determined by GC, as stated in the certificate of analysis of the manufacturer;^b Determined by GC.

Vapor pressures and phase transition thermodynamic properties

Table 4.133. Temperatures, molar enthalpies and entropies of fusion of 2,6-di-*tert*-butylnaphthalene available in the literature.

T_{fus} (onset)	$\Delta_{\text{cr}}^{\text{l}} H_{\text{m}}^{\circ}(T_{\text{fus}})$	$\Delta_{\text{cr}}^{\text{l}} S_{\text{m}}^{\circ}(T_{\text{fus}})$
K	kJ·mol ⁻¹	J·K ⁻¹ ·mol ⁻¹
420.2 ± 0.2 ^a	18.5 ± 0.2 ^a	44.0 ± 0.5
420.45 ^b		
419 ^c		

^a Ref. [66], mass fraction purity 0.9993;^b TCI Europe, certificate of analysis;^c Ref. [68], no information regarding minimum purity.

Table 4.134. Vapor pressures of 2,6-di-*tert*-butylnaphthalene determined by the Knudsen effusion method.^a

T / K	t / s	Orifices	m / mg			p / Pa			
			m_{small}	m_{medium}	m_{large}	p_{small}	p_{medium}	p_{large}	p_{mean}
323.11	24677	A ₁ '-B ₄ '-C ₇ '	6.37	8.13	9.88	0.109	0.113	0.109	0.110
325.19	24677	A ₂ '-B ₅ '-C ₈ '	8.13	9.94	12.13	0.140	0.138	0.134	0.137
327.18	24677	A ₃ '-B ₆ '-C ₉ '	9.97	12.44	15.17	0.172	0.173	0.168	0.171
329.11	18057	A ₁ '-B ₄ '-C ₇ '	9.10	11.01	13.83	0.215	0.210	0.210	0.212
331.18	18057	A ₂ '-B ₅ '-C ₈ '	11.31	13.84	16.88	0.268	0.265	0.257	0.263
333.17	18057	A ₃ '-B ₆ '-C ₉ '	13.86	17.16	20.84	0.329	0.330	0.319	0.326
335.12	10314	A ₁ '-B ₄ '-C ₇ '	9.55	11.78	14.50	0.398	0.397	0.389	0.395
337.18	10314	A ₂ '-B ₅ '-C ₈ '	11.60	14.56	17.74	0.485	0.493	0.478	0.485
339.18	10314	A ₃ '-B ₆ '-C ₉ '	14.31	17.89	21.93	0.600	0.607	0.592	0.600
341.11	10787	A ₁ '-B ₄ '-C ₇ '	18.54	22.59	28.17	0.746	0.735	0.730	0.737
343.16	10787	A ₂ '-B ₅ '-C ₈ '	22.88	27.98	34.43	0.923	0.913	0.895	0.910
345.17	10787	A ₃ '-B ₆ '-C ₉ '	27.58	33.63	42.26	1.116	1.101	1.101	1.106

^a $u(T/K) = \pm 0.01$, $u(p/\text{Pa}) = \pm 0.01$.

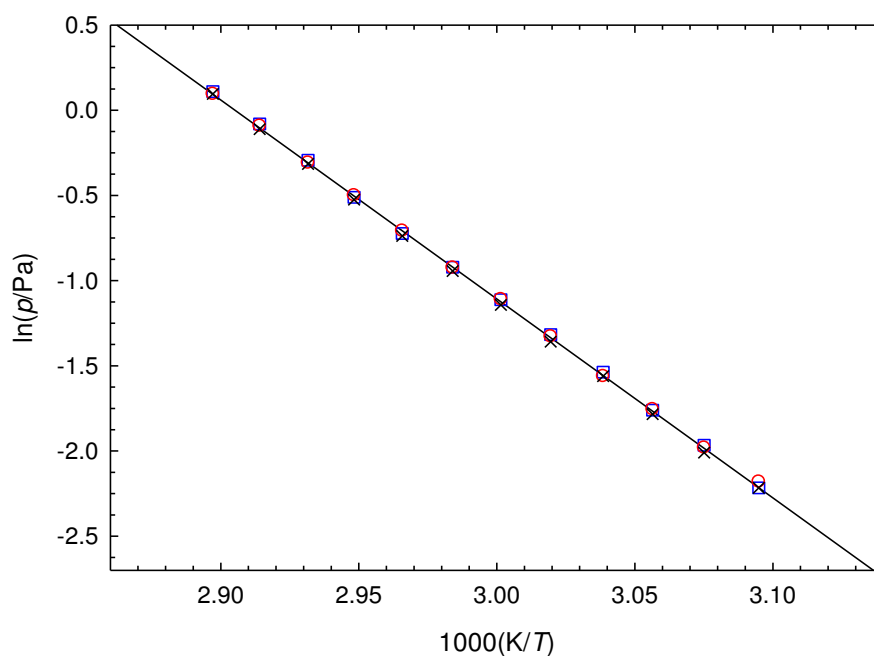


Figure 4.25. Plots of $\ln(p/\text{Pa})$ against $1000(K/T)$ of 2,6-di-*tert*-butylnaphthalene: effusion vapor pressures for the different effusion orifices - \square , small; \circ , medium; \times , large.

Table 4.135. Standard ($p^\circ = 0.1$ MPa) molar properties of sublimation of 2,6-di-*tert*-butylnaphthalene, derived from the experimental vapor pressure results.

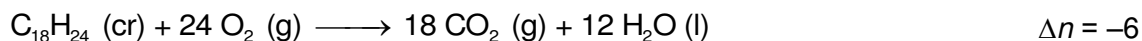
$\Delta T / K$	θ / K	$\frac{\Delta_{cr}^g G_m^\circ(\theta)}{kJ \cdot mol^{-1}}$	$\frac{\Delta_{cr}^g H_m^\circ(\theta)}{kJ \cdot mol^{-1}}$	$\frac{\Delta_{cr}^g S_m^\circ(\theta)^a}{J \cdot K^{-1} \cdot mol^{-1}}$	$\frac{p(\theta)^b}{Pa}$	R^2	$\frac{\Delta_g^{cr} C_{p,m}^\circ}{J \cdot K^{-1} \cdot mol^{-1}}$	s^d
<i>Crystalline phase, effusion method</i>								
323.11-345.17	298.15	41.64 ± 0.04	99.14 ± 0.35	192.9 ± 1.2	$5.1 \cdot 10^{-3}$	0.9999	57.8	0.009
	334.14^e	34.82 ± 0.01	97.06 ± 0.35	186.3 ± 1.0	$3.6 \cdot 10^{-1}$			

^a Calculated through equation 4.14; ^b Calculated through equation 4.15; ^c Estimated value; ^d Standard deviation of the fit defined as $s = \sqrt{\left(\sum_{i=1}^n (\ln p - \ln p_{calc,i})^2\right) / (n - m)}$, where n is the number of experimental points used in the fit and m is the number of adjustable parameters in the Clarke and Glew equation; ^e Mean temperature.

The value of $C_{p,m}^\circ(g, 298.15K) = 323.3 J \cdot K^{-1} \cdot mol^{-1}$ [66] was calculated at the B3LYP/6-31G(d) level of theory, and inserted into equation 4.12, yielding the result $\Delta_{cr}^g C_{p,m}^\circ = -57.8 J \cdot K^{-1} \cdot mol^{-1}$.

Combustion calorimetry and thermodynamic properties of formation

Combustion equation:



The study of 2,6-di-*tert*-butylnaphthalene by static bomb combustion calorimetry was performed by another researcher [66], whose results were used to derive the standard molar enthalpies of formation in crystalline and gaseous phases presented in table 4.136.

 Table 4.136. Standard ($p^\circ = 0.1$ MPa) molar energy and enthalpy of combustion, and derived standard molar enthalpies of formation of the crystalline and gaseous phases of 2,6-di-*tert*-butylnaphthalene, at $T = 298.15$ K.

$-\langle \Delta_c U^\circ \rangle$	$-\Delta_c U_m^\circ(cr)$	$-\Delta_c H_m^\circ(cr)$	$-\Delta_f H_m^\circ(cr)$	$\Delta_{cr}^g H_m^\circ$	$-\Delta_f H_m^\circ(g)$
$J \cdot g^{-1}$	$kJ \cdot mol^{-1}$	$kJ \cdot mol^{-1}$	$kJ \cdot mol^{-1}$	$kJ \cdot mol^{-1}$	$kJ \cdot mol^{-1}$
42997.0 ± 7.1	10335.8 ± 4.7	10350.7 ± 4.7	162.4 ± 5.3	99.14 ± 0.35	63.3 ± 5.3

Table 4.137. Standard ($p^\circ = 0.1$ MPa) molar absolute entropies and standard molar entropies, enthalpies and Gibbs energies of formation of the crystalline and gaseous phases of 2,6-di-*tert*-butylnaphthalene, at $T = 298.15$ K.

Phase	S_m°	$-T\Delta_f S_m^\circ$	$-\Delta_f H_m^\circ$	$\Delta_f G_m^\circ$
	J·K ⁻¹ ·mol ⁻¹	kJ·mol ⁻¹	kJ·mol ⁻¹	kJ·mol ⁻¹
g	566.37 ^a	329.5	63.3 ± 5.3	266.2 ± 5.3
cr	373.5 ± 1.2 ^b	387.0 ± 0.4	162.4 ± 5.3	224.6 ± 5.3

^a Calculated at the B3LYP/6-31G(*d*) level [66];

^b $S_m^\circ(\text{cr}) = S_m^\circ(\text{g}) - \Delta_{\text{cr}}^g S_m^\circ$.

4.3. Photoluminescence properties

4.3.1. General remarks

The photoluminescence study of the compounds was initiated during the last year of this doctoral project. Due to the late acquisition of the equipment and a hard familiarization period with the technique, it was not possible to advance as much as was expected and some of the experimental results obtained so far are still exploratory. Also a number of setbacks regarding the equipment occurred during this period which further delayed the work. For instance, the sample holder was contaminated, was replaced by a new one, and it was only possible to resume the work a couple of months later.

Initially it was intended to focus on the solid state fluorescence study. During the first few months, several tests were performed with the new equipment using loose powder samples of pyrene (used as a test substance, results are provided in annex C.2.3.), fluorene, fluorenone, and naphthalene, as well as some of their derivatives studied in this project. Additionally, 9-fluorenone and fluoranthene were also tested.

From all the compounds studied, the ones presenting very small or no fluorescent emission in powder form are listed in table 4.138. For the compounds that presented more promising quantum yield results (larger than 0.1, for the maximum absorbance), the solid state study was later repeated using different conditions of amount of sample and different excitation wavelengths. As we advanced with this technique, there was a need to understand the fluorescence behavior of the compounds in solution as a complement to the fluorescence results in the solid state. Employing an optimized procedure (section 3.4.6.1.), the solution fluorescence study of the parental molecules, fluorene and naphthalene, and some of their derivatives was performed.

The detailed fluorescence spectral data of the solution and powder studies of the most promising compounds are presented in section 4.3.2.

Table 4.138. Fluorescence quantum yields of the weakly/non fluorescent compounds, in powder form, studied in this work (approximately 40 % of the area of the base of the dish covered by powder sample).

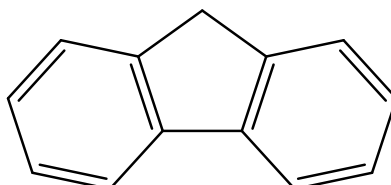
Compound	[λ_{exc}] / nm	$\lambda_{\text{max}}^{\text{Abs } a}$ / nm	ϕ_{F}^b
2-Fluorencarboxaldehyde	280 - 400	360	0.00
2-Nitrofluorene	280 - 380	380	0.00
2-Bromofluorene	280 - 380	310	0.01
2-Iodofluorene	280 - 380	320	0.00
2,7-Di- <i>tert</i> -butylfluorene	280 - 380	310	0.09
2,7-Difluorofluorene	300 - 400	320	0.03
2,7-Dichlorofluorene	300 - 400	320	0.02
2,7-Dibromofluorene	280 - 400	320	0.01
2,7-Diodofluorene	280 - 380	320	0.00
9-Fluorenol	300 - 450	310	0.00
9-Fluorencarboxylic acid	280 - 400	310	0.06
9-Phenyl-9-fluorenol	280 - 380	310	0.00
9-Benzylidene fluorene	280 - 400	370	0.00
9-Fluorene methanol	280 - 400	310	0.06
9-Chlorofluorene	280 - 380	320	0.00
Fluorenone	400 - 500	450	0.07
2-Aminofluorenone	300 - 420	420	0.00
2-Hydroxyfluorenone	280 - 400	400	0.00
2-Fluorofluorenone	280 - 380	380	0.02
2,7-Dibromofluorenone	280 - 400	350	0.01
2,6-Diethylnaphthalene	300 - 350	320	0.02

^a Maximum absorption wavelength of the range studied, determined using the Quantaaurus apparatus;^b Determined using the maximum absorption wavelength as the excitation wavelength.

4.3.2. Experimental results

4.3.2.1. Fluorene and fluorene derivatives

4.3.2.1.1. Fluorene



Molecular formula	CAS Number	Molar Mass	Density
C ₁₃ H ₁₀	86-73-7	166.2176 g·mol ⁻¹	1.20 [69]

Table 4.139. Source, purification and analysis details of fluorene.

Source	Lot	Minimum initial purity	Purification method	Final mass fraction purity ^a
Sigma-Aldrich	STBC4093V	0.986 ^b	Recrystallization; Sublimation under reduced pressure	0.9843
Supelco ^c	LC08752V	0.991 ^b 0.999 ^d 0.9825 ^e	Sublimation under reduced pressure	0.9842

^a Determined by GC; ^b Determined by GC, as stated in the certificate of analysis of the manufacturer; ^c Analytical standard;

^d Determined by HPLC with UV detection at 254 nm, as stated in the certificate of analysis of the manufacturer;

^e Determined by GC, previous to purification process.

Table 4.140. Literature results for the fluorescence quantum yield of fluorene in different solvents.

Solvent	C / mol·L ⁻¹	λ_{exc} / nm	ϕ_F	Method	Source
Hexane			0.54	Relative	Weber & Teale [70]
Ethanol			0.53	Relative	Weber & Teale [70]
Ethanol	2.0·10 ⁻²	300	0.50	Relative	Ellis & Solomon [71]
Ethanol	Infinite dilution ^a	254	0.68 ± 0.04	Relative	Dawson & Windsor [72]
Cyclohexane	6·10 ⁻⁴	265	0.80	Relative	Berlman [73]
Methylcyclohexane		265	0.71 ± 0.03	Relative	Williams <i>et al.</i> [74]
Hexane		254	0.68	Relative	Palmer & Parmar [75]

^a Fluorescence data extrapolated to zero concentration.

Table 4.140 provides literature results for the quantum yield of fluorene (listed in chronological order). As mentioned before, fluorescence quantum yield depends on physical conditions, such as the solvent, the sample concentration, and the excitation wavelength. Therefore when available these parameters are also specified in table 4.140. The literature data refers to measurements performed at room temperature using relative methods. Dawson and Windsor [72] have used the same relative measuring method reported by Weber and Teale [70], in which the intensities of fluorescence are compared with the intensities of excitation light scattered from non-absorbing, colloidal reference solutions. The fluorescence spectra reported by Dawson and Windsor were corrected for self-absorption by measuring the spectra at several concentrations and extrapolating to the fluorescence spectra at zero concentration. Berlman [73] and Williams *et al.* [74] used a solution of 9,10-diphenylanthracene ($\phi_F = 1.0$ [76]), while Palmer and Parmar [75] used a solution of $5 \cdot 10^{-3} \text{ mol} \cdot \text{dm}^{-3}$ of quinine bisulfate in 1 N sulphuric acid ($\phi_F = 0.546$ [77]).

Table 4.141. Fluorescence spectroscopic data of fluorene in cyclohexane solutions, at room temperature.

	$\lambda_{\text{exc}}^a / \text{nm}$	$\lambda_{\text{max}}^F{}^b / \text{nm}$	ϕ_F^c
1 st Sample			
$1 \cdot 10^{-5} \text{ mol} \cdot \text{L}^{-1}$		303.4	0.32 ± 0.01
$1 \cdot 10^{-4} \text{ mol} \cdot \text{L}^{-1}$	265	310.2	0.30 ± 0.01
$1 \cdot 10^{-3} \text{ mol} \cdot \text{L}^{-1}$		317.0	0.29 ± 0.01
2 nd Sample			
$1 \cdot 10^{-6} \text{ mol} \cdot \text{L}^{-1}$		302.6	0.43 ± 0.01
$1 \cdot 10^{-5} \text{ mol} \cdot \text{L}^{-1}$	265	303.4	0.32 ± 0.01
$1 \cdot 10^{-4} \text{ mol} \cdot \text{L}^{-1}$		310.2	0.30 ± 0.01

^a Excitation wavelength corresponding to the maximum absorption determined using UV-Vis spectrometry for the concentration $1 \cdot 10^{-5} \text{ mol} \cdot \text{L}^{-1}$;

^b Wavelength at the maximum fluorescence emission intensity;

^c Mean values and standard deviations of the mean of six independent measurements.

Table 4.142. Absorption and fluorescence spectroscopic data of fluorene in powder form (Supelco), for different amounts of sample.

Sample amount ^a	λ_{exc} / nm	Abs ^b	λ_{max}^F ^c / nm	ϕ_F
15 %		0.169		0.37
40 %	260 ^d	0.606	407.9	0.30
100 %		0.705		0.29
15 %		0.203		0.60
40 %	320 ^e	0.606	407.9	0.49
100 %		0.708		0.47

^a Rough estimate of the percentage of area of the base of the quartz dish covered by sample;

^b Determined by the Quantaurus apparatus;

^c Wavelength at the maximum fluorescence emission intensity;

^d Excitation wavelength corresponding to the maximum absorption determined using UV-Vis spectrometry;

^e Excitation wavelength corresponding to the maximum absorption determined using the Quantaurus apparatus.

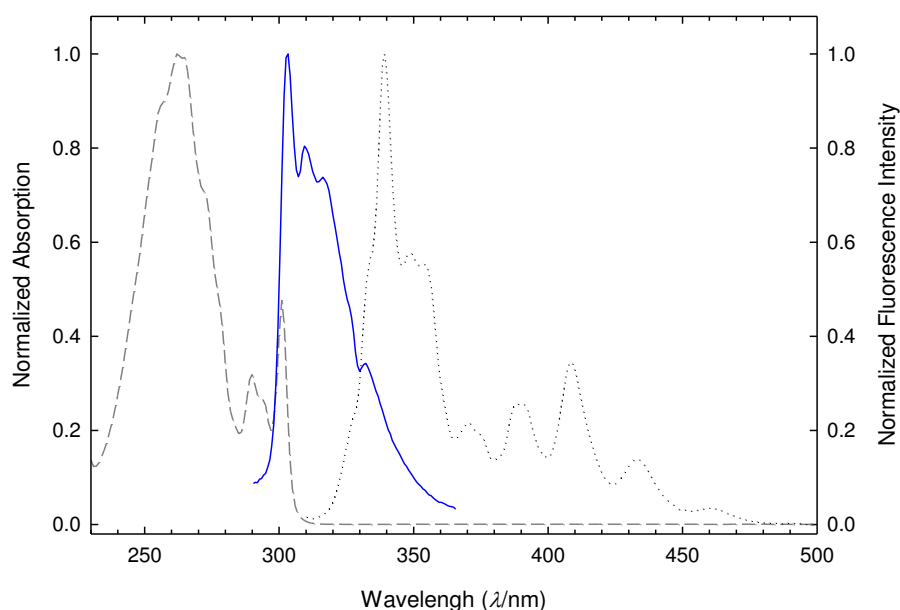


Figure 4.26. Normalized UV-Vis absorption and fluorescence emission spectra of fluorene: dashed line - absorption spectra ($1 \cdot 10^{-5} \text{ mol} \cdot \text{L}^{-1}$); solid line - solution fluorescence spectra ($1 \cdot 10^{-6} \text{ mol} \cdot \text{L}^{-1}$); dotted line - powder fluorescence spectra (1st sample).

Table 4.141, reports the experimental results obtained with the two different fluorene samples studied. The fluorescence quantum yield results do not agree with the value determined by Berlman [73]. This may be due to self-absorption problems, as it will be discussed in section 5.3.1., or to impurities of the samples. Commercial fluorene generally contains impurities very difficult to remove, such as benz[*f*]indane, anthracene

and carbazole [78-80]. Initially, the sample that had been previously used for a thermodynamic study [81] was tested. The purity of the sample was analyzed by GC and a small impurity of similar volatility to fluorene was detected. Further purification by reduced pressure sublimation was attempted without improving the purity degree. A second sample, an analytical standard, was commercially acquired from Supelco. This sample was equally sublimed under reduced pressure and analyzed by GC and its purity didn't differ much from that of the first sample. The obtained fluorescence spectra and quantum yield in cyclohexane solution was consistent with that obtained for the first sample. The results for the solid state, however, were slightly different. As can be observed in figure 4.27, the relative intensity of the bands shown above 370 nm is higher in the second sample than in the first sample which leads to a shift of the maximum emission to longer wavelengths ($\lambda_{\text{max}}^{\text{F}} = 408.7 \text{ nm}$). Other purification techniques and further measurements will be explored in the future as it is crucial to characterize in detail the parental molecules in order to evaluate the effect of the different substituents, both quantitatively and qualitatively.

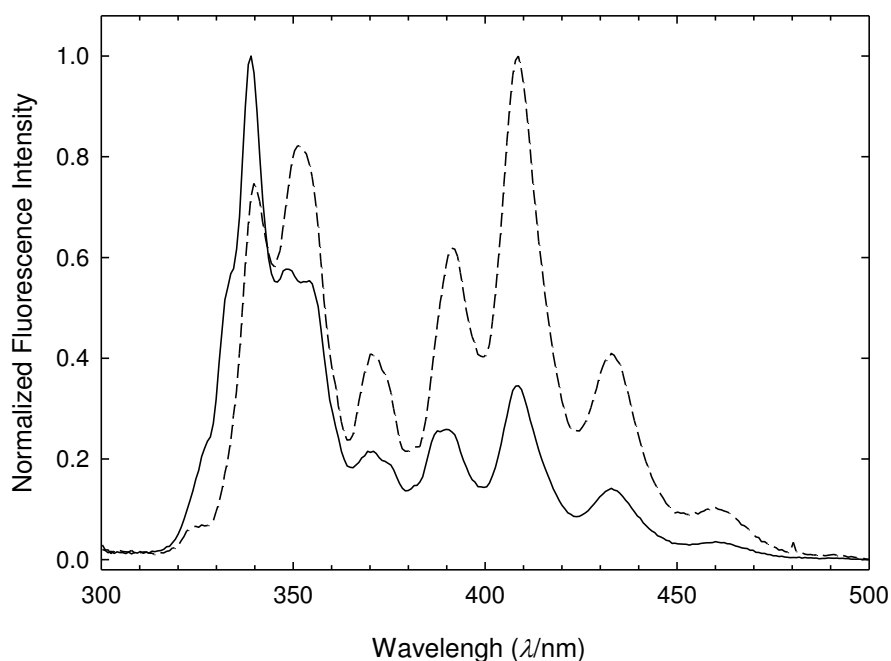
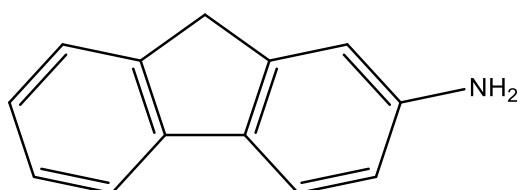


Figure 4.27. Normalized fluorescence emission spectra of fluorene powder samples: solid line - first sample; dashed line - second sample (Supelco).

4.3.2.1.2. 2-Aminofluorene



Details regarding the source, purity and physical properties of 2-aminofluorene are reported in section 4.2.2.1.2.

Table 4.143. Absorption and fluorescence spectroscopic data of 2-aminofluorene in powder form, for different amounts of sample.

Sample amount ^a	λ_{exc}^b / nm	Abs ^c	λ_{max}^F ^d / nm	ϕ_F
15 %		0.564		0.30
40 %	350	0.671	387.2	0.26
100 %		0.746		0.19

^a Rough estimate of the percentage of area of the base of the quartz dish covered by sample;

^b Excitation wavelength corresponding to the maximum absorption determined using the Quantaurus apparatus;

^c Determined using the Quantaurus apparatus;

^d Wavelength at the maximum fluorescence emission intensity.

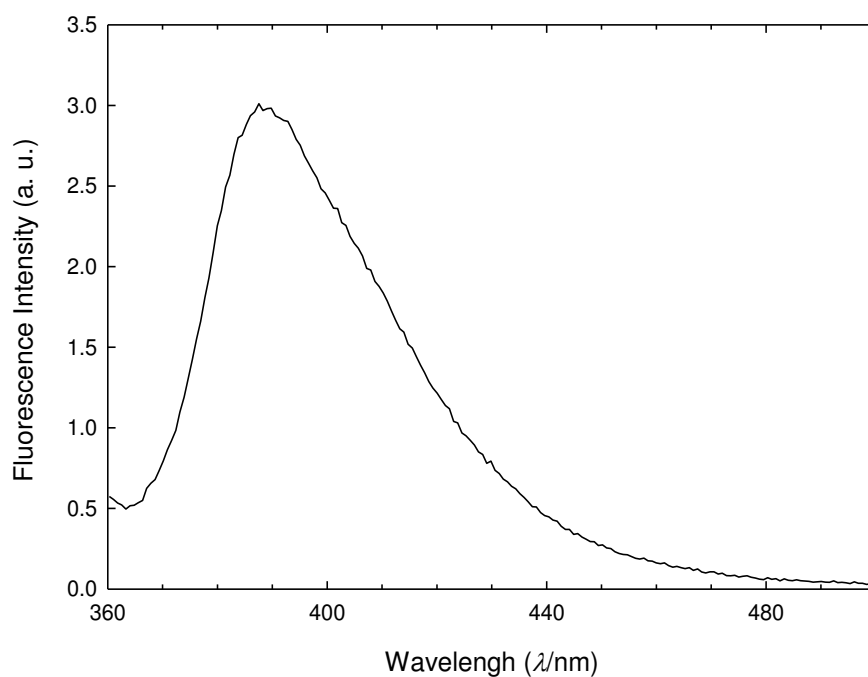
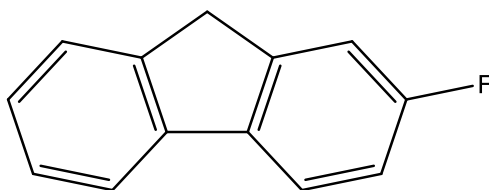


Figure 4.28. Fluorescence emission spectra of 2-aminofluorene in powder form ($\lambda_{exc} = 350$ nm).

4.3.2.1.3. 2-Fluorofluorene



Details regarding the source, purity and physical properties of 2-fluorofluorene are reported in section 4.2.2.1.4.

Table 4.144. Absorption and fluorescence spectroscopic data of 2-fluorofluorene in powder form, for different amounts of sample.

Sample amount ^a	λ_{exc} ^b / nm	Abs ^c	λ_{max}^F ^d / nm	ϕ_F
15 %		0.254		0.32
40 %	310	0.685	356.6	0.32
100 %		0.746		0.28

^a Rough estimate of the percentage of area of the base of the quartz dish covered by sample;

^b Excitation wavelength corresponding to the maximum absorption determined using the Quantaurus apparatus;

^c Determined using the Quantaurus apparatus;

^d Wavelength at the maximum fluorescence emission intensity.

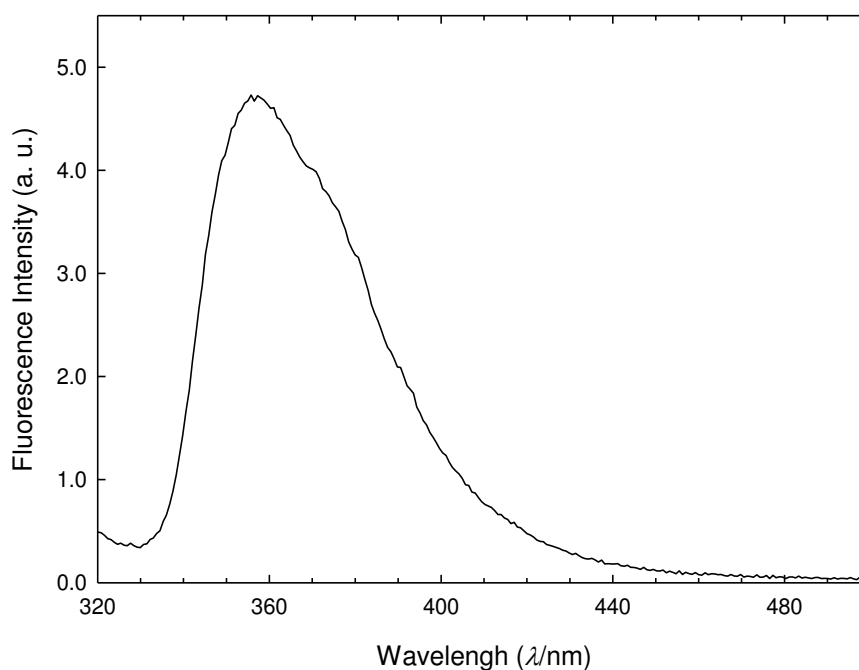
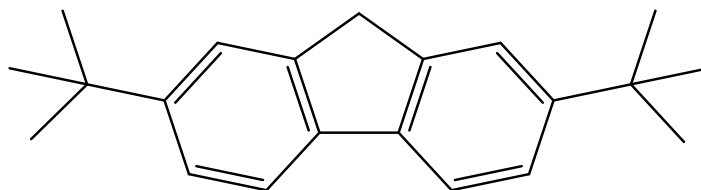


Figure 4.29. Fluorescence emission spectra of 2-fluorofluorene in powder form ($\lambda_{exc} = 310$ nm).

4.3.2.1.4. 2,7-Di-*tert*-butylfluorene


Details regarding the source, purity and physical properties of 2,7-di-*tert*-butylfluorene are reported in section 4.2.2.2.1.

 Table 4.145. Fluorescence spectroscopic data of 2,7-di-*tert*-butylfluorene in cyclohexane solutions, at room temperature.

Sample	$\lambda_{\text{exc}}^a / \text{nm}$	$\lambda_{\text{max}}^F{}^b / \text{nm}$	ϕ_F^c
$1 \cdot 10^{-5} \text{ mol} \cdot \text{L}^{-1}$		322.3	0.49 ± 0.01
$1 \cdot 10^{-4} \text{ mol} \cdot \text{L}^{-1}$	273.0	323.1	0.43 ± 0.01
$1 \cdot 10^{-3} \text{ mol} \cdot \text{L}^{-1}$		324.6	0.43 ± 0.01

^a Excitation wavelength corresponding to the maximum absorption determined using UV-Vis spectrometry for the concentration $1 \cdot 10^{-5} \text{ mol} \cdot \text{L}^{-1}$;

^b Wavelength at the maximum fluorescence emission intensity;

^c Mean values and standard deviations of the mean of six independent measurements.

 Table 4.146. Absorption and fluorescence spectroscopic data of 2,7-di-*tert*-butylfluorene in powder form, for different amounts of sample.

Sample amount ^a	$\lambda_{\text{exc}}^b / \text{nm}$	Abs ^c	$\lambda_{\text{max}}^F{}^d / \text{nm}$	ϕ_F
15 %		0.277		0.09
40 %	310	0.419	334.5	0.07
100 %		0.712		0.07

^a Rough estimate of the percentage of area of the base of the quartz dish covered by sample;

^b Excitation wavelength corresponding to the maximum absorption determined using the Quantaurus apparatus;

^c Determined using the Quantaurus apparatus;

^d Wavelength at the maximum fluorescence emission intensity.

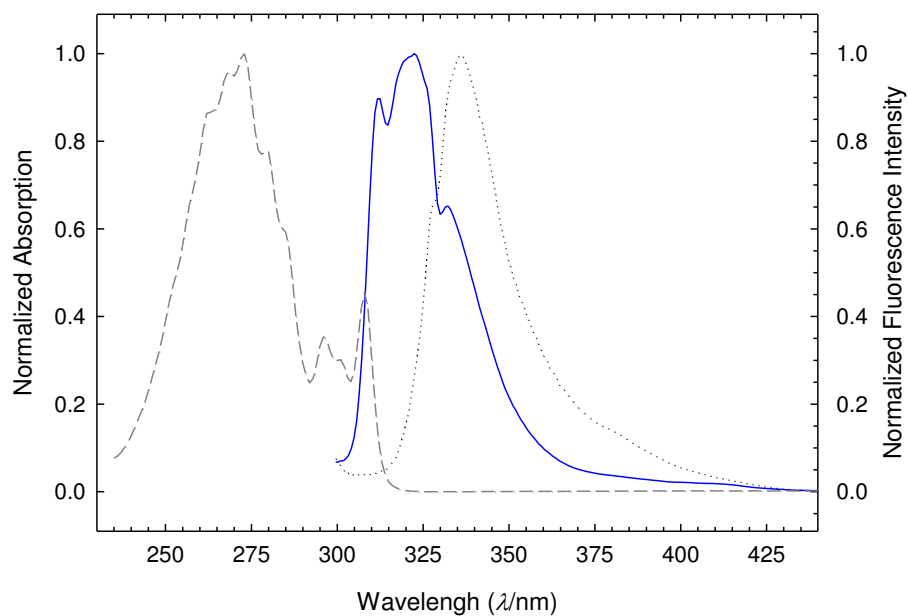
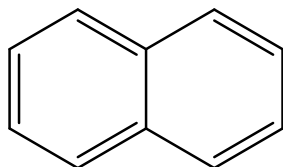


Figure 4.30. Normalized UV-Vis absorption and fluorescence emission spectra of 2,7-di-*tert*-butylfluorene: dashed line - absorption spectra ($1 \cdot 10^{-5} \text{ mol} \cdot \text{L}^{-1}$); solid line - solution fluorescence spectra ($1 \cdot 10^{-5} \text{ mol} \cdot \text{L}^{-1}$); dotted line - powder fluorescence spectra.

4.3.2.2. Naphthalene and naphthalene derivatives

4.3.2.2.1. Naphthalene



Molecular formula	CAS Number	Molar Mass	Density
C ₁₀ H ₈	91-20-3	128.1698 g·mol ⁻¹	1.037 [82]

The sample used for the photoluminescence study was already available at the lab and no information regarding the supplier, lot and initial purity was available. The sample had been sublimed twice under reduced pressure (by another researcher) and the purity was checked by GC previously to the photoluminescence study.

Table 4.147. Source, purification and analysis details of naphthalene.

Source	Mass fraction purity
Commercial ^a	0.9998 ^b

^a Sublimed twice under reduced pressure.

^b Determined by GC.

Table 4.148. Literature results for the fluorescence quantum yield of naphthalene in different solvents.

Solvent	<i>C</i> / mol·L ⁻¹	λ_{exc} / nm	ϕ_F	Method	Source
Hexane			0.10	Relative	Weber & Teale [70]
Ethanol			0.12	Relative	Weber & Teale [70]
Ethanol	Infinite dilution ^a	254	0.205 ± 0.014	Relative	Dawson & Windsor [72]
Cyclohexane	7.3·10 ⁻³	265	0.23 ± 0.02	Relative	Berlman [73]
Cyclohexane	7.0·10 ⁻⁵	270	0.23 ± 0.01	Absolute ^b	Suzuki <i>et al.</i> [83]

^a Fluorescence data extrapolated to zero concentration;

^b Integrating sphere.

Table 4.148 provides literature results for the quantum yield of naphthalene (listed in chronological order). The literature data refers to measurements performed at room temperature. Dawson and Windsor [72] have used the same relative measuring method reported by Weber and Teale [70]. The fluorescence spectra reported by Dawson and Windsor were corrected for self-absorption extrapolating the fluorescence spectra to zero concentration. Berlman [73] used a solution of 9,10-diphenylanthracene ($\phi_F = 1.0$ [76]) as standard.

The absorption and fluorescence emission spectra as well as the fluorescence quantum yield in cyclohexane solution obtained in this work are consistent with those reported in the literature, with the exception of those reported by Weber and Teale [70]. To the best of our knowledge, no quantum yield results have been published for naphthalene in the solid state.

Table 4.149. Fluorescence spectroscopic data of naphthalene in cyclohexane solutions, at room temperature.

Sample	λ_{exc}^a / nm	λ_{max}^F ^b / nm	ϕ_F ^c
$1 \cdot 10^{-4} \text{ mol} \cdot \text{L}^{-1}$	276	336.0	0.21 ± 0.01
$1 \cdot 10^{-3} \text{ mol} \cdot \text{L}^{-1}$		336.8	0.22 ± 0.01

^a Excitation wavelength corresponding to the maximum absorption determined using UV-Vis spectrometry for the concentration $1 \cdot 10^{-4} \text{ mol} \cdot \text{L}^{-1}$;

^b Wavelength at the maximum fluorescence emission intensity;

^c Mean values and standard deviations of the mean of five independent measurements.

Table 4.150. Absorption and fluorescence spectroscopic data of naphthalene in powder form, for different amounts of sample.

Sample amount ^a	λ_{exc}^b / nm	Abs ^c	λ_{max}^F ^d / nm	ϕ_F
15 %	320	0.205	339.0	0.23
40 %		0.532		0.21
100 %		0.712		0.20

^a Rough estimate of the percentage of area of the base of the quartz dish covered by sample;

^b Excitation wavelength corresponding to the maximum absorption determined using the Quantaurus apparatus;

^c Determined using the Quantaurus apparatus;

^d Wavelength at the maximum fluorescence emission intensity.

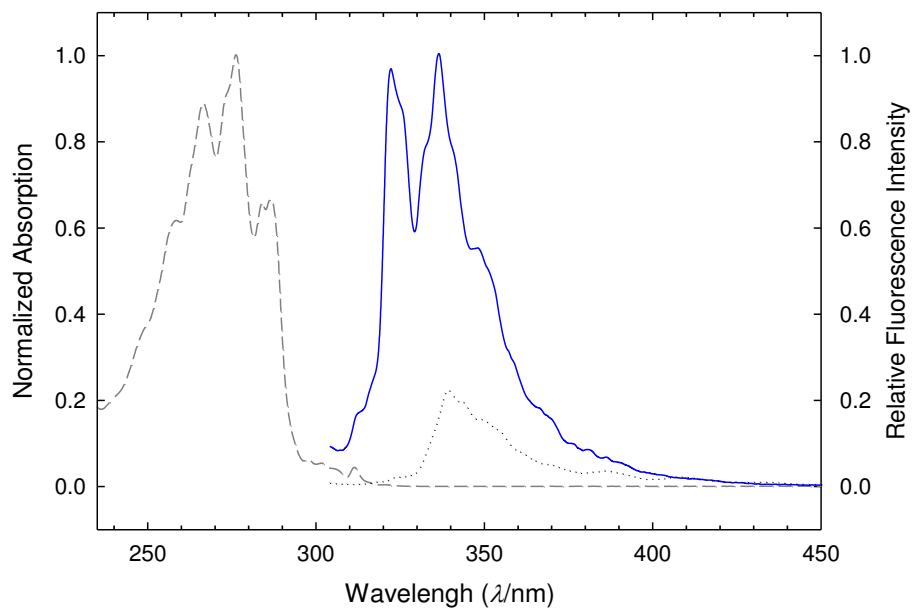
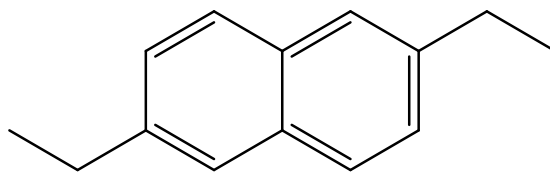


Figure 4.31. Normalized UV-Vis absorption and relative fluorescence emission spectra of naphthalene: dashed line - absorption spectra ($1 \cdot 10^{-4}$ mol·L $^{-1}$); solid line - solution fluorescence spectra ($1 \cdot 10^{-4}$ mol·L $^{-1}$); dotted line - powder fluorescence spectra.

4.3.2.2.2. 2,6-Diethylnaphthalene



Details regarding the source, purity and physical properties of 2,6-diethylnaphthalene are reported in section 4.2.2.6.1.

Table 4.151. Fluorescence spectroscopic data of 2,6-diethylnaphthalene in cyclohexane solutions, at room temperature.

Sample	λ_{exc}^a / nm	λ_{max}^F ^b / nm	ϕ_F ^c
$1 \cdot 10^{-4} \text{ mol} \cdot \text{L}^{-1}$	323	339.8	0.46 ± 0.01
$1 \cdot 10^{-3} \text{ mol} \cdot \text{L}^{-1}$			0.45 ± 0.01

^a Excitation wavelength corresponding to the maximum absorption determined using UV-Vis spectrometry for the concentration $1 \cdot 10^{-4} \text{ mol} \cdot \text{L}^{-1}$;

^b Wavelength at the maximum fluorescence emission intensity;

^c Mean values and standard deviations of the mean of five independent measurements.

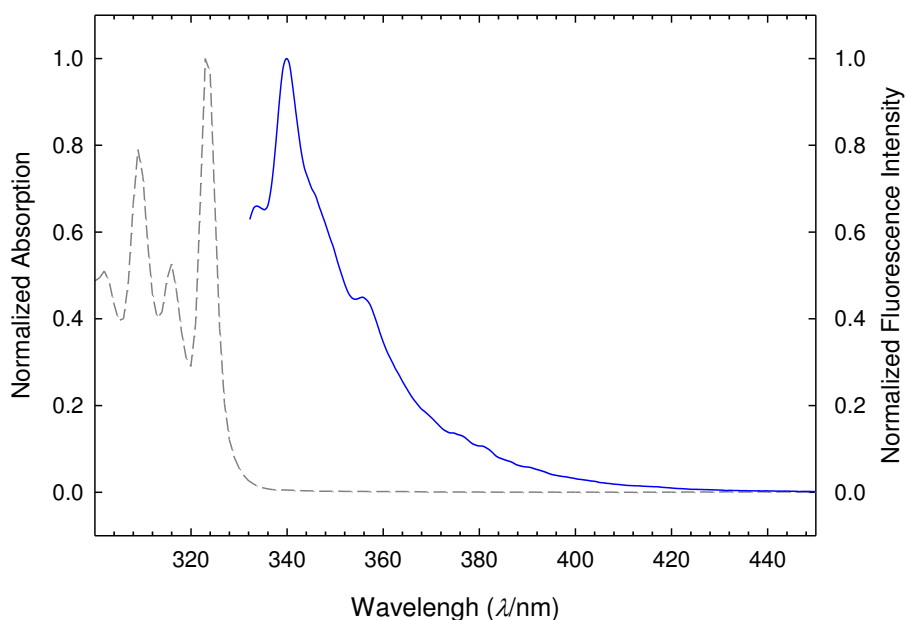
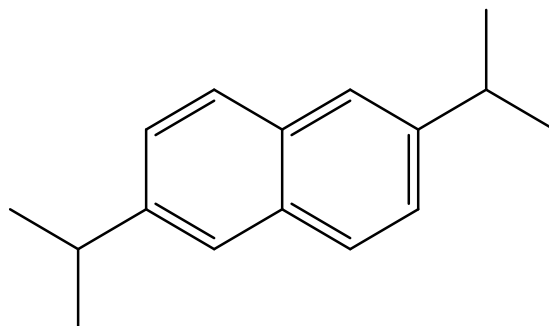


Figure 4.32. Normalized UV-Vis absorption and relative fluorescence emission spectra of 2,6-diethylnaphthalene: dashed line - absorption spectra ($1 \cdot 10^{-4} \text{ mol} \cdot \text{L}^{-1}$); solid line - solution fluorescence spectra ($1 \cdot 10^{-3} \text{ mol} \cdot \text{L}^{-1}$).

4.3.2.2.3. 2,6-Diisopropylnaphthalene



Details regarding the source, purity and physical properties of 2,6-diisopropylnaphthalene are reported in section 4.2.2.6.2.

Table 4.152. Fluorescence spectroscopic data of 2,6-diisopropylnaphthalene in cyclohexane solutions, at room temperature.

Sample	$\lambda_{\text{exc}}^a / \text{nm}$	$\lambda_{\text{max}}^F{}^b / \text{nm}$	ϕ_F^c
$1 \cdot 10^{-4} \text{ mol} \cdot \text{L}^{-1}$	320	339.1	0.42 ± 0.01
$1 \cdot 10^{-3} \text{ mol} \cdot \text{L}^{-1}$			0.40 ± 0.01

^a Excitation wavelength corresponding to the maximum absorption determined using UV-Vis spectrometry for the concentration $1 \cdot 10^{-4} \text{ mol} \cdot \text{L}^{-1}$;

^b Wavelength at the maximum fluorescence emission intensity;

^c Mean values and standard deviations of the mean of five independent measurements.

Table 4.153. Absorption and fluorescence spectroscopic data of 2,6-diisopropylnaphthalene in powder form, for different amounts of sample.

Sample amount ^a	$\lambda_{\text{exc}}^b / \text{nm}$	Abs ^c	$\lambda_{\text{max}}^F{}^d / \text{nm}$	ϕ_F
15 %	320	0.222	345.8	0.38
40 %		0.606		0.37
100 %		0.727		0.36

^a Rough estimate of the percentage of area of the base of the quartz dish covered by sample;

^b Excitation wavelength corresponding to the maximum absorption determined using the Quantaurus apparatus;

^c Determined using the Quantaurus apparatus;

^d Wavelength at the maximum fluorescence emission intensity.

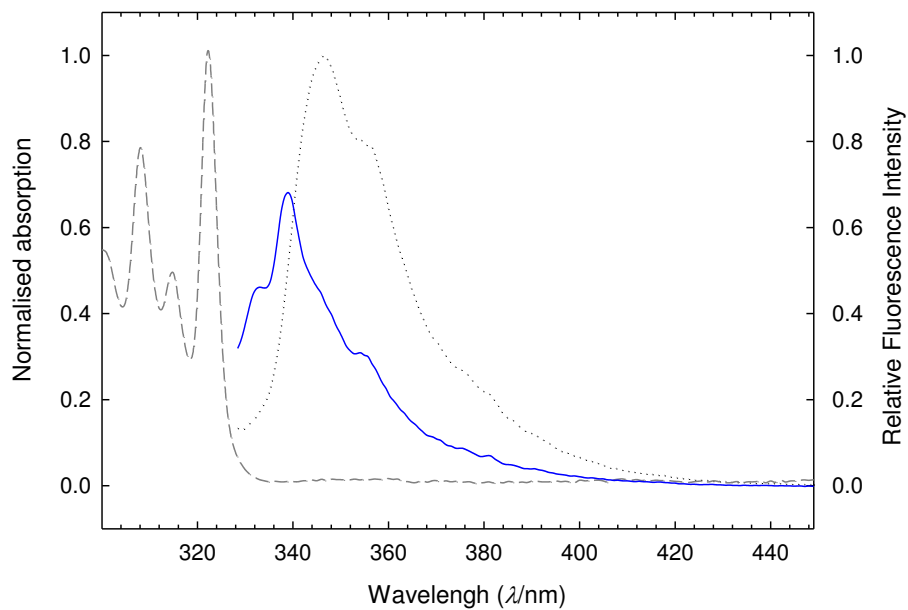
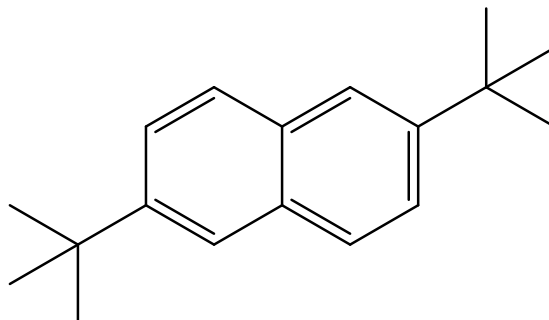


Figure 4.33. Normalized UV-Vis absorption and relative fluorescence emission spectra of 2,6-diisopropylnaphthalene: dashed line - absorption spectra ($1 \cdot 10^{-4} \text{ mol} \cdot \text{L}^{-1}$); solid line - solution fluorescence spectra ($1 \cdot 10^{-3} \text{ mol} \cdot \text{L}^{-1}$); dotted line - powder fluorescence spectra.

4.3.2.2.4. 2,6-Di-*tert*-butylnaphthalene


Details regarding the source, purity and physical properties of 2,6-di-*tert*-butylnaphthalene are reported in section 4.2.2.6.3.

Table 4.154. Fluorescence spectroscopic data of 2,6-di-*tert*-butylnaphthalene in cyclohexane solution and in powder form, at room temperature.

Sample	$\lambda_{\text{exc}}^a / \text{nm}$	$\lambda_{\text{max}}^F{}^b / \text{nm}$	ϕ_F^c
$1 \cdot 10^{-4} \text{ mol} \cdot \text{L}^{-1}$	320	336.8	0.39 ± 0.01
$1 \cdot 10^{-3} \text{ mol} \cdot \text{L}^{-1}$		337.5	0.34 ± 0.01

^a Excitation wavelength corresponding to the maximum absorption determined using UV-Vis spectrometry for the concentration $1 \cdot 10^{-4} \text{ mol} \cdot \text{L}^{-1}$;

^b Wavelength at the maximum fluorescence emission intensity;

^c Mean values and standard deviations of the mean of five independent measurements.

Table 4.155. Absorption and fluorescence spectroscopic data of 2,6-di-*tert*-butylnaphthalene in powder form, for different amounts of sample.

Sample amount ^a	$\lambda_{\text{exc}}^b / \text{nm}$	Abs ^c	$\lambda_{\text{max}}^F{}^d / \text{nm}$	ϕ_F
15 %	320	0.354	342.3	0.57
40 %		0.608		0.55
100 %		0.731		0.52

^a Rough estimate of the percentage of area of the base of the quartz dish covered by sample;

^b Excitation wavelength corresponding to the maximum absorption determined using the Quantaurus apparatus;

^c Determined using the Quantaurus apparatus;

^d Wavelength at the maximum fluorescence emission intensity.

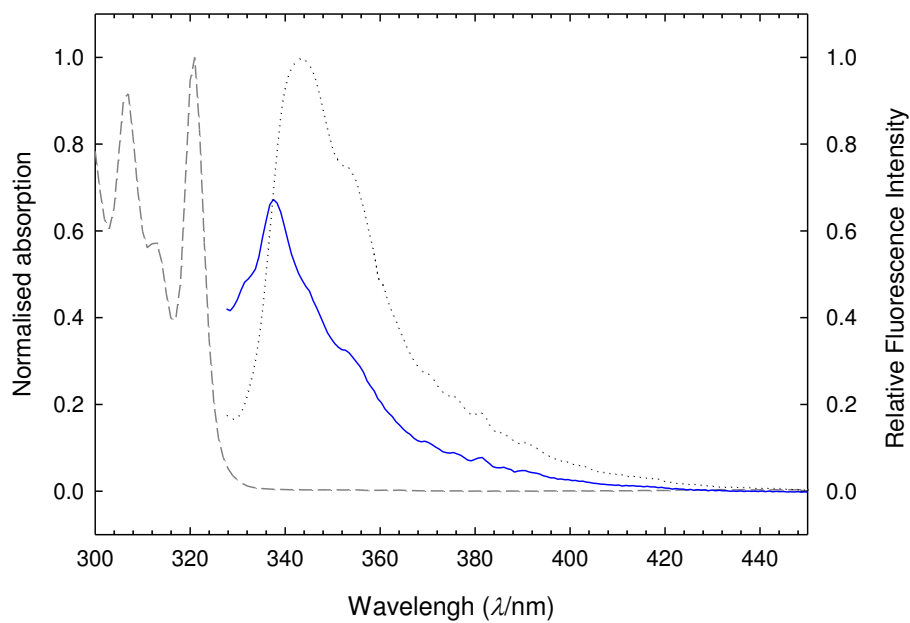
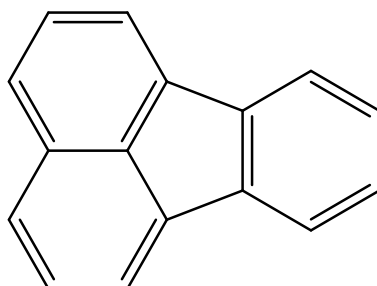


Figure 4.34. Normalized UV-Vis absorption and relative fluorescence emission spectra of 2,6-di-*tert*-butyl-naphthalene: dashed line - absorption spectra ($1 \cdot 10^{-4} \text{ mol} \cdot \text{L}^{-1}$); solid line - solution fluorescence spectra ($1 \cdot 10^{-3} \text{ mol} \cdot \text{L}^{-1}$); dotted line - powder fluorescence spectra.

4.3.2.3. Fluoranthene



Molecular formula	CAS Number	Molar Mass	Density
C ₁₆ H ₁₀	206-44-0	202.2494 g·mol ⁻¹	1.243 [84]

Table 4.156. Source, purification and analysis details of fluoranthene.

Source	Lot	Initial purity ^a	Purification method ^b	Final mass fraction purity ^c
Sigma-Aldrich	14128DD	0.996	Recrystallization	0.9989

^a Determined by HPLC, as stated in the certificate of analysis of the manufacturer;^b Ref. [85];^c Determined by GC.

Table 4.157. Absorption and fluorescence spectroscopic data of fluoranthene in powder form, for different amounts of sample.

Sample amount ^a	λ_{exc} ^b / nm	Abs ^c	λ_{max}^F ^d / nm	ϕ_F
15 %		0.399		0.50
40 %	400	0.529	460.7	0.48
100 %		0.690		0.46

^a Rough estimate of the percentage of area of the base of the quartz dish covered by sample;^b Excitation wavelength corresponding to the maximum absorption determined using the Quantaurus apparatus;^c Determined using the Quantaurus apparatus;^d Wavelength at the maximum fluorescence emission intensity.

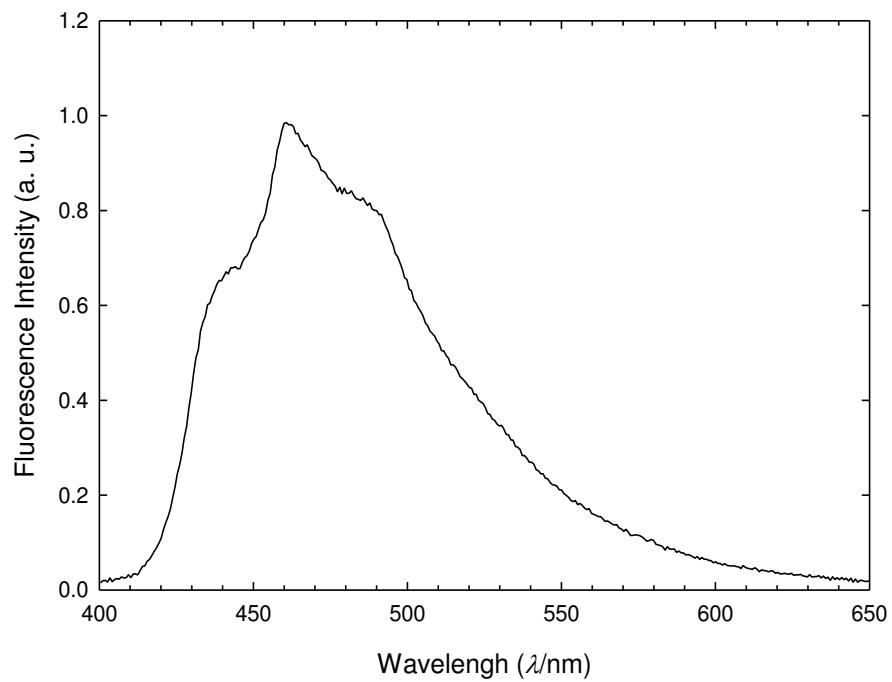


Figure 4.35. Fluorescence emission spectra of fluoranthene in powder form ($\lambda_{\text{exc}} = 400$ nm).

References

- [1] V.L.S. Freitas, *Ph. D. Thesis*, Faculty of Sciences, University of Porto (2009);
- [2] I. Rocha, *Ph. D. Thesis*, Faculty of Sciences, University of Porto (2013);
- [3] E.W. Washburn, *J. Res. Nat. Bur. Stand. (US)* 10 (1933) 525-558;
- [4] W.N. Hubbard, D.W. Scott, G. Waddington, chapter 5, in: F.D. Rossini (Ed.), *Experimental Thermochemistry*, vol. 1, Interscience, New York (1956);
- [5] M.L.C.C.H. Ferrão, G. Pilcher, *J. Chem. Thermodyn.* 19 (1987) 543-548;
- [6] M.A.V. Ribeiro da Silva, A.I.M.C. Lobo Ferreira, *J. Chem. Thermodyn.* 42 (2009) 499-505;
- [7] L. Bjellerup, chapter 3, in: H.A. Skinner (Ed.), *Experimental Thermochemistry*, vol. 2, Interscience, New York (1962);
- [8] L. Bjellerup, *Acta Chem. Scand.* 11 (1957) 1761-1765;
- [9] P. Sellers, S. Sunner, *Acta Chem. Scand.* 18 (1964) 202-206;
- [10] L.M.N.B.F. Santos, M.T. Silva, B. Schröder, L. Gomes, *J. Therm. Anal. Cal.* 89 (2007) 175-180;
- [11] F.D. Rossini, chapter 14, in: F.D. Rossini (Ed.), *Experimental Thermochemistry*, Vol. 1, Interscience, New York (1956);
- [12] G. Olofsson, chapter 6, in: S. Sunner, M. Månsson (Eds.), *Experimental Chemical Thermodynamics*, Vol. 1, Pergamon Press, Oxford (1979);
- [13] <http://www.chemspider.com/>;
- [14] C.L. Yaws, chapter 5, in: C.L. Yaws, D.H. Chen, *Thermophysical Properties of Chemicals and Hydrocarbons*, William Andrew Inc. (2008);
- [15] J.D. Cox, G. Pilcher, *Thermochemistry of Organic and Organometallic Compounds*, Academic Press, London/New York (1970);
- [16] M.J.S. Monte, *Ph. D. Thesis*, Faculty of Sciences, University of Porto (1990);
- [17] J.R. Taylor (Ed.), chapter 6, in: *An Introduction to Error Analysis: The Study of Uncertainties in Physical Measurements*, 2nd ed, University Science Books, Sausalito (1996);
- [18] J.S. Chickos, S. Hosseini, D.G. Hesse, J.F. Liebman, *Struct. Chem.* 4 (1993) 271-278;

- [19] M.J.S. Monte, A.R.R.P. Almeida, M.A.R. Matos, *J. Chem. Eng. Data* 55 (2010) 419-423;
- [20] J.A.S.A. Oliveira, A.F.L.O.M. Santos, M.D.M.C. Ribeiro da Silva, M.J.S. Monte, *J. Chem. Thermodyn.* 89 (2015) 134-141;
- [21] E.S. Domalsky, E.D. Hearing, *J. Phys. Chem. Ref. Data* 22 (1993) 805-1159;
- [22] J.S. Chickos, D.G. Hesse, J.F. Liebman, *Struct. Chem.* 4 (1993) 261-269;
- [23] O.V. Dorofeeva, *Thermodynamic Properties of Gaseous Polycyclic Aromatic Hydrocarbons Containing Five-Membered Rings*, Institute for High Temperatures, USSR Academy of Sciences, Preprint No.1-263, Moscow (1989) (as cited in: <http://webbook.nist.gov/cgi/cbook.cgi?ID=C86737&Units=SI&Mask=1#ref-5;10-08-2011>);
- [24] M.V. Roux, M. Temprado, J.S. Chickos, Y. Nagano, *J. Phys. Chem. Ref. Data* 37 (2008) 1855-1996;
- [25] H.L. Finke, J.F. Messerly, S.H. Lee, A.G. Osborn, D.R. Douslin, *J. Chem. Thermodyn.* 9 (1977) 937-956;
- [26] M.J.S. Monte, R. Notario, M.M.G. Calvinho, A.R.R.P. Almeida, L.M.P.F. Amaral, A.I.M.C. Lobo Ferreira, M.D.M.C. Ribeiro da Silva, *J. Chem. Eng. Data* 57 (2012) 2486-2496;
- [27] *Selected Values of Properties of Chemical Compounds*, Thermodynamics Research Center, Texas A&M University, College Station, Texas (1997) (as cited in: <http://webbook.nist.gov/cgi/cbook.cgi?ID=C71432&Units=SI&Mask=1#Thermo-Gas>);
- [28] D. Ambrose, *J. Chem. Thermodyn.* 7 (1975) 1143-1157;
- [29] R.H. Smith, D.H. Andrews, *J. Am. Chem. Soc.* 53 (1931) 3644-3660;
- [30] O.V. Dorofeeva, *J. Phys. Chem. Ref. Data* 15 (1986) 437-464;
- [31] V.V. Diky, G.J. Kabo, A.A. Kozyro, A.P. Krasulin, V.M. Sevruck, *J. Chem. Thermodyn.* 25 (1993) 1169-1181;
- [32] J.D. Cox, D.D. Wagman, V.A. Medvedev, *CODATA key values for Thermodynamics*, Hemisphere Publishing Corp., New York (1989);
- [33] G.K. Johnson, P.N. Smith, W.N. Hubbard, *J. Chem. Thermodyn.* 5 (1973) 793-809;
- [34] M.W. Chase Jr., *NIST-JANAF Thermochemical Tables*, 4th Edition, *J. Phys. Chem. Ref. Data*, Monograph 9 (1998) 1-1951;

- [35] <http://www.chemspider.com/Chemical-Structure.32028.html>, accessed in October 2011;
- [36] J.L. Goldfarb, E.M. Suuberg, *Environ. Toxicol. Chem.* 27 (2008) 1244-1249;
- [37] W.J. Schmitt, R.C. Reid, *J. Chem. Eng. Data* 31 (1986) 204-212;
- [38] J.A.S.A. Oliveira, M.J.S. Monte, R. Notario, M.D.M.C. Ribeiro da Silva, *J. Chem. Thermodyn.* 76 (2014) 56-63;
- [39] <http://www.lookchem.com/9H-Fluorene-2-fluoro-/>, accessed in January 2016;
- [40] T.S.M. Oliveira, *M. Sc. Thesis*, Faculty of Sciences, University of Porto (2013);
- [41] L.M.P.F. Amaral, private communication;
- [42] J. Fu, E.M. Suuberg, *Environ. Toxicol. Chem.* 31 (2012) 486-493;
- [43] <http://www.lookchem.com/2-Iodo-9H-fluorene/>, accessed in January 2016;
- [44] <http://www.chemspider.com/Chemical-Structure.3304489.html>, accessed in July 2012;
- [45] J.A.S.A. Oliveira, V.L.S. Freitas, R. Notario, M.D.M.C. Ribeiro da Silva, M.J.S. Monte, *J. Chem. Thermodyn.* 101 (2016) 115-122;
- [46] A.F.L.O.M. Santos, J.A.S.A. Oliveira, M.J.S. Monte, *J. Chem. Thermodyn.* 90 (2015) 282-293;
- [47] H.A. Skinner, A. Snelson, *Trans. Faraday Soc.* 56 (1960) 1176-1183;
- [48] F.M. Fraser, E. Prosen, *J. Res. Natl. Bur. Stand. (US)* 55 (1955) 329-333;
- [49] http://www.lookchem.com/product_2-7-difluoro-9H-fluorene/13754978.html, accessed in January 2016;
- [50] B.M. York Jr., *Spiro-(fluoren-9,4'-imidazolidine)-2',5'-diones*, Patent US4438272 (1984);
- [51] L.A. Carpino, *J. Org. Chem.* 45 (1980) 4250-4252;
- [52] <http://www.chemnet.com/cas/en/16218-28-3/2,7-diiodofluorene.html>, accessed in May 2014;
- [53] R. Anémian, Y. Morel, P.L. Baldeck, B. Paci, K. Kretsch, J.-M. Nunzic, C. Andraud, *J. Mater. Chem.* 13 (2003) 2157-2163;
- [54] C.J. Kelley, A. Ghiorghisa, J.M. Kauffman, *J. Chem. Research (M)* 1997, 2701-2733;

- [55] J.A.S.A. Oliveira, M.M. Calvinho, R. Notario, M.J.S. Monte, M.D.M.C. Ribeiro da Silva, *J. Chem. Thermodyn.* 62 (2013) 222-230;
- [56] C.J. Whitman, *J. Chem. Phys.* 20 (1952) 161-164;
- [57] K. Motzfeldt, *J. Phys. Chem.* 59 (1955) 139-147;
- [58] <http://www.chemspider.com/Chemical-Structure.124573.html>, accessed in May 2011;
- [59] S.P. Pinto, *M. Sc. Thesis*, Faculty of Sciences, University of Porto (2010);
- [60] <http://www.chemspider.com/Chemical-Structure.120928.html>, accessed in March 2012;
- [61] M.M.G. Calvinho, *M. Sc. Thesis*, Faculty of Sciences, University of Porto (2010);
- [62] <http://www.chemnet.com/cas/en/6630-65-5/9-Chlorofluorene.html>, accessed in December 2015;
- [63] <http://www.chemnet.com/cas/en/3096-57-9/2-Amino-9-fluorenone.html>, accessed in November 2013;
- [64] <http://www.chemnet.com/cas/en/14348-75-5/2,7-dibromo-9-fluorenone.html>, accessed in October 2014;
- [65] <http://www.chemnet.com/cas/en/59919-41-4/2,6-diethylnaphthalene.html>, accessed in January 2015;
- [66] A.F.L.O.M. Santos, J.A.S.A. Oliveira, M.D.M.C. Ribeiro da Silva, M.J.S. Monte, *Chemosphere* 146 (2016) 173-181;
- [67] <http://www.chemnet.com/cas/en/24157-81-1/2,6-diisopropylnaphthalene.html>, accessed in January 2015;
- [68] H.M. Crawford, M.C. Glesmann, *J. Am. Chem. Soc.* 76 (1954) 1108-1109;
- [69] R.E. Gerkin, A.P. Lundstedt, W.J. Reppart, *Acta Crystallogr. C* 40 (1984) 1892-1894;
- [70] G. Weber, F.W.J. Teale, *Trans. Faraday Soc.* 53 (1957) 646-655;
- [71] D.W. Ellis, B.S. Solomon, *J. Chem. Phys.* 46 (1967) 3497-3501;
- [72] W.R. Dawson, M.W. Windsor, *J. Phys. Chem.* 72 (1968) 3251-3260;
- [73] I.B. Berlman, *Handbook of Fluorescence Spectra of Aromatic Molecules* (2nd Ed.), Academic Press, New York (1971);
- [74] A.T.R. Williams, S.A. Winfield, J.N. Miller, *Analyst* 108 (1983) 1067-1071;

- [75] T.F. Palmer, S.S. Parmar, *J. Photochem.* 31 (1985) 273-288;
- [76] E.J. Bowen, J. Sahu, *J. Phys. Chem.* 63 (1959) 4-7;
- [77] W.H. Melhuish, *J. Phys. Chem.* 65 (1961) 229-235;
- [78] P. Di Marco, G. Giro, *Phys. Stat. Sol. (a)* 30 (1975) K143-K146;
- [79] E.A. Johnson, *J. Chem. Soc.* (1962) 994-997;
- [80] S.A. Jadhav, S.R. Patil, *Mater. Chem. Phys.* 60 (1999) 204-210;
- [81] M.J.S. Monte, S.P. Pinto, A.I.M.C. Lobo Ferreira, L.M.P.F. Amaral, V.L.S. Freitas, M.D.M.C. Ribeiro da Silva, *J. Chem. Thermodyn.* 45 (2012) 53-58;
- [82] <http://www.chemnet.com/cas/en/91-20-3/Naphthalene.html>, accessed in January 2015;
- [83] K. Suzuki, A. Kobayashi, S. Kaneko, K. Takehira, T. Yoshihara, H. Ishida, Y. Shiina, S. Oishi, S. Tobita, *Phys. Chem. Chem. Phys.* 11 (2009) 9850-9860;
- [84] L.F. Fieser, F.C. Novello, *J. Am. Chem. Soc.* 62 (1940) 1855-1859;
- [85] M.J.S. Monte, R. Notario, S.P. Pinto, A.I.M.C. Lobo Ferreira, M.D.M.C. Ribeiro da Silva, *J. Chem. Thermodyn.* 49 (2012) 159-164.

Chapter

5

Discussion and conclusions

- 5.1. Introduction
- 5.2. Thermodynamic properties
- 5.3. Photoluminescence properties
- 5.4. Conclusions

References

5.1. Introduction

After the detailed presentation of the experimental results of the compounds studied in the previous chapter, the thermodynamic properties are now discussed in terms of volatility and thermal stability, and the photoluminescence properties are discussed in terms of fluorescence spectral details and quantum efficiency.

The influence of the different substituents in the thermodynamic and photoluminescence properties of the fluorene, fluorenone and naphthalene derivatives was evaluated by comparison with the properties of the parental molecules.

Additionally, the thermodynamic properties were employed in several correlations and, using similar approaches to others published recently by our research group [1,2], estimation equations were developed to predict the vapor pressure and thermodynamic properties of sublimation and vaporization of some of the fluorene, fluorenone and naphthalene derivatives studied.

5.2. Thermodynamic properties

5.2.1. Thermodynamic properties of fusion

Table 5.1 presents a summary of the temperatures of fusion and of the enthalpies and entropies of fusion, at this temperature, of fluorene, fluorenone, naphthalene and its derivatives. Estimated values derived using correlations to be discussed ahead are also presented in this table (inside parenthesis).

Table 5.1. Temperatures, molar enthalpies and entropies of fusion of the compounds studied, determined by DSC.

Compound	T_{fus} (onset)	$\Delta_{\text{cr}}^{\text{l}} H_{\text{m}}^{\circ}(T_{\text{fus}})$	$\Delta_{\text{cr}}^{\text{l}} S_{\text{m}}^{\circ}(T_{\text{fus}})$
	K	$\text{kJ}\cdot\text{mol}^{-1}$	$\text{J}\cdot\text{K}^{-1}\cdot\text{mol}^{-1}$
Fluorene [3]	388.0 ± 0.2	20.3 ± 0.1	52.3 ± 0.3
2-SUBSTITUTED FLUORENES			
2-Fluorencarboxaldehyde	357.61 ± 0.07	22.05 ± 0.05	61.7 ± 0.1
2-Aminofluorene	400.9 ± 0.1	23.81 ± 0.05	59.4 ± 0.1
2-Nitrofluorene	429.9 ± 0.4	24.75 ± 0.05	57.6 ± 0.1
2-Fluorofluorene	373.11 ± 0.09 (373.2) ^a	22.40 ± 0.03	60.04 ± 0.08
2-Chlorofluorene	369.7 [4] (370.6) ^a		
2-Bromofluorene	387.39 ± 0.03 (385.7) ^a	17.0 ± 0.1	43.9 ± 0.3
2-Iodofluorene	404.13 ± 0.04 (404.9) ^a	17.53 ± 0.05	43.4 ± 0.1
2,7-DISUBSTITUTED FLUORENES			
2,7-Di- <i>tert</i> -butylfluorene	395.9 ± 0.2	15.6 ± 0.3	39.4 ± 0.8
2,7-Difluorofluorene	356.4 ± 0.3 (356.4) ^b	18.05 ± 0.04	50.6 ± 0.1
2,7-Dichlorofluorene	396.90 ± 0.06 (397.6) ^b	18.4 ± 0.2	46.4 ± 0.5
2,7-Dibromofluorene	438.8 ± 0.1 (437.3) ^b	22.72 ± 0.04	51.78 ± 0.09

.../...

.../...

2,7-Diodofluorene	490.9 ± 0.1 (491.5) ^b	24.28 ± 0.09	49.5 ± 0.2
9-SUBSTITUTED FLUORENES			
9-Fluorenicarboxylic Acid	503.8 ± 0.3	30.2 ± 0.3	59.9 ± 0.6
9-Phenyl-9-fluoreneol	382.7 ± 0.1	22.7 ± 0.1	59.3 ± 0.3
9-Benzylidene fluorene	348.69 ± 0.05	17.0 ± 0.1	48.8 ± 0.3
9-Fluorene methanol	377.1 ± 0.1	27.9 ± 0.2	74.0 ± 0.5
9-Chlorofluorene	362.2 ± 0.3	17.6 ± 0.1	48.6 ± 0.3
Fluorenone [5]	356.2 ± 0.2	17.6 ± 0.7	49.4 ± 2.0
2-SUBSTITUTED FLUORENONES			
2-Aminofluorenone	429.5 ± 0.1	24.06 ± 0.09	56.0 ± 0.2
2-Hydroxyfluorenone	482.3 ± 0.2	29.4 ± 0.1	61.0 ± 0.2
2-Fluorofluorenone	388.51 ± 0.02	18.93 ± 0.05	48.7 ± 0.1
2,7-DISUBSTITUTED FLUORENONES			
2,7-Dibromofluorenone	477.8 ± 0.3	26.9 ± 0.2	56.3 ± 0.4
Naphthalene [6]	353.4	19.07 ± 0.08	54.0 ± 0.2
2,6-SUBSTITUTED NAPHTHALENES			
2,6-Dimethylnaphthalene [7]	383.32 ^c	25.06 ± 0.01	65.38 ± 0.03
2,6-Diethylnaphthalene	322.5 ± 0.1	22.36 ± 0.06	69.3 ± 0.2
2,6-Diisopropylnaphthalene	343.0 ± 0.2	18.8 ± 0.1	54.8 ± 0.3
2,6-Di- <i>tert</i> -butylnaphthalene	420.2 ± 0.2	18.5 ± 0.2	44.0 ± 0.5

^a Values estimated through equation 5.4;

^b Values estimated through equation 5.5;

^c Triple point temperature.

The thermodynamic properties of fusion – temperature, enthalpy and entropy – are important characteristics of pure compounds. They are related to the intermolecular forces presented in both crystalline and liquid phases. So, they are somewhat related to the compound's crystalline structure. As can be seen in figure 5.1, the enthalpies of fusion tend to increase with increasing temperatures of fusion, for the compounds studied.

Interestingly this tendency seems to be in accordance with the Walden's rule [8]. From the experimental study on the fusion of 15 aromatic compounds formed by “non-associated” molecules, Walden calculated a mean value of the entropy of fusion of these compounds as $\langle \Delta_{cr}^l S_m^o \rangle = 56.5 \text{ J}\cdot\text{K}^{-1}\cdot\text{mol}^{-1}$. Similarly to the Trouton's rule for the normal entropy of

vaporization of “non-associated” liquids [9], this mean value has been used for rough estimations of the enthalpy of fusion when values of temperatures of fusion are available.

The entropy of fusion of the compounds studied, represented in figure 5.2, may be represented by the mean value $\langle \Delta_{\text{cr}}^{\text{l}} S_{\text{m}}^{\text{o}}(T_{\text{fus}}) \rangle = (53.0 \pm 7.1) \text{ J}\cdot\text{K}^{-1}\cdot\text{mol}^{-1}$ (the quoted uncertainty is the standard deviation of the mean) where the value of 9-fluorenemethanol is excluded (two hydrogen bonds per molecule, as shown in section 5.2.2.1.).

The correlation presented in figure 5.1 is well defined by the equation 5.1:

$$\Delta_{\text{cr}}^{\text{l}} H_{\text{m}}^{\text{o}}(T_{\text{fus}})/\text{K}\cdot\text{mol}^{-1} = 0.0530 (T_{\text{fus}}/\text{K}) \quad (5.1)$$

The values of the enthalpy of fusion estimated according to this equation for the compounds studied present a standard deviation of $2.8 \text{ J}\cdot\text{K}^{-1}\cdot\text{mol}^{-1}$.

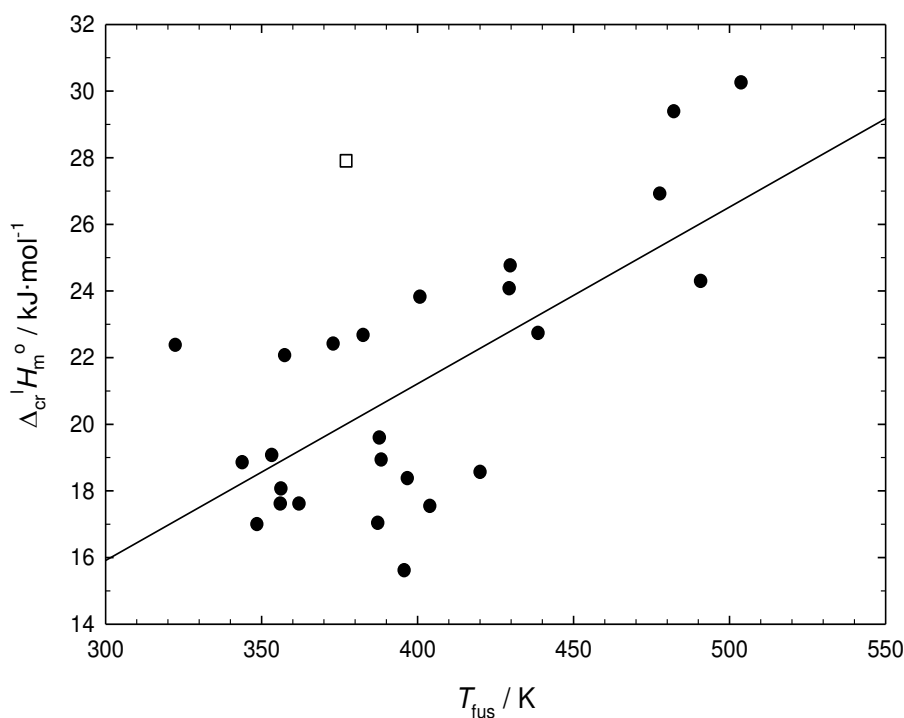


Figure 5.1. Correlation between the temperature (T_{fus}) and enthalpy of fusion ($\Delta_{\text{cr}}^{\text{l}} H_{\text{m}}^{\text{o}}$) of the compounds studied (\square , 9-fluorenemethanol).

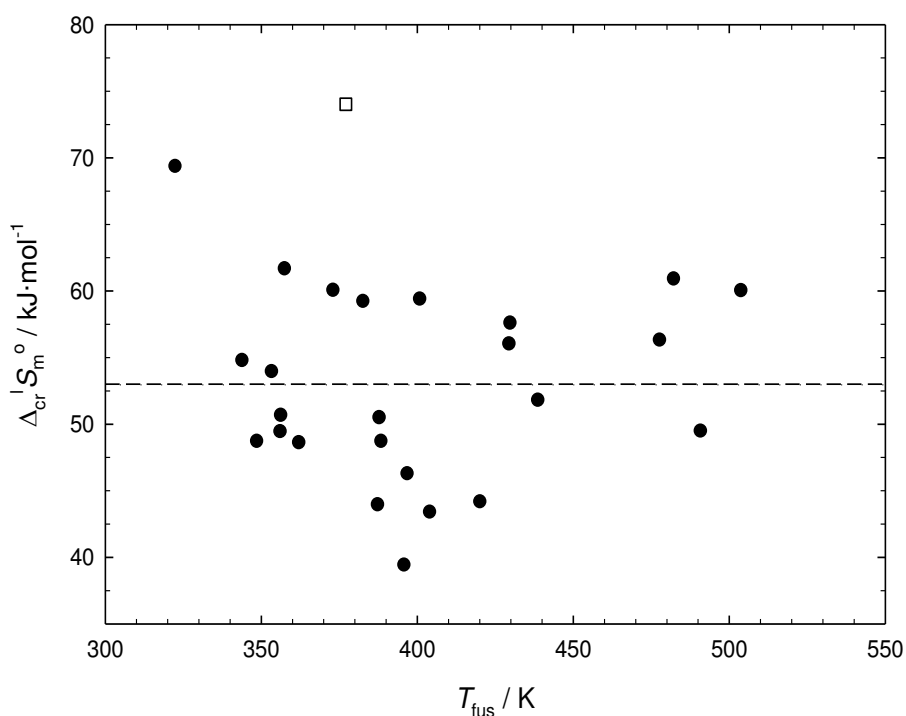


Figure 5.2. Temperature of fusion versus entropy of fusion of the compounds studied (□, 9-fluorene-methanol).

Accurate estimations of the temperature of fusion are admittedly difficult and no general procedure has proven successful for its prediction based on correlations with other physical and structural properties [10].

In this work, we attempted to establish a correlation between the temperatures of fusion of halogenated fluorenes and the combined influence of the excess volumes and excess electron affinity of halogen atoms, as recently applied by Monte *et al.* [2] for the estimation of the thermodynamic properties of vaporization of halogenated benzenes. The previously referred excess properties, presented in table 5.2, are calculated as the difference between the properties of the halogen substituents (X), and the respective properties of the hydrogen atom being replaced.

$$V^{XS}(X)/nm^3 = V(X)/nm^3 - V(H)/nm^3 \quad (5.2)$$

$$EA^{XS}(X)/eV = EA(X)/eV - EA(H)/eV \quad (5.3)$$

Correlating the temperatures of fusion with the referred to above atomic properties of each halogen, equations 5.4 and 5.5 reproduce rather well the temperatures of fusion of the fluorenes halogenated in positions 2 and 2,7, respectively. The results estimated from these equations are listed in table 5.1.

$$T_{\text{fus}}(2\text{-Xfluorene}) / \text{K} = 492.75 + 0.813(10^3 V^{\text{XS}}(\text{X})/\text{nm}^3) - 47.05(EA^{\text{XS}}(\text{X})/\text{eV}) \quad (5.4)$$

$$R^2 = 0.994; \sigma = 2.1 \text{ K}$$

$$T_{\text{fus}}(2,7\text{-X}_2\text{fluorene})/\text{K} = 481.30 + 5.95(10^3 V^{\text{XS}}(\text{X})/\text{nm}^3) - 60.89(EA^{\text{XS}}(\text{X})/\text{eV}) \quad (5.5)$$

$$R^2 = 0.9997; \sigma = 1.8 \text{ K}$$

Table 5.2. Bondi radius, and absolute and excess volumes and electron affinities of the halogen atoms (reported in ref. [2]).

Atom	r^a	$10^3 V$	$10^3 V^{\text{XS}}$	$EA^{b,c}$	$EA^{\text{XS}c}$
	nm	nm ³	nm ³	eV	eV
H	0.120	7.23	0	0.75419	0
F	0.147	13.3	6.1	3.401290	2.647
Cl	0.175	22.4	15.2	3.612724	2.859
Br	0.185	26.5	19.3	3.363588	2.609
I	0.198	32.5	25.3	3.059038	2.305

^a Bondi radius reported in ref. [11];

^b Ref. [12];

^c 1 eV = 1.602176565(35) · 10⁻¹⁹ J.

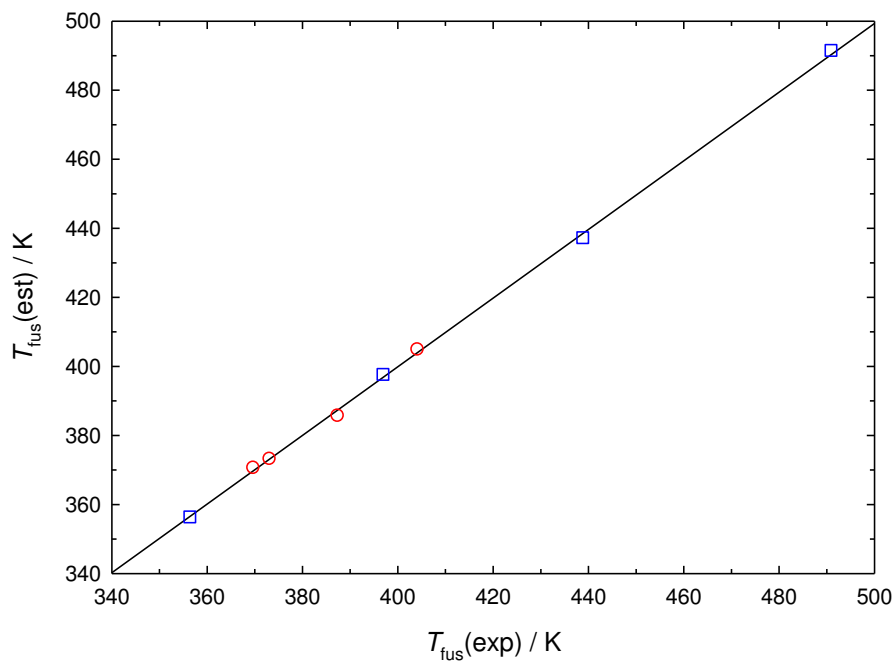


Figure 5.3. Correlation between experimental and estimated results of T_{fus} of halogenated fluorenes: \circ , 2-halogenated fluorenes (2-fluorofluorene, 2-chlorofluorene, 2-bromofluorene, 2-iodofluorene); \square , 2,7-dihalogenated fluorenes (2,7-difluorofluorene, 2,7-dichlorofluorene, 2,7-dibromofluorene, 2,7-diiodofluorene).

The quality of each estimation equation may be defined by the statistic parameters presented above: the standard error of the estimate (σ) and the square correlation coefficient (R^2). Figure 5.3 shows the correlation between the experimental and estimated results for the temperature of fusion, highlighting the excellent estimated results yield by equations 5.4 and 5.5. Similar correlations may eventually be established for fluorenes halogenated in position 9, however there was only one result available (9-chlorofluorene). For halogenated fluorenones the only two available results (2-fluorofluorenone and 2,7-dibromofluorenone didn't allow checking if experimental results of fusion may be described by such correlations.

5.2.2. Thermodynamic properties of sublimation and vaporization

5.2.2.1. Fluorene and fluorene derivatives

Table 5.3 presents a summary of the thermodynamic properties of sublimation and vaporization of fluorene and its derivatives, at $T = 298.15$ K, including their vapor pressures. Estimated values derived using correlations to be discussed ahead are also presented in this table (inside parenthesis).

Table 5.3. Thermodynamic properties of sublimation and vaporization of fluorene and its derivatives, as well as their vapor pressures at $T = 298.15$ K. Values inside parenthesis are estimations.

Compound	Phase	$\Delta_{cr/l}^g G_m^o$	$\Delta_{cr/l}^g H_m^o$	$T \Delta_{cr/l}^g S_m^o$	$p(cr/l)$
		kJ·mol ⁻¹			Pa
Fluorene [3]	cr	34.49 ± 0.02	87.8 ± 0.5	53.3 ± 0.5	9.1·10 ⁻²
	l	30.43 ± 0.04	72.1 ± 0.2	41.7 ± 0.2	4.7·10 ⁻¹
2-SUBSTITUTED FLUORENES					
2-Fluorencarboxaldehyde	cr	45.94 ± 0.08 (44.8) ^a	110.1 ± 0.6	64.3 ± 0.6	8.9·10 ⁻⁴
2-Aminofluorene	cr	48.97 ± 0.06 (49.5) ^a	112.3 ± 0.4	63.3 ± 0.4	2.6·10 ⁻⁴
2-Nitrofluorene	cr	53.49 ± 0.06 (53.9) ^a	116.2 ± 0.3	62.7 ± 0.3	4.7·10 ⁻⁵
.../...					

.../...					
2-Fluorofluorene	cr	35.13 ± 0.01 (35.1) ^b (36.7) ^a	91.72 ± 0.08 (91.4) ^c	56.59 ± 0.08	7.0·10 ⁻²
	l	30.89 ± 0.03 (30.5) ^d	71.9 ± 0.3 (72.5) ^e	41.0 ± 0.3	3.9·10 ⁻¹
2-Chlorofluorene	cr	(38.7) ^b	(92.5) ^c	(53.8)	(1.6·10 ⁻²)
	l	(35.3) ^d	(79.1) ^e	(43.8)	(6.5·10 ⁻²)
2-Bromofluorene	cr	42.25 ± 0.03 ^f (42.5) ^b (42.0) ^g (40.4) ^a	96.6 ± 0.1 ^f (97.7) ^c	54.3 ± 0.1	4.0·10 ⁻³
	l	38.44 ± 0.03 (37.9) ^d	81.7 ± 0.1 (82.6) ^e	43.3 ± 0.1	1.8·10 ⁻²
	cr	46.66 ± 0.02 ^f (46.7) ^b (46.3) ^g (44.8) ^a	102.5 ± 0.1 ^f (102.0) ^c	55.8 ± 0.1	6.7·10 ⁻⁴
2-Iodofluorene	l	42.18 ± 0.02 (41.6) ^d	87.41 ± 0.09 (87.6) ^e	45.2 ± 0.09	4.1·10 ⁻³
	2,7-DISUBSTITUTED FLUORENES				
2,7-Di- <i>tert</i> -butylfluorene	cr	51.57 ± 0.06 (53.3) ^a	121.1 ± 0.4	68.9 ± 1.0	9.2·10 ⁻⁵
	l	46.61 ± 0.04	101.2 ± 0.2	54.6 ± 0.2	6.8·10 ⁻⁴
2,7-Difluorofluorene	cr	34.79 ± 0.02 (34.9) ^b (35.3) ^a	91.8 ± 0.4 (91.7) ^c	57.0 ± 0.4	8.0·10 ⁻²
	l	(30.6) ^d	(73.0) ^e		
	cr	46.03 ± 0.03 (46.1) ^b (46.3) ^g (44.3) ^a	102.7 ± 0.1 (102.5) ^c	56.7 ± 0.1	8.6·10 ⁻⁴
2,7-Dichlorofluorene	l	(40.2) ^d	(86.1) ^e		
	cr	54.15 ± 0.06 ^g (54.2) ^b (55.0) ^g (53.9) ^a	114.6 ± 0.2 ^g (114.1) ^c	60.5 ± 0.2	3.3·10 ⁻⁵
2,7-Dibromofluorene	l	(45.4) ^d	(93.1) ^e		
	.../...				

.../...

2,7-Diiodofluorene	cr	64.1 ± 0.2 (64.1) ^b (63.6) ^g (64.3) ^a	126.5 ± 0.7 (126.2) ^c	62.4 ± 0.7	5.9·10 ⁻⁷
	l	(52.8) ^d	(103.1) ^e		
9-SUBSTITUTED FLUORENES					
9-Fluorenol [5]	cr	46.32 ± 0.06 (47.0) ^h	108.3 ± 0.5	62.0 ± 0.5	7.7·10 ⁻⁴
	l	40.32 ± 0.07	91.6 ± 0.4	51.3 ± 0.4	8.6·10 ⁻³
9-Fluorencarboxylic acid	cr	62.3 ± 0.2 (61.2) ^h	130.4 ± 0.8	68.1 ± 0.8	1.2·10 ⁻⁶
9-Phenyl-9-fluorenol	cr	54.79 ± 0.06	125.0 ± 0.3	70.2 ± 0.3	2.5·10 ⁻⁵
9-Benzylidene fluorene	cr	53.8 ± 0.1	117.7 ± 1.1	63.9 ± 1.1	3.8·10 ⁻⁵
9-Fluorenemethanol	cr	48.14 ± 0.03 (48.4) ^h	118.8 ± 0.2	70.7 ± 0.2	3.7·10 ⁻⁴
	l	42.98 ± 0.01	97.8 ± 0.1	54.8 ± 0.1	3.0·10 ⁻³
9-Chlorofluorene	cr	37.80 ± 0.03 (36.5) ^h	95.0 ± 0.5	57.2 ± 0.5	2.4·10 ⁻²

^a Values estimated through equation 5.11; ^b Values estimated through equation 5.6; ^c Values estimated through equation 5.7; ^d Values estimated through equation 5.8; ^e Values estimated through equation 5.9; ^f Weighted mean of results derives from vapor pressures measured by effusion and static methods; ^g Values estimated through equation 5.10; ^h Values estimated through equation 5.12.

5.2.2.1.1. Correlations and estimation equations

It has been recently shown by Monte and Almeida [1] that thermodynamic properties of sublimation of substituted benzenes can be predicted using estimating equations based on the respective temperature of fusion (T_{fus}) and the number and quality of substituents. Using a similar approach, estimating equations were derived by multiple linear regression from the experimental results determined in the present work in order to estimate the thermodynamic properties of sublimation of halogenated fluorenes in positions 2 and 2,7. The standard Gibbs energies (and subsequently derived vapor pressures) and enthalpies of sublimation, at $T = 298.15$ K, were estimated using equations 5.6 and 5.7, respectively, involving T_{fus} of the halogenated fluorenes and the number and quality of halogen substituents. In these equations, n_F , n_{Cl} , n_{Br} , n_I , represent, respectively, the number (one or two) of fluorine, chlorine, bromine and iodine atoms that replace hydrogen in the fluorene molecule.

$$\Delta_{\text{cr}}^{\text{g}} G_{\text{m}}^{\circ}(298.15 \text{ K}) / \text{kJ} \cdot \text{mol}^{-1} = 1.9 + 0.086(T_{\text{fus}}/\text{K}) + 1.15n_{\text{F}} + 5.02n_{\text{Cl}} + 7.27n_{\text{Br}} + 9.99n_{\text{I}}$$

$$R^2 = 1.000; \sigma = 0.2 \text{ kJ} \cdot \text{mol}^{-1} \quad (5.6)$$

$$\Delta_{\text{cr}}^{\text{g}} H_{\text{m}}^{\circ}(298.15 \text{ K}) / \text{kJ} \cdot \text{mol}^{-1} = 20.1 + 0.182(T_{\text{fus}}/\text{K}) + 3.38n_{\text{F}} + 5.09n_{\text{Cl}} + 7.06n_{\text{Br}} + 8.39n_{\text{I}}$$

$$R^2 = 0.999; \sigma = 0.9 \text{ kJ} \cdot \text{mol}^{-1} \quad (5.7)$$

As mentioned previously, Monte *et al.* [2] also developed equations for the estimation of vapor pressures and enthalpies of vaporization of liquid halogenated benzenes, which consider calculated contributions to each halogen substituent based on the combined influence of the respective volumes and electron affinities. The proposed method was also tested for other polycyclic aromatic compounds, including a few fluorene and fluorenone derivatives. Using the halogen contributions proposed by Monte *et al.* [2] and the thermodynamic properties of vaporization of the parent compound – fluorene – given in table 5.3, the standard Gibbs energies and enthalpies of vaporization, at $T = 298.15 \text{ K}$, of the halogenated fluorene derivatives were estimated, at $T = 298.15 \text{ K}$, using equations 5.8 and 5.9 respectively.

$$\Delta_{\text{l}}^{\text{g}} G_{\text{m}}^{\circ}(298.15 \text{ K}) / \text{kJ} \cdot \text{mol}^{-1} = \Delta_{\text{l}}^{\text{g}} G_{\text{m}}^{\circ}(\text{fluorene}) / \text{kJ} \cdot \text{mol}^{-1} + 0.09n_{\text{F}} + 4.9n_{\text{Cl}} + 7.5n_{\text{Br}} + 11.2n_{\text{I}}$$

$$R^2 = 0.999 \quad (5.8)$$

$$\Delta_{\text{l}}^{\text{g}} H_{\text{m}}^{\circ}(298.15 \text{ K}) / \text{kJ} \cdot \text{mol}^{-1} = \Delta_{\text{l}}^{\text{g}} H_{\text{m}}^{\circ}(\text{fluorene}) / \text{kJ} \cdot \text{mol}^{-1} + 0.43n_{\text{F}} + 7.0n_{\text{Cl}} + 10.5n_{\text{Br}} + 15.5n_{\text{I}}$$

$$R^2 = 0.997 \quad (5.9)$$

The estimated results obtained from equations 5.6 to 5.9, also presented in table 5.3, were correlated with the ones obtained experimentally as can be observed in figure 5.4, showing excellent agreement.

Given that it was not possible to experimentally determine the thermodynamic properties of sublimation and vaporization of 2-chlorofluorene (section 2.3.1.4.), these properties were estimated using the previously mentioned equations and the literature temperature of fusion ($T_{\text{fus}} = 369.7 \text{ K}$ [4]), yielding the estimated results included in table 5.3. The properties of vaporization the dihalogenated fluorene derivatives were also estimated using equations 5.8 and 5.9.

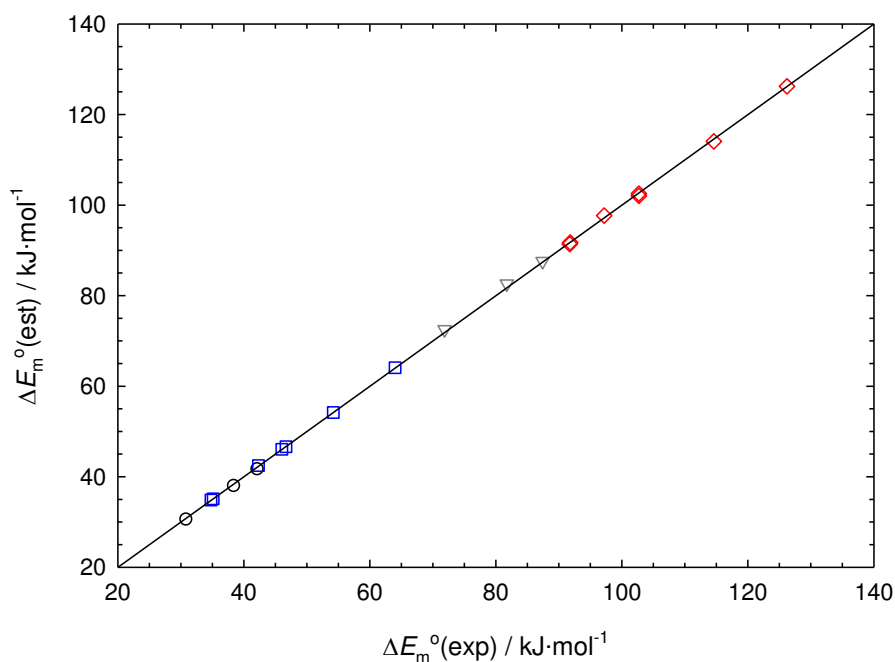
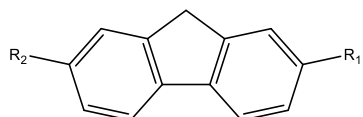


Figure 5.4. Correlation between experimental and estimated results of thermodynamic properties of sublimation or vaporization for the halogenated fluorenes studied: \square , $\Delta_{cr}^{\circ}G_m^{\circ}$; \diamond , $\Delta_{cr}^{\circ}H_m^{\circ}$; \circ , $\Delta_l^{\circ}G_m^{\circ}$; ∇ , $\Delta_l^{\circ}H_m^{\circ}$.

The regular dependence of the standard Gibbs energies with the enthalpies of sublimation and vaporization has been used as an estimation method for some groups of aromatic compounds with different substituents [13-15]. When plotting the standard Gibbs energies of sublimation of fluorene and fluorene derivatives studied in this work as a function of the respective enthalpies of sublimation, represented in figure 5.5, there is a tendency correlating these thermodynamic properties that seems to be applicable only for the mono and di halogenated fluorenes, although the fluoro derivatives results look to be outliers.



- $R_1 = \text{Br, I}; R_2 = \text{H}$
- $R_1 = R_2 = \text{H, Cl, Br, I}$

$$\Delta_{cr}^{\circ}G_m^{\circ} / \text{kJ}\cdot\text{mol}^{-1} = -27.95 + 0.724(\Delta_{cr}^{\circ}H_m^{\circ} / \text{kJ}\cdot\text{mol}^{-1}) \quad (5.10)$$

$$R^2 = 0.996; \sigma = 0.7 \text{ kJ}\cdot\text{mol}^{-1}$$

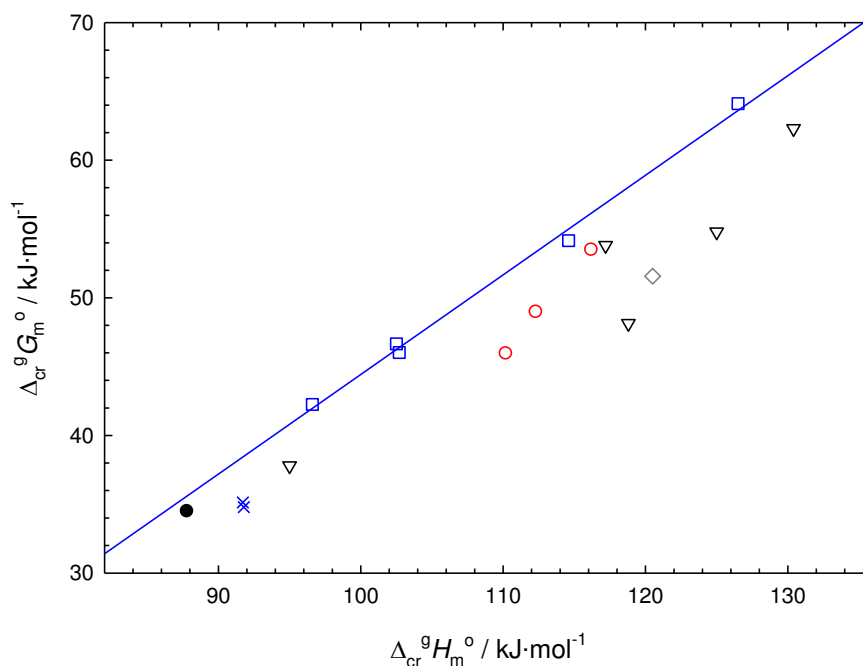
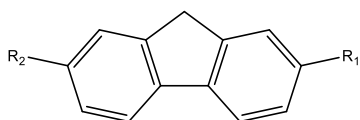


Figure 5.5. Correlation between $\Delta_{\text{cr}}^g H_m^o$ and $\Delta_{\text{cr}}^g G_m^o$ determined experimentally: ●, fluorene; □, 2-halogenated and 2,7-dihalogenated fluorenes (2-bromofluorene, 2-iodofluorene, 2,7-dichlorofluorene, 2,7-dibromofluorene, 2,7-diiodofluorene); ×, 2-halogenated and 2,7-dihalogenated fluorene outliers (2-fluorofluorene, 2,7-difluorofluorene); ○, 2-substituted fluorenes (2-fluorencarboxaldehyde, 2-aminofluorene, 2-nitrofluorene); ◇, 2,7-di-*tert*-butylfluorene; ▽, 9-substituted fluorenes (9-fluorencarboxylic acid, 9-phenyl-9-fluorene, 9-benzylidene-fluorene, 9-fluorene-methanol, 9-chlorofluorene).

Including the temperature of fusion as an additional independent variable while attempting to correlate the enthalpies and standard Gibbs energies of sublimation, two tendencies were distinguished for the following groups of compounds: 2-substituted and 2,7-disubstituted fluorenes, defined by equation 5.11, and 9-substituted fluorenes defined by equation 5.12. The estimated results obtained by these equations are compiled in table 5.3.



- $R_1 = \text{CHO}, \text{NH}_2, \text{NH}_2, \text{F}, \text{Br}, \text{I}; R_2 = \text{H}$
- $R_1 = R_2 = \text{H}, \text{F}, \text{Cl}, \text{Br}, \text{I}, \textit{tert}\text{-butyl}$

$$\Delta_{\text{cr}}^g G_m^o / \text{kJ} \cdot \text{mol}^{-1} = -41.25 + 0.506(\Delta_{\text{cr}}^g H_m^o / \text{kJ} \cdot \text{mol}^{-1}) + 0.085(T_{\text{fus}} / \text{K}) \quad (5.11)$$

$$R^2 = 0.978; \sigma = 1.5 \text{ kJ} \cdot \text{mol}^{-1}$$

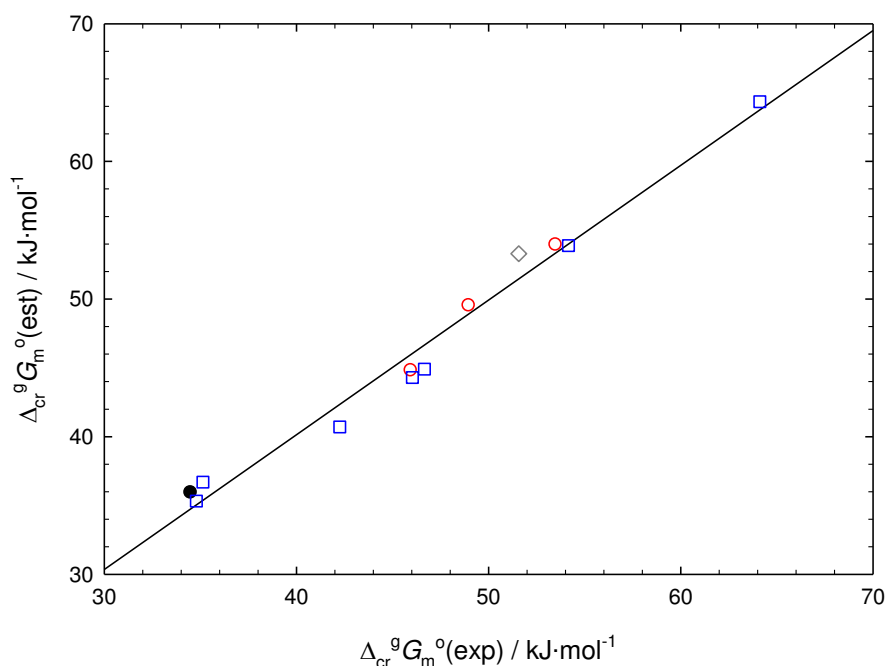
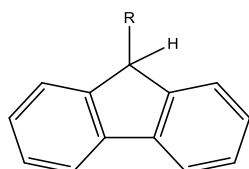


Figure 5.6. Correlation between experimental and estimated results of $\Delta_{\text{cr}}^{\text{g}}G_{\text{m}}^{\text{o}}$ for the 2-substituted and 2,7-disubstituted fluorenes: ●, fluorene; ○, 2-substituted fluorenes (2-fluorencarboxaldehyde, 2-aminofluorene, 2-nitrofluorene); □, 2-halogenated and 2,7-dihalogenated fluorenes (2-fluorofluorene, 2-bromofluorene, 2-iodofluorene, 2,7-difluorofluorene, 2,7-dichlorofluorene, 2,7-dibromofluorene, 2,7-diiodofluorene); ◇, 2,7-di-*tert*-butylfluorene.



- **R** = H, COOH, CH₂OH, Cl, OH

$$\Delta_{\text{cr}}^{\text{g}}G_{\text{m}}^{\text{o}} / \text{kJ} \cdot \text{mol}^{-1} = -29.74 + 0.461(\Delta_{\text{cr}}^{\text{g}}H_{\text{m}}^{\text{o}} / \text{kJ} \cdot \text{mol}^{-1}) + 0.062(T_{\text{fus}} / \text{K}) \quad (5.12)$$

$$R^2 = 0.995; \sigma = 1.1 \text{ kJ} \cdot \text{mol}^{-1}$$

In the latter correlation were included the 9-fluorene derivatives in which only one of the two hydrogens in position 9 is substituted by a functional group, including 9-fluorenol using literature results [5]. The 9-substituted fluorenes in which both hydrogens in position 9 were substituted by either two functional groups (9-phenyl-9-fluorenol) or one functional group linked by the double bond (9-benzylidene fluorene) were not included in this correlation.

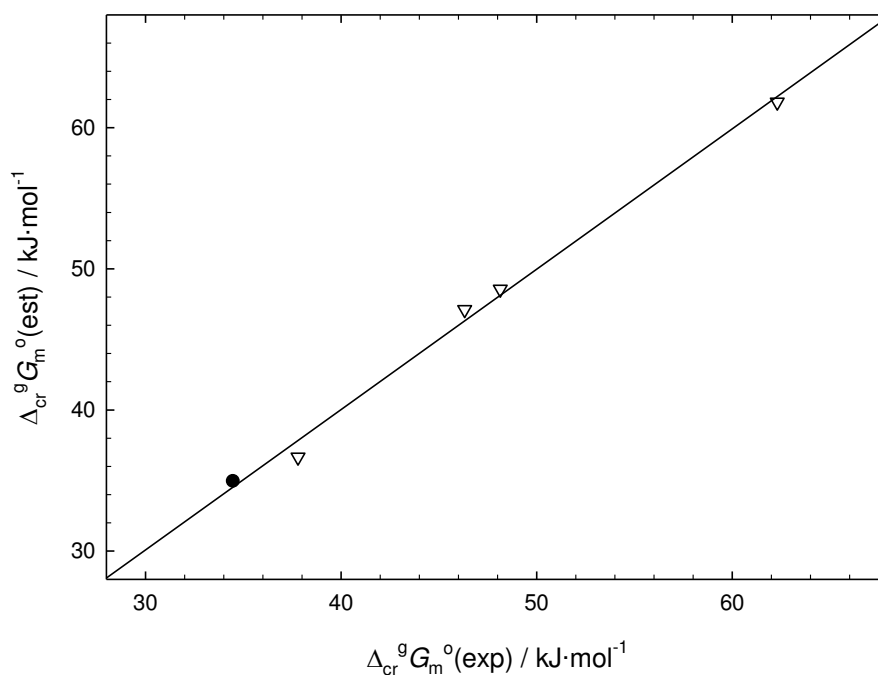


Figure 5.7. Correlation between experimental and estimated results of $\Delta_{cr}^g G_m^o$ for the 9-substituted fluorenes: ●, fluorene; ▽, 9-substituted fluorenes (9-fluorenicarboxylic acid, 9-fluorenemethanol, 9-fluoreneol, 9-chlorofluorene).

5.2.2.1.2. Enthalpic and entropic contributions to the standard Gibbs energies of sublimation and vaporization

Aiming to rationalize the volatility results of the crystalline and liquid phases of the compounds studied, the standard Gibbs energies of sublimation and vaporization were analyzed in terms of their corresponding enthalpic and entropic contributions. Whenever possible the interpretation of the experimental results will be supported by the available crystalline structures of the compounds.

i) 2-Fluorenicarboxaldehyde, 2-aminofluorene and 2-nitrofluorene

Figure 5.8 presents the thermodynamic properties of sublimation of 2-fluorenicarboxaldehyde, 2-aminofluorene, and 2-nitrofluorene. As the three compounds present similar values of the standard entropy of sublimation, the differences observed in their volatility follow the differences of their enthalpies of sublimation.

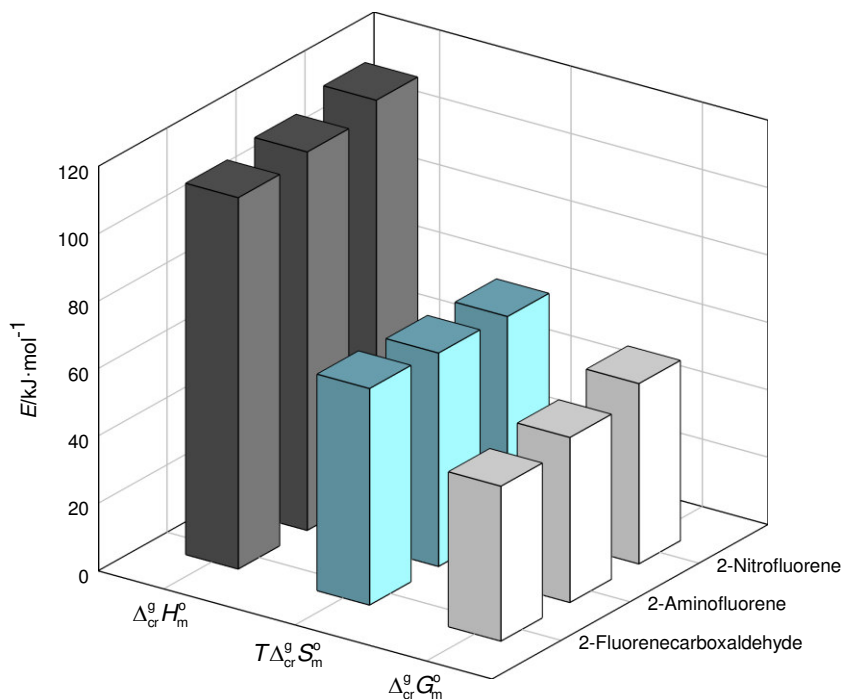


Figure 5.8. Relation between the enthalpic ($\Delta_{cr}^{\circ} H_m^{\circ}$) and entropic ($T\Delta_{cr}^{\circ} S_m^{\circ}$) contributions to $\Delta_{cr}^{\circ} G_m^{\circ}$ of the carboxaldehyde, amine and nitro derivatives of fluorene in position 2.

No crystal structure data was found for 2-nitrofluorene. Crystalline structural data are, however, available for the other two compounds. For 2-fluorencarboxaldehyde [16], the observed C–H...O interactions result in the formation of a cyclic dimer about a center of symmetry, as schematized in figure 5.9.

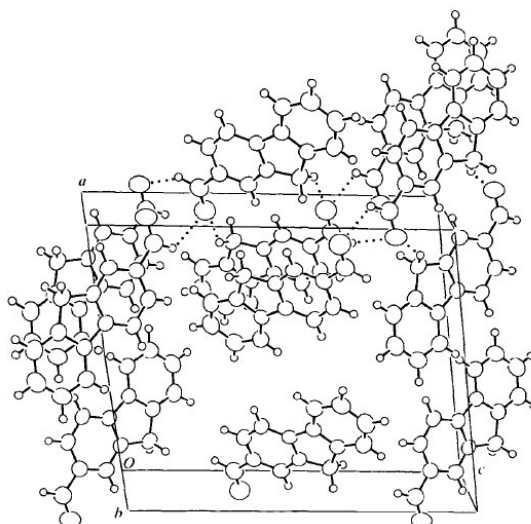


Figure 5.9. Packing diagram of 2-fluorencarboxaldehyde, C–H...O interactions are represented as dashed lines (image adapted from ref. [16]).

For 2-aminofluorene, the amine group does not form N–H...N hydrogen bonds (that would strongly diminish its volatility), but is only engaged in weaker N–H... π interactions, where the N–H vector points to the faces of the aromatic rings of neighboring molecules [17].

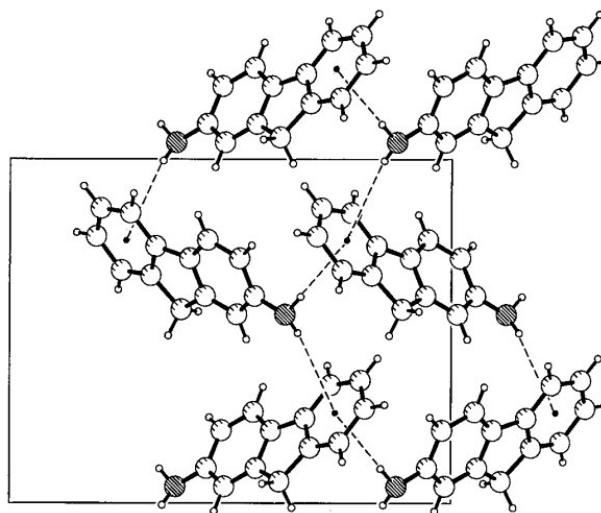


Figure 5.10. Packing diagram of 2-aminofluorene, N–H... π interactions are represented as dashed lines (image adapted from ref. [17]).

ii) 2- and 2,7- halogenated fluorenes

The enthalpic and entropic contributions to the standard Gibbs energy of sublimation of the monohalogenated and the dihalogenated derivatives of fluorene are schematized in figures 5.11 and 5.12, respectively, in order of decreasing volatility. The volatilities of the crystalline phase of both series of halogenated derivatives decrease with increasing halogen size. This decrease is more accentuated in the case of the dihalogenated compounds. As was the case for the aldehyde, amine and nitro fluorene derivatives, the volatility of the halogenated derivatives seems to be predominantly led by enthalpic contributions. This is particularly evident for the dihalogenated fluorenes.

Both the fluorinated derivatives seem to present larger entropic contributions when compared to the other halogenated fluorenes (figure 5.13). This larger entropic contribution seems to be the reason for their discrepancy concerning the correlation given by equation 5.10. The inclusion of the temperature of fusion (equation 5.11) seems to attenuate this divergence as can be observed in figure 5.6.

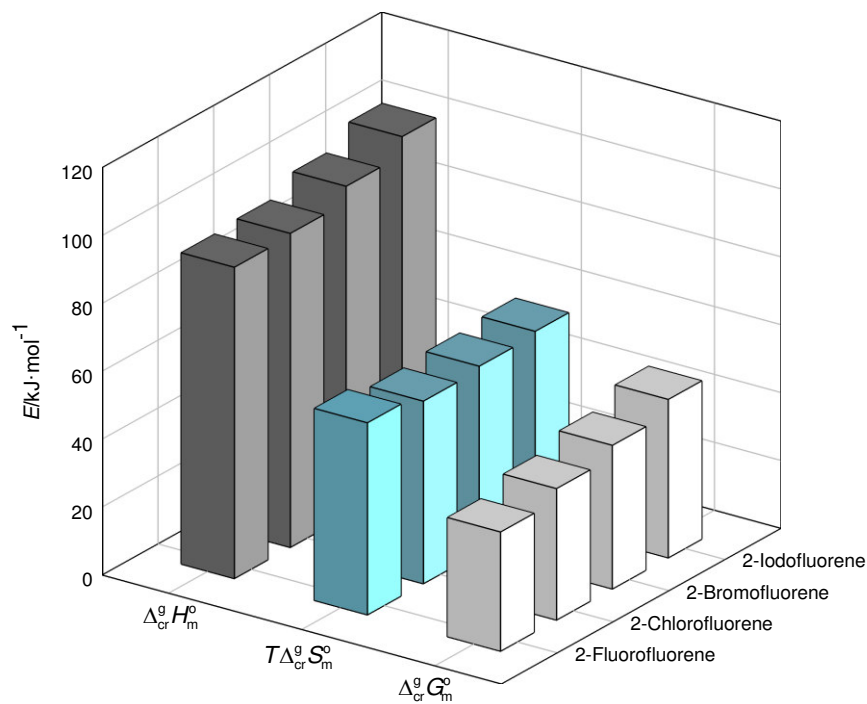


Figure 5.11. Relation between the enthalpic and entropic contributions to $\Delta_{cr}^{\circ} G_m^{\circ}$ of the monohalogenated derivatives of fluorene in position 2.

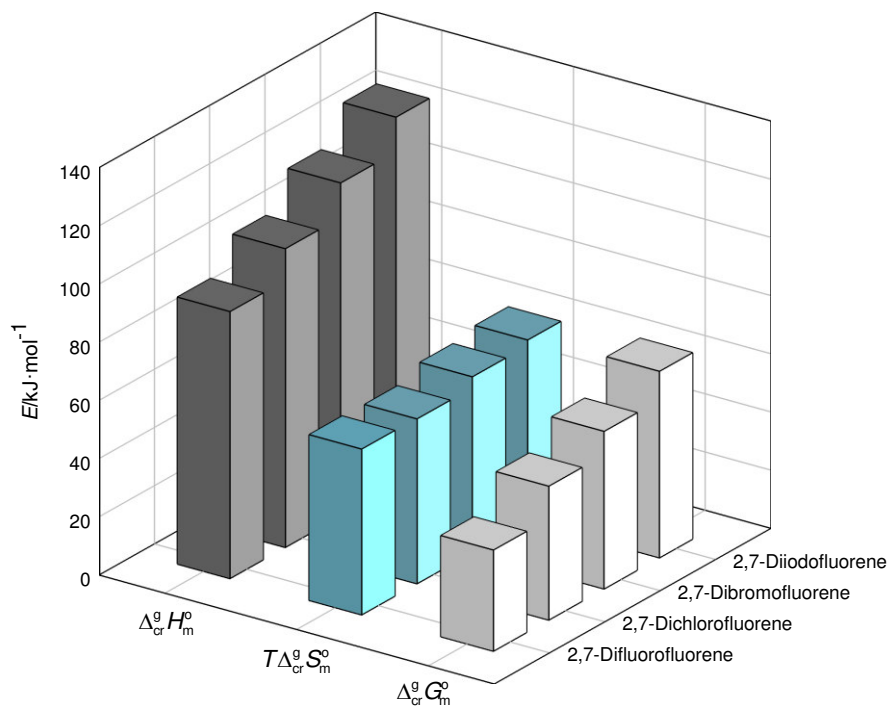


Figure 5.12. Relation between the enthalpic and entropic contributions to $\Delta_{cr}^{\circ} G_m^{\circ}$ of the dihalogenated derivatives of fluorene in positions 2,7.

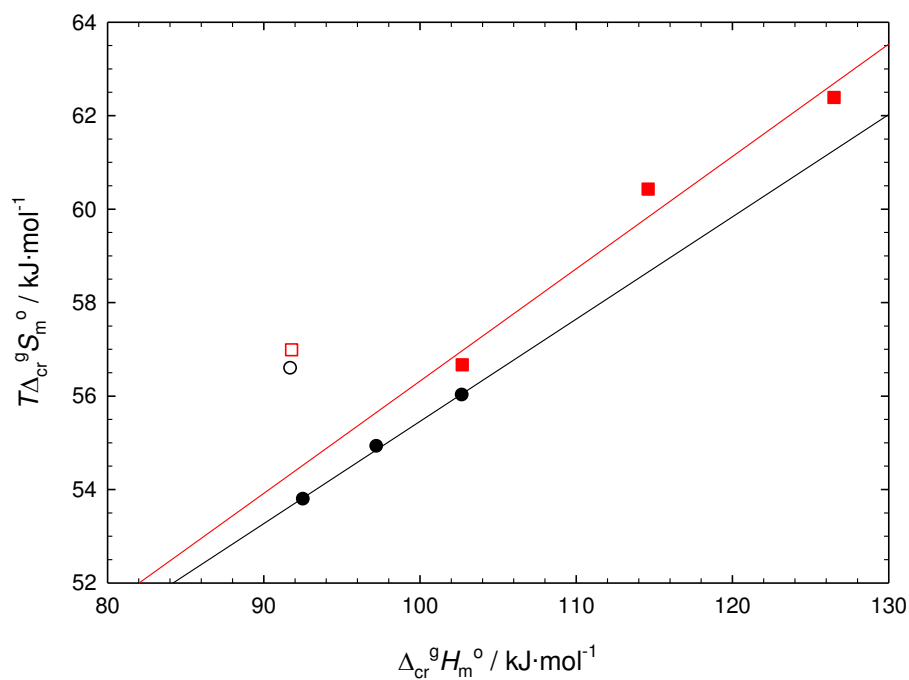


Figure 5.13. Correlation between the enthalpies and entropies of sublimation of the monohalogenated (●) and the dihalogenated (■) derivatives of fluorene.

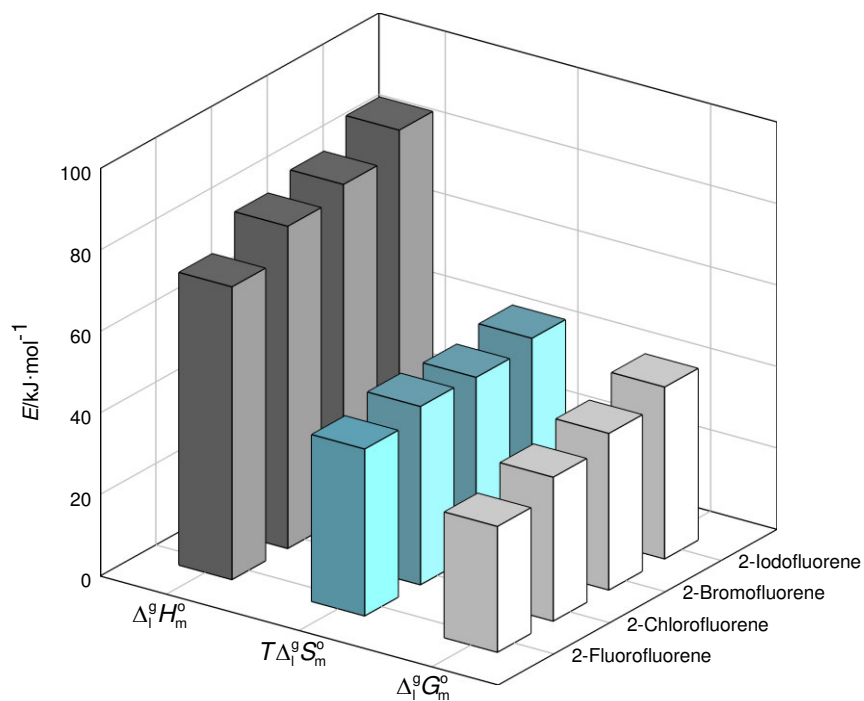


Figure 5.14. Relation between the enthalpic and entropic contributions to $\Delta_l^g G_m^o$ of the monohalogenated derivatives of fluorene in position 2.

When considering the liquid phase, the volatility of the monohalogenated derivatives schematized in figure 5.14, replicates what was observed in the crystalline phase. While in the crystalline phase the entropy of sublimation of the fluoro derivatives appeared to be higher than that of the other halogenates, the same is not observed in the entropy of vaporization.

iii) 9-Substituted fluorenes

The enthalpic and entropic contributions to the standard Gibbs energies of sublimation of the 9-fluorene derivatives studied are schematized in figure 5.15.

9-Fluorenemethanol, 9-phenyl-9-fluorene and 9-fluorencarboxylic acid present similar entropies of sublimation and their differences in volatility is thus related to enthalpic contributions. The crystalline packing of these compounds are further stabilized by strong hydrogen bonds O–H...O. Most likely the presence of the hydrogen bonding and π -stacking interactions decreases their entropy of the crystalline phase.

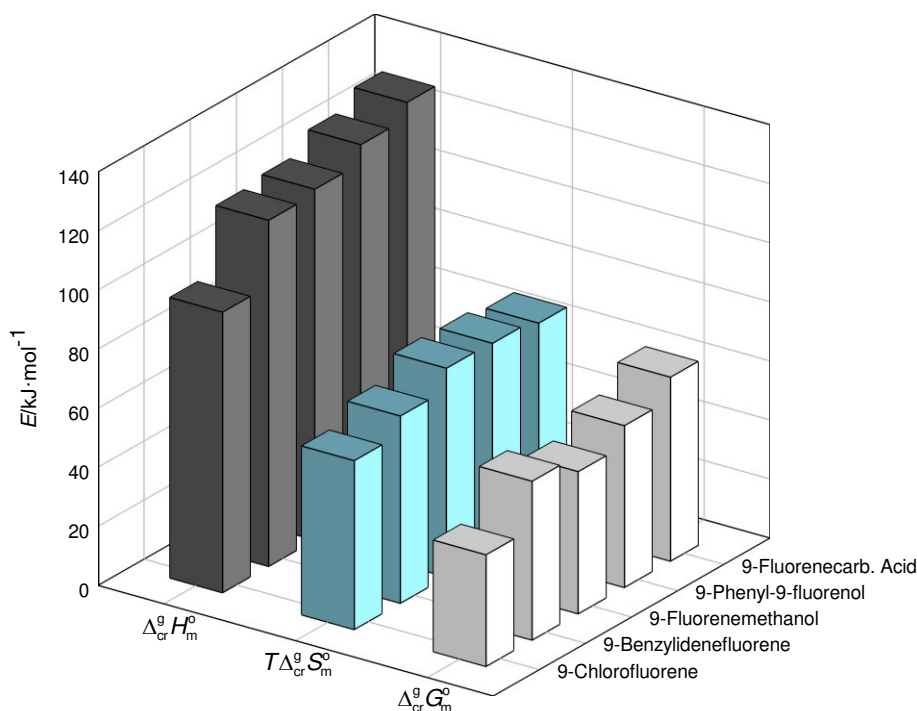


Figure 5.15. Relation between the enthalpic and entropic contributions to $\Delta_{cr}^g G_m^o$ of the 9-fluorene derivatives.

In the crystalline structure of 9-fluorenemethanol [18], the molecules are arranged in two dimensional layers linked by hydrogen bonds, as referred to above, and also benefit from nonparallel π -stacking interactions between the flat fluorenyl systems (figure 5.16).

Csöregi *et al.* [19] reported that the crystal packing of 9-phenyl-9-fluorenol contains hydrogen bonded dimers involving one of the hydroxyl groups as a proton acceptor and the other as both proton donor and acceptor (figure 5.17). The packing of the 9-phenyl-9-fluorenol dimers seems to be further stabilized by π interactions between neighboring fluorene moieties. More recently, Hosseinzadeh *et al.* [20] reviewed the structure reported by Csöregi and suggested the existence of additional weaker O–H \cdots π and C–H \cdots O hydrogen bond type interactions involving neighboring molecules.

Among the 9-substituted fluorenes studied, 9-fluorencarboxylic acid is the least volatile. According to Blackburn *et al.* [21], the crystalline structure of fluorene-9-carboxylic acid contains two sets of cyclic dimers (A and B, as shown in figure 5.18) dimers each exhibiting hydrogen bonding about a center of symmetry. An additional disordering of the carboxyl oxygen atoms observed in A molecules distinguishes them from B molecules.

These three compounds present higher entropies of sublimation when compared to those of 9-chlorofluorene and 9-benzylidene fluorene.

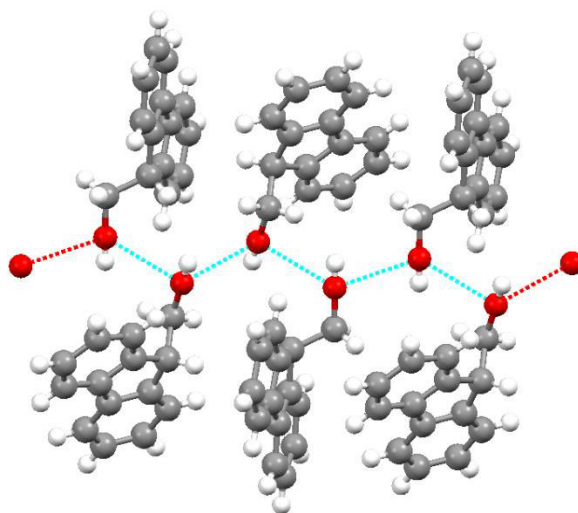


Figure 5.16. Scheme of the crystalline structure of 9-fluorenemethanol. Hydrogen bonds (O–H \cdots O) are represented as dashed lines (image adapted from ref. [18]).

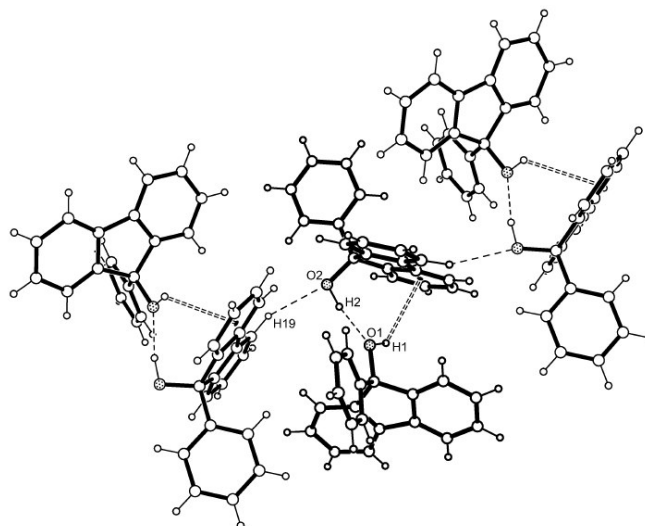


Figure 5.17. Scheme of the crystalline structure of 9-phenyl-9-fluorene. Hydrogen bonds are represented as dashed lines and O–H... π interactions as double dashed lines (image adopted from ref. [20], crystal structural data available from ref. [19]).

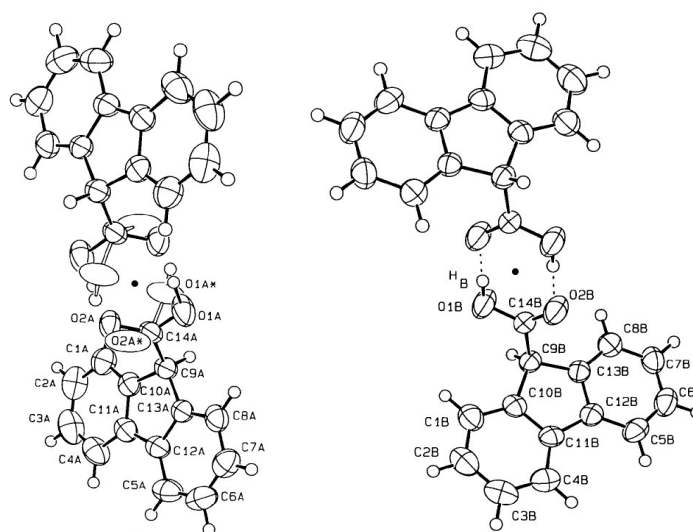


Figure 5.18. Scheme of the crystalline structures of A and B fluorene-9-carboxylic acid cyclic dimers. Hydrogen bonds are represented as dashed lines and centers of symmetry as dots (image and numbering scheme adopted from ref. [21]; for clarity, depiction of the hydrogen bonding of the two A-molecule carboxyl groups has been omitted).

9-Benzylidene fluorene and 9-fluorene methanol present similar enthalpies of sublimation, however 9-fluorene methanol is more volatile due to the higher entropic contribution referred to above. The absence of hydrogen bonding and π -stacking interactions in 9-benzylidene fluorene is confirmed in its crystalline structure reported by Chan *et al.* [22]. To the best of our knowledge, no structural data has been

reported for 9-chlorofluorene that is the most volatile of the group of the 9- substituted fluorenes studied, although it is not clear if its the volatility is mainly due to enthalpic or entropic factors.

5.2.2.2. Fluorenone and fluorenone derivatives

Table 5.4 presents a summary of the thermodynamic properties of sublimation and vaporization of fluorenone and its derivatives, at $T = 298.15$ K, including their vapor pressures. Estimated values derived using correlations to be discussed ahead are also presented in this table (inside parenthesis).

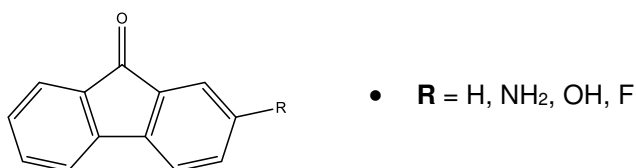
Table 5.4. Thermodynamic properties of sublimation and vaporization of fluorenone and its derivatives, as well as their vapor pressures at $T = 298.15$ K. Values inside parenthesis are estimations.

Compound	Phase	$\Delta_{cr/l}^g G_m^o$	$\Delta_{cr/l}^g H_m^o$	$T \Delta_{cr/l}^g S_m^o$	$p(cr/l)$
		kJ·mol ⁻¹			Pa
Fluorenone [5]	cr	38.82 ± 0.03	95.1 ± 0.5	56.3 ± 0.5	1.6·10 ⁻²
	l	36.25 ± 0.02	80.6 ± 0.2	44.4 ± 0.2	4.5·10 ⁻²
2-SUBSTITUTED FLUORENONES					
2-Aminofluorenone	cr	58.8 ± 0.2 (58.6) ^a	123.7 ± 0.7	64.9 ± 0.7	5.0·10 ⁻⁶
	cr	64.8 ± 0.2 (65.0) ^a	132.9 ± 0.8	68.1 ± 0.8	4.4·10 ⁻⁷
2-Fluorofluorenone	cr	40.38 ± 0.02 ^b (40.3) ^a	97.1 ± 0.1 ^b	56.7 ± 0.1	8.4·10 ⁻³
	l	(36.4) ^c	(82.2) ^c	(45.8)	(4.2·10 ⁻²)
		(36.3) ^d	(81.0) ^e		
2,7-DISUBSTITUTED FLUORENONES					
2,7-Dibromofluorenone	cr	60.37 ± 0.09	121.9 ± 0.4	61.5 ± 0.4	2.7·10 ⁻⁶
	l	(51.7) ^c	(103.8) ^c	(52.1)	(8.7·10 ⁻⁵)
		(51.3) ^d	(101.6) ^e		

^a Values estimated through equation 5.13; ^b Weighted mean of results derived from vapor pressures measured by effusion and static methods; ^c Values derived indirectly from the experimental results of fusion and sublimation; ^d Values estimated through equation 5.14; ^e Values estimated through equation 5.15.

5.2.2.2.1. Correlations and estimation equations

Following what was previously discussed for the fluorene derivatives, we attempted to correlate the standard Gibbs energies and enthalpies of sublimation for fluorenone and its derivatives studied in this work. This correlation, defined by equation 5.13, yields very good results for the 2-substituted fluorenone derivatives studied, and includes the results of fluorenone.



$$\Delta_{\text{cr}}^{\text{g}} G_{\text{m}}^{\circ} / \text{KJ} \cdot \text{mol}^{-1} = -26.59 + 0.689 (\Delta_{\text{cr}}^{\text{g}} H_{\text{m}}^{\circ} / \text{KJ} \cdot \text{mol}^{-1}) \quad (5.13)$$

$$R^2 = 0.9999; \sigma = 0.2 \text{ kJ} \cdot \text{mol}^{-1}$$

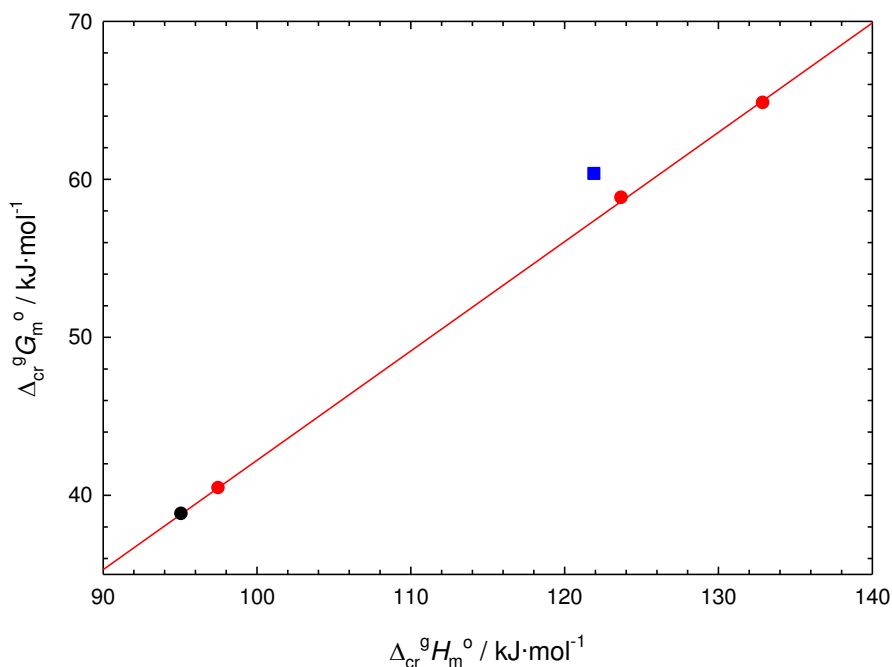


Figure 5.19. Correlation between $\Delta_{\text{cr}}^{\text{g}} H_{\text{m}}^{\circ}$ and $\Delta_{\text{cr}}^{\text{g}} G_{\text{m}}^{\circ}$ determined experimentally: ●, fluorenone; ●, 2-substituted fluorenones (2-aminofluorenone, 2-hydroxyfluorenone, 2-fluorofluorenone); ■, 2,7-dibromofluorenone.

This correlation doesn't yield satisfactory results for the di-substituted derivative studied, 2,7-dibromofluorenone. Even when considering the temperature of fusion as an added variable, this compound behaves like an outlier of the correlation.

As previously mentioned, the method proposed by Monte *et al.* [2] for the estimation of vaporization thermodynamic properties of haloaromatics was also found successful for the estimation of these properties of some halogenated fluorenones. Considering the properties of vaporization of fluorenone, listed in table 5.4, equations 5.14 and 5.15 were respectively used to estimate standard Gibbs energy and enthalpy of vaporization of two halogenated fluorenones (2-fluorofluorenone and 2,7-dibromofluorenone) whose sublimation was studied in this work.

$$\Delta_1^g G_m^o(298.15 \text{ K}) / \text{kJ} \cdot \text{mol}^{-1} = \Delta_1^g G_m^o(\text{fluorenone}) / \text{kJ} \cdot \text{mol}^{-1} + 0.09n_F + 4.9n_{Cl} + 7.5n_{Br} + 11.2n_I \quad (5.14)$$

$$\Delta_1^g H_m^o(298.15 \text{ K}) / \text{kJ} \cdot \text{mol}^{-1} = \Delta_1^g H_m^o(\text{fluorenone}) / \text{kJ} \cdot \text{mol}^{-1} + 0.43n_F + 7.0n_{Cl} + 10.5n_{Br} + 15.5n_I \quad (5.15)$$

The so-estimated results were in good agreement with the values of the standard Gibbs energies and enthalpies of vaporization derived indirectly from the experimental results of fusion and sublimation.

5.2.2.2.2. Enthalpic and entropic contributions to the standard Gibbs energies of sublimation

The enthalpic and entropic contributions to the volatilities of the fluorenone derivatives are schematized in figure 5.20. All the fluorenone derivatives studied are less volatile than the parental compound, fluorenone.

The crystalline packing of 2-aminofluorenone has been reported by Eakins *et al.* [23]. Like 2-aminofluorene, hydrogen bonding is not observed between neighboring amine groups. Also, probably due to the approximately planar orientation of the hydrogen and nitrogen atoms of the amine groups relative to the fluorenyl fragment, no π -stacking interactions were observed, as opposed to what was the case in the fluorene derivative (21° angle between amine group and fluorenyl fragment [17]). No crystalline

structure data were found in the literature for the remaining fluorenone derivatives studied in this work.

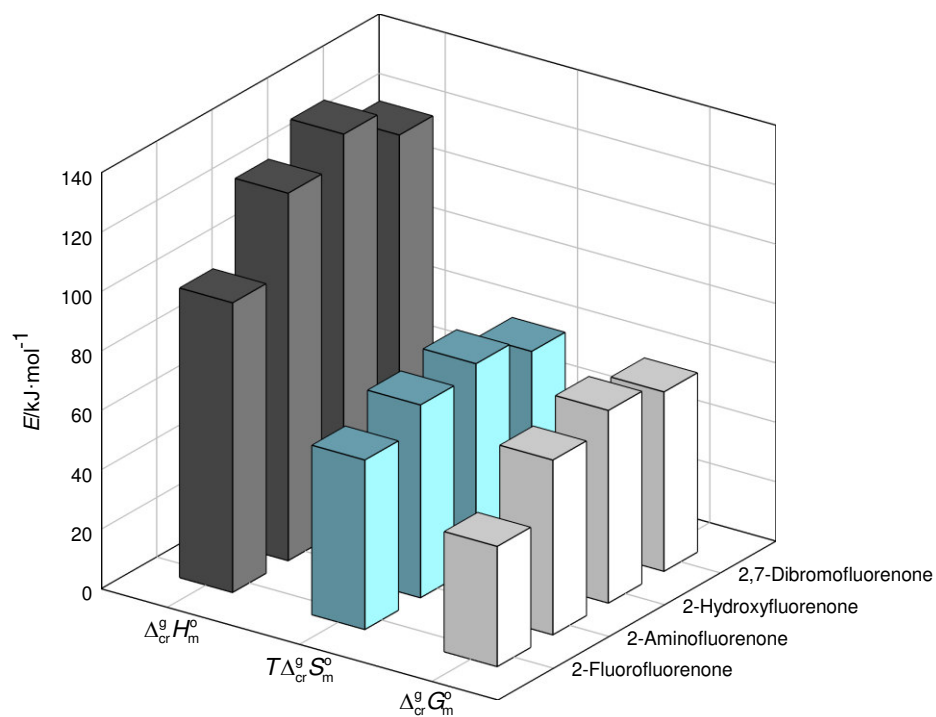


Figure 5.20. Relation between the enthalpic and entropic contributions to $\Delta_{cr}G_m^\circ$ of the fluorenone derivatives.

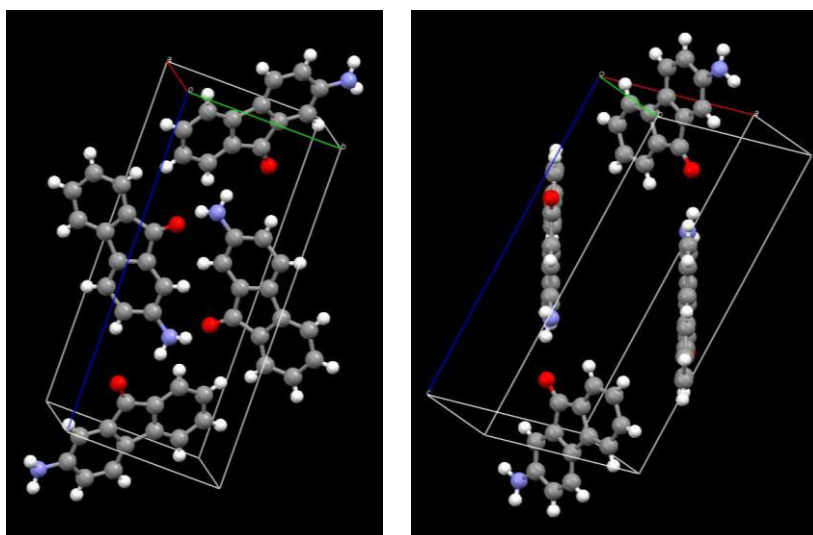


Figure 5.21. Packing arrangement of 2-aminofluorenone within the unit cell (image adapted from ref. [23]).

5.2.2.3. Naphthalene and naphthalene derivatives

Table 5.5 presents a summary of the thermodynamic properties of sublimation of naphthalene and the alkyl derivatives, at $T = 298.15$ K, including their vapor pressures. Estimated values derived using correlations to be discussed ahead are also presented in this table (inside parenthesis).

Table 5.5. Thermodynamic properties of sublimation and vaporization of naphthalene and its derivatives, as well as their vapor pressures at $T = 298.15$ K. Values inside parenthesis are estimations.

Compound	Phase	$\Delta_{cr/l}^g G_m^o$	$\Delta_{cr/l}^g H_m^o$	$T \Delta_{cr/l}^g S_m^o$	$p(cr/l)$
		kJ·mol ⁻¹			Pa
Naphthalene [24]	cr	22.58 ± 0.01	72.70 ± 0.04	50.12 ± 0.04	1.1·10 ¹
2,6-SUBSTITUTED NAPHTHALENES					
2,6-Dimethylnaphthalene [25]	cr	30.96 ± 0.01	86.7 ± 0.2	55.7 ± 0.2	3.8·10 ⁻¹
2,6-Diethylnaphthalene	cr	32.03 ± 0.01 (32.2) ^a	93.63 ± 0.09	61.6 ± 0.1	2.4·10 ⁻¹
2,6-Diisopropylnaphthalene	l	30.49 ± 0.01	73.42 ± 0.04	42.9	4.6·10 ⁻¹
2,6-Diisopropylnaphthalene	cr	35.94 ± 0.01 (36.0) ^a	98.0 ± 0.2	62.1 ± 0.2	5.1·10 ⁻²
2,6-Di- <i>tert</i> -butylnaphthalene	cr	41.64 ± 0.04 (41.8) ^a	99.1 ± 0.4	57.5 ± 0.4	5.1·10 ⁻³

^a Values estimated through equation 5.16.

5.2.2.3.1. Correlation between enthalpy and standard Gibbs energy of sublimation

The standard Gibbs energies of sublimation of the alkylnaphthalene derivatives, presented in table 5.5, did not linearly depend on the respective enthalpies of sublimation. Considering the temperature of fusion as an additional independent variable, the standard Gibbs energies of sublimation of the alkyl derivatives studied in this work and of naphthalene are perfectly defined by equation 5.16.

$$\Delta_{cr}^g G_m^o / \text{KJ} \cdot \text{mol}^{-1} = -41.3 + 0.554(\Delta_{cr}^g H_m^o / \text{KJ} \cdot \text{mol}^{-1}) + 0.067(T_{fus} / \text{K}) \quad (5.16)$$

$$R^2 = 0.9998; \sigma = 0.1 \text{ kJ} \cdot \text{mol}^{-1}$$

Osborn and Douslin [25] have reported the vapor pressures and enthalpies of sublimation and vaporization of four dimethylnaphthalene isomers, including 2,6-dimethylnaphthalene. The reported crystal vapor pressures for 2,6-dimethylnaphthalene, measured using an inclined-piston pressure gauge, were fitted to the Clarke and Glew equation (eq. 3.72) using $\Delta_{\text{cr}}^{\text{g}}C_{p,m}^{\circ} = -33.7 \text{ J}\cdot\text{K}^{-1}\cdot\text{mol}^{-1}$ [26], and the derived standard Gibbs energy and enthalpy of sublimation at $T = 298.15 \text{ K}$ are included in table 5.5.

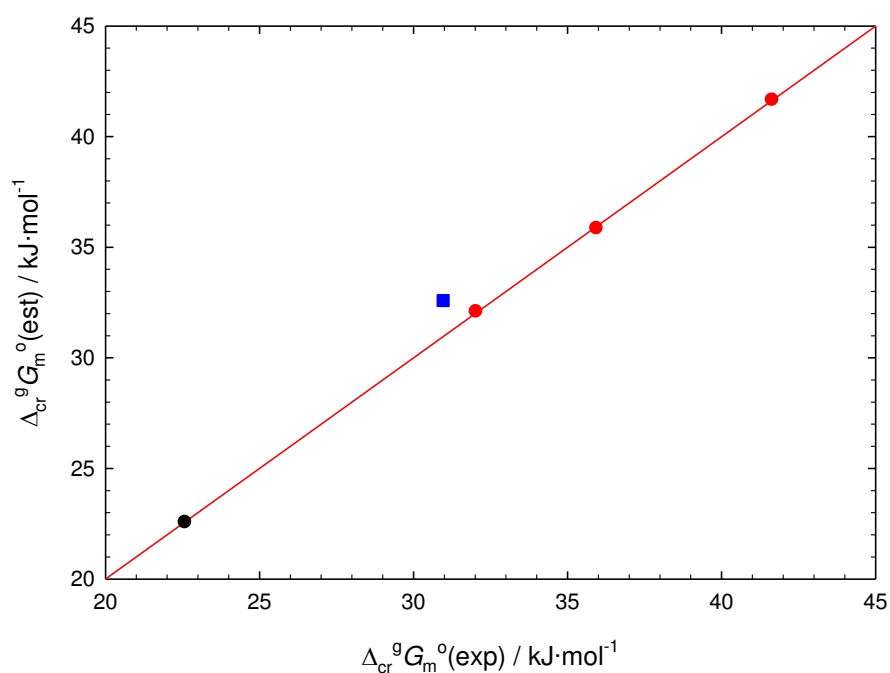


Figure 5.22. Correlation between experimental and estimated results of $\Delta_{\text{cr}}^{\text{g}}G_m^{\circ}$: ●, naphthalene; ●, 2,6-substituted naphthalenes studied in this work (2,6-diethylnaphthalene, 2,6-diisopropylnaphthalene, 2,6-di-*tert*-butylnaphthalene); ■, 2,6-dimethylnaphthalene [25].

Equation 5.16 did not yield a good estimation for 2,6-dimethylnaphthalene, as can be observed in figure 5.22. Considering the value $T_{\text{fus}} = 383.3 \text{ K}$ [7], the estimated standard Gibbs energy of sublimation, $32.4 \text{ kJ}\cdot\text{mol}^{-1}$, is $1.4 \text{ kJ}\cdot\text{mol}^{-1}$ larger than the value derived in this work from the reported vapor pressures by Osborn and Douslin [25].

No significant correlation was observed between the properties of phase transition and the increase in molar mass of the alkyl substituent.

5.2.2.3.2. Enthalpic and entropic contributions to the standard Gibbs energies of sublimation

The enthalpic and entropic contributions to the volatilities of naphthalene and the 2,6-dialkyl naphthalene derivatives are schematized in figure 5.23, including those of 2,6-dimethylnaphthalene, in order of decreasing volatility.

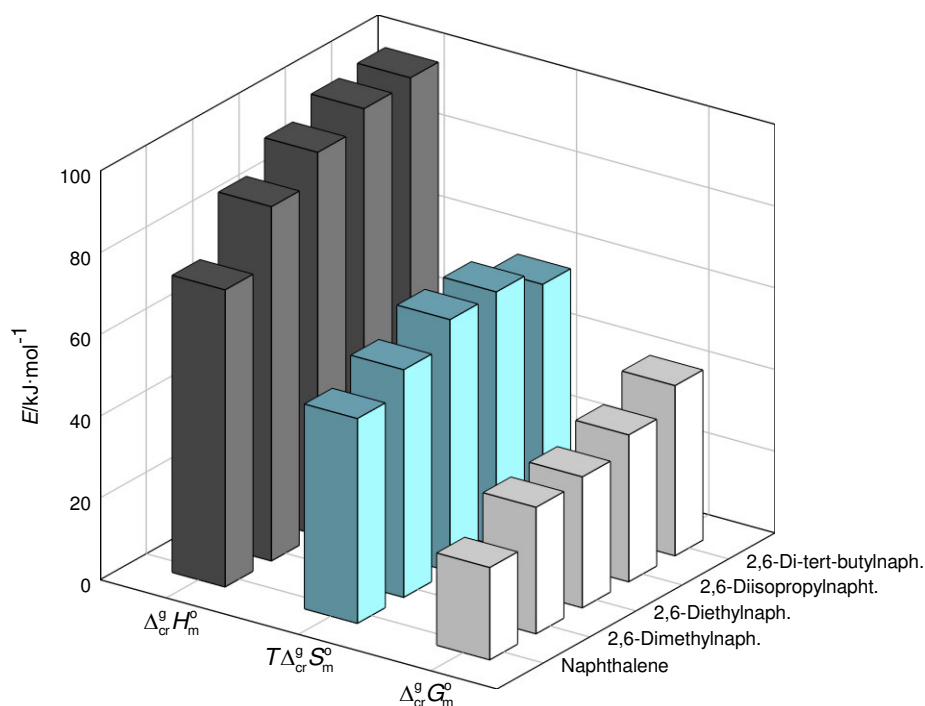


Figure 5.23. Relation between the enthalpic and entropic contributions to $\Delta_{\text{cr}}^{\text{g}}G_{\text{m}}^{\circ}$ of naphthalene, 2,6-dimethylnaphthalene and of the 2,6-dialkyl naphthalene studied in this work.

All the dialkyl derivatives presented in figure 5.23 are less volatile than the parental compound, naphthalene, and the volatility of the dialkyl derivatives decreases with increasing molar mass of the alkyl substituents. The diethyl and the diisopropyl derivatives present similar entropic contributions and their difference in volatility seems to be influenced mainly by enthalpic factors. 2,6-Di-*tert*-butylnaphthalene exhibits a decrease in the entropy of sublimation, that contributes to a decrease in volatility when compared to the other two dialkyl naphthalenes studied.

5.2.3. Thermodynamic properties of formation

A compound's thermodynamic stability can be evaluated by its standard molar Gibbs energy of formation. Besides being an important parameter for calculating equilibrium constants of reactions, it measures the thermodynamic tendency towards decomposition into their constituent elements under standard conditions – smaller values indicate greater stability. In order to compare the thermodynamic stability of some of the compounds studied, with that of the parental molecules, we determined their standard molar Gibbs energies of formation in the crystalline and gaseous phases.

Table 5.6 presents a summary of the thermodynamic properties of formation of some of the fluorene and naphthalene derivatives studied in this work, at $T = 298.15$ K. In this table are also included the results of fluorene [3], naphthalene [6,24], and 2,6-dimethylnaphthalene [25,27], which were taken or derived from literature results. The standard molar entropies and Gibbs energies of formation of fluorene, naphthalene and 2,6-dimethylnaphthalene, in the crystal and gaseous phases, were derived considering the respective values of the absolute gaseous entropies, S_m° (fluorene, g) = $381.0 \text{ J}\cdot\text{K}^{-1}\cdot\text{mol}^{-1}$ [5], S_m° (naphthalene, g) = $346.84 \text{ J}\cdot\text{K}^{-1}\cdot\text{mol}^{-1}$ [28] and S_m° (2,6-dimethylnaphthalene, g) = $422.42 \text{ J}\cdot\text{K}^{-1}\cdot\text{mol}^{-1}$ [26], determined computationally.

Table 5.6. Thermodynamic properties of formation, in the crystalline and gaseous phases, of fluorene, naphthalene and some of its derivatives studied in this work, at $T = 298.15$ K.

Compound	Phase	$\Delta_f H_m^{\circ}$	$-T\Delta_f S_m^{\circ}$	$\Delta_f G_m^{\circ}$
		kJ·mol ⁻¹		
Fluorene [3,5]	cr	91.6 ± 3.0	156.9 ± 0.3	248.5 ± 3.0
	g	179.4 ± 3.0	103.5	282.9 ± 3.0
2-SUBSTITUTED FLUORENES				
2-Fluorencarboxaldehyde	cr	$-(45.7 \pm 3.1)$		
	g	64.5 ± 3.2		
2-Aminofluorene	cr	81.3 ± 2.7	205.6 ± 1.4	286.9 ± 3.0
	g	193.6 ± 2.7	142.3	335.9 ± 2.7
2-Nitrofluorene	cr	48.2 ± 3.9	217.9 ± 1.0	266.1 ± 4.0
	g	164.4 ± 3.9	155.2	319.6 ± 3.9
2-Bromofluorene	cr	110.8 ± 2.2	144.8 ± 0.1	255.6 ± 2.2
	g	207.4 ± 2.2^a	90.4	297.8 ± 2.2

.../...

.../...

2,7-DISUBSTITUTED FLUORENES				
2,7-Di- <i>tert</i> -butylfluorene	cr	$-(141.7 \pm 6.5)$	432.4 ± 0.4	290.7 ± 6.5
	g	$-(20.6 \pm 6.5)$	362.9	342.3 ± 6.5
2,7-Dibromofluorene	cr	114.7 ± 2.5	141.3 ± 0.2	256.0 ± 2.5
	g	229.3 ± 2.5^a	80.9	310.2 ± 2.5
9-SUBSTITUTED FLUORENES				
9-Fluorencarboxylic acid	cr	$-(302.5 \pm 3.4)$	213.4 ± 0.8	$-(89.1 \pm 3.5)$
	g	$-(172.1 \pm 3.5)$	145.3	$-(26.8 \pm 3.5)$
9-Phenyl-9-fluorene	cr	5.3 ± 2.7		
	g	130.3 ± 2.7		
9-Benzylidene-fluorene	cr	246.6 ± 4.0		
	g	364.3 ± 4.1		
9-Fluorene-methanol	cr	$-(109.6 \pm 2.9)$	229.1 ± 0.7	119.5 ± 2.9
	g	9.2 ± 2.9	158.5	167.7 ± 2.9
Naphthalene [6,24,28]	cr	78.0 ± 1.5	119.7 ± 0.4	197.7 ± 1.5
	g	150.7 ± 1.5	69.6	220.3 ± 1.5
2,6-SUBSTITUTED NAPHTHALENES				
2,6-Dimethylnaphthalene [25-27]	cr	$-(5.7 \pm 1.7)$	184.0 ± 0.3	178.3 ± 1.7
	g	81.0 ± 1.7	128.4	209.4 ± 1.7
2,6-Diethylnaphthalene	cr	$-(61.9 \pm 3.1)$	254.0 ± 0.1	192.1 ± 3.1
	g	31.7 ± 3.1	192.4	224.1 ± 3.1
2,6-Diisopropylnaphthalene	cr	$-(122.1 \pm 3.9)$	321.1 ± 0.2	199.0 ± 3.9
	g	$-(24.1 \pm 3.9)$	259.1	235.0 ± 3.9
2,6-Di- <i>tert</i> -butylnaphthalene	cr	$-(162.4 \pm 5.3)$	387.0 ± 0.4	224.6 ± 5.3
	g	$-(63.3 \pm 5.3)$	329.5	266.2 ± 5.3

^a Derived from the weighted mean of the standard molar enthalpies of sublimation determined in this work using the effusion and static methods.

5.2.3.1. Thermodynamic stability

The standard molar Gibbs energies of formation of fluorene, naphthalene and of the derivatives listed in table 5.6, in the crystalline and gaseous phases, were plotted in figure 5.24 in order of increasing thermodynamic stability of the crystals of each family of compounds.

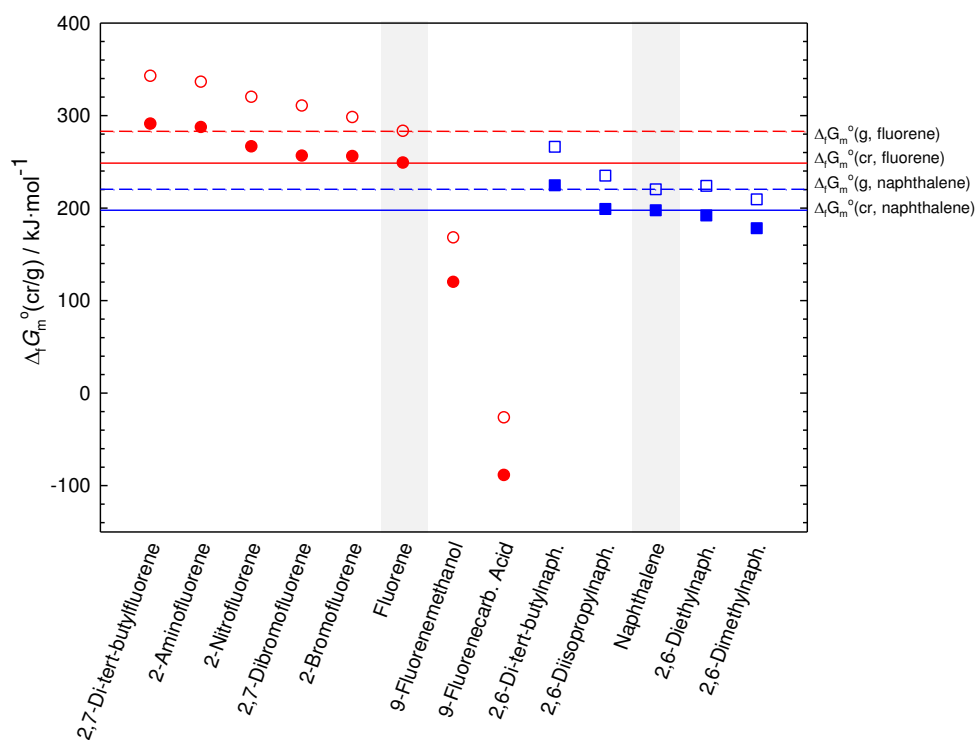


Figure 5.24. Standard molar Gibbs energies of formation, in the crystalline phase (filled symbols) and in the gaseous phase (open symbols), of fluorene, naphthalene and some of their derivatives, plotted in order of increasing thermodynamic stability of the crystals.

Obviously, the difference between the standard molar Gibbs energies of formation in the crystalline and gaseous phases is the standard molar Gibbs energy of sublimation, which is related to the vapor pressure of the crystal compound. Accordingly, the standard molar Gibbs energies of formation provide additional insight on the role of volatility in the further stabilization of crystalline phase with respect to gaseous phase.

Among the fluorene derivatives studied, only the two 9-substituted fluorenes – 9-fluorenamethanol and 9-fluorencarboxylic acid – are thermodynamically more stable than fluorene, in both crystalline and gaseous phases. Despite the differences of the standard Gibbs energy of sublimation, the thermodynamic stability of the considered fluorenes follows the same order in both crystalline and gaseous phases.

As for the alkyl naphthalene derivatives, the high volatility of naphthalene contributes to a decrease in stability in its crystalline phase, relative to that of 2,6-dimethylnaphthalene and 2,6-diethylnaphthalene which are thermodynamically more stable in the crystalline phase. In the gaseous phase, the relative stability of naphthalene and 2,6-diethylnaphthalene is inverted. For the same reason, the reduced stability of 2,6-

diisopropylnaphthalene in the gaseous phase relative to that of naphthalene, is partially compensated in the crystalline phase where both compounds present similar stability.

The relative thermodynamic stability of the dialkyl derivatives decreases with increasing molar mass of the alkyl substituent, in both crystalline and gaseous phases. Significant and regular variations of the standard molar enthalpy and entropy of formation with increasing molar mass of the alkyl groups are evident in both crystalline and gaseous phases for the dialkyl derivatives. These variations partially compensate resulting in more discrete differences in the standard molar Gibbs energies of formation. The exception to this tendency is naphthalene, remaining slightly less stable than the 2,6-dimethyl and 2,6-diethylnaphthalene derivatives, due to a stronger enthalpic contribution verified in both phases (figure 5.25).

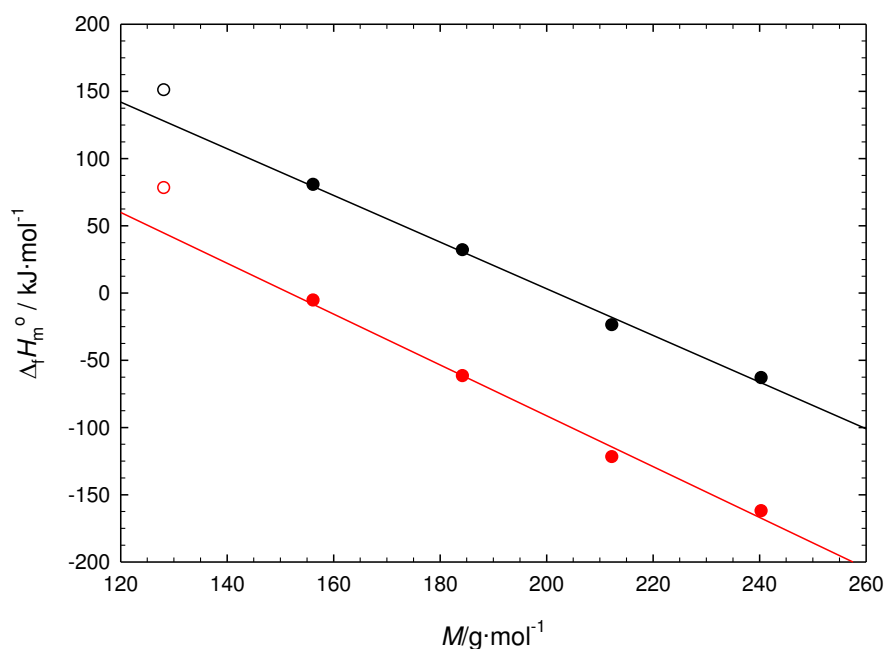


Figure 5.25. Decrease of the standard molar enthalpies of formation, in the gaseous (●) and crystal (●) phases, with increasing molar mass of naphthalene (open symbols) and the 2,6-dialkylnaphthalenes (filled symbols) studied in this work.

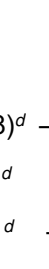
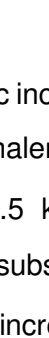
5.2.3.2. Enthalpic increments

The enthalpic increments in the gas phase enthalpies of formation related to the insertion of the different substituent groups in fluorene and naphthalene were determined

and, when possible, compared with the respective increments in the simple aromatic ring, benzene, to check for transferability of the enthalpic contributions. These increments may also be useful in establishing prediction schemes for standard molar enthalpies of formation, in the gas phase, of structurally similar compounds.

Table 5.7 reports the estimated enthalpic increments in the gas phase enthalpies of formation associated with the insertion of different substituent groups on benzene, as well as on positions 2,6 of naphthalene and on positions 2,7 of fluorene.

Table 5.7. Gaseous phase increments on enthalpies of formation associated to the insertion of different substituents in benzene, in positions 2,6 of naphthalene and in positions 2,7 of fluorene (all values in $\text{kJ}\cdot\text{mol}^{-1}$).

Substituent groups							
R ₁	R ₂	$\Delta_f H_m^\circ$	$\Delta H_m^\circ(\text{inc})$	$\Delta_f H_m^\circ$	$\Delta H_m^\circ(\text{inc})$	$\Delta_f H_m^\circ$	$\Delta H_m^\circ(\text{inc})$
H	H	82.9 ± 0.9^a		150.7 ± 1.5^b		179.4 ± 3.0^c	
CH ₂ CH ₃	H	30.0 ± 1.0^d	$-(52.9 \pm 1.3)$				
CH(CH ₃) ₂	H	4.0 ± 1.0^d	$-(78.9 \pm 1.3)$				
C(CH ₃) ₃	H	$-(24.4 \pm 0.8)^e$	$-(107.3 \pm 1.2)$				
CH ₂ CH ₃	CH ₂ CH ₃			31.7 ± 3.1	$-(59.5 \pm 3.4)^f$		
CH(CH ₃) ₂	CH(CH ₃) ₂			$-(24.1 \pm 3.9)$	$-(87.4 \pm 4.2)^f$		
C(CH ₃) ₃	C(CH ₃) ₃			$-(63.3 \pm 5.3)$	$-(107.0 \pm 2.8)^f$	$-(20.6 \pm 6.5)$	$-(100.0 \pm 3.6)^f$
CHO	H	$-(36.7 \pm 2.8)^d$	$-(119.6 \pm 2.9)$			64.5 ± 3.2	$-(114.9 \pm 4.4)$
NH ₂	H	87.1 ± 1.1^d	4.2 ± 1.3			193.6 ± 2.7	14.2 ± 4.0
NO ₂	H	67.5 ± 0.5^d	$-(15.4 \pm 1.1)$			164.4 ± 3.9	$-(15.0 \pm 4.9)$
Br	H	105.4 ± 4.1^d	22.5 ± 4.2	175.6 ± 2.3^g	24.9 ± 2.7	207.4 ± 2.2	28.0 ± 3.7
Br	Br					229.3 ± 2.5	25.0 ± 2.0^f

^a Value taken from ref. [6]; ^b Value derived from data in ref. [6,24]; ^c Value taken from ref. [3]; ^d Value taken from ref. [29];

^e Value taken from ref. [30]; ^f Enthalpic increment per substituent; ^g Value taken from ref. [31].

The mean enthalpic increments associated to the insertion of ethyl or isopropyl groups in positions 2,6 of naphthalene ($\Delta H_m^\circ(\text{inc}) = -59.5 \text{ kJ}\cdot\text{mol}^{-1}$ and $\Delta H_m^\circ(\text{inc}) = -87.4 \text{ kJ}\cdot\text{mol}^{-1}$) are $6.6 \text{ kJ}\cdot\text{mol}^{-1}$ and $8.5 \text{ kJ}\cdot\text{mol}^{-1}$ larger (in absolute value) than the corresponding increments for the alkyl substituents in benzene ($\Delta H_m^\circ(\text{inc}) = -52.9$ and $\Delta H_m^\circ(\text{inc}) = -78.9 \text{ kJ}\cdot\text{mol}^{-1}$). The enthalpic increment for the insertion of *tert*-butyl group in *tert*-butylbenzene ($\Delta H_m^\circ(\text{inc}) = -107.3 \text{ kJ}\cdot\text{mol}^{-1}$), however, is in agreement with the mean enthalpic increment

observed in 2,6-di-*tert*-butylnaphthalene ($\Delta H_m^o(\text{inc}) = -107.0 \text{ kJ}\cdot\text{mol}^{-1}$). For 2,7-di-*tert*-butylfluorene, the mean increment *per tert*-butyl group ($\Delta H_m^o(\text{inc}) = -100.3 \text{ kJ}\cdot\text{mol}^{-1}$) is ca. $7 \text{ kJ}\cdot\text{mol}^{-1}$ smaller (in absolute value) than the values referred to above. A smaller increment is also observed for fluorene substituted in position 2 with an aldehyde group ($\Delta H_m^o(\text{inc}) = -114.9 \text{ kJ}\cdot\text{mol}^{-1}$), when compared to that in benzene ($\Delta H_m^o(\text{inc}) = -119.6 \text{ kJ}\cdot\text{mol}^{-1}$). In opposition, larger increments are observed when considering the substitution by an amine group ($\Delta H_m^o(\text{inc}) = 14.2 \text{ kJ}\cdot\text{mol}^{-1}$) or a bromine atom ($\Delta H_m^o(\text{inc}) = 28.6 \text{ kJ}\cdot\text{mol}^{-1}$) in fluorene comparatively to those in benzene ($\Delta H_m^o(\text{inc}) = 4.2 \text{ kJ}\cdot\text{mol}^{-1}$ and $\Delta H_m^o(\text{inc}) = 22.5 \text{ kJ}\cdot\text{mol}^{-1}$, respectively). The increment for a bromine atom in position 2 of naphthalene ($\Delta H_m^o(\text{inc}) = 25.0 \text{ kJ}\cdot\text{mol}^{-1}$) is also larger than in benzene. The enthalpic increments for the nitro group in benzene and in position 2 of fluorene are in close agreement ($\Delta H_m^o(\text{inc}) \approx 15 \text{ kJ}\cdot\text{mol}^{-1}$).

5.3. Photoluminescence properties

5.3.1. Challenges and technical difficulties

As mentioned previously, several difficulties appeared in applying the used method and related technique. The instruction's manual of the apparatus is not always clear and it was sometimes hard to correctly use the equipment that the manufacturer considers easy-to-use and intuitive [32]. Other researchers have complained about these setbacks. On a recent publication regarding integrating sphere theory [33], Valenta comments on the use of commercial apparatus including the Quantaaurus: "their users often struggle with lack of detailed information on the quantum yield (QY) determination procedure and the technique background". Actually, it was quite hard to achieve consistent experimental conditions in order to guaranty reproducibility of results, particularly for determining the QY of powder samples. One of the issues that might affect results is the self-absorption effect, which is a major concern for integrating sphere setups [34-36]. Emitted light can be reabsorbed by the fluorophore in the region of the spectral overlap between absorption and emission (small Stokes shift), leading to a reduction of the fluorescence QY and a distortion of the fluorescence spectrum. The dedicated software of the equipment provides an option for self-absorption correction only for concentrated solutions. This functionality was not simple to implement and yielded non-reliable results, reason why it was decided to present the obtained results without self-absorption correction. Instead it was used a range of concentrations to test for spectral and QY dependence on the concentration. The least concentrated solutions were accepted to yield the most reliable results of QY. Information available in the literature also states that it should be relatively easy to avoid erroneous QY results in solution by using very low concentrations [36,37], however, in the solid state this is more difficult to achieve. When studying powder samples, we found that QY results also depended on the area of the sample contained in the Petri dish. Again, we opted for studying different amounts of sample to infer on the self-absorption effect on the solid state QY results. For the reasons referred to above the obtained results of QY of powder samples are somewhat exploratory and will be further developed in future work.

5.3.2. Fluorescence properties of the compounds studied

The nature and position of substituent groups influence both the emission spectra and the QY of fluorescent molecules. The effect of substituents, however, can be complex and no generalization should be assumed [38,39].

The results presented in the previous chapter for the solid state fluorescence properties of fluorene and its derivatives, show that all substituents studied seem to have a quenching effect on the fluorescence emission¹ of crystalline fluorene. Within the 2-substituted fluorene derivatives, only 2-aminofluorene and 2-fluorofluorene show appreciable QY results. As for the 2-substituents aldehyde, nitro, bromine, and iodide no significant emission was detected in the respective fluorene derivatives. In general, the presence of heavy atoms (like bromine and iodine) results in fluorescence quenching, known as internal heavy atom effect, because the increased probability of intersystem crossing favors the occurrence of phosphorescence instead of fluorescence [37,40,41].

Substitution in positions 2,7 and in position 9 of fluorene in general lead to very small or undetectable QY results in the solid state. From the di-substituted derivatives studied, 2,7-di-*tert*-butylfluorene is the one that shows the greatest QY. While for 2-fluorofluorene, the emission was only partially quenched when compared to that of fluorene, in 2,7-difluorofluorene the quenching effect is stronger and the observed QY is irrelevant.

Fluorenone shows very weak emission in the solid state as do all of its derivatives studied.

Naphthalene and the dialkyl derivatives studied, with the exception of 2,6-diethylnaphthalene, are strongly fluorescent in the solid state. The isopropyl and *tert*-butyl substituents lead to higher QY in the solid state than that determined for crystal naphthalene.

5.3.2.1. Fluorene and 2,7-di-*tert*-butylfluorene

Figure 5.26. shows the emission spectra of fluorene and 2,7-di-*tert*-butylfluorene in cyclohexane solution and in powder form. In cyclohexane solution, both compounds emit in the UV region. In the solid state, fluorene presents a broader emission range and continues emitting in the visible region of the spectrum.

¹ From this point forward whenever "emission" is mentioned, it refers to fluorescence emission.

The emission spectrum of fluorene in solution is characterized by the maximum emission band at 303 nm and three smaller shoulders at longer wavelengths. The spectra of 2,7-di-*tert*-butylfluorene is located at longer wavelengths, with a maximum emission at 336 nm. In the solid state, 2,7-di-*tert*-butylfluorene presents a less structured emission spectra when compared to that of fluorene.

The emission spectra of fluorene in cyclohexane solution are quite consistent with those published by Berlman [37] and Nakamizo and Kanda [42]. The determined QY in solution, however, is not in agreement with the result reported by Berlman [37] (section 4.3.2.1.1.), which may be due to the presence of impurities in the samples studied and to eventual self-absorption effects. The impurities don't seem to be relevant in the absorption spectra, for the concentration range studied.

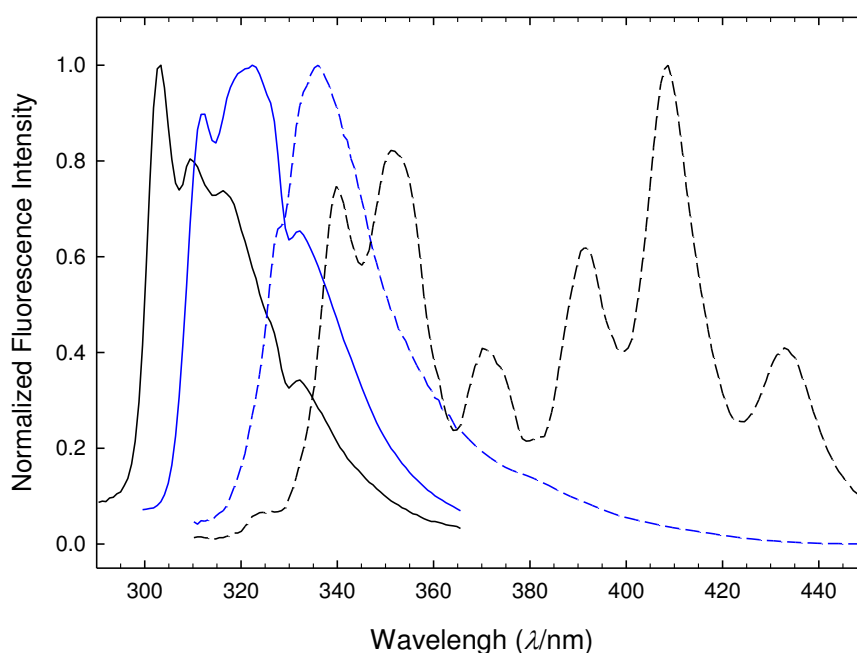


Figure 5.26. Normalized fluorescence emission spectra of fluorene (in black) and 2,7-di-*tert*-butylfluorene (in blue): solid lines, - cyclohexane solution ($1 \cdot 10^{-6}$ mol·L $^{-1}$); dashed lines - powder form.

In the solid state, the emission spectra at wavelengths above 370 nm are consistent with those published by Sangster and Irvine [43] (λ_{exc} not specified) and Pujari *et al.* [44] ($\lambda_{exc} = 363$ nm). However, Di Marco and Giro [45] ($\lambda_{exc} = 265$ nm) report a simpler, less structured emission spectra for ultrapure fluorene crystals, with maximum emission ca. 320 nm. These authors consider that bands that may appear above 370 nm are usually a

consequence of impurities (anthracene and benz[*f*]indane) in the sample, which seems to be the case of the other literature results [43,44]. So, it seems that the results obtained in this work for solid fluorene may be affected by the presence of impurities of the studied samples as referred before.

In the solid state, the quantum efficiency of fluorene is much higher than that of 2,7-di-*tert*-butylfluorene.

Table 5.8. Fluorescence quantum yields of fluorene and 2,7-di-*tert*-butylfluorene in cyclohexane solution and in powder form.

Compound	ϕ_F		
	Solution (max. C) ^a	Solution (min. C) ^b	Powder
Fluorene	0.29 ^c	0.43 ^d	0.60 ^e
Fluorene (literature)	0.80 ^f		
2,7-Di- <i>tert</i> -butylfluorene	0.43	0.49	0.09

^a Result for the least dilute solution;

^b Result for the most dilute solution;

^c 1st sample;

^d 2nd sample;

^e 2nd sample (approximately 15 % of area of the base of the quartz dish covered by sample);

^f Ref. [37], for 6·10⁻⁴ mol·L⁻¹.

A distortion of the emission spectrum at shorter wavelengths and a red shift of the emission maximum with increasing concentration are spectral indications of reabsorption [36,46]. To visualize the reabsorption effect, the emission spectra of fluorene and 2,7-di-*tert*-butylfluorene were normalized to the maximum emission of the most concentrated solution. Figures 5.27 and 5.28 clearly show the dependence of the emission spectra of fluorene and 2,7-di-*tert*-butylfluorene with solution concentration, as the bands at shorter wavelengths are completely suppressed. The increase in QY for more dilute solutions (less self-absorption) is also evident, from the data compiled in table 5.8.

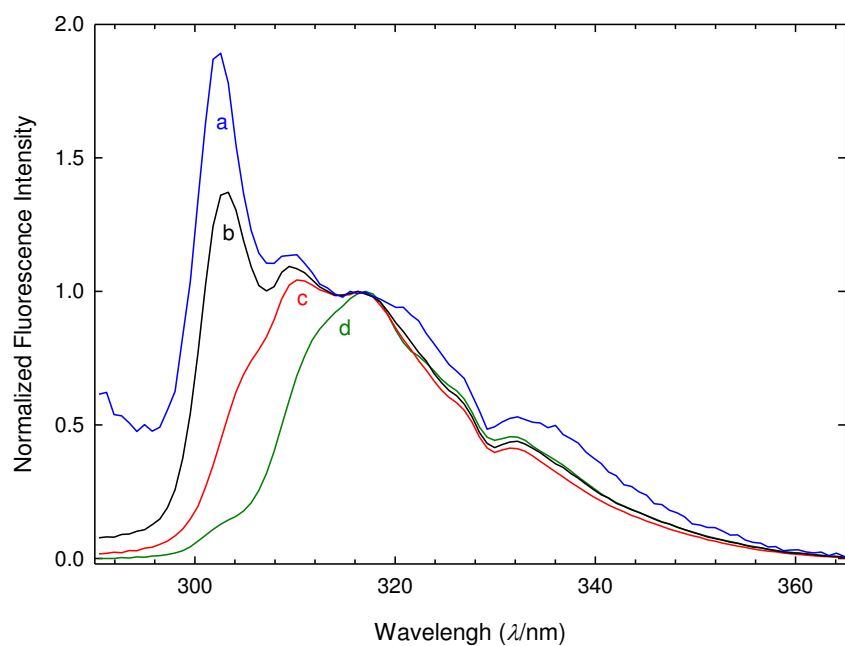


Figure 5.27. Normalized fluorescence emission spectra of fluorene in cyclohexane solution at different concentrations: a. $1 \cdot 10^{-6} \text{ mol} \cdot \text{L}^{-1}$; b. $1 \cdot 10^{-5} \text{ mol} \cdot \text{L}^{-1}$; c. $1 \cdot 10^{-4} \text{ mol} \cdot \text{L}^{-1}$; d. $1 \cdot 10^{-3} \text{ mol} \cdot \text{L}^{-1}$ (spectral data normalized to the maximum emission of the most concentrated solution).

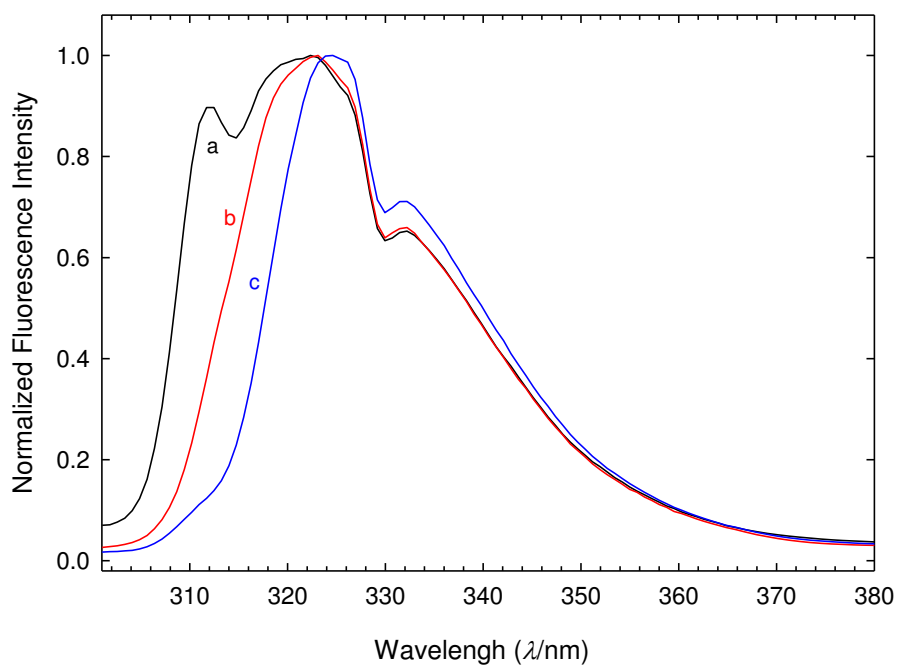


Figure 5.28. Normalized fluorescence emission spectra of 2,7-di-*tert*-butylfluorene in cyclohexane solution at different concentrations: a. $1 \cdot 10^{-6} \text{ mol} \cdot \text{L}^{-1}$; b. $1 \cdot 10^{-5} \text{ mol} \cdot \text{L}^{-1}$; c. $1 \cdot 10^{-4} \text{ mol} \cdot \text{L}^{-1}$.

5.3.2.2. Naphthalene and naphthalene derivatives

Naphthalene and its 2,6-dialkyl derivatives studied emit in the UV region, either in solution or in the solid state. The emission spectrum of naphthalene in cyclohexane solution is characterized by two major bands at 322 and 337 nm (maximum emission), and two shoulders at 313 and 348 nm. The obtained spectra are in agreement with that published by Berlman [37], but the maximum emission reported by this author corresponds to the band at 322 nm.

Naphthalene, as many aromatic hydrocarbons, can form excited dimers (excimers) in the solid state [47]. In solution, however, excimer fluorescence only occurs at relatively high concentrations ($>0.1 \text{ mol}\cdot\text{L}^{-1}$ [48]) or at very low temperatures [49], reasons why it is not evident in the present results.

The solid state fluorescence spectra of naphthalene is characterized by a broad band with a maximum emission at 339 nm, showing a slight red-shift when compared to that in cyclohexane solution, and two shoulders at about 342 and 350 nm.

The shape of the fluorescence spectra of the three 2,6-dialkyl naphthalenes studied in cyclohexane solution is identical. It is characterized by a dominant band around 340 nm, slightly shifted to shorter wavelengths with increasing molar mass of the alkyl substituent, and two shoulders at about 333 and 354 nm. The emission spectra of naphthalene and of the 2,6-dialkyl naphthalenes was also recorded at more diluted concentrations ($<10^{-4} \text{ mol}\cdot\text{L}^{-1}$). For these concentrations, the absorption was very low and the emission was not efficiently detected by the fluorimeter.

The absorption and emission spectra of 2,6-dimethylnaphthalene in cyclohexane solution has been reported by Berlman [37]. The quantum yield ($\phi_f = 0.45$, $C = 1.3\cdot 10^{-3} \text{ mol}\cdot\text{L}^{-1}$) and the maximum emission wavelength ($\lambda_{\text{max}}^f = 340 \text{ nm}$) reported by this author are consistent with those determined in this work for the other dialkyl naphthalenes.

Some alkyl aromatic compounds show noticeable shifts of the fluorescence spectra toward longer wavelengths when compared to the parent compound [37,50]. This is however not the case for the alkyl naphthalenes studied when considering the obtained results for naphthalene, as can be observed in figure 5.29.

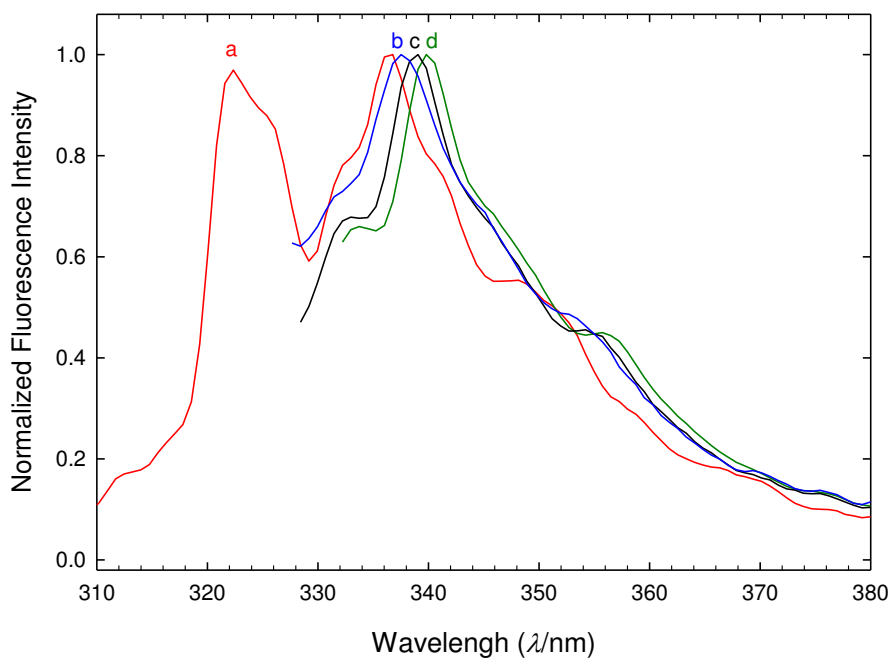


Figure 5.29. Normalized fluorescence emission spectra of naphthalene and of the 2,6-dialkyl derivatives studied in cyclohexane solution: a. Naphthalene; b. 2,6-di-*tert*-butylnaphthalene; c. 2,6-diisopropylnaphthalene; d. 2,6-diethylnaphthalene.

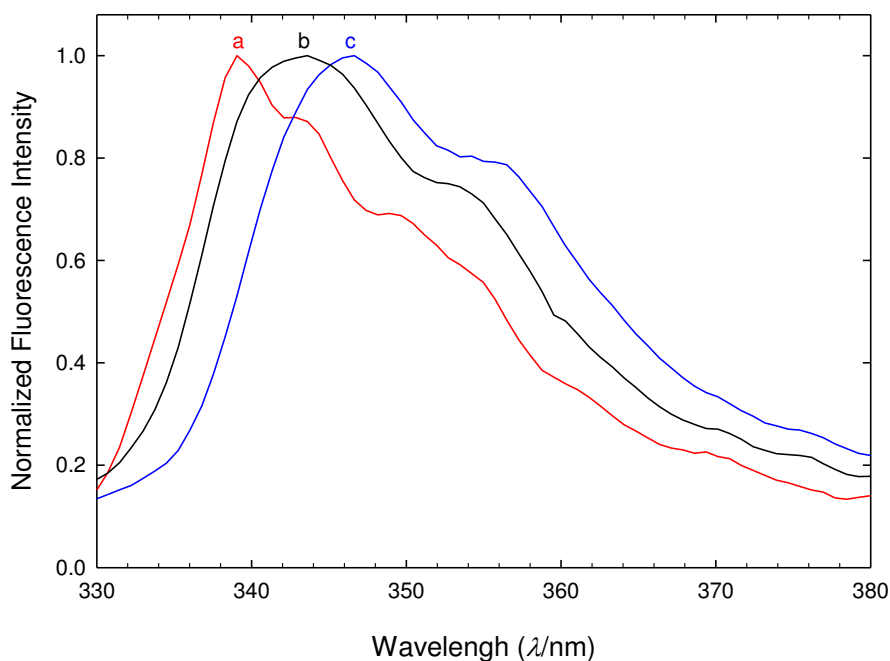


Figure 5.30. Normalized fluorescence emission spectra of naphthalene and of the 2,6-dialkyl derivatives studied in the solid state: a. naphthalene; b. 2,6-di-*tert*-butylnaphthalene; c. 2,6-diisopropylnaphthalene.

The fluorescence spectra of 2,6-diisopropylnaphthalene and 2,6-di-*tert*-butylnaphthalene powders, with a maximum emission at around 346 nm and 344 nm respectively, show a similar profile to that obtained for naphthalene, as can be observed in figure 5.30. The solid state fluorescence spectra of 2,6-di-*tert*-butylnaphthalene is shifted to shorter wavelengths compared to 2,6-diisopropylnaphthalene, as was the case in the solution fluorescence spectra. It does not reveal the existence of excimers, probably because the alkyl substituents sterically hinder the excimer formation.

Table 5.9. presents a compilation of the QY results in cyclohexane solution and in powder form for naphthalene and for the 2,6-dialkyl derivatives studied. The QY's of the 2,6-dialkyl derivatives are in general larger than that of naphthalene in solution and in powder form. The exception is 2,6-diethylnaphthalene that, while revealing important fluorescence in cyclohexane solution, shows no significant fluorescence emission in the powder form. Considering the results obtained for the other dialkyl derivatives, this near complete quenching effect was unexpected. The reason behind this surprising result is still unclear.

Table 5.9. Fluorescence quantum yields of naphthalene and of the 2,6-dialkyl derivatives studied in cyclohexane solution and in powder form.

Compound	ϕ_F (solution) ^a	ϕ_F (powder)
Naphthalene	0.22	0.23
2,6-Dimethylnaphthalene	0.45 ^b	
2,6-Diethylnaphthalene	0.45	0.02
2,6-Diisopropylnaphthalene	0.40	0.38
2,6-Di- <i>tert</i> -butylnaphthalene	0.34	0.57

^aFor $1 \cdot 10^{-3}$ mol·L⁻¹;

^bRef. [37].

For the dialkyl derivatives studied, the QY in solution decreases with increasing molar mass of the alkyl substituent. In the solid state, despite the absence of QY results of 2,6-methylnaphthalene, the tendency seems to be inverted as these results increase with increasing molar mass of the alkyl substituent. No fluorescence data were found in the literature regarding the three 2,6-dialkylnaphthalenes studied for comparison purposes.

5.4. Conclusions

- This work is a contribution to further expand the knowledge of thermodynamic properties of fluorene, fluorenone and naphthalene derivatives, whose available literature data is scarce or often inaccurate. The combination of the different thermodynamic properties determined in the course of this work has, therefore, allowed a more thorough and comprehensive understanding of the molecular energetics of these polycyclic aromatic hydrocarbons.
- Additionally, useful correlations (5.4 - 5.16) were developed based on the obtained results that allow the estimation of thermodynamic properties of compounds whose experimental study was not possible.
- Keeping in mind that these compounds are acknowledged environment pollutants, the collected data regarding the dependence of vapor pressure with temperature and consequently derived properties of phase transitions are crucial to better understand and control their environmental impact.
- When considering the eventual application of these compounds in optoelectronic devices, this work provides important information regarding the thermodynamic stability of some of the compounds in the crystalline phase. The assessment of thermodynamic stability is important to evaluate the reactivity of these compounds, in order to predict convenient routes leading to their degradation in the environment.
- Even though so far the study of photoluminescence properties may be considered exploratory, it opened a new research possibility that will be explored in the future.

References

- [1] M.J.S. Monte, A.R.R.P. Almeida, *Struct. Chem.* 24 (2013) 2001-2016;
- [2] M.J.S. Monte, A.R.R.P. Almeida, J.F. Liebman, *Chemosphere* 138 (2015) 478-485;
- [3] M.J.S. Monte, S.P. Pinto, A.I.M.C. Lobo Ferreira, L.M.P.F. Amaral, V.L.S. Freitas, M.D.M.C. Ribeiro da Silva, *J. Chem. Thermodyn.* 45 (2012) 53-58;
- [4] Lookchem, 2016. <http://www.lookchem.com/2-Chlorofluorene/>, accessed in March 2016;
- [5] M.J.S. Monte, R. Notario, M.M.G. Calvino, A.R.R.P. Almeida, L.M.P.F. Amaral, A.I.M.C. Lobo Ferreira, M.D.M.C. Ribeiro da Silva, *J. Chem. Eng. Data* 57 (2012) 2486-2496;
- [6] M.V. Roux, M. Temprado, J.S. Chickos, Y. Nagano, *J. Phys. Chem. Ref. Data*, 37 (2008) 1855-1996;
- [7] H.L. Finke, J.F. Messerly, S.H. Lee, A.G. Osborn, D.R., Douslin, *J. Chem. Thermodyn.* 9 (1977) 937-956;
- [8] P. Walden, *Z. Elektrochem.* 14 (1908) 713-728, cited in: A.S. Gilbert, *Thermochim. Acta* 339 (1999) 131-142;
- [9] F. Trouton, *Philos. Mag.* 18 (1884) 54-57;
- [10] J.S. Chickos, G. Nichols, *J. Chem. Eng. Data* 46 (2001) 562-573;
- [11] R.S. Rowland, R. Taylor, *J. Phys. Chem.* 100 (1996) 7384-7391;
- [12] J.C. Rienstra-Kiracofe, G.S. Tschumper, H.F. Schaefer, S. Nandi, G.B. Ellison, *Chem. Rev.* 102 (2002) 231-282;
- [13] M.J.S. Monte, L.M.N.B.F. Santos, J.M.S. Fonseca, C.A.D. Sousa, *J. Therm. Anal. Calorim.* 100 (2010) 465-474;
- [14] A.R.R.P. Almeida, M.J.S. Monte, *J. Chem. Thermodyn.* 57 (2013) 160-168;
- [15] A.R.R.P. Almeida, M.J.S. Monte, *J. Chem. Thermodyn.* 65 (2013) 150-158;
- [16] A.J. Dobson, R.E. Gerkin, *Acta Cryst.* C54 (1998) 1890-1892;
- [17] T. Steiner, *Acta Cryst.* C56 (2000) 874-875;
- [18] W. Nuansing, A. Rebollo, J.M. Mercero, J. Zuñiga, A.M. Bittner, *J. Raman Spectrosc.* 43 (2012) 1397-1406;

- [19] I. Csöreg, M. Czugler, E. Weber, *J. Phys. Org. Chem.* 6 (1993) 171-178;
- [20] R. Hosseinzadeh, Z. Lasemi, W. Seichter, E. Weber, *Cryst. Eng. Comm.* 11 (2009) 1331-1337;
- [21] A.C. Blackburn, A.J. Dobson, R.E. Gerkin, *Acta Cryst.* C52 (1996) 2638-2641;
- [22] K.-T. Chan, Y.-H. Tsai, W.-S. Lin, J.-R. Wu, S.-J. Chen, F.-X. Liao, C.-H. Hu, H.M. Lee, *Organometallics* 29 (2010) 463-472;
- [23] G.L. Eakins, J.S. Alford, B.J. Tiegs, B.E. Breyfogle, C.J. Stearman, *J. Phys. Org. Chem.* 24 (2011) 1119-1128;
- [24] M.J.S. Monte, L.M.N.B.F. Santos, M. Fulem, J.M.S. Fonseca, C.A.D. Sousa, *J. Chem. Eng. Data* 51 (2006) 757-766;
- [25] A.G. Osborn, D.R. Douslin, *J. Chem. Eng. Data* 20 (1975) 229-231;
- [26] A.F.L.O.M. Santos, J.A.S.A. Oliveira, M.D.M.C. Ribeiro da Silva, M.J.S. Monte, *Chemosphere* 146 (2016) 173-181;
- [27] W.D. Good, *J. Chem. Thermodyn.* 5 (1973) 715-720;
- [28] A.F.L.O.M. Santos, private communication;
- [29] J.B. Pedley, *Thermochemical Data and Structures of Organic Compounds*, Thermodynamics Research Center, College Station, Texas, U.S.A. (1994);
- [30] S.P. Verevkin, *J. Chem. Thermodyn.* 30 (1998) 1029-1040;
- [31] M.A.V. Ribeiro da Silva, M.L.C.C.H. Ferrao, A.J.M. Lopes, *J. Chem. Thermodyn.* 25 (1993) 229-235;
- [32] K. Suzuki, (Application Note) *Nature Photonics* 5 (2011);
- [33] J. Valenta, *Nanosci. Methods* 3 (2014) 11-27;
- [34] J.C. de Mello, H.F. Wittmann, R.H. Friend, *Adv. Mater.* 9 (1997) 230-232;
- [35] T.-S. Ahn, R.O. Al-Kaysi, A.M. Müller, K.M. Wentz, C.J. Bardeen, *Rev. Sci. Instrum.* 78 (2007) 086105;
- [36] C. Würth, M. Grabolle, J. Pauli, M. Spieles, U. Resch-Genge, *Nat. Protoc.* 8 (2013) 1535-1550;
- [37] I.B. Berlman, *Handbook of Fluorescence Spectra of Aromatic Molecules* (2nd Ed.), Academic Press, New York (1971);

- [38] G.G. Guilbault, *Practical Fluorescence* (2nd Ed.), Marcel Dekker, Inc., New York (1990);
- [39] B. Valeur, *Molecular Fluorescence: Principles and Applications*, Wiley-VCH Verlag GmbH, Weinheim, Germany (2001);
- [40] J.R. Lakowicz, *Principles of fluorescence spectroscopy* (3rd Ed.), Springer, New York (2006);
- [41] A. Ghodbane, N. Saffon, S. Blanc, S. Fery-Forgues, *Dyes Pigm.* 113 (2015) 219-226;
- [42] M. Nakamizo, Y. Kanda, *Spectrochim. Acta* 19 (1963) 1235-1248;
- [43] R.C. Sangster, J.W. Irvine Jr., *J. Chem. Phys.* 24 (1956) 670-715;
- [44] S.R. Pujari, S.A. Jadhav, S.R. Patil, *Indian J. Chem. A* 40 (2001) 933-938;
- [45] P. Di Marco, G. Giro, *Phys. Stat. Sol. (a)* 30 (1975) K143-K146;
- [46] K. Suzuki, A. Kobayashi, S. Kaneko, K. Takehira, T. Yoshihara, H. Ishida, Y. Shiina, S. Oishi, S. Tobita, *Phys. Chem. Chem. Phys.* 11 (2009) 9850-9860;
- [47] K. Uchida, M. Tanaka, M. Tomura, *J. Lumin.* 20 (1979) 409-414;
- [48] I.B. Berlman, A. Weinreb, *Mol. Phys.* 5 (1962) 313-319;
- [49] E. Döller, T. Förster, *Z. Physik. Chem.* 34 (1962) 132-150 (as cited in ref. [37]);
- [50] B.L. Van Duuren, *Anal. Chem.* 32 (1960) 1436-1442.

Chapter

Annexes

A

A.1. Units and conversions

A.2. Constants

B

B.1. Abbreviation, acronym and symbol list

C

C.1. ^1H NMR, ^{13}C NMR and mass spectral data

C.2. Experimental results of test substances

References

Annex A.

A.1. Units and conversions

The relative atomic masses used for the elements in the calculation of all molar quantities throughout this work were those recommended by the IUPAC Commission in 2011 [1]. In this work, the International System of Units (SI) [2] was adopted. Multiples and submultiples of SI units were used when necessary, based on the order of magnitude of the values to which these units referred to. Some conversions were necessary to adapt literature values to the SI and are described as follows, accompanied by the conversion ratio of the corresponding SI unit:

- The temperature values in degrees Celsius ($^{\circ}\text{C}$) were converted into Kelvin (K) according to the relation:

$$T / \text{K} = T / ^{\circ}\text{C} + 273.15 \quad (\text{A.1})$$

- The energy, when expressed in calories (cal), were converted to joules (J) according to the relation:

$$1 \text{ cal} = 4.184 \text{ J} \quad (\text{A.2})$$

- The vapor pressure values, when expressed in millimeters of mercury (mmHg), were converted to Pascal (Pa) according to the relation:

$$1 \text{ mmHg} = 133.322 \text{ Pa} \quad (\text{A.3})$$

A.2. Constants

- Gas constant: $R = 8.3144598(48) \text{ J}\cdot\text{K}^{-1}\cdot\text{mol}^{-1}$ [3]
- Avogadro constant: $N_{\text{A}} = 6.022140857(74)\cdot 10^{23}$ [3]

Annex B.

B.1. Abbreviation, acronym and symbol list

Table B.1. List of abbreviations, acronyms and symbols used and respective meanings.

Abbreviation, acronym or symbol	Meaning
a	y-axis intercept
A_0	Area of the effusion orifice
Abs	Absorbance
aux	Auxiliar
b	Slope
BA	Benzoic acid
C	Concentration ($\text{mol}\cdot\text{L}^{-1}$), or Capacitance of the capacitor
cal	calibration
carb	Carbon
CAS	Chemical Abstracts Service
cert	Certificate
corr	Corrected
cpd	compound
cr	Crystalline
C_B	Benzenic carbon (Benson notation)
C_v	Molar heat capacity, at constant volume
c_p	Specific heat capacity, at constant pressure
$C_{p,m}^{\circ}$	Standard molar heat capacity, at constant pressure
$\Delta_{cr/l}^g C_{p,m}^{\circ}$	Difference between the standard molar heat capacities of the gas phase and the crystalline/liquid phase, at constant pressure
d	Doublet
dd	Doublet of doublets
ddd	Doublet of doublet of doublets
dt	Doublet of triplets
ddt	Doublet of doublet of triplets
E	Energy, or Energy equivalent

.../...

.../...	
E_f	Energy equivalent of the final state
E_i	Energy equivalent of the initial state
exp	Experimental
FID	Free induction decay
GC	Gas Chromatography
G_m	Molar Gibbs energy
$\Delta_f G_m^\circ$	Standard molar Gibbs energy of formation
$\Delta_{cr/l}^g G_m^\circ$	Standard molar Gibbs energy of sublimation/vaporization
h	Height, or Planck constant
HPLC	High Pressure Liquid Chromatography
$\Delta_c H_m^\circ$	Standard molar enthalpy of combustion
$\Delta_f H_m^\circ$	Standard molar enthalpy of formation
$\Delta_{cr/l}^g H_m^\circ$	Standard molar enthalpy of sublimation/vaporization
I	Intensity of electric current
IBP	Isothermal bomb process
ign	Ignition
J	Coupling constant
k	Cooling constant of the calorimeter
k_{cal}	Calibration constant
K_{hp}	Hiby and Pahl correction factor
K_n	Knudsen number
K_p	Equilibrium constant, expressed in terms of pressure
l	Liquid
l	Thickness
lit	Literature
m	Mass, or Multiplet
Δm	Mass variation
M	Molar Mass
min	Minimum, or Minute
max	Maximum
n	Number of independent determinations, or Number of hydration molecules, or Number of molecules per unit of volume

.../...

.../...	
Δn	Variation of the number of moles of gaseous species
NMR	Nuclear magnetic resonance
p°	Reference pressure
p_{tp}	Pressure of the triple point
ppm	Parts per million
Q	Amount of heat
r	Radius, or Heat of rotation
R^2	Correlation coefficient
s	Singlet
sol	Solution
S_{m}	Molar entropy
$\Delta_{\text{f}} S_{\text{m}}^\circ$	Standard molar entropy of formation
$\Delta_{\text{cr/l}}^{\text{g}} S_{\text{m}}^\circ$	Standard molar entropy of sublimation/vaporization
t_{f}	Final instant of the main period
t_{i}	Initial instant of the main period
t_{r}	Instant when the bomb rotation is initiated
T_{s}	Temperature of the surroundings
T_{∞}	Convergence temperature
T_{fus}	Temperature of fusion
T_{tp}	Temperature of the triple point
T_{f}	Final temperature
T_{i}	Initial temperature
T_{m}	Mean temperature
ΔT	Temperature variation, or Experimental temperature range
ΔT_{corr}	Thermal corrective term
ΔT_{ad}	Variation of temperature in adiabatic conditions
td	Triplet of doublets
tdd	Triplet of doublet of doublets
u	Variation in temperature caused by heat of stirring
ΔU	Internal energy variation
$\Delta_{\text{c}} U^\circ$	Standard massic energy of combustion
$\Delta_{\text{c}} U^\circ$	Standard molar energy of combustion

.../...

.../...

ΔU_{Σ}	Energy variation associated to the Washburn corrections
ν	Frequency
V	Volume
V_i	Initial voltage of the capacitor
V_f	Final voltage of the capacitor
V_m	Molar volume
$\Delta_{\text{cr/l}}^g V_m$	Molar volume variation between the gas phase and the crystalline/liquid phase
w_0	Transmission probability factor
x_i	Individual value
\bar{x}	Mean value
α	Condensation coefficient
δ	Chemical shift
ε_{cal}	Energy equivalent of the calorimeter with an empty combustion bomb
ε_f	Energy equivalent of the combustion bomb containing only the products formed
ε_r	Energy equivalent of the combustion bomb containing only the reactants
θ	Reference temperature
λ	Mean free path of gas molecules, or Wavelength
λ_{exc}	Excitation wavelength
$\lambda_{\text{max}}^{\text{Abs}}$	Maximum absorption wavelength
$\lambda_{\text{max}}^{\text{F}}$	Maximum fluorescence emission wavelength
μ	Chemical potential
ν	Vibrational energy level, or Stoichiometric coefficients
π	Pi
ρ	Density
σ	Diameter of molecular collision, or Standard deviation of the mean
Σ	Summation
ϕ	Heat flow, or Diameter
ϕ_{F}	Fluorescence quantum yield
%	Percentage
®	Registered trademark

Annex C.

C.1. ^1H NMR, ^{13}C NMR and mass spectral data

The ^1H NMR and ^{13}C NMR data were acquired at room temperature using deuterated chloroform (CDCl_3) as solvent. Chemical shifts (δ) are expressed in ppm values relative to tetramethylsilane used as internal reference, and coupling constants (J) are expressed in Hz. Electron impact mass spectral data (EI-MS) are reported as m/z (% of relative intensity) of the most important fragments, where M^+ refers to the molecular ion.

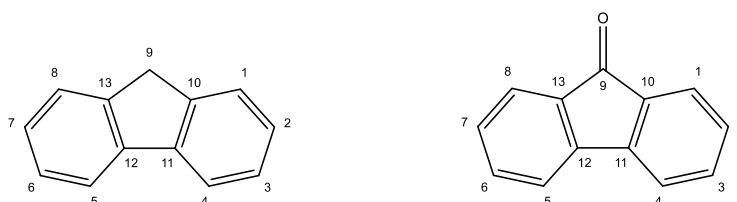


Figure C1. Structures, and IUPAC numbering, of fluorene and fluorenone.

C.1.1. 2,7-Difluorofluorene

^1H NMR (400 MHz, CDCl_3) δ = 7.63 (2H, *dd*, J = 8.4, 5.0 Hz, H4, H5), 7.22-7.19 (2H, *m*, H1, H8), 7.10-7.02 (2H, *m*, H3, H6), 3.86 (2H, *s*, H9, H9').

^{13}C NMR (100 MHz, CDCl_3) δ = 163.06 (*d*, $^1J_{\text{CF}}$ = 244.4, 1.1 Hz, C2, C7), 145.91 (C10, C13), 137.81 (C11, C12), 121.27 (C4, C5), 114.98 (*d*, $^2J_{\text{CF}}$ = 23.1 Hz, C3, C6), 113.24 (*d*, $^2J_{\text{CF}}$ = 23.1 Hz, C1, C8), 37.87 (C9).

EI/MS m/z (%): 203 (26), 202 (M^+ , 100), 201 (93), 199 (12), 181 (16), 101 (13), 101 (14).

C.1.2. 2,7-Dichlorofluorene

^1H NMR (400 MHz, CDCl_3) δ = 7.66 (2H, *d*, J = 8.2 Hz, H4, H5), 7.53 (2H, *s*, H1, H8), 7.37 (2H, *dd*, J = 8.2, 1.9 Hz, H3, H6), 3.89 (2H, *s*, H9, H9').

^{13}C NMR (100 MHz, CDCl_3) δ = 145.49 (C10, C13), 140.16 (C11, C12), 133.67 (C2, C7), 128.21 (C4, C5), 126.31 (C1, C8), 121.69 (C3, C6), 37.53 (C9).

EI/MS m/z (%): 238 ($[\text{M}+4]^+$, 25), 237 (24), 236 ($[\text{M}+2]^+$, 77), 235 (46), 234 (M^+ , 93), 233 (33), 202 (24), 201 (83), 200 (57), 164 (47), 163 (67), 99 (59), 82 (46).

C.1.3. 2,7-Diiodofluorene

^1H NMR (400 MHz, CDCl_3) δ = 7.87 (2H, *d*, J = 0.9 Hz, H1, H8), 7.72 - 7.67 (2H, *m*, H3, H6), 7.49 (2H, *d*, J = 8.0 Hz, H4, H5), 3.83 (2H, *s*, H9, H9').

^{13}C NMR (100 MHz, CDCl_3) δ = 144.84 (C10, C13), 140.41 (C11, C12), 136.01 (C1, C8), 134.18 (C3, C6), 121.59 (C4, C5), 92.44 (C2, C7), 36.30 (C9).

EI/MS m/z (%): 418 (M^+ , 100), 291 (32), 164 (40), 163 (38).

C.1.4. 9-Chlorofluorene

^1H NMR (400 MHz, CDCl_3) δ = 7.71 (2H, *d*, J = 7.5 Hz, H4, H5), 7.68 (2H, *ddt*, J = 7.3, 1.3, 0.7 Hz, H1, H8), 7.44 (2H, *tdd*, J = 7.5, 1.2, 0.5 Hz, H3, H6), 7.38 (2H, *td*, J = 7.5, 1.2 Hz, H2, H7), 5.83 (*s*, H9).

^{13}C NMR (100 MHz, CDCl_3) δ = 144.70 (C10, C13), 140.92 (C11, C12), 130.26 (C1, C8), 128.93 (C2, C7), 126.73 (C3, C6), 121.03 (C4, C5), 58.44 (C9).

EI/MS m/z (%): 202 ($[\text{M}+2]^+$, 14), 200 (M^+ , 42), 166 (29), 165 (100), 163 (25), 83 (21).

C.1.5. 2-Bromofluorenone

^1H NMR (400 MHz, CDCl_3) δ = 7.80 (*d*, J = 1.8 Hz, H1), 7.69 (*dt*, J = 7.4, 0.9 Hz, H8), 7.64 (*dd*, J = 7.9, 1.9 Hz, H3), 7.56 - 7.50 (2H, *m*, H5, H6), 7.42 (*d*, J = 7.9 Hz, H4), 7.39 - 7.31 (*m*, H7).

^{13}C NMR (100 MHz, CDCl_3) δ = 193.31 (C9), 144.61 (C12), 143.94 (C11), 138.02 (C3), 136.71 (C10), 135.94 (C6), 134.64 (C13), 130.34 (C1), 128.50 (C7), 125.54 (C8), 123.84 (C2), 122.63 (C4), 121.35 (C5).

C.1.6. 2-Iodofluorenone

^1H NMR (400 MHz, CDCl_3) δ = 7.99 (*dd*, J = 1.6, 0.5 Hz, H1), 7.85 (*dd*, J = 7.8, 1.6 Hz, H3), 7.68 (*dt*, J = 7.4, 0.9 Hz, H8), 7.55 - 7.50 (*m*, H5, H6), 7.36 (*ddd*, J = 7.4, 6.1, 2.5 Hz, H7), 7.31 (*dd*, J = 7.8, 0.4 Hz, H4).

^{13}C NMR (100 MHz, CDCl_3) δ = 192.42 (C9), 143.78 (C12), 143.66 (C11), 143.12 (C3), 135.77 (C10), 135.01 (C1), 133.37 (C13), 133.36 (C6), 129.61 (C7), 124.57 (C8), 122.02 (C4), 120.47 (C5), 93.92 (C2).

EI/MS m/z (%): 307 (23), 306 (M^+ , 100), 179 (16), 151 (71), 150 (35).

C.1.7. 2,7-Dichlorofluorenone

^1H NMR (400 MHz, CDCl_3) δ = 7.62 (2H, *dd*, J = 1.9, 0.6 Hz, H1, H8), 7.47 (2H, *dd*, J = 8.0, 1.9 Hz, H3, H6), 7.44 (2H, *dd*, J = 8.0, 0.6 Hz, H4, H5).

^{13}C NMR (100 MHz, CDCl_3) δ = 191.98 (C9), 142.72 (C11, C12), 136.33 (C10, C13), 136.30 (C2, C7), 135.44 (C3, C6), 125.89 (C1, C8), 122.40 (C4, C5).

EI/MS m/z (%): 252 ($[\text{M}+4]^+$, 18), 250 ($[\text{M}+2]^+$, 80), 249 (24), 248 (M^+ , 100), 220 (16), 150 (38), 111 (17), 99 (18), 85 (30), 84 (19), 69 (20), 57 (47).

C.1.8. 2,7-Diiodofluorenone

^1H NMR (400 MHz, CDCl_3) δ = 7.99 (2H, *dd*, J = 1.6, 0.4 Hz, H1, H8), 7.86 (2H, *dd*, J = 7.8, 1.6 Hz, H3, H6), 7.30 (2H, *dd*, J = 7.8, 0.4 Hz, H4, H5).

^{13}C NMR (100 MHz, CDCl_3) δ = 191.88 (C9), 144.34 (C3, C6), 143.88 (C11, C12), 135.75 (C10, C13), 134.46 (C1, C8), 123.03 (C4, C5), 95.34 (C2, C7).

EI/MS m/z (%): 433 (24), 432 (M^+ , 100), 277 (29), 150 (55), 85 (15), 71 (18), 57 (23).

C.2. Experimental results of test substances

C.2.1. Benzoic Acid

Table C.1. Vapor pressures of benzoic acid determined by the Knudsen effusion method.^a

<i>T</i> / K	<i>t</i> / s	Orifices	<i>m</i> / mg			<i>p</i> / Pa			
			<i>m</i> _{small}	<i>m</i> _{medium}	<i>m</i> _{large}	<i>p</i> _{small}	<i>p</i> _{medium}	<i>p</i> _{large}	<i>p</i> _{mean}
302.16	21857	A ₁ '-B ₄ '-C ₇ '	6.89	8.43	10.32	0.181	0.179	0.174	0.178
302.16	21211	A ₁ '-B ₄ '-C ₇ '	6.74	8.15	10.19	0.182	0.178	0.177	0.179
302.16	21059	A ₁ '-B ₄ '-C ₇ '	6.74	8.16	10.10	0.183	0.180	0.177	0.180
304.31	21857	A ₂ '-B ₅ '-C ₈ '	8.79	11.16	13.45	0.231	0.237	0.228	0.232
304.21	21211	A ₂ '-B ₅ '-C ₈ '	8.39	10.68	12.94	0.227	0.234	0.226	0.229
304.21	21059	A ₂ '-B ₅ '-C ₈ '	8.38	10.61	12.84	0.229	0.234	0.226	0.230
306.18	21857	A ₃ '-B ₆ '-C ₉ '	10.83	13.29	16.46	0.286	0.284	0.280	0.283
306.28	21211	A ₃ '-B ₆ '-C ₉ '	10.76	13.02	16.36	0.293	0.286	0.287	0.289
306.28	21059	A ₃ '-B ₆ '-C ₉ '	10.65	13.09	16.24	0.292	0.290	0.286	0.289
311.14	14144	A ₁ '-B ₄ '-C ₇ '	12.76	15.49	18.87	0.523	0.521	0.498	0.514
311.15	14503	A ₁ '-B ₄ '-C ₇ '	12.90	15.67	19.23	0.515	0.514	0.495	0.508
311.15	14635	A ₁ '-B ₄ '-C ₇ '	13.13	15.87	19.45	0.522	0.510	0.498	0.510
314.19	14144	A ₂ '-B ₅ '-C ₈ '	17.39	21.51	26.36	0.716	0.717	0.699	0.711
314.21	14503	A ₂ '-B ₅ '-C ₈ '	17.75	22.44	26.90	0.713	0.729	0.696	0.713
314.21	14635	A ₂ '-B ₅ '-C ₈ '	17.94	22.69	27.28	0.716	0.733	0.701	0.717
317.27	14144	A ₃ '-B ₆ '-C ₉ '	24.24	29.68		1.003	0.994		0.999
317.27	14503	A ₃ '-B ₆ '-C ₉ '	24.80	30.24		1.001	0.987		0.994
317.27	14635	A ₃ '-B ₆ '-C ₉ '	25.08	30.66	38.63	1.006	0.995	0.998	1.000

^a $u(T/K) = \pm 0.01$, $u(p/Pa) = \pm 0.01$.

Table C.2. Vapor pressures of benzoic acid determined by the static method with capacitance manometers. ^a

<i>T</i> /K	<i>p</i> /Pa	100Δ <i>p</i> / <i>p</i> ^{<i>b</i>}	<i>T</i> /K	<i>p</i> /Pa	100Δ <i>p</i> / <i>p</i> ^{<i>b</i>}	<i>T</i> /K	<i>p</i> /Pa	100Δ <i>p</i> / <i>p</i> ^{<i>b</i>}
<i>Crystalline phase, static method</i>								
315.19	0.831	0	331.01	4.264	0.3	346.85	19.17	0
319.05	1.249	0	334.89	6.213	0.1	350.66	26.96	0.2
323.10	1.905	0	338.91	9.065	-0.1	354.75	38.06	-0.2
327.00	2.823	-0.1	342.90	13.37	0			

^a $u(T) = \pm 0.01$ K, $u(p) = 0.01 + 0.0025p$ Pa;^b $\Delta p = p - p_{\text{calc}}$, where p_{calc} is calculated from the Clarke and Glew equation with parameters given in table C.3.Table C.3. Standard ($p^\circ = 0.1$ MPa) molar properties of sublimation of benzoic acid, derived from the experimental vapor pressure results.

ΔT /K	θ /K	$\Delta_{\text{cr}}^{\text{g}} G_{\text{m}}^{\circ}(\theta)$ kJ·mol ⁻¹	$\Delta_{\text{cr}}^{\text{g}} H_{\text{m}}^{\circ}(\theta)$ kJ·mol ⁻¹	$\Delta_{\text{cr}}^{\text{g}} S_{\text{m}}^{\circ}(\theta)$ ^{<i>a</i>} J·K ⁻¹ ·mol ⁻¹	$p(\theta)$ ^{<i>b</i>} Pa	R^2	$\Delta_{\text{g}}^{\text{cr}} C_{p,m}^{\circ}$ ^{<i>c</i>} J·K ⁻¹ ·mol ⁻¹	s ^{<i>d</i>}
<i>Crystalline phase, effusion method</i>								
302.16-317.27	298.15	34.01 ± 0.01	90.9 ± 0.2	190.8 ± 0.7	1.1·10 ⁻¹	0.9999	20.8	0.007
	309.72 ^{<i>e</i>}	31.81 ± 0.01	90.7 ± 0.2	190.1 ± 0.6	4.3·10 ⁻¹			
<i>Crystalline phase, static method</i>								
315.19-354.75	298.15	33.94 ± 0.02	91.0 ± 0.2	190.4 ± 0.7	1.1·10 ⁻¹	1.0000	20.8	0.008
	334.97 ^{<i>e</i>}	26.94 ± 0.02	90.2 ± 0.2	188.9 ± 0.6	6.3			

^a Calculated through equation 4.14; ^b Calculated through equation 4.15; ^c Estimated value. ^d Standard deviation of the fit defined as $s = \sqrt{(\sum_{i=1}^n (\ln p - \ln p_{\text{calc}})_i^2) / (n - m)}$, where n is the number of experimental points used in the fit and m is the number of adjustable parameters in the Clarke and Glew equation; ^e Mean temperature.

The value $\Delta_{\text{cr}}^{\text{g}} C_{p,m}^{\circ} = -20.8$ J·K⁻¹·mol⁻¹ was estimated in this work from the difference between the values of $C_{p,m}^{\circ}(\text{g}, 298.15 \text{ K}) = 126.0$ J·K⁻¹·mol⁻¹ [4] and $C_{p,m}^{\circ}(\text{cr}, 298.15 \text{ K}) = 146.8$ J·K⁻¹·mol⁻¹ [5]. The results of $\Delta_{\text{cr}}^{\text{g}} H_{\text{m}}^{\circ}(298.15 \text{ K})$ thus obtained are in very good agreement with the review of literature values for benzoic acid presented by Ribeiro da Silva *et al.* [6] ($\Delta_{\text{cr}}^{\text{g}} H_{\text{m}}^{\circ}(298.15 \text{ K})/\text{kJ}\cdot\text{mol}^{-1} = 90.2 \pm 1.9$, mean of 23 values).

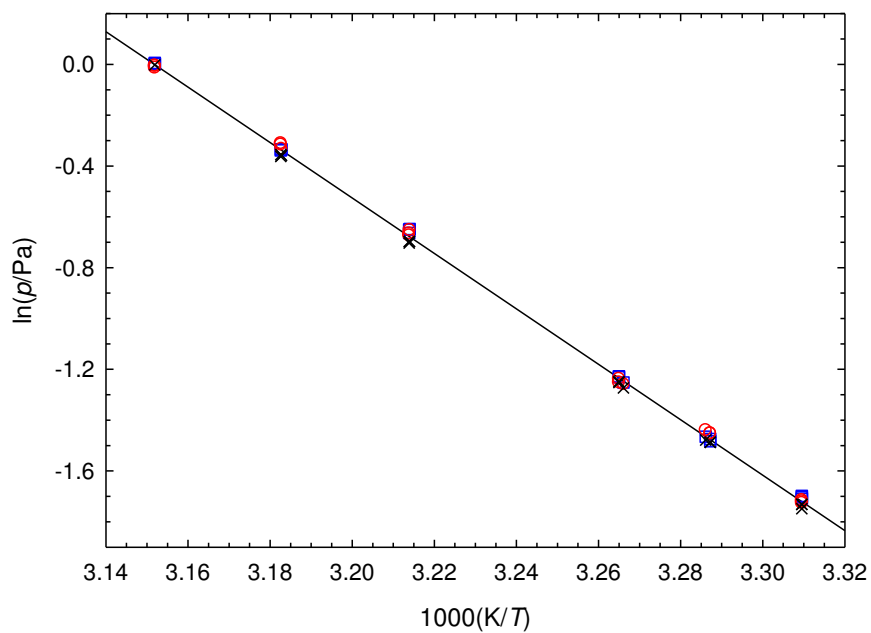


Figure C.2. Plots of $\ln(p/\text{Pa})$ against $1000(K/T)$ of benzoic acid: effusion vapor pressures for the different effusion orifices - \square , small; \circ , medium; \times , large.

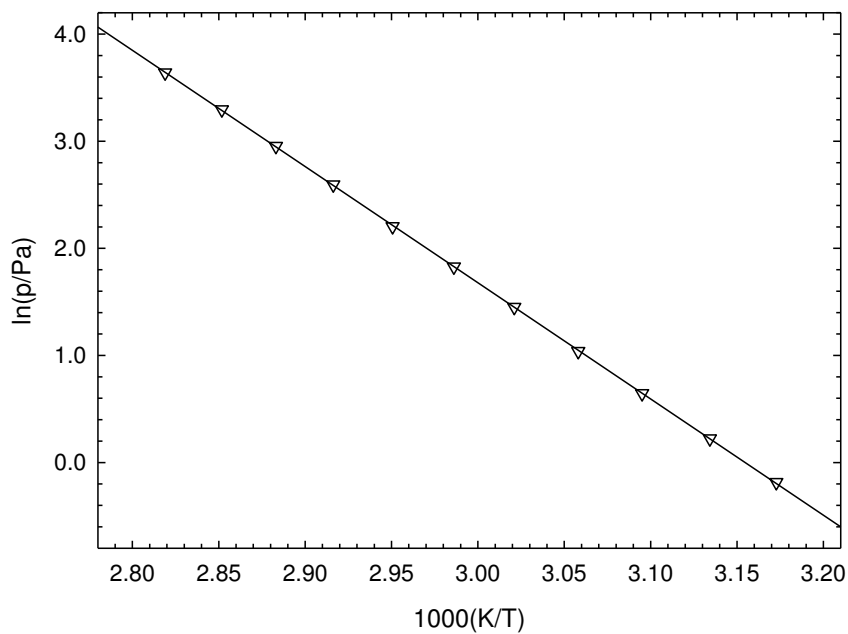


Figure C.3. Plots of $\ln(p/\text{Pa})$ against $1000(K/T)$ of benzoic acid: ∇ , static crystal vapor pressures.

C.2.2. *N*-Methylnicotinamide

Table C.4. Vapor pressures of *N*-methylnicotinamide determined by the Knudsen effusion method. ^a

T / K	t/s	Orifices	m / mg			p / Pa			
			m_{small}	m_{medium}	m_{large}	p_{small}	p_{medium}	p_{large}	p_{mean}
329.17	28628	A ₂ '-B ₅ '-C ₈ '	5.28	6.58	8.16	0.104	0.105	0.104	0.105
331.27	28628	A ₃ '-B ₆ '-C ₉ '	6.77	8.20	10.23	0.134	0.132	0.131	0.132
333.15	21342	A ₁ '-B ₄ '-C ₇ '	6.15	7.48	9.31	0.164	0.162	0.160	0.162
335.17	21342	A ₂ '-B ₅ '-C ₈ '	7.68	9.76	12.10	0.206	0.211	0.209	0.209
337.27	21342	A ₃ '-B ₆ '-C ₉ '	9.70	12.02	15.00	0.261	0.261	0.259	0.260
339.15	14545	A ₁ '-B ₄ '-C ₇ '	8.30	10.27	12.56	0.328	0.328	0.320	0.325
341.16	14545	A ₂ '-B ₅ '-C ₈ '	10.20	12.91	15.82	0.404	0.414	0.404	0.407
343.27	14545	A ₃ '-B ₆ '-C ₉ '	12.91	15.86	19.72	0.513	0.510	0.505	0.510
345.13	10761	A ₁ '-B ₄ '-C ₇ '	11.63	14.19	17.65	0.627	0.619	0.613	0.619
347.16	10761	A ₂ '-B ₅ '-C ₈ '	14.26	17.94	22.30	0.771	0.784	0.776	0.777
349.27	10761	A ₃ '-B ₆ '-C ₉ '	17.91	21.97	27.42	0.971	0.964	0.957	0.964

^a $u(T/K) = \pm 0.01$, $u(p/\text{Pa}) = \pm 0.01$.

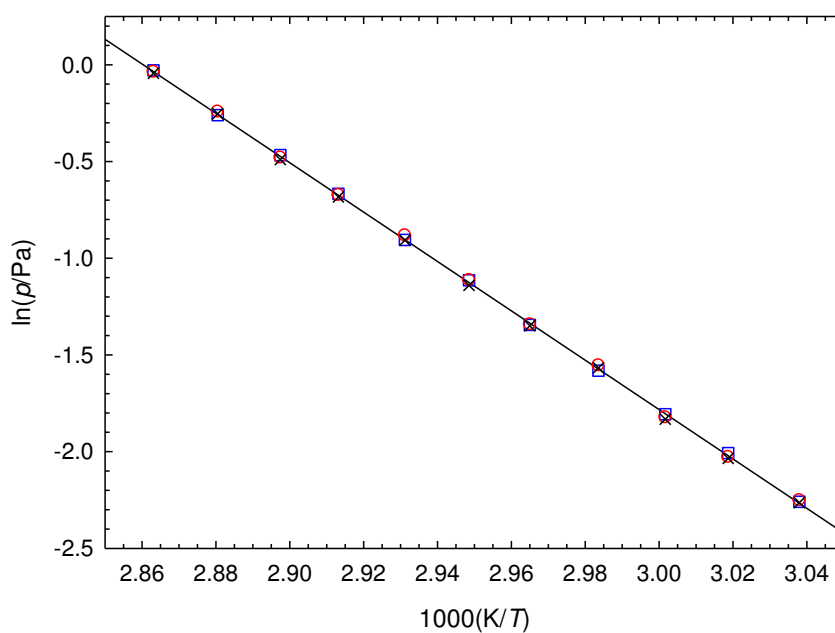


Figure C.4 Plots of $\ln(p/\text{Pa})$ against $1000(K/T)$ of *N*-methylnicotinamide: effusion vapor pressures for the different effusion orifices - \square , small; \circ , medium; \times , large.

Table C.5. Standard ($p^\circ = 0.1$ MPa) molar properties of sublimation and vaporization of *N*-methylnicotinamide, derived from the experimental vapor pressure results.

$\Delta T / \text{K}$	θ / K	$\frac{\Delta_{\text{cr}}^{\text{g}} G_{\text{m}}^{\circ}(\theta)}{\text{kJ}\cdot\text{mol}^{-1}}$	$\frac{\Delta_{\text{cr}}^{\text{g}} H_{\text{m}}^{\circ}(\theta)}{\text{kJ}\cdot\text{mol}^{-1}}$	$\frac{\Delta_{\text{cr}}^{\text{g}} S_{\text{m}}^{\circ}(\theta)^{\text{a}}}{\text{J}\cdot\text{K}^{-1}\cdot\text{mol}^{-1}}$	$p(\theta)^{\text{b}}$ Pa	R^2	$\frac{\Delta_{\text{g}}^{\text{cr}} C_{\rho, \text{m}}^{\circ \text{c}}}{\text{J}\cdot\text{K}^{-1}\cdot\text{mol}^{-1}}$	s^{d}
<i>Crystalline phase, effusion method</i>								
329.17-349.27	298.15	44.24 ± 0.04	107.4 ± 0.4	211.8 ± 1.3	1.8·10 ⁻³	0.9999	27.4	0.008
	339.22 ^e	35.62 ± 0.01	106.2 ± 0.4	208.1 ± 1.3	3.3·10 ⁻¹			
<i>Crystalline phase, literature [7]</i>								
347.78-377.39	298.15	44.13 ± 0.03	107.1 ± 0.2	211.2 ± 0.7	1.8·10 ⁻³	1.0000	27.4	0.006

^a Calculated through equation 4.14; ^b Calculated through equation 4.15; ^c Estimated value [7]; ^d Standard deviation of the fit defined as $s = \sqrt{\left(\sum_{i=1}^n (\ln p - \ln p_{\text{calc}})_i^2\right) / (n - m)}$, where n is the number of experimental points used in the fit and m is the number of adjustable parameters in the Clarke and Glew equation; ^e Mean temperature.

C.2.3. Pyrene

Table C.6. Literature results for the fluorescence quantum yield of pyrene in different solvents, and in powder form.

Sample	Solvent	$C / \text{mol}\cdot\text{L}^{-1}$	$\lambda_{\text{exc}} / \text{nm}$	ϕ_{F}	Method	Source
Solution	Ethanol	$2\cdot 10^{-6}$	313	0.65	Relative ^a	[8]
Solution	Ethanol		313	0.72	Relative ^b	[9]
Solution	Ethanol	Infinite dilution ^c	313	0.53 ± 0.02	Relative ^d	[10]
Solution	Benzene	Infinite dilution ^c	313	0.60 ± 0.03	Relative ^d	[10]
Solution	Cyclohexane	Infinite dilution ^c	313	0.58 ± 0.01	Relative ^d	[10]
Solution	Cyclohexane	$5\cdot 10^{-5}$	313	0.32	Relative ^e	[11]
Solution	Cyclohexane		266	0.69	Relative ^e	[12]
Solution	Cyclohexane		241	0.31	Relative ^e	[13]
Solution	Cyclohexane			0.66 ± 0.02	Absolute ^f	[14]
Solid				0.68	Absolute ^f	[15]

^a Standard solution of anthracene in ethanol ($\phi_{\text{F}} = 0.27$ [16]);

^b Standard solution of anthracene in ethanol ($\phi_{\text{F}} = 0.30$ [17]);

^c Fluorescence data extrapolated to zero concentration;

^d Intensities of fluorescence are compared with the intensities of excitation light scattered from non-absorbing, colloidal reference solutions;

^e Standard solution of 9,10-diphenylanthracene ($\phi_{\text{F}} = 1.0$ [18]);

^f Integrating sphere.

Solution fluorescence

Table C.7. Fluorescence spectroscopic data of pyrene in cyclohexane solutions, at room temperature.

	$\lambda_{\text{exc}}^a / \text{nm}$	$\lambda_{\text{max}}^{\text{F}b} / \text{nm}$	ϕ_{F}^c
$5\cdot 10^{-7} \text{ mol}\cdot\text{L}^{-1}$		383.8	0.43 ± 0.01
$1\cdot 10^{-5} \text{ mol}\cdot\text{L}^{-1}$	335	383.8	0.44 ± 0.01
$1\cdot 10^{-4} \text{ mol}\cdot\text{L}^{-1}$		383.8	0.45 ± 0.01

^a Excitation wavelength corresponding to the maximum absorption determined using UV-Vis spectrometry for the concentration $1\cdot 10^{-5} \text{ mol}\cdot\text{L}^{-1}$;

^b Wavelength at the maximum fluorescence emission intensity;

^c Mean values and standard deviations of the mean of three independent measurements.

Pyrene is known to present excimer emission in concentrated solutions [19] so, in order to quantify solely the monomer emission quantum yield, only diluted solutions ($<1 \cdot 10^{-4} \text{ mol} \cdot \text{L}^{-1}$) were studied. The quantum yield results reported in references 11 and 12 refer to dilute solutions that have not been degassed prior to measurement and the reported quantum yield results are smaller when compared to the remaining literature data. Even though the fluorescence spectra obtained in this work are quite consistent with those reported in the literature, the determined quantum yields seem to be consistently smaller than the ones found in the literature for cyclohexane solutions (not considering the literature results reported by in references 11 and 13).

Solid state fluorescence

Table C.8. Absorption and fluorescence quantum yield results of pyrene in powder form, for different amounts of sample.

Sample amount ^a	λ_{exc} / nm	Abs ^b	λ_{max}^F ^b / nm	ϕ_F ^c
40 %	330 ^d	0.488	476.5	0.69
15 %		0.354		0.53
40 %	330 ^d	0.569	470.5	0.51
100 %		0.719		0.50
15 %		0.350		0.40
40 %	380 ^f	0.689	470.5	0.40
100 %		0.742		0.39

^a Rough estimate of the percentage of area of the base of the quartz dish covered by sample;

^b Determined by the Quantaurus-QY;

^c Wavelength at the maximum fluorescence emission intensity;

^d Excitation wavelength corresponding to the maximum absorption determined using UV-Vis spectrometry;

^f Excitation wavelength corresponding to the maximum absorption determined using the Quantaurus apparatus.

The solid state emission spectrum shows a single broad unstructured band corresponding to the excimer, red-shifted in relation to the monomer (figure C.5). The first value reported in table C.8. for the solid state quantum yield of pyrene is in agreement with that reported in reference 12. This determination was repeated a few months later to test the dependence of quantum yield with amount of sample and eventual self-absorption effects in the solid phase, and the repeated results were smaller than the original one. The difference in quantum yield could be due to eventual sample degradation.

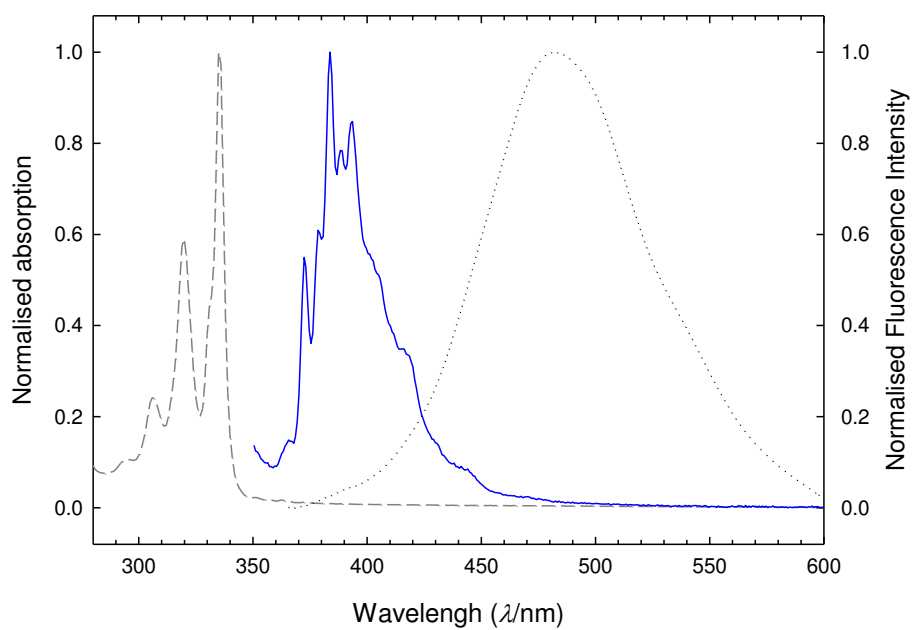


Figure C.5. Normalized UV/vis absorption and fluorescence emission spectra of pyrene ($\lambda_{\text{exc}} = 335$ nm): dashed line - absorption spectra ($1 \cdot 10^{-5}$ mol·L⁻¹); solid line - solution fluorescence spectra ($5 \cdot 10^{-7}$ mol·L⁻¹); dotted line - powder fluorescence spectra.

References

- [1] M.E. Wieser, N. Holden, T.B. Coplen, J.K. Böhlke, M. Berglund, W.A. Brand, P. De Bièvre, M. Gröning, R.D. Loss, J. Meija, T. Hirata, T. Prohaska, R. Schoenberg, G. O'Connor, T. Walczyk, S. Yoneda, X.-K. Zhu, *Pure Appl. Chem.* 85 (2013) 1047-1078;
- [2] A. Thompson, B.N. Taylor, 2008. *NIST Special Publication 811. Guide for the use of the International System of Units (SI)*, National Institute of Standards and Technology, Gaithersburg (<http://physics.nist.gov/cuu/pdf/sp811.pdf>);
- [3] P.J. Mohr, B.N. Taylor, D.B. Newell, 2015. *The 2014 CODATA recommended values of the fundamental physical constants* (Web Version 7.0);
- [4] L.M.N.B.F. Santos, M.A.A. Rocha, L.R. Gomes, B. Schröder, J.A.P. Coutinho, *J. Chem. Eng. Data* 55 (2010) 2799-2808;
- [5] D.C. Ginnings, G.T. Furukawa, *J. Am. Chem. Soc.* 75 (1953) 522-527;
- [6] M.A.V. Ribeiro da Silva, M.J.S. Monte, L.M.N.B.F. Santos, *J. Chem. Thermodyn.* 38 (2006) 778-787;
- [7] A.R.R.P. Almeida, J.A.S.A. Oliveira, M.J.S. Monte *J. Chem. Thermodyn.* 82 (2015) 108-115;
- [8] C.A. Parker, C.G. Hatchard, *Trans. Faraday Soc.* 59 (1963) 284-295;
- [9] C.A. Parker, T.A. Joyce, *Trans. Faraday Soc.* 62 (1966) 2785-2792;
- [10] W.R. Dawson, M.W. Windsor, *J. Phys. Chem.* 72 (1968) 3251-3260;
- [11] I.B. Berlman, *Handbook of Fluorescence Spectra of Aromatic Molecules* (2nd Ed.), Academic Press, New York (1971);
- [12] M.E. Abu-Zeid, J.A. Moreno-Bernal, J.R. Lopez, *J. Photochem.* 10 (1979) 221-230;
- [13] A.T.R. Williams, S.A. Winfield, J.N. Miller, *Analyst* 108 (1983) 1067-1071;
- [14] S.A. Ruetten, J.K. Thomas, *J. Phys. Chem. B* 102 (1998) 598-606;
- [15] R. Kato, K. Suzuki, A. Furube, M. Kotani, K. Tokumaru, *J. Phys. Chem. C* 113 (2009) 2961-2965;
- [16] W.H. Melhuish, *J. Phys. Chem.* 65 (1961) 229-235;

- [17] T. Medinger, F. Wilkinson , *Trans. Faraday Soc.* 61 (1965) 620-630;
- [18] E.J. Bowen, J. Sahu, *J. Phys. Chem.* 63 (1959) 4-7;
- [19] J.B. Birks, L.G. Christophorou, *Spectrochim. Acta* 19 (1963) 401-410.